Third Edition

Wire Bonding

IN MICROELECTRONICS

CD includes all the book's full-color figures plus animations

George Harman

Wire Bonding in Microelectronics

About the Author

George G. Harman is a retired Fellow of the National Institute of Standards and Technology (NIST). He has a BS in industrial physics from Virginia Polytechnic Institute & State University and an MS in physics from the University of Maryland (1959). Harman is a former President of IMAPS (1995–1996) and Chair of the IEEE CPMT Fellow Committee (1988–2002). He is a life fellow of both IMAPS and of the IEEE. He has held many other elected and appointed positions in those societies, and is a member of the ITRS Roadmap Committee for Assembly and Packaging (for more than 10 years).

He is widely considered to be the world's foremost authority on wire bonding. Harman has published more than 60 papers, 3 books on wire bonding (the 3 editions of *Wire Bonding in Microelectronics*), 8 book chapters, 4 patents, and has given about 100, 8-hour, short courses on wire bonding around the world (over the past 30 years). He has received numerous awards, both domestically and internationally. His most recent were the IMAPS "Lifetime Achievement Award" (2006) and the IEEE "Field Award for Components, Packaging, and Manufacturing Technology" (2009).

Wire Bonding in Microelectronics

George Harman

Third Edition

New York Chicago San Francisco
Lisbon London Madrid Mexico City
Milan New Delhi San Juan
Seoul Singapore Sydney Toronto

The McGraw-Hill Companies

Copyright © 2010, 1997, 1989 by The McGraw-Hill Companies, Inc. All rights reserved. Except as permitted under the United States Copyright Act of 1976, no part of this publication may be reproduced or distributed in any form or by any means, or stored in a database or retrieval system, without the prior written permission of the publisher.

ISBN: 978-0-07-164265-1

MHID: 0-07-164265-X

The material in this eBook also appears in the print version of this title: ISBN: 978-0-07-147623-2, MHID: 0-07-147623-7.

All trademarks are trademarks of their respective owners. Rather than put a trademark symbol after every occurrence of a trademarked name, we use names in an editorial fashion only, and to the benefit of the trademark owner, with no intention of infringement of the trademark. Where such designations appear in this book, they have been printed with initial caps.

McGraw-Hill eBooks are available at special quantity discounts to use as premiums and sales promotions, or for use in corporate training programs. To contact a representative please e-mail us at bulksales@mcgraw-hill.com.

Information contained in this work has been obtained by The McGraw-Hill Companies, Inc. ("McGraw-Hill") from sources believed to be reliable. However, neither McGraw-Hill nor its authors guarantee the accuracy or completeness of any information published herein, and neither McGraw-Hill nor its authors shall be responsible for any errors, omissions, or damages arising out of use of this information. This work is published with the understanding that McGraw-Hill and its authors are supplying information but are not attempting to render engineering or other professional services. If such services are required, the assistance of an appropriate professional should be sought.

TERMS OF USE

This is a copyrighted work and The McGraw-Hill Companies, Inc. ("McGraw-Hill") and its licensors reserve all rights in and to the work. Use of this work is subject to these terms. Except as permitted under the Copyright Act of 1976 and the right to store and retrieve one copy of the work, you may not decompile, disassemble, reverse engineer, reproduce, modify, create derivative works based upon, transmit, distribute, disseminate, sell, publish or sublicense the work or any part of it without McGraw-Hill's prior consent. You may use the work for your own noncommercial and personal use; any other use of the work is strictly prohibited. Your right to use the work may be terminated if you fail to comply with these terms.

THE WORK IS PROVIDED "AS IS." McGRAW-HILL AND ITS LICENSORS MAKE NO GUARANTEES OR WARRANTIES AS TO THE ACCURACY, ADEQUACY OR COMPLETENESS OF OR RESULTS TO BE OBTAINED FROM USING THE WORK, INCLUDING ANY INFORMATION THAT CAN BE ACCESSED THROUGH THE WORK VIA HYPERLINK OR OTHERWISE, AND EXPRESSLY DISCLAIM ANY WARRANTY, EXPRESS OR IMPLIED, INCLUDING BUT NOT LIMITED TO IMPLIED WARRANTIES OF MERCHANTABILITY OR FITNESS FOR A PARTICULAR PURPOSE. McGraw-Hill and its licensors do not warrant or guarantee that the functions contained in the work will meet your requirements or that its operation will be uninterrupted or error free. Neither McGraw-Hill nor its licensors shall be liable to you or anyone else for any inaccuracy, error or omission, regardless of cause, in the work or for any damages resulting therefrom. McGraw-Hill has no responsibility for the content of any information accessed through the work. Under no circumstances shall McGraw-Hill and/or its licensors be liable for any indirect, incidental, special, punitive, consequential or similar damages that result from the use of or inability to use the work, even if any of them has been advised of the possibility of such damages. This limitation of liability shall apply to any claim or cause whatsoever whether such claim or cause arises in contract, tort or otherwise.

Disclaimer:
This eBook does not include the ancillary media that was packaged with the original printed version of the book.

Contents

Introduction to Third Edition

The new material in this book was introduced because of new technical areas. (Examples are fine-pitch bonding, Cu wire bonding, as well as different pad metallurgies.) Also, many practical questions have been posed to the author by phone calls, plant visits, e-mails, and during many short courses taught for the University of Arizona, ISHM (IMAPS), SMI, IEEE, and other organizations. Material has been included/updated to answer the most frequently asked of these questions.

In 1970, wire bonds caused a large proportion—sometimes as high as one-third of all semiconductor-device field-failures. However, the number of recognized failure mechanisms at that time was quite limited. Typically, they were cited as "purple plague," underbonding, overbonding, and nonspecified contamination-induced corrosion. Currently (2009), dozens of chemical, metallurgical, and mechanical failure mechanisms have been identified. Part of these new mechanisms were discovered because of greatly improved analytical methods and equipment (e.g., Auger and SIMS analysis), part because of the many trillions of bonds made (and millions to billions failed), and part because of the changing technology (e.g., new metallurgies, plastic encapsulation). A study of recent Au and Al wire bond failure papers indicates that the discovery of new failure mechanisms has slowed, although the rediscovery of old ones, or variations of them, has continued. Thus, it was felt that it is appropriate to review the known failure modes and mechanisms of wire bonds, categorize them, and where possible, explain and/or give solutions to them. (New bond metallurgies are still fertile fields of investigation.)

Since failures are generally revealed by testing, the bond pull and shear tests are still described, but *updated(!)* such as for fine pitch, new mold compounds, etc. The book also discusses mechanical, metallurgical, chemical, and miscellaneous failure mechanisms. Some of these overlap and were placed in the most appropriate sections.

This book is primarily concerned with understanding failures and yield problems originating from chip-to-package wire bonds, although other wire bonds, such as crossovers and PC board bonds, are included as appropriate. Flip chip, TAB, lead-frame bonding, etc., are discussed briefly in Chap. 2 and are included elsewhere when wire bond-type interfaces and failure mechanisms have been observed. Newer pad metallurgies, such as Ni based (Chap. 6B) are fully discussed, and the increasingly popular Cu wire bonding (Chap. 3 and throughout) is described. Discussions of chip cleaning, gold plating, and gold-aluminum intermetallics are still important. The wirebonders themselves are not discussed in detail since they are updated yearly and are usually proprietary, specialized autobonders, and the manufacturers offer courses on their setup and use.

This book has been written to serve as a text to accompany courses taught by the author and others, as well as a stand-alone book. The color CD was introduced, since increasingly, modern figures are difficult to understand without color. The book is written at a practical level and is also intended for use by production line engineers in solving, or avoiding, bonding problems. However, enough detail and *many references* are included for failure analysis personnel or others who are interested in doing design and research on the subject. Today most published references are available for *quick downloading from the Internet* (further explained in the Bibliography).

Areas where more research is needed are clearly indicated. It is hoped that workers will study and fill in these gaps in the near future rather than spend time adding extra decimal points to well-characterized and understood problems. The author freely offers opinions, which the reader is, of course, free to ignore!

This third edition has several invited authors who have contributed special appendixes and chapters. This brings more diverse knowledge, than the (main) author alone could contribute. These contribution-authors are acknowledged, including their current (2009) addresses. These new contributions are greatly appreciated and should increase the areas of knowledge encompassed by this book!

It is assumed that all readers have a basic knowledge of wire bonding, single or multiple device packaging, and/or hybrid/SIP circuit assembly technology. Terms in general usage in these fields are not defined in the text, but many are in the Glossary. The book is divided into relatively independent chapters, and its Index can be used to look up specific problems.

Manuscript organization. Each chapter of this book is self-contained with its own references and numbering system. In some cases, this results in the same reference appearing in two or more chapters. This was thought to be the most convenient for readers. The chapters are coupled together by referring in the text from one to another for greater detail or explanation, where appropriate.

Manuscript style. The style is that of a technical paper, rather than the informal style used by the author in his presentations and courses on this subject. Chemical symbols are used rather than the full element name for compactness. In general, knowing that aluminum = Al, copper = Cu, and gold = Au, will take care of the majority of the usage. However, the Glossary translates most other symbols.

Units. The choice was again (reluctantly) made to use both SI and English units since parts of the American semiconductor assembly community still use the latter. However, many figures were reproduced directly from technical papers and their units may be in either system alone. Mixed units are still frequently used in English language publications. The units of force are probably the most confusing. Grams-force (gf) is most often used in this text. The reader can convert 1 gf = 9.8 mN (millinewtons). For any remaining unconverted length units, it should be noted that 1 mil = 0.001 in = 25.4 μm. Some additional conversion factors are included in the text where appropriate.

Please note: Certain commercial equipment, instruments, or materials are identified in this book in order to adequately specify an experimental procedure. Such identification does not imply recommendation or endorsement by the author(s), nor does it imply that the materials or equipment identified are necessarily the best available for the purpose at any given time.

Acknowledgments

This book could not have been written without the editorial and organizational, contributions of Erik Secula. His help is immensely appreciated. I also wish to acknowledge The Semiconductor Electronics Division management's support and dedication of resources for researching/editing the book.

Various sections of the book have benefited by the technical reviews and/or contributing comments of William J. Boettinger, Curt A. Richter, Neil Zimmerman, *NIST*; Peter Douglas, *Custom Chip Connections*; Alfaro Callejas, *Gaiser Precision Tools*; and Robert Chylak, *Kulicke and Soffa*. **Direct Contributors:** Yong Liu, *Fairchild Semiconductor* (Chapter 11); Jamin Ling, *Kulicke and Soffa* and Luke England, *Fairchild Semiconductor* (Chapter 6B); Lee Levine, *Process Solutions Consulting* (two appendixes), and Narendra Noolu, *Intel* (appendix). Many technical authors have graciously contributed original copies of their figures (and some animations) incorporated in this book. Their contributions were essential and acknowledged in the captions.

Introduction to CD

The figures on the CD are in color, when available, and a few are animated. Many of the figures and captions are not entirely "stand-alone", since it is assumed that these will be viewed along with the book. Some of the book captions had to be condensed or rewritten for space limitations, and several figures are not in the book but added to the CD to enhance understanding.

A number of the book figures should be seen in color to fully understand their meaning, which necessitated the color CD. In addition, all figures whether they have color or not, are included for convenience. These are in the order of their chapter and figure number, so that a reader can view them on a large computer screen when reading the book, or project them. The original JPG figures for the book were converted into power point slides, original figure captions from the book (or condensed) are added and converted into PDF format, which can be searched by figure number or title and can be easily viewed. In several cases when animations were available, they will follow the associated color figure slide. These may have to be clicked or double-clicked to see the animation. Readers may also have to click a security warning before the first animation, and each time if read directly from the CD.

In some cases more extensive explanation is added, or an additional figure from the author's talks/papers may follow the referenced figure, to further clarify/explain. Some long captions had to be condensed to fit the space. (Only one table, requiring color, is included.)

[Reference numbers] following the captions are those in the book, and with the same notation. Some source references and permissions are included in the captions (if not, they were made at NIST or by that section author). It is assumed that references in the printed-book captions are adequate and vice versa. It is also assumed that the figures (captions) will be viewed on a computer screen rather than projected, so the print can be small.

A title-bar color code is used to identify the different sections. Those by invited authors are GREEN. Normal chapters are RED. Animations are YELLOW with red borders. This allows the reader to find them quickly.

Cited references and copyright notices in the figure captions refer to those at the end of the appropriate chapter in the book. In a few cases, full publication references are included in "slide notes" at the bottom of the figure or in an orange box in the upper left of the slide. A cursor touch or double clicking will open it up.

CHAPTER 1

The Technical Introduction to the Third Edition

Currently (2008), there are over 8 to 9 billion wires bonded per year on the planet. Most were used in the 160 billion ICs produced, but many more are in interconnect transistors, LEDs, etc. The number of wires (with two bonds on each wire) has increased every year, including recessions to the present, from two or three bonds in 1947 (see Fig. 1-1). The infrastructure is so extensive that no other chip-interconnection method can displace wire bonds in the foreseeable future, although other technologies, particularly flip chip and its variations, are growing at a faster rate. The industry is driving wire-bonding technology toward: (1) increased yields (<25 ppm defects) (see Chap. 9), (2) decreased pitch (approaching 20 μm for both wedge and ball bonds), and (3) lowest possible and ever decreasing cost. However, many new specific technical and material issues will be involved in achieving these goals. Some examples are new bond-pad metals (e.g., palladium, see Chap. 5; various Ni-based metallizations, see Chap. 6), higher-frequency ultrasonic energy (how high, how to optimize and for what materials, see Chap. 2), the lack of quantitative understanding of the ultrasonic bonding mechanism, the reality of real-time bond monitoring, as well as continuing new failure modes resulting from wafer fabrication (e.g., bond pad lift-up), and reliability problems in new plastic molding compounds (e.g., "green" mold compounds), as well as increasing wire-sweep problems (potential solution Cu ball bonding?). The above issues result in an expanding, but technically challenging future for this method of chip interconnection.

Some of the history and references of early wire bonding development are given in Sec. 2.5. Also, the bonding machine components, such as the transducer and bonding tools, are described in that section, along with a description of the ultrasonic-bonding mechanism.

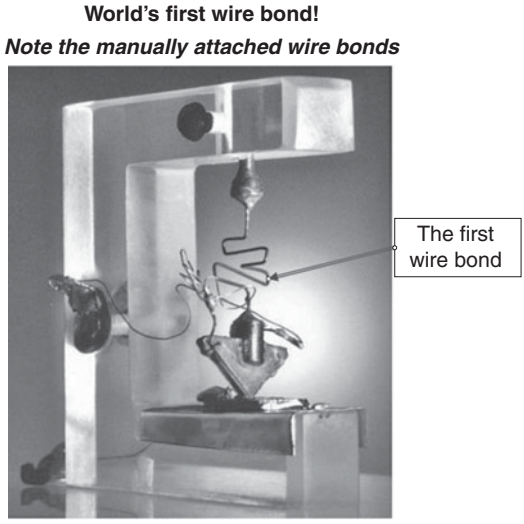

FIGURE 1-1 Replica of the first transistor, Bell Labs, December 23, 1947, indicating the first wire interconnection. (*Courtesy Bell-Labs/Lucent, 1947.*)

A discussion of the differences between various bonding systems with a table comparing the advantages and disadvantages of each is given in Table 2-1, Chap. 2, to help choose the appropriate wire bonding, as well as alternative technologies. Tab, and Beam Leads, which were once considered leading edge technologies, have almost vanished.

1.1 The Wedge- and Ball-Bonding Machine Operations

Figure 1-2 is the simplified step-by-step procedure of the wedge-bonding machine operation and Fig. 1-3 is the same for a ball bonder. The captions are self-explanatory. These procedures have not changed for more than 30 years, and new diagrams are unnecessary. Some Web sites give animations of the bonding process, http://www.kns.com/_flash/cap_bonding_cycle.swf (see Bibliography). Autoball bonders are several times faster than autowedge bonders, since after making the ball bond, the wire can be moved, with the capillary, in any direction to make the second bond; whereas, for wedge bonds, either the device (or transducer) must be mechanically oriented in an approximately straight-line direction between the two bonds before the first bond is made. If not, the thinned heel of the first wedge bond may be bent sideways (stressed and weakened or cracked) as the wire moves toward an angled second-bond position. Currently, wire-looping methods can bend the wire in a smooth radius as it proceeds from the first to the second bond, and such wedge-bonding rates increase somewhat, but it seems to have achieved limited application.

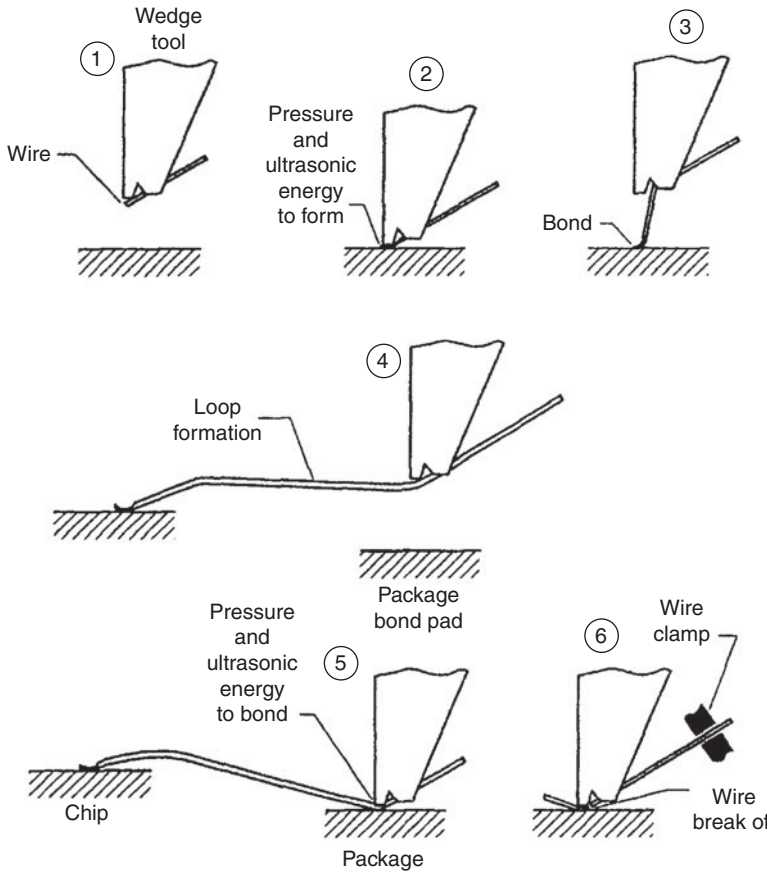

FIGURE 1-2 Simplified procedure for making an ultrasonic-wire bond between a chip-bond pad and the package with a typical wedge-type tool. (1) Wire is located between the bonding surface of the tool and the bond. When used on a manual bonding machine, the tool is lowered to its first search position (75 to 125 m above the bonding surface). This height is chosen by the operator. Autobonders eliminate the search position entirely. (2) The tool is lowered and presses the wire against the bonding surface with a predetermined force. Ultrasonic energy is applied for a preset time to make the first bond. (3) The tool is raised while the wire is paid out from the spool of wire (not shown). (4) The work holder moves the second bonding site under the tool (if an autobonder, usually the transducer and tool moves), the loop is formed and the tool is lowered to its second search position (similar to steps described in 1). (5) The tool is lowered to the bonding pad, and the second bond is made, as in 2. (6) After the second bond has been made, a wire clamp (behind the tool) closes and pulls back on the wire to break it at the heel of the bond. The tool is then raised, and the end of the wire is fed out underneath the tool until the end is located somewhat beyond the front of the tool (the tail length), as shown in 1. The bonder is then ready to repeat the cycle. Updated and redrawn from Ref. [1-2].

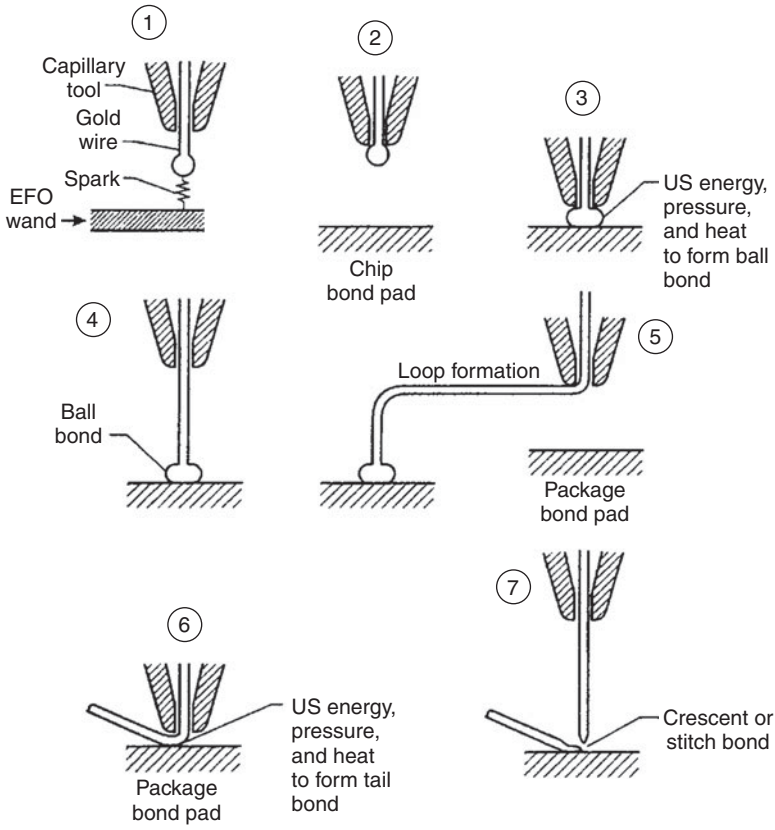

Figure 1-3 Simplified procedure for making a ball-stitch wire interconnection with a capillary tool. (1) Gold wire is fed through the capillary, and an EFO spark melts the wire. A gold ball forms at the end of the wire. (The ball typically consumes about a 300 μm length of a 25 μm dia. wire, but will be less for fine-pitch bonding.) (2) The wire is retracted so that the ball is positioned against the bottom of the capillary. (3) The tool is lowered to the bond pad, and the gold ball is pressed against it. The interface rises to the bonding temperature (from the heated workholder), US energy is applied, and the ball bond is formed. (4) The tool is raised, leaving the ball welded to the surface, and forming the wire loop as it moves toward the second bond position. (5) The bond pad is positioned beneath the bonding tool (or capillary). (6) The tool is lowered, as in step 3, to make a bond. This bond (and any subsequent bonds made before the wire is broken off) is called a stitch bond. Sometimes the final bond is called the crescent bond because of its shape. (7) After the stitch bond is made, the capillary tool is raised, and a wire clamp above the capillary tool (not shown) pulls and breaks the wire free. The tool rises up, the clamp lowers the wire sufficiently to allow another ball to be made, and the bonder is ready to repeat the bonding cycle.

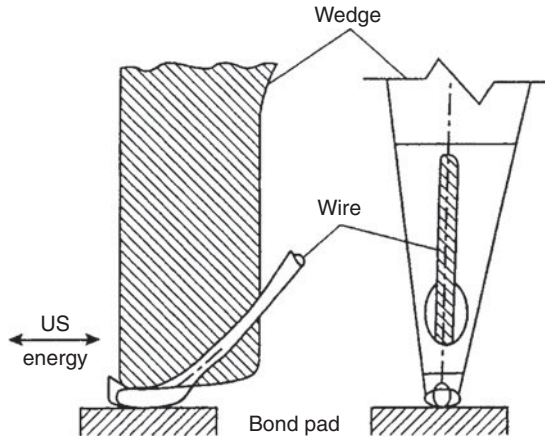

FIGURE 1-4 A close-up of the bonding tool and wire for an ultrasonic (US) wedge bond. Arrows indicate the direction of the US energy. The tool is usually made of WC, but some are made of other hard materials such as TiC [1-3].

Figure 1-4 gives a close-up of the bonding tool and wire during the process of making an ultrasonic (US) wedge-wedge wire-bond. Arrows indicate the direction of the US energy tool motion. Figure 1-5 is similar for a ball bond. In either case, if heat is added to assist the ultrasonic-bonding process, then it is called thermosonic (TS) bonding.

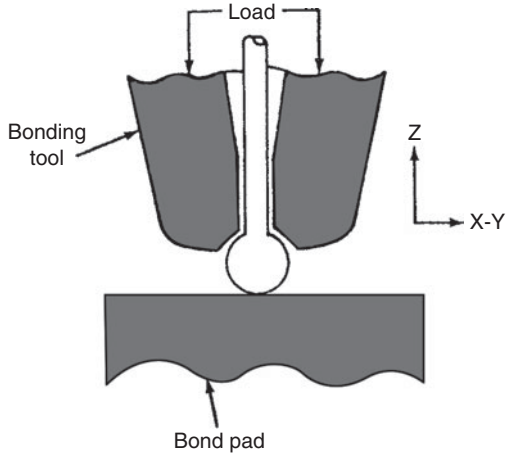

FIGURE 1-5 A close-up of a ball-bonding capillary tip (cutaway) with the ball resting on the bond pad (before the bonding load is applied). Arrows indicate the direction of the bonding load (force). Capillaries are usually made of hardened, scintered Al_2O_3, but many other materials have been used [1-3].

This heat usually comes from the machine workholder (the base to which the package is clamped), but in some cases, it can be a heated-bonding tool or capillary. TS bonding usually takes place at greater than or equal to 150°C, but there are many cases where lower or higher temperatures are used. When the temperature approaches 300°C, a gold wire bond can often be made without any ultrasonic energy. This is called thermocompression (TC) bonding. The bonding sequence is the same as for TS bonding, Fig. 1-3, except that no US energy is applied, a longer bond time is required, and the stage temperature is higher (≥300°C). Thermocompression bonding is rarely used today because the high temperatures may harm plastic packaging materials, and also, the bonding process is more affected by contamination than is TS bonding (see Chap. 7), and the TS bond time (10–15 ms) is much shorter, a requirement of modern high-speed autobonders. Animations of the tool motions are available from the Web sites of several autobonder companies and impart considerable understanding that still photographs cannot. See, Further readings.

1.2 How to Approach Bonding Problems?

1.2.1 Which Metals Can Be Ultrasonically Bonded?

There may be cases when an unusual metal pad must be US bonded, and it is not obvious whether this is possible. The *Welding Handbook* [1-3] gives a figure, reproduced as Fig. 1-6, that shows which metallurgical combinations have been ultrasonically welded (bonded) with fine wire. The caveat is that there was no information on the reliability or potential bond yield of such welded couples. Gold wire can be TS bonded to Pd films (a recent high-volume process discussed in Chap. 5), and Cu is also TS (ball) bonded to Al in volume IC production. Large-diameter Al wire is readily bonded to stainless steel and Ni, as well as directly to Si. Annealed Nb wire has also been bonded to Nb film [1-4] for use in superconducting devices. Creativity abounds in the area of US bonding with new materials.

Data in Table 1-1 is useful when approaching a new bonding situation such as often occurs in sensors, MEMS, high-temperature devices, superconductors, and the like. This figure, developed by the ASW, was not designed for microelectronics bonding, but rather US welding in general. Many of these metals require special preparation, such as in Ref. [1-4]. Some require temperatures above those acceptable for microelectronics. In general, hard refractory metals cannot be used as wire in microelectronics. However, the table shows the wide range of materials that it is possible to bond.

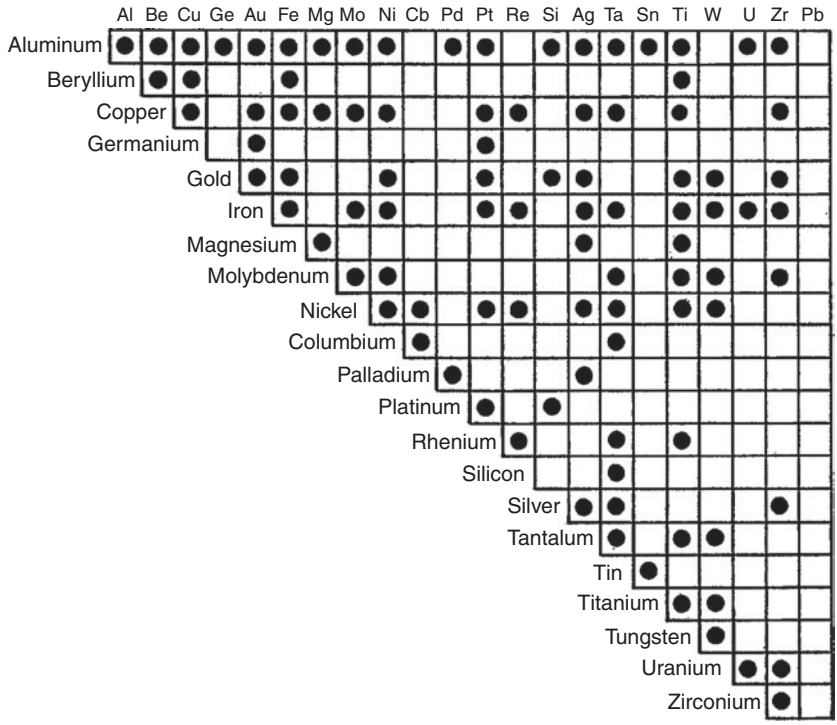

Figure 1-6 Metals which have been successfully joined together by ultrasonic welding or in which welding feasibility has been demonstrated. (*Used with permission of the American Welding Society (AWS) Welding Handbook Committee, A. OBrien and C. Guzman, ed. 2007, Welding Handbook, 9th Edition, Volume 3*).

Reaction	Standard Reduction Potential (V)
$Au^{+} + e \leftrightarrow Au$	1.69
$Au^{+++} + 2e \leftrightarrow Au^{+}$	1.4
$AuCl_4^{-} + 3e \leftrightarrow Au + 4Cl^{-}$	1.0
$Al^{+++} + 3e \leftrightarrow Al$	–1.66
$Cu^{+} + e \leftrightarrow Cu$	0.52
$Ag^{+++} + 2e \leftrightarrow Ag^{+}$	1.9
$Ni^{++} + 2e \leftrightarrow Ni$	–0.26

Note: This table is only indicative.

Table 1-1 The electrochemical series: These values are measured with respect to the potential of a standard hydrogen electrode. However, for bond pads, there may be water, electrolytes, and especially voltages present, which can cause worst case reactions on chips. Therefore, this table is only indicative. Also see App. 5B for corrosion reactions.

1.2.2 Assessing the Bondability and Reliability of Proposed New Bond Systems

There are times (particularly in the MCM, MEMS, and sensor industries), when a new metallization system or wire must be bonded together. The following is a list of steps to consider when approaching such problems. Table 1-2 outlines the steps and these are described in detail below, with examples.

1. Can it be welded by ultrasonic, TS, and or possibly TC methods? As a first cut, see tables of ultrasonically bondable materials in the *Welding Handbook*, [1-3] Fig. 1-6. For device metallization, consider how any possible dopants (e.g., Cu and Si in Al) might affect bondability and cratering. Very frequently, someone has worked out the problems you face, and their publication will save time (and money). For example, in order to bond a 50-μm diameter superconducting niobium wire to niobium thin films [1-4], it was necessary to anneal the wire at ~ 2200°C (by passing current through it in a vacuum), which softened (annealed) it from a Vickers hardness value of 180 down to 80 kgf/mm^2. To prevent oxidation of the thin-film pads before using, a thin coating (4 nm) of Pd was sputtered onto the wire. After those

1) Is it known to be weldable by ultrasonic, TC, or TS method? (See Fig. 1-6.)
2) How can possible metal dopants affect bondability cratering or reliability? (Cu or Ti in metal?) (See Chaps. 8 and 9.)
3) Are there any potential bondability or handling problems that could occur for high-volume production (Cu oxidizes easily)?
4) Does the metal form a soft or hard oxide *compared to itself*? (Hard is best for bonding!)
5) Is the new wire (or metallization) harder than Al or Au? There may be cratering or bondability problems. (See Chap. 8.)
6) Are there numerous intermetallic compounds that may form—if so are their melting points high or low?—look it up in phase diagrams. (High, >600°C is more stable.) (See Chap. 5.)
7) Are the individual materials easily corroded? Does the bond couple form a corrosion couple? Check the electrochemical series. (See Table 1-1.)
8) Is either metal easily attacked by halogens or sulfur compounds? (They are everywhere.) (See App. 5B, Chap. 5.)

TABLE 1-2 Assessing the Reliability of a Proposed New Bond-Metal-System

treatments, bond parameters of 90 gf (880 mN), plus normal power and time produced good strong bonds. As in this example, a great deal of ingenuity may be called for, but in most cases, good bonds can be made.

2. Are there any potential bondability or handling problems for high-volume production? Does the metallization form a soft oxide during long storage or normal chemical treatment? As an example, Ni and Cu are bondable by Al and Au, but each has a soft oxide (covering a hard metal) that reduces the bondability and must be removed or else special bond schedules or techniques developed. Aluminum is soft, but has a hard-brittle oxide which easily shatters and is pushed aside into debris zones during bonding. (See Fig. 2-7 that pictorially shows this process.) This type of oxide does not present a bonding problem.
3. Is the new wire harder than Al or Au (e.g., Cu)? If so, when bonding to pads over Si, GaAs, or most other low-fracture toughness semiconductor chips, the cratering probability is increased and may require special bonding techniques, schedules, or modification of the under-pad structure by adding hard barriers such as Ti, Ti-W, Ti-N, or Ta (see Sec. 5.1.5).
4. Are there numerous intermetallic compounds that may form and affect reliability? Look up the phase diagram. If such intermetallic compounds exist and have high melting points (e.g., >1000°C), then they are stable and should not significantly affect reliability. If low (500°C), then they are less stable, and their constituents will continue to diffuse, and their reliability is in question. The activation energy of individual compounds can be approximated from the following empirical equation:

$$\text{Activation energy} \sim \frac{\text{melting point (K) (kcal/mol)}}{A}$$

where $A \approx 35$ for face-centered cubic metals but $A \approx 50$ for Au-Al intermetallic compounds (Note: 1 eV ≈ 23 kcal/mol). There are many complications in using such a formula because the nucleation and other properties of different compounds vary, but it is a beginning. As an example, Ni-Al compounds have a very high melting point. They are refractory and are stable at jet turbine blade temperatures: Ni-Al bonds do not fail from intermetallic problems.

Even if there are no intermetallics in a bimetallic bond system there may still be interdiffusion which could lead to

Kirkendall-type voids. As an example, Au bonds to Ag (as discussed in Sec. 2.3.5) and may or may not be a problem, depending upon the thermal environment of the device and the type of metallurgical defects present (thick-film silver is less reliable than electroplated silver for Au bonds). As another example, one might consider Au-ball bonds to platinum. This is a completely miscible metallurgical system, but because the activation energy for interdiffusion is high, platinum is not likely to diffuse into the Au. Data given by Hall (Chap. 6, Fig. 6-9) indicates that temperatures in the range of 400°C would be required for significant interdiffusion, whereas Ni can diffuse into Au by grain boundary diffusion in the 100 to 200°C range (as discussed in Sec. 3.4.1).

5. Are the individual materials easily corroded? Does the bond couple have a high probability of making a corrosion couple with Cl? Halogens and sulfur compounds are omnipresent, so look up their effect on the bare metals. Look up the electrochemical series potentials as in Fig. 1-6 (which is a simplified version) [1-5]. If the most common reduction reactions of the metals are widely separated, then corrosion is probable in the presence of halogens and moisture. As an example, Al is strongly negative, –1.66, and Au positive, +1.69, making a good battery that corrodes easily consuming the Al. Gold and Ag, however, are both strongly positive; thus, one would not expect corrosion on these bonds. Such corrosion has been discussed in several chapters of the book. On the other hand, most Ni reactions are negative except one, whose occurrence is less probable. Thus, the Ni-Al couple has not been observed to corrode. The electrochemical series must be used with caution since the measurements are made under very specific conditions. However, such information can be useful in prediction of possible problems in some new metallurgical combination.

1.2.3 Some Unusual Uses of Wire Bonds

Bonds can be used for many different purposes other than simply making electrical connection through wires. Figure 1-7 gives a creative application of ball bonding that forms an electrical connection between conductors in two different planes. Soldering was not practical in this case [1-6]. Ball bonds are also used as a fab-less way of bumping chips (frequently called stud bumps—see Chap. 9) for flip-chip bonding, and every manufacturer of autobonders makes specialized machines for that purpose, and even for whole wafer bumping (see Chap. 9).

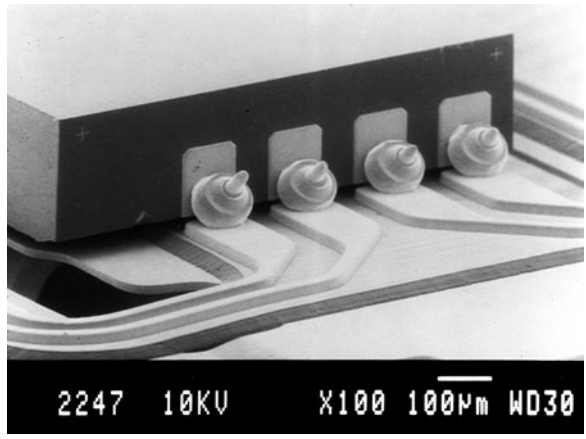

FIGURE 1-7 An unusual application of ball bonding that forms an electrical connection between conductors in two different planes. In this case, the ultrasonic energy (tool motion) is parallel to the length of the component. Both bonding surfaces were Au plated (over Ni/Cu). The ball (wire) is Au, 1% Pd. Creative (oriented to angle the package) clamping was also necessary to hold the unit in place. (*Reprinted with permission from Hutchinson Technology, Hutchinson, MN, USA.*)

References

1-1 Wesselmann, C., "Flip Chip off the Dime," an editorial in *Advanced Packaging*, V-5 (March/April 1996), p. 7.

1-2 Schafft, H. A., Modified from Testing and Fabrication of Wire-Bond Electrical Connections—A Comprehensive Survey, National Bureau of Standards (NIST) Tech. Note 726 (September 1972), pp. 1–129.

1-3 Ultrasonic Welding, In: *Welding Handbook*, 9th Ed, Vol 3, Welding Processes, Part 2, Miami: American Welding Society, 2007. ISBN 0-978-87171-053-6.

1-4 Jaszczuk, W, ter Brake, H. J. M., et. al., "Bonding of a Niobium Wire to a Niobium Thin Film", *Measurement Science and Technology*, v-2 (1991), pp. 1121–1122.

1-5 Any chemical handbook or the Handbook of Chemistry and Physics (CRC Press) contains such tables.

1-6 Houk, G. D., private communication Hutchinson Technology, Hutchinson, Minnesota.

This page intentionally left blank

CHAPTER 2

Ultrasonic Bonding Systems and Technologies, Including a Description of the Ultrasonic Wire Bonding Mechanism

2.1 Introduction

Currently (2008), the interconnections to >90% of integrated circuit (IC) and other semiconductor chips are ultrasonically welded in some manner. The exception being the devices that have solder bumps, or other variations of flip chips (C4), as well as a few thermode-bonded TAB devices (see Fig. 2-20). Aluminum-to-aluminum cold ultrasonic (US) welds are usually made with Al, 1% Si wire (25–50 μm in diameter) to various Al alloy (1% Si, 1–2% Cu, etc.) bonding pads on semiconductor chips, or often Ni-Au, Pd, etc. on the package. Larger diameter Al wire (up to ~0.75 mm, usually supplied in the fully annealed condition) is used to interconnect power devices that may require many amperes of current. Aluminum ribbon wire is gaining acceptance for very high-current interconnections, and major manufacturers of large wire bonders offer ribbon capabilities (see Sec. 2.7.1). However, Au-ball thermosonic bonding is used for the overwhelming

number of interconnections in microelectronics today. (Because of price and some mechanical/electrical properties, Cu wire is replacing Au in some applications, see Chap. 3.)

The ultrasonic transducer is the heart of all types of wire-bonding machines and, therefore, is described first in this section. The various wire-bonding technologies, as well as the competing interconnection technologies, are also described and compared.

2.2 Ultrasonic Transducer and Tool Vibration Modes

The ultrasonic transducer and bonding tool (inserted to the proper length) together form a mechanical resonant structure. The operating frequency is chosen so that both components can be made compatible with the size of the welding structures (i.e., generally, the higher the frequency, the smaller the components). Small, low-mass/inertia transducers speed up the mechanical movement. Most current autobonder systems operate over 100 kHz and typically from 120 to 140 kHz. (Experiments have been carried out as high as 250 kHz.) An example of a traditional older (60 kHz) transducer used in microelectronics bonding, including the capillary (or bonding tool), is given in Fig. 2-1. There are five main parts to the transducer. The first, (A), is the electrical-to-mechanical energy transducer. This is usually a piezoelectric element* and it converts the 60 kHz (or higher frequency) electrical energy (from the ultrasonic power supply) into mechanical vibrations that travel to the tool. The second, (B), is the clamp. It is located on a vibration node and is the part that is clamped or held by the bonding machine. If it happens to be located off the node, then part of the ultrasonic energy will be fed into the machine housing instead of the bonding tool. The third, (C), is often referred to as the horn, and it usually has a taper that magnifies the ultrasonic wave amplitude as an electrical transformer that can step up voltage. The fourth, (D), is the ultrasonic wave amplitude. The tool, or capillary, (E), is clamped perpendicular to the axis of the horn, so it is driven in a front-to-back vibration mode. The electrical energy from the ultrasonic power supply is stabilized by a phase-lock circuit to minimize drift and keep the ultrasonic system close to its resonance during bonding. Application of the energy to the transducer may be sharp or slowly ramped up, depending on the particular manufacturer and application. A modern 120 kHz autobonder transducer is shown in Fig. 2-2. It performs the same function as in Fig. 2-1, but because of design and higher frequency, is very small [~4 cm (~1.6 in) long] with low mass and thus low-mechanical inertia. Both features are essential

*These elements generally have a high impedance, and, in some cases, the vibration amplitude will decrease during the bonding load.

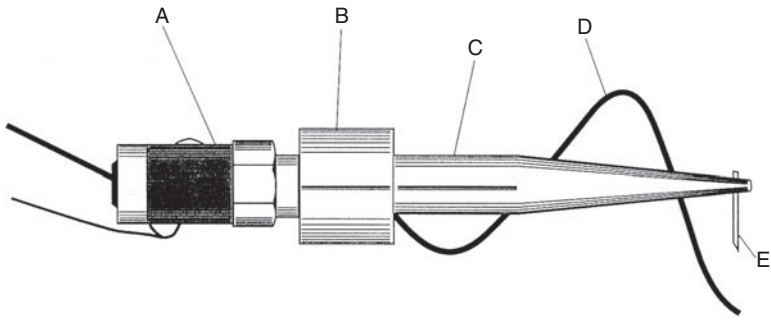

Figure 2-1 An example of a typical ultrasonic transducer used for manual microelectronics wire bonding (welding). The bonding tool (capillary) is shown near the tip. (A) is the transducer element; (B) is the mounting clamp, which is located on a vibration node and is clamped to the bonding machine; (C) is referred to as the horn (tapered to amplify the ultrasonic wave); (D) represents the ultrasonic wave amplitude; and (E) is the tool, or capillary, which is clamped perpendicular to the axis of the horn. This 60 kHz unit is about 12 cm (~5 in) long.

for the ever-increasing speed of autobonder operation. Some other autobonder manufacturers' transducers are shaped more like Fig. 2-1, but reduced to a size similar to Fig. 2-2.

The vibration modes of wedge-bonding tools were extensively studied around 1970, primarily by IBM [2-1 to 2-4], NIST (NBS) [2-9 to 2-11, 2-14, 2-15], and Takeda [2-17]. Currently, most major autobonder manufacturers design their own transducers and use some form of measurement system to characterize them. Laser interferometers, nonlaser fiber optic probes, capacitor microphones, and magnetic pickups have all been used to study tool vibrations. The typical 60 kHz tool vibration modes [2-8 to 2-12, 2-14, 2-15], both unloaded

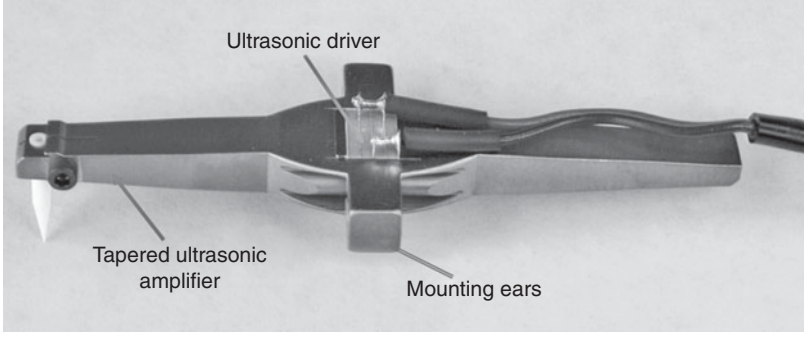

Figure 2-2 An example of a transducer from a high-speed autobonder. It is low mass and only about 4 cm (1.6 in) long (resulting in low inertia) to allow high-speed movements. The US drive is at ~120 kHz. (*Courtesy of K&S.*)

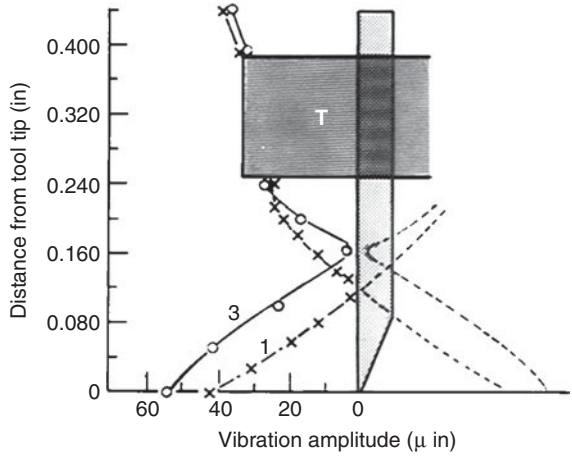

Figure 2-3 Wedge bonding–tool vibration modes for 60 kHz excitation. The vibration amplitude (peak to peak) was measured with a laser interferometer (as shown in Figs. 2-3 to 2-5). The dark portion with the *T* in it represents the position and the vibration amplitude of the transducer horn. The transducer frequency was 60 kHz. Modal patterns for a short, 30° (angle of wire entering the tool) WC too (1) shown unloaded and during the actual bonding of 25-μm Al, 1% Si wire. The bonding force was 25 g: curve 1, (×), unloaded; curve 3, (o), near end of an actual bonding cycle. The symmetry of the vibration is indicated by the dotted curves on the back side of the tool; these mirror-image amplitude curves are omitted for subsequent figures for clarity, showing only the front portion of the vibration. The large dark area (*T*) represents the position and vibration amplitude of the transducer horn. (Note: 10 mil = 0.254 mm) [2-9 to 2-11].

and during bonding, are shown in Figs. 2-3 to 2-5, in curves 1 to 3. These absolute vibration amplitude measurements were made with a laser interferometer. The US power supply used to drive the transducer for these studies maintained a fixed frequency of ~60 kHz and constant amplitude during bonding.* In these figures, "*T*" indicates the end of the transducer.

The loaded vibration nodes are seldom as sharp (usually rounded) or as complete as the unloaded ones. The nodal position during bonding is dependent upon the mechanical loading of the tool tip, which is primarily a function of the bond deformation (~1.6 wire diameters). A smaller deformation, such as 1.2, may result in a nodal rise of only 0.50 to 0.64 mm (20–25 mils) from the unloaded position. This tool showed no significant change in tip amplitude during bonding, but such changes would be expected if the bonding force and/or the bond

*Modern U.S. power supplies are phase-locked and can change the frequency a few hundred hertz or so during bonding to keep the resonant system optimally tuned. This should not significantly alter the modal patterns or the tool-loading effects.

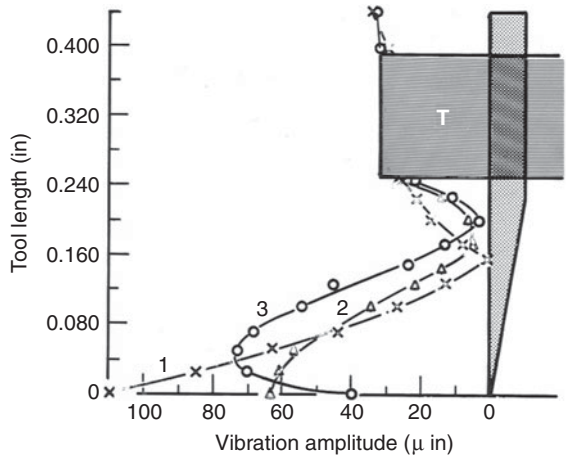

Figure 2-4 Modal patterns for a 60° tool shown unloaded and during actual bonding of 25 μm Al, 15% Si wire. The bonding force was 25 g. Modal patterns: curve 1, unloaded; curve 2, 7 ms after beginning of bonding cycle; curve 3, 5 ms before end of bonding, showing the tool vibration loading down near the end of bonding. Each point on the loaded curves (2 and 3) is an average obtained from three bonds. The tool is clamped into "*T*" with the indicated extension. The vertical axis is to the scale of the component dimensions; however, the horizontal axis is to a much smaller scale, since it represents the ultrasonic tool vibration amplitude as measured by the laser. The vibration envelopes are plotted as solid and dotted lines in front of the tool. These tool vibration measurements were published in [2-7 to 2-11].

deformation were increased. Each plotted point represents an average of three measurements. The measurement details, as well as the laser interferometer, were described in [2-11 to 2-15]. Recently, different laser techniques have been used to characterize bonding tool/capillary motion, and examples are given below.

Characteristics of a thin, 60° tungsten-carbide (WC) tool are shown in Fig. 2-4. This tool is intended to fit into small spaces and also to be used in reverse (package-to-die) bonding. Preliminary studies suggested that this tool had rather unusual bonding characteristics, so the study of loading effects was more thorough than that undertaken for other tools, with data taken near both the beginning and the end of the bonding cycle.

As noted above, the node rises up the tool during bonding, and, for the 60° tool, the vibration amplitude of its thin tip decreases significantly throughout the bonding period. This effect results from increased loading of the tool as the bond deforms. Such tool-loading effects were modeled [2-2]. These measured results suggest that the 60° tool may have some ability to compensate for slight differences in the bond pad or the wire characteristics by loading down to a greater or lesser degree.

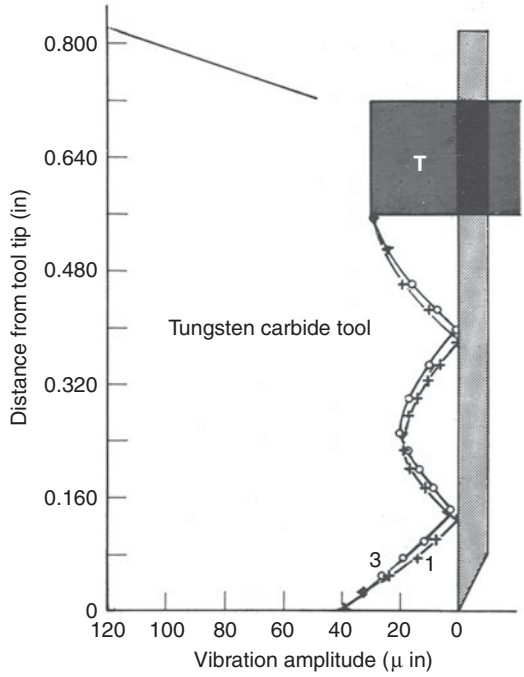

Figure 2-5 The modal patterns of a long WC wedge bonding tool shown unloaded and during actual bonding of 25 μm Al, 1% Si wire. The bonding force was 25 g. Curve 1, (+), is for free vibration, and curve 3, (o), is made during the last 5 ms of a 50 ms bonding cycle.

The modal patterns of a longer WC bonding tool shown unloaded and during bonding of 25 gm Al, 1% Si wire, are given in Fig. 2-5. Although the node moves up during bonding, it has little effect on the tip amplitude.

The vibration modes of tools made with different materials (or dimensions) can change the vibration patterns. For example, titanium carbide tools (sometimes used for Au wedge bonding) have a much lower density and are more flexible than WC. Such tools have their nodal position approximately 0.5 mm (20 mil) above that of a WC tool with the same geometry. As a result, the vibration amplitude of the unloaded tool tip is about 20% greater for the same transducer drive [2-15].

For comparison, the 60 and 80 kHz [2-16] free vibration modes of typical WC tools used for bonding large-diameter wire, 0.2 mm (8 mil), are given in Fig. 2-6. The tool extensions for this wire are longer (5 vs. 1.9 cm) than the one in Fig. 2-5, and their diameter is also larger (0.32 vs. 0.16 cm) so it will have a similar vibration pattern at 60 kHz.

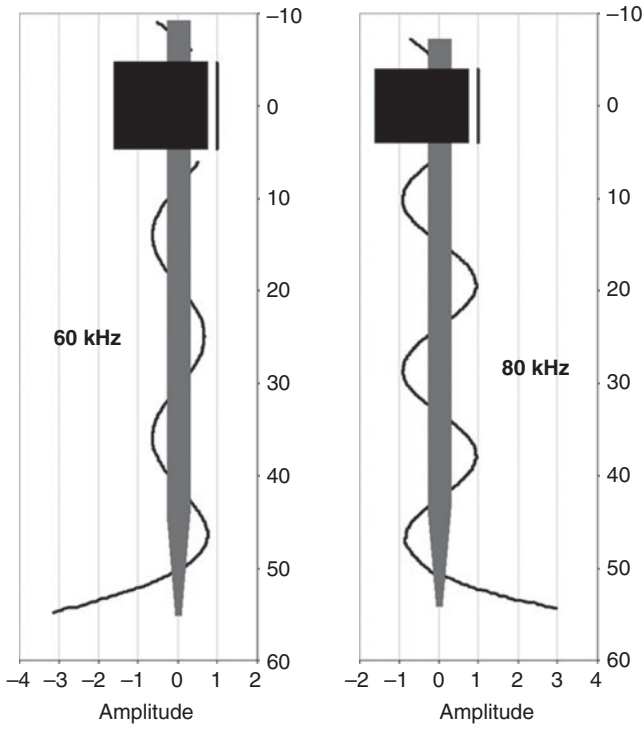

Figure 2-6 The unloaded (free) vibrations of two modern WC wedge-bonding tools used for bonding 200 µm (8 mil) wire. The vertical scale is in mm, and the horizontal is relative amplitude The mechanical taper at the bottom of the tools amplifies the vibration motion. The bottom tip of the 60 kHz tool happened to be moving left when the instantaneous interferometer measurement was made, and the 80 kHz one was moving to the right. The vertical scale is in millimeters. Data were taken with a laser interferometer. The amplitude measurements are relative. The ultrasonic frequency is indicated on each figure [2-16]. (*Courtesy of Orthodyne Electronics.*)

The US frequency of some large-diameter wire bonder transducers has been increased from the standard 60 kHz, up to ~80 kHz to improve bond quality. The equivalent tool vibrations at both frequencies are given in Fig. 2-6.

The equivalent vibration modes of ceramic ball-bonding capillaries were studied. These measurements were made with a capacitor microphone, which is described in Ref. [2-14]. The free (unloaded) tool vibration measurements are shown in Fig. 2-7. The position of the single node is given, and the increased amplitude near the tip is inferred by correcting the data. The microphone's resolution (100 µm

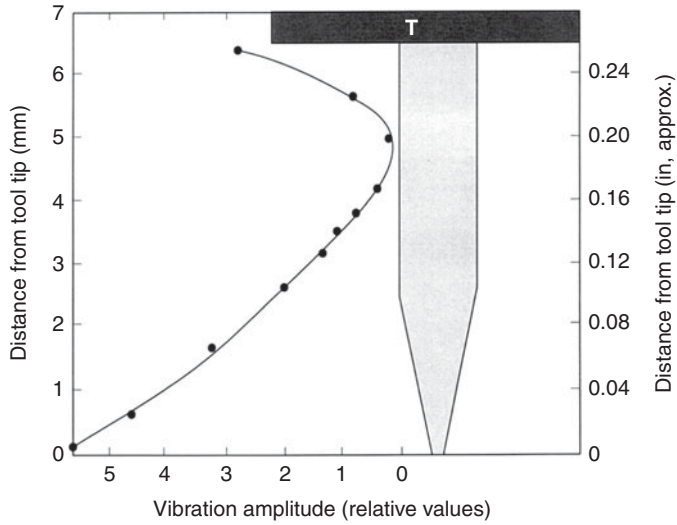

Figure 2-7 The unloaded vibration pattern of a typical ceramic capillary used for ball bonding. Vertical scale is in mm and in (extension below transducer is 6.5 mm). Data were taken with a capacitor microphone, so the amplitude measurements are relative. The ultrasonic frequency was approximately 60 kHz.

on a flat surface) limited the accuracy near the capillary tip. Different capillaries used in different transducers have shown some displacement of the node, usually upward rather than downward. Unusual capillaries, such as bottleneck designs, are more difficult to measure during bonding, but can be modeled using finite element analysis (FEA) software or analytical methods [2-2, 2-9]. Such capillaries would be expected to load down even more than the 60° tool during bonding.

An early study of transducer and tool vibration modes by Wilson was carried out using a laser holographic interferometer [2-4]. This method displayed the vibration maxima and minima along the horn, as well as showing the effect of nonuniform tool-bond loading on both the transducer and the tool.

Currently, the complete amplitude vibration modes of bonding tools and transducers can be measured with available commercial equipment [2-7]. Capillary and transducer motion/velocity are displayed giving maximum details of amplitude, off-axis vibration and rotation. An example is given in Fig. 2-9. One such instrument, a laser vibrometer, also can plot the frequency versus vibration velocity of tools and transducers over a chosen frequency range, allowing optimization of transducer/system performance, as demonstrated in Figs. 2-8 and 2-9.

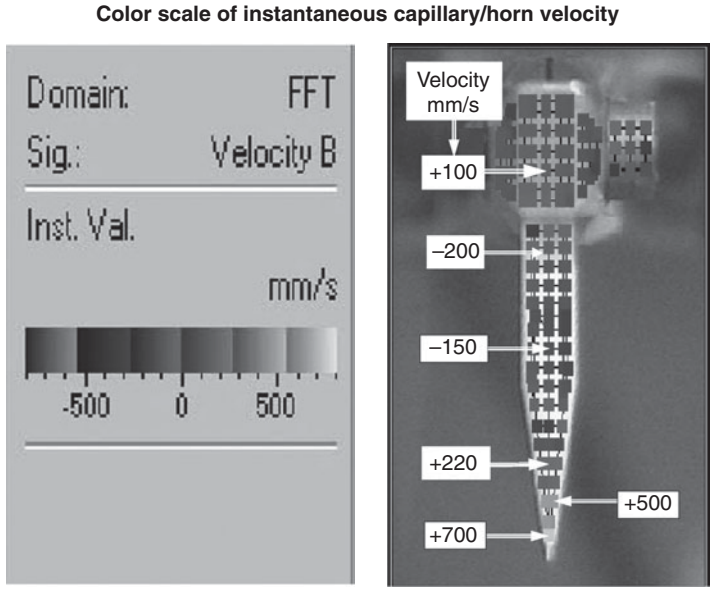

Figure 2-8 An output from a laser vibrometer monitoring a bonding capillary and transducer tip velocity. The section velocity (mm/s) is read from its color from the FFT figure (left), but for this grey-scale book picture, values were added in boxes. This color figure appears in the CD attached to the book and should be referred to for clearer understanding of these patterns. From the color it is noted that values often change horizontally across the tool and transducer. The US drive frequency was 250 kHz for this special transducer test. (*Courtesy of K&S.*)

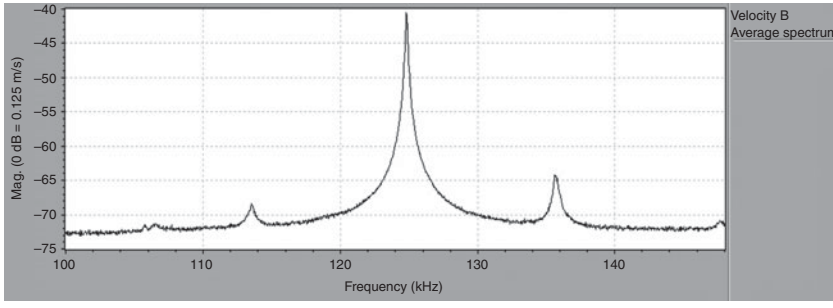

Figure 2-9 Example of a transducer frequency sweep (fast Fourier transform) from data obtained on the same measurement system as in a, but using a different experimental transducer peaked at about 125 kHz. Additional smaller resonance peaks are apparent. (*Courtesy of K&S.*)

2.3 How Ultrasonic Bonds Are Made (Empirical Description)

Small-ultrasonic welds used in microelectronic interconnections are usually made with soft, face-centered cubic metal wires (e.g., Al, Cu, Au) of 25 to 33 μm diameter. There is no generally accepted mathematical model of the ultrasonic welding process. It is a complex process, and the physics is not fully understood. However, many efforts have been made to study and/or explain the process [2-1, 2-9, 2-10, 2-18 to 2-21] (and modeled in Chap. 11) so an empirical description of the observed bonding process follows. This treatment is mostly adapted from Harman [2-9] and Harman [2-10].

Ultrasonic Al (25 μm diameter) wedge-bond formation was studied by examining the bond foot prints left on normal Al bond pads by bonds that did not stick. These are called bond lift-off patterns and represent the best method of studying the early stages of bond formation. Such patterns are made by maintaining the clamping force and the ultrasonic power constant. The normal bond time is then progressively decreased below the point that the wire will adhere, and it lifts off. The pattern in Fig. 2-10(A) results from pressing the wire against

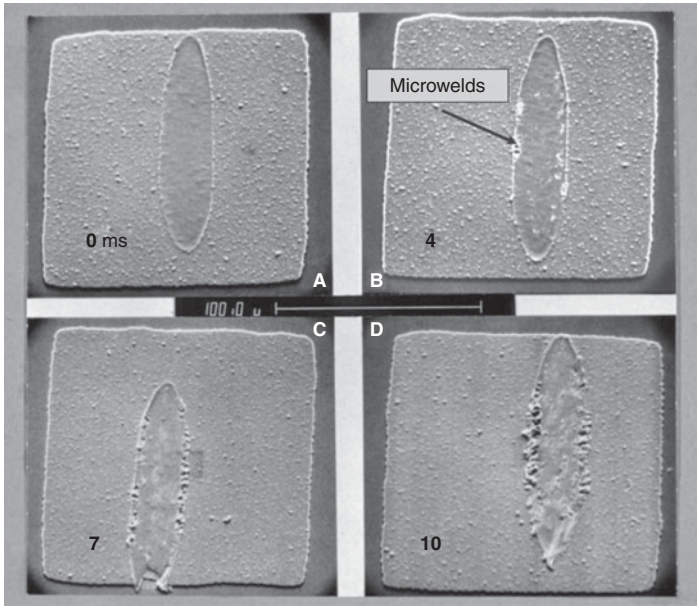

Figure 2-10 Wedge bond lift-off patterns. Patterns are made by maintaining the clamping force (25 g) and ultrasonic amplitude 0.88 μm (~35 μin) constant and progressively decreasing the weld time (optimized for 50 ms) below the point that the wire will adhere. (A) Zero weld time (no ultrasonic energy); (B) 4 ms weld time; (C) 7 ms weld time; and (D) 10 ms weld time.

the pad with the normal clamping weight of 25 g, but with no ultrasonic energy applied. Figure 2-10(B) shows the lift-off pattern made by applying ultrasonic energy for a 4 ms period. The wire-to-pad microwelds have formed at points near the perimeter. The lift-off pattern in Fig. 2-10(C) resulted from a 7 ms bonding time. The welded area has spread part of the way around the perimeter. Figure 2-10(D) shows the bond formation at 10 ms. The welding has increased considerably, but is still primarily confined to the perimeter. At longer bond times, the wire could not be lifted up without tearing the pad or breaking the wire. Examination of many such patterns shows that weld formation begins around the perimeter, but that no two time-equivalent patterns are exactly the same. The amount and location of the welding around the perimeter may show considerable variation. However, the examples given in Fig. 2-10 were chosen to be typical of those observed for each indicated bonding time and power setting. A further verification that ultrasonic wedge welding progresses around the perimeter is shown in Fig. 2-11. These are photographs taken of disrupted metallization, as seen through the back side of an Al-metallized fused quartz substrate [2-11 in SP]. In each photograph, the bond parameters were held constant except for the power. Note that the third bond (c), made at the highest US power, has cracked the quartz. This is an example of cratering caused by excessive US energy (see Chap. 8 for a discussion on cratering). Studies of evolution of the bond interface on Au/Ni/Cu bond pads, obtained by etching the Al, 1% Si wedge bonds off, have revealed growth patterns similar to

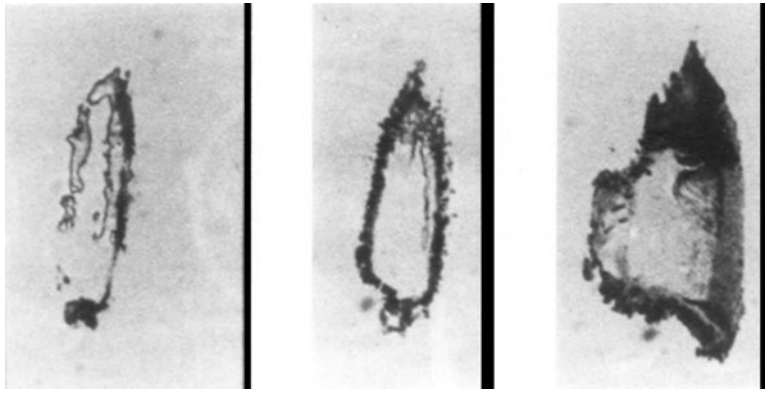

Figure 2-11 "Through the underside of a bond pad." The disruption of the bond pad observed from the underside of a thin (~0.2 μm) evaporated Al pad, which was deposited on a clear fused quartz substrate. These three patterns were made by increasing the ultrasonic power for each Al wedge bond, while holding force and time constant. Power-supply dial settings were, from left to right, (a) 4.5; (b) 5.5; (c) 9.5. The third bond, made at the highest US power, has cracked the quartz, an example of cratering discussed in Chap. 8 [2-11].

Figs. 2-10 and 2-11 except that as the bonds mature the center also became welded [2-12].

The Au-Au crescent-wedge (after ball bond) weld formation patterns were studied by Zhou [2-13] and found to be similar to US Al wedge growth (starting around the perimeter and generally growing inward with power/time). Thus most bonds start around the perimeter and mature inwardly, but there are many reported variations.

Although the initial welds on TC-ball bonds form around the perimeter, as with US wedge bonds, TS bonds appear to follow a more random pattern, as shown in Fig. 2-12 [2-22]. The microwelds may be elongated in the direction of the ultrasonic vibration motion. The welding time in this figure ranged from 2 to 16 ms at 100 kHz. No equivalent comparison has been made at 60 kHz bonding frequency. However a fully welded bond from a recent mfg's bonder is shown for comparison in Fig 2-12(E), where the intermetallic appeared in swirl patterns, and these have been observed by others as well. Thus each bonder can develop welding in different patterns (as revealed by etching*).

2.3.1. Brief Phenomenological Explanation of the Ultrasonic and Thermosonic Bonding Process

Ultrasonic welding is a type of deformation weld in which the metal is first softened by the ultrasonic energy. The clamping force deforms the softened wire or ball against the equivalently softened bonding pad, sweeping aside brittle surface oxides and contaminants, leaving clean surfaces in contact. A pictorial cartoon demonstrating this process for a ball bond is given in Fig. 2-13, but it is also appropriate for a wedge bond as in Fig. 2-14. The modeling of the ultrasonic bonding process is detailed in Chap. 11.

Little deformation takes place in the center of the weld, so the oxides and contaminants mostly remain there, and this area is often observed to remain unwelded, as shown for wedge bonding in Fig. 2-14. Presumably, the same energy transfer mechanism that softens the metals without significant heat generation also supplies the required activation energy for metal-metal interdiffusion and, for Au-Al bonds, the formation of intermetallic compounds. This forms these metal-to-metal (atomic) bonds within a few milliseconds. Note

*The amount of Au-Al intermetallic formation is often used to demonstrate the extent of welding [2-25, 2-36, 2-52,] to ensure reproducibility. The amount of intermetallic in the bond interface is implied by observing the disruption (roughness) of the Au-ball bonded surface after etching the Al pad (from under the ball) with a 20% solution of KOH or other etchant that does not attack gold. In some cases, however, more sophisticated failure-analysis techniques are used to examine, identify and analyze the actual intermetallics that forms. Although these techniques give excellent visual evidence of the welded area, they are too slow and expensive to be used to execute a designed experiment or even to set up a bonder. The ball shear test is a quicker, more quantitative method to use for these purposes, and its results have been correlated with the amount of welded area in as-made bond interfaces [2-36, 2-52] to assure reproducibility.

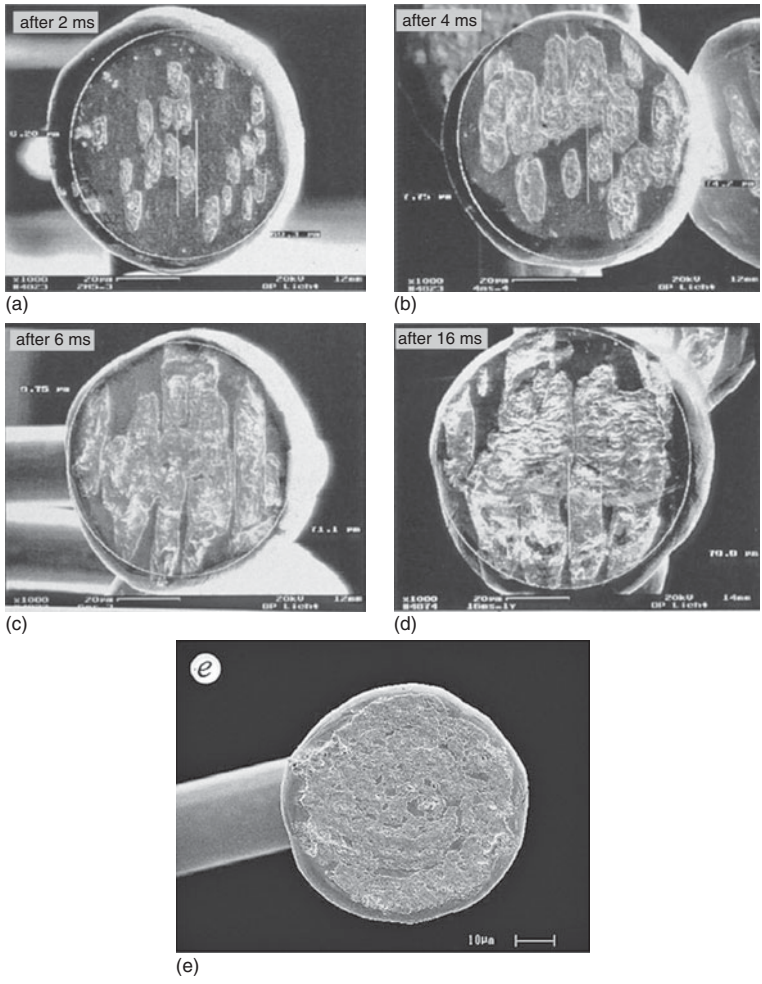

FIGURE 2-12 (a,b,c,d,e) Thermosonic ball-bond welding patterns at different welding times, revealed by etching the ball free from the Al bond pad. Bonds were welded with 46 gf (450 mN) force, 10 kHz ultrasonic energy, and a stage temperature of 250°C. For (a), the weld time was 2 ms; (b) 4 ms; (c) 6 ms; and (d) 16 ms. After the bond is mature, long weld times did not increase the welded area for this type of bond [2-22]. (*Courtesy of ESEC.*) The etch–removed bond [(e), lower] is a modern approximately fully welded bond on a 70 µm pitch, made at 120 kHz, showing swirl-shaped intermetallic patterns [2-23]. (*Courtesy of K&S.*) Some others have swirls, but with an unwelded center [2-20]. (Also see Chap. 5, App. 5A, Fig. 5A-1.)

that an equivalent wire deformation can be made with higher clamping force, but with no US energy or heat, it does not result in a weld, and the wire will easily lift off.

Ultrasonic softening and the subsequent deformation (under stress) has been studied by Langenecker [2-23] over the range of

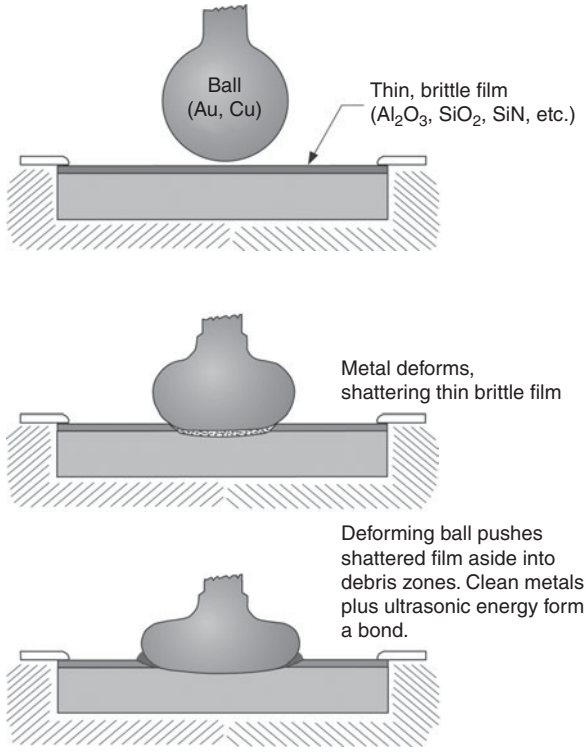

Figure 2-13 The bonding force and US energy breaks through thin surface-oxide-films, pushes them aside, and US energy forms the weld.

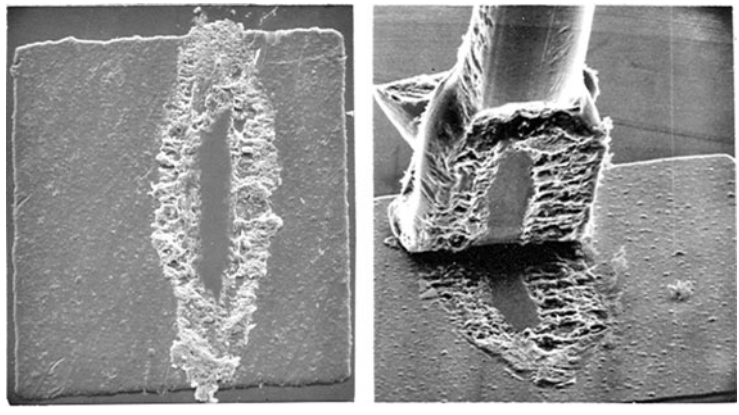

Figure 2-14 An ultrasonic wedge bond made with normal parameters for a manual wedge bonder using 25 μm diameter Al, 1% Si wire. The bond (on the left) has been partially lifted up so that the weld pattern may be seen. The center remained unwelded. On the right, is a bond pad with a similar bond completely removed.

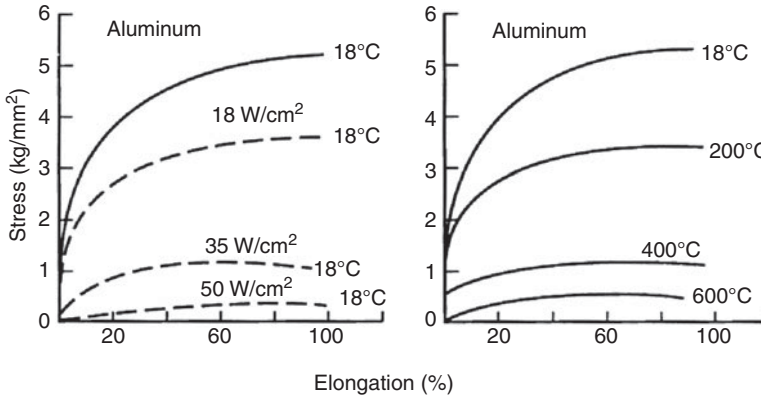

Figure 2-15 Stress versus elongation for Al single crystals. The left curve indicates strain (elongation) during irradiation at 20 kHz ultrasonic energy (dashed lines). The right-hand curves show comparable stress-strain behavior resulting from heating alone. The solid curves indicate no applied ultrasonic energy only the indicated temperature (from Langenecker [2-23]) (© *IEEE*). (The author notes that this work has not been duplicated with modern measurement equipment/techniques, and although believed to be correct, it should be verified, a good university thesis subject.)

15 kHz to 1 MHz, with most of his work being done at 20 kHz. He has compared the similarity of the stress versus elongation in Al single crystals (with 20 kHz ultrasonic energy at constant temperature) to equivalent elongations resulting from heat. His results are reproduced in Fig. 2-15. It should be noted that Langenecker did not study or even consider ultrasonic bonding or welding, only the ultrasonic softening of metals, metal forming, and heating. However, the ultrasonic softening process that he described has been incorporated into several explanations of the bonding process [2-1, 2-9, 2-21]. The stress versus elongation is essentially equivalent to deformation under a compressive load, such as occurs in metal forming and ultrasonic welding. From this, it is clear that either ultrasound or heat can independently cause equivalent deformations with a given stress. However, significant differences exist between the two types of excitation, the major one being that the ultrasonic energy density required to produce deformation in Al is about 10 million times less than is required for an equivalent deformation resulting from thermal energy alone, although some heating is a by-product of any such US process. After US softening and deformation of the weldments occur, and the US energy is removed, the metals are left work-hardened (acoustic hardening), whereas equivalent thermal deformations leave the metal permanently softer (annealed). Such work hardening in Al ultrasonic wedge bonds has been experimentally verified by Coucoulas [2-24] and on bonded Au balls by Pantaleon [2-25] and recently by Srikanth

for copper wire [2-26]. However, Krazanowski [2-19] observed that a wide range of structures can remain after bonding, depending on the metals involved, so this hardening may not be universal in all materials and/or produced by all bonding equipment.

There is little experimental evidence that US bonding process occurs because of heat generated by the US energy. Various in-process bonding measurements have shown less than ~10 to 100°C maximum temperature rise [2-1]. More recently, Mayer [2-27] as well as Suman [2-28] measured only small changes in interface temperatures (~10°C) using surrounding sensors. (M), or Al, topped under-the-pad sensors that allowed experiments to take place at bonding temperatures of ~150°C for Au ball bonds.

However, one study inferred an interface temperature of 250°C from observations of crystallographic defect microstructures in wedge-bonded larger diameter Al wires [2-19]. Another study, bonding Au balls directly to sputtered type-K thin film thermocouples, obtained a rise from 240 to 320°C. Other bonding conditions were omitted [2-29]. The temperature rise was attributed to friction; however, it is unlikely that any welding (bonding) ever took place, considering the bond was to the thermocouple as the pad. These results cannot be compared to actual bonding measurements where microwelds would presumably begin to minimize slippage/friction-generated heat after a few milliseconds.

In no case where bonding actually took place, did the interface temperature approach the melting point of either weldment or more than or equal to 300°C normally required for TC bonding. Also, US Al-Al wedge bonds have been made immersed in liquid N_2 at a temperature of 77 K [2-1, 2-9]. Since high heat is not necessary, the activation energy to form the metal-metal bond may possibly be transmitted in the form of phonon-lattice interactions. Lower clamping forces have been shown to increase the interface temperature by ~25°C, implying that there is increased interfacial scrubbing during some portion of the bonding cycle (note that similar low bonding forces have also been shown to result in cratering and poor bonding). Some papers have attributed the entire bonding process to the frictional rubbing and propose melting temperatures in the interface, [2-30] but there is little analytical evidence for such where actual welding occurred.

When Langenecker's softening mechanism is incorporated into the above observations, Al wedge bonding to a typical Al IC bond pad can be summarized as follows: Some wire-to-pad interfacial motion (scrubbing) certainly occurs upon first application of ultrasonic energy, resulting in some interfacial cleaning action and modest frictional temperature rise. A few milliseconds later, small microwelds form just inside the perimeter of the mated surfaces as in the lift-off patterns of Figs. 2-10 and 2-12, and, at this point, the wire-to-pad

interfacial motion ceases.* Ultrasonic energy is then absorbed into the entire weldment area (wire, interface, and bond pad). As a consequence of deformation cleaning, the center of the bond area is left relatively unwelded in wedge bonds. This may not occur if there are orbital or sideways tool vibration modes present during bonding causing some center welding to occur.

Extensive microstructural details of bond interfaces were obtained with a transmission electron microscope [2-19] as well as some using a SEM [2-1]. Those taken along the interface of monometallic US welds showed, variously, grain boundaries, no grain boundaries, debris zones of oxides, and contaminants, as well as numerous crystallographic defects. However, in general, the monometallic bonding process results in interface formation that is similar to grain boundaries in polycrystalline materials, but continuous along the interface. Au-Al US welds, made at room temperature, show debris zones as well as clear metallic boundaries (similar to grain boundaries). There are also intermetallics along this boundary, which are a normal part of such Au-Al bond formation [2-31]. As a consequence of deformation cleaning, the center of the bond area is left unwelded (minimum mass motion occurs in the center of a compressed, deforming ball/wire). This may not occur if there are orbital or sideways tool (capillary) vibration modes present during bonding. Such modes can be easily revealed by modern laser vibrometer measurements as was shown in Fig 2-9.

Contaminants in the bond interface can inhibit weld formation by preventing the deforming metal surfaces from coming into intimate contact. A thin, hard oxide on a soft metal, such as 0.5 to 1 nm (50–100 A) of Al_2O_3 on Al, will break up and be thinly dispersed or pushed into "debris" zones with little effect on the average welded area. However, soft oxides on harder metals, such as NiO on Ni (which is used in large-wire power device packages), appear to serve as a lubricant during initial weldment contact and deformation, remaining on the surface and preventing weld formation. This holds true for soft oxides (e.g., Cu_xO_y) on soft metals (e.g., whereas Au does not have an oxide, diffused-to-the-surface Cu will oxidize and has been shown to significantly increase the activation energy required for Au-to-Au TC bonding [2-32]). Also, as little as 0.2 nm (20 A) of a carbonaceous contaminant has been shown to reduce bondability on any bonding surface (see Chap. 7). Thus, it is important to understand the nature of a

*Joshi [2-1] used a laser interferometer and observed that the tool, the bond, the pad, and the *laminated* polymer substrate moved in unison during most of the bonding process. This substrate motion would not occur on hard, brittle substrates, such as silicon or ceramic. Here the final motion must be between the tool and the wire, as was found in [2-9]. Ultrasonic energy is then absorbed into the entire weldment volume (wire, interface, and bond pad).

surface contaminant or oxide on a given bond-pad metal to understand its effect on bondability and reliability.

2.4 Bonding with High(er) Frequency Ultrasonic Energy

The original reasons for choosing 60 kHz are obscure, but fine-wire bonding machines have used that frequency for bonding from the 1960s to the present. This resonance frequency resulted in transducers and tools that were appropriate to microelectronic dimensions and were stable during the bonding load. However, other frequencies (e.g., 25 kHz) have been used for bonding large-diameter Al wires in power devices. The possibility of US welding over a wide frequency range has been known for some time. The *Welding Handbook* [2-33] cites ultrasonic welding frequencies as ranging from 0.1 up to 300 kHz. Also, the ultrasonic softening process was verified up to 1 MHz by Langenecker, so it is not surprising that higher frequencies would find use in microelectronics bonding if an advantage could be demonstrated. The present interest in using high frequency (HF) for microelectronics wire bonding was started by Ramsey and Alfaro [2-34]. They studied thermosonic Au ball bonding on IC pads using US energy in the range of 90 to 120 kHz and reported that such frequencies produced better welding at lower temperatures and in shorter bonding times. This also resulted in more complete Au-Al intermetallic formation and thus, more complete weld formation. More recently, several papers have given additional advantages for using HF (>60 kHz) for both ball and wedge bonding [2-35], as discussed in the following paragraph.

There have been no large-scale (published) implementations and design of experiment (DOE) comparisons between different frequencies, and for the many possible bonding problem situations (cratering, contamination, metallic oxides, soft substrates, etc.). Nevertheless, all small-diameter-wire autobonders since approximately the year 2000, have incorporated transducer frequencies between ~100 and 140 kHz drive for the transducers. The lower mass (inertia) of the small HF transducers allows bonding machines to run faster. The other advantage is that strong HF wedge bonds can be made with low deformation and with shorter welding time [2-34]. All of these are desirable for high-speed and fine-pitch bonding. However, one study [2-36] compared Al wedge bonding at 60 and 120 kHz in a DOE study and found little low-deformation advantage. The authors did find that less metal splash occurred around the bond perimeter at 120 kHz, and higher yields were achieved in shorter bonding times. In other studies [2-37], a range of higher frequencies (100, 140, 250 kHz) were reported to produce good Au ball-bonds at low temperature (50°C) compared to 60 kHz. The best shear strength and the shortest bonding time were obtained at 250 kHz. However, the bonding window

was very narrow at such low temperatures, requiring much closer control over machine parameters, heat stage temperature, and materials. Such low temperature studies have not been implemented in production. Charles [2-38] has published the only carefully designed experiments comparing 60 and 100 kHz Au ball bonding. His studies concluded that 60 kHz had a larger bonding window than 100 kHz for Au ball bonds, but was not as effective in bonding pads that were difficult to bond, such as ones over soft substrates (e.g., PTFE). One hundred kHz bonded in a shorter time for both Au ball and Al wedge bonds. Outside of these studies it has been found that the Au crescent (second bond) of a ball bond has a very narrow bonding window at high frequencies, sometimes requiring a higher temperature for high yield. At least one company produced a dual frequency transducer (second harmonic used for the ball and the fundamental frequency for the crescent bond).

Another paper reported wedge bonding with 100 μm diameter. Al wire to Cu plates using 60, 190, and 330 kHz bonding frequencies [2-39]. The authors reported that 330 kHz produced stronger bonds in a shorter time and with lower vibration amplitude. Other workers reported that 90 to 120 kHz US energy resulted in better ball bonds to pads on polyimide that were placed over active areas of IC chips [2-40]. There have also been statements (unpublished) that HF improves bonding to pads over soft polymers such as PTFE. If verified, it may imply that the polymer absorbs less energy at high frequencies, leaving more for the bond interface. However, little is known about US energy absorption in polymers. Thus, a particular frequency could be either more or less effective than another when used for bonding over a particular polymer. Hundreds of DOE comparison studies will be required before all materials used as substrates are characterized and a general understanding is achieved. Since the use of such HF is relatively new in 1996, one can expect that limitations as well as advantages will appear in the future. This is a very dynamic area.

One explanation of the differences in wedge bonding at higher US frequencies has been proposed by Shirai [2-35] and incorporated in [2-21]. In this explanation, the HF tool-to-wire vibration produces a higher strain-rate and, therefore, a much higher stress in the Al wire. The wire becomes strain-rate hardened, deforms less, and more energy transmits to the weld interface. This results in a strong Al wedge bond with lower deformation. From Ramsey [2-34], the higher frequency increases the rate of metallic interdiffusion and makes a better metal weld. This explanation appears to be reasonable; however, there are many unanswered questions, and much more must be learned about the HF bonding mechanism. The explanation used by Shirai is based on a strain-rate model for single crystal LiF, Ge, and Si [2-41]. These are brittle ionic and covalent materials. Wire bonding is done with soft, polycrystalline, face-centered cubic metals (Au and Al) that respond to stress by deforming easily, although they would

have some (unknown) high-strain-rate-modified response. Compilations of strain-rate hardening in Al [2-42] would not support the proposed mechanism. Furthermore, Langenecker has verified his US softening mechanism up to 1 MHz, implying that the strain-rate hardening is not significant below that frequency. However, that paper omits many measurement details and itself leaves questions. Shirai's proposed mechanism, which may be qualitatively correct, should be further studied. In particular, its theory should be rederived around the known properties of soft, polycrystalline, face-centered cubic metals. Most of our understanding of the US softening and welding mechanism is based on fundamental studies carried out in the early to mid-1960s. These experiments should be repeated with current measurement methods and high-speed computers for mathematical computation (verification) of models. Full understanding is the necessary basis for continued advancement of US bonding, as we push towards the limits of speed, fine pitch (~20 μm), and especially, high yield. Our present understanding is mostly empirical, and that knowledge has been pushed to its limits.

2.5 In-Process (Real-Time) Bond Monitoring

There has long been a desire for an electrical or a mechanical real-time (in-process) quality control system to increase the bond yield. Efforts, which to date have been mostly empirical, include measuring an electrical parameter from the US power supply, the transducer's impedance, the tool-drop (related to bond deformation) during bonding, tool lift-up force after bonding, the amount of US energy transmitted through the package, second and third harmonic output from sensors on the transducer. In some cases, the bonding time can be extended until the defined parameter is achieved or the power input altered. Modern high-speed computers (incorporated in advanced autobonders) make several of these possible and practical. Some of these methods have been published, others patented, and others have appeared only in internal company or military contract reports (see [2-43 to 2-51]). Many are slight variations of earlier publications or patents. The details of current systems are usually proprietary, and a thorough review of these and other bond-monitoring systems is beyond the scope and intent of this book. Bonder manufacturers will discuss their particular system with customers, and some have more detailed information on their Internet Web sites.

Bond-monitoring systems are essentially empirical, since there is no accepted quantitative theory of ultrasonic/thermosonic bonding. The electrical-signal systems require defining or establishing some empirically determined bond quality window. (In general, a process control based solely on windowing will fail some good bonds and/or pass some weak ones.) Other systems measure and control the bond

deformation. In each case, the bond-monitoring systems can contribute to improved quality control. However, a complete understanding of the US welding process is necessary before a true in-process bond monitor can be made, although the empirical ones do contribute to improved quality control. There have been a number of ultrasonic bonding mechanism studies as discussed above, but there is no accepted and validated mathematical model to guide a designer of bond-monitoring equipment.

Currently, wire bonds can be produced at very high yields using the means described in Chaps. 4, 7, and 9, such as molecular cleaning and carefully optimizing bonding parameters with DOE. By following these procedures, it is currently possible to bond with ≤25 ppm defectives [2-52] in medium-to-high-volume production. Under such conditions, it could be hard to justify an expensive system added onto each autobonder if it slowed the bonding process, or only reduced those defect numbers by a few parts per million. However, low-volume hybrids, SIPSs, and other technologies that use multiple chips from different sources seldom achieve such high yields. For those and other cases in which the defects can range from several hundred to several thousand ppm, a currently available bond monitor could pay for itself. Low-production volumes make it difficult to establish that there is a real decrease in defectives into the <50 or 100 parts per million range. To prove such requires a better understanding of small-sample statistics, or by making 100,000 setup and test bonds (see Chap. 9). Thus, incorporating an expensive bond monitor in each autobonder might not be practical for all uses, but certainly can enhance many.

2.6 Wire-Bonding Technologies

2.6.1 Thermocompression Bonding

Thermocompression (TC) wedge and ball bonding for microelectronics was developed by Bell Laboratories in 1957 [2-53]. This method was used until US wedge bonding largely replaced it in the mid-1960s. Although Au-Au TC welds can be made in high vacuum at room temperature, such welds require a high-force and a high-interface temperature to take place in a normal manufacturing environment. TC bonding is a type of solid-phase welding that combines heat and force to plastically deform the weldments, sweeping aside surface contaminants (air, carbonaceous impurities, oxides, etc.), resulting in intimate contact between cleaned surfaces. At this point, short-range interatomic forces with heat supplying the metal-metal activation energy result in a metallic welded bond. The primary process variables (time, temperature, and deformation) follow an Arrhenius relationship, and their activation energies have been studied [2-32].

This activation energy is supplied by the high-interface temperature, which for most TC bonding is around 300°C. The temperature is usually supplied by heating the entire device, that is, placing it in contact with the heated work holder (WH). However, variations that heat the bonding tool alone (≥400°C) or in combination with WH heating, have also been used. Ball-bonding technologies normally feed the wire through a capillary, and the tool can move in any direction after making the ball bond. This results in current autoball-bonding machines being several times faster than ones designed for wedge bonding.

A majority of the TC bonding-mechanism studies were done at Bell Laboratories and Western Electric. [2-32, 2-54 to 2-56]. However, important work was also done by others [2-57, 2-58]. Thermocompression bonding is more sensitive to surface contaminants than any other bonding method (see Sec. 7.2), the bonding time is much longer, and the interface temperature is higher. Because of these, this process is seldom used in microelectronics today, having been replaced by thermosonic bonding.

2.6.2 Ultrasonic Wedge Bonding (Small- and Large-Diameter Wires)

Ultrasonic wedge bonding was introduced to the microelectronics industry in about 1960 and became dominant in device production, until gold-ball thermosonic autobonders took over. Ultrasonic wedge bonding is normally done at room temperature (if heated, it is also called thermosonic bonding). It is primarily used to bond Al wire to either Au or Al bond pads, although it can bond Au wire with special "gold bonding" tools (cross-grooved or roughened). Large-wire Al US bonding is the dominant method of interconnecting power devices. The US weld is formed by the application of ultrasonic energy through a resonating transducer-tool combination while applying a clamping force. An example of the transducer and bonding tool configuration and vibration modes were given in Figs. 2-1 and 2-2 and the bonding sequence in Chap. 1, Fig. 1-2. The wedge-bonding system (transducer-tool combination) must be oriented in approximately a straight line from the first bond to the second, before the first bond is made. This is a disadvantage for autobonders, since it requires mechanically aligning the package or the transducer for each wire. This slows down the wire bonding process by more than 50%, requiring several times more autobonders (and their overhead costs) to bond the same number of devices as thermosonic ball bonders.

Large-diameter Al wire bonding is used primarily in power devices and hybrids that require more than several amperes per wire. Such wire bonding is addressed in various parts of this book in appropriate context, rather than in a separate section. Large-Al wires are bonded by cold ultrasonic welding methods, using 60 or 80 kHz US power supplies, although in earlier times some used 25 kHz. Large wire is usually

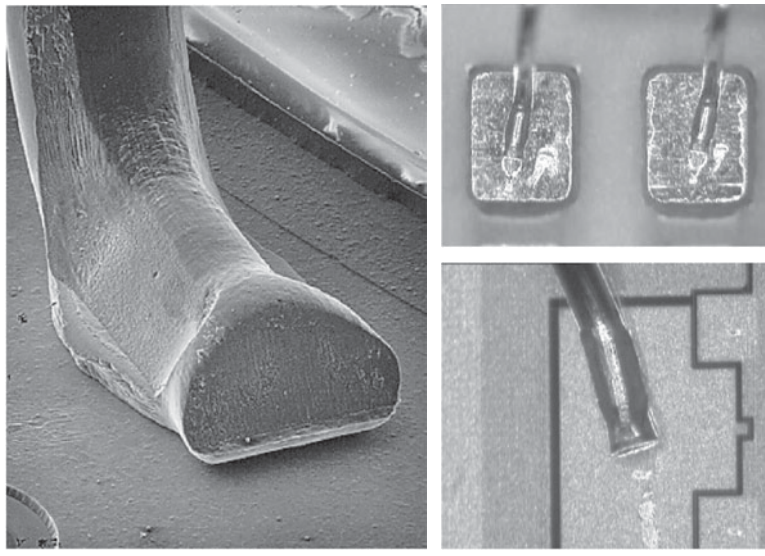

Figure 2-16 Modern large-wire aluminum bonds left is 250 μm (~10 mil); right ones are 150 μm (~6 mil), bonding frequency was 80 kHz. (*Courtesy of Orthodyne Electronics.*)

considered to range from about 75 or 100 μm to over 0.5 mm in diameter (3–30 mil). Figure 2-16 shows large-wire Al bonds. They typically use either 99.99% Al or Al, 1% Si wire. A discussion of large-wire metallurgy and burnout characteristics is included in Chap. 3. The current large-wire technology includes both manual and autobonders. Earlier, such bonders used manual or electrically activated scissors or a blade to cut off the wire after the second bond. In some cases, that bond was made by tweezer welding (see Sec. 2.7.2). However, the development of a special bonding tool that both bonded and cut off the wire advanced the field significantly so that both bonds and the cut-off could be made ultrasonically. This increased the speed of the process and made autobonders possible. Present-day bonding tools developed by Orthodyne confine the wire in a parallel inverted V-groove during bonding, which leaves the bond neck strong [2-59], see Fig. 2.9. This is quite different from the relatively flat bonding tools used for fine-wire wedge bonding. Even though large-diameter wires are usually fully annealed, they are very stiff and the bonding forces are far greater than those required for small-wire wedge bonding (up to ~1 kgf vs. 25–35 gf). The ultrasonic energy required is equivalently higher also, up to ~25 W versus <1 W for fine wire. Most power device packages are usually plated with Ni, and large-diameter Al wire bonds very well to that metallization, if it is free of oxides. Large-wire bonds can have the same reliability problems as small-diameter Al bonds; however, a well set-up process

experiences few such failures. Since such bonds have a high profile, they can be tested with both the pull test and the shear test (see Chap. 4).

2.6.3 Thermosonic Ball and Wedge Bonding

Coucoulas was the first to combine ultrasonic energy with heat to produce thermosonic bonding in 1970. As such, he is the father of thermosonic bonding. He called it "Hot Work Ultrasonic Bonding" [2-60]. Today, the vast majority of interconnections to integrated circuits are made with Au thermosonic (TS) ball bonding. It is also occasionally used for Au wedge-wedge bonding. This bonding method is a combination of ultrasonic and thermocompression welding that optimizes the best qualities of each for microelectronic usage. TC welding usually requires interfacial temperatures in the order of 300°C. This temperature can damage some modern die-attach plastics, packaging materials, laminates, and some sensitive chips. However, in thermosonic welding, the interface temperature can be much lower, typically between 125 and 220°C (but may vary over a wide range), which avoids such problems. Also the bonding time is much shorter than for TS bonding, often <10 ms versus >100 ms. The ultrasonic energy helps disperse contaminates during the early part of the bonding cycle and helps mature the weld in combination with the thermal energy. This combination also allows the US energy to be kept small enough to minimize cratering damage to the semiconductor chip (see Chap. 8). For ball bonding, the wire is threaded through a capillary-shaped tool, and a spark melts the end of the wire forming a ball at the bottom of the tool. The bond (weld) is formed when the tool under load presses (deforms) the ball against the heated bonding pad (~150°C) and ultrasonic energy is applied completing the process as in Fig. 2-13.

2.6.4 Choosing a New/Different Wire-Bonding Technology

There may be times when one must choose a wire-bonding technology for some new application or perhaps change an established technology used on a current product. The three wire bonding methods—thermocompression, ultrasonic, and thermosonic have many advantages and disadvantages. These are compared in Table 2-1, which can be used to help choose an appropriate bonding technology.

There are numerous options within the above bonding technologies. Some of these are to change the conventional bonding wire or bond pad metallurgy, such as using Cu or Pd ball bonding, perhaps Pd-plated pads, or possibly increasing the ultrasonic bonding frequency (see above). Under some circumstances, round wire may be replaced with ribbon (Sec. 2.7.1). In general, a currently used, well-understood, high-yield process should not be changed unless there is a compelling reason to do so. For example, if the device operates at very high frequency (multi-GHz range) or very close chip placement (tiling) is required, then a change from wire bonding to flip chip may

(A) Thermocompression (Gold) TC Ball Bonding (Rarely Used In 2008)	
Advantages	**Disadvantages**
Excellent reliable Au-Au bonds	High interface temperature required (interface 300°C)
Simple 2+ parameter machine setup	Very susceptible to contamination
All direction bonding from ball*	Large-bonding pads required
Autobonders are faster than wedge	Forms plague with Al-chip pads
Negligible cratering compared to US and TS	Lower yield than US wedge or TS
(B) Thermosonic (Gold and Copper Wire) TS Ball Bonding (Dominant Technology in 2008)	
Medium interface temperature (~150°C)	Somewhat susceptible to contamination, >US but <TC
Lower ultrasonic energy (than US wedge)	Some cratering potential, >TC
All direction bonding from ball[a]	4-Parameter machine setup
Autobonders are fast	
Excellent, reliable Au-Au bonds	
Lower cratering than US wedge	Forms plague with Al-chip pads
(C) Ultrasonic Wedge (Aluminum and Gold Wire) US (~5% Usage in 2008)	
Least susceptible to contamination	Autowedge bonders slower (<1/2) than autoball bonders
Al bonds reliably at room temperature	X-Y wire-pad orientation required, (slows bonding processes)
Fine pitch, <50 μm	Larger cratering potential, >TC, TS
Excellent, reliable Al-Al bonds	Special tools (wedges) needed for Au-Au, Cu, room temperature bonding
Highest yield potential, <20 ppm	3-Parameter machine setup
Large-wire Al bonding	Al Wire unreliable on Ag
Lowest loops available, <75 μm	Au-Wire bonds poorly without heat

[a]After the ball bond is made, the loop can be formed in any direction; thus this is a non-directional bonding method which is ideal for fast autobonders.

Table 2-1 Comparison of Wire Bonding Technologies

be justified. However, remember that any technology change (even within the three wire-bonding technologies) requires new equipment, operator training, long learning curve, and extensive (expensive) requalification of the existing product. Some non-wire-bond technology options are briefly described in Table 2-2.

2.7 Variations of Fine-Wire Bonding Technology

Although the vast majority of all wire bonding is done by TS, or cold US methods using round wire, there is a smaller amount of specialized bonding using US Al and thermosonically bonded Au ribbon wire. There is also some electrical-discharge parallel-gap (split-electrode) welding of wires of intermediate to large diameter, especially for Pt and other wires that do not bond readily by conventional ultrasonic means. Such wires have been bonded with focused lasers, but this usually involves melting and is not a part of solid-phase and US welding, as discussed in this book.

2.7.1 Ribbon Wire Bonding

Ribbon wire has been used in hybrid microcircuits, mostly as crossovers, for decades. It is also used in microwave circuits, since its larger, rectangular perimeter results in lower losses. Initially, all ribbon wire was Au and was bonded by thermocompression or parallel gap welding (see below). However, in 1969, Kessler [2-11, 2-61] and later others [2-62, 2-63] investigated both Al and Au US ribbon wedge bonding. Figure 2-17 is an SEM photograph of US wedge-bonded Al

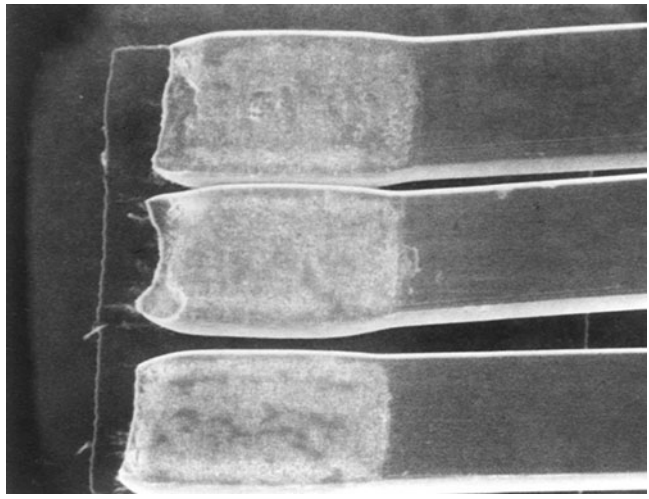

Figure 2-17 An SEM photograph of three US wedge-bonded Al, 1% Si ribbon wires, 12.5 × 38 μm (0.5 × 1.5 mil). Note the low bond deformation.

ribbon wires. One advantage of ribbon over round wire is that its high-frequency impedance is lower, depending on the width-to-thickness ratio which reduces both the inductance and the skin-effect losses. As such, it is often used in microwave devices and hybrids with w/t ratios of 5 to 10, or even higher. The inductance, L, in nH, of a straight ribbon wire is given by Eq. (2-1) [2-64].

$$L = 2 \times 10^{-4}\, \ell(1n[2\ell/(t+w)] + 0.5 + 0.2235 \times [t+w]/\ell) \qquad (2\text{-}1)$$

where t is the ribbon thickness, w is its width, and ℓ is the length of the wire, all in micrometers.

The skin effect will decrease the inductance (in the range of 2–6%) at high frequencies but can increase the impedance considerably (see Chap. 9). The high-frequency losses of ribbons with large w/t ratios can be much lower than that of TAB leads (which are almost square) as well as round wire.

There are two correctable problems encountered when bonding ribbon wires. As the w/t ratio is increased (>5), the tool and substrate must be maintained extremely parallel (within less than one degree), or one side of the ribbon will be poorly welded. (To avoid this for very wide ribbons, bonding is often done with a small tool and using multiple welds across the width.) Also, there is seldom a very large deformation of the ribbon during bonding, so there is little surface cleaning of oxides and contaminants from the interface. Thus, to obtain good welding, the bond pads should be plasma or UV-ozone cleaned shortly before bonding (see Chap.7). The above reasons imply that it is extremely important to use good bondable metal on the pads and to carefully optimize the bonding-machine parameters. If thermosonic bonding Au ribbon/wire, then using the highest practical interface temperature is helpful. Currently, there are several suppliers of ribbon wires.

Recently, the use of large Al ribbon [e.g., 80×10 mils (2×0.25 mm)] for high power devices has increased and autobonders have been made to increase throughput. Also special *textured* bonding tool shapes have been developed that help deform the wire and clean the surfaces during bonding increasing the yield. Ribbon reduces the number of individual interconnections, reducing the wire bonding time required for high power chips and also facilitates spreading the current across a large die surface/metallization (see Fig. 2-18). These large ribbons need special techniques for pull-testing and otherwise evaluate their strength. See Ref. [2-65].

2.7.2 Parallel Gap and Tweezer Welding

Parallel-gap electrode welding (PGW) (sometimes called split electrode welding) is often used for resistive and harder metal wires, both round and ribbon, as well as for special metallizations. As an example,

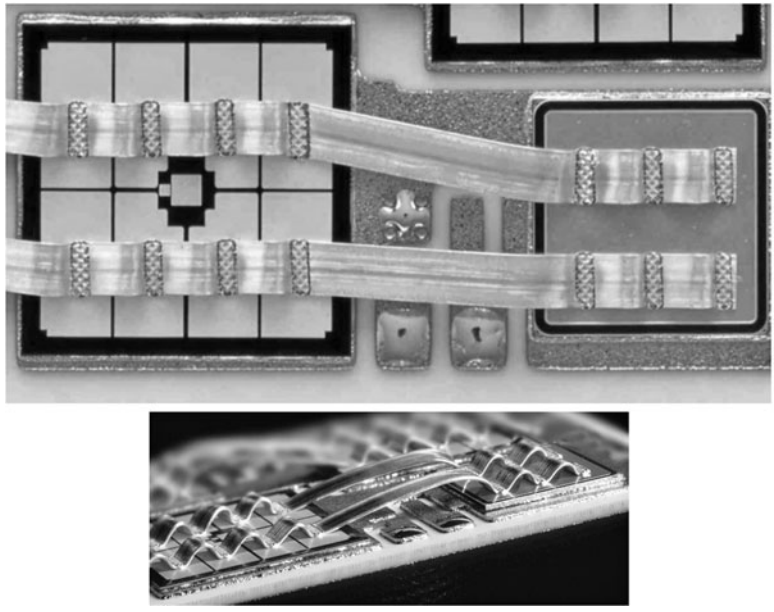

Figure 2-18 Photograph of devices bonded with large Al ribbon [80 × 8 mil (2 × 0.2 mm)], using a waffle pattern ultrasonic bonding tool. The upper picture is taken directly from the top and clearly reveals the patterned tool, and how such bonding can be oriented to connect die or pads that are displaced from a straight line. Lower figure is tipped to show the stress-relief looping between bonds. (*Courtesy of Orthodyne Electronics.*)

Pt wire work-hardens significantly during cold ultrasonic wedge bonding. So, it is often bonded by parallel-gap (electrical discharge) welding [2-66 to 2-68], which is a form of thermocompression (TC) bonding (no melting takes place). Figure 2-19 shows a typical setup for parallel gap welding. Platinum has a high resistivity and low thermal conductivity, which are helpful properties for this welding method. The electrical discharge, between two closely spaced electrodes through the wire, heats it to appropriate TC bonding temperatures (several hundred degrees), while the clamping force presses it against the pad metallization. This forms the thermocompression (deformation) bond.

PGW is typically used for larger diameter wires [e.g., ≥100 (4 mil)]. It is not adaptable for high-speed bonding and is usually performed manually, one wire at a time. This bonding method is frequently used in high-temperature electronics. Johnson and Fendrock [2-67, 2-68] describe the methods of setting the bonding parameters (i.e., force, electrical power, and time), as well as other welding setup information. In one example, a 125 μm (5 mil) diameter Pt wire was welded to a 0.5 μm Pt bond pad on a sapphire substrate. For such situations, a heated stage (at ~200°C) was recommended.

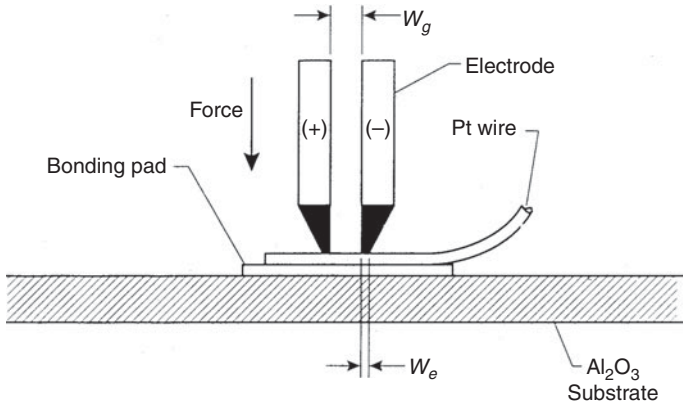

Figure 2-19 Diagram of a parallel gap welder used for small-diameter wire welding showing the electrode-wire-pad arrangement [2-68]. (*Used with kind permission of Springer Science and Business Media.*) W_g is the parallel gap width and W_e is the individual electrode width (related to the impression it leaves in the wire). A capacitor discharge is passed between the two electrodes heating the wire and forming the thermocompression weld.

Tweezer Welding

It is an old manual wire-bonding technique used for bonding large-diameter Al wires to high posts on power-device packages. However, some power-device specialty companies may still be making such welds. An example of devices having tweezer welds was given in Chap. 4, Fig. 4-6. The package must have a tall, usually Au-plated, alloy 42 post that extends through a glass-metal seal for external electrical connections. The chip bond is made by an ultrasonic weld (similar to modern large-wire ultrasonic bonding). The wire is either precut to length or cut after the first bond with special scissors. The unbonded end is then manually moved by the operator to the side of an Au-plated bonding post. An operator-positioned spring- tensioned "clip lead" (tweezer) clamps the wire tightly against the post. An electrical discharge is passed through the clip lead, heating the Al wire (below its melting point), and to an extent the post, forming an electrical discharge (TC) weld. Optical examination of the weld usually reveals significant Au-Al intermetallic compound formation around the perimeter. This is often used as indication of good bonding. As with most TC bonds, the center is left unwelded. There have been a number of reliability problems resulting from tweezer welds, although when properly made they are quite reliable. These problems arise because the bonding process is completely operator-dependent. The clamping force is dependent upon the spring tension in a modified clip-lead, as well as the proper placement by the operator. The bond strength (interface) is difficult to test. The best method is to cut the wire and do a 90° peel in the plane of the weld (sideways).

In some cases, after bonding, the extending wire tail is peeled back as a NDPT. This author is not aware of any published papers on this method of bonding, and most of the equipment still in use is well over 20 years old.

2.8 Major Chip Interconnection Alternatives to Wire Bonding (Flip Chip and TAB)

As the off-chip speed increases and the bond pitch decreases, the inductance and crosstalk of wire bonds limits their use (see Sec. 10.6). Also, some high-silicon-density requirements cannot be met with wire-bond interconnections. As the chip-power increases along with lower operating voltage (down to one volt) and finer pitch, wire bonds will not be able to carry the required current. Some projections state that individual high-performance chips will draw over 100 A, requiring hundreds of 25 μm diameter wire bonds just to distribute the power. Also, as the I/O (input/output) pad-pitch decreases and the number of peripheral pads increases, at some point area-array pads will be required for interconnections. ITRS [2-69] projections predict the finest wire-bondable pitch that can be achieved (at high bond yields and adequate current carrying capacity), will be somewhere between 20 and 25 μm in single-row peripheral bond pads. (Multiple rows, called area array bonding, over 4 μm deep, are possible with modern autobonders, but crosstalk can limit performance.) At some point, a change to flip chip (C4, microballs, conductive polymers, etc.) or some as yet undiscovered technology will be required to solve future I/O interconnection limitations.

The most obvious alternatives to wire bonding are some variation of flip-chip interconnections. A thorough discussion of these technologies and their many variations is beyond the scope of this wire-bonding book, but some brief comments and comparisons are described further in this chapter.

2.8.1 Flip Chip

Solder Ball Flip Chip

The most used, advanced interconnection alternative to wire bonding is the flip chip (called C4, Controlled Collapse Chip Connection or just FC). See Ref. [2-70]. This technology was invented in the mid 1960s at IBM. It has the lowest possible inductance per lead, ~0.05 to 0.1 nH (compared to ~1 nH/m for 25 mm diameter wire) and thus the highest frequency response as well as the lowest crosstalk and simultaneous switching noise. Flip chips also offer the highest packaged Si density. They can be "tiled" as close together as 125 μm (5 mils) on ceramic substrates in hermetic packages. For laminate substrates

that require epoxy underfills, flip chips are spaced ~0.5 mm (20 mil) apart. A reasonable amount of heat can be conducted out through the chip's front surface by the solder bumps to the package below. However, very high heat (generated in the fastest devices) must be removed from the back of the die (which faces upward). This can involve elaborate heat-conducting fins/rods and expensive packages, although heat-sink attachment with silicone grease or polymer has become a cheaper alternative. The package and the I/O pads must be designed around the specific intended bumped die, and this implies very high volume or high costs. Recently, flip chips have been used on laminate (PCB) substrates with polymer under-filling to correct the CTE mismatch. These polymer substrates reduce the package cost, but may further limit the heat dissipation. Other efforts to reduce the process costs have led to bond-pad bumping with TS ball bonds (and removing the wire) to the existing peripheral Al bond pads. Also, conductive polymers or microballs have been used. To take full advantage of flip-chip technology, it is necessary to redesign existing chips for area-array I/O FC pads, which cannot then be effectively wire bonded for use in normal packages (although area array autobonding is being developed). Such redesigning originally slowed the use of flip-chip technology, although there have long been programs to redistribute the peripheral bond pads into area-array format [2-71]. This has poorer heat transfer (through the bumps) and more crosstalk than a chip originally designed for area-array I/Os, so it is only an interim step. However, the massive use of portable devices, such as cell phones, has overcome this problem because of small size and high frequency requirements. Currently, more high-performance chips and higher Si density (tiling) are required for such use, and many more chips are currently designed in true area-array, flip-chip format. This interconnection method is growing at a faster rate than wire bonds and eventually (in many years) will presumably overtake them as the preferred interconnection method for many applications.

Ball Bumped/Stud Bumped Flip Chip

Recently, the use of ball bumped (stud-bumped) flip chip has become increasingly used. For instance, there are billions/year of SAW filters interconnected with them and hundreds of millions of ICs. It allows a ball bonder to attach Au (or Cu) flip-chip bumps to existing wafers or chips designed for normal wire bonding. The volume has become so high that almost every manufacturer of autobonders produces a dedicated ball bumping machine that can attach tens of thousands of ball bumps to entire wafers rapidly. These are dices and are ready for flip chipping (usually with conductive epoxy or other bonding method). Some of these techniques/applications are discussed and shown in other parts of the book. A publication describes the techniques for making these, as well as the economics [2-77].

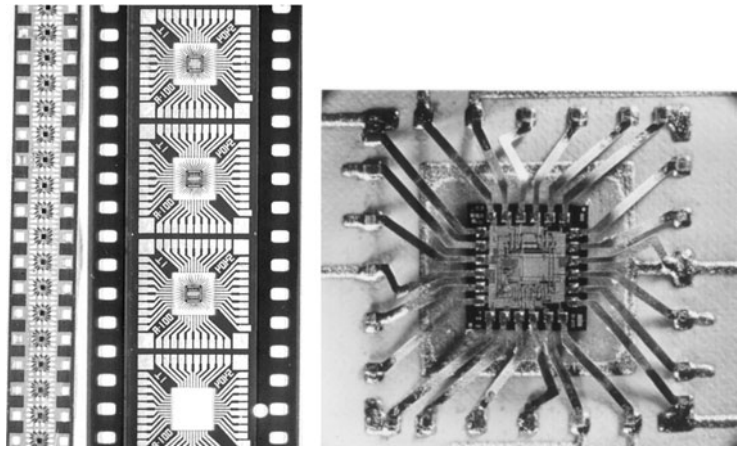

Figure 2-20 Two TAB tapes, 12 mm and 35 mm (left) and a TAB solder-bonded chip (right).

2.8.2 Tape-Automated Bonding

Tape-automated bonding (TAB) was invented in the 1960s.* It consists of rectangular (or ribbon-like, tin-plated) Cu beams held in place by a thin polymer tape (usually polyimide), often in 35 mm film-type format. Typically, the beams are mass soldered (alloyed) to Au bumps plated over normal peripheral bond pads on chips. Neither TAB nor wire bonding is appropriate for area-array bonding as are flip chips. TAB leads can also be TS bonded [2-72] to the plated bumps or to ball-bonded bumps [2-73]. They have even been directly bonded to the normal pads (bumpless TAB) using converted wire autobonders [2-74]. TAB leads have also been laser welded to bumps [2-75]. The rectangular leads normally have slightly lower high-frequency impedance than round wires [see Eq. (2-1)], and until ~1990 could have finer pitch than wedge and ball bonds (see Sec. 2.9). Two-metal-layer TAB can have lower inductance and crosstalk (than wire bonds), but is very expensive. TAB usually requires at least as much space as wire bonds (no tiling possible), and similarly passes heat out the back of the die into the substrate, the exception being flip-TAB where the leads can be short and the inductance low. But heat must then be taken off through the exposed back side of the die, rather than through solder bumps, as for flip chips. This requires more expensive packages as with high-powered flip chips. It is similar to standard flip-chip technology except that it uses gold bumps rather than solder bump interconnection. Photographs of older TAB tapes (35 and 12 mm) and a TAB chip soldered to a substrate are given in Fig. 2-20.

*Generally thought of as originating at General Electric and referred to as the "GE minimod," but the first patent was filed in 1966 by Francis Hugel (U.S. Patent 3,440,027).

TAB offers the advantage of testability and burn-in of chips before committing them to expensive SIP or other multichip packages. This advantage has diminished as known-good-die or tested chip-sized-packages became more available. In general, TAB tape is expensive and inflexible, requiring new tape (and masks) for every small change in chip or package pad location. As with flip chips, to be economical, TAB requires either very high-volume or very high-cost chips, where packaging costs are insignificant. An example of the latter could be in flat-panel displays. TAB is a niche technology and will continue to find such uses, but not in mainstream chip packaging.

2.9 Wire-Bonding Technology: A Comparison and Future Directions

Wire bonding is the most flexible of all IC interconnection technologies. If the die undergoes a downsizing or has other pad-dimensional changes, the autobonder can be reprogrammed (taught) in a short time. Once taught and recorded, the same die can be wire-bonded by the same machine simply by inserting the appropriate floppy disk. Short wire bonds have acceptable low inductance (~1 nH/mm), and, by surrounding signal leads with ground-power leads, they can approximate a transmission line in some cases. Nevertheless, inductance and crosstalk at high frequencies are the main drawbacks for using wire bonds on high-performance chips. Wire bonds are cost-effective for both low- and high-device volumes. Chips are bonded face up, so heat can be conducted out from the back through the die-attach material into the substrate. There are many combinations of basic wire-bond technology with other interconnection methods as described above; for example, ball-bumped TAB and a variation used for applying Au or Cu FC bumps (generically called stud bumps), TAB leads bonded to chips with TS wire bonders, and wire bonds on top of cut-off TAB leads for package interconnections after TAB was used on the die for KGD testing. Thus, even if other interconnection technologies are used, the knowledge and equipment of wire bonding are often required to make the interconnections. A comparison of the three technologies is given in Table 2-2.

The ITRS packaging roadmap (2007) predicts that ball bonds will have bond pad pitches ~20 μm by 2013 [2-76]. For wedge bonds, the pitch is expected to decrease to 20 μm by 2009. Over 10^{13} wire bonds are expected to be made in 2008. This number has increased by 12 to 14% per year in recent years. A huge materials and equipment infrastructure for wire bonds is in place worldwide, with many thousands of workers already trained. As a result, one should expect momentum to keep wire bonds the dominant interconnection method for many years.

Considering the above interconnection technologies (and the many possible variations of each), it is likely that both wire and flip-chip technologies will be used, often side-by-side in the same facility

Unit to Compare	Best	Middle	Worst
Cost	WB	Low performance, FC	FC, TAB
Manufacturability	WB	FC (especially if underfill required)	TAB
Flexibility for changes	WB	FC, TAB	
Reliability	FC (process dependent)	WB (materials dependent)	TAB (>process dependent)
Performance (high speed)	FC	Ribbon wire	WB (round wire)
Silicon density (tiling chips)	FC	Flip-TAB	WB, TAB

WB is round-wire bonding; if ribbon were used, the performance should be better than TAB. FC is flip chip—here only solder-bump C4 rather than other FC variations are considered. Note that TAB is barely a niche technology in 2008.

Table 2-2 Major Interconnection Technology Comparison

for many years to come. These may be in the same packages, as in SIPS, stacked chips, BGA's, and so forth. High performance technologies, such as high-density interconnect (chips first), MCMs, etc. are niche categories, at least for the present. Other as-yet uninvented interconnection technologies may appear, perhaps applied at the wafer level (which are related to FC technology). Some older, discarded technologies, such as "beam leads," may be reborn (e.g., for chip-sized packages). Manufacturers of the future will choose the interconnection technologies that are cheapest, and/or give the required performance, or otherwise optimized for a given application. There should be no preconceived constraints on this choice.

References

2-1 Joshi, K. C., "The Formation of Ultrasonic Bonds Between Metals," *Welding Journal*, Vol. 50, 1971, pp. 840–848.

2-2 Dushkes, S. Z., "A Design Study of Ultrasonic Bonding Tips," *IBM J. Res.*, Vol. 15, May 1971, pp. 230–235.

2-3 Crispi, F. J., Maling, G. C., and Rzant, A. W., "Monitoring Microinch Displacements in Ultrasonic Welding Equipment," *IBM J. Res.*, Vol. 16, May 1971, pp. 307–312.

2-4 Wilson, A. D., Martin, B. D., and Strope, D. H., "Holographic Interferometry Applied to Motion Studies of Ultrasonic Bonders," *IEEE Trans. on Sonics and Ultrasonics*, Vol. SU-19, Oct. 1972, pp. 453–461.

2-5 Hu, C. M., Guo, N. Q., Yu, J. D., and Ling, S. F., "The Vibration Characteristics of Capillary in Wire Bonder," *Proc. IEEE CPMT Electronics Packaging Technology Conference*, Singapore, 1998, pp. 202–208.

2-6 Osterwald, F., Lang, K.-D., and Reichl, H., "Increasing Bond Quality by Ultrasonic Vibration Monitoring," *Proc. 1996 ISHM/IMC*, Denver, CO, pp. 426–431.
2-7 Fritzsche, H., "Improvements in monitoring ultrasonic wire bonding process by simultaneously monitoring vibration amplitude and bonding friction using lasers and analytical models," *VTE* (Germany) Vol. 3, (2002), pp. 119–126.
2-8 Polytec, Inc. Tustin, California 92780.
2-9 Harman, G. G. and Leedy, K. O., "An Experimental Model of the Microelectronic Ultrasonic Wire Bonding Mechanism," *10th Annual Proc. Reliability Physics*, Las Vegas, Nevada, Apr. 5–7, 1972, pp. 49–56.
2-10 Harman, G. G. and Albers, J., "The Ultrasonic Welding Mechanism as Applied to Aluminum and Gold Wire-Bonding in Microelectronics," *IEEE Trans. on Parts, Hybrids, and Packaging*, Vol. PHP-13, 1977, pp. 406–412.
2-11 NBS Technical Notes in the series *Methods of Measurement for Semiconductor Materials, Process Control and Devices:* TN 495 (June 1969); TN 520 (Sept. 1969); TN 527 (Dec. 1969); TN 571 (Sept. 1970); TN 788 (Mar. 1973); TN 806 (June 1973); Special Publication 400-4 (Mar. 31, 1974).
2-12 Ji, H., Li, M. C., Wang, J. Guan, and H. S. Bang, "Evolution of the Bond Interface during Ultrasonic Al–Si Wire Wedge Bonding Process," *Journal of Materials Processing Technology*, Vol. 182, Issues 1–3, 2 Feb. 2007, pp. 202–206.
2-13 Zhou, Y., Li, X., and Noolu, N. J., "A Footprint Study of Bond Initiation in Gold Wire Crescent Bonding," *IEEE Trans. Packaging Technologies*, Vol. 28, Dec. 2005, pp. 810–816.
2-14 Harman, G. G. and Kessler, H. K., "The Application of Capacitor Microphones and Magnetic Pickups to the Tuning and Trouble Shooting of Microelectronic Ultrasonic Bonding Equipment," NBS *TN 573*, May 1971, pp. 1–22 (some availability in 2007).
2-15 Harman, G. G., (Editor/contributor), "Microelectronic Ultrasonic Bonding," *NBS Special Publication 400-2*, Jan. 1974, pp. 1–103, which summarized 5 years of this work (some availability in 1996).
2-16 McKeown, M. and Voronel, "A. 80 kHz as an Alternate Frequency for Large Aluminum Wire Bonding," *Proc. IMAPS*, San Diego, CA, Oct. 8–12, 2006, pp. 659–702.
2-17 Takeda, K., Ohmasa, M., Kurosu, N., and Hosaka, J., "Ultrasonic Wirebonding Using Gold Plated Copper Wire onto Flexible Printed Circuit Board," *Proc. 1994 1MC*, Apr. 20–22, 1994, pp. 173–177.
2-18 Chen, G. K. C., "The Roll of Micro-Slip in Ultrasonic Bonding of Microelectronic Dimensions,"*1972 Intl. Microelectronic Symposium (ISHM)*, Washington, D.C., Oct. 30–31 Nov. 1, 1972, pp. 5-A-1-1 to -9, (has 66 early references to bonding and mechanisms).
2-19 Krazanowski, J. E., "A Transmission Electron Microscopy Study of Ultrasonic Wire Bonding," *IEEE Trans. CHMT*, Vol. 13, Mar. 1990, pp. 176–181.
2-20 Qi, J., Hung, N. C. Li, M., and Liu, D. "Effects of Process Parameters on Bondability in Ultrasonic Ball Bonding," *Scripta Materialia* 54 (2006), pp. 293–297.
2-21 Levine, L., "The Ultrasonic Wedge Bonding Mechanism: Two Theories Converge," *ISHM 1995 Proceedings*, Los Angeles, CA, Oct. 24–26, 1995, pp. 242–246.
2-22 Carrass, A., and Jaecklin, V. P., *Analytical Methods to Characterize the Interconnection Quality of Gold Ball Bonds*, *Proc. EuPac '96*, Essen, Germany, Jan. 31–Feb. 2, 1996, pp. 135–139.
2-23 Langenecker, B., "Effects of Ultrasound on Deformation Characteristics of Metals,"*IEEE Trans. Sonics and Ultrasonics SU-13*, 1966, pp. 1–8.
2-24 Coucoulas, A.,"Ultrasonic Welding of Aluminum Leads to Tantalum Thin Films," *Trans. Metallurgical Soc. of AIME*, Vol. 236, 1966, pp. 587–589.
2-25 Pantaleon, R., and Manolo, M., "Rationalization of Gold Ball Bond Shear Strengths," *44th Electronic Components & Technology Conference*, May 1–4, Washington, D.C., 1994, pp. 733–740.
2-26 Srikanth, N, Murali, S, Wong, YM, and Vath, CJ, "Critical study of thermosonic copper ball bonding," *Thin Solid Films*, Vol. 462, 2004, pp. 339–345.
2-27 Mayer, M., Paul, O., and Baltes, H.,"In-situ Measurement of Stress and Temperature under Bonding Pads During Wire Bonding Using Integrated Microsensors", *Proc EMIT '98*, Bangalore, India, Feb 17–19, 1998, pp. 129–133.

2-28 Suman, S, Gaitan, M, Joshi, Y, and G. Harman, "Wire Bonding Process Monitoring using Thermopile Temperature Sensor," *Proc. IEEE Trans. Adv. Packaging, Part B: Advanced Packaging*, Vol. 28, 2005, pp. 685–693.
2-29 J-R. Ho, C-C. Chen, C-H. Wang, "Thin film thermal sensor for real time measurement of contact temperature during ultrasonic wire bonding process," *Sensors and Actuators*, Vol. 111, 2004, pp. 188–195.
2-30 Karpel, G. Gur, Z. Atzmon, W. D. Kaplan, "TEM microstructural analysis of As-Bonded Al–Au wire-bonds," *J Mater Sci*. Vol. 42, 2007, pp. 2334–2346.
2-31 Ramsey, T., Alfaro, C., and Dowell, H.," Metallurgy's Part in Gold Ball Bonding," *Semiconductor. Intl.* Vol. 14, No. 5, Apr. 1991, pp. 98–102.
2-32 Spencer, T. H., "Thermocompression Bond Kinetics—The Four Principal Variables," *Proc. Intl. J. Hybrid Microelectronics*, Vol. 5, Nov. 1982, pp. 404–408.
2-33 Ultrasonic Welding, In: *The Welding Handbook*, Eighth (and earlier also) Edition, Vol. 2, Chapter 25, 1991, pp. 784–812.
2-34 Ramsey, T. H., and Alfaro, C.," The Effect of Ultrasonic Frequency on Intermetallic Reactivity of Au-Al Bonds," *Solid State Technology*, V34, Dec. 1991, pp. 37–38.
2-35 Shirai, Y., Otsuka, K., Araki, T., Seki, I., Kikuchi, K., Fujita, N., and Miwa, T., "High Reliability Wire Bonding Technology by the 120 kHz Frequency of Ultrasonic," *Proceedings of 1993 Intl. Conf. on Multichip Modules*, Denver, CO, Apr. 14–16, 1993, pp. 366–375.
2-36 Gonzalez, B., Knecht, S., and Handy, H., "The Effect of Ultrasonic Frequency on Fine Pitch Al Wedge Wirebond," *Proc. 1996 ECTC*, Orlando, FL, May 28–31, 1996, pp. 1078–1087.
2-37 Jaecklin, V. P., "Room Temperature Ball Bonding Using High Ultrasonic Frequencies," *Proc. Semicon/Test, Assembly & Packaging*, Singapore, May 2–4, 1995, pp. 208–214.
2-38 H. K. Charles, Jr., K. J. Mach, S. J. Lehtonen, A. S. Francomacaro, J. S. DeBoy and R. L. Edwards, "Wirebonding at higher ultrasonic frequencies: reliability and process implications," *Microelectronics Reliability*, Vol. 43, Issue 1, Jan. 2003, pp. 141–153.
2-39 Tsujino, J., Mori, T., and Hasegawa, K., "Characteristics of Ultrasonic Wire Bonding Using High Frequency and Complex Vibration Systems," *Proc. 25th Ann. Ultrasonic Industry Assn*., Columbus, OH, Oct. 26–27, 1994, pp. 17–18. (abstract only).
2-40 Heinen, G., Stierman, R. J., Edwards, D., and Nye, L., "Wire Bonds Over Active Circuits," *Proc. 44th Electronic Components and Technology Conf*, Washington, D.C., May 1–4, 1994, pp. 922–928.
2-41 Johnson, W. G., "Yield Points and Delay Times in Single Crystals," *J. Appl. Phys*., Vol. 33, Sept. 1962, pp. 2716–2730.
2-42 "Mechanical Testing, Effect of Strain Rate on Flow Properties," in *Metals Handbook*, 9th ed., Vol. 8, 1985. pp. 38–46.
2-43 See U.S. Patent 3,636,456, Jan. 8, 1972; U.S. Patent 3,693,158, Sept. 19, 1972; U.S. Patent 3,852,999, Dec. 10, 1974; U.S. Patent 4,815,001, Mar. 21, 1989.
2-44 Salzer, T. E., and Martin, C. T., Monitoring and Control Means for Evaluating the Performance of Vibratory-Type Devices, U.S. Pat. 3,794, 236, Feb. 26, 1974.
2-45 Rodionov, V. A., "The Stabilization of the Quality of Ultrasonic Welded Joints," *Svar. Proiz*. (Weld Production, USSR) No. 3, 1979, pp. 14–16.
2-46 Salzer, T. E., Method and Apparatus for Ultrasonic Bonding, U.S. Patent 4,373,653, Feb.15, 1983.
2-47 Raben, K-U., Monitoring Bond Parameters During Bonding, U.S. Patent 4,854,494, Aug. 8, 1989; German Patent 3,701,652, Jan. 21, 1987.
2-48 Jensen, J., and Bradner, D., "Monitoring Ultrasonic Wire Bonders with a Dynamic Signal Analyzer," *Solid State Technology*, Vol. 33, June 1990, pp. 53–55.
2-49 Gibson, 0. E., Gleeson, W. J., Burkholder, L. D., and Benton, B. K., Bond Signature Analyzer, U.S. Patent 4,998,664, Mar. 12, 1991.
2-50 Pufall, R., "Automatic Process Control of Wire Bonding," *Proc. 43th Electronic Components and Technology Conf*, Orlando, Florida, June 1–4, 1993, pp. 159-162.

2-51 Ingle, L., and Koontz, J., "Directly Bonded Interconnect Method and Adaptive Feedback Bond Signature Analysis System," *Proc. 1993 Intl. Conf on Multichip Modules*, Denver, Colorado, Apr. 14–16, 1993, pp. 384–390.
2-52 Short, R., "Fine Pitch Wedge Bonding for High Density Packaging," *Proc. 1994 Intl. Conf on Multichip Modules*, Denver, Colorado, Apr. 13–15, 1994, pp. 50–55.
2-53 Anderson, 0. L., and Christianson, H., "Technique for Attaching Electrical Leads to Semiconductors," *J. Appl. Phys*., Vol. 28, 1957, pp. 923–924.
2-54 English, A. T., and Hokanson, J. L., "Studies of Bonding Mechanisms and Failure Modes in Thermocompression Bonds of Gold Plated Leads to Ti-Au Metallized Substrates," *9th Annual Proc. IRPS*, Las Vegas, Nevada, Mar. 31–April 2, 1971, pp. 178–186.
2-55 Ahmed, N., and Svitak, J. J., "Characterization of Au-Au Thermocompression (TC) Bonding," *Proc. Electronic Components Conf*, Washington, D.C., May 1975, pp. 52–63. Also In: Solid State Technology, Vol. 18, Nov. 1975, pp. 25–32.
2-56 Condra, L. W., Svitak, J. J., and Pense, A. W., "The High Temperature Deformation Properties of Gold and Thermocompression Bonding," *IEEE Trans. on Parts, Hybrids and Packaging*, Vol. 11, Dec. 1975, pp. 290–296.
2-57 Jellison, J. L., "Kinetics of Thermocompression Bonding to Organic Contaminated Gold Surfaces,"*Proc. 26th Electronic Components Conf*., San Francisco, California, Apr. 26–28, 1976, pp. 92–97.
2-58 Antel, W. K., "Determining Thermocompression Bonding Parameters by a Friction Technique," *Trans. Met. Soc. AIME*, Vol. 236, Mar. 1966, pp. 392–396.
2-59 Smith, M., "Quality Assurance Issues Associated with Large-Wire Ultrasonic Bonding," *ASTM Committee F-1.07*, Jan. 26, 1995. Also see "*Hybrids: Designing for Maximum Yield in Power, Microwave and RF Devices*." Both available from Orthodyne Electronics Corp, 2300 Main St., Irvine, California 92714.
2-60 Coucoulas, A., "Hot Work Ultrasonic Bonding? A Method of Facilitating Metal Flow by Restoration Process," *Proc. 20th IEEE Electronic Components Conf*, Washington, D.C., May 1970, pp. 549–556.
2-61 Kessler, H. K., and Sher, A. H., "Microelectronics Interconnection Bonding with Ribbon Wire," NBS Technical Note 767, Apr. 1973, pp. 1–24.
2-62. Guidici, D. C., "Ribbon Wire vs. Round Wire Reliability for Hybrid Microcircuits," *IEEE Trans. Parts, Hybrids and Packaging*, Vol. PHP-11, June 1975, pp. 159–162.
2-63 Beck, D., "The Case for Ribbon Bonding of Large Packages to PCBs," *Surface Mount Tech*., Vol. 8, Apr. 1994, pp. 38–44.
2-64 Terman, F. E., *Radio Engineers' Handbook*, McGraw-Hill, New York, 1943, pp. 47–57.
2-65 Wong, G., and Oftebro, K., "Bond Test Methodologies for Large Aluminum Ribbon," *Intl Symp. Microelectronics (IMAPS)*, San Jose, CA, Nov. 11–15, 2007, pp. 933–940.
2-66 Knowlson, P. M., "Fundamentals of Parallel Gap Joining," *Microelectronics and Reliability*, Vol. 5, Pergamon Press, 1966, pp. 203–206.
2-67 Johnson, D. R., and Knutson, R. E., "Parallel Gap Welding to Thick Film Metallization," *Proc. 26th Electronic Components Conf*., San Francisco, California, Apr. 26–28,1976, pp. 66–73.
2-68 Fendrock, J. J., and Hong, L. M., "Parallel Gap Welding to Very Thin Metallization for High Temperature Microelectronic Interconnects," I*EEE Trans. on CHMT*, Vol. CHMT-13, June 1990, pp. 376–382.
2-69 International Technology Roadmap for Semiconductors. International Technology Roadmap for Semiconductors. http://www.itrs.net/home.html
2-70 "Solder Ball Technology," (multiple papers and authors), *IBM J. Res. and Dev.*, Vol. 37, Sept. 1993, pp. 581–675. Also, ibid, Vol. 13, May 1969, pp. 226-284.
2-71 Kromann, G. B., Gerke, R. G., and Huang, W. W., "Hi-Density C4/CBGA Interconnect Technology for a CMOS Microprocessor," *IEEE Trans. on CPMT-Part B*, Vol. 19, Feb. 1996, pp. 166–173.
2-72 Silverberg, G., "Single Point TAB (SPT): Versatile Tool for TAB Bonding," *1987 Proc. ISHM, Minn*., MN, Sept. 28–30, 1987, pp. 449–456.
2-73 Larson, E. N., and Brock, M. J., "Development of a Single Point Gold Bump Process for TAB Applications," *Proc. 1993 Intl. Conf on Multichip Modules*, Denver, Colorado, Apr. 14–16, 1993, pp. 391–397.

2-74 Jacobi, J. W., Process for Bonding Integrated Circuit Components, U.S. Patent 4842662, June 27, 1989. Also see Deeney, J. L., Halbert, D. B., and Laszo, H., "TAB as a High-Leadcount PGA Replacement," *IEEE Trans. on CHMT*, Vol. 14, Sept. 1991, pp. 543–548.
2-75 Zakel, E., Azdasht, G., and Reichl, H., "Investigations of Laser Soldered TAB Inner Lead Contacts," *Proc. 41st Electronic Components and Technology Conf.*, Atlanta, Georgia, May 1–16, 1991, pp. 497–506.
2-76 ITRS, The International Technology Roadmap for Semiconductors, 2007. http://www.itrs.net/home.html
2-77 Evans, D., Couts, P., "Gold Stud Bumping for High Density Flip Chip Interconnect," *Proc IMAPS 2007 Symposium*, San Jose, CA, Nov. 11–15, 2007, pp. 1184–1190.

CHAPTER 3

Bonding Wire Metallurgy and Characteristics That Can Affect Bonding, Reliability, or Testing

3.1 Introduction

Various parts of this book use materials science and metallurgical characteristics of bonding wire to explain different bonding phenomena. This chapter includes the stress-strain characteristics, fatigue, wire hardness, and other properties that affect the results of bond tests, bondability, and reliability. This chapter also presents wire burn out, and aging characteristics, as well as a review of the various recent ASTM standards* appropriate to bonding wire in App. 3A. This chapter also gives actual data on wires and defines the necessary metallurgical terms in the context of wire bonding. It is recommended that a reader having no familiarity with metallurgy/materials science read an introductory text on that subject to better understand the

*American Society for Testing Materials 100 Barr Harbor Drive, West Conshohocken, PA 19428.

concepts.* Such understanding will be helpful in other parts of this book, as well.

Ribbon wire applications are discussed in Chap. 2 and will not be separately discussed here, with the exception of some fatigue data in Sec. 3.8. It is assumed to be similar in metallurgical properties to round wire of comparable size (99.99% Au—without dopants).

3.2 Stress-Strain Characteristics of Bonding Wires

Bonding wire is generally specified by its elongation and breaking load (sometimes incorrectly referred to as its tensile strength). Presumably there are other properties that influence the bonding process, but those are not understood and cannot be called out or practically measured. They may be related to uniformity, surface finish and hardness, crystal structure, heat treatment, etc. (e.g., a similar specified Al or Au wire from a different manufacturer often requires different bonding parameters to achieve equivalent bonding).

The basic metallurgical stress-strain properties of typical bonding wires are shown in the curves of Fig. 3-1. Such data are obtained by following ASTM F 219 specifications (see App. 3A), and pulling (applying force to) a 25.4 cm (10 in) length of wire while continuously recording the elongation (stretching) and its actual breaking-load (force). The stress axis represents the applied force (usually in gms or mN), while the horizontal axis, the strain, represents the wire's response to the pulling stress/force and appears as the wire elongation (stretching). Curves represent data from the same (large-diameter) Al bonding wire in two different states of anneal. However, the curves are generic for both large- and small-diameter wires made of either Al or Au. Specific wires may yield slightly different shapes (e.g., be flatter in region 3, etc.). Data for the stress ordinate are normalized since the stress-relieved curve could be two or three times higher (stronger) than the annealed one. Curve A is fully annealed and B is stress-relieved (slightly annealed). Region 3 denotes the plastic deformation, where the wire permanently stretches. The breaking load of each wire is shown at point 4 and would be read from the vertical stress (applied force) axis. Note that gold wire for use in thermosonic and thermocompression bonding is annealed and would generally have stress-strain characteristics nearer to those of curve A in Fig. 3-1.

---

*See for instance, *Understanding Materials Science: History, Properties, Applications (Hardcover)*, by Rolf E. Hummel Springer-Verlag; 2d ed. (May 1998). Also see, *Fundamentals of Materials Science and Engineering: An Integrated Approach*, 3d ed. William D. Callister, Jr. and David G. Rethwisch, December 2007. For data, formulas, etc. see *CRC Materials Science and Engineering Handbook*, by J. F. Shackelford and W. Alexander (eds), 3d ed., 2001.

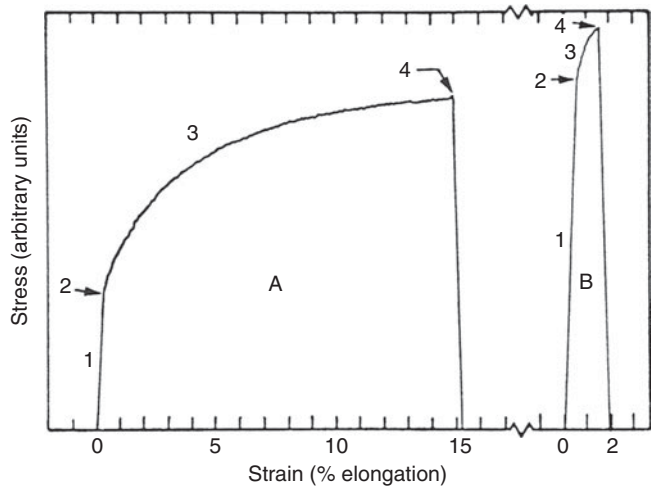

Figure 3-1 Typical stress (pulling force) versus strain (elongation) curves for aluminum bonding wire in two states of hardness: wire (A) is annealed and is typical of large-diameter aluminum bonding wire, but also similar to those of Au used in TS bonding; (B) is stress-relieved (partially annealed). Its characteristics are similar to those used for small-diameter ultrasonic wedge bonding (either Al or Au wire). In order to display both curves on the same chart, the stress axis was made arbitrary [the breaking load of (A) was approximately one-half that of (B)]. On both curves (1) is the elastic region where the stress is proportional to the strain, (2) is the proportional or elastic limit, (3) is the region of inelastic or plastic deformation, and (4) is the breaking load of the wire. The elongation at the breaking point is 15% for (A) and 1.5% for (B).

If the wire is nondestructively pulled (NDPT), the force must not exceed the elastic limit (point 2 in both curves). This produces irreversible metallurgical changes in the wire, which by definition cannot be nondestructive (see Sec. 4.3).

3.3 The Shelf-Life Aging of Bonding Wires

High-volume manufacturers receive their wire on "just-in-time" delivery, and use wire within a week or month of receiving shipment, and they are not concerned about aging properties. However, small organizations and those that only occasionally use a particular type/size of wire need to be concerned about the long-term storage (aging) properties of many types of bonding wire. Some discard wire after an arbitrary period, such as 3 or 6 months. They are not willing to risk a change in its metallurgical properties which could affect yield from an existing bonding machine setup. In the mid-1980s, ASTM (Committee F 1.07) had several wire manufacturers systematically study the actual aging properties of both Au and Al, 25 μm (1 mil) diameter

bonding wires. These were stored on 5 cm (2 in) spools at 22.8 ± 1.6°C (73 ± 3 EF) for 2 years and tested periodically. In conjunction with updating the ASTM bonding wire standards, wire manufacturers were recently contacted and they agreed that the general aging characteristics of current wires are expected to remain generally valid today. This should hold even with the major metallurgical changes that have been made in wires for gold ball bonding, as discussed extensively in the next paragraph.

The original data was published in ASTM standards, F 72 and F 487. In 2006, those documents were updated and reballotted, soliciting comments from four current wire manufacturers and other experts. Aluminum fine wire still primarily consists of Al, 1% Si and has approximately the same characteristics as shown in the original measurements. The main difference being in more controlled/reproducible characteristics due to manufacturing improvements. Gold bonding wire for high-speed autobonders now contains differing and often much higher percentages (up to 1%) of stabilizing/intermetallic-inhibiting additives. Although no equivalent multicompany aging tests have been made, these new alloys are expected to be at least as stable over time as the wires of the mid-80s period.

In general, the breaking load of hard, as-drawn wire decreased rapidly (from 5 to 15%) within 6 weeks after manufacture (thus, hard-wire is seldom recommended for volume production, where reproducibility is required). It continued to decrease, but more slowly, over the 2-year period as it self-annealed at room temperature. All stress-relieved and annealed wires of both gold and aluminum stayed within their breaking load specification for the entire 2-year test period. The elongation characteristics for Al, 1% Si wire were more ambiguous than the breaking load, changing upward or downward but within the specification extremes, and generally recovering to the median by the end of the test. The data were compiled and published in ASTM standards, F 487 (for Al, 1% Si) and in F 72 (for Au alloys, Be and Cu doped). The aging data for aluminum (1% Si) and gold (<10 ppm beryllium doped) are given in Figs. 3-2 and 3-3, respectively. Other aging charts, Al, 1% Mg, and Au + Cu, are not reproduced here because these wires are seldom used today and have been dropped from the ASTM standards. However, they were included in the original ASTM study (ASTM F 638 and F 72, respectively). The reader is directed to the ASTM standards for more detailed data on the specifications and properties of bonding wire (see App. 3A for a listing).

The conclusion drawn from the shelf-life study is that, in general, small-diameter annealed or stress-relieved wire (not hard, as drawn) can be used for up to 2 years with only minimal change in its breaking load, although Al wire elongation may vary over its entire specified range. The caveat is that the wire must be stored at approximately constant room temperature, and exposure to direct sunlight, drafts from an open door, or possible heat sources must be avoided.

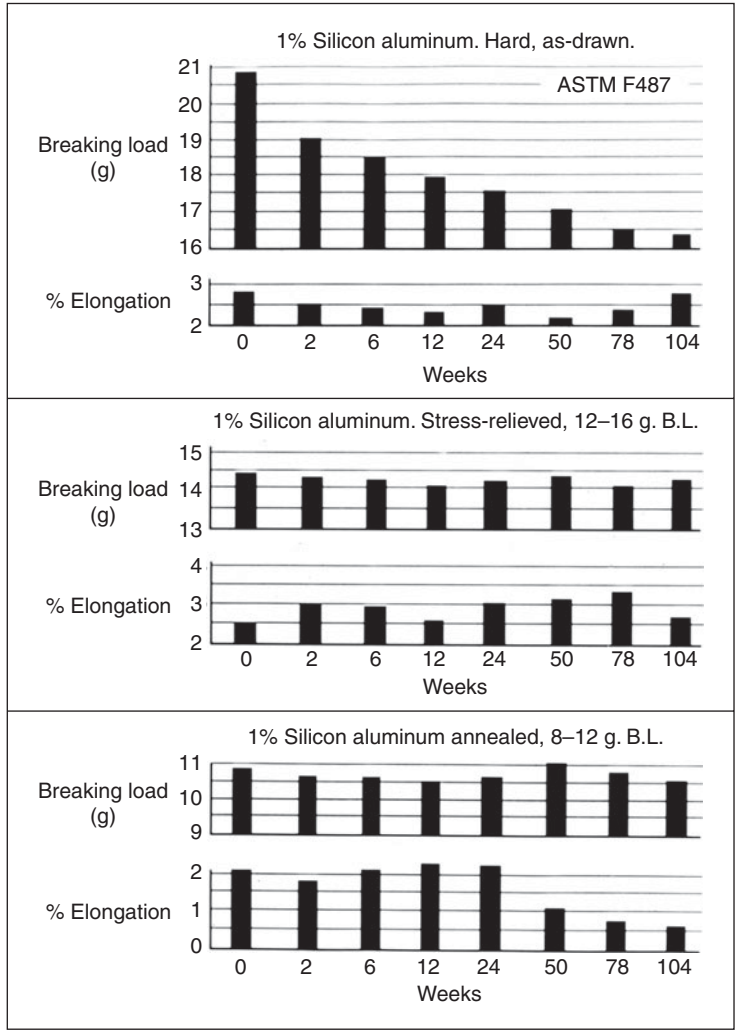

Figure 3-2 The shelf-life aging of bonding wire for 25-µm diameter, Al 1% Si, wire in hard as-drawn, stress relieved, and annealed condition.
[*From ASTM F 487-revised in (2006). Copyright ASTM. Reprinted with permission.*]

Even after the ASTM tests, some occasional users prefer to dispose of wire within 6 months or so. One rationale is that the ambient as well as the general handling of the wire cannot always be assured over a 2-year period. Another is that the micrometallurgy of modern Au wire has changed since the ASTM data were taken and its aging characteristics have not been studied. We note small-diameter Au-wire has improved considerably in that time (more stable, stronger,

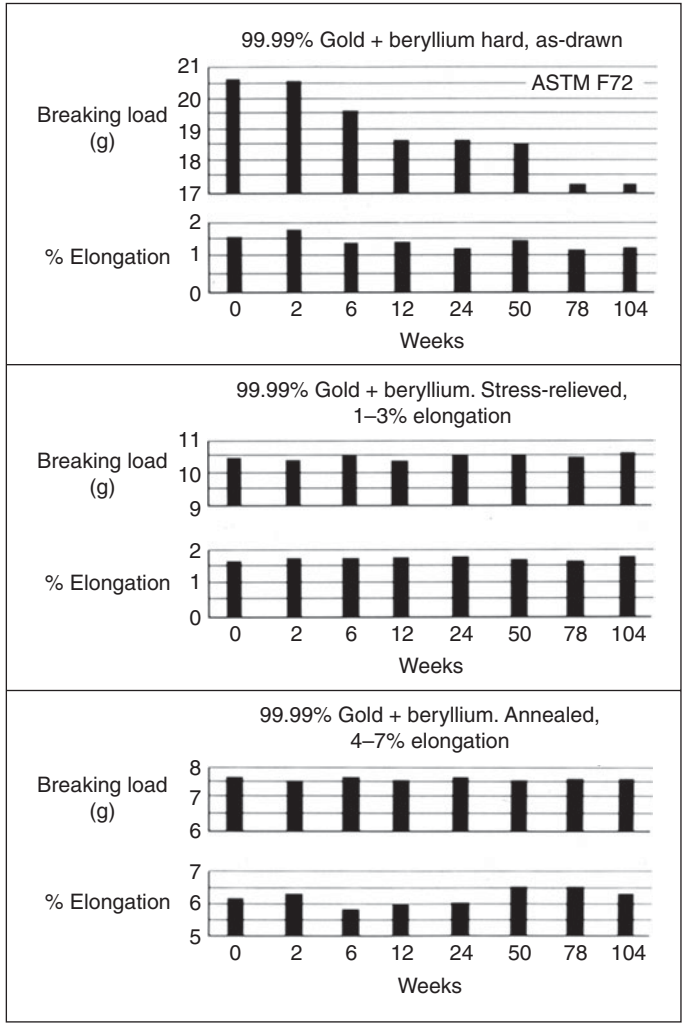

Figure 3-3 The shelf-life aging of bonding wire for 25 μm diameter, gold wire with <10 ppm Be, in hard as-drawn, stress relieved, and annealed condition. [*From ASTM F 72-revised in (2006). Copyright ASTM. Reprinted with permission.*]

better neck and looping characteristics, etc.). In contrast, Al wire primarily still uses the same 1% Si alloy, and thus has changed little, improving primarily in uniformity and reproducibility.

No equivalent aging studies have been conducted on larger-diameter bonding wire, (~100 μm, 4 mil) diameter and larger. However, most large-diameter aluminum wires currently used for power devices are of 99.99% Al. These wires are generally used in the

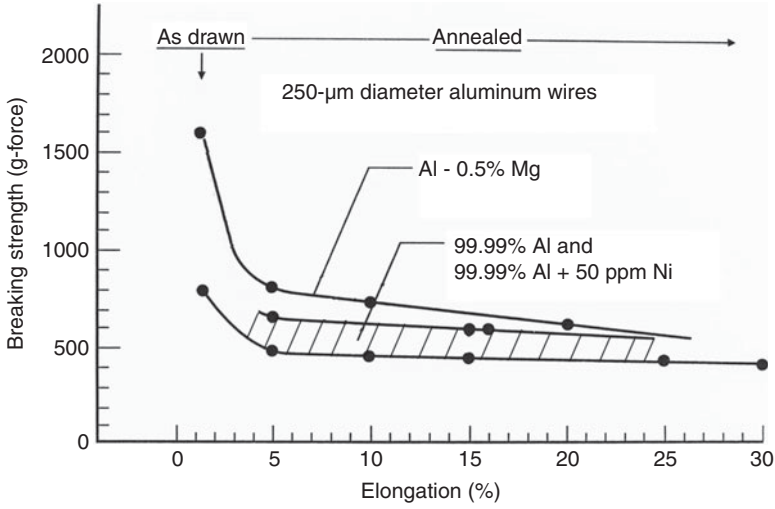

Figure 3-4 Typical annealing curves (heat-treatment) of modern 250-μm diameter aluminum bonding wires. The top curve contains 0.5% Mg. The lower banded-together curves represent the user/manufacturer specification range of 99.99% Al and the 99.99% Al, plus 50 ppm of Ni dopant. The metallurgical characteristics of the two can overlap[3]. The user specifications (BL and elongation) will determine the position on the curve that the manufacturer anneals the wire to produce the desired characteristics. (*Courtesy of Custom Chip Connection, 2008.*)

annealed condition (>5% elongation). Based on the above aging tests for small-diameter wire, it can be assumed that the breaking load of such annealed wire is not apt to change over a 2-year period. An example of typical breaking loads and elongations for large-diameter wires is given in the annealing curves shown in Fig. 3-4. To make such curves the wire is annealed at various times. Points on the left side of the curve take shorter times and lower temperatures than on the right. For example, to produce a typical large-diameter bonding wire, it could be annealed at 250°C for 45 min (99.99% curve producing ~15% elongation).* The process is repeated with different times and temperatures to complete the curve. Most large-diameter Al wire is used in the high-elongation (>5%), flat breaking-load region of the curve, and should remain very stable at normal handling temperatures.

The large-diameter wire, containing ~50 ppm Ni as a dopant is used to enhance corrosion resistance for plastic encapsulation. We note, however, that a majority of all large-wire applications still use standard 99.99% Al wire. This is also the primary large-diameter wire used in industry up to 500 μm (20 mil) diameter with elongations from 10 to 20%, in 2008.*

*Dr. Peter Douglas, Custom Chip Connection, Huntsville, AL, Private Communication.

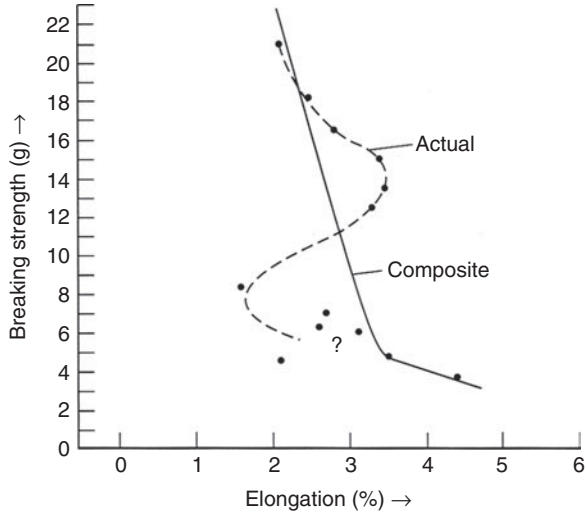

Figure 3-5 The breaking strength versus elongation for 25 µm (1 mil) diameter 1% Si Al wire. There may be variation in elongation in the intermediate range which results in drift of that parameter during aging, as shown in Fig. 3-3 [3-1].

An annealing curve for Al, 1% Si, 25 µm (1 mil) diameter wire is given in Fig. 3-5 [3-1]. The small-diameter silicon-doped wire is quite different from the large wire. The exact shape of such curves for this type of wire will vary with annealing temperature, cooling time, and the individual manufacturer's process. In some cases, the changes (swings) in elongation of the wire can be several times larger than shown in Fig. 3-5. The explanation for these elongation swings is related to crystallographic structural change of the wire's fiber axis from <110>, as drawn, to <111>, during recrystallization (heat treatment). Details of such crystallographic behavior is beyond the scope of this book,* and the reader is referred to other general metallurgy books [3-2] for a more complete understanding.

3.4 General Discussion of Gold Bonding Wire

Small-diameter gold bonding wires for ball bonding come in two distinctly different types. The first was originally used for manual wire bonders. Its breaking load is in the range of 6 to 8 g, annealed,

*See for instance, *Understanding Materials Science: History, Properties, Applications (Hardcover)*, by Rolf E. Hummel Springer-Verlag; 2d ed. (May 1998). Also see, *Fundamentals of Materials Science and Engineering: An Integrated Approach*, 3d ed. William D. Callister, Jr. and David G. Rethwisch, December 2007. For data, formulas, etc. see *CRC Materials Science and Engineering Handbook,* by J. F. Shackelford and W. Alexander (eds), 3d ed., 2001.

with an elongation of –4 to 7% (for 25 μm diameter). Such a wire is usually stabilized with copper and silver dopants, at less than 100 ppm by weight. High-speed autobonders require a much stronger wire with the (annealed) breaking loads in the 8 to 12 g range and elongations of 3 to 6%. This extra strength is necessary to prevent breakage or stretching when the wire is rapidly pulled through the bonding capillary, but especially to supply increased strength in the heat-affected neck region (just above the ball), giving better loop formation and thermal cycle performance. The high strength also gives added wire-sweep resistance for plastic encapsulation (see Sec. 8.1.7). Many different dopants can be used to stabilize these wires. Such original dopant was beryllium, introduced first in the general 10 to 100 ppm range but more recently used in the 5 to 8 ppm range [3-3]). Later calcium (5–7 ppm) and then other dopants, usually in proprietary amounts, were added to improve the wire and neck characteristics. As above, the total dopant concentration does not exceed 100 ppm, and all wires are specified as 99.99% Au. Recently more impurities have been added to further strengthen the wire or the neck above the ball and also to reduce intermetallic compound failures in fine pitch applications. In some cases (in 2008), the purity has been lowered to 99.9% Au often with Pd or proprietary dopants). Discussions of the wire neck region (its length, hardness, grain structure changes, etc.) have been given by several investigators [3-4, 3-5, 3-6]. Although stronger wires were designed to meet the needs of high-speed autobonders, they can also be used quite well with manual bonders.

Gold wires for ball bonding are supplied in the annealed condition. If the wire were left hard (as drawn), the portion immediately above the ball would become annealed during wire melting and ball formation. This zone would thus be much weaker than the rest of the wire, bending sharply (like a hinge) above the ball and preventing smooth loop formation. (This phenomenon, which allows easy break-off at the neck, is used for ball-bumped flip chip applications and also for uses requiring very low loops such as TSOPs, smart cards, and stacked-chips, see Chap. 9.) Even with special additives to improve the strength and minimize the length (38 to 100 μm, 1.5 to 4 mils) of the neck, this zone is still the weakest part of the wire bonding system [3-4]. It is called the HAZ (heat affected zone) and has a hardness about 20% lower than the rest of the wire. A sketch of the grain structure in this zone, after ball formation, is shown in Fig. 3-6*a,* and an actual wire section is in Fig. 3-6*b*. It should be noted that the HAZ has a larger grain structure than the rest of the wire, making it the weakest part of the bond system. It usually breaks there in a pull test. There is continuing research by the wire manufacturers to strengthen this region in order to improve looping, and increase its resistance to fatigue and wire sweep.

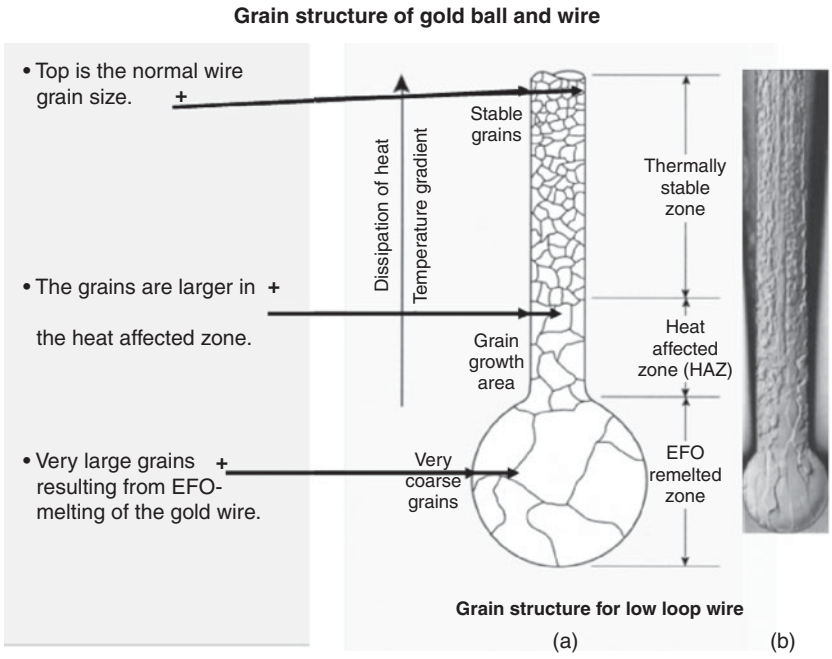

Figure 3-6 (*a*) Sketch of the grain structure for a gold wire before and after ball formation, showing the heat-affected zone. (*Courtesy of H. Chia, AFW, Inc.*) (*b*) An etched gold wire and ball revealing the actual grain structure. (*Courtesy of K&S wire.*)

Some of the metallurgical problems associated with gold ball bond formation and wire looping have long been studied [3-5]. Those problems are (1) clubbed ball formation (ball not centered on wire); (2) grain growth and weakness of wire above ball; (3) neckdown formation and leadframe tie bar severance; and (4) wire scratching. These do not occur often in usual situations, and most autobonders are normally programmed to avoid them (3). Also, in some cases (2) and (3) wire metallurgy is being improved to limit the problems. Normal maintenance usually eliminates wire surface damage (4). Nevertheless such problems do occur enough to note and Table 3-1 can be used indicate some of the approaches for troubleshooting.

Specific troubleshooting information on wire and bond tool problems can often be obtained from the wire and bonding tool manufacturers. Several of these have extensive catalogues that devote part of the space to such problems as well as to general technical explanations. Often they have very useful Web sites, some are listed in further reading at the end of the book.

Problems	Possible Solutions
Clubbed ball	Increase tail length, lower EFO position, avoid, capillary or machine sideways motion
Wire grain growth (weakness in HAZ)	Shorten EFO spark time, use improved (doped) wire
Neckdown above ball, tie bar severance	Use reverse looping
Wire scratching or marks	Clean clamps, replace/clean capillary

TABLE 3-1 Gold Ball Bonding Problems/Solutions

3.5 Aluminum Wire for Ultrasonic Wedge Bonding

Small-diameter Al wire for ultrasonic (US) wedge bonding normally has 1% Si added to increase its strength (pure Al is too soft to draw to small-wire dimensions). This alloy was adopted in the 1960s as having the right mechanical properties and has proved satisfactory ever since. It is not greatly changed today, although it is much more uniform and reproducible. Silicon is not in solid solution below 500°C and thus it appears in these wires as finely divided particles. These particles can grow with heat treatments, and large particles can serve as stress risers, initiating cracks and causing the wire to break during device thermal cycling (see Sec. 8.2). However, in practice Al, 1% Si wire has proven quite reliable in billions of devices. Its ASTM standard (F-487) was upgraded in 2006. Aluminum alloys, containing 1 or 0.5% Mg, are in uniform solid solution at room temperature. As such they might have been a better choice for the industry. However, it has dropped out of use for fine wire bonding, and that ASTM standard (F-638) was discontinued in 2006. We note that at the 0.5% level, Mg is still in limited use for some large-diameter wire interconnections, up to 250 μm (10 mil) diameter.

Small-diameter aluminum wire for ultrasonic wedge bonding has quite different mechanical properties from similar diameter gold wire for ball bonding. The former is generally supplied in the stress-relieved condition, meaning that it is not fully annealed (only partially so), see Fig. 3-2. Wire with breaking loads as high as 21 and as low as 12 g (for 25-μm diameter Al wires) have been used for US bonding. Fully annealed Al, 1% Si wire would be in the range of ~4 to 7 g BL with the elongation about 10%. This is too soft to be (usefully) US wedge bonded to normal Al IC metallization. Typically, 25-μm diameter Al wire is specified as having a breaking load of 14 to 16 g and an elongation in the range of ~0.5 to 2%, the same specification as used 25 years ago. The low elongation is needed to allow clamp-pull-breakoff of the wire after the second bond. High-elongation wire

would stretch rather than break and stop the bonding operation, often loosing the threading of the wire. However, large-diameter wire having high elongation is cut off by a specially designed bonding tool and bonded with an inverted V-shaped, parallel-grooved tool that limits deformation. Examples of bonded large-wire are given in Chap. 2. Thus, large-Al wire can be fully annealed, have very high elongations, and still be bonded, as shown in Chap. 2, Fig. 2-16. Most large-diameter Al wire is either specified as 99.99% Al, or a few may contain 0.5% Mg. However, 99.99% wires have been offered with ~50 ppm of Ni additive, which is intended to make them less subject to corrosion in plastic packages as discussed previously. These wires are reputed to withstand up to 700 h in a pressure cooker test (121°C, 100% RH). This wire alloy is not offered in small diameters. Any possible effect on Au-Al intermetallic compound formation has not been a problem since large wire is usually bonded to Ni on the package and Al pads on the device.

3.6 Wire and Metallization Hardness

The hardness values of wires and balls are often needed to assess the possibility of cratering and to match the hardness of metallization for best bonding.* Such data are scattered throughout the book and are collected together in the cratering section (Sec. 5.1) in Table 5-2 for convenience. These data are often in different units and may not be directly converted, since, necessary information is often not published. Values of typical metallization hardness are not included in that table because they depend on heat treatment and any alloying agents. For instance, Al metallizations containing Cu can increase in nanohardness (UMH, or ultramicrohardness, see glossary) by up to a factor of 4 (1 to 4 GPa) as the concentration of Cu increases from 0 to 10% [3-7]. Another UMH test [3-8] found that pure Al films ranged from ~0.45 to 0.6 GPa. The 2 to 4% Cu range (sometimes used in IC metallization) is about 2 GPa. This alloy is noted for age hardening, so its actual hardness will depend on heat treatment and age. Hardness measurements made on thin (~1 μm) metallization require special UMH testers using very low forces (~0.2 g load) and cannot be performed without special knowledge and training. However, hardness measurements on wires and balls have been made with standard microhardness testers, typically using loads of ~1 to 4 g.

Two studies have measured the correlation between metallization hardness and bondability. Nabatian [3-9] (thick films and wedge bonding) and Klein [3-10] (IC metallization and ball bonding) found

*There is also a hardness difference between as-made undeformed balls and bonded balls, with the latter being about 40% harder (Chap. 8, Table 8-3), but differences depend on the metal (e.g., Au, Cu).

that bondability decreases as the metallization hardness increases, all other conditions being equal. (See Chap. 9 for an example of bondability as a function of hardness.) In addition, others found that the best bondability occurs when both the wire and the metallization are about equal in hardness [3-11]. Typically pure bondable Au and Al wire and films range in hardness from ~50 to 90 HKn, (a metal hardness scale, see glossary) but can increase in hardness rapidly with impurity and gas (oxygen) content.

3.7 The Effect of EFO Polarity on Gold Wire and Its Metallurgy

Around 1984, the industry began to change from using a positive electronic flame-off spark (EFO) to a negative EFO for gold ball formation [3-12]. One reason for the change was that the negative EFO resulted in more uniform ball formation (important for today's high yield and fine pitch bonding requirements). Another was that foreign (carbonaceous) particles were not attracted to the wire and the capillary. Also, gold is not sputtered from the wire and deposited on the capillary. Thus, using the negative EFO stopped the deposits, and significantly increased capillary life, minimizing capillary-related machine down-time. In addition, extensive theoretical studies of ball formation at the University of Pennsylvania [3-13] showed that a negative EFO produced more effective and uniform heat transport from the spark to the wire.

There were also some "claimed" benefits for the EFO polarity change. As an example, it was claimed that the ball was softer and, therefore, resulted in less cratering. However, limited studies of ball hardness resulting from positive and negative EFOs showed that the latter actually resulted in a slightly harder ball, probably because it produced smaller grain structure [3-14]. Values reported were (average) 39.3 HKn for –EFO and 37.3 HKn for +EFO. Thus, any EFO polarity effect on cratering, which was never documented, remains unexplained.

3.8 Metallurgical Fatigue of Bonding Wires

Wire bond reliability problems resulting from temperature and power cycling are extensively discussed and explained in Figs. 8-17 to 8-19 (Sec. 8.4). However, no metallurgical stress versus number of cycles failure data are given there. Metal fatigue is defined and some typical S-N failure curves are shown. Several authors have studied the wire fatigue problem in Au and Al wires, and some have given S-N curves in their publications [3-15 to 3-20]. The information presented below covers Au and Al wire alloys. Copper-alloy wire S-N experiments have also been described [3-19].

When a metal (wire) is subjected to a repetitive stress, such as bending back and forth, it may eventually fail even though that stress is much lower than is required to fracture it in one single bend or pull. **This is called fatigue**. Data on material fatigue are usually given as stress versus the number of cycles (S-N) required to cause failure. Most wire (bond) fatigue data have been obtained in an accelerated manner by mechanically flexing short lengths of wire at some constant operating temperature (usually room temperature). However, field failure conditions are seldom so simple. Power (on/off) and other temperature cycling involves various periods of heating, holding at temperature for various times, and cooling at various rates. In real devices, this thermal cycling flexes the wire, which introduces work damage. But, it may also partially anneal that damage during periods of continuous high-temperature operation.

There has been relatively little actual fatigue data published for bonding wires, and much of the data are calculated from other data or presented in different forms [3-16, 3-17]. Some use deflection, longitudinal strain, stress, etc., without enough information given to convert units and directly compare data. That which is available can only be assumed accurate for the specific (often unstated, and usually proprietary) wire metallurgy that was used in the study, typically comparing wire A, B, C. Often the manufacturing process (including dopant and annealing) may have changed since the data were published. Nevertheless, (very) approximate estimations of wire bond life due to fatigue can be made from such generic data. The following three S-N curves, Figs. 3-7 to 3-9, are thought to be

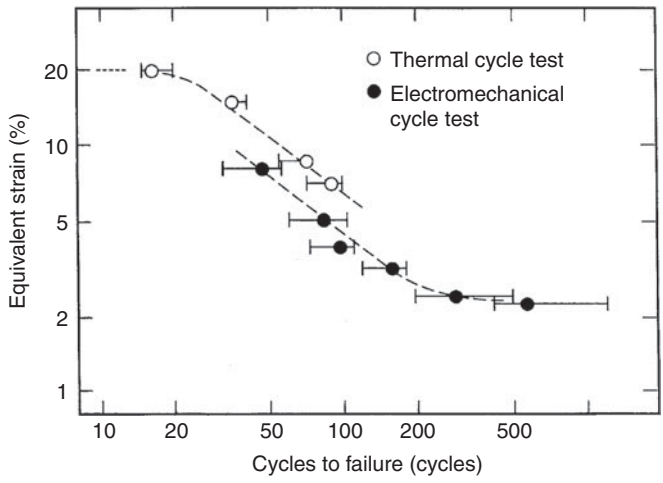

Figure 3-7 The relationship between equivalent strain and the cycles to failure for 20 × 350 μm, thermocompression bonded, Au ribbon. The top curve results from thermal cycling (–55–85°C), and the lower results from mechanical cycling to equivalent displacements [3-18].(© *IEEE*.)

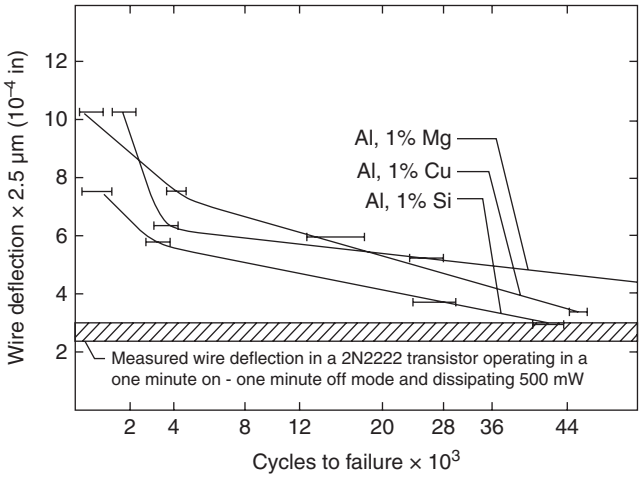

Figure 3-8 Fatigue curves (basically S-N curves) for different 25 μm diameter for various Al alloy wires that were US wedge-bonded. These data were obtained by a mechanical accelerated fatigue test on the wires. The dashed bar below represents the measured wire deflection that occurred in an actual device under temperature cycling conditions. Note that the Mg-doped wire is more fatigue resistant than the Cu-or Si-doped wires [3-15]. (© *IEEE*.)

appropriate for both understanding and life estimates of bare wires. In addition, Uebbing [3-16] studied encapsulated Au wire fatigue, using the S-N curve from wrought gold, and the reader is referred to his paper for those data. Some wire manufacturers currently have fatigue data on their Web site, see Bibliography.

One direct comparison of the S-N lifetime of Au (ribbon wire, no purity data given, but usually 99.99%) between mechanical flexing (MF) and thermal cycling (T-Cy) were given [3-18]. It was found that for the same strain, the cycles-to-failure were ~60% greater for T-Cy than for MF (at room temperature), as shown in Fig. 3-7.

The broadest general study of wire fatigue was carried out by a group from Cornell University. They built a special apparatus that could study the cycles to failure at various temperatures (20°C, 75°C, and 125°C), and at three different strain amplitudes [3-20]. Both Al and Au wires, at 25 μm diameter, were used. The Al was standard 1% Si and those results should be valid today, while the Au results should still be indicative. The two types of Au wire were unspecified, and currently can be quite different. The strain amplitudes were 0.7%, 5%, and 10%. Normally one would expect low-strain repetitive amplitudes in microelectronic systems. For this, the (0.7%) strain data, gave a cycles-to-failure range of 1000 to 10,000 cycles, with a longer life at the lower temperatures. For the Au samples, one type had a higher and the other type, a lower, cycles to failure than Al. The data is too complex to combine and plot in one or two figures, and an interested reader should use the original reference (available for download through IEEE *Xplor*. and libraries).

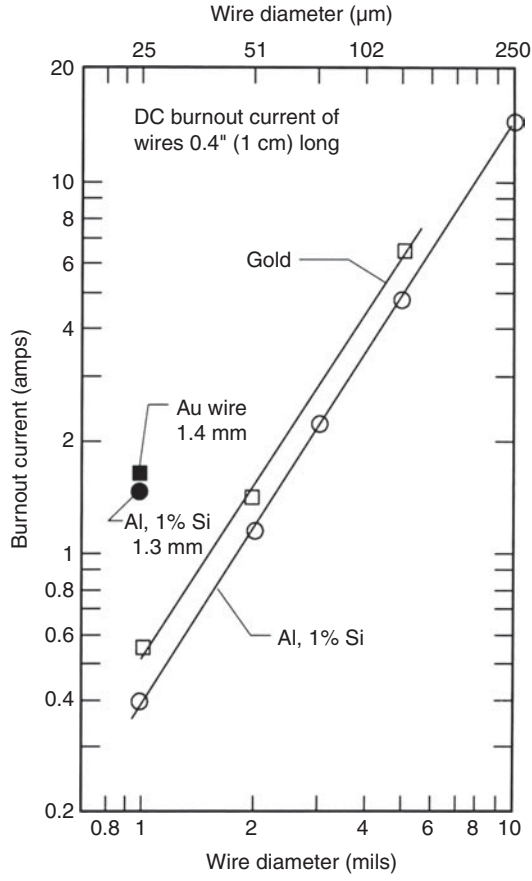

Figure 3-9 Wire burnout for DC-ramped current measured for 1 cm lengths of Au and Al wire of indicated diameter, except for shorter lengths shown by black data points.

During high-temperature exposure, Al, 1% Si wire may grow large silicon aggregates and develop a weak bamboo structure. The Si aggregates can serve as stress risers (causing cracks) and shortening the fatigue life. Because of this, the T-Cy life of such Si-doped Al wire could be shorter than its expected life without such long high-temperature exposure. Thus, as with Au wire, an accurate value of wire fatigue life in a real device is difficult to estimate. A study of fatigue life of several specified Al wire alloys was made by Ravi [3-15]. His data are reproduced as Fig. 3-9 and indicate that Al, 1% Mg wire has the superior CF fatigue life. (Temperature cycle fatigue was not measured.) He also compares the deflection against the actual measured value from a working device. Aluminum wire alloys have changed minimally since his work, so the comparison should still be valid, but should be

compared to the above Cornell study, which used more precise equipment. Considering all of these uncertainties discussed previously, wires do fail during thermal cycles, whether they are in open cavity or plastic packages. Therefore, this problem must be considered when designing interconnection systems subject to significant temperature variations, and the designer may be forced to make fatigue life estimates based on limited data. Clearly more work is needed to better characterize the relative mechanical properties of bonding wires by using similar equipment [3-20]. The practical solution to wire fatigue in open cavity packages is to increase the loop-height to bond-length ratio. This minimizes the amount of flexing in a given ΔT situation (see Sec. 8.2), and as such affects both Au and Al wires. Other environmental factors such as humidity have been shown to reduce the fatigue life of Al wires [3-17]. However, since most chips/wires are plastic encapsulated, where the strain must be estimated and can vary around a chip/package, the only practical method is to use temperature cycling to establish a realistic life. This has become standard in all packaging development.

3.9 Copper Wire for Ball Bonding

Copper wire has been studied for over 20 years, but only recently has been incorporated in actual volume production (**see Chap. 5**). It is very different from Au wire. It oxidizes and thus requires an inert atmosphere during "EFO" ball formation, it is harder and more crater prone etc. However, the renewed interest has been driven primarily by the high cost of Au, Cu's lower resistivity (for carrying more current), as well as its resistance to wire sweep in plastic encapsulation. Its intermetallic reliability and increased hardness on Al pads have been well established and are discussed in Chap. 5 with appropriate references. In addition, thermosonic bonded Cu balls reveal a much higher hardness of 111 HVN than that of initial Cu balls (84 HVN). This can and does lead to cratering (see Chap. 8) [3-21]. Most Cu ball bond production is at 50 μm (2 mil) diameter and larger wire sizes used for small power devices. This author is not aware of high-volume production at 25 μm sizes or less. However, with Au approaching $1000 per troy ounce (2008), it surely will be when metallurgical problems, such as neck and stitch-fatigue in plastic encapsulation, have been solved. All bonding wire manufacturers make Cu wire, and autobonders designed for it are readily available. There are no ASTM or international standards for it, as yet, but many of those listed below for Au wire should be helpful.

Several comments from the packaging industry indicate that problems have occurred in plastic encapsulated Cu wire less than 50 μm (generally <40 μm) diameter. Cu is sensitive to cold working or recrystallization. It has been observed that a higher incidence of heel cracks as well as ball neck cracks result from temperature cycling

and are frequently associated with 25 μm or less diameter wire that is plastic encapsulated. Cu wire can crack near the stitch heel and at the ball neck during temperature cycling.* Therefore, there are still studies going on to implement 25 μm or smaller diameter wire. Additional industry comments indicate that other problems may be equally important to metallurgical ones. Examples are that to optimize for wire bonding, it is necessary to harden the bond pads, and this presents manufacturing problems for companies that have their chips bonded in foundries. Tools wear faster, and threading at finer pitch (≥40 μm) is slower. Complex metallurgy pad areas (i.e., Cu/Lo-k) are easily damaged. [C*urrently there is some production using fine (~25 μm) Cu wire in plastic encapsulation for low-end amusement devices, where only limited temp cycling is encountered.*] Thus, even with all the listed problems Cu wires cost, advantages are so great over Au that, in time, the remaining problems should be solved.

A concise summary of Cu wire, advantages and problems, was given in a technical bulletin published by Gaiser Tools. It is reproduced in App. 3B.

Insulated Bonding Wire

The concept of insulating bonding wire to prevent shorts between adjacent wires has been around for many years [3-21, 3-23]. One such coating system was applied to Al wire by heavily anodizing it. This was effective for wedge bonding, but without the need for fine pitch, it offered few advantages. Other coatings were tried later, but there was little demand for such products in the course-pitch wire bonding era, and they were not implemented. There have been many patents for such technology. Recently, [3-24] developed a coating compatible with Au ball bonding. This is currently available from at least one wire supplier. As such, with very fine pitch (to 20 μm) advancing rapidly, it is possible that such will be used significantly in the future.

3.10 Conductor Burn Out (Fusing)

3.10.1 Bonding Wires

The current-carrying capacity of interconnection wires in semiconductor devices is an important packaging design parameter, and many papers have been written on the subject [3-25 to 3-35]. Wire burn out (fusing) is a complex subject that is influenced by the metallurgy and length of the wire, the ambient gas, or (if used) the plastic encapsulant, as well as the duty cycle of the current, the type of bonds (ball or wedge), and the degree of heat-sinking out through the bonds to the chip or package. Several other factors influencing wire burn

*Summarized from comments made by Cesar Chavez, private communication.

out are the wire resistivity, thermal conductivity, temperature coefficient of resistance, and melting point. Other possible factors such as the deformation of the wedge bond and the quality of the bond (the percent of welded interface) can also affect the burn out of short wires. These latter have never been evaluated or even considered in the published literature.

Heat conductivity from the wire to the chip or package, as well as the I^2R heat generated by the given length of wire are important factors in changing the burnout current. Thus, in an open cavity package, assuming a minimally deformed perfectly welded bond interface, the longer the wire, the lower the burnout current (more I^2R heating and less of it conducted out the ends), up to some length in which thermal conduction out the bonded ends is insignificant. As the wire is lengthened, convection and radiation losses into the ambient, control the heat loss process more than thermal conduction out the bonded ends. However, this is very different for plastic encapsulated devices.

Aluminum wire responds differently in oxygen (or air) than in inert gasses or in vacuum. A rapid burn out (in a millisecond or less) in oxygen may result in distorted ball formation on each side of the wire. However, when heated slowly by a current ramp-up (longer than a few seconds), a thick aluminum oxide sheath is produced which changes the heat transfer into the ambient, protects the liquid metal from further oxidation, and holds it in place. Thus, the Al wire temperature can rise hundreds of degrees above its melting point, which results in an apparent artificially high burnout current. When the current is removed, the liquid metal cools and contracts. Sometimes an open circuit will result (if no continuous metal remains inside the Al_2O_3 sheath). At other times, the wire survives and, for practical purposes, has a higher burnout current than its temperature would predict. The first observation of this phenomenon was reported by Kessler [3-25] and later verified [3-29].

Gold wire, which does not oxidize, burns out neatly at its melting point, leaving gold balls on each open wire end. Assuming that the heat conducted out through each weld is the same, such wire will burn out approximately in the center of the span. Gold wire has both a higher melting point and a lower resistivity, and thus has a higher burnout current than Al.* Unfortunately, there is little experimental

*Al, 1% Si, 25 μm diameter, bonding wire has a resistivity of approximately 3.1 mΩ-cm @ 20°C, which results in a resistance of about 60 Ω/m or 0.06 Ω/mm (40 mil length). Its melting point is in the range of 600 to 655°C. The same diameter gold wire, 99.99% pure, has a resistivity of approximately 2.4 mΩ-cm @ 20°C, and a resistance of about 45 Ω/m or 0.045 Ω/mm. Its melting point is 1063°C. In practice, the exact resistivity varies somewhat with added impurity, especially when at the 99.9% level. Also, the measured resistance is very dependant on the accuracy of the actual wire diameter. (Most specifications allow ~5% variation.) Since the resistance varies as $1/r^2$, these specifications can result in about a 10% variation of burnout current for a 25-μm diameter wire, everything else being equal.

data on varying bare-wire length in the short length region less than ~1 mm (where more heat is conducted out through the welds on the end). Also, the shorter the wire, the less total I^2R heating is produced in that wire, as stated previously.

A graph of experimental data for DC-ramped-current wire-burn out for both gold and aluminum wires having wedge bonds (or equivalent) at each end is given in Fig. 3-9. Two short-wire-length data points are included in the figure for comparison. The bond-length versus current transition is actually a continuous one. The data that are available indicate that for 25-μm diameter bare gold wire, the burnout current decreases continuously as the wire is lengthened (from ~1.8 A at 1 mm length) and reaches approximate equilibrium for lengths more than or equal to 5 mm (at ~0.6 A). The long-wire minimum burnout current is similar to that reported in [3-25, 3-30, 3-33]. See Fig. 3-10 for a calculated example of the burn-out current versus length for both Au and Al wires, showing clearly the decrease in burn-out current with increased length. Normally one may assume that wires containing the traditional <10 ppm impurities will have the same burn-out properties as pure Au (calculated in Fig. 3-10 (up to 1%) which increases the resistivity and can reduce the burn-out current for a given situation. Note also that burn-out current can be much greater when wires are plastic encapsulated.

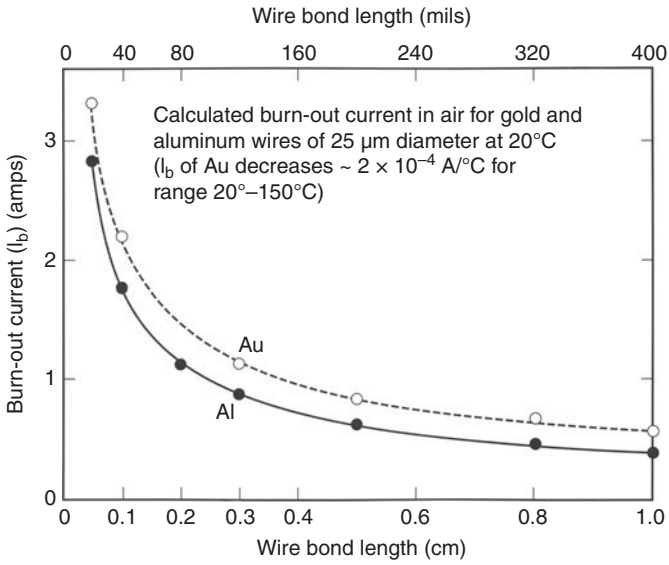

Figure 3-10 Wire burnout calculated for pure Au and Al, 25 μm wires using the resistivity of pure Al and Au. This compares adequately with data in Fig. 3-9, considering that both measured material were doped, and the diameters may vary by 3–5%, whereas the curves use pure metal data and exactly 25 μm diameters.

The bonding method, as well as bond quality, can also affect the burn-out current. Shorter lengths of gold ball-bonded wire will burn out at a higher current than an equivalent length of gold wedge-wedge bonded wire. This results from the wedge-bond neck constricting the wire and limiting the thermal flow, whereas the large ball serves as a heat spreader, making good thermal contact with the chip. As an example, everything else being equal, a 25-µm diameter gold wedge-wedge bond burned out at 0.6 A DC, but a similar ball-wedge bond burned out at 1 A DC. The burn-out point would be displaced (from the center) toward the wedge bond since there is better heat conductivity out through the ball, cooling that side of the wire. If heat flow was symmetrical, then burn out would occur at the center of the wire.

Some wire manufacturers give tables of burnout data for their product, usually identified only by letters or other code, so it may not be applicable to an other manufacturer's product. Nevertheless it can be useful and points out that different wire dopants can influence both the burn-out and resistivity. See Web sites in further reading.

Plastic-encapsulated devices comprise over 95% of integrated circuits. Thus, it is surprising that there have been minimal studies of (gold) wire burn-out in such conditions. Some organizations have made limited studies for internal use, but not published them. One such study contracted to a university, is available as an unpublished report [3-33], and some of its conclusions are used in this section. Encapsulated wires will carry considerably more current than open-air wires due to the increased thermal conductivity of the surrounding plastic compound (with respect to air). However, at some point, as the current increases, it heats the wire sufficiently to affect the thermal characteristics of the adjacent encapsulant (glass transitions, melting, charring, volatilization, etc.). Ultimately this leaves an air gap between the wire and the plastic, or, the plastic otherwise become thermally insulating, and the wire burns out quickly. The report [3-33] finds that the voltage drop across the wire (an indication of temperature) increases erratically as if there were a series of plastic (thermal-characteristics) transitions. Some encapsulated 30-µm (1.2-mil) diameter gold wires sustained currents of several amperes for over an hour before failure. As with bare wires, longer encapsulated ones failed at lower current levels.

As stated above, gold wire burns out in air by forming neat balls on each side of the open wire. However, when encapsulated, interaction with the plastic and the filler results in complex failures, generally of the type shown in Fig. 3-11 [3-34]. Here, no definable ball was formed (or else any ball fragments fell off during decapsulation) and particles of the inorganic filler adhere to the wire. The burn-out current for the 25-µm diameter gold wire in this particular case was 1.1 A (data obtained by slowly, manually, increasing the current) which was about twice as high as expected for a 25-µm diameter Au wire of equivalent length in air. Another difference between open cavity and

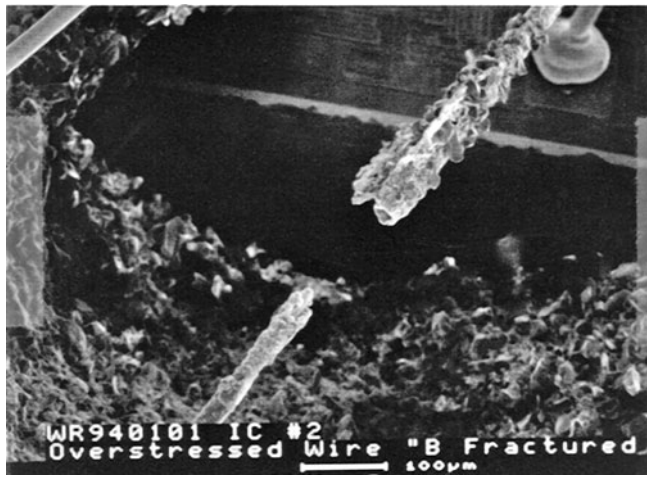

Figure 3-11 SEM photograph of a burned-out 25-µm diameter Au wire that had been plastic encapsulated. The particles adhering to the wire are silica filler from the plastic molding compound [3-34].

plastic encapsulation burn out is the response to transients and current pulses. This is often modeled and well understood for open cavities [3-27 to 3-31], but the heat capacity and thermal conductivity of the plastic encapsulant can greatly increase the transient burn-out current. Because of these difficulties, it is not surprising that there are no modeling papers on the subject, whereas there are many of them for the more readily modeled (free-air) situation.

Considering the complexities of accurately determining the maximum current a wire can carry, it is not surprising that many designers simply derate the burn-out current, such as obtained from Fig. 3-11, by a factor of 2 or 3, increase the wire diameter, or use multiple wires (for power devices). Therefore, wire burn out is seldom encountered in devices that reach the field, and when it is, it usually results from a device or system failure such as a short or transient which might destroy the device anyway, even if the wire did not burn out. More experimental studies are needed to fully understand burn out in plastic-encapsulated wires and also for various bond-related heat sinking (ball, wedge, poor welding, etc.) at the ends of open cavity wires.

3.10.2 The Maximum Allowable Current for PCB and MCM Conductors

Although the maximum allowable current for PCBs is not directly related to bonding wire burn out, it is interesting to consider these familiar packaging situations that have different current limitations. In addition to PC boards, MCMs, SOPs, SIPs, etc., fall in this different

category. Whereas, the current carrying capacity of typical PC board conductors may be large (several amperes), MCM conductors over thin film dielectrics, may have small cross sections (8 to 25 μm widths by 4 to 10 μm thickness) and can be embedded in thermally insulating polyimide, BCB, etc. These can heat up rapidly as the current increases. However, long before conductor burn-out occurs, the adhesive that bonds the conductor to a PC board, or the polymer surrounding the device conductors, may be thermally damaged and cause future reliability problems. Thus, specifications are usually given in terms of maximum permissible temperature rise rather than maximum current. The current capacity of vias and other constrictions must also be considered, as well as solder joints which could melt. Under worse conditions, the PC board or SIP insulating material could burst into flames. There have been many studies of the safe current carrying capacities of PC boards. See, for example, Refs. [3-36 to 3-38].

A concise summary of Cu wire advantages and problems was given in a technical publication by Coors/Gaiser/Tool. It is included as App. 3B. Many studies are going on to implement 1.0 mil or less diameter wire.

Appendix 3A

A LISTING OF USEFUL ASTM* STANDARDS AND SPECIFICATIONS ON BONDING WIRE AND BOND TESTING (All of these were updated in 2006 and reballoted.)

(1) ASTM F 72-06, Standard Specification for Gold Wire for Semiconductor Lead Bonding. (Lists typical chemical dopants, breaking loads, elongation, dimensional tolerance, metal spool dimensions, permissible curling and twisting and in an appendix, lists the aging characteristics—discussed above. Note that many new Au wire dopants are proprietary and are not given in this specification and some may be added up to 1% concentration by weight.)

(2) ASTM F 205, Standard Test Method for Measuring Diameter of Fine Wire by Weighing. (Discusses calibration, precision and calculations for both Au and Au, as well as for other materials.)

(3) ASTM F 219, Standard Test Methods of Testing Fine Round and Flat Wire for Electron Devices and Lamps. Describes methods of measuring the tensile strength and elongation, electrical resistivity, and out of roundness, using 25.4 cm (10 in) lengths.

*American Society for Testing Materials 100 Barr Harbor Drive, West Conshohocken, PA 19428.

(4) ASTM F 487-06, Standard Specification for Fine Aluminum-1% Silicon Wire for Semiconductor Lead Bonding. (Most of the same information as in F 72 above but for Al, 1% Si wire.)

(5) ASTM F 584-06, Standard Practice for Visual Inspection of Semiconductor Lead-Bonding Wire. (This may be discontinued but is useful as it gives manual procedures and photographs of acceptable and unacceptably cleaned bonding wires.)

Appendix 3B

Copper Wire Bonding, a Low-Cost Solution to Gold Wire Bonding?

From Industry Newsletter & Technical Publication, Volume III, Issue 4, July 2005. (Used with Permission of COORS TEK/GAISER precision bonding tools.)

Introduction: Part one of this discussion covered aspects of the ball formation; the various ways to achieve size and shape consistency. In this section, the material properties in particular the hardness and the impact on ball bonding will be discussed. The copper bonding process is not simply about how to make a good free-air ball but how to achieve good product quality and reliability.

The Facts*:*

Copper is a good electrical and thermal conductor, better than gold (see Table 3B-1).

Copper wire is harder than gold (see Table 3B -1).

Copper as a raw material is cheaper and more abundant than gold (>$0.20/oz. vs. >$800/oz).

Copper oxidizes easily, gold does not.

Copper wire bonding uses a limited number of specially designed capillaries, gold wire does not.

Copper processing requires special hardware to prevent oxidation, gold does not.

Copper when bonded to Aluminum pads forms thin intermetallic layers, Gold forms thick intermetallic layers (see gold in Fig. 3B-1).

Typical Parameter	Cu	Au
Resistivity ($\times 10^{-6}$ ohm/cm)	1.6	2.3
Wire Hardness (HK)	>64	<60
Ball Hardness (HK)	>50	<39
Looping	Excellent	Excellent

(HK) = Knoop Hardness

Table 3B-1 Characteristics of Cu and Au Wires

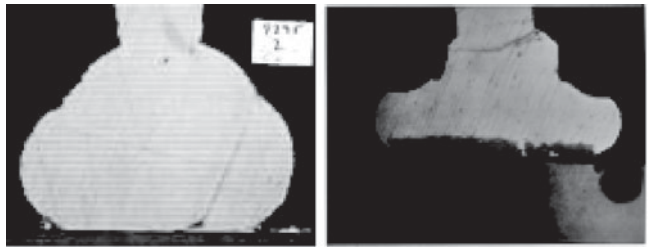

FIGURE 3B-1

Copper work hardens easily, gold does not (see copper in Fig. 3B-1).

Issues: Some of the most important ones are cratering, oxidation and long-term reliability.

The Bonding Process: The copper wire bonding process has to be tailored around the physical properties of the material, the hardness. The significant differences between copper and gold require much higher bonding parameters in order to achieve similar quality factors (pull and shear strength, ball size, and shape). The increase in bonding parameters such as ultrasonic power and force signifies a significant increase in capillary wear therefore reducing effective life of the tool. This is the reason Gaiser Tool Co. recommends special ceramic material for this application.

The capillary material acoustical and wear resistance are key to maximize life and reduce ultrasonic power requirements.

The impact of the copper hardness is most significant during the ball bond process, when copper alloys with the aluminum pad. This can result in bond pad subsurface damage (cratering, chip outs). The most common solution to this problem is either increase bond pad thickness or use a protective under layer (TiW most common). Many times the solution is to implement both, metal thickness and a protective under layer.

Copper oxidizes rapidly when exposed to oxygen, therefore special care must be taken to protect it. The use of enclosed containers in the wire bonder are encourage to keep the wire spool free of oxidation as well as to the use of inert gases such as argon (Ar) or nitrogen (N).

Copper oxide is a layer that prevents the pure copper from alloying or diffusing or bonding with the surfaces in contact.

Long-term reliability, especially when devices are exposed to high-pressure high-humidity temperature cycling, has yielded mixed results. Some claim no problems while others reported multiple failures beyond 500 cycles.

One of the failure modes associated to copper's work-hardening ability is neck breaks, commonly seen during temperature cycling test (see Fig. 3B-2).

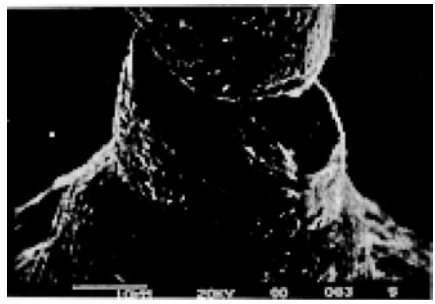

Figure 3B-2 A temperature cycled Cu ball bond (encapsulated) that developed a neck crack.

There are however manufacturing facilities that currently manufacture copper wire products but mostly limited to power devices where large diameter wire is used.

Small-diameter wire (<33 μm) is still a challenge not because of bonding capability but because of reliability concerns as indicated above.

Conclusion

There is no question copper is a cheaper material but also one that brings new challenges to the bonding engineers. It may also be a cost-effective process in the eyes of a product manager but when the extra care and attention is required, it is weighed against the existing gold process and then we should ask ourselves, are the net savings worth?

References

3-1 Douglas, P., Custom Chip Connection, private communication. For a discussion of some small diameter bonding wire characteristics, see also, New Bonding Wire Developments, Microelectronic Packaging Technology: Materials and Processes, *Proc. of the 2nd ASM International Electronic Materials and Processing Congress*, Philadelphia, PA, Apr. 24–28, 1989, pp. 8902–8908.

3-2 Jones, W. K., Liu, Y. and Morrone, A., "The Effect of Thermal Exposure on the Structure and Mechanical Properties of Al-1% Si Bonding Wire," *Proc. of the 1993 International Symposium on Microelectronics (ISHM)*, Nov. 9–11, Dallas, TX, 1993, pp. 445–450.

3-3 U.S. Patent 3,272,625, Sept. 13, 1966. Beryllium-Gold Alloy and Article Made Therefrom, Brenner, Bert, assigned to Sigmund Cohn Corp.

3-4 Ohno, Y., Ohzeki, Y., et, al. "Factors Governing The Loop Profile in Au Bonding Wire.," *Proc. 1992 Electronic Components & Technology Conf.*, San Diego, CA, May 18–20, 1992, pp. 899–902.

3-5 Hu, S. J., Lim, R. K. S., and Sow, G. Y., "Gold Wire Weakening in the Thermosonic Bonding of the First Bond", *IEEE Trans. on CPMT-Part A*, Vol. 18, Mar. 1995, pp. 230–234.

3-6 Levine, L. and Sheaffer, M., "Wire Bonding Strategies To Meet Thin Packaging Requirements," *Part 1,Solid State Technology*, Vol. 36, Mar. 1993, pp. 63–70, Part 2 is in July 1993, pp. 103–109.

3-7 Dirks, A. G., Wierenga, P. E., and van den Broek, J. J., "Ultramicrohardness of Aluminum and Aluminum Alloy Thin Films," *Thin Solid Films*, Vol. 172, 1989, pp. 51–60.
3-8 Bangeri, H., Kaminitschek A., and Wagendristel, A., "Ultramicrohardness Measurements On Aluminum Films Evaporated under Various Conditions", *Thin Solid Films*, Vol. 137, 1986, pp. 193–198.
3-9 Nabatian, D, & Nguyen, P. H., "The Effect of Mechanical Properties of Thick Film Inks on Their Ultrasonic Bondability," *Proc. of ISHM*, Atlanta, GA, 1986 pp. 65-71.
3-10 Klein, H. P., Durmutz, U, Pauthner, H., and Rohrich, "Aluminum Bond Pad Requirements for Reliable Wirebonds," *Proc. IPFA Symposium*, Nov. 7–9, Singapore, 1989, pp. 44–49.
3-11 Hirota, J., Machida, K., Okuda, T., Shimotomai, M., and Kawanaka, R., "The Development of Copper Wire Bonding for Plastic Molded Semiconductor Packages," *35th Proc. IEEE Electronic Components Conference*, Washington, D.C., May 20–22, 1985, pp. 116–121.
3-12 Dreibelbiss, J., Kulicke & Soffa Co. The first production test was in March 1984 at a facility in Bangkok. Private Communication, Lee Levine.
3-13 Huang, L. J., Jog, M. A., Cohen, I. M., and Ayyaswamy, P. S., "Effect of Polarity on Heat Transfer in the Ball Formation Process," *J. Elect. Materials*, Vol. 113, Mar. 1991, pp. 147–153. Also see same authors, "Ball Formation in Wire Bonding", Part II "Real Scale Experimental Studies," *ISHM Journal*, Vol. 13, June 1990, pp. 29–34.
3-14 Douglas, P., and Davies, G., American Fine Wire Company, Technical Report #9. This series of reports, #1-9, also show grain structure of wires and give considerable other technical information.
3-15 Ravi, K. V., and Philofsky, E. M., "Reliability Improvement of Wire Bonds Subjected to Fatigue Stresses," *10th Annual Proc. IEEE Reliability Physics Symposium*, Las Vegas, Nevada, Apr. 5–7, 1972, pp. 143–149.
3-16 Uebbing, J., "Mechanisms of Temperature Cycle Failure in Encapsulated Optoelectronic Devices," *Proc. IRPS*, 1981, pp. 149–156.
3-17 Maguire, D,, Livesay, B. R., and Srivatsan, T. S., "The Effect of Humidity and Electric Current on the Fatigue Behavior of Aluminum Bonded Wire," *Proc. ISTFA*, Long Beach, CA, Oct. 21–23, 1985, pp. 372-377.
3-18 Tomimuro, H., Jyumonji, H., "Novel Reliability Test Method for Ribbon of Interconnections Between MIC Substrates," *Proc. 1986 ECC*, May 5–7, 1986, pp. 324–330.
3-19 Onuki, J., Koizumi, M., and Suzuki, H., "Investigation on Enhancement of Copper Ball Bonds During Thermal Cycle Testing," *IEEE Trans. on CHMT*, Vol. 14, June 1991, pp. 392–395. Also see *J. Appl Phys*, Vol. 68, 1990, p. 5610.
3-20 Deyhim, A., Yost, B., Lii, M., and Li, C-Y., "Characterization of the Fatigue Properties of Bonding Wires," *Proc. 1996 ECTC*, Orlando FL, May 28–31, 1996, pp. 836–841.
3-21 Srikanth, N., Murali, S., Wong, Y.M., Vath III, C. J.," Critical study of thermosonic copper ball bonding", *Thin Solid Films* , Vol. 462–463, 2004, 339–345.
3-22 Otto, Alex J., "Insulated Aluminum Bonding Wire For High Lead Count Packages," *ISHM Journal*, Vol. 9, No-1, 1986, pp 1–8.
3-23 Susumu Okikawa, Michio Tanimoto, Hiroshi, Watanabe, Hiroshi, Mikino, and Tsuyoshi Kaneda, "Development of a Coated Wire Bonding Technology," *IEEE Trans. Comp. Hybrids and Manuf. Tech.* Vol. 12, No. 4, 1989, pp 603–608.
3-24 Christopher Carr, Juan Munar, William Crockett, Robert Lyn, "Robust Wirebonding of X-Wire Insulated Bonding Wire Technology," *Proc. IMAPS Symposium*, 2007, pp. 911–917.
3-25 Kessler, H. K.,National Bureau of Standards Special Publication 400-1, Semiconductor Measurement Technology: (March 1974) Burn-out Characteristics of Fine Bonding Wire, pp. 35-39.
3-26 Loh, E., "Physical Analysis of Data on Fused-Open Bond Wires," *IEEE Trans. on CHMT*, Vol. CHMT-6, No. 2, June 1983, pp. 209–217.
3-27 Loh, E., "Heat Transfer of Fine-Wire Fuse," *IEEE Trans. on CHMT*, Vol. CHMT-7, No. 3, Sept. 1984, pp. 264–267.

3-28 Coxon, M., Kershner, C,. and McEligot, D. M., "Transient Current Capacities of Bond Wires in Hybrid Microcircuits," *IEEE Trans. CHMT*, Vol. CHMT-9, No. 3, Sept. 1986, pp. 279–285.
3-29 King, R., Schaick, C. V., and Lusk, J., "Electrical Overstress of Nonencapsulated Aluminum Bond Wires," *27th Annual Proc., Reliability Physics*, Phoenix, Arizona, Apr. 11–13, 1989, pp. 141–151.
3-30 May, J. T., Gordon, M. L., Piwnica, W. M., and Bray, S. B., "The DC Fusing Current and Safe Operating Current of Microelectronic Bonding Wires," *Proc. Intl. Society for Testing and Failure Analysis (ISTFA)*, Los Angeles, CA, Nov. 6–10, 1989, pp. 121–131.
3-31 Ham, R. E., "Prediction of Bond Wire Temperatures Using an Electronic Circuit Analogy," *Hybrid Circuit Technology*, Ap, 1990, pp. 53–54.
3-32 The military standard, MIL-M-3851O J, 15 Nov. 1991. has a section on current carrying capacity wire burnout. It is *Internal Lead Wires*, Paragraph 3.5.5.3. The simplified formula is not entirely correct, but it can be a general guide.
3-33 Lage, J. (Faculty Advisor), Design of an Apparatus and Test Procedure for the Fusing Current of Gold Wire in Bare and Encapsulated Condition, Southern Methodist University, ME Dept., CME 4381—senior Design (sponsored by Texas Instruments-Semiconductor Group), Apr. 29, 1993 pp. 1–124.
3-34 Fitzsimmons, Ray, Raytheon Company, Private communication.
3-35 Mertol, A., "Estimation of Gold Bond Wire Fusing Current and Fusing Time," *IEEE Trans. on CPMT-Part B*, Vol. 18, No. 1, Feb. 1995, pp. 210–214.
3-36 Rainal, A. J., "Current Carrying Capacity of Fine-Line Printed Conductors," *Bell System Tech J.*, Vol. 60, Sept. 1981, pp. 1375–1389. Also see, "Temperature Rise at a Constriction in a Current-Carrying Printed Conductor," ibid., Vol. 55, Feb. 1976, pp. 233–269.
3-37 IPC Guidelines for Multichip Module Technology Utilization, IPC-MC-790, Aug. 1992, p. 47.
3-38 Pan, T-Y., Poulson, R. H., and Blair, H. D., "Current Carrying Capacity of Copper Conductors in Printed Wiring Boards," *Proc. 43rd IEEE Electronics Components and Tech. Conf.*, Orlando, FL, June 1–4, 1993, pp. 1061–1066.

CHAPTER 4
Wire Bond Testing

4.1 Introduction

The measurement methods, techniques, and equations used for evaluating wire bonds were developed many years ago and described in earlier editions of this book. Few modern papers present new approaches, except for the testing of fine pitch ball bonds. Therefore, this chapter has been brought up to date, by noting changes required by finer pitch (*more fully described in Chap. 9*), or by changing/adding appropriate figures and references when needed rather than completely rewriting for the sake of change. Only when a newer figure or reference is judged to be better or clearer, will it be added here. Several original figures have been redrawn/modified for more complete or extended understanding and the Web-available EIA shear test specification is included and discussed. Many of the recent advances have resulted from improvements in the test equipments' precision and convenience, rather than fundamental new measurement methods or principles. The author has added judgments and comments thought to be helpful for those new to the field. The latest Mil-Std 883G/H criteria are discussed in this chapter, but it is realized that today **there is minimal military-driven production**. Commercial in-house *specifications* vary widely but are frequently based on the web-available military specifications and measurement methods which are used internationally. They are a good starting point, but often have lower quantitative (compromise) specifications than used by many organizations.

Autobonders have extended their capability to make very long wire loops for small diameters, and techniques have been developed to make very low loops. Both of these affect wire bond testing, but the equations describing the bond-pull test are still valid in these extreme cases, with a few caveats to detail their use/limits.

Although the major part of this book is concerned with the yield and reliability of wire bonds, the normal method for evaluating these problems involves some form of testing. The most common method for evaluating wire bonds is still the pull test, primarily destructive, but, to a much smaller extent, nondestructive. Details of these tests

are addressed below. While the pull test is valid for wedge bonds, it is necessary to use a shear test, or, in some cases, a thermal stress test to evaluate Au ball bonds (on Al pads) adequately. Therefore, the ball-shear test is extensively described. The theory and applications of these bond tests are fully understood, and the pull as well as the ball-shear tests have become standard ASTM [4-1] test methods (see the appropriate sections below for details). The pull tests and thermal stress tests are currently described in U.S. military specifications (Std 883-G/H). The shear test is called out in that updated document later. It is based on the JEDEC commercial standard EIA/JESD22-B116 [4-2] described in this chapter in Sec. 4.3.11. Various additional bond evaluation tests are described. There are numerous warnings about the differences or limitations of the various tests as they might be applied to fine pitch bond testing, although the main technical discussion of that subject is in Chap. 9 along with the details of fine pitch bonding technology.

The nondestructive bond-pull test is currently in use only for some very special purposes, mostly satellite and space probes, but also occasionally for human-implanted devices. It is included in this edition as an appendix of the present chapter, rather than dropping it, since its data and statistics are otherwise unavailable. However, remember that this test is never used today in any high volume production process, but all such do use some form of statistical process control.

4.2 The Destructive Bond Pull Test

The wire-bond pull test is the most universally accepted method for controlling the quality of the wire bonding operation. It was introduced to evaluate the strength of wire bonds to semiconductor devices in the 1960s. Similar tests have been used for welded, soldered, and other wire connections for many years. The objective of this section is to examine the variables of the bond pull test, both theoretically and experimentally, and from them determine the most likely sources of problems and errors inherent in the test as it is typically performed. Where possible, suggestions for better utilization of the test are included.

4.2.1 Variables of the Bond Pull Test

Numerous papers have been written on the subject of the wire-bond pull test. Derivations of the equations, standard test methods, and, in one case, their validation in round-robin tests have been given [4-1, 4-3 to 4-5]. To understand the intricacies of the pull test, it is necessary to consider the geometrical configuration as well as the several equations that define the resolution of forces. [Note that the introduction of the pull angle, φ, complicates the calculation, see below Eq. (4-3). When the hook is pulled straight up, it is better to simplify Eqs. (4-1) and (4-2) by

making φ = 0.] The force in *each* wire, (f_{wt}) and (f_{wd}) at wire break, with a specified pull force, *F*, at the hook is

$$f_{wt} = F\left[\frac{(h^2+\epsilon^2 d^2)^{1/2}\left((1-\epsilon)\cos\phi + \frac{(h+H)}{d}\sin\phi\right)}{h+\epsilon H}\right] \tag{4-1}$$

$$f_{wd} = F\left[\frac{\left(1+\frac{(1-\epsilon)^2 d^2}{(H+h)^2}\right)^{1/2}(h+H)\left(\epsilon\cos\phi - \frac{h}{d}\sin\phi\right)}{h+\epsilon H}\right] \tag{4-2}$$

If the hook is applied as close as practical to one of the bonds, the vertical (peel) component of the pull force can approach the force of a 90° pull test (described in MIL STD 883G/H, Method 2011 [4-7] and illustrated in Fig. 4-3).

When an over-the-ball position of the hook is chosen (to pull ball bonds vertically), it will break in the HAZ for course pitch. However, this position is preferred for testing fine pitch ball bonds (not wedges) to avoid pulling the metallization up (see Chap. 9, fine pitch discussion). These equations can also be used when testing ribbon bonds.

If, from Fig. 4-1, both bonds are on the same level ($H = 0$), and the loop is pulled vertically ($\varphi = 0$), in the center ($\varepsilon = 0$), and ($\theta_t = \theta_d$), then the more familiar equation is obtained

$$f_{wt} = f_{wd} = \frac{F}{2}\sqrt{1+\left(\frac{d}{2h}\right)^2} = \frac{F}{2\sin\theta} \tag{4-3}$$

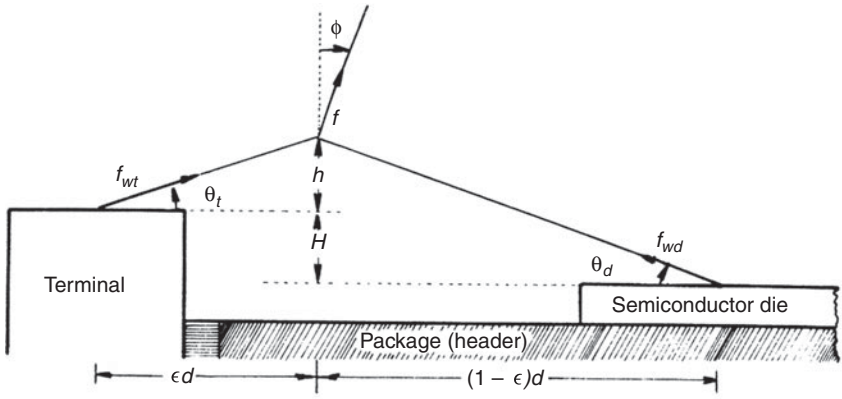

Geometric variables for the bond-pull test

Figure 4-1 Geometric variables for wire-bond pull test in the plane of the bond loop, as used in Eqs. (4-1) to (4-4) [4-5]. Note that the angle φ is included here for cases when the substrate may be tipped or otherwise must be pulled at an angle.

If both bonds are on the same level ($H = 0$), and the loop is pulled vertically ($\varphi = 0$), in the center ($\varepsilon = 0$), and ($\theta_t = \theta_d$), then the more familiar equation is obtained:

$$f_{wt} = \frac{F}{\sin\theta_t + \cos\theta_t \tan\theta_d} \tag{4-4}$$

where $\theta_t = \theta_d = \theta$. Note that, in general, for bonds of a given strength, larger values of *h/d* will result in higher pull force, *F,* values. Equivalent equations using angles θ_t, θ_d, and *F* are:

$$f_{wd} = \frac{F}{\sin\theta_d + \cos\theta_d \tan\theta_t} \tag{4-5}$$

Note that all of the above equations are solved for the *force or tension in the wire,* f_{wt} and f_{wd} (usually at break). If a reader wants to calculate the actual *pull force,* then the equations must be solved for *F*. A wire will break when either f_{wt} or f_{wd} first reaches its breaking strength. This entails assigning a breaking strength (value) to each side of the wire. Typically, this is about 60 to 75% of the manufacturer-specified breaking load of the wire for Al wedge bonds (due to heel deformation and metallurgical overworking), but is nearer 90% for Au bonds (either ball or crescent bond break). The wire normally breaks just above the ball in the heat-affected zone (see Chap. 3).

A plot of the calculated pull force (*F*) at wire rupture for wedge bonds is given for a typical two-level semiconductor device-bond configuration in Fig. 4-2, pulled straight up ($\varphi = 0$) at the center of the loop. With everything else being equal, it is apparent that the higher the loop height, the higher the bond pull force will be. For a given bond-to-bond spacing, *d,* lowering the loop will result in a force multiplier, increasing the values of f_{wt} and f_{wd} for a given force at the hook, *F,* and thus yielding a lower force at wire rupture.

The position of the hook (indicated as εd in Fig. 4-1) and the pull angle, 4, will significantly affect the distribution of forces at the bonds. One can choose a ε or φ value that will give equal forces on each bond, and it will result in a more equal test of both bonds. This is possible with some automated pull testers. However, manual pull-test operators would be significantly slowed by such a procedure. In addition, most specifications (such as ASTM F459-06 [4-1] and MIL-STD-883 G/H, Method 2011) [4-7], and most in-house requirements specify that the hook be placed in the center between the bonds. So this is considered the standard hook-placement position for normal testing of wedge bonds, but not for fine pitch ball bonds which may peel the bond pad (see Chap. 9 and its references). We note that major accepted specifications must be changed to allow such hook placement for Cu/Lo-k devices and other fine pitch pull tests! (MIL-STD-883G/H now allows non-center hook placement.) Whenever the hook is moved close to a wedge bond, a higher proportion of the wire force is applied

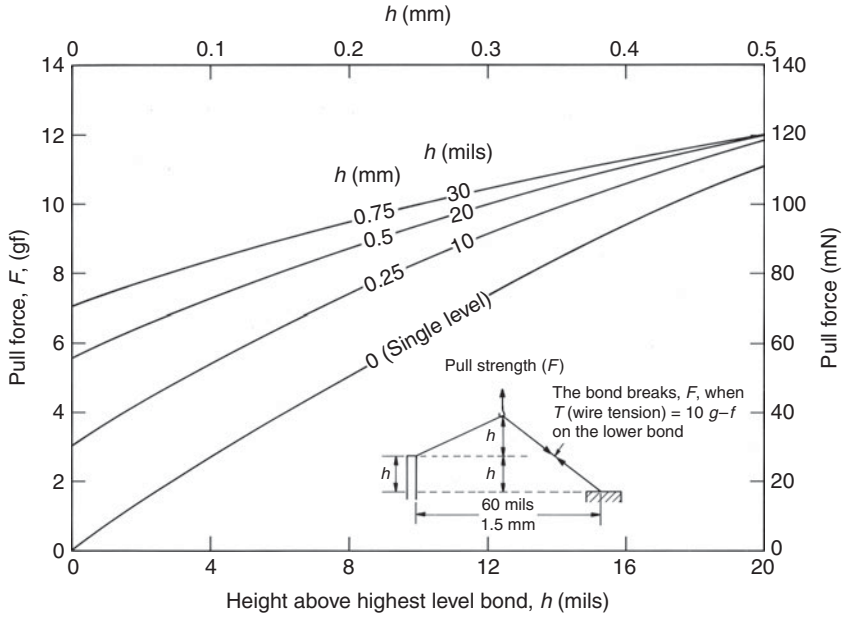

Figure 4-2 Bond pull force calculated with Eqs. (4-1) and (4-2) for various loop heights and package pad heights, pulled in the center of the loop.

in the vertical (or peel) direction. If bonds have a tendency to peel, then a significantly lower pull force will result, as demonstrated in Fig. 4-3. Details of this and other special pull-test pitfalls (e.g., pulling out of the plane of the bond, the effect of one weak and one strong bond, etc.) are given in [4-4, 4-5]. Note: this does not apply to ball bonds.

4.2.2 Peeling (Tweezer Pulling) for "Quality Tests" and Troubleshooting of Wedge Bonds and Crescent (Tail) Bonds

Simply moving the pull hook toward a wedge or crescent bond (Fig. 4-3) changes the distribution of forces from tensile breaks to peeling the bond, which can reveal weak welding. A simple "tweezer" peel can also reveal poorly welded wedge and crescent bonds in the as-made condition. For this, the loop is cut or tweezer-pull broken near the other (ball) with a manual tweezer (or electrical operated one). The wire is then pulled in the vertical direction and, if weak, will peel revealing a weak bond. Such is defined as a 90° pull. If the wire is advanced further over the weld nugget (bonded part) then it is called a 120° pull/peel, etc. It is seldom quantitatively measured but is a good qualitative test for gold (or copper) crescent bonds. Al wedge bonds usually break for greater than 90° pulls because of the brittle nature of the heel. Peeling completely, without breaking and

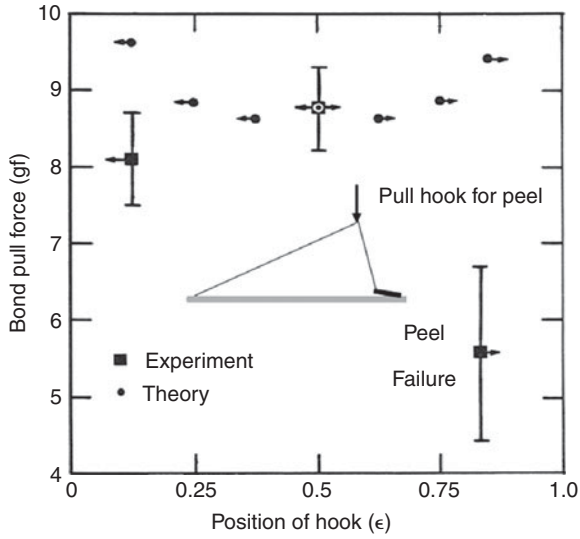

FIGURE 4-3 Figure included to emphasize both the effect of moving the pull hook from the first to the second wedge bond, and the major weakening effect of peel failures on wedge bonds, as revealed by this pull test. This was a controlled experiment in which the hook is moved toward the less welded wedge bond. Note that potentially peelable wedge bonds may not result in weaker pull force if pulled from center position. Note also that error bars increase in the peel region. Measured and calculated pull force as a function of hook position for single-level, 25 μm (1 mil) diameter ultrasonic aluminum wedge bond pairs having first and second bonds with equal breaking strengths, d = 1.5 mm (60 mils) and h = 0.35 mm (14 mils). First bond is located at $\varepsilon = 0$ and second bond at $\varepsilon = 1$, peeling position $\varepsilon = \sim 0.85$. Experimental data is designated by an arrow with box. Each point is the mean of 25 to 30 bonds pulled at indicated hook position. Error bars represent ±1 standard deviation of mean. Failure occurred at bond indicated by arrows. Center position breaks ($\varepsilon = 0.5$, bond angle = 25°) were all tensile failures, 60% of which occurred at heel of first bond. All second bonds lifted (peel failure) when pulled in position $\varepsilon = 0.85$ (second bond angle = 60°). Theoretical prediction ='arrow with dot.' Each point is calculated from Eqs. (4-1) and (4-2) assuming that both first and second bonds are of equal strength and all failures are by tensile-mode breaks. Arrow points to position of bond that would break; center position breaks are evenly divided between two bonds [4-5]. The peeling problem versus hook placement position is illustrated in the center figure. Note that the peeling problem also exists for the crescent (wedge)bond of a ball bond, but will have little effect if the hook is placed over the ball bond—also discussed in Chap. 9.

leaving a nugget, also leaves the footprint on the pad that can be examined with a microscope for details of welding (like the lift-off patterns in Chap. 2, Figs. 2-10 and 2-11) and is an excellent trouble-shooting or studying procedure for setup purposes. For example, tail pulling has recently been used to study Cu-ball tail-bonding conditions on both Au and Ag bond pads [4-6].

The peel test has been used for years and is completely described in MIL-STD-883G/H, Method 2011.7. This test method is short and reproduced here to further clarify the above discussion:

> "3.1.1: Test condition A—Bond peel. The lead or terminal and the device package shall be gripped or clamped in such a manner that a peeling stress is exerted with the specified angle between the lead or terminal and the board or substrate. Unless otherwise specified, an angle of 90 degrees shall be used. When a failure occurs, the force causing the failure and the failure category shall be recorded. 3.1.2 Test condition C—Wire pull (single bond). This test is normally employed for internal bonds at the die or substrate and the lead frame of microelectronic devices. The wire connecting the die or substrate shall be cut so as to provide two ends accessible for pull test. In the case of short wire runs, it may be necessary to cut the wire close to one termination in order to allow pull test at the opposite termination. The wire shall be gripped in a suitable (tweezer-like) device and simple pulling action applied to the wire or to the device (with the wire clamped) in such a manner that the force is applied approximately normal to the surface of the die or substrate. When a failure occurs, the force causing the failure and the failure category shall be recorded."

4.2.3 Failure Predictions That Are Based on Pull Test Data Must Have Confirmed Normality

Many organizations use the pull test average ($\bar{x}$) range (r), and standard deviation (σ) distribution charts for production control purposes. The data are plotted continuously giving a running chart for SPC. In addition, the operators usually record the bond failure modes. The latter are helpful when bonding problems are encountered. Modern pull testers can store the failure mode and pull force and can generate the statistics, which are often coupled directly into a PC or other larger computer. From these data, predictions are often made as to the number of pull test (force values below the specified control limit) failures to be expected each day. LTPD and confidence levels are also calculated.

One might assume that such predictions of pull-test failures could be calculated from the distribution curve as defined by the average and standard deviation of the test values. However, because there are usually several test failure modes [e.g., bond lift from either end, wire break in the span, heel break, neck break (above ball), cratering, and metallization failure], the distribution is often not normal. When this occurs, such predictions may be invalid. **Before attempting to make such calculations, a test for normality, such as the Chi Square statistic, should be used on the data**. Frequently, when using non-normal data, the predicted number of test failures can appear higher (or lower) than the number that actually occurs. For example, in one case,

assuming a normal distribution, the prediction was that 2.27% of the bonds should have pull forces in the range of less than or equal to 34.3 mN (≤3.5 gf). However, experimental data revealed only 0.4% in that low range. The Chi Square statistic confirmed that normality was absent [4-8].

4.2.4 Effect of Metallurgy and Bonding Processes on the Bond Pull Force

In a production-line environment where speed is essential, pull-test operators seldom ascertain that the hook is at the exact center of the bond loop. Often, the hook will slip toward the highest point of the loop. This point is determined by the type of bonding machine or by the device package. If the package has one very high or low bond pad, then hook slippage* can lead to peel-mode failures as previously described. If both bonds are well made, however, the method of bonding will generally dominate the results, as discussed below.

Gold ball bonds (thermosonic) are normally bonded with a capillary-type tool. Assuming a normal loop, the wire rises straight up from the center of the ball to a peak near the ball, bends, and progresses linearly downward towards the second bond, which is the wedge or crescent bond (see Fig. 4-4). If the pulling hook rises to the peak, most of the force is applied directly to the ball, which, because of its large bonded area, is stronger than the wire. [Above the ball bond peeling or tearing does not occur with off-center hook placement as it does for wedge bonds (but it could if the bond pitch spacing is below ~50 μm—see Cu/Lo-k, Chap. 10).] Typically, the wire breaks in the recrystallized (heat-affected) zone immediately above the ball. The wedge or crescent bond is usually weaker than the ball bond. However, when the hook is located near the peak of the loop (nearer the ball), relatively little force is applied to the wedge bond, and it seldom breaks. Thus, only the heat-affected zone (neck) of the stronger bond (the ball) is tested (see Sec. 4.3 on shear testing of ball bonds). For single-level ultrasonic wedge bonds, Fig. 4-4, the case is reversed. The wire rises from the edge of the first bond (which is the weaker bond), peaks somewhat before the center of the relatively low loop, and then goes down continuously to the second, stronger bond. Thus, if the hook rises to the peak of the loop, more of the force is applied to the weaker bond, which breaks. In this case, the stronger bond remains untested. It is apparent that the combination of a high-bond loop as well as a force distribution that tests the stronger bond is one reason why Au ball bonds are specified to have, and do give, a higher pull force than Al

*Most modern pull testers have stiff hooks that eliminate slippage and pull vertically regardless of the shape of the loop. These are preferable but might lead to some other problems in dealing with complex loops generated by autobonders.

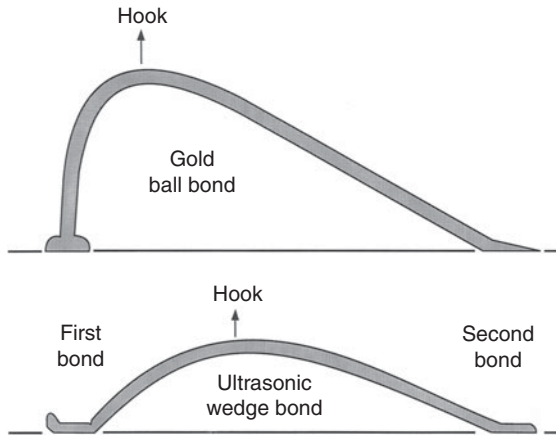

Figure 4-4 Typical geometrical configuration and position (for single level bonds) of the pulling hook for gold ball bond (top) and ultrasonic wedge bond (bottom). Pulling hook tends to slip toward the peak of the loop.

wedge bonds. However, in both cases, a pull in the center of the loop for single-level bonding would provide a more reliable quality control for the total bonding process.

Advanced autobonders are capable of making loops in almost any shape and extreme lengths (see App. 9A, Chap. 9 for a description of autobonder "Looping" by Lee Levine). There will be no special discussion on pull testing such long, unusually shaped loops, except to note that during pulling the wire straightens and reaches a peak at the hook position. If one measures the final peak of the loop before break, (the loop parameters, H, ε, etc.) then the pull force can be calculated with Eqs. (4-1) to (4-3). However, some unusual loops have been designed to miss other chips or structures along their path. Straightening could cause the wire to contract, snag, etc., on those obstacles and give erroneous pull data. Thus observing the wire on a slowed pulling is important before committing to use the pull test on any particular unusually "shaped" loop.

Gold ball bonds generally yield a higher pull force than Al wedge bonds for the reasons cited. But ultrasonic Au wedge bonds made with wire having the equivalent breaking force and elongation of Al wire will yield approximately equivalent pull forces to Al wedge bonds when the bond deformation is in the low to medium range (~1.5 wire diameters), as shown in Fig. 4-5. At higher deformations, however, Al ultrasonic wedge bonds become metallurgically overworked, which weakens the heel region and lowers the pull force dramatically, often by a factor of 2, as the bond deformation increases above 2 wire diameters. The different metallurgical characteristics of Au wire permit deformations up to about 2.5 wire diameters with

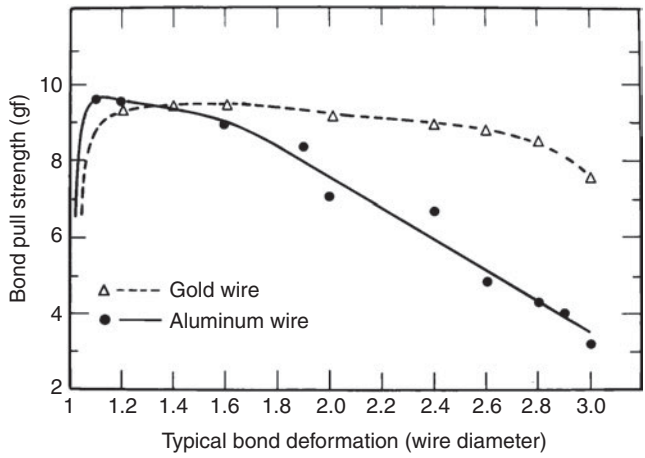

Figure 4-5 Bond pull force versus bond deformation for 25 μm (1 mil) diameter aluminum and gold wires, both having 13 gf breaking force. All bonds were made on the same bonding machine using the same bonding tool. Other bonding parameters were optimized for each metal to produce the best overall pull force and the lowest standard deviation. All bonds were made on a single level. The loop heights were approximately 0.3 mm (12 mil) and the bond-to-bond spacing was 1 mm (40 mil). The loop-height-to-bond-spacing ratio is much larger than that generally found in device production. Thus, a scaling down of the bond-pull force axis by a factor of about two would be more typical of values obtained from integrated circuits [4-9].

little decrease in the pull force. Unfortunately, dependence of the pull force on bond deformation is not recognized in some specifications. MIL-STD-883G, Method 2017.8 [4-7], permits bond deformations of 3 wire diameters for both Au and Al ultrasonic wedge bonds and 5 wire diameters for the crescent (wedge) bond following an Au ball bond. This is not generally permitted by commercial (in-house) specifications.

4.2.5 Effect of Wire Elongation on Bond Pull Force (Primarily for Large-Diameter Al, but also for Au Wire Used in Ball Bonding)[4-9]

As is evident from Eqs. (4-1) through (4-3), the bond pull force is strongly dependent on the ratio of the loop height to bond spacing. This loop height can increase during pulling if the wire elongates significantly. Small-diameter wire made for ultrasonic wedge bonding, either Au or Al, normally has an elongation of less than 2%, and this has little effect on the measured pull force. However, small-diameter Au wire, for TS ball bonding, or Al wire that has been annealed can have elongations of approximately 5 to 10%, and large-diameter annealed Al bonding wire, up to approximately 30%. During bond pulling,

the *h/d* ratio increases significantly, yielding a pull force higher than one would expect if only the breaking load of the wire and the initial bond geometry were considered. This effect will be even more significant if the initial value of *h* was low.

Figure 4-2 showed that loop height is an important factor in determining the bond pull force. Thus, it is apparent that significant wire elongation during bond pulling will change the loop height and affect the magnitude of the pull force. Figure 4-6 gives a pictorial example of the loop height change versus elongation for three bond-to-bond lengths, and Fig. 4-7, a calculation starting with the same initial loop height. The geometries were chosen to cover those often encountered in medium- to high-power transistors with large-diameter Al wires, but they can be linearly scaled down to appropriate microelectronic dimensions as long as the ratio of loop-height-to-bond spacing is kept constant.

Figure 4-8 shows the effect of this wire elongation (incorporating the resulting loop height increase) on the bond-pull force, assuming the same initial geometry as used in Fig. 4-7. In this calculation, all bonds break when the force in the wire reaches 500 gf. (See Chap. 3 for the properties of such wire.) For simplicity, the calculation was made for single-level bonds. From Fig. 4-8, it is apparent that the tendency of the bond-pull force to decrease with decreasing wire-breaking load can be partially offset by the increase in wire geometry when the wire has

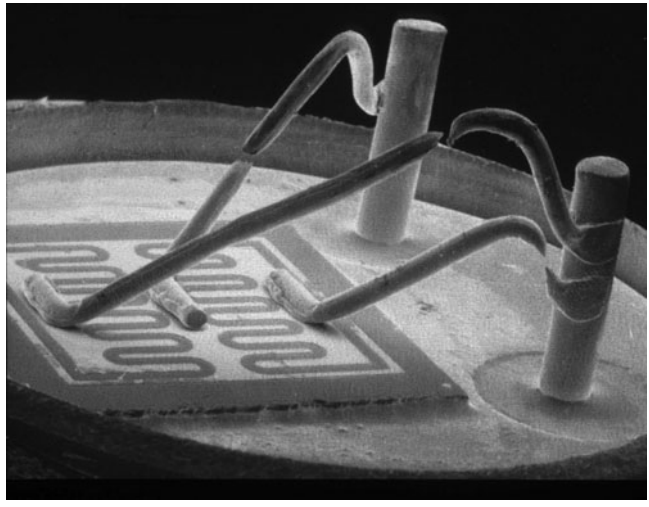

Figure 4-6 An actual example of wire elongation during pull testing of large diameter (tweezer welded) wire bonds, where the elongation is usually from 15 to 30%. Ductile fractures are shown. These are older devices, but the same wire metallurgy is used today (Chap. 3). As-made, these wires went in approximately a straight line from the chip to the post.

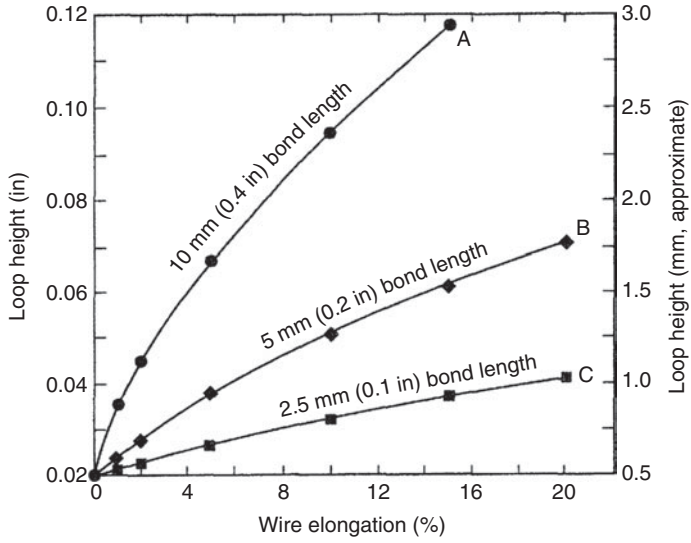

Figure 4-7 The effect of wire elongation on the final loop height at the point of wire rupture during a bond pull test. All bonds had the same initial loop height, 0.5 mm (20 mils), but three different bond-to-bond lengths were used as indicated.

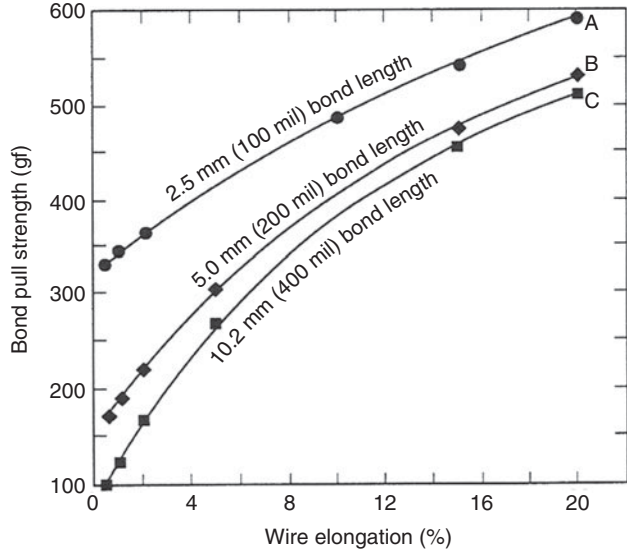

Figure 4-8 Bond-pull force and wire breaking force versus wire elongation. The solid curves are bond-pull forces based on the geometries of similar lettered curves in Fig. 4-7.

increased elongation. Therefore, the pull force tends to be independent of the specific wire-breaking load for many common device geometries. These results may be scaled down for integrated circuits, except that small 25 μm (1 mil) diameter annealed Al wire elongates less than approximately 10%, and then only after high-temperature exposure or significant *annealing*. Otherwise it's typically ~2%.

There will be special cases where the effect of large wire elongations can change the bond-pull geometry and, hence, the measured pull force, even more than indicated in Figs. 4-7 and 4-8. This occurs when the pulling probe (the hook and arm) is misplaced, is flexible, or is free to pivot where it is joined to the force gauge or load cell.

The effect may occur even if the hook does not slip in the case where a high package bond pad (post) is involved. Here, the wire span will be considerably longer on the chip side of the hook than on the package side. The relatively greater increase in length (elongation) of the chip-side span during the test will result in moving (swinging) the hook nearer the package pad and in pulling on the wire at some angle, φ, from the vertical. The effect will be enhanced if the pulling hook was initially placed nearer to the package bond than to the chip bond. These changes in the bond-pull geometry, which can result in lower measured values of pull force, must be taken into account in any pull-test calculations involving wires with high elongations.

Stress-strain type measurements have been made during pull testing on a number of large-diameter power-device wire bonds to determine any unique characteristics that could influence the pull test. Both the measurement and its interpretation are much more difficult for pulling a typical wire-bond loop than for measuring the stress-strain relationship of a long piece of wire. In pulling a standard 250 mm (10 in) length of wire, the elongation is normally read directly from a recorder (see Sec. 3.2, Fig. 3-1 for examples of stress-strain curves.). However, in pulling a large-diameter wire-bond loop, the total length of wire is generally less than 6.25 mm (0.25 in), and, in addition, the measurement indicated by the apparatus is in reality the increase in loop height (which is nonlinear with wire elongation) and is very small compared to the elongation of the standard length of wire. Thus, when determining wire-bond-loop elongation, the sensitivity of the measurement apparatus must be increased to its maximum, and any system nonlinearities, such as a slight irregularity of the screw-thread pitch on the stress-strain machine or bending of the pulling hook, will have a greater effect and must be corrected for in each curve.

A typical, corrected force versus rise-in-pulling-hook curve for a 200 μm (8 mil) diameter emitter wire bond from a power device is shown in Fig. 4-9. There are three distinct regions in this curve.

Region 1 is the triangular loop formation and elastic wire-tensioning region. Although the curve increased linearly for this bond, other bonds often showed variations as the loop formed into a triangle, generally within the dotted curves. Point 2 denotes the elastic

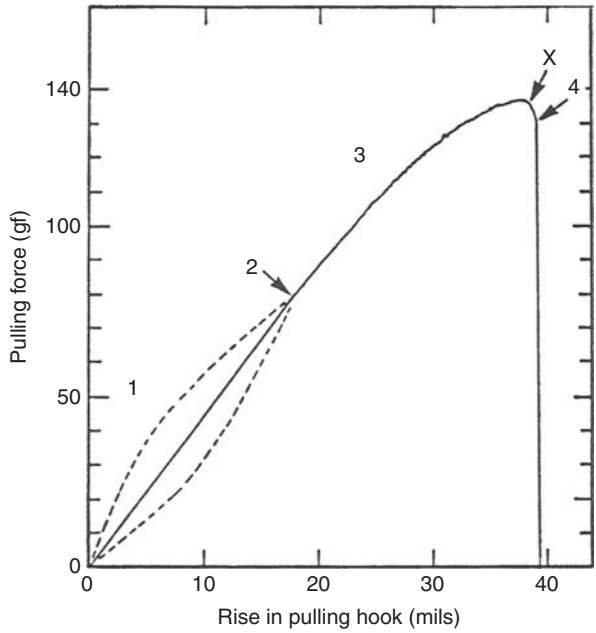

Figure 4-9 Bond-pulling force (related to stress) versus rise in pulling hook after wire contact (related to strain and elongation) for a 200 μm (8 mil) diameter aluminum wire bond on a power device. (1) is the triangular loop formation and elastic wire tensioning region—the dotted lines indicate the typical variations that are observed in this region; (2) is the wire elastic limit; (3) is the region of inelastic wire deformation; (X) is the region where the wire necks down rapidly and then breaks at (4). This curve was corrected for measuring apparatus nonlinearities.

limit of the wire, and point 3 is the region of inelastic (plastic) elongation, which, in this case, begins at approximately 60% of the bond pull force. At point X, the wire necks down rapidly and then breaks at point 4. The elongation of the wire in region 3 was determined to be 10.5% by using data from Fig. 4-7 and the measured bond geometry. More explanation, as well as stress-strain curves of typical bonding wires, is given in Sec. 3.2.

4.3 Ball-Bond Shear Test

4.3.1 Introduction

The wire-bond pull test is universally used to assess the strength and to determine bonding machine setup parameters of wire bonds used in microelectronics (see Sec. 4.1). Often, technicians and engineers assume that pull test data, which are adequate to determine wedge-bonding

machine setup parameters, are also sufficient to set up the ball-bonding machine parameters. However, considering that most ball bonds can have interfacial welded areas in the order of 3 to 6 times the cross-section area of the wire (fine pitch ball bonds excepted), it is apparent that the wire will break in pull testing before even a poorly welded ball will lift* [4-11, 4-12]. In addition, the wire just above the neck of the ball bond is totally annealed, recrystallized (the heat affected zone), and generally becomes the weakest part of the ball-bond wire wedge-bond system. In a pull test, the wire often breaks at this point, depending on the placement of the hook and the bond geometry (see Sec. 4.2). Thus, little information is gained on the breaking strength of the ball-to-bonding-pad interface if the ball is welded over more than 10 to 20% of its interfacial area.

Considering the above, it is apparent that some type of push-off or shear test offers the best possibility of assessing the quality of a ball-bond interface and, thus, properly setting up a ball-bonding machine.

The ball-shear test was independently introduced to the microelectronics industry in 1967 [4-13, 4-14]. However, it appears to have been ignored or forgotten for almost 10 years until Jellison [4-15, 4-16] and, later, Shimada [4-17] designed precision shear testers and used them in a series of laboratory experiments that clearly demonstrated the usefulness of the test. Since that time, there have been numerous studies of the ball-shear test. Today, it has been almost universally adopted for production control, and there is excellent equipment available, as well as several published standards (see Sec. 4.3.11).

4.3.2 Apparatus

The equipment used to perform the ball bond-shear test has ranged from tweezers and other hand-held probes [4-11, 4-18] to dedicated shear-test machines with strain-gage force sensors, automatic height positioning, and various electronic methods of data recording/presentation. In principle, the ball-shear test is simple and consists of bringing some form of a shear tool up to the side of a bonded ball, applying a force sufficient to push it off, and recording that force. The test is illustrated in Fig. 4-10.

---

*Consider a ball bond on a 25 μm (1 mil) diameter gold wire. The diameter of a well-bonded normal pitch ball is usually in the 65 to 90 μm (2.5 to 3.5 mil) diameter range, and the wire-to-bonded-area ratio in this case is from about 4 to 10 in favor of the ball. (It would be lower for fine-pitch ball bonds, see Table 4-3.) Thus, in a wire-bond pull test, the wire will break even if the ball is weakly welded. Arguments similar to this were first pointed out by Gill [4-14], and variations of them have appeared in most of the later studies involving the ball-shear test. For instance, Stafford [4-12] calculated the force that the wire can apply on the ball-metallization interface in the pull test and verified the above conclusion quantitatively.

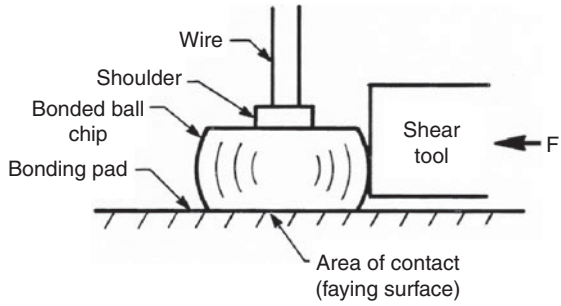

Figure 4-10 Schematic drawing of the ball-shear test. The bonded (welded) area is often less than the faying area (area of intimate contact). The typical outside diameter of a bonded ball from a 25 μm (1 mil) diameter Au wire is from about 50 to 100 μm (3.0 to 4.5 mil). The height of the ball above the bonding pad is usually less than 25 μm (1 mil) but << for fine pitch.

Jellison [4-15] designed an early precision mechanical system with strain-gauge force readouts. The design details are appropriate for any dedicated ball-shear tester. A sketch of his apparatus is shown in Fig. 4-11. This tester employed a rigid, low-friction, linear bearing to transmit the load from the tool to the strain gauge. The sample was placed in the horizontal position and viewed from above with a

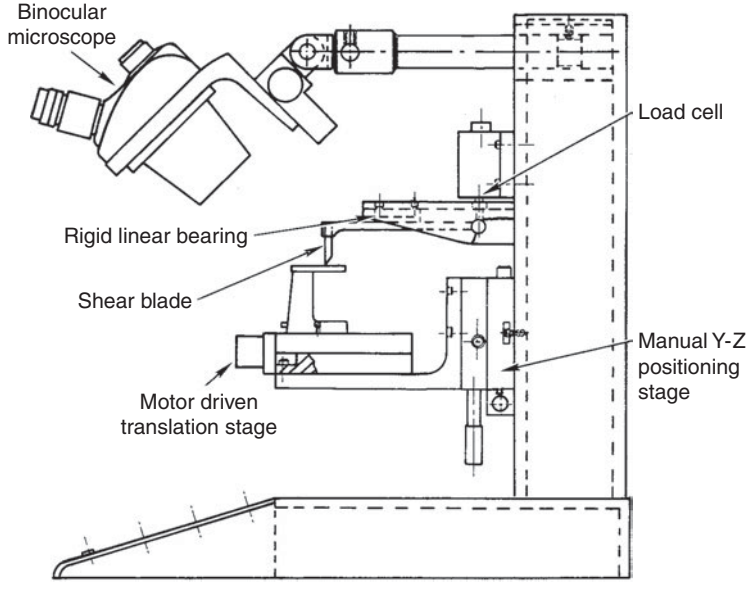

Figure 4-11 Sketch of the first precision ball-bond shear tester. (*After Jellison [4-15];* © IEEE.)

microscope. The shear tool extended downward from its clamp so that it could operate in a deep package. A motor drive moved the test sample work holder to perform the shear test at a fixed rate of 0.2 mm/s (8 mil/s). (This rate is not critical, since the rate of shear force application does not affect the shear force value over the range of from 0.13 to 3.3 mm/s (5 to 130 mil/s [4-19]).

Currently, there are several commercial ball-shear testers available. The most sophisticated of these* have automatic vertical position finders, record data and failure modes, and can be interfaced with computers and printers for final data analysis. The main mechanical difference between modern ones and that of Fig. 4-11 is that Jellison moved the stage and current ones move the shear tool. Of course, current testers have greater position accuracy and measurement precision, are semiautomated, and much easier to use.

4.3.3 A Manual Shear Probe As an Aid in Setting Up Ball Bonder (For Laboratory Use)

It is always desirable to have a quantitative, precision shear tester. However, if such is not available, a simple substitute can be made that will give information, that, while not quantitative, will nevertheless allow one to quickly set up ball-bonding machine parameters and qualitatively evaluate bonds for laboratory or other nonproduction purposes.

The simplest and most readily available tool for manually pushing off large (non-fine pitch) ball bonds is the blunted end of one tine of a tweezer, and production personnel have used such for this purpose for years [4-18]. However, tweezers are relatively awkward to use, particularly if the ball is strongly welded. A simple manual shear probe has been designed for this purpose [4-11]. Figure 4-12, detail A, is a drawing of a probe tip that is appropriate for use on balls made from wire of up to 33 μm (~1.3 mil) in diameter and of course pitch. The tip can be made by a machinist or a precision tooling company. However, a reasonably satisfactory one can be made in a few minutes using the smallest blade from a standard jeweler's screwdriver set. This blade, while still in the jeweler's screwdriver set as a holder, can be manually narrowed and thinned on very fine emery paper to the approximate dimensions of Fig. 4-12, detail A. (*Note the use of a manual shear probe is not practical for typical ball bonds on pads having pitches finer than ~100 μm.*)

In use, the sample is placed on a holder at a height such that the probe, when held like a pencil, will approach the surface at an angle of about 20 to 25°. This matches the angle on the tip of the tool. The ball

*Some manufactures are Dage Precision Industries Inc., UK, Aylesbury, Buckinghamshire, HP19 8RG, and Royce Instruments Inc., 500 Gateway Drive Napa CA 94558. Both have sales/service offices worldwide.

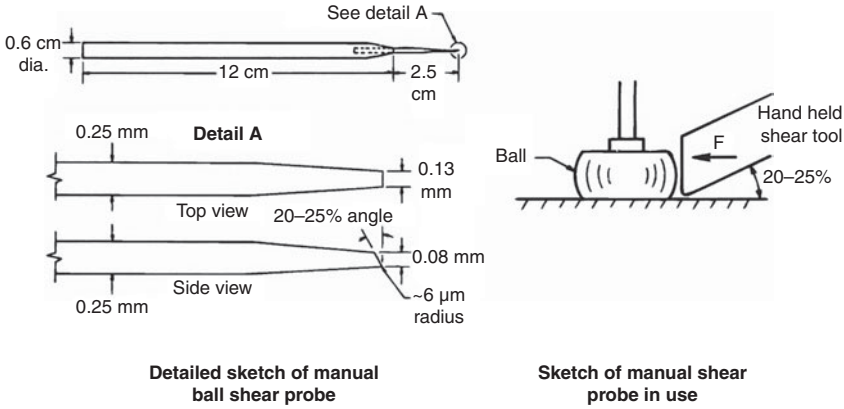

Figure 4-12 Left is the detailed sketch of a manual ball shear probe and to the right is a sketch of the probe in use.

bond is then contacted approximately perpendicular to its radius. A binocular microscope with no less than 30X magnification should be used. Practice should start with strong ball bonds. These will generally have a shear force greater than 50 gf. For comparison, some weak balls can be made by using the same bonding-machine settings as for the strong ones but locating half or more of the ball off the bonding pad. If the pads are on an IC, this will place part of the bond on passivation where it will not weld, reducing the shear force proportionately. An indication of the bond strength can often be obtained by observing the deformation or smearing of the ball (see Fig. 4-13). (Such techniques are appropriate for a variety of experiments on bonding.)

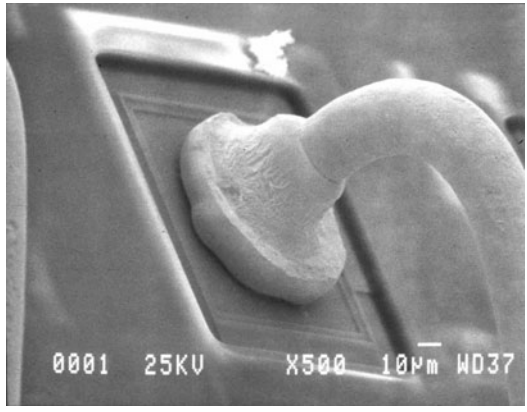

Figure 4-13 Ball bond on pad lower than polyimide or other passivation (hard to shear).

A manual shear probe is never used to obtain quantitative data. It is primarily used to quickly set up a manual bonder on the machine, for bonding one-of-a-kind experimental systems/chips (done often in R&D laboratories, but never in production areas). Such manual probes cannot be used for fine-pitch ball bond evaluation.

4.3.4 Interferences to Making Accurate Ball-Shear Test Measurements

As with any test method, there may be problems in performing the ball-shear test that can produce incorrect or misleading data. The general ball-shear test failure modes are given in App. 4A [4-47]. Others are summarized below:

Summary of Interferences in Making Ball-Shear Tests
Shear tool drag (incorrect tool height) and recessed pads
Gold-gold friction rewelding
Metallization adhesion problems-thick film example, and bond pad below top surface passivation
Shear tool cleanliness (accumulation after many tests)
Substrate flatness (tipped nonlevel substrate)

Shear tool drag (*and modern recessed pads*)*:* One of the most common problems is the improper vertical positioning of the tool. The tool should not drag on the substrate. It should approach normally deformed balls from ~2 to 5 μm (~0.1 to 0.2 mil) above the substrate and for large, high balls, no higher than 13 μm (~0.5 mil). (The bottom of the tool must be kept clean to permit such positioning.) If the tool is positioned higher, it may ride over or smear over the top of the ball, depending on the height of the ball. If substrate dragging occurs on thin and especially thick films, then the indicated shear force can increase by 10 to 20 gf. Some chips are not attached horizontally, and additional care must be taken to prevent the shear tool from contacting the bond-pad metallization during the test. (See App. 4A, failure mode 2.)

Shear tool drag becomes a more critical problem for finer pitch. For example, one 70 μm pitch ball bonding process (see Table 4-1) produces bonded balls that are only 6 μm high, and the bond pads were recessed below the 1^{+} μm of passivation, which overlapped the edges. If multilayer interconnects are used, the pad can be recessed even further, leading to great difficulty in performing the shear test as shown in Fig. 4-14. *Also, at very fine pitch (<50 μm) the shear test itself is difficult to perform and the pull test is used in industry* (see Chap. 9, Sec. 9.1.10).

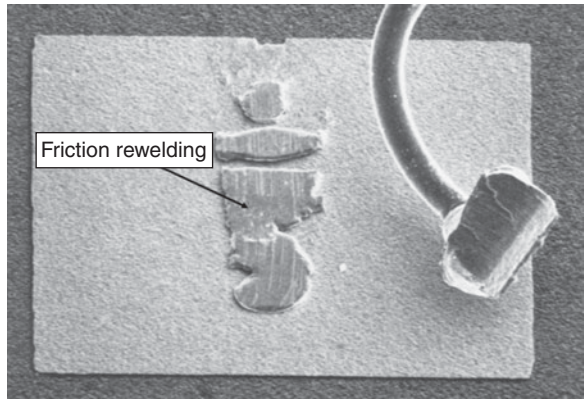

Figure 4-14 An example of a gold ball strongly bonded to gold metallization that underwent friction rewelding to the pad. Note also the gross deformation of the ball resulting from shear testing a strongly welded ball bond. This TS bond was made from 25 μm (1 mil) diameter wire. (*After Weiner [4-35]; © IEEE.*)

Gold-to-gold friction rewelding: Shearing Au bonds on Au substrates can lead to an unusual interference. Gold is capable of friction welding to Au surfaces at room temperatures. An SEM photograph of a deformed Au ball and Au bonding pad showing the results of multiple friction rewelding is given in Fig. 4-13. Rewelding problems may be eliminated by using a shear tool design that is slightly ground-back from the forward edge. This will lift the ball, preventing rewelding [4-20]. Friction rewelding seldom occurs while shearing bonds on Al metallized IC pads, where the small size of the pad, as well as the passivation surface film adjacent to the pad, prevents it.

Interferences when shearing bonds on thick films (*and a method of determining weak metallization adhesion problems*): Several potential interferences can occur when shearing ball bonds on thick-film metallization. One would normally assume that balls of a given diameter would yield shear forces somewhat lower when bonded to thick films than when bonded to thin films, since thick films contain pits and voids, and, in some cases, glass or oxide occlusions on the surface. There have been a number of shear test studies of ball bonds on thick-film metallization in the literature [4-21, 4-22, 4-23].

However, there was not enough information given on the welded ball size, or the actual welded area, to compare directly with the extensive laboratory data published on thin films. One might expect to use the same experimental procedure in shearing bonds made to thick films as for thin films. However, the thick films themselves are often higher than the recommended vertical position of the tool above the substrate when set for shearing bonds on

thin films. Therefore, ball-shear tests made on thick-film circuits may present problems in vertical positioning of the tool. It is, therefore, possible that the tool will drag across the thick film during the shear process. This will result in a high-apparent value for the ball-shear force and may explain why some reported values of ball-shear force from thick-film tests are higher than the shear force expected from thin film Au [4-21].

Even if the vertical positioning of the shear tool is correct, shear tests made on bonds welded to thick films, as well as to thin films, can yield much lower shear values than expected if the metallization adheres poorly to the substrate [4-11, 4-14]. An example of shearing a ball on a poorly adherent thick film is given in Fig. 4-15. In addition, when bonding to pads on semiconductor chips, it is possible to fracture (crater) the semiconductor. Application of the shear test to balls that damaged and cracked the silicon during bonding may result in cratering and low-shear forces during the test. The shear test can, therefore, be used to evaluate bonding machine setup parameters, to minimize semiconductor damage (cratering) not detectable with the pull test, as well as to test metallization adherence. Data from such tests is usually required for DOE evaluation and determining the optimal bonding machine setup (see Chap. 8, App. 8B by Lee Levine [4-36]).

Interferences when shearing compound bonds (*ball on ball*)*:* In the past, rework occasionally required stacking ball bonds. This was done with manual bonders. There has been only one published work on a

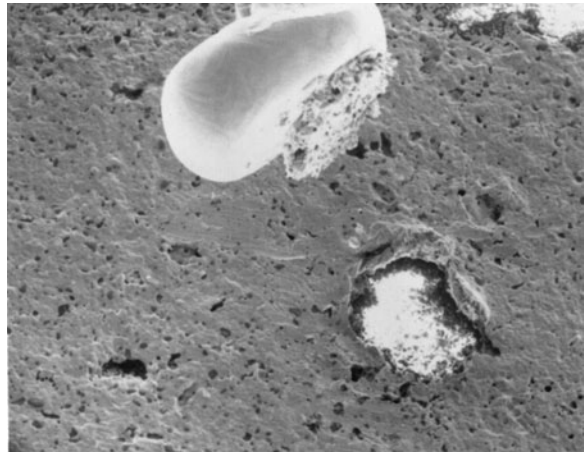

Figure 4-15 An example of a TC ball bond sheared from a poorly adherent gold thick film. This ball sheared at 24 gf, whereas equivalent sized bonds to adherent thin-film gold sheared in the 70 to 80 gf range. The bond was made from 32 μm (1.3 mil) diameter gold wire, with bonding parameters typical of 120 μm pitch on a chip.

shear test evaluation of compound-thermosonic bonds [4-24]. This work found that centering of the top ball bond on the bottom ball was very important. There was an increased tendency to crater in cases where the top ball bond was misaligned on the bottom one (as revealed by the ball-shear test). Some bonding machines resulted in more craters than others without apparent reason. Increased ultrasonic energy also significantly increased cratering, which is normally to be expected. However, when ball on ball cratering occurred, the energy could be minimized (also temperature increased) and essentially cure the cratering problem. When optimized, the bond shear force of the lower ball was statistically unchanged from that of a single ball bond. Therefore, the use of compound bonds on chips, made with manual bonders, should be minimized. Autobonders precisely center a ball on a ball, and craters from them have not been observed. Stacked ball bonds made by autobonders are used in making compound ball bonds for use as standoff bumps when converting devices with Al bond pads into flip chips (ball bumped flip chips). In most cases, only one ball bond is used, but there are examples of stacking several to obtain increased height [4-24]. This offers stress relief against fatigue failure in thermal cycling (see Fig. 4-16). These stacked bonds applied with autobonders would be well centered on one another. As such, they do not pose cratering problems. However, the correct procedure for shear test evaluation of the stacked bonds is not obvious. Most likely, the Au-Au bond interfaces will be strong and cause no reliability problems (see Chap. 5), so testing the lower (Au-Al) interface alone should be sufficient.

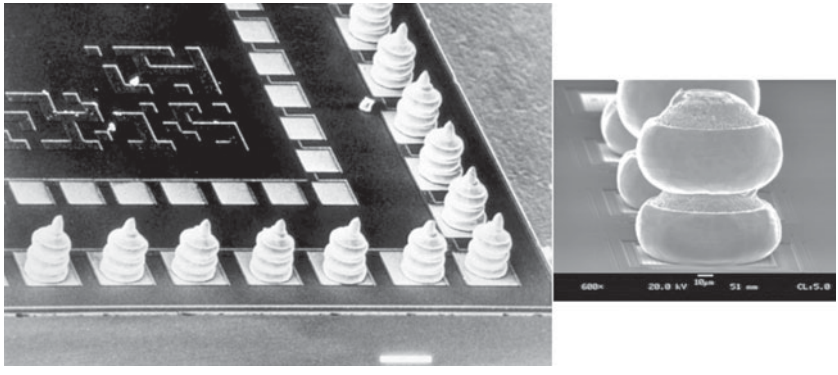

(a) (b)

Figure 4-16 An example of stacked-ball bonds that could be used for stress relief in flip chips. (*a*) is a full triple "ball bumped" chip, and (*b*) is an example of a double "accu-bump/chopped-bump." (Made by moving the tool sideways across the wire neck after the ball is welded. See animation in color Fig. 4-16*a* in the CD.) (*Courtesy of K&S.*)

Cleanliness and wear of shear tools: Since a shear tool should be positioned within ~2.5 to 5 μm (~ 0.1 to 0.2 mil) from the chip or substrate (and even closer for fine-pitch situations), its bottom surface must be kept clean. Metallic smears, bits of Al, Au, glassivation, Si, etc., can stick to the bottom and prevent proper vertical positioning. This problem is most significant when shearing very flat (low-profile) balls with tools that are several times wider than the diameter of those balls. A narrow tool (about 1-ball-diameter wide) tends to clean itself off as it shears through metal, but not if the entire ball pushes off.

Shear tools wear during long use and/or mishandling. The front and bottom surfaces must be smooth, polished, and rectangular in shape, with no chipouts permitted on the shearing edge. To obtain reproducible test results, shear tools must be monitored and replaced with the same urgency as bonding tools and capillaries. Tools used for finer-pitch balls require more frequent monitoring than tools for coarser pitch, but the test becomes increasingly impractical for pitches less than 50 μm.

4.3.5 Ball-Shear Force versus Bonded Area

Experimental shear force data versus actual bonded area for ball bonds have been published by two independent sources [4-16, 4-17] and verified [4-11]. The shear strength of both Cu- and Ag-doped (<10 ppm) Au wires was measured to be 90 MPa (13,100 psi). Beryllium-doped and recent proprietary Au alloy wires could be 10 to 20% higher. The ultimate shear strength for the hard and annealed 1% Si, Al wires, respectively, were 139 and 84 MPa (20,200 and 12,200 psi). Some shear strength values of the hard and annealed Al wires bracketed those of Au, indicating that a ball-bond weld can fail either on the Al or Au side depending on the particular characteristics of the Al pad. These data are plotted in Fig. 4-17 as shear force versus diameter of the bonded area.

The wires used in this experiment contained Cu and Ag impurities at the parts per million level. Gold wire used in automatic bonding machines is usually stabilized with Be, Ca, and proprietary elements, which results in a 10 to 30% stronger wire in a stress-strain test. One might assume that such Au wire would produce higher gold-ball shear values, but this has not been experimentally observed.* Values obtained from Fig. 4-17 should be considered maximum theoretically obtainable values, rather than expected values, since all of the area under a ball is not welded. Thermosonic ball bonds on an Al

*Comparisons using 25 μm wire with breaking loads ranging from 8 to 13 gf showed no statistical difference in ball-shear values for the same size balls [4-26]. Apparently, the "burnout annealing" that occurs during EFO ball formation leaves the balls in a similar metallurgical condition.

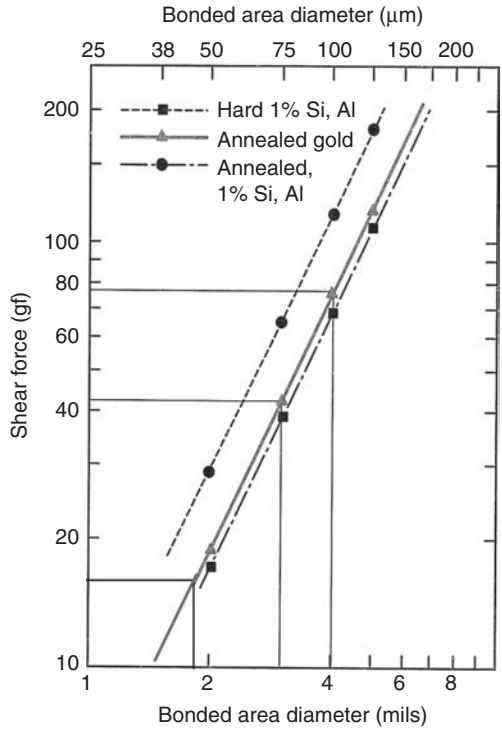

Figure 4-17 Shear force versus bonded area for evaluating the maximum expected values to be obtained from the ball-shear test. Only one curve is given for gold because the ball is fully annealed and less affected by any dopants. However, since the joint will fail in its weakest member, the shear-strength range of aluminum is given for guidance as to the possible strengths of aluminum metallization. For use, the diameter of the tool impression in the ball is measured with a microscope or if fine pitch, the entire diameter is used. Note that below ~50 μm diameter, the shear force drops rapidly below 20 gf and becomes increasingly harder to shear, requiring finer shear tools and greater skill in positioning. At some point the shear test becomes impractical and the pull test is used (see Chap. 9, Sec. 9.1.10).

film are typically only welded over about 65% of the area of an average 75 g shear force (3 mil) diameter ball deformed 50% during bonding 11. [Some investigators have obtained welded areas over 80%, as revealed by observing the KOH etch-revealed intermetallics in the bond interface (see Table 4-1).] Thus, the entire area under a bond will not be welded (although fine pitch ball bonds are usually very high). In addition, one may expect greater amounts of welded area for optimized bonds to clean metallization versus contaminated ones, as well as the method of bonding. For instance, when testing bonded balls of 75 to 90 μm (3.0 to 3.5 mil) diameter, it was found that shear-force values of well-made bonds to Au metallization were approximately 40 gf (very near the value in Fig. 4-17) and to Al metallization

Machine or Test Parameter	100 μm Avg. of 5 Machine[a]	Observed Range, 100 μm Process[a]	90 μm Process 1 type of Machine[b]	80 μm Process, 1 type of Machine[c]	70 μm Process, 1 type of Machine[d]
Free-Air Ball Dia. (μm)	50	45.4 to 56.3	_	43.2	40.6
Bonded Ball Dia. (μm)	74	67.7 to 78.6	61.3	55.8	47
Bonded Ball Height (μm)	16.1	12 to 17.2	13.5	12.5	5.9
Shear Force (gf)	35.4	27.2 to 43	32.4	25.7	19.2
Shear Strength (gf/mil^2)[e]	5.36	3.7 to 6.4	7.06	6.5	7.04
Intermetallics Under Ball (% interface area)	65.6	79.6 to 47	_	79.5	>80

[a]Five Different Mfg. Machines, (averaged) data obtained over 8 h runs [4-26].
[b]One Type of Machine [4-26].
[c]ESEC, Several Identical Machines [4-27].
[d]K&S and SEMATECH, Several Identical Machines (private communication) Also see [4-28].
[e]Milli-Newton (mN) units may be substituted for grams-force (gf), 1 gf = 9.8 mN. Also, 1 mil = 25.4 μm. (1 gf/mil^2 = 0.0152 mN/μm^2).
Note: Data in table (4-3) were summarized from a SEMATECH study. Since the test was extensive, the range of each parameter is given to alert the reader that different autobonders can be quite different. The machines and parameters were typical of a 100 μm bonding process at that time. Today, advanced bonders can produce much finer pitch and closer tolerances than indicated in this table.

TABLE 4-1 Averaged Autobonding Machine Parameters for Four Ball Bonding Processes Using 25 μM Diameter Gold Wire

were ~30 gf (~70% of values in Fig. 4-17 and closer to other predictions) [4-12].

Mixed units are used in the industry for shear strength (SS) because SI units (μm or mm) result in values so high or low that they are not intuitively comprehendible. The reader can use the conversion factor above to convert data. Note: All machines, except one in the 100 μm process, bonded with 60 kHz US energy and on Al chip pads. Observation of numerous cross-sections of ball bonds at this laboratory (NIST) indicates that the outer boundary of the tool imprint on top of the ball corresponds closely to the perimeter of the actual bonded area. It is, therefore, recommended that the welded area should be estimated by measuring the outer diameter of the tool imprint in the ball, rather than the outside diameter of the (non-fine pitch*) ball. This value should then be used to obtain the maximum expected shear force in Fig. 4-17, and it may be 15 to 20% lower than that obtained by using the outer diameter of the ball, as was used in Table 4-1. However, some fine pitch capillaries do not produce bonds with the traditional squashed-ball shape. They may be an inverted conical shape (see Fig. 4-18), or a minimally squashed classical shape. Fine pitch balls tend to be welded over a very high percentage of the interface, and the outside perimeter is typically used for calculations.

The curves of Fig. 4-18 can be used to establish the maximum shear force obtainable in as-made ball bonds. However, no minimum acceptable value can be deduced from that curve, but it has been addressed by comparing wire pull and ball-shear data [4-19] and in one standard (Sec. 4.4.11). If the mean pull force is plotted against the mean shear force, a minimum shear force will be found in which no ball bond lifts occur during pull testing. Such a procedure requires thousands of bonds to obtain meaningful data. In this study with large diameter balls by today's standards, the mean shear force of good bonds was approximately 80 gf, and the crossover shear force, where some ball-lifts occurred during pull testing, was 40 gf shear force. Therefore, by this criterion, a minimum acceptable shear force appears to be approximately one-half the indicated shear force value in Fig. 4-17. [However this does not consider the thermal stress reliability requirements of Au-Al bonds, which require higher shears of about 5.5 g/mil^2 (84 MPa). See Fig. 4-23 and its top curve along with its discussion.] Fine pitch appears to result in higher values, but is more subject to thermal degradation.

The microelectronics industry has been moving toward fine-pitch ball bonding (<50 μm pitch), as well as experimenting with high-frequency ultrasonic energy. To compare the shear strength (amount of welding) from one ball size (or US frequency) to another, the industry has begun to use normalized shear-test values [4-25, 4-26, 4-27]. For this

*Capillary imprints on fine pitch balls often extend to the outer diameter of the ball, depending on the specific tip design. For these, the outer diameter should be used in calculations.

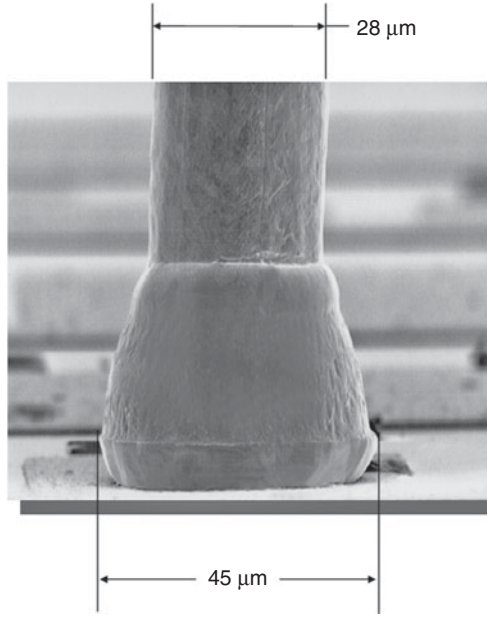

Figure 4-18 The minimal (conical) shape of some fine pitch ball bonds. (*Courtesy of K&S.*)

case, the shear strength is calculated by dividing the measured shear force (SF) by the area of the ball (calculated from optical measurements of the outer bond diameter). As used in one study [4-26], two optical measurements of bonded-ball diameter are made at right angles in an "effort" to correct for noncircular balls. The equation is

$$\text{SS} = \left(\frac{\text{SF}}{\frac{\pi}{4} \times \left(\frac{d_x + d_y}{2} \right)^2} \right) \tag{4-6}$$

where d_x = ball diameter in the x direction and d_y = ball diameter in the y direction.

When the ball appears to be mostly round, the d_x and d_y can be replaced simply by a single diameter measurement, D.

$$\text{SS} = \frac{\text{SF} \times 4}{\pi \times D^2} \tag{4-6a}$$

Typical values of SS range from 5 gf/mil^2 to greater than 7 gf/mil^2. The intermetallic measurement (welded area) is usually obtained by etching the bond pad from under the ball with some etchant that does not attack the ball (e.g., 25% solution of KOH) and then observing the intermetallic (metal disruption) on the bottom of the ball. A high-power metallurgical or other microscope can be used for this purpose.

Table 4-1 was summarized from extensive data from several sources to show the bond characteristics and values obtained by this method. Shear force, SS values, and intermetallic percentages are compared for bonds intended for a range of fine-pitch processes. The correlation between the amount of intermetallic, or metal disruption, on the ball and the shear strength has been established [4-26, 4-27], and, thus, the actual amount of intermetallic is only determined occasionally (e.g., for a major change in metallization or Au wire dopant).

One would assume that a simple square-law equation (related to the bonded-ball area) using the data from Table 4-1 could be used to predict the expected shear force of fine pitch bonds, knowing the actual welded area (percentage of intermetallics). This could then be related back to Fig. 4-17. However, the actual curve-fitting equation using data from Table 4-1 turned out to be less than square law.* It is

$$\mathrm{SF}_{(\text{welded area dia.})} = 0.024\,D^{1.78} \tag{4-7}$$

where SF is the shear force in gf, and D is the equivalent diameter of the actual welded area in micrometers. The correlation coefficient is: $r^2 = 0.999$. This equation can be used on fine-pitch bonds (≤100 μm) to determine the equivalent welded diameter (and from that the percent that are intermetallics) or the shear force if the percentage of intermetallics is known. Also, using the data from Table 4-1, one can project that, for a 60-μm pitch process, the effective bonded-ball diameter would be 34 μm (for 80% welded area and represents an actual diameter of 38 μm) and the shear force would be 13.4 gf. From Fig. 4-17 it would be nearer 12 gf, not a bad approximation. (See Chap. 9 for further fine pitch details.)

Using the actual measured bonded-ball diameter (in micrometers), the equation becomes:

$$\mathrm{SF}_{(\text{ball dia.})} = 0.023\,D^{1.75} \tag{4-7a}$$

where $r^2 = 0.98$. Equation (4-7*a*) assumes ~80% welded area under the bonds, and the diameter is measured optically as the outer perimeter. This equation is easier to use than Eq. (4-7), since only the measured diameter of the bonded ball is required. However, since the welded area under production bonds normally varies, results on any experiment may also vary. Still, this equation is an adequate approximation for most finer-pitch (≤70 μm) situations (see testing of fine pitch bonds, Chap. 9).

---

*Since the actual bonded area was used, a square-law behavior related to the increased cross-section should have been observed. The reasons for fine-pitch bonded balls producing a shear-force-to-bonded-area relationship different from larger diameter bonds are not understood, and more study is indicated. Very fine pitch bonds have been observed to have a larger percentage of welded area (shear strengths consistently >7 gf/mil^2 than equivalent larger diameter balls).

4.3.6 Effect of Gold-Aluminum Intermetallics on the Shear Force

When Au is thermosonically bonded to Al, intermetallic compounds form in the interface. In fact, it has become a normal procedure to evaluate the amount of weld formation by observing the amount and distribution of those compounds as described above. Considering this, one may wonder what effect intermetallics have on the shear test. In the as-made condition, these are thin and have no effect on the shear force [4-26, 4-27] except that they are essential for strong Au-Al welding. However, after thermal exposure (thermal stress test, high-temperature environment life, etc.) the compounds will grow. They may appear as spikes into the ball bond in poorly welded interfaces (see Sec. 4.3.7) and have some effect on the shear test.

There appears to be minimal data on either the tensile or the shear strength of intermetallic compounds. However, Philofsky [4-29] made estimates of the tensile strength as a result of tensile testing Kirkendall-void-free Au-Al couples and concluded that all of the intermetallic compounds are at least three times as strong as annealed Au or Al. (Also see Table 5-1, Chap. 5, for many properties of these intermetallics.)

Considerations of the binding energy of the compounds would suggest that these compounds could be 10 times as strong as either Au or Al, and this is generally verified by hardness measurements [4-30]. Even though such compounds are brittle, we conclude that they should not result in lowering the ball-bond shear force as long as the interface is void-free. As they spread laterally in the interface, they can actually increase the shear force (equivalent to more complete welding). Such an increase in strength (10% or more) during the early part of high-temperature tests has often been observed [4-17], and this explains why bonds made at relatively high temperature are reported to be initially the strongest.

The formation of intermetallic compounds under a ball bond can produce considerable stress on the silicon [4-31]. The added stress of a ball-shear test can then result in silicon damage (cratering). See Sec. 8.1 for a discussion of this problem and App. 4A, Failure Mode 3, for an example.

4.3.7 Pluck Test, Pry Test, Flip Test, etc. (Failure Analysis Technique)

If an Au ball bond to Al is poorly welded and subsequently undergoes thermal stress, then intermetallic spikes may form that will extend into the Au and Al [4-32]. Figure 4-19 is a drawing of such a bond. These spikes can add lateral strength to the bond when it undergoes shear testing and yield a deceptively high shear force. A failure analysis procedure to examine such bonds can be used to reveal this.

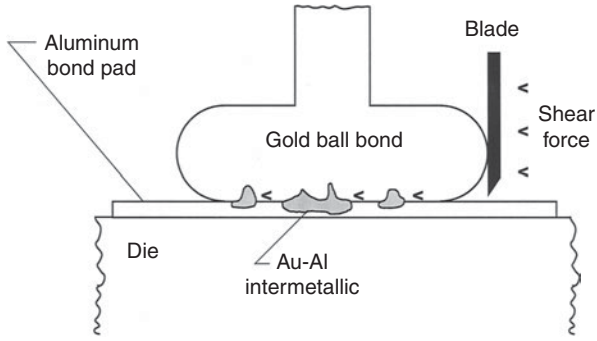

Figure 4-19 Schematic of a ball bond with isolated intermetallic growths. These growths can offer considerable resistance to a ball-shear probe, but can often be "pried" up with a scalpel or will lift with low force in a pull test [4-32].

A fine scalpel blade is used to pry or "flip" the bond up, leaving the intermetallic spikes on the pad and on the lifted ball for examination. This was called the "pluck test." Weak, "as-made," bonds could more easily have been revealed by a shear test during production (before any spikes were thermally generated), and the problems of poor bonding machine setup or contamination could have been solved at that time. But when it does occur, failure analysis may be required. Thermal stress experiments on intentionally weak bonds (shear force <50% of optimum) made on clean pads by Harman (unpublished) indicate that, when the shear force has decreased to about half its original value (<25% of normal), the described mechanism becomes significant. In some cases, bonds with shear forces of 10 to 15 gf will lift in a pull test at 3 to 5 gf. This happened frequently enough to require application of the nondestructive pull test at various stages of the ball-shear, thermal-stress experiments to remove bonds with this failure mechanism. It should be noted that strongly welded Au ball bonds that are thermally stressed result in relatively uniform intermetallic formation and have not been observed to fail by this mechanism. An example of this phenomenon would be similar to that shown in Fig. 5A-1 in Chap. 5, App. 5A.

Such failure analysis methods have not been applied to fine pitch balls, because of the difficulty of inserting a probe under them. Almost as much information can be obtained from etching the Al pad out from the ball with 20% potassium hydroxide and examining the "turned over" ball. However since the pull test is often applied to these bonds, one occasionally sees spikes remaining in the pad after thermal stress test lift-offs.

4.3.8 Comparison of the Ball-Shear and the Bond-Pull Tests

The most effective comparison between the ball-shear and the bond pull test was given by White [4-33]. Strong Au ball bonds were made to Al integrated circuit metallization, and they were put on temperature test at 200°C for 2688 h. The degradation of the Au-Al interface was studied by monitoring both the shear and pull test at various time intervals. White's data are replotted in Fig. 4-20. The bond interface strength decreased by a factor of 2.6, presumably due to Au-Al intermetallic formation and possibly some Kirkendall voiding. However, these were not sufficient to impair the electrical operation of the devices (adding only a few milliohms). During this time, the pull force actually increased slightly, presumably due to changes in the Au wire metallurgy. Thus, the pull force is not a valid indicator of a ball bond's interface strength. It should be noted also that this severe thermal stress, which consumed all of the available Al (the flat portion of the ball-shear curve), did not result in device failure.

4.3.9 Applications of the Ball-Shear Test

Bonding Machine Setup Parameters, Thermocompression Bonding

Thermocompression (TC) bonding has fallen into disuse because of its high temperature requirements and long bonding times. A synopsis of the setup parameters is included for any occasional continuing usage of

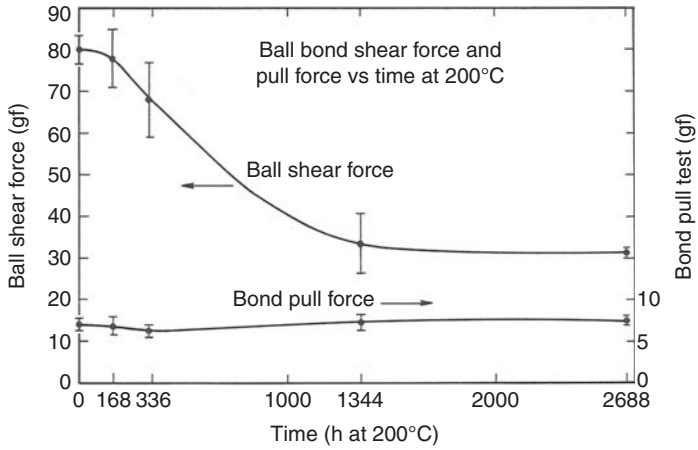

Figure 4-20 Gold-ball bond-shear force-and-pull force versus time at 200°C. The ball bonds were made with 25 μm (1 mil) diameter gold wire, were approximately 100 μm in diameter. They were bonded to pure Al integrated-circuit bonding pads. Note the change of scale from shear force (left) to pull force (right). Error bars were observed to narrow as the intermetallic growth stabilized. (*Curve is a **replot** including private data from White [4-33]*; © *IEEE*.)

this technology. It was used for much early work that is still part of the basis of our understanding of bonding and was essential in developing the ball-shear test. Directly or indirectly, the majority of published work on the ball-shear test has resulted in improving the setup parameters of bonding machines. Generally, for TC bonding, the machine is set up for a bond interface temperature of 300°C, a bonding time of 0.2 s, and a bonding force of 100 to 125 gf to obtain strong thermocompression ball bonds from 25 μm (1 mil) diameter gold-wire on either Al or Au metallizations. These parameters offer good shear strength, even in the presence of a moderate amount of organic contamination [4-14, 4-16]. Typically, the higher the temperature the greater the bond strength if some contamination is present, see Chap. 7.

Bonding Machine Setup Parameters, Thermosonic Bonding

Jellison [4-21] studied thermosonic bonding characteristics of both thin and thick Al films and is further discussed in Cleaning, Chap. 7. In general, early workers found that the shear force improved significantly with increased ultrasonic power and temperature. Weiner [4-35] studied TS bonding the effect of US power on ball bonding setup with both Al and Au metallizations, using manual bonders. His data is plotted in Fig. 4-21. It shows greater US power sensitivity of the shear force for Al metallization than for Au.

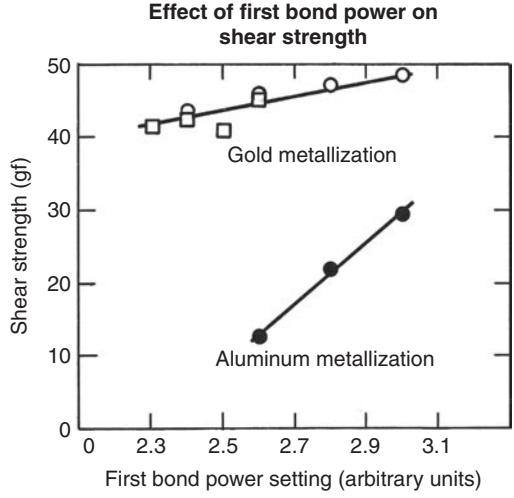

Figure 4-21 The effect of ultrasonic power on ball-shear force. Bonds made with 25 μm (1 mil) diameter gold wire. The stage temperature for these measurements was 125°C, and the bonding force was 30 gf. This may be appropriate for one set of conditions/bonder and is given as an example. (*After Weiner [4-35]; © IEEE.*)

Currently most organizations use design of experiment methods (DOE) obtained for ball-shear force encompassing machine variables are described in Chap. 8, App. 8B, DOE for modern autobonder setup by Lee Levine. There are significant differences between the older results on manual bonders and ones obtained using modern autobonders. This is not resolved, but may result from autobonders using short bonding times (8 to 15 ms vs. 50 or so ms for manual ones, and the force may change) whereas current autobonders use high frequency US energy. At any rate DOE setup (above) must be used for current autobonders!

The order of priority of the bonding machine parameters
Power is the most important variable.
Bond force and impact are important on ball diameter, especially in ultrafine pitch, and maybe for reliability.
Temperature is important, especially for second bond (crescent) strength.
Time is a minor variable.

Although values are different, their relationship is approximately similar for 60 and 120 kHz. One study, Charles, IMAPS 2002, found that for short thermal aging times, 100 kHz gave better shear strength than 60 kHz. Thus the effect of frequency on reliability of Au-Al bonds must still be studied to find its limits.

Earlier investigators have described DOE methods for setting up TS bonders [4-37, 4-38, 4-39] and obtained differing coefficients. It is clear that, at the present time, each machine type may have enough variability to require its own DOE setup procedure. Currently transducers within a single manufacturer are very similar. However, different manufactures often run at different frequencies (90 to 135 kHz typical) with experimental transducers above 250 kHz. They may use shorter bonding times for higher speed/throughput, etc.

For TC bonding, it was possible to assemble published data and give typical bonding parameters. This is not possible for TS bonding, partly because the published data or parameters do not overlap, and partly because of the reasons cited above and further development into fine pitch. Since there are no clearly defined universal parameters, it is extremely important to use DOE along with the ball-shear test to optimize bonding machine setup which is done with modern software.

Evaluation of Production Bond Quality

The major use of the ball-shear test, as with the pull test, lies in the area of production quality control. This test was slow to gain acceptance after its introduction in the 1970s, due to the lack of commercial testing equipment and standards for its use. Both problems have long

been corrected (see Secs. 4.3.2 and 4.3.11), and currently (2008) all major semiconductor assembly and MCM/hybrid/SIP facilities are using the shear test to control their ball bond production.

Historically, the first published use of the ball-bond shear test (in 1967) was to monitor and control aspects of microelectronic (chip) production rather than to evaluate bonding. Gill [4-14] used it to monitor adhesion of the "then" new molybdenum-gold metallization system. Weak adhesion of Au to molybdenum was revealed by the Au peeling from the molybdenum during the bond-shear test. The shear test is still an excellent method to determine the quality of metallization adhesion (see 4-15) and has also been used to evaluate the tendency of different metal and bond systems to crater under plastic package generated shear and thermal stresses.

It is apparent that the high stresses applied to ball bonds in plastic-encapsulated devices during molding and later during thermal cycling (and also the thermal shock during surface-mount soldering) make it essential to use the ball-shear test for production-bond quality control. When used as a continuing production test, the shear test will reveal the degrading effects of recently introduced contamination, as well as any variation in the metallization or glassivation removal process. This information can be obtained quickly enough to take corrective action before large amounts of a failed product are made. Several studies have shown a correlation between ball-shear test results and the reliability of the devices [4-40 to 4-43].

The nondestructive ball-shear test was investigated only twice [4-19, 4-39], and it was found that balls can be stressed to 75% of their destructive shear force without significant final shear force degradation. In principle, this test could be used to assure production-bond quality as can be done with the nondestructive bond-pull test. However, great care is required in positioning the shear tool. As a result, the test is slow and, therefore, costly, which has prevented its further consideration. A worse problem, however, is probable damage to the top surface chip passivation, and in the case of fine pitch, it becomes impossible to use. Thus, although this was an interesting investigation historically, it cannot be recommended for production and absolutely cannot be used on fine pitch bonds.

4.3.10 Shear Test for Wedge Bonds

The shear test is clearly useful for evaluating ball bonds, but is it also useful on small-diameter ultrasonic Al wedge bonds? A cooperative experiment between NIST and Sandia National Laboratories (reported in [4-44]) was designed to determine this. The test consisted of three groups of 25 μm diameter Al, 1% Si wire, [BL = 12 to 14 gf (× 9.8 for mN)] ultrasonic wedge bonds on a single wafer substrate made at NIST. Half of the bonds (randomly selected) were pulled to destruction, and then the wafer was sent to Sandia where the remaining bonds were shear tested. The data are shown in Fig. 4-22.

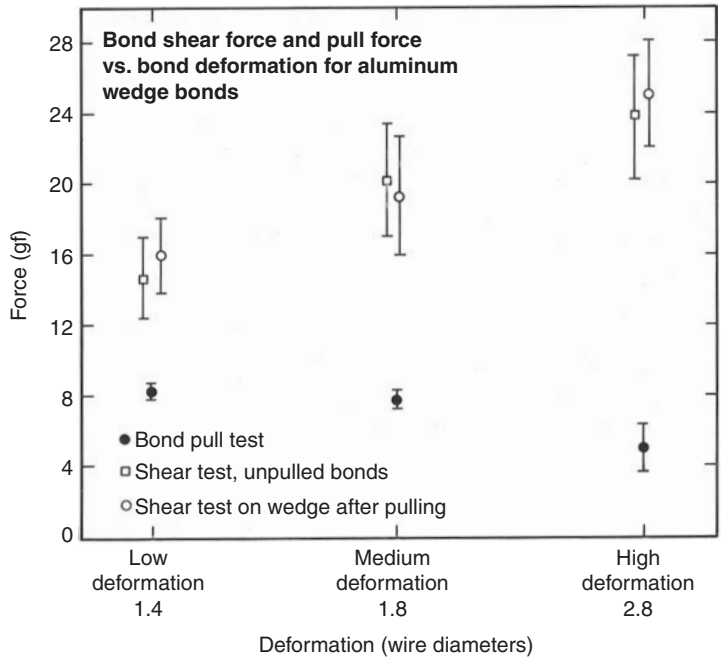

Figure 4-22 Data from bond-pull tests and bond-shear tests on ultrasonic aluminum wedge bonds of 25 μm (1 mil) diameter wire on aluminum metallization. The error bars represent one standard deviation of the mean above and below the mean breaking strength ~20 bonds [4-9].

These results may be understood if the metallurgical nature of the bond is considered. For Al ultrasonic wedge bonds, the bond heel becomes metallurgically overworked and weakens as the bond deformation increases, but the amount of the welded area increases simultaneously. The pull test is particularly sensitive to the weakening of the bond heel. Therefore, the pull force decreases as the deformation increases. The shear test, on the other hand, is completely independent of the condition of the heel; it is sensitive only to the actual amount of welded area. A high-shear value could be obtained from a wedge bond with a cracked or completely broken neck (heel). From the above, it is apparent that the shear test is not very useful for evaluating Al wedge bonds made from small-diameter wire, particularly as the bond deformation increases above two wire diameters. However, since current shear testers can be easily positioned within several micrometers, they are occasionally used to evaluate the welded interface on small Al wedge bonds when the problems described above are understood. The minimum wedge bond deformation recommendation for high frequency bonds (made with ≥ 100 kHz) is approximately 1.25 × wire diameters. Thus, shearing such with modern equipment is generally feasible

unless the wire diameter is less than or equal to 25 μm. See Levine [4-45] for a concise discussion of fine pitch and ribbon testing.

The greatest use of the shear test on wedge-wedge bonds takes place on large-diameter Al wire wedge bonds, such as are used in power devices. These are usually made with parallel, V-grooved tools and stand relatively high. Such bonds can be successfully evaluated with a shear tester. For example, if a 250 μm (10 mil) diameter Al wire is deformed 20% (at the interface) and has a foot length of 750 μm (30 mil), then the shear force will be approximately 1.6 kgf (3.5 lbf) if the interface was fully welded.* A well-bonded Al wedge bond from large wire [diameter ≥ 100 μm (≥4 mil)] on a power device should yield a shear force value on the order of 2 to 4 times the pull force value (depending on the length of the bond), thus greatly increasing the sensitivity for bonding machine setup purposes. A shear strength value [see Eqs. (4-6) and (4-6*a*) in Sec. 4.3.5] can be defined for large wedge bonds by substituting the wedge-pad contact area (bond length times width) in place of the ball area, as in Eq. (4-9). This will make it possible to compare bonding quality between different-sized wires, foot lengths, or possibly different metallurgies.

$$SS_{(\text{wedge bond})} = \left(\frac{SF}{L \times W}\right) \tag{4-9}$$

where SF is in gf, W is the interface width, and L is the bond length. Both are normally in mils, but as in Eq. (4-6) could equally well be in SI units. In the example above, the SS = 4.4 gf/mil^2 (0.07 mN/μm^2). This is one random example but real experimental data should be higher.

An interesting testing change has occurred now that ball-bond pitch has decreased below 50 μm. First, the shear test is increasingly hard to apply due to interference with adjacent bonds. Second, the bonded area will be reduced to the point that a bond pull test will adequately evaluate the strength of a ball bond. A pull test criterion can be based on 75% welded area (percentage of intermetallics) of the ball. When this area becomes equivalent to the wire diameter, then the pull test will adequately evaluate the ball-bond strength, and that test can be substituted for the shear test. (We note here that the adhesion of the bond pad metallization to the substrate can further lower the pull-failure force and may result in lifted metallization—a condition that many current specifications reject. The need for such changed pull criteria/specifications will be discussed in Chap. 9.)

Ribbon bonds with a height of 12 μm (~0.5 mil) or higher can also be successfully tested with a shear tester. Optimum shear test values for both ribbon and large-diameter wire can be obtained from the curves of Fig. 4-17 by correcting for the rectangular bonded area.

---

*Based on 700 kg/cm^2 (10,000 psi) shear force of annealed Al and a wire-breaking load of ~500 g (1.1 lb).

Shear testing has been used for years to test the integrity of TAB bumps at the wafer level. It was also used to measure the strength of the bonding between the TAB lead and the bump as well as the lead buckling force [4-46]. Typically, such tests were performed with a wire-bond ball-shear tester. The shear test is universally used to determine the strength of solder balls on chips for flip-chip attachment.

4.3.11 Ball-Shear Test Standardization

The ball-shear test is used in essentially all major semiconductor assembly facilities around the world to control ball-bond production for all but the finest pitch. There are two published standards on its usage, as well as many internal company manufacturing specifications. The first standard specification was published by ASTM in 1990. It is ASTM F 1269, and was updated in 2006. It is test methods for shear testing of ball bonds. This test was originally documented by a round robin involving six cooperating laboratories [4-47]. The EIA JEDEC committee JC-14.1 has issued a shear test standard which is available on the Internet as a JEDEC (commercial) standard (www.jedec.org/download/search/22b116.pdf): Wire Bond Shear Test Method, EIA/JESD22-B116. This test contains recommended shear test values, see Fig. 4-23. It is now called out in MIL-STD. 883G/H.

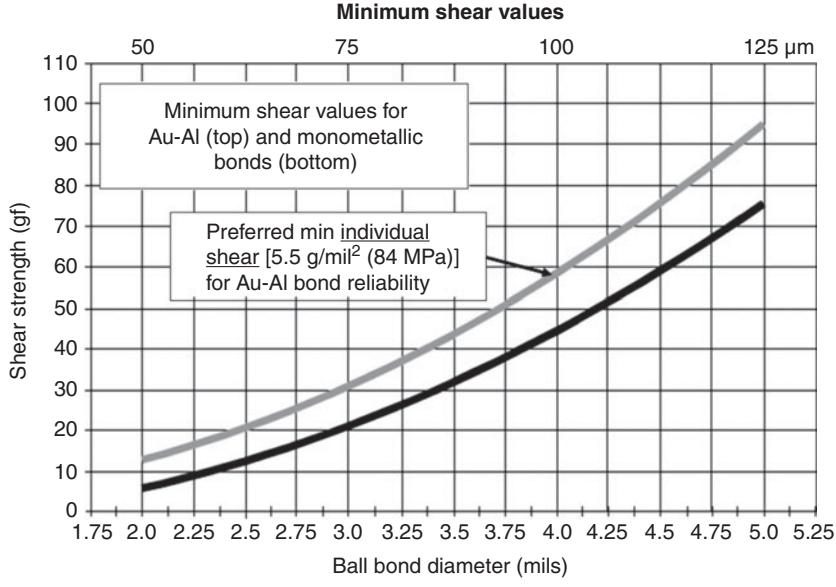

Figure 4-23 Modified minimum recommended ball-shear test values given in the EIA/JESD22-B116 document. The recommendation would be improved if the top curve at 84 MPa (5.5 g/mil^2) was the minimum shear reading for Au-Al bonds. However, monometallic bonds should be reliable on the lower line. (This Document is on the Web. It may be subject to revision.)

Thus, adequate standards are available to implement the ball-bond shear test. The recommended values (below) do need to be eventually modified in the future. The top curve in Fig. 4-23 [5.5 g/mil^2 (84 MPa)] should be chosen as the minimum individual shear reading for Au ball bonds on Al pads, when long-term reliability (1000 h at 175°C or equivalent) is required [4-48]. This is typically a required test for some important industries.

4.4 Evaluating Both the Ball and the Wedge Bond on a Single Wire

The wedge (or crescent) bond of a ball-wedge bonded wire, as with a wedge-wedge bonded wire, is best evaluated with a pull test. One study found that there was only negligible degradation of the ball-shear force after bond pulling and concluded that the pull test can therefore be done first [4-39]. Similar statements are made in ASTM F 1269-06. Thus, the ball can be sheared after the loop is pull tested, allowing data to be obtained from both bonds of a single wire and minimizing the required sample size.

4.5 Thermal Stress Test for Au-Al Wire Bond Reliability

Gold bonds on Al pads (or the reverse) have long been observed to fail beyond some level of thermal stress (see Chap. 5, Intermetallics). However, Horsting [4-49] (see Chap. 6 for Al bonds on Au) found that, if the bond is well made and there are no impurities present in the bond interface, the bond will remain strong even after long times at high temperatures. If impurities are in the interface or the bond is poorly welded, then the bond-strength may degrade rapidly during such stress. To reveal potential problems in a new gold-plated package lot, Horsting applied a stress test that consisted of a 390°C bake for 1 h, followed by a pull test. If the bonds lifted (interface separation) in a pull test, the entire package lot was rejected. Ebel [4-50] introduced an entire bake schedule as a screening procedure to reveal similar potential bond failures for hybrids. Later, MIL-STD-883, Method 5008 for hybrids, specified a similar, though less severe, test of 30°C for 1 h and a pull-test value specified as greater than or equal to 1.5 gf (14.7 mN)—post seal. Currently (2008), this is in MIL-PRF-38534. The time, temperature, and other conditions of these various stress tests are given in Table 4-2. It should be emphasized that this stress test is only useful for bimetallic bonds that diffuse and react readily (e.g., Au-Au and noble metal bonds improve with temperature, and Al-Al bonds stay about the same—see Chap. 5, Sec. 5.3.7).

Time (h)	T °C	Pull Test Failure Criteria	Reference
1	390°	Weak or lifts@	[4-49]
1 4 24 200 3000	350 300 250 200 150	Less than one half the minimum acceptable post seal pull force of (MIL-STD 883, Method 2011)	[4-50]
1	300°C	<1.5 gm for 1 mil 25 μm wire <1 gm for smaller wire	MIL-PRF-38534F App. C [4-7]

TABLE 4-2 Various Thermal Stress Tests for Au-Al Bond Reliability Assessment

4.6 Future Issues in Wire Bond Testing

Bond testing in the future will be influenced by the increasingly finer pitch of IC bond pads and the corresponding decreasing size of the bonds. For the pull test, as package sizes and loop heights decrease, it has become increasingly difficult to get the hook under the wire. The problems described above of pulling wires in multiple-tier packages applies to decreasing pitch and loop height as well. This further complicates application of the destructive pull test. The normal procedure for multiple-tiered packages is to pull test each tier, from the top down, but some loops may be too low to insert a hook underneath them. The NDPT becomes impossible to apply.

The ball-shear test will be applied to smaller diameter balls, as well as ones that are not as high. This requires flatter substrates, more precise shear-tool height adjustment, and narrower shear blades (which will wear out more rapidly). Modern shear testers have the capability of shearing with the required precision. However, in many cases similar test methods can be used, but with more care. One is substituting SPC as an alternative to extensive destructive pull testing. SPC must be applied as the pitch decreases. High volume autobonders make bonds very uniformly and in general require less testing, as long as DOE (Chap. 8, App. 8B, by Lee Levine) is used for setting them up.

An important testing change has occurred as ball-bond pitch has decreased below 50 μm and the shear test becomes impractical.* The

*ITRS predictions are that both ball bonds and wedge bonds will decrease in size to 20 μm pitch.

bonded area will be reduced to the point that a bond pull test will adequately evaluate the strength of a ball bond. A pull test criterion can be based on 75% welded area (percentage of intermetallics) of the ball. When this area becomes equivalent to the wire diameter, then the pull test will adequately evaluate the ball-bond strength, and then that test can be substituted for the ball-shear test. (We note here that low adhesion of the bond pad metallization to the substrate can further lower the pull-failure force and may result in lifted metallization; a condition that many current specifications reject.) Such changed pull criteria for Cu/Lo-k and fine pitch chips will be discussed in detail in Chap. 9.

Area array bonding has recently been introduced (see Chap. 9). Testing them is similar to testing multiple tiers of bonds in a package. The hook can only be inserted by pulling the top layer, then going to the next layer down. It can be further complicated by fine pitch. Usually the bond numbers are so great that it becomes impractical to pull or shear test them, except on test structures, and then bonded only on one layer. This method is also applicable ball shear testing of area array ball bonds.

Visual inspection, which in the past has been used for some high-reliability and space devices, was often carried out along with mechanical testing. It is much more difficult or impossible to perform on fine-pitch bonds, and also the acceptance criteria are changed. Fine-pitch ball and wedge bonds may appear different from past accepted requirements for courser pitch. The former have smaller diameters and bond height, and they may be conical instead of squashed ball shape (Fig. 4-19). Wedge bonds made with high frequency US can be narrower, but still strong. Both would be rejected under older course pitch visual inspection criteria (e.g., in MIL- STD-883G/H and earlier editions). Such criteria has been recently (2008) revised, and any visual criteria can now be compatible with testing new fine pitch bonds, as well as many contemporary commercial specifications. (See Chap. 9 for pull testing of ball bonds on Cu/Lo-k and other fine pitch bonds.)

Appendix 4A Typical Failure Modes of the Ball-Shear Test (Failure Mode 2 Is the Normal Desired Test Result)

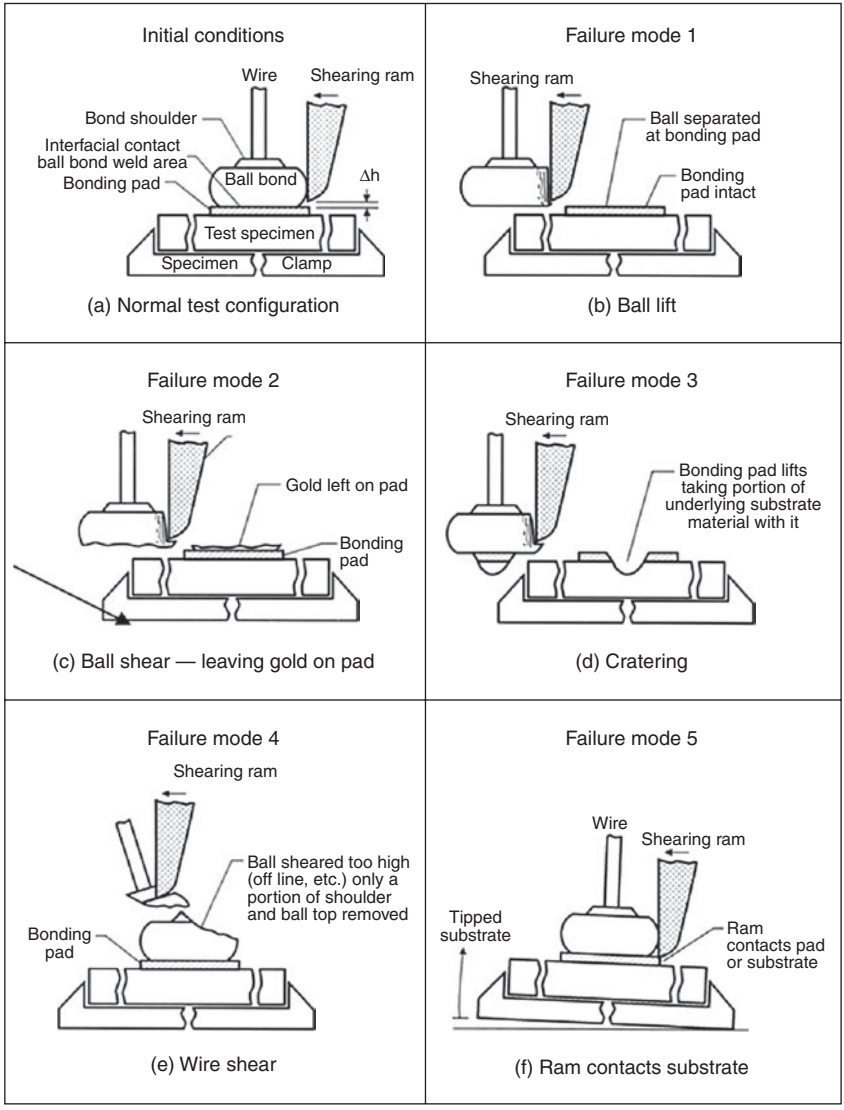

Figure 4A-1 Shear test failure modes. (*After Charles [4-47] and ASTM F 1269-06, with modifications.*) (*© ASTM 2006*)

Appendix 4B The Nondestructive Bond Pull Test

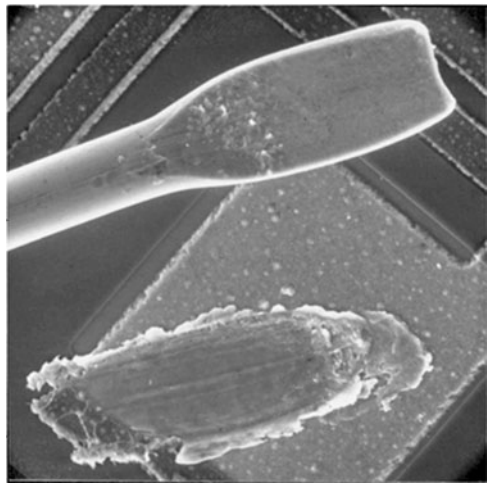

Figure 4B-1 Of what value is a nondestructive pull test? It can reveal cosmetically perfect wedge (and ball) bonds that would lift, as above, in a low-force pull test (in this case ~0.2 gm).

4B.1 Introduction

In 2008, the nondestructive wire-bond pull test (NDPT) was only used in specialized circumstances, such as for planetary space missions, and a few in similar critical situations. It is expensive and cannot be used in some circumstances, such as for fine pitch bonds. This test is performed similar to the destructive pull test, but it is intended to reveal weak bonds while avoiding damage to acceptable bonds. Figure 4B-1 is an example of an NDPT on a weak, Al wedge bond. As with the destructive test, it is only useful on wedge bonds or the wedge bond of a ball-wedge bond (see ball-shear test in Sec. 4.3). For the NDPT, the maximum applied force to the bond loop is limited to some predetermined value that is below the normal destructive pull test value. The resolution of forces Eqs. (4-1) to (4-5) apply and are important for understanding when a weak bond does break. The test is usually applied on a 100% basis to all wires in a multichip module or IC, but in some cases it may be limited to areas or to specific pads of a chip found to have repeated bonding problems. From the late 1960s until about 1990, the NDPT was used for many hermetic, high-reliability (mostly military and space) electronic devices. The test was a requirement for all class-S/K (space) devices. Around the end of this period, high-lead-count fine-pitch multitiered pin grid array and similar packages came into common use. It was difficult, if not

impossible, to nondestructively pull the overlapping wires without the hook damaging some wires and/or causing shorts between wire layers. Thus, NASA and the U.S. military undertook an alternative statistical process control (SPC) method for wire bonding as a substitute for the NDPT. SPC was allowed for devices with packages having 84 or more external terminations and with nominal bonding wire pitch at the package post of less than or equal to 305 μm (12 mils). Early evaluation studies of the NDPT were carried out by a number of organizations, but often the information was obtained for in-house purposes and remains unpublished. The several early published reports [4-51 to 4-54] indicate that the NDP test is valid under the specific conditions of each particular experiment. Of these, only Polcari [4-51]recognized and discussed the importance of bond geometry. He also repeatedly stressed a number of bonds to their chosen NDP force and found that some did not fail during 100 applications of this force, whereas others failed after only four or five trials. The average bond withstood about 50 successive applications of force before failure. However, the standard deviations of the destructive bond pull force for the bonds available to them were quite large. Many of the bonds would have been stressed beyond their elastic limits (see Sec. 4B.2). All of the bonds were stressed at forces higher than those recommended in the present work.

The nondestructive pull force is usually specified for a given wire diameter and metallurgy (see ASTM F 458-06, MIL–STD-883 G/H, Method 2023.5 [4-55] and MIL-PRF-38535). Typical values for 25 μm (1 mil) diameter wire are 2.0 gf for Al and 2.4 gf for Au. Various in-house specifications have ranged from 0.8 to 3 gf for the same wire size. However, such specific values make no allowance for bonds having widely different geometries. The test will break a strongly welded wire bond when (because of package or other limitations) it has a very low loop. Likewise, fixed-pull values apply relatively less testing force to bonds with high loops.

A more scientific approach to deriving the NDP force is to consider the metallurgical characteristics of the specific wire (obtainable from the manufacturer) in addition to the bond geometry. Figure 3-1 in Chap. 3 showed two differing elongations of wire used for bonding. Although those curves are for Al wire, equivalent data for Au wire would be similar. Note that Au wire for use in thermosonic and thermocompression bonding is annealed and would generally have stress-strain characteristics nearer to those of curve A in Fig. 3-1. To avoid metallurgical change or damage to wires during pulling, the wire must not be stressed beyond its elastic limits, region 1 of the stress-strain curves.

4B.2 Metallurgical and Statistical Interpretation of the NDP Test

The metallurgical and statistical interpretation of the NDPT was given by Harman [4-56] and the following treatment is taken from

that work. A normal distribution destructive bond-pull control limit of $(\bar{x} - 3\sigma)$, often used in the electronics industry, assures that only one normal distribution bond out of 740 will have a pull force below that value (note that bond pull forces in a large population may not be normal, see Sec. 4.2.2). Reducing the NDP force 10% to $0.9(\bar{x} - 3\sigma)$, where $\sigma \leq 0.25\ x$, will assure that no bond within the normal $(\bar{x} - 3\sigma)$ distribution is stressed past its elastic limit, whereas any freaks (bonds with low, non-normal, bimodal, etc., pull forces) will be weeded out. Only those bonds whose pull force lies in the range of $(\bar{x} - 3\sigma)$ to $0.9(\bar{x} - 3\sigma)$ may be stressed, to some degree, beyond their elastic limits. All bonds with pull forces below that range will be broken, and all bonds with pull forces above it will only be stressed within their elastic limits. The actual percentage of bonds that lie within the inelastic stress range will depend on the relationship between $\bar{x}$ and σ.

In cases where very low standard deviations are encountered ($\sigma \leq 0.15\ \bar{x}$), as may happen in volume production using autobonders, the NDP force can be changed to $0.9(\bar{x} - 4\sigma)$. In this case, no more than one normal distribution bond out of ~30,000 would be stressed past its elastic limits. In a situation where $\bar{x} = 6$ gf and $\sigma = 0.15\ \bar{x}$, the NDP force would be approximately 2.1 gf, and only one normal-distribution bond in 45,000 would be stressed beyond its elastic limits. Table 4B-1 gives the percentage of those bonds whose pull force will lie in the inelastic stress range for both the normal and the low criteria. For low elongation wire, the maximum safe NDP force is $0.9(\bar{x} - 3\sigma)$, where $0.25k > 0.15\bar{x}$, and $0.9(\bar{x} - 4\sigma)$ when $\sigma \leq 0.15\,\bar{x}$. No NDP testing

Standard Deviation as Percentage of 0	Percentage of Bonds with Pull Strengths Lying in the Range	
	$(\bar{x} - 3\sigma)$ to 0.9 $(\bar{x} - 3\sigma)$	$(\bar{x} - 4\sigma)$ to 0.9 $(\bar{x} - 4\sigma)$
25	0.038	—
20	0.066	—
15	0.1	2.2×10^{-3}
10	0.12	3.0×10^{-3}
5	0.13	3.2×10^{-3}

[a]This table is calculated on the assumption that the bond pull strengths (excluding freaks, which usually have very low pull strengths) fall approximately within a normal distribution rather than, for example, a bimodal one. If more bonds than predicted have pull strengths falling below that of normal distribution, particularly in the range of 0-3 to $0.9(\bar{x} - 3\sigma)$, then more bonds may be damaged than are indicated in the table, and conversely. Plots of bond data on normal probability paper can be used as a simple means of determining the normality of the distribution (see Sec. 4.2.3) or data entered into a statistical program.

Table 4B-1 Percentage of Bonds in the Inelastic Stress Range[a]

Type of Production	WIRE Composition	Elongation	Relation Between ($\bar{x}$) and σ on the Bond Pull Test	NDP Force Recommendation
Normal	Al	<3%	$(0.25 \leq \sigma > 0.15)\ \bar{x}$	$0.9\ (\bar{x}) - 3\sigma)$
High Rel.	Al	<3%	$\sigma \leq 0.15\ \bar{x}$	$0.9\ (\bar{x}) - 3\sigma)$
All	Al	0.5 to 20%	$\sigma \leq 0.25\ \bar{x}$	$[(\bar{x} - 3\sigma)]/2$
All	Al	>20%	$\sigma \leq 0.25\ \bar{x}$	$[(\bar{x} - 3\sigma)]/3$
All	Au	Use same elongation and σ rules as aluminum, except that the elastic limit is less predictable from one manufacturer to the next.		

TABLE 4B-2 Summary of NDP Force Recommendations Relation

is recommended for cases where $\sigma > 0.25\ \bar{x}$, since this indicates that some aspects of the bonding procedure are out of control and either a low, meaningless NDP force would have to be used or too many bonds would be stressed beyond their elastic limits and/or broken. Table 4B-1 gives a summary of the NDPT recommendations for wire with various elongations.

4B.3 Assessment of Any NDP Test-Induced Metallurgical Defects

During the NDP test, with the NDP force limits derived above, the wire is only subjected to approximately one metallurgical stress-fatigue cycle. Bulk Al and Au will normally withstand hundreds of thousands of such cycles when the stress is kept below the elastic limit. The stress during the NDP test is primarily along the wire; thus, there are essentially no outer-fiber-strains (from bending) in the bond heel area to enhance the probability of unannealable crack formation.

Under these conditions, any stress-fatigue developed below the elastic limits of the bond-loop system during the NDP test should be small. Also, almost all devices whose reliability is critical enough to require NDP tests (usually space applications) will routinely undergo thermal screens, such as burn-in (~125°C for 168 h or equivalent), or such screens could be added if desired. These screens should anneal any threshold level of NDP-test-induced fatigue occurring below the elastic limits, and they can also anneal some, if not all, of the stress-fatigue which might occur above the elastic limit, assuming no crack has formed. Thus, only a small fraction of the NDP-tested bonds, whose breaking strength is in the inelastic stress range of Table 4A-2.1, would retain a significant number of test-induced metallurgical defects after a typical burn-in or other annealing period. Even for a case where a small non-annealable crack remains in the bond heel, it would not

normally be detrimental to the subsequent operating life of the device. A reliability problem would arise only if severe high-frequency vibrations (such as ultrasonic cleaning) were encountered or if the bonds had low loops and were subject to temperature cycling (see Secs. 8.3 and 8.4).

Forty years after the invention of the nondestructive pull test at Autonetics (Rockwell), the idea of the nondestructive pull is still controversial. Some people worry about possible metallurgical damage to the neck or heel of the bond, and others are concerned that the hook might hit and damage an adjacent wire as it is being positioned. (Note discussion of the substitution of SPC during bonding for the NDPT on high pincount packages at the beginning of this section and in Sec. 4B.1.)

At the time of this writing (2008) there have been hundreds of millions of nondestructive wire pull tests performed, [4-57], which have been a requirement for some military and space (K) devices. All of the evidence available indicates that the test is nondestructive. In addition, it has been shown that the NDP test does not lower the bond-force distribution of devices that later undergo the usual military qualification tests of temperature cycle, burn-in, shock, and vibration [4-58]. With regard to damage to adjacent wire bonds (on a single-tier package), a trained operator is less apt to damage a wire with the hook while positioning for a pull than an equivalently trained operator is to misplace or otherwise damage a wire while actually making a bond with a manual bonder. Automatic nondestructive pull testers have been made to specifically avoid touching adjacent wires. In such cases, the hook turns parallel to the wire for placement and then perpendicular to it for pulling. (However, even this is not adequate for fine pitch or packages with bonds in several tiers—where SPC must be used.) The NDPT is often used for automatically testing large diameter wedge bonds in high volume assembly.

The nature of immature and otherwise poorly bonded interfaces has been fully described in Chap. 2. They consist of a series of unconnected microwelds. When an appropriate force is applied, the interface begins to separate, first breaking the microwelds nearest to the bond heel, resulting in a crack. This crack propagates rapidly along the microwelded interface with characteristics similar to those of a (modified) "Griffith crack" and completely breaks the interface within a few milliseconds. If the force is below a threshold value (too low to break the first few microwelds at the heel), then no break or damage occurs to the interface. Thus, the NDP test is largely a go, no-go test, and any possible marginal damage can be assessed by the statistical methods outlined above.

4B.4 Limitations of the NDP Test

Regardless of all of the comments above, the user of NDP-tested devices must be aware of the limitations of this test. The test will only perform one function. It will remove weak, poorly made bonds with pull

forces below the chosen force level at the time the test is performed. There is no assurance against later bond strength degradation due to Au-Al intermetallic and subsequent void formation, ultrasonic-cleaner-induced wire-bond vibration fatigue, or wire-bond flexure fatigue due to temperature or power cycling, etc. Such possible failure mechanisms are described elsewhere in this book (see Chaps. 5, 7, and 8).

The effect of post-NDP-test screens and environments on bonds should be thoroughly understood by the device user. These are discussed elsewhere in this book. In some cases, the devices could be chosen or designed to minimize post-NDP-test degradation, such as using monometallic wire and bond-pad systems and using high bond loops. The NDP test, as well as the destructive pull test, is not appropriate for screening the quality of ball bonds. The welded area of a ball bond would have to be less than the cross section of the wire to fail during a standard NDP test [pulled at 3 gf for a 25 μm (1 mil) diameter wire]. This could only happen if the bonding process were completely out of control.

4B.5 The Current Status of the NDPT (2008) for Critical Space Applications

The NDPT is expensive and costs about as much as manually making the bonds in the first place—and much more if the bonds were made on an autobonder and NDP tested manually. Therefore, the NDPT is performed only on critical high-reliability military or class K for space (equivalent) and some implanted medical devices. Currently, there is pressure to reduce costs of all systems, military and commercial, and the NDPT is an area of concern. In addition, with the introduction of fine-pitch, costs and time as well as mechanical problems in implementing the NDPT tend to reduce its use. The chosen approach for critical military and space applications (with limitations) is to use statistical process control for devices with more than 84 terminations and package-pad-pitch of ≤305 μm (12 mils) (see MIL-STD-883G/H, Method 2023.5, paragraph 3.2). This specification is adequate to serve as an alternative to the NDPT. There is no mention of multitiered packages, which are a primary NDPT problem, as well as the chip pad fine pitch. The entire procedure depends upon the bond pull test for both Al wedge and Au ball bonds; thus, there is no ball-shear test evaluation required for SPC of ball bonds. [Note, the JEDEC Shear test is now (2008) called out in MIL-STD-883G/H, [4-7] and hopefully, this will also be added to any SPC requirements.]

The difficulty of performing the NDPT under multitiered and/or fine-pitch (<150 μm on the package and ~60 μm on the chip) conditions is real, and the above (Method 2023) is helpful. However, the problem with any SPC approach is that one must choose which parameters to control and how to measure them. There are few specific details given in this test method. Cleaning with UV-ozone, plasma, or with

unspecified solvents (see Chap. 7) is given as an option rather than a requirement. Normal distributions are assumed, but may not exist in many devices. In addition, many space parts are still made in small numbers on manual bonders, but need wirebond yield loss and failure rates to be in the low ppm (near 4.5 σ) range. Any statistical monitoring system will, of necessity, have to assume normal distributions, but most bond failures in a well-controlled high yield process are better described as "freaks" or "outliers" (see discussion in Sec. 9.4 on small-sample statistics). Assessment of process capability depends on the normality of the underlying failure mode distribution. If different simultaneous failure modes are present, then it is unlikely that the normality assumption will be fulfilled, and estimates of product quality based on the expected failure mode will not necessarily reflect the true defect levels in devices. Thus, it is not clear that the chosen SPC approach and variables will yield the bond quality essential for high reliability in the small quantities of individual devices or SIPs needed for typical satellite or other space applications. The most encouraging aspect of current bonding technology is that modern autobonders make very reproducible bonds in high volume production. Unless there is a metallization or cleaning problem, the bonds made will be more uniform and reliable than obtainable with manual bonders. If plasma or UV-ozone cleaning were added to the SPC preparation, then that condition would be adequate for high-reliance use.

References

4-1 ASTM, 100 Barr Harbor Drive, West Conshohocken, Pennsylvania, 19428–2959. [ASTM Standard Test Methods with Round Robin test verifications: F 459-06 (Pull Test), and F 1269–06 (Ball shear test).]

4-2 JEDEC, 2500 Wilson Blvd., Suite 220, Arlington, VA 22201–3834, USA.

4-3 Schafft, H. A., Testing and Fabrication of Wire-Bond Electrical Connections—A Comprehensive Survey, National Bureau of Standards Tech. Note 726, Sept. 1972.

4-4 Albers, J. H., Ed., "Semiconductor Measurement Technology. The Destructive Bond Pull Test," *NBS Spec.*, Pub. 400–18, Feb. 1976.

4-5 Harman, G. G. and Cannon, C. A., "The Microelectronic Wire Bond Pull Test, How to Use It, How to Abuse It," *IEEE Trans. on Components, Hybrids, and Manufacturing Technology CHMT-1*, Sept. 1978, pp. 203–210.

4-6 John Beleran, Alejandro Turiano, Dodgie R. M. Calpito, Dominik Stephan, Saraswati, Frank Wulff, Breach, C., "Tail Pull Strength of Cu Wire on Gold and Silver-plated Bonding Leads," Proc. Semicon, May 4–6, 2005, Suntech Center, Singapore.

4-7 MIL-STD-883G, 28 February 2006, Test Methods and Procedures for Microelectronics, and MIL-PRF-38534F, 2006. (Both have been revised in version "H" November 2008 in Initial Draft of MIL-STD-883, Revision H.

4-8 Owens, N. L., "Wire Pull and Normality Assumptions," *9th Ann. Proc. IEPS*, San Diego, California, Sept. 11–13, 1989, pp. 595–601.

4-9 Harman, G. G., Ed., "Semiconductor Measurement Technology. Microelectronic Ultrasonic Bonding," *NBS Spec.*, Pub. 400–2, Jan. 1974.

4-10 Harman, G. G., "The Use of Acoustic Emission as a Test Method for Microelectronic Interconnections," *Proc. International Conference on Soldering and Welding in Electronics*, Munich, Germany, Nov. 11–12, 1981, pp. 104–110.

4-11 Harman, G. G., "The Microelectronic Ball-Bond Shear Test - A Critical Review and Comprehensive Guide to Its Use," *The Int. J. Hybrid Microelectronics*, 6, 1983, pp. 127–141. Also pub. in *Solid State Tech.*,Vol. 27, May 1984, pp. 186–196.
4-12 Stafford, J. W., "Reliability Implications of Destructive Gold-Wire Bond Pull and Ball Bond Shear Testing," *Semiconductor International*,Vol. 5, May 1982, pp. 83–90.
4-13 Arleth, J. A. and Demenus, R. D., "A New Test for Thermocompression Microbonds," *Electronic Products*, Vol. 9 May 1967, pp. 92–94.
4-14 Gill, W. and Workman, W., "Reliability Screening Procedures for Integrated Circuits," *Physics of Failure in Electronics* ,Vol. 5, *RADC Series in Reliability*, Shilliday, T. S., and Vaccaro, J., Eds., June 1967, pp. 101–142.
4-15 Jellison, J. L., "Effect of Surface Contamination on the Thermocompression Bondability of Gold," *Proc. 28th IEEE Electronic Components Conference*, Washington, D.C., May 11–12, 1975, pp. 271–277; also *IEEE Trans. on Parts, Hybrids, and Packaging* Vol. 11, 1975, pp. 206–211.
4-16 Jellison, J. L., "Kinetics of Thermocompression Bonding to Organic Contaminated Gold Surfaces," *Proc. 29th IEEE Electronics Components Conf.*, San Francisco, California, Apr. 26–28, 1976, pp. 92–97; also *IEEE Trans. Parts, Hybrids, and Packaging* Vol. 13, 1977, pp. 132–137.
4-17 Shimada, W., Kondo, T., Sakane, H., Banjo, T., and Nakagawa, K., "Thermo-Compression Bonding of Au-Al System in Semiconductor IC Assembly Process," *Proc. Int. Conf. on Soldering, Brazing, and Welding in Electronics*, DVS, Munich, Germany, Nov. 25–26, 1976, pp. 127–132.
4-18 Thompson, R. J., Cropper, D. R., and Whitaker, B. W., "Bondability Problems Associated with the Ti-Pt-Au Metallization of Hybrid Microwave Thin Film Circuits," *IEEE Trans. on Components, Hybrids, and Manufacturing Technology,* Vol. 4 1981, pp. 439–445.
4-19 Panousis, N. T. and Fischer, M. K. W., "Non-Destructive Shear Testing of Ball Bonds," *Intl. J. Hybrid Microelectronics,* Vol. 6, 1983, pp. 142–146.
4-20 Charles, H., Johns Hopkins University, Applied Physics Laboratory, private communication.
4-21 Jellison, J. L. and Wagner, J. A., "The Role of Surface Contaminants in the Deformation Welding of Gold to Thick and Thin Films," *Proc. 29th IEEE Electronics Components Conference*, Cherry Hill, New Jersey, May 14–16, 1979, pp. 336–345.
4-22 St. Pierre, R. L. and Reimer, D. E., "The Dirty Thick Film Conductor and Its Effect On Bondability," *Proc. 25th IEEE ECC,* 1976, pp. 98–102.
4-23 Johnson, K. I., Scott, M. H., and Edson, D. A., "Ultrasonic Wire Welding, Part II, Ball-Wedge Wire Welding," *Solid State Technology* Vol. 20, 1977, pp. 91–95.
4-24 Schultz, G. and Chan, K., "A Quantative Evaluation of Compound Ball Bonds," *Proc. Intl. Symposium on Microelectronics (ISHM*), Seattle, Washington, Oct. 12–19, 1988, pp. 238–245. Also, for the use of stacked bumps for flip chip see: Suwa, M., Takahashi, H., Kamada, C. and Nishiuma, M.," Development of a New Flip-Chip Bonding Process using Multi-Stacked μ-Au Bumps," *Proc. 44th Electronic Components and Technology Conference*, Washington, D.C., May 1–4, 1994, pp. 906–909.
4-25 Ramsey, T., Alfaro, C., and Dowell, H., "Metallurgy's Part in Gold Ball Bonding," *Semicon. Intl.*, Vol. 14, no. 5, Apr. 1991, pp. 98–102.
4-26 Data abstracted and summarized from SEMATECH machine benchmarking studies, Used with permission.
4-27 Jaecklin, V. P., "Room Temperature Ball Bonding Using High Ultrasonic Frequencies," *Proc. Semicon Test, Assembly & Packaging*, May 2–4, 1995, pp. 208–214.
4-28 Leonhardt, D. A., "Ultrafine Pitch Gold Ball Bonding," *Semiconductor International*, Vol. 19, July 1996, pp. 311–318.
4-29 Philofsky, E., "Purple Plague Revisited," *Solid-State Electron*, Vol. 13, 1970, pp. 1391–1399.
4-30 Kashiwabara, M. and Hattori, S., "Formation of Al-Au Intermetallic Compounds and Resistance Increase for Ultrasonic Al Wire Bonding," *Review of the Electrical Communication Laboratory (NTT)*, Vol. 17, Sept. 1969, pp. 1001–1013.

4-31 Clatterbaugh, G. V., Weiner, J. A., and Charles, H. K., Jr., "Gold-Aluminum Intermetallics: Ball Bond Shear Testing and Thin Film Reaction Couples," *IEEE Trans. on Components, Hybrids, and Manufacturing Technology* Vol. 7, 1984, pp. 349–356. Also see earlier publications by Charles and Clatterbaugh, *Int. J. Hybrid Microelectronics*, Vol. 6, 1983, pp. 171–186.
4-32 Devaney, J. R. and Devaney, R. M., "Thermosonic Ball Bond Evaluation by a Bond Pluck Test," *Proceedings ISTFA Conference*, Los Angeles, California, 1984, pp. 237–242.
4-33 White, M. L., Serpiello, J. W., Stringy, K. M., and Rosenzweig, W., "The Use of Silicone RTV Rubber for Alpha Particle Protection on Silicon Integrated Circuits," *19th Annual Proc., Reliability Physics* , Orlando, Florida, Apr. 7–9, 1981, pp. 43–47.
4-34 Michaels, D., Burroughs Corp. (UNISYS), comments made at ASTM Committee F-1 Meeting, San Diego, California, Feb. 1–2, 1983.
4-35 Weiner, J. A., Clatterbaugh, G. V., Charles, H. K., Jr., and Romenesko, B. M., "Gold Ball Bond Shear Strength, Effects of Cleaning, Metallization, and Bonding Parameters," *Proc. 33rd IEEE Electronics Components Conf.*, Orlando, Florida, May 16–18, 1983, pp. 208–220.
4-36 Sheaffer, M. and Levine, L., "How to Optimize and Control the Wire Bonding Process: Part 1," *Solid State Technology*, Vol. 33, Nov. 1990, pp. 119–123, and Part 2, Vol. 34, Jan. 1991, pp. 67–70.
4-37 Hu, S. J., Lim, G. E., Lim, T. L., and Foong, K. P., "Study of Temperature Parameter on the Thermosonic Gold Wire Bonding of High Speed CMOS," *IEEE Trans. On CHMT*, Vol. 14, Dec. 1991, pp. 855–858.
4-38 Chen, Y. S. and Fatemi, H., "Gold Wire Bonding Evaluation By Fractional Factorial Designed Experiment," *Int. J. Hybrid Microelectronics*, Vol. 10, Number 3, 1987, pp. 1–7.
4-39 Charles, H. K. and Clatterbaugh, G. V., "Ball Bond Shearing - A Complement to the Wire Bond Pull Test," *Intl. J. Hybrid Microelectronics,* Vol. 6, Oct. 1983, pp. 171–186.
4-40 Basseches, H. and D'Altroy, F., "Shear Mode Wire Failures in Plastic-Encapsulated Transistors," *IEEE Trans. Components, Hybrids, Manufacturing Technology,* Vol. 1, 1978, pp. 143–147.
4-41 Shell-De Guzman, M., Mahaney, M., and Strode, R., "The In-Process Bond Shear Test: Its Relationship to Ball Bond Reliability and Its Application to the Reduction of Wirebond Process Variation," *Microelectronics Reliability*, Vol. 33, No. 11/12, 1993, pp. 1935–1946. Also, see Mahaney, M., Shell, M. K., and Strode, R., "Use of the In-process Bond Shear Test for Predicting Gold Wirebond Failure Modes in Plastic Packages," *29th Proc. IRPS*, 1991, pp. 44–51.
4-42 Clarke, R. A. and Lukatela, V., "Inadequacy of Current MIL-STD Wire Bond Certification Procedures," *Intl J. Microcircuits & Electronic Packaging*, Vol. 15, 1992, pp. 87–96.
4-43 Pantaleon R. and Manolo, M., "Rationalization of Gold Ball Bond Shear Strengths," *Proc. 44th Electronic Components & Technology Conference*, Washington, D.C., May 1–4, 1994, pp. 733–740.
4-44 NBS Special Publication 400-19, Semiconductor Measurement Technology Quarterly Report, January 1 to June 30, 1975, Bullis, W. M., Ed., April 1976, p. 51. The NBS portion of the work was done by G. G. Harman and C. A. Cannon and the Sandia portion by W. Vine.
4-45 Levine, L., "Should We Pull Test and Shear Test Fine-Pitch Wedge and Ribbon Bonds?" *Chip Scale Review*, May/June 2003, pp. 13.
4-46 Kim, Y-G., Pavuluri, J. K., White, J. R., B-Vishniac, I. J., and Masada, G. Y., "Thermocompression Bonding Effects on Bump-Pad Adhesion," *IEEE Trans CPMT-Part B*, Vol. 18, Feb. 1995, pp. 192–200.
4-47 Charles, H. K.," Ball Bond Shear Testing: An Interlaboratory Comparison," *Proc. 1986 Intl Symp. for Microelectronics (ISHM)* , Atlanta, Georgia, Oct. 6–8, 1986, pp. 265–274.
4-48 Kumar, S., Florendo, M, Dittmer, K., "A Wire Bond Process Optimization Strategy for Very Fine Pitch Development," *Proceedings of Assembly Seminar, Semicon Singapore Conference*, Singapore, 1999, pp. 67–75.

4-49 Horsting, C. W., "Purple Plague and Gold Purity," *10th Annual Proc. IEEE Reliability Physics Symposium*, Las Vegas, Nevada, Apr. 5–7, 1972, pp. 155–158.
4-50 Ebel, G. H.," Failure Analysis Techniques Applied in Resolving Hybrid Microcircuit Reliability Problems," *15th Annual Proceedings Reliability Physics*, Las Vegas, Nevada, Apr. 12–14, 1977, pp. 70–81.
4-51 Polcari, S. M. and Bowe, J. J., "Evaluation of Non-Destructive Tensile Testing," *Report No. DOT-TSC-NASA-71-10*, June 1971, pp. 1–46.
4-52 Ang, C. Y., Eisenberg, P. H., and Mattraw, H. C., "Physics of Control of Electronic Devices," *Proc. 1969 Annual Symposium on Reliability*, Chicago, Illinois, Jan. 1969, pp. 73–85.
4-53 Slemmons, J. W., "The Microworld of Joining Technology," *The American Welding Society 50th Annual Meeting, Proceedings*, Philadelphia, Pennsylvania, Apr. 1969, pp. 1–48.
4-54 Bertin, A. P., "Development of Microcircuit Bond-Pull Screening Techniques," *Final Technical Report RADC-TR-73-123,* Apr. 1973, AD762–333.
4-55 MIL-STD-883G/H, 28 February 2006 and Initial Draft of MIL-STD-883, Revision H,, November 2008; Test Methods and Procedures for Microelectronics, and MIL-PRF-38534F, 2006.
4-56 Harman, G. G., "A Metallurgical Basis for the Non-Destructive Wire-Bond Pull-Test," *12th Annual Proc. IEEE Reliability Physics*, Las Vegas, Nevada, Apr. 2–4, 1974, pp. 205–210.
4-57 Roddy, J., Spann, N., and Seese, P., *IEEE Trans. on Components, Hybrids, and Manufacturing Technology*, Vol. 1, Sept. 1978, pp. 228–236.
4-58 Blazek, R. S., "Development of Nondestructive Pull Test Requirements for Gold Wires on Multilayer Thick Film Hybrid Microcircuits," *IEEE Trans. on Components, Hybrids, and Manufacturing Technology,* Vol. 6, Dec. 1983, pp. 503–509.

This page intentionally left blank

CHAPTER 5

Gold-Aluminum Intermetallic Compounds and Other Metallic Interface Reactions in Wire Bonding

5.1 Gold-Aluminum Intermetallic Compound Formation and Classical Wire-Bond Failures

5.1.1 Introduction

Gold-aluminum intermetallic compound formation and associated Kirkendall voids have resulted in more documented wire-bond failures than any other problem over the years. There have been hundreds of papers on this subject, and this chapter can only present an overview of them. Modern packaging and device environments do not (or need not) involve the high temperatures (≥300°C) that produced most of the classical failures. The compounds are typically referred to as "purple plague (the Al-rich phase)." This term comes from the characteristic color of the $AuAl_2$ intermetallic compound that often occurs around the perimeter of an Au bond on an Al pad. (Such colored intermetallic compounds are quite commonly found in metallurgy, and, as an example, Au and In also form a purple-colored intermetallic compound.) Most present day Au-Al related failures are

more properly referred to as impurity-driven or corrosion reactions. These are discussed in Sec. 5.2, but an understanding of the classical failures is essential to comprehend the nature of present day ones.

The most definitive early work on Au-Al compounds, oriented toward microelectronic bonding was done by Philofsky [5-1, 5-2, 5-3], and those interested in more details are referred to his publications. The compounds will occur in the bonded interface between Au wire and Al metallization, and vice versa. Such compounds begin to form during the actual process of Au-Al thermosonic or ultrasonic bonding. (It is considered to be a necessary part of the Au-Al bonding/welding mechanism.) The compounds will continue growing during the cure of plastic molding compounds (typically at 175°C for 3 to 5 h) and grow during qualification screening (burn-in, stabilization bakes), or at any time when high temperatures are encountered during the life of the device. A few monolayers of such compounds will even form at room temperature if clean metal surfaces are brought into intimate contact (such as evaporated films).

Even though Au-Al intermetallics have been associated with many bond failures, and many people are *"frightened to death of them,"* the fact is they are always present in Au-Al bonded interfaces. While they are considered to be the basis for Au-Al bonding, ultrasonic welding certainly does take place in monometallic Au-Au and Al-Al bonds. Ramsey [5-4] has studied this phenomenon in Au-Al wire bonding and first reported that the compounds appear during the actual bonding process. Approximately 95% of all IC devices have Au-Al bonding, are plastic encapsulated and, in the resin curing process, are subjected to the above high temperatures. This curing can drive the initial intermetallics completely through some thin Al bond pads. Thus, the IC industry has learned to live with plague. Bond failures usually occur because of impurities in the bond interface (or in the plastic encapsulant), poor welding (which produces isolated micro-welds, see App. 5A), and/or extreme thermal exposure.

Wire bonds are made both to and with non-Au or Al metals. Depending on the possible metallic alloys, these also may develop various intermetallic compounds in the interface, and are discussed below (see Sec. 5.3). These include several noble metals, such as Pd, as well as Ni and Cu.

5.1.2 Intermetallic Compound Formation in the Au-Al System

There are five Au-Al intermetallic compounds, as shown in the phase diagram of Fig. 5-1 [5-5]. These are Au_5Al_2, Au_4Al, Au_2Al, $AuAl_2$, and AuAl. We note that recent interpretation of crystal structure has changed the designation of Au_5Al_2 used in the past, to Au_8Al_3 [5-6]. This chapter has retained the older designation since the early quoted works/figures use it, and using both in the same chapter would be

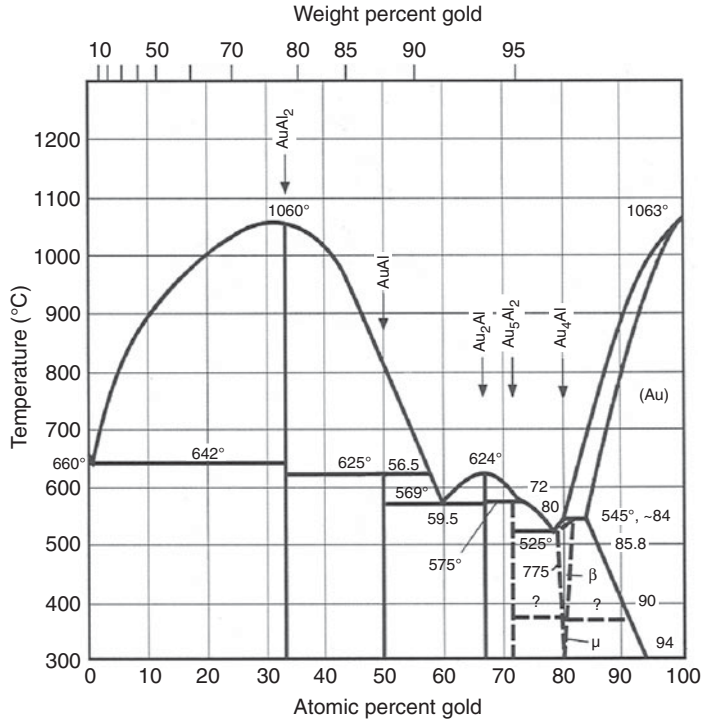

Figure 5-1 Aluminum-gold phase diagram with the five Au-Al intermetallic compounds indicated. (*After Hansen [5-5].*) Note that this is an older diagram and is retained because it is easier to read and identify the intermetallic compounds. Newer versions show them broadened and split into α and β phases. These complicate reading the display and offer little additional knowledge for bond reliability. Metallurgists are referred to the ASM Alloy Phase Diagrams Center Web site. It also has extensive explanations of phase diagrams for those not familiar with them.

confusing. The small difference would not affect understanding of bonding problems, nor would the broadening of the intermetallic lines as shown in recent phase diagrams. We also retain the Au in first position, which is reversed in some modern metallurgy texts (Al first), for the same reasons.

These compounds, as with many other intermetallics, are colored, with $AuAl_2$ being purple (*purple-plague* gets its name from this one) with the rest being tan or white, as indicated in Fig. 5-2. Since the phases are usually mixed in a bond interface, the observed color is often gray, brown, or black. The Al-rich $AuAl_2$ compound has a high melting point and, therefore, is relatively stable (once formed). In general, however, under continued thermal exposure, diffusion continues (especially through the low melting-point compounds) until all of the Au or the Al is reacted. (See App. 5B, Noolu, for some interdiffusion

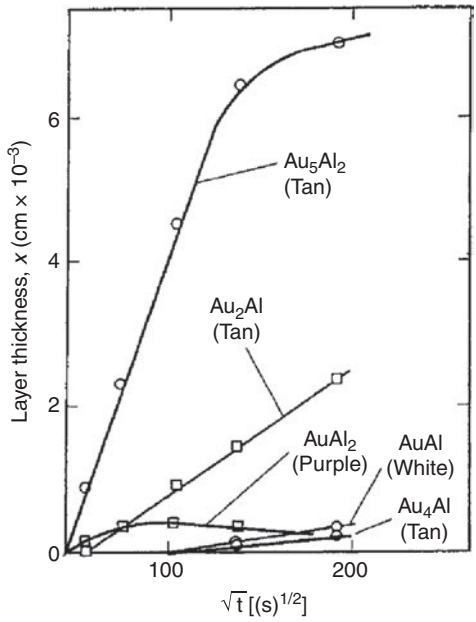

Figure 5-2 Layer thickness of the five Au-Al intermetallic phases versus the square root of time at 400°C. Data were obtained on large butt-welded couples having unlimited and equal supplies of Au and Al. (*After Philofsky [5-1] ; © 1970, with permission from Elsevier.*) Note that generally a 1 μm Au ball-bonded Al pad will completely convert into intermetallic in 24 h at 175°C. See App. 5B for a table of conversion times and temperature versus Al thickness.

and failure modes of such compounds related to cell volume changes as the compounds continue to diffuse.)

After this, there can be a rearrangement toward the excess metal-rich compounds (Au-rich in the case of a ball bond on thin Al metallization). But, in general, the reaction slows, as was demonstrated by the ball-shear test shown in Fig. 4-17 of Chap. 4.

Observations suggest that the initial growth rate of the intermetallic compounds usually follows a parabolic relationship

$$x = K\,t^{1/2} \tag{5-1}$$

where x is the intermetallic layer thickness, t is the time, K is the rate constant, and

$$K = C\,e^{-E/KT} \tag{5-2}$$

where C is a constant, E is the activation energy for layer growth (in electron volts), k is the Boltzmann constant, and T is the absolute

temperature (in Kelvins).* The value of K changes for each intermetallic phase, and is also dependent upon the neighboring phases, which supply additional Au and Al for continued compound formation.

Because of this, Philofsky lists nine different rate constants for the five Au-Al compounds. Figure 5-2 shows the relative rates of intermetallic formation. From this, it is apparent that Au_5Al_2 grows much faster than the other phases. (Because of this, it is also the phase most often cited as resulting in Kirkendall voiding and bond failures.)

The mechanical properties of the five compounds differ among themselves and vary widely from those of the Au and Al. The crystallographic lattice constants are larger (see Table 5-1), so they occupy a larger volume, and thus, plagued bonds often appear to be lifted up. The thermal expansion coefficients are considerably lower for the compounds than for either Au or Al, and some reliability implications for both of these differences are discussed in Noolu's App. 5B of this chapter. Temperature cycling can be used to reveal potential failures† resulting from these property differences [5-7].

The compounds are also much harder (and more brittle), so, plagued bonds can crack during temperature cycling or other stresses. Some detailed properties of these Au-Al compounds are given in Table 5-1.

The rate of diffusion of one metal into the other (or into itself) is dependent on the number of defects in the crystal lattice. Defects can be vacancies, dislocations, and grain boundaries. During diffusion, one atom moves into an empty lattice position (vacancy), and another atom moves into the empty position of the first. Grain boundaries and surfaces, because the lattice has more open structures, have many vacancies and they increase the diffusion rate by orders of magnitude compared to diffusion in the bulk or a single crystal. Poorly welded bonds consist of numerous isolated microwelds which contain large surface area-to-volume ratios, as well as mechanical stresses that result in numerous lattice defects. Thick-film metallizations also contain many grain boundaries, stresses, and impurities, all of which result in lattice defects. Thus, it is not surprising that poorly welded bonds or Al-wire bonds to thick films fail rapidly, see App. 5A for a discussion on this problem.

A generic activation energy, E (one that combines the effects of all five compounds and/or Kirkendall voids), for various bond failures is often measured by workers. As a result, the literature abounds with different values of (E) for various properties thought to be related to

---

*In chemical or metallurgical literature, one often sees the equation written as: $K = C \exp(-Q/RT)$, where Q is the activation energy in kilocalories/mole (1 eV ≈ 23 K). Cal/mole), R is the gas constant (1.98), and T = temperature in Kelvins.

†Intermetallic problems were revealed in plastic encapsulated devices in several hundred temperature cycles from −40 to 140°C (1% cumulative failures occurred at 300 cycles, and 2% at 800). Four times as many cycles were required for 0 to 125°C testing.

Phase	Structure	Lattice Parameters (Å)	Composition at % Au	Vicker's Hardness (5 Kg)	Specific Resistance (Ohm–cm)	Coefficient of Linear Expansion (10^{-5})	Color of the Phase	Heats of Formation at 400K (cal +/–500)
Au	FCC	a = 4.08	84–100	60–90	2.3	1.42	Gold	
Au_4Al	Cubic	a = 6.92	80–81.2	334	37.5	1.2	Tan	
Au_8Al_3 Au_5Al_2	Rhombohedral	a = 14.68, α = 30.5	72.7	271	25.5	1.4	Tan	
	HCP	a = 7.71 c = 41.9						
Au_2Al	Orthorhombic	A = 3.36 B = 8.84 C = 3.21	65–66.8	130	13.1	1.3	Tan	–8300
AuAl	Monoclinic	A = 6.40 B = 3.33 C = 6.32 β = 92.99	50	249	12.4	1.2	White	–9200
$AuAl_2$	FCC	A = 5.99	32.33 –33.92	263	7.9	0.94	Purple	–10100
Al	FCC	A = 4.05	0–0.6	20–50	3.2	2.3	Lustrous	

[a]See Refs [5-102 to 5-104]
Note: This figure was assembled by N. Noolu, see App. 5B.

TABLE 5-1 Structure and Properties of Au-Al Intermetallic Compounds[a]

intermetallic-compound formation. A compilation of activation energies [5-8] reported for various types of Au-Al wire-bond failures is given in Table 5-2. It is not possible to explain the wide variation in values, except that the measurements were made by different methods and were not necessarily related to the same type or definition of failure. Different metallurgical couples were used (Al wire bonded to various Au films, Au wire to various IC metallizations) resulting in Al- or Au-rich couples (see reversing metallurgical interfaces, Sec. 5.1.4). Also, some activation energies reported for bond failures may have resulted from impurities in the interface or from poor welds as in App. 5A.

The diffusion coefficient has not been discussed above. However, it determines the actual rate of diffusion and varies considerably, depending on whether that diffusion proceeds via grain boundary or bulk (interdiffusion). It is also dependent on the number of defects

References	Specimen	Observed Quantity	Activation Energy
8	Au-Al-films	Au-Al-growth rate	1 eV
9	Au-Al-films	Sheet resistance	1 eV
10, 11	Au-Al-wire couples	Au-Al-growth rate	0.78 eV
1	Au-Al-wire couples	Au-Al-growth rate	0.69 eV
2	Au-Al-wire couples	Mechanical degradation	1 eV
12	Au-wire, Al-film	Au-Al-growth rate	0.88 eV
13	Au-wire, Al-film (1.4 μm) on Ta	Contact resistance, $\Delta R = 50\%$	0.55 eV
13	Au-wire, Al-film <0.3 μm 0.5, 1 μm	Contact resistance, $\Delta R = 1\ \Omega$ Contact resistance, $\Delta R = 1\ \Omega$ Pull strength (time to failure)	0.7 eV 0.9 eV 0.2 eV
16	Al wire, Au-film	Resistance drift to $\Delta R = 15\ m\Omega$	0.73 eV
8	Au-balls, Al-films 1 μm, Al-Si 1.3 μm, Al 2.5 μm, Al	Resistance (peripheral voiding)	0.9 eV ≥0.8 eV 0.6 eV
14, 15	Au-balls, Al-film	Ball shear strength	0.4 to 0.56 eV

(After Gerling [5-8] with later additions; © IEEE.)

Table 5-2 Various Thermal Activation Energies Reported for Bond Failures and Growth of Au-Al Compounds

available (the more defects, the faster diffusion proceeds). Aluminum and other metals diffuse very rapidly into Au by grain-boundary diffusion. A discussion of this is given in Sec. 6A.4. It should be noted that the specific intermetallic compounds in a bond-interface area are related to the relative amounts of Au and Al present and can be different if Al metallization contains Cu or Si in the 1 to 2% level. In addition, some compounds may be absent because of a low nucleation probability (they do not get started) or they may grow very slowly and are not observed.

Figure 5-3 gives the compounds observed to form in Au- and Al-rich areas, and in areas with Au and Al in equal amounts [5-17]. One of the consequences of the change in specific compounds shown in Fig. 5-3 is the accompanying intermetallic cell volume change. Each compound occupies a different volume, and as the changes occur, stresses may lead to cracks and ultimately result in bond failure.

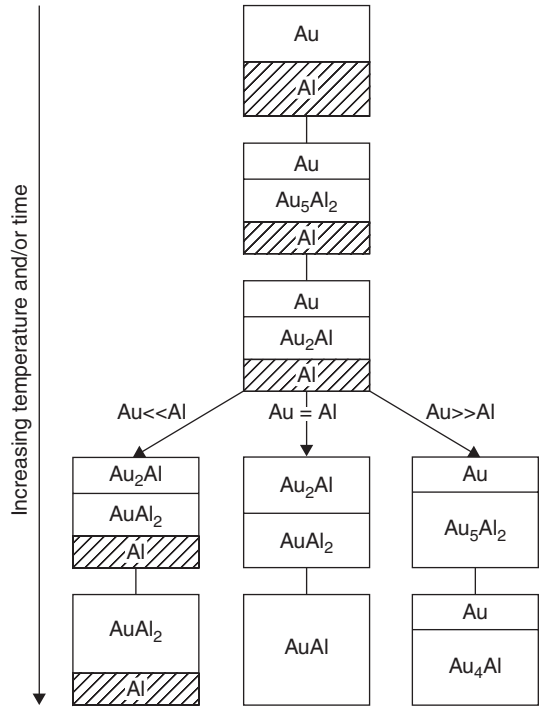

Figure 5-3 Schematic representation of compound formation in gold-aluminum thin-film systems. The identity of the final compounds is determined by the annealing temperature and by the proportions of the starting materials. The final compounds result from the reaction being driven to completion (stability), with one component being completely consumed. This occurs only after long times at high temperatures. (*After Majni [5-17]*; *© 1970, with permission from Elsevier.*) Note that these compound changes are accompanied by volume changes that can cause stress and bond failure, see App. 5B.

Noolu studied these volume transformations during Au-Al phase changes. The essence of his work on intermetallics is that there are major differences in the five intermetallic lattice sizes. During thermal stress, a specific compound may transform into other compounds. In most cases the second compound is smaller or larger (by up to ~20%) than the first, and leaves cracks or stress behind. Once formed, a crack can propagate during temperature cycling. Also excess Al or Au can be released (or absorbed) as the compounds change. See the Noolu's App. 5B for a description of this phenomena.

Silicon may form ternary compounds with Au and Al, but, as shown by Philofsky, these are no more detrimental to bond quality than the pure Au-Al compounds by themselves, and, in some cases, may be helpful.

These intermetallic compounds are not the normal cause of failure. They are mechanically strong (although brittle) and electrically conductive. Bond failures result from the formation of Kirkendall voids, as well as from the susceptibility of Au-Al couples to degradation by impurities or corrosion. The latter two causes are extensively discussed in following sections. Kirkendall voids form when either the Al or Au diffuses out of one region faster than it diffuses in from the other side of that region. Vacancies pile up and condenses to form voids, normally on the Au-rich side along the Au_5Al_2-to-Au interface. The rates of diffusion vary with temperature and with different phases and are dependent upon the adjacent phases, as well as the number of vacancies in the original metals.

Classical Kirkendall voids require bake times greater than an hour at temperatures greater than 300°C to occur on the Au-rich side (Au_5Al_2), and greater than 400°C on the Al-rich side ($AuAl_2$), or much longer times at lower temperatures [5-2, 5-3]. Such temperatures and times are seldom reached during modern bonding or modern device and systems packaging. Thus, it is rare that well-made bonds on integrated circuits used in normal environments actually fail due to the formation of *classical* Kirkendall voids. However, the failures resulting from impurities (see Sec. 5.2), poor welding (see App. 5A), hydrogen, or other defects in plated Au layers (see Chap. 6) can appear to have resulted from classical Kirkendall voiding. Thus, it is essential to understand the classical failure modes.

5.1.3 The Classical Au-Al Compound Failure Modes

An example of Au-Al compound formation is shown in Fig. 5-4. Here, a poorly formed ball-bond was subjected to high temperature, and the reaction generated considerable intermetallic compound. This particular bond was both electrically conductive and mechanically strong (as later shown by a ball-shear test). Thus, the presence of these compounds will not necessarily cause bonds to fail. However, even if such bonds do not fail, the interface strength does degrade. The typical degradation of

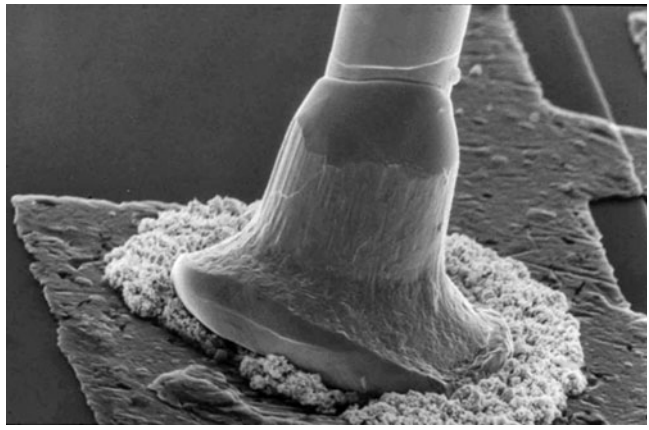

Figure 5-4 An SEM photograph of Au-Al intermetallic compound formation (white and fluffy) around the perimeter of the bond and under the grossly deformed ball. Even with its poor appearance, the bond was mechanically strong and electrically conductive.

the Au-Al ball bond interface during high-temperature storage has been studied [5-18]. Strong Au ball-bonds were made to Al integrated-circuit metallization and then put on temperature test at 200°C for 2688 h. The degradation of the interface was observed by monitoring the ball-shear force at various time intervals. These data were replotted in Fig. 4-17 in Chap. 4. The bond interface strength decreased by a factor of 2.5, presumably due to brittle Au-Al intermetallic formation and some Kirkendall voiding. However, the voiding was not sufficient to impair the electrical operation of the device for this period and temperature. This work demonstrates that when the available constituents are converted into the intermetallic compound, the process slows down. Thus, well-made Au ball-bonds on thin-film Al pads, without impurities in their interfaces, can be reliable during short-to-medium-term exposure to high temperatures.

There are three classical bond-failure modes associated with the formation of Au-Al intermetallics. In the first, the bond may be mechanically strong, but can have a high-electrical resistance or may even be open-circuited. In this case, which typically occurs with Au wire-bonded to thin Al bond pad, Kirkendall voids form around the bond periphery restricting the available electrical conduction path. The voids are indicated by the arrows in Fig. 5-5 and, as another example, clearly around the perimeter in Fig. 5-6. The resistance change results in device failure when it increases enough to drive the circuit out of its electrical specification range. An example of this resistance increase, as a function of time and temperature, is given in Fig. 5-7. Initially, the resistance of the Au ball bonds to the Al pads was a few milliohms. However, the compounds have a higher resistivity

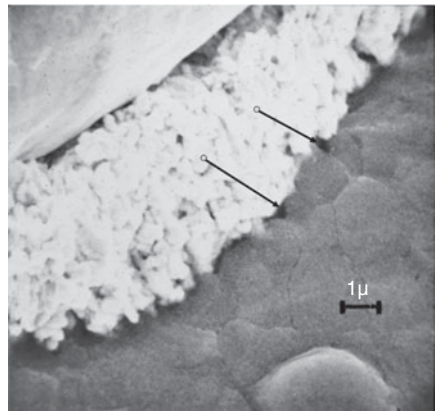

Figure 5-5 An SEM photograph of an Au wire wedge-bond to Al metallization, aged at 450°C for 10 min, illustrating the voids, indicated by arrows, which form around the periphery of the bond. (*After Philofsky [5-1, 5-2]; © 1970, with permission from Elsevier.*)

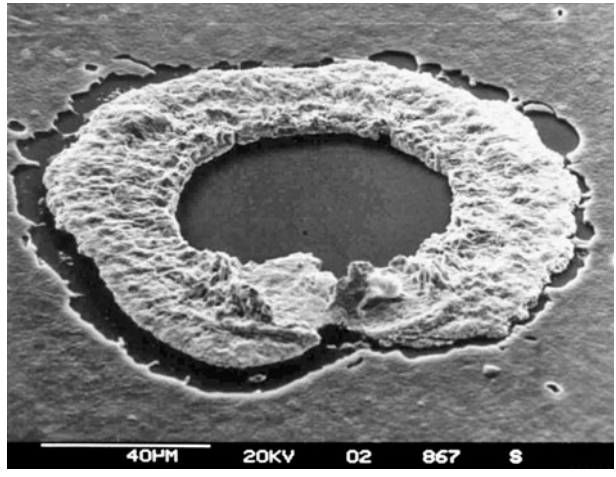

Figure 5-6 A closeup of "ultimate" Kirkendall voids around the perimeter. The gold ball bond was in the center. It dewetted after thermal stress and fell off. (*After Gerling [5-8].*)

than either Au or Al; thus, as the compounds form under the bond (during the first hundred hours or so) the initial resistance increases by about 8 mΩ [5-15]. This initial resistance increase (< 1000 h) had an activation energy of 0.4 eV.* Such slight increases are not accompanied

*This reported activation energy for initial resistance increase is lower than others reported in Table 5-12 but this author (GGH) considers the lower value, resulting from a well-designed experiment to specifically study this increase, to be more accurate.

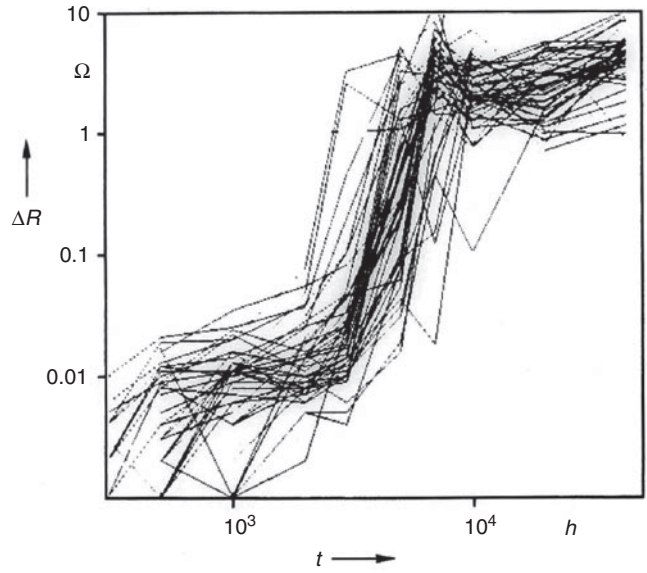

Figure 5-7 The change in contact resistance of multiple Au ball bonds on 1.3 μm Al pads as a function of time at 200°C. The initial bond resistance was a few milliohms. (*After Gerling [5-8]; © IEEE.*)

by Kirkendall voids, pose no reliability hazards, and, in fact, are always present during TS bonding and increase after burn-in or any plastic encapsulation-curing process.

The second resistance increase occurs as the intermetallic compound continues forming outside the actual bond area and around the perimeter. Later, as Kirkendall voids form (e.g., several thousand hours at 150°C), the resistance increases rapidly and device electrical failure occurs. Many studies made over the years and under various conditions have demonstrated similar increasing resistance patterns. Some are related to Al bonds on Au-plated surfaces and are discussed in Chap. 6.

In the second type of failure, the voids lie beneath the bond, as illustrated in the metallurgical cross-section of an Al wedge-bond over an Au plating, shown in Fig. 5-8. In this case, the bond can fail due to mechanical weakness, although its resistance will also increase. An equivalent section of an Au ball, bonded to Al IC metallization, is shown in Fig. 5-9.

Note that the intermetallic compounds, as well as the voids, rise up just inside the bond perimeter. (No welding takes place on the perimeter.) The diffusion rate inside the perimeter is enhanced due to the large number of defects left in this region during the stress and deformation of bonding. It is also the first Au area to be reached by in-diffusing Al from the outer bond pad. Void-free Au-Al intermetallic

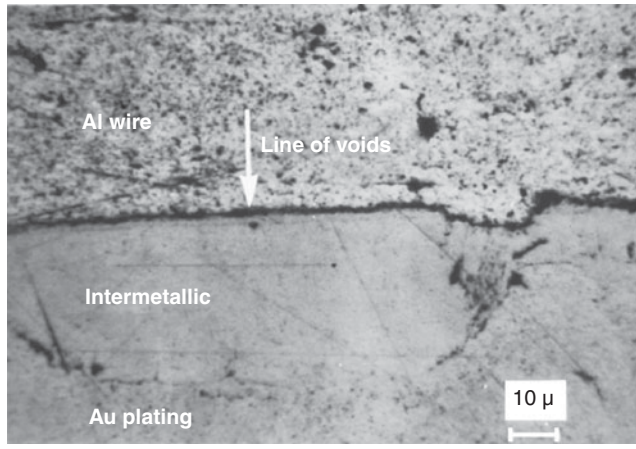

Figure 5-8 Aluminum wedge bond on a plated Au film. The unit was aged at 460°C for 100 min. The arrow points to the continuous line of Kirkendall voids that would cause a weak or zero pull-strength bond. (*After Philofsky [5-2];* © *IEEE*.)

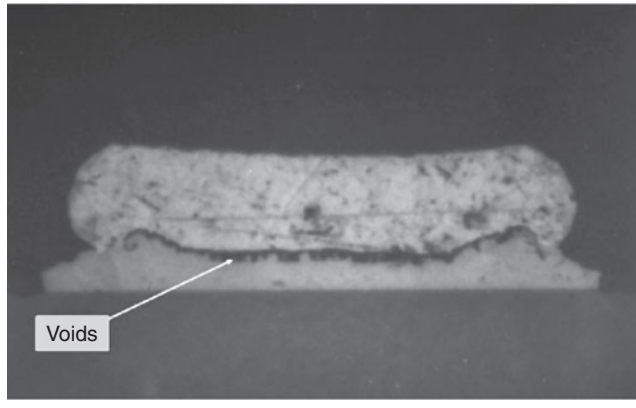

Figure 5-9 An Au ball bond to Al metallization heated at 180°C for 98 h in an atmosphere containing Br. Note that the line of voids and the intermetallic compound both rise up just inside the perimeter of the bond. Welding begins just inside that perimeter.

compounds are stronger than the pure metals [5-1]; however, they are also more brittle [5-2]. Thus, if a wire-bond system contains intermetallics, that system is far more susceptible to brittle fracture during temperature-cycle-induced flexure than Au or Al wires alone. An example of a plagued, fatigued, Au crescent-stitch-bond to Al metallization, which had been cycled only 20 times, is given in Fig. 5-10. In addition to brittleness, the growth of intermetallic compounds is enhanced by the stress of temperature cycles. Thus, it is important to

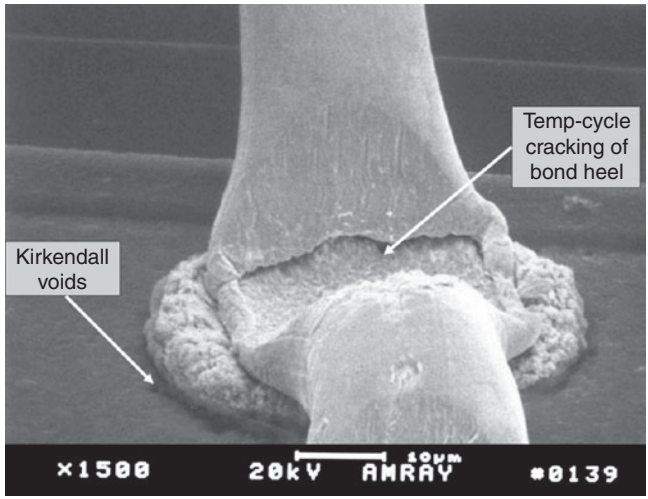

Figure 5-10 An SEM micrograph of TS Au crescent, wedge-stitch-bond to 1 μm of aluminum, then thermal stressed for 6 h at 155°C, and temp-cycled 20 times between −65 and l55°C. This reveals two major intermetallic failure modes. Kirkendall voids are seen around the perimeter, and a brittle fracture crack formed at the thin heel as a result of the temp-cycling of intermetallic diffused up from the Al pad.

be aware of this problem in devices that are likely to be temperature-cycled, such as under-the-hood automotive electronics.

Philofsky [5-2] published metallurgical design limits for avoiding bond failures due to the formation of intermetallic compounds. A condensed version of his diagnostic tables is given in Table 5-3.

Thinner metallization has been cited to limit Kirkendall voiding by restricting the availability of one of the intermetallic components [5-2, 5-10]. Similar observations have been made more for Al wire bonds on 1-μm plated Au films in which resistance drift failures occurred, but when the same composition films were thinner, 0.25 μm (10 μin), they were reliable [5-16].

5.1.4 Reversing the Au-Al Metallurgical Interfaces

Often, one may have reliability data for, say, a ball bond of one metal, bonded to a thin-film pad of the other; however, some new bonding situations may call for the reverse, in which the wire is of the former pad metallurgy and the pad, of the former wire. Intuitively, one might think that it would make no difference metallurgically in the bondability or the reliability of the bond. Intuition is often wrong, and when one examines the metallurgical conditions that exist during and after bonding, it becomes apparent that significant differences may occur. Basically it is equivalent to changing the bottom two left and right hand blocks in Fig. 5-3, resulting in entirely different

Symptom	Cause	Remedy
Open metallization around bonding pad (A)[a] Zero pull strength - bond peeled off pad - fracture surface purple, (B)[b]	Voiding in $AuAl_2$	Keep circuit below 400°C.
Zero pull strength - bond peeled off pad - fracture surface tan, (A)[a] and (B)[b]	Voiding in Au_5Al_2. Thermal cycling will aggravate.	Make metallization thinner or reduce time at temperature.
Zero pull strength - break at heel, fracture surface, - tan (A)[a] - Tan or purple, (B)[b]	Intermetallic formation in heel of bond fatigues during thermal cycling.	Make metallization thinner or use thicker wire or reduce time at temperature.

[a](A) Au wire to Al metallization
[b](B) Al wire to Au plating

TABLE 5-3 Failure Modes Associated with Intermetallic Formation (*Condensed from Philofsky [5-2]*).

intermetallic compounds under the bond. ($AuAl_2$ + Al), goes to (Au_5Al_2 + Au), and an entirely different amount of stress remains there (see Noolu's App. 5B).

Consider first the bonding method. The thermosonic ball bonding of Au balls at *relatively* high temperature (~150 to 200°C) to Al 1% Si thin-film pads is quite different from room-temperature ultrasonic wedge bonding of Al 1% Si, wire to thin- (or thick-) film Au pads. The machine is different, the bonding tools are different, and the thermosonic ball-bond is formed differently (part ultrasonic and part thermocompression). During such bonding, the package may be at high temperature for several minutes, and significant amounts of the *initially formed-intermetallics* will continue to grow in the interface, whereas for cold ultrasonic bonds only the amount generated during actual welding will be present.

For Au ball bonding to Al pads on semiconductor chips, the Al metal is much thinner (≤ 1 μm) than the deformed Au ball (~3 to 10 μm for fine pitch, larger for course pitch). Thus, Au-rich intermetallics form during the plastic mold compound cure, burn-in, or lifetime environment, and at different rates from Al bonds on Au thin films. Also, Kirkendall voiding is often associated with specific intermetallics (e.g., Au-rich, Au_5Al_2, and Au_4Al, for an Au bond on Al metallization) [5-1, 5-2], and these may not be present in the reverse metallurgical combination. This can lead to lower reliability than for an Al wedge bond to a pure

1. **The bonding method may be different for different wires, so complete welding may occur only with one wire choice or with one bonding technology.**
   - Thermosonic ball bonding vs. 25°C ultrasonic wedge-bonding. (Melted balls are softer than its wire, so Au wedge bonds are harder than ball bonds and require more US energy.)
   - Machine setup method may not be comparable. (TS has one more variable than US wedge-bonding, TC less.)
   - Choice of bonding tool (grooved tool vs. flat tool vs. capillary).
2. **Thickness of the metal in the bonded wire is >>than the metal on most pads, so:**
   - Different intermetallics form and at different rates.
   - Kirkendall voiding is usually associated with specific intermetallics, which may not be present with one combination.
3. **The wire may be harder or softer than the pad when the metallurgy is reversed.**
   - Al-wire bonds to Ni but Ni-wire is too hard to bond to Al.
4. **Oxide and contamination on bond pads may be more prevalent and interfere with bonding more readily than when it is on the wire.**
   - Copper balls are formed in a neutral/reducing atmosphere and are oxide free. Copper pads usually have some oxide on their surface, which interferes with bondability.
   - Hard oxides on soft metal (e.g., Al_2O_3 on Al) pads break up and are pushed aside during bonding, the reverse situation (Ni oxide on Ni) lowers bondability.

TABLE 5-4 Reversing the Bonded Metallurgical Interface

Au thin film. A detailed schematic and discussion of these metallurgical differences (Au-rich, Al-rich, and AuAl equal) are given in Fig. 5-3. Other cases that cannot be reversed may be related to the hardness of the metals. Soft Al wire can be US bonded to hard Ni films. However, the reverse will not result in a weld. The hard Ni wire will sink into the soft Al pad and push it aside. The US energy required to deform Ni is so great that it would crater and destroy any semiconductor underneath. A number of these nonreversible bonding or reliability situations are given in Table 5-4 (see also Sec. 5.1.2). Some metals simply do not bond well without heat (e.g., Al wire US wedge bonds easily to Au at 25°C, but not Au wire to Au—requires special grooved tools, and then for high yield, heat should be added).

5.1.5 The Effect of Diffusion Inhibitors and Barriers

Au-Al intermetallic growth was found to be inhibited by including H_2 in an open-cavity hermetic device package [5-19]. It was postulated that the H_2 filled vacancies in the Al and prevented or slowed its

diffusion into the Au. Since 95% of current devices are plastic encapsulated, such a procedure is not an option, and even for hermetic devices one would have to assure hermeticity or the H_2 could leak out.

In the past, Al bonds to thick-film Au metallization were more subject to failure by Kirkendall voiding than Al bonds to thin films. Presumably this was because thick films contain more grain boundaries, vacancies, and impurities, all of which enhance diffusion. In the late 1970s, Pd was added to Au thick-films for use in Al ultrasonic bonding [5-20, 5-21]. This resulted in either a relatively stable Au-Al-Pd ternary compound or a concentration of Pd at the interface* that slowed both the Au and Al diffusion and lengthened the life of Al wire bonds. Several applications requiring Al-wire bonding currently employ such Pd-doped Au thick films. As an example, 1 and 2% Pd, Au wires have been used for the ball bumping of Al bond pads for flip-chip [5-22] and TAB [5-23] bonding. Reliability and screening tests were run, and the long-term reliability was calculated to be 100,000 h at 85°C for the TAB devices. Thus, the Pd additive in Au ball bonds apparently serves as a diffusion or reaction inhibiter, as it does in thick-film Au. Palladium has recently been added to Au bonding wire (at about 1%) to slow intermetallic growth in fine pitch wire bonds, as well as other (proprietary) dopants, see Chaps. 3 and 9.

Titanium-tungsten metallurgical barriers have long been used to prevent Au-bump diffusion into Al bond pads to protect the integrity of TAB bonds. For this purpose, the Ti-W is "pumped" (diffused) with nitrogen to improve its resistance to Au and Al-diffusion [5-24], Problems arise when the barrier is penetrated by defects or cracked during the TAB-bonding process. The Au and Al interdiffuse, swelling the interface and further cracking the barrier [5-25, 5-26]. The reliability then becomes worse than that of a Au ball bond directly on the Al.

There have been cases when Ti, Ti-W, Ti-N, or Ta films are sandwiched between layers of Al metallization to inhibit electromigration or for other purposes [5-27]. If Au ball bonds are welded to such pads, then it is very important that care is taken during bonding-machine setup to prevent cracking of the barrier layer to prevent swelling as above. Also, there is a possibility that the top Al (when converted into intermetallic) can dewet from the barrier and result in a lifted-off bond. This is sometimes referred to as "pad lift," but technically that term refers to a separation of the entire bond pad from the chip's surface. Aluminum is frequently deposited on Cu pads in Cu/Lo-k chips for easy wire bonding. To prevent interdiffusion of Al into the Cu, Ta, Ti, or other diffusion barrier is first deposited on the Cu pads, followed by the Al bonding layer.

*The literature is not clear on which occurs.

5.2 Impurity-Accelerated Au-Al Bond Failures

The previous section (Sec. 5.1) described metallurgical diffusion, intermetallic compound formation, and Kirkendall voiding in pure bulk welds, as well as wire bonds made to uncontaminated pads. These can result in Au-Al weld failures, but usually only when subjected to very high temperatures for long times. Horsting [5-28] was the first to discover that voiding-type wire-bond failures can be accelerated by impurities. He found that a number of impurities (e.g., Ni, Fe, Co, B) in Au-plated films may result in rapid Kirkendall-like-voiding and Al wire-bond failures. His model proposed that during a high-temperature bake (for an impurity-free Au-Al bond interface), the intermetallic diffusion front moves through the Au plating down to the Ni underplating, and the bond remains strong. For impure Au, the impurities became concentrated ahead of the intermetallic growth. At some concentration, precipitation of these impurities occurs. These particles then act as sinks for vacancies produced by the diffusion reaction, resulting in Kirkendall-like voids and leading to weak or zero-strength bonds. He introduced a thermal-stress test (390°C for 1 h followed by a pull test) as a pragmatic means of detecting Au films containing impurities. Horsting's failure model was derived from plated films and is treated more completely in Chap. 6A, see Fig. 6A-1. Comparisons of his and other thermal-stress tests for bond reliability are given in Table 4-4 in Chap. 4.

After Horsting's work showed that contaminants can accelerate bond failure, a number of other contaminants in Au-plated films, as well as from plastics, ambient atmospheres, etc., have been shown to degrade bond reliability.

5.2.1 The Effect of Halogens on the Au-Al Bond System

Halogens are pervasive and are well known to corrode Al metallization in integrated circuits [5-29] (see App. 5B). However, the first observation that halogen compounds could degrade the strength of previously made Au bonds on Al metallization was by Thomas [5-30]. He cured various epoxies in the caps of TO-18 headers and sealed them to the package base that contained wire-bonded devices. Groups of these sealed packages were then stored at 150, 180, and 200°C for up to 1000 h. Massive wire-bond failures occurred within 24 h at 200°C in devices with epoxies containing brominated flame retardants (tetrabromobispheonol-A). The Au-Al bonds failed after developing a weak lamellar microstructure as shown in Fig. 5-11. This structure is not characteristic of normal, intermetallic growth, but is more characteristic of a single-phase alloy that has grown unstable and separated. Apparently, the outgassing products from the epoxy attacked the intermetallic compound, diffusing in from the sides or other areas where the compound was exposed. No corrosion of the Al-bond pad

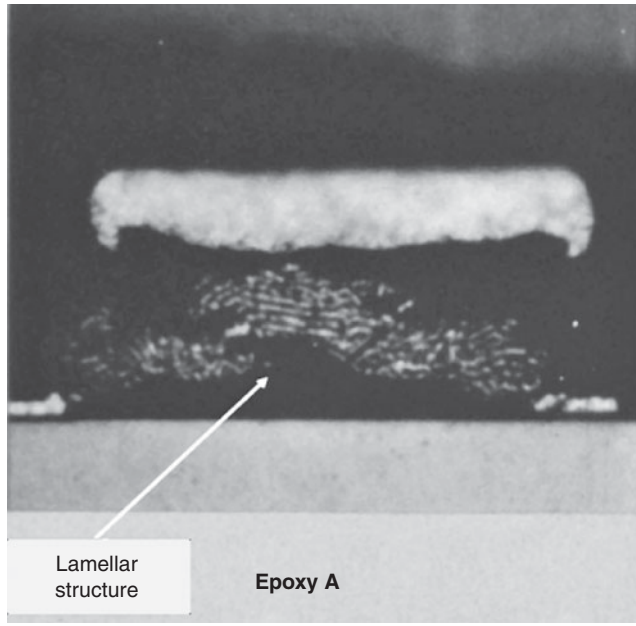

Figure 5-11 A lamellar structure in the intermetallic region for 32 μm diameter Au wire ball-bonded to a 1 μm thick Al metallization. The chip was then hermetically sealed and aged at 200°C for 24 h in the presence of epoxy, which outgassed halogens. This metallurgical structure is typical of two-phase regions commonly observed for eutectic and eutectoid microstructures (i.e., Pearlite). (*After Thomas [5-30]; © IEEE.*)

material outside the bond area was observed, implying that it only attacked the intermetallics. Controls containing no epoxy in the caps resulted in strong bonds having normal, intermetallic growth.

Analysis of the outgassed products from these epoxies showed the presence of methyl bromide and ethyl chloride. Additional experiments verified that each of these pure gasses produced identical lamellar-structure bond failures. In addition, some Al metallization corrosion by the gasses was observed. Thus, Thomas observed this lamellar-structure bond failure mechanism occurring with both Cl^- and Br^- containing gasses. The same structure was found in devices that were exposed to CF_4/O_2 plasma treatment (100 W, 1 Torr, 5 to 30 min) [5-31]. These devices were die-bonded (both eutectic and epoxy), molded in plastic, and autoclaved [121°C, 10,545 kg/m^2 (15 psi) steam]. Thus, fluorine will also produce the weak-lamellar structure at the Au-ball to Al-pad interface. In addition, the work also revealed more rapid synergistic failures when Cl (from contaminated die-attach epoxy) was in the bond interface.

Many other investigators have observed rapid Au-Al bond failures in the presence of brominated resins, elevated temperature, and usual humidity. Not all have reported finding the lamellar-intermetallic

structure, however, gross void formation has been found, and it was postulated that such voids may result from Al removal in the form of volatile halides [5-32]. The activation energy for mechanical bond failure due to brominated epoxies was found to be 0.8 eV. Others [5-33], however, found much lower activation energies for resistive bond failure (as opposed to mechanical) ranging from 0.2 to 0.5 eV. Thomas applied the brominated resin directly to the bond areas. He also gave a chain of chemical reactions that can lead to the resistive bond failures. The conclusions were that most of the reaction occurred with free bromine ions and that if the resins were purified of them, then failures, while not eliminated, would be significantly reduced.

Still other studies of ball-bond degradation from outgassed products of die-attach epoxies in hermetic packages caused ball-bond failures [5-34]. An example of a failed bond in a hermetic package (presumed to contain about 10,000 ppm of moisture) is shown in Fig. 5-12. This appears to be typical of this type of failure. The author concluded that the early degradation process of Au-Al bonds is a catalytic corrosion process requiring humidity levels of ~10,000 ppm. Such levels may be present in hermetic packages that have leaks, had epoxy die attach, or in plastic packages in humid atmospheres.

Currently, many high-quality molding compounds contain tightly bound bromine and do not release it at *normally encountered* device temperatures, but may do so under HAST or high-temperature conditions. However, it has also been found that small amounts of Sb_2O_3 (often added to molding compounds) can combine with the remaining

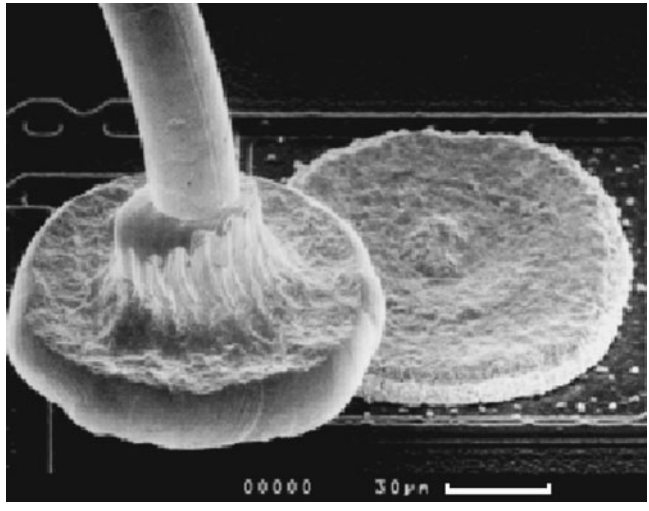

Figure 5-12 An example of a failed bond from outgassed products of die-attach epoxies in an hermetic package (presumed to contain about 10,000 ppm of moisture). The Arrow indicates a magnification of the intermetallic/corrosion area, revealing its complexity. (*After Klein [5-34].*)

amounts of free Br and cause bond corrosion [5-35]. In addition to eliminating Sb_2O_3, recent compounds have included proprietary "ion scavengers" to eliminate background levels of free Br and Cl. Devices molded with such compounds were reported to withstand 1400 h of autoclave [207 kPa (30 psi) at 135°C] without bond failure.

There is still a lack of agreement in the literature in both observations and interpretation, for example, a corrosion mechanism producing $Al(OH)_3$ [5-33], metallurgical phase separation) [5-30], oxidation of the Al in the intermetallic (Al_2O_3) [5-36], and volatile metal halide removal [5-32]. It is quite possible that all of these mechanisms occur under various conditions that have not been clearly defined, or understood.

The role of H_2O in the bond-degradation process is not clear, Klein [5-34] did the most conclusive work on this (≈ 10,000 ppm required) and suggested that H_2O serves as a catalyst. However, it could also be an oxidant, resulting in Au-Al voiding or a lamellar structure to proceed at the lower temperatures of an autoclave. Even if no autoclave is used, the high-temperature (approximately 180 to 200°C) begins the breakdown of epoxy encapsulants which release water [5-37]. Thus, Thomas' [5-30] sealed-device experiment could have contained enough released H_2O (from the epoxy) to affect the results. Other cases that introduced pure gasses were presumed to be dry, so this is not a complete explanation. A summary of bond failures resulting from halogens is given in Table 5-5. Fluorine, Cl, Br, and C were introduced onto bond pads before bonding (without subsequent plastic encapsulation), and only the normally expected interface degradation after thermal stress tests was observed [5-46].

Very large contamination was required to cause failures, and generally these occurred when the contamination layer was thick enough to limit bond formation, rather than to chemically degrade a well-made one. Most of the stress tests were run at high temperatures where no liquid H_2O is possible. Most were baked near 300°C and in N_2, with one run at 175°C. High-humidity environments encountered in plastic devices, HAST, or in hermetic enclosures containing H_2O were not included. Nevertheless, by not finding halogen degradation under clearly stated conditions, this work is supportive of the requirement for significant H_2O (or vapor) before halogen failures will occur. For a discussion of how Au-Al bond failures may occur when non-halogen films are in the interface, see App. 5A.

Many experiments have been run in an effort to understand the complex Au-Al plastic-induced contamination interactions. No complete understanding has emerged. Thus, more work is still needed.

5.2.2 Recommendations for Removing or Avoiding Halogen Contamination

It has been well established that halogens in an Au-Al bond interface or even in the environment after bonding (as long as some moisture

Source of Contamination	Contributing Causes	Negative Effect on wire Bonds[a]	Corrective Action
Silox etch (Fluoride)	Static DI wash	B,R	Agitated DI wash
F or Cl residue on pads from RIE	May leave fluorocarbon polymer films, F or Cl	B,R>6 atomic % R<6 atomic %	Possible argon sputtering
Photo resist stripper	Dichlorobenzene residue	B,R,C	Complete removal
Wafer sawing in city water	Cl in water	B,R	DI water with surfacant
Trichlorethane (TCA)	Water contamination releases HCl	B,R,C	Use different solvent or better–plasma clean
CF4/O_2 plasma clean	Autoclave	R,C	Use O_2 or Ar plasma
Cl from burn-in oven chloroprene gasket	Copper-bonded gold thick film, surface Cu–>$CuCl_2$ (Al wire bonds)	R	Change gaskets to non- halogen elastomer
Cl from plastic	85°C/85% RH, autoclave	R	Use plastic <IO ppm Cl
Br from encapsulation fire retardant	High temp (175–200°C) or 125°C autoclave	R	Avoid autoclave, high temperature, or free Br

[a]B = Reduces bondability; R = Reduces reliability; C = Corrosion failures.
See Refs. [5-39, 5-40, 5-41, 5-43; 5-44, 5-45, 5-46, 5-47]

TABLE 5-5 Problems from Halogens on Bond Pads

is present) can degrade Au-Al bond strength. The quoted experiments were run with halogen-free controls, and all controls survived much longer at any temperature and humidity than the contaminated devices. Halogens from wafer processing may become chemically bound to the Al and, depending on concentration, may cause a brown appearance [5-38] that is difficult to remove. The fluorine coloration was removed and *bondability restored by Ar plasma cleaning* [5-39]. However, radiation damage (see Chap. 7) destroyed the device's electrical characteristics. Most normal devices should survive such cleaning, see Chap. 7. A 30 s rinse in acetone has been used to remove F-ions from silicon surfaces [5-47]. The effectiveness of this cleaning method has not been verified on bond-pad surfaces when the F has reacted and become chemically bound. Chlorine has been removed from bond pads, at the wafer level, by heating the wafers to 300°C in O_2 for 30 min [5-40]. This method is not generally applicable at the packaging level, but could be used before die attach. Outgassed halogens (mostly chlorine) from epoxy die attach are generally not chemically bound to the bond pads and, if so, are readily removable by plasma or UV-ozone cleaning. If the halogens are reacted/chemically bound, then only plasma sputtering (with argon) will remove them.

5.2.3 Nonhalogen Epoxy Outgassing Induced Bond Failures

There have been reports of Au-Al wire-bond failures resulting from nonhalogen epoxy die-attach outgassed products and other organic contamination [5-37, 5-38, 5-48, 5-50]. Problems resulting from these products were very elusive, because failures occurred only occasionally, and made failure analysis as well as a full understanding very difficult. In one case [5-33], bond pads were directly exposed to the epoxy solvents and reactive dilutants. It was found that the reactive dilutants caused organic deposits on the bond pad, which sometimes polymerized, reinforcing the oxide layer and preventing optimum bonding. (These conclusions are supported by other work [5-46].) Such weak (as-made) bonding problems should be detected in production by the use of a ball-shear test or prevented by plasma or UV-ozone cleaning before bonding (see Chap. 7).

5.2.4 Green Mold Compound Problems

The most recent changes to mold compounds have been the result of the "*Green*" environmental movement and the many international laws mandating such changes. These resulted in removing elements thought to pollute the environment (i.e., halogens, heavy metals, etc.) when the devices were discarded, similar to the removal of Pb from solder. However, the first such "*pure*" mold compounds introduced new failure modes in Au-Al "*fine pitch*" wire bonds and resulted in several published studies [5-51, 5-52].

These include SEMs of bond sections identifying the intermetallic compounds, and will be further discussed in Chap. 9. Regardless of the "green" pollution state, it must be remembered that all mold compounds contain resin, hardeners, catalysts, fillers, some form of flame retardants, adhesion promoters, ion scavengers, etc. **The green requirements cannot remove these functions.** In new compounds there is always the possibility that some, or one of these, will *attack* or *accelerate* Au-Al intermetallic formation. Thus, as long as chips use these metallic interconnections, there is always the possibility of problems. In the future, new mold compounds must be a prime failure suspect when unexpected corrosion/metallurgical bond failures occur. It should be noted that some of the mold compound as well as other problems are increased by various "Green" requirements, such as using no-lead solders. These have increased many package-processing temperatures, which in turn can degrade the chemistry of mold compounds and accelerate intermetallic formation.

5.3 Nongold-Aluminum Bond Interfaces

5.3.1 Aluminum-Copper Wire-Bond System

In recent years, wires and metallizations other than pure Au or Al have been in production. Copper ball bonding to Al pads has long received attention [5-53 to 5-62]. Recently Cu wire bond usage has become important [5-64, 5-65] for reasons of economy with respect to Au (Au → $900/troy oz). Cu has higher electrical conductivity, higher resistance to wire sweep during plastic encapsulation, and minimal intermetallic problems. Copper is harder than Au; thus more care is required during bonding to avoid cratering (see Table 8-3 in Chap. 8) to compare the metallurgical properties of Au and Cu. The hardness results in a tendency to push the softer Al pad metal aside, requiring harder metallization such as that described in Refs. [5-54, 5-62]. Some bonding-machine parameters for Cu ball bonding are given in Fig. 8-4 in Chap. 8, and wire characteristics are discussed in Chap. 3, along with some ball neck and crescent problems in plastic encapsulation, in Chap. 3, and its App. 3B.

Since Cu oxidizes readily, ball bonds must be formed in an inert atmosphere, requiring modification of the bonder. Therefore, many older studies of Cu ball bonding have been concerned with ball formation, bondability, and cratering. These problems have been solved by the bonder manufacturers. and all offer dedicated Cu ball bonders. The Al-Cu phase diagram shows the existence of five intermetallic compounds favoring the Cu-rich side. Thus, there could be the possibility of various intermetallic failures similar to those of the more familiar Al-Au system, and there have been many comparisons between Au-Al and Cu-Al bonds, see for instance Refs. [5-64, 5-65].

All showed less, generally negligible, intermetallic formation and strong bonding to Al pads.

Olsen [5-61] studied the thermal aging effects of Al wedge bonds to OFHC* Cu metallization. He found completely different aging characteristics, depending on the ambient.

When the bonds were thermally aged in air at 150°C for 1600 h, they remained strong. However, aging in vacuum resulted in a rapid decrease in bond strength in the time frame between 1200 and 1600 h with an activation energy of 0.45 eV. The study found that even though intermetallic compounds grew at the same rate as in vacuum, Cu oxide apparently prevented or inhibited the growth of void-like grooves under the bond, increasing bond reliability. One study of Al wedge bonds to Cu pads found that this bond interface is more vulnerable to corrosion and less reliable in thermal stress tests than Al bonds to Au pads. In this case, the bond resistance rose rapidly after baking for 1000 h at 135°C [5-62].

Intermetallic growth for Cu ball bonds to Al metallization was studied, and it was found that the growth rate was less than half that of Al-Au bonds [5-55, 5-57]. The latter study found only $CuAl_2$ and CuAl compounds in bonds aged (apparently in air) at 150 to 200°C. The activation energy for this growth was 1.2 eV. Both found no Kirkendall voiding, but rather a weakening of the shear strength due to *growth of the brittle* $CuAl_2$.

Copper ball-bond strength (to Al metallization), in the presence of Br flame retardant and Cl in plastics, was also studied [5-57]. The bonds were aged in proximity to epoxies, similar to the earlier studies of Thomas for Au-Al bonds [5-30]. The Cu-Al bonds were strong after 1245 h at 200°C, whereas Au-Al bonds failed after 700 h. An extensive reliability study of Cu ball bonds to Al metallization (which involved all aspects of plastic IC production processing) found that Cu ball bonding was equal to or surpassed the reliability of Au ball bonds, both stressed in air [5-59].

Copper ball bonding to Al metallization in plastic packages appears to be adequately reliable, except in plastic encapsulation temperature cycling. The amount of oxygen in open-cavity packages should be limited so that oxidation of Cu wires [5-58] will not be a long-term reliability problem, but this is not a problem in plastic. Aluminum wedge bonding to Cu pads appears to be less robust than the reverse [5-61, 5-62]. This may be a case of the differences resulting from reversing the bonded interfaces (see Sec. 5.1.4).

The bondability of Cu balls to Al pads has proven excellent, and the reliability of bonds to Al pads under high temperature is very good, see above. For thin soft Al metallizations (< 0.6 μm) the harder Cu ball may push the Al metallization aside, so the Al pad should be

*Oxygen-free high conductivity.

made harder, or a TiW layer put under the pad. This will also reduce any cratering problem due to the Cu-ball hardness (compared to Au balls). Devices using Cu-Al bonds should be tested in various ambients (see App. 5C). Aluminum metallization containing Cu-Al intermetallics corrode with Cl and F contamination plus water (see Sec. 5.3.2). In production, such corrosion may become a factor in Cu-Al bonds, although such problems have not been observed in laboratory experiments [5-57].

Even though Cu ball bonding has been thoroughly studied and used in production, it has failed to achieve significant fine-wire (< 38 μm, 1.5 mil) IC production (2007). It is commonly used in small-power device production (usually ≥ 50 μm diameter). Many companies are working on the problem. (See Chap. 3 for a discussion of problems using fine Cu wire.)

5.3.2 Aluminum Bond Pads Containing Copper, Causing Bonding Problems

Aluminum integrated-circuit bond pad metallization may contain 1 to 2% percent Cu to inhibit electromigration or make the metallization harder (see above). Isolated Cu-Al intermetallic aggregates can form if the sintering (heat treatment) is incorrect. These aggregates have different electrochemical potentials from pure Al, and also from other Cu-Al phases (~0.1 V difference) [5-63]. Corrosion is usually attributed to the theta phase (Al_2Cu) aggregates. The combination of moisture and traces of a halogen (that is usually present) will result in corrosion on the bond pad, and can discolor the metal (see App. 5B). A detailed discussion of the microcorrosion of such Al-Cu and Al-Cu-Si was given by Weston [5-66]. These conditions are sometimes referred to as the "brown" or "black" metal problem [5-38, 5-66].

Figure 5-13 is an example of a pitted-bond pad that resulted in weak TS bonding. The problem can be eliminated during processing if a homogeneous distribution of Cu is obtained or by careful cleaning to remove halogens after such manufacturing steps as wafer sawing and washing. If "brown metal" is observed during the assembly operation, such chips should not be used. When Cu is added to Al, depending on wafer processing, as much as 40 Å layers of Cu_2O have been observed to form on the surface [5-68], seriously degrading bondability. High bondability can only be assured when that layer is < 5 Å. Thus, when Cu is added to Al bond pads, it has been observed to cause corrosion, make the bond pad harder (*sometimes useful when ball bonding with Cu wire*), and can result in Cu_2O on the surface. All of these can present bondability problems, lower the reliability, and require more ultrasonic energy for bonding. The latter can increase the probability of cratering (see Chap. 8, Sec. 8.1). In general, some loss of bondability is experienced when the Cu content of Al metallization is increased over approximately 1.5%. The Cu content, as well

Figure 5-13 Scanning electron micrograph of pitted Al-1.5% Cu bonding-pads following ball shearing showing the lack of bonding (i.e., no Au residue or any evidence of bonding) in the corrosion halo areas as compared with the normal areas. (*After Thomas [5-68] 67; © IEEE.*)

as the proper heat treatment of the IC metallization to minimize its effects, cannot be controlled at the assembly and packaging level. However, it is necessary for packaging personnel to understand the potential problems when dealing with chips containing Cu in the metallization, as well as to recognize its effects when failures are experienced.

5.3.3 Copper-Gold Wire Bond System

The possibility of using Au wires bonded to bare Cu IC bond pads and lead frames, as well as to Cu thick films, has led to interest in the reliability of this metallurgical system. (Note that this is also discussed in the Cu/Lo-k Chap. 10) The phase diagram shows three ductile intermetallic-like phases (Cu_3Au, AuCu, Au_3Cu) with overall activation energies of 0.8 to 1 eV. Kirkendall-like voiding has also been reported [5-69, 5-70, 5-71]. Temperature-time studies of thermocompression lead-frame bonds [5-72] in both air and vacuum show a significant decrease in strength as a result of void formation. Figure 5-14 (based on a 40% bond-strength decrease) predicts a life of about 5 years continuously at 100°C. The lifetime would be longer if the failure criteria had been a 50 or 60% decrease in strength. In either case, the lifetime is adequate for most commercial devices. Others studied Au TS bonds to thick-film Cu and found little strength degradation at 150°C for up to 3000 h, and no failures at 250°C over this period [5-73].

The reliability of fully welded Au bonds on Cu, based on autoclave for 1000 h, temperature cycling (– 65 to 150°C for 8000 cyc.), and

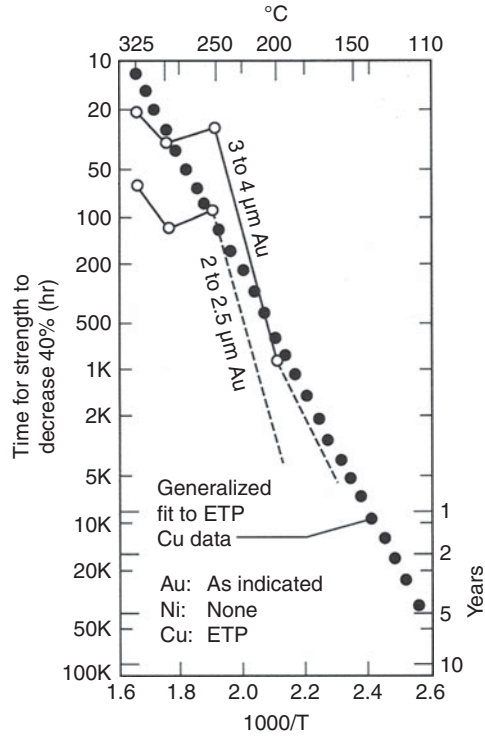

Figure 5-14
Temperature dependence of time to decrease Cu-Au gold-bond strength 40% below the as-bonded strength. Dotted line represents generalized fit to the Cu data. (*After Hall [5-72]; © IEEE.*)

temperature aging (150°C, 1000 h), has been adequately verified for commercial devices [5-75]. The bond strength of Au-Cu bonds is apparently influenced by the microstructure, weld quality, and impurity content of the Cu. The greatest problem in bonding to Cu lead frames is assuring adequate cleaning (grease and **copper-oxide** removal) [5-74, 5-75] before and during bonding. This would entail a neutral or reducing atmosphere to prevent oxidation, which is expensive for production. In addition, if a polymer die attach is used on lead frames, the polymer must be cured in an inert atmosphere to prevent Cu oxidation while still maintaining significant gas flow to carry off the plastic outgas products. If this is not done, then Cu pads on the chip and the lead frame will present serious bondability or reliability problems. Such potential problems have supported the continuing use of spot-plated Ag or possibly thin Pd films for bonding areas on lead frames. For Cu/Lo-k devices, the Cu pad has a diffusion barrier with an Al bondable layer on top.

5.3.4 Palladium-Au and -Al Bonding System (Used Primarily for Lead Frames)

Palladium-plated lead frames were introduced into the IC industry to replace spot-plated Ag for bond pads, to promote adhesion of the

plastic molding compounds, and to serve as a noble metal surface to enhance surface-mount soldering to the external leads [5-76]. The Pd film is plated over a 1.5 μm (60 μin) Ni film on the Cu lead frame. The Pd is so thin, 0.076 μm (3 μin), that it dissolves in solder without forming brittle Pd-Sn intermetallic compounds. Thermosonic Au wire bonding to these Pd films is similar to bonding to the usual Ag spot-plating, except that reoptimization of the bonding parameters is required (higher power, force, and/or time). Also, capillary life is shorter because the Pd-Ni surface is much harder than that of the spot-plated Ag. The reliability of this metallurgical bonding system for commercial grade product has been established in volume production. Palladium and Au are completely miscible, and no intermetallic compounds exist. Both Au and Pd have strongly positive electrochemical potentials, so bond interface corrosion is unlikely. Palladium will slowly form a green oxide in air at about 400°C, which presumably would reduce bondability. Therefore, it would be safest to bond Pd at interface temperatures < 300°C or in a neutral atmosphere. Palladium is mildly subject to corrosion by halogens and sulfur, so lead frames should be protected from them. Also, exposure to HAST may oxidize Pd surfaces.

Palladium diffuses rapidly into Au by grain-boundary diffusion [5-77] and might be similar to an Au bond on thick-film Ag. (No data are available on Au diffusion into Pd.) Therefore, a potential problem might result if the device was in a long-term, high-temperature environment, and the thin Pd layer was absorbed (diffused) into the Au of the wire bond. This could result in dewetting under the crescent bond at the Ni interface. Such has not been studied and probably will not occur in the thermal environment of typical commercial plastic-encapsulated devices. Also, Pd absorbs ~900 times its volume of hydrogen; in the process it expands and becomes brittle and could separate from the Ni base. Any absorbed hydrogen would be liberated with heat. If used in a sealed hermetic package, it could combine with any oxygen and form water vapor. If plasma cleaning is used before wire bonding, then the plasma cannot contain either O_2 or H_2 (Ar is best), and UV-ozone cannot be used for the same reasons. (The Pd is applied so thin that it would not absorb much H_2.)

The use of Pd-plated lead frames is in high volume, especially in packaging memory chips. However, there are several potential assembly problems that a user should consider. To avoid brittle Sn-Pd intermetallics during soldering, the Pd must be plated so thin (about 0.075 μm, 3 μin) that it can be easily scratched, leading to solderability or bondability problems. Thus, all lead-frame handling processes, such as trim-and-form, must be improved. Shipping containers and board loading equipment must also be designed to avoid scratching. The plating process is more expensive than spot plating of Ag, and thus, the entire cost of ownership must be considered to make the process pay off (e.g., no solder-dipping or spot-plating process is required).

In addition to lead-frame coatings, Pd is being used as a surface (bondable) finish for use on PWBs for surface-mount soldering. It is logical to conclude that if successful for PWBs, then Pd-coated metallization can also be used for COB die attach and wire bonding, and this should be satisfactory. However, if surface-mount soldering Pd-plated device leads to equivalent Pd-plated PWB boards, there could be enough Pd in a thin solder joint to form $PdSn_4$ (a brittle intermetallic), leading to failure in temperature cycling [5-78]. Thin Pd platings are currently (2008) an important protection and bondable surface for increasingly used Ni platings (to replace very expensive Au), see Chap. 6.

Ball Bonding with Pd Wire

Two early studies [5-79, 5-80] have shown that Pd wire can be ball bonded to Al pads. Another study of the metallurgical diffusion of Pd-Al butt-welded couples suggested that the apparent activation energy for Pd-Al intermetallic compound formation is ≈1.25 eV [5-81]. This is much higher than for any of those in the Au-Al system (see Table 5-2). Thus, compound formation and voiding would be expected to proceed very slowly. This study also thermosonically ball bonded Pd wire to Al metallization. In both cases, the same intermetallic compounds, $PdAl_3$ and Pd_2Al_3, were found after thermal baking. Voiding occurred in the Pd_2Al_3 after 100 h at 400°C. The AlPd phase diagram is complex and has numerous intermetallic compounds; however, none are on the Al-rich side, which contains a benign eutectic at 8 atm% Pd. We note that when Al wedge bonding to thin Pd films, the Al dominates the reaction.

Palladium is harder than Au (~200 vs. ~90 hKn, respectively), so cratering would be a problem when ball-bonding Pd to Al pads on Si chips. In addition, Pd has less than one-fourth the thermal and the electrical conductivity of Au (which is of no consequence for the thin lead-frame plating described above) and would require larger diameter wires to carry a given current. A limited study of Al ultrasonic-wedge-bonding, as well as Au thermocompression ball-bonding to 1 μm thick electroplated Pd films found that bondability was similar to that of Au plating [5-82]. Also, no reliability problems were revealed during temperature bakes at 200°C for 50 h. These are summarized in Table 5-6.

5.3.5 The Silver-Aluminum Wire Bond System

Silver is used as a bond-pad plating on lead frames [5-83, 5-84] and as metallization in commercial thick-film hybrids (usually in alloy form with Pt or Pd) [5-85]. Silver has also been tried as a substitute for Au wire for ball-bonding integrated circuits [5-86], but revealed many reliability problems.

The Ag-Al phase diagram is complex with numerous intermetallic phases. However, only the intermediate mu- and zeta-phases have

Advantages
1. Thin Pd (0.076 μm, 3 μin) is plated over Ni platings on lead frames and as the top surface for protection and bondability on packages, PC boards, etc.
2. Au crescent and Al wedge-bonds to thin palladium films are reported to have **no reliability problems**. Al wire-bond reliability to 1 μm Pd films reported to have similar bondability to Au plating.
3. Gold crescent-bondability to thin Pd films different from silver-plated lead frames, but **high yields** achieved with higher power, etc.
4. **No intermetallic compounds** exist between Pd and Au (miscible system).
5. Pd has high-surface free-energy giving **good adhesion of plastic-mold** compounds and die-attach epoxies.
6. **Good solderability** (Very thin Pd dissolves in solder, so no intermetallics grow.)
Potential Problems
1. Many **intermetallic compounds** exist between Pd and Al (but not on the Pd-rich or Al-rich side of the phase diagram). Thin Pd coatings result in harmless solid solutions rather than brittle intermetallic compounds.
2. Pd rapidly **absorbs H_2**, expands and embrittles. Care must be taken to prevent exposure until all assembly is completed.
3. Pd oxidizes at ~400°C, which lowers bondability (~300°C is maximum safe).
4. Pd may oxidize if cleaned with UV-ozone or O_2-plasma, lowering bondability. Argon plasma is best cleaning method.
5. Cost of Pd-plating > Ag spot-plating. Must use total packaging costs (COO) to justify.
6. **Thin Pd scratches** easily, so trim-and-form and handling processes must be improved. Also, capillaries wear out faster during crescent bonding.
7. Soldering Pd-plated lead frames to Pd-plated PC-boards requires DOE setup.

TABLE 5-6 The Palladium, Aluminum, and Gold Wire Bond System

been observed in Ag-Al wire-bond interfaces [5-84, 5-87]. The intermetallic phases had an activation energy for growth of 0.75 eV. Some Kirkendall voiding has been observed in this metal system [5-9, 5-88, 5-89], but generally at higher temperatures than experienced by microelectronic circuits. Failure of Ag-Al electrical contacts due to interdiffusion was first discovered by Hermansky [5-89]. However, the rapid humidity-induced degradation mechanism in wire bonds is the major reason that the Ag-Al metal combination is seldom used [5-87]. Chlorine was identified as the main driving element of the corrosion process.*

*Presumably, other halogens would cause the same effect.

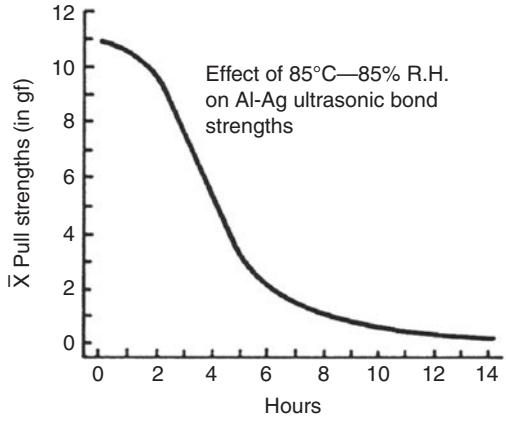

Figure 5-15 Degradation of aluminum-wire bonds to silver-plated surfaces by temperature and humidity. Each data point represents the average of 10 wire pull-test strengths for 99.99% Al wire of 50 μm diameter. (*After James [5-83]; © IEEE.*)

When it was removed from the Ag surface in an NH_4OH-H_2O ultrasonic-cleaning bath, subsequently made Al-Ag bonds remained reliable below 100°C. The humidity-corrosion mechanism has been extensively verified [5-83, 5-86, 5-90]. Wire-bond strength degradation of Al-Ag wire bonds is shown in Fig. 5-15. Failure analysis of the sample revealed $Al(OH)_3$ in the failed-bond interface. This led to the proposed mechanism that failure occurred by the classical aluminum-chlorine corrosion, which regenerates the chlorine to continue the reaction (see App. 5C).

Sections of failed bonds revealed that the corrosion actually took place in the zeta intermetallic phase [5-86]. It is not clear why the Ag-Al bond system corrodes more readily than the Au-Al system, unless the Ag or its oxide acts as a catalyst or an intermediate reaction exists in addition to the galvanic reaction.* The activation energy for bond-strength degradation due to this corrosion process was reported to be 0.3 eV [5-90], and thus, it is not strongly temperature dependent. Two authors [5-83, 5-87] verified that there is no comparable corrosion reaction under similar conditions for Al-Au bonds or for Au-Ag bonds.

An additional failure mechanism of the Ag-Al wire-bond system has also been described [5-90]. Aluminum wires bonded to Ag metallization in CERDIPs failed catastrophically due to high electrical resistance (not because they were weak mechanically). This was

*In the electrochemical series, Au^+ is more positive than Ag^+, and one would assume the Au-Al couple would corrode as readily as the Ag-Al couple. However, Ag^{++} is more positive than gold. No similar information was found for the conductive oxides of silver which may play a role.

attributed to a selective oxidation of the Ag-Al intermetallic layer that resulted in an insulating-oxide barrier in the interface. The activation energy for this reaction was given as 1.4 eV, and the mechanism was active above 400°C. This type of reaction was also reported for Al bonds on thick-film Ag [5-91]. Here, the bonds were heated for 10,000 h at 85, 100, 150, and 200°C. A step increase in resistance occurred at 4800 h at 200°C and 10,000 h at 150°C. These reactions would not be expected to affect devices processed and operated at normal temperatures, but could occur in some very long-term or worst-case situations.

Large-diameter Al wires have been bonded to Pd-Ag thick-film metallization in automotive hybrids [5-85]. However, preparation required washing with solvents, followed by careful resistivity-monitored (ionagraph) cleaning in deionized water and a solvent. After that, the hybrids were covered with a silicone gel for further protection. It is not clear whether the Pd additive to the Ag thick-film, the careful cleaning, the silicone gel, or the combination prevents the Ag-Al bond-corrosion problems described above. Each is helpful, but until the corrosion mechanism is fully understood, the use of thick-film Ag for Al bonding should be undertaken with caution, qualifying the devices in autoclave or 85°C/85% RH. However, most automotive companies stopped using the Ag-Al bonding metallurgy. The conclusion of this section is that the Ag-Al interface is unreliable under any conditions. It should not be used without considerable reliability testing, as well as a compelling reason to use it.

5.3.6 Aluminum-Nickel Wire Bond System

When the price of Au (platings) increased dramatically during the 1970s, Ni-coatings were substituted for Au on power devices. Large-diameter Al wires were easily bonded to the Ni and were found to be reliable under the various environments. Such in-house work by device manufacturers apparently was not published in the open literature, so most information has been obtained informally or in a few high-temperature electronics studies. Large-diameter wire, ≥75 μm (3 mil), Al wires bond well to Ni platings or inlays (assuming there is no Ni oxide present). This metallurgy has been used in high-volume production on power devices for over 25 years with no significant reliability problems reported. In most cases, the Ni is deposited from electroless boride or sulfamate solutions. Low-stress films electroplated from sulfamate baths also produce reliable bonds. However, phosphide electroless Ni solutions that codeposit more than 6 or 8% of phosphorus can result in both reliability and bondability problems.

Aluminum-nickel bonds are much more reliable than Al-Au bonds. The Al-Ni phase diagram is complex with numerous intermetallic phases and transitions. However, the system is generally refractory and is used in high-temperature applications, such as aircraft turbine blades. Apparently, the activation energy for the growth of these

(intermetallic) phases is high (> 1 eV, from melting point data), and Kirkendall voiding does not take place at temperatures and times encountered by power devices. Researchers [5-92, 5-93 and 5-94] observed no mechanical degradation of the Al-Ni bond in limited thermal stress tests at 300°C for 100 h. They found only about a 1% increase in bond-interface resistance during that test. The electrochemical series indicates that most Ni+ and Al+ reactions have negative potentials, and thus, galvanic corrosion is far less likely with Al-Ni bonds than with Al-Au ones.

The main difficulty encountered during Al wire bonding to Ni platings is bondability rather than reliability. Nickel surfaces will slowly oxidize, producing the same bondability problems that will be discussed in Chap. 6. Thus, packages should be bonded soon after they are Ni-plated, protected in an inert atmosphere, or chemically cleaned before bonding. (Often, thin Pd with an immersion Au coating is applied for protection and bondability.) Changing bonding machine schedules, such as impacting the tool-wire plating with the ultrasonic energy applied, has been reported to improve bondability to slightly oxidized Ni surfaces, but this is not desirable. Various surface preparation techniques (such as sandblasting) are sometimes applied before or after Ni plating to increase bondability, but the Ni-Pd-Au platings are best (Chap. 6).

5.3.7 Au-Au, Al-Al, Au-Ag, and Some Less-Used Monometallic Bonding Systems

The Au-Au system is extremely reliable. It is not subject to interface corrosion, intermetallic formation, or other bond-degrading conditions. A poorly welded Au-Au bond will improve in strength with time and temperature [5-95], as shown in Fig. 5-16. Gold-gold interconnections have been tested for 1000 h at 500°C and no interface degradation was found [5-92, 5-93]. Cold ultrasonic Au-Au wedge bonds can be made using cross-grooved, special-surfaced bonding tools, or possibly with HF ultrasonic generators (see Chap. 2). However, Au welds best and has the highest bond-yields when some heat is applied during bonding process. Thermosonic bondability is affected by surface contamination, and appropriate cleaning procedures must be used before bonding (see Chap 7). Most Au ball bonding-wire is stabilized with 5 to 7 ppm of Be, Ca, and other proprietary additives, such as Pd up to 0.1% total for fine pitch. It is annealed before it is sold. As such, it will show little metallurgical change with thermal aging. For the above reasons, the Au-Au bonding system is capable of reliable performance up to ~300°C or higher for long periods. Small-diameter wire (~25 μm diameter) as used in integrated circuits is effective but becoming more expensive, and Cu wire is being considered in some cases (see Chap. 3). Large Au wire (up to 500 μm diameter and 1 cm long) used in the past to interconnect some

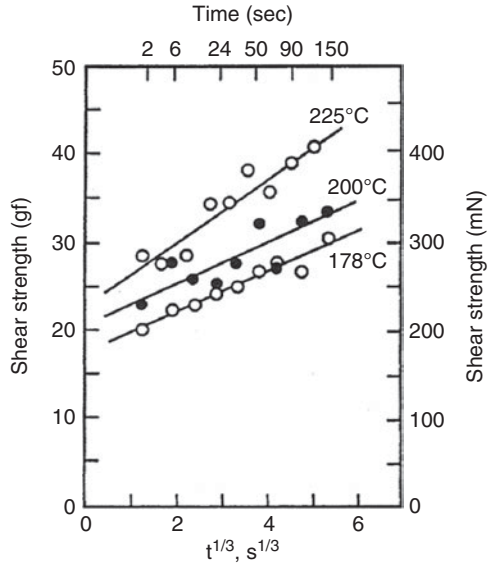

FIGURE 5-16 The improvement in shear force (with temperature and force) of TC Au ball bonds made to photoresist-contaminated Au metallization. This shows that the Au-Au interface strength can improve with temperature and time after the bonds have been made. (*After Jellison [5-95]; © IEEE.*)

special power devices is expensive, costing > $2.00 per wire. With Au approaching $900 per troy ounce it is not used today in those applications. **The small diameter Au-Au bonding system is a proven and preferred metallurgical system, and for reliability in all critical environments. It should be the metallurgy of choice.**

The Al-Al bonding system is also very reliable. This metal junction is not subject to interface corrosion, and in a corrosive environment, the surrounding pad will often be digested, but the bond interface will remain intact. While thermocompression Al-Al bonds can be made with high deformation, Al welds best ultrasonically at room temperature, and heat does not significantly improve the weld quality. Studies similar to that of Fig. 5-16 for Au-Au bonding have not been made to determine whether Al-Al bond interfaces improve with temperature and time. However, Al-wire bonded to Al pads and aged at 300°C for 1000 h showed negligible interface resistance change, even though the wire (decreased strength) annealed considerably [5-92, 5-93, 5-94]. Also, such interfaces in high-volume production do not weaken, as evidenced by the reliability of billions of Al-Al bonds in high-reliability CERDIPs and other devices that were exposed to temperatures as high as 400°C for 30 min during sealing. Electromigration in Al, 1% Si wires has been reported in 25 μm diameter wire under long operation. This required several hundred milliamperes of current for 5 to 6 years in open-cavity packages [5-96]. No failures

were found at the bond interfaces, but a bamboo structure appeared on the failed wires. Considering the above, the Al-Al wire bond system is extremely reliable and can be used in any thermal environment that is expected for normal semiconductor devices

The Au-Ag system has been shown to be reliable by James [5-83] and *it has been used on more than billions of lead frames*. No interface corrosion has been reported, and no intermetallic compounds form. Gold-wire bonds to Ag-plated lead frames have been successfully used in high-volume production for hundreds of billions of plastic-encapsulated devices for many years. Bondability problems can result if the Ag-plating is heavily tarnished by sulfur compounds, but this tarnish can be easily prevented or removed. In high-volume production, thermosonic bonding is often performed if the stage temperatures in the order of 250°C, which dissociates thin silver-sulfide films and otherwise increases bondability. Although reliable for long-term use in plastic-encapsulated devices, there can be an interdiffusion problem for long-term use at higher temperatures. Silver was observed to diffuse rapidly into Au by grain-boundary diffusion* with an activation energy of about 0.6 eV. Silver depletion, or channeling, has been observed around the peripheries of Au wires bonded to thin films of Ag and then baked at 350°C for 500 h. Such Au wires bonded to the Ag films showed large Ag decorated-grain boundaries, extending well up the wire above the ball bond [5-83, 5-97]. If the Ag film is deposited over metal, as in the case of lead frames, then a longer life is expected since the peripheral channels must extend under the bond to cause mechanical or electrical failure. Temperature cycling, using low (−40°C) temperature extremes revealed poor Au-Ag bonds better than ones emphasizing high temperatures [5-98].

Small-diameter Au wires bonded to thick-film Ag (with Pd or Pt additives) often fail a stress test (300°C for 1 h followed by a pull test). Thick-film metallization generally contains more defects and vacancies, as well as impurities, than vacuum-deposited or plated films. Thus, interdiffusion will proceed faster, resulting in the observed failures. The development of better thick-film Ag alloys may inhibit such diffusion. Possible solutions might be to add a few percent of Au to the thick-film Ag or Ag to the Au wire.

---

*There are differences in the literature as to the activation energy and diffusion coefficients. James obtained 0.6 eV activation energy from experiments with real (polycrystalline) wire bonds and polycrystalline silver films. Mallard obtained 40 kcal/mol (1.75 eV) for Ag into Au, and 48.3 (2.1 eV) for Au diffusion in pure Ag in single crystal specimens. Diffusion usually proceeds orders of magnitude faster via grain boundary diffusion than bulk or single crystal diffusion, see Chap. 6. Thus, the present author would pick the work of James to be more relevant to wire bonding than other work, such as the paper by Mallard. (Mallard, W. C., Gardner, A. B., Bass, R. F., and Slifkin, L. M., "Self Diffusion in Silver-Gold Solid Solutions," *Phys. Rev.*, Vol. 129, 1963, pp. 617–625.)

The Pd-Pd and Pt-Pt bonding systems (and other noble metals as well) are very reliable metallurgical bonding systems. The potential problems that may affect reliability in the Pd system were discussed above (oxidation, hardness, and hydrogen absorption). Bonding with Pd wire can be done by ultrasonic or thermosonic methods, and Pd wire may also be used for bonding to Al pads on semiconductors (see Sec. 5.3.4).

Platinum wire is hard and also work hardens significantly during cold ultrasonic wedge bonding and may harm tools, so it is more easily bonded by parallel-gap (electrical discharge) welding (see Sec. 2.7.2), which is a form of thermocompression bonding (no melting takes place). This method is typically used for larger diameter wires (e.g., 100 μm). Fine wires can be ball bonded by thermocompression or thermosonic methods, but at relatively high temperatures and in the latter case, minimum ultrasonic energy should be used to minimize work-hardening during bonding. Platinum is much harder than Au and could damage (crater) a semiconductor beneath the bond pad. For this reason, Pt is usually bonded to Pt or other noble metal pads on ceramic, usually in larger wire diameters (e.g., 100 μm) rather than for integrated-circuit chip bonding. For best results high temperature (~300 C) is used in conjunction with US energy. It has a low thermal conductivity and is only used for very special, usually space, applications. Platinum is more than twice the price of Au and is prohibitive for most systems.

Just as the same noble metals are reliable when bonded together, combinations of them are considered to be also reliable. For example, gold ribbon wire, parallel-gap welded to Pt-Au thick-film conductors showed no electrical degradation in 1000 h at 500°C [5-93]. This would presumably be the case for other noble-metal combinations. It is also assumed that the various noble-metal bond interface strengths will improve similar to the Au-Au interface of Fig. 5-16.

Table 5-7 shows the general relative reliability of the various metallurgical bond systems discussed above. (Also, see Chap. 3 for metallurgical comments on Cu bonds.)

Interface Reliability			
	High →	Au - Au Al - Al Au - Ag Al - Ni Au - Al	Reliability established by high-volume production.
	← Low	Au - Cu Ag - Au Al - Cu	Reliability established by laboratory experiments or low-volume production only. Acceptable for commercial production. Copper wire bonds may crater Si.
		Al - Ag	Use only with great caution.

TABLE 5-7 Wire Bond Interface Reliabilty

Appendix 5A Rapid Bond Failure in Poorly Welded Au-Al Wire Bonds

Bond failures, due to Au-Al intermetallic growth and void formation, were described earlier in this chapter. Such failures in plastic-encapsulated devices are often assumed to result from the synergistic effect of ionic impurities (often halogens) in the plastic and moisture. However, halogen-free, but poorly welded bonds have been observed to fail much more rapidly than strongly welded bonds [5-21, 5-49, 5-85, 5-99]. These failing bonds may have nonreactive impurities in the interface. In that case, diffusion cannot spread laterally and improve the bond strength (as some poorly welded bonds on cleaned surfaces appear to), but must spread vertically into the Au and Al, emphasizing the isolated-microweld nature such of bonding. Such a failed bond is shown in Fig. 5A-1 [5-99].

To explain this problem, it is necessary to understand early (immature) bond formation. The initial welding of US wedge and ball bonds consists of isolated microwelds around the bond perimeter. Some examples of these were shown in Figs. 2-10 and 2-11 in Chap. 2 for the early stages of Al-Al US bonds and in Fig. 2-12 for TS ball bonds. Initial welding for US bonds takes place near the perimeter where the metal motion (deformation) is maximum. This deformation

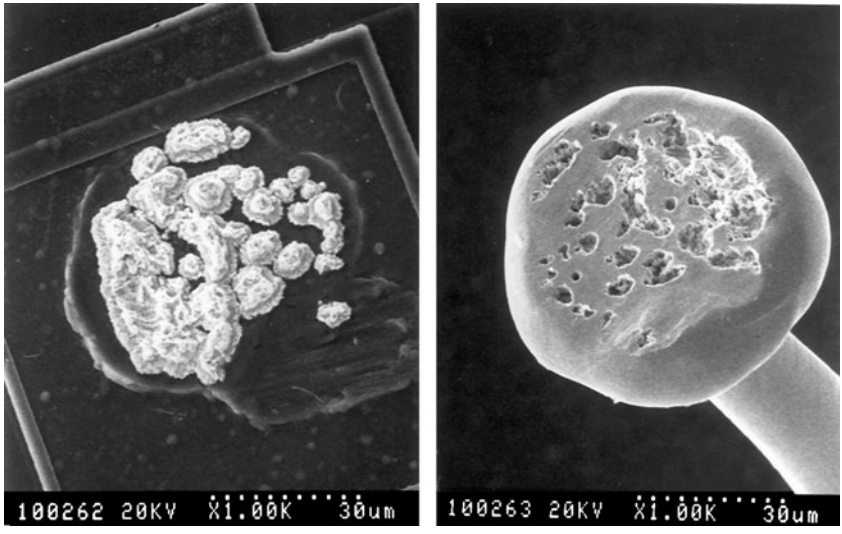

Figure 5A-1 SEM micrograph of the surfaces of a failed Au ball bond to Al metallization. Carbonaceous impurities are presumed to have inhibited uniform welding. Bonds were subjected to a 300°C bake for 1 h. (*After Clarke [5-99]; © ISHM/IMAPS.*)

sweeps surface oxide and contaminants aside into debris zones, allowing intimate contact between the two metallic interfaces. As the weld matures, the perimeter microwelds grow, join together, and spread inward (this was shown pictorially in Figs. 2-10 to 2-12, Chap. 2). Thermosonic Au-ball bonds to Al are somewhat different and the microwelds have been observed to start and spread randomly. However, all immature welds consist of isolated microwelds,* and these can result either from poor bonding machine setup (underbonding), or from some form of contaminant in the interface that prevents intimate contact between surfaces.

Wilson developed a two-dimensional finite-element model for Au-Al diffusion in structures with microweld dimensions [5-100] to explain why poorly welded bonds fail rapidly. Metallic diffusion takes place rapidly by way of defects. Surfaces and grain boundaries result in rapid diffusion for several reasons, one of which is that they contain large numbers of defects. The actual stress and excess defect level within these microwelds is unknown, so assumptions had to be made to create a model. Microwelds are generally too small to contain several grains, and, thus, internal grain boundaries. They are assumed to be one grain for modeling purposes. Thus, the model assumed that most vacancies were on the microweld surfaces. The welded interface was assumed to contain the vacancies that were on the original surfaces. The seven diffusion coefficients between the Au, Al, and five Au-Al compounds for layer growth were obtained from Philofsky [5-2, 5-3]. Microweld shapes that were observed in actual failed bonds (Figs. 2-4 and 2-5) were modeled, as well as simple butt-junctions. Results from equivalent time-temperature soaks of about 20 min at 200°C were given.

Thus, according to this model, diffusion can be several times more rapid in most microweld geometries than it would be in large, completely welded couples, supporting some observations that poorly welded Au-Al bonds fail more rapidly than well-welded ones. As stated above, the model also explained bonds having nonreactive impurities in the interface that limited initial welding to a few isolated microwelds.

Since this work was published, there have been no experiments run to directly verify it. Until this happens, the above approach remains one possible explanation for the observed rapid failure of some poorly welded Au-Al bonds, and refinements in the calculation as well as further experiments to verify (or disprove it) are still needed.

---

*Isolated microwelds offer more surface area and lattice defects for rapid diffusion, as well as for attack by halogens, than do strong, uniformly welded bonds.

Appendix 5B Thermal Degradation in Au-Al Ball Bonds

Naren Noolu,* Kevin Ely,† John Lippold,‡ and William Baeslack III§ (E-mail contact: narendra.j.noolu@intel.com)

Review of the available literature [5-102, 5-103] suggests that Kirkendall porosity formed due to the differential interdiffusion rates of Al and Au across the bond is the most widely accepted mechanism for the failure of Au-Al ball bonds. Formation of brittle intermetallic compounds is one other broadly accepted mechanism for the degradation of Au-Al ball bonds. This appendix summarizes a detailed study of the phase transformations in Au-Al ball bonds that lead to their degradation and failure at elevated temperatures [5-101 to 5-105].

Figure 5B-1 presents various stages of thermal degradation that lead to the failure of Au-Al ball bonds.

Stage 1: *As-bonded* interface typically consists of an alloyed zone (AZ) formed between the Au bump and the Al pad with a void line in it and these regions are shown in Fig. 5B-1*a* and *b*. Possible reasons for the formation of the void line are unbonded regions and impurities trapped between the Au bump and the Al pad. Formation of the void line is not very likely to be due to Kirkendall porosity as this void line was noted in bonds removed from the bonder heat stage in less than 3 sec (typically a chip is on the bonder heat stage for a few minutes to complete bonding of all the Al pads).

Stage 2: *Growth of Au-Al phases* becomes apparent during thermal exposure and Fig. 5B-1*c* shows all the five Au-Al phases formed in a Au-Al ball bond thermally exposed at 250°C for 15 min. Growth of these phases continues as long as the Al or the Al alloy below the Au bump is available and this growth is accompanied by volume changes. Based on a theoretical model, that explains growth and shrinkage of Au-Al phases with interdiffusion reactions taking place at the interphase boundaries, the calculated volumetric changes associated with each of the phase transformations are listed in Table 5B-1. It can be noted from Table 5B-1 that the theoretical model predicts volumetric shrinkage with the growth of Au_8Al_3, Au_2Al, and AuAl, but negligible change with that of Au_4Al and volumetric expansion due to the growth of $AuAl_2$. Fig. 5B-1 1*c* shows that Au_8Al_3 and Au_2Al are the predominant phases between an Au bump and an Al pad. This suggests that growth of Au-Al phases across a ball bond results in volumetric shrinkage.

Stage 3: *Reverse transformation* of the Au-Al phases across the bond initiates once the Al/Al alloy below the Au bump is completely consumed. The phase immediately next to the Ti diffusion barrier is

*Sr. Packaging Engr., Intel Corporation, Chandler, AZ 85224 E-mail: narendra.j.noolu@intel.com
†Manager, Edison Welding Institute, Columbus, OH 43221
‡Professor, Edision Joining Technology Center, Columbus, OH 43221
§Dean of Engineering, The Ohio State University, Columbus, OH 43221

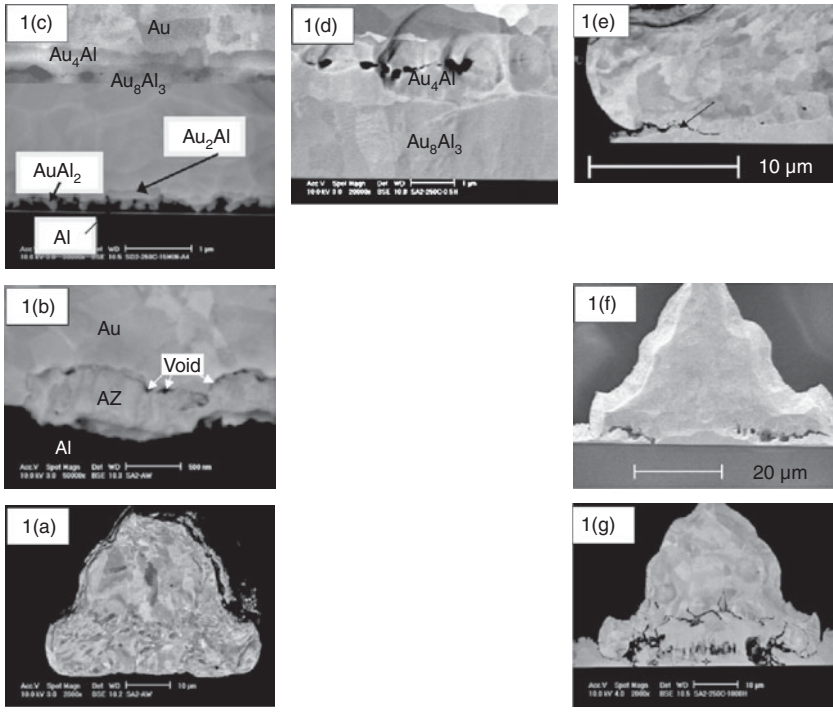

Figure 5B-1 SEM images of the Au-Al ball bond cross-sections showing various stages of thermal degradation sequentially. (*a*) Ball bond in the as-bonded condition. (*b*) High magnification image of the interface between the Au bump and Al pad showing the various regions of the interface in the as-bonded condition. (*c*) Au-Al phases grown across a bond thermally exposed for 15 min at 250°C. (*d*) Intermediate stage of a reverse transformation of Au_8Al_3 to Au_4Al in a ball bond thermally exposed for 30 min at 250°C. (*e*) Initiation of cracks of crack at the edge of a ball bond thermally exposed for 2 h at 250°C. (*f*) Crack propagation well into a ball bond thermally exposed for 150 h. (*g*) Cavity growth, crack propagation well into a ball bond thermally exposed for 1000 h.

the first to reverse transform. In reverse transformations, the highest Al containing compound is consumed giving rise to the growth of the next Al richest phase as per the Au-Al phase diagram. Reverse transformation of all the Au-Al phases eventually leads to the growth of Au_4Al across the entire reaction zone. Based on the theoretical model and calculated volume changes associated with reverse transformations presented in Table 5B-2, it is evident that all the reverse transformations result in volumetric shrinkage.

Stage 4: *Growth of cavities* at the void line becomes apparent only in high-resolution SEM imaging during initial periods of thermal exposure. Similar to the phase transformations that take place across the ball bond, growth and reverse transformation of Au-Al phases also occur lateral to the ball bond. These lateral phase transformations take

Interphase Boundary	Partial Reaction(s) at the Interphase Boundary	Product Phase	% Volume Change
Au-Au_4Al	$5Au \Rightarrow Au_4Al + Au(Au_4Al)$	Au_4Al	+19.1
Au_4Al-Au_8Al_3	$4Au(Au_4Al) + Au_8Al_3 \Rightarrow 3Au_4Al$	Au_4Al	+0.25
	$3Au_4Al \Rightarrow Au_8Al_3 + 4Au(Au_8Al_3)$	Au_8Al_3	−27.15
Au_8Al_3-Au_2Al	$2Au(Au_8Al_3) + 3Au_2Al \Rightarrow Au_8Al_3$	Au_8Al_3	+1.04
	$Au_8Al_3 \Rightarrow 3Au_2Al + 2Au(Au_2Al)$	Au_2Al	−19.49
Au_2Al-AuAl	$Au(Au_2Al) + AuAl \Rightarrow Au_2Al$	Au_2Al	−3.79
	$Au_2Al \Rightarrow AuAl + Au(AuAl)$	AuAl	−30.45
AuAl-$AuAl_2$	$Au(AuAl) + AuAl_2 \Rightarrow 2AuAl$	AuAl	−18.1
	$2AuAl \Rightarrow AuAl_2 + Au(Al)$	$AuAl_2$	−2.8
$AuAl_2$-Al	$Au(Al) + 2Al \Rightarrow AuAl_2$	$AuAl_2$	+30.4
	$AuAl_2 \Rightarrow 2Al + Au(Al)$	Al	−23.9

Table 5B-1 Calculated Volume Changes Associated with the Growth of Phases Across Au-Al Ball Bonds. There is no Au-Au_4Al Interphase Laterally and Hence no Interdiffusion Reactions.

Interphase boundary	Partial Reaction(s) at The Interphase Boundary	Product Phase	% Volume Change
AuAl-$AuAl_2$	$Au(AuAl) + AuAl_2 \Rightarrow 2AuAl$	AuAl	−18.1
Au_2Al-AuAl	$Au(Au_2Al) + AuAl \Rightarrow Au_2Al$	Au_2Al	−3.79
Au_8Al_3-Au_2Al	$2Au(Au_8Al_3) + 3Au_2Al \Rightarrow Au_8Al_3$	Au_8Al_3	−1.07
Au_4Al-Au_8Al_3	$3Au_4Al \Rightarrow Au_8Al_3 + 4Au(Au_8Al_3)$	Au_8Al_3	−27.15
Au-Au_4Al	$Au_4Al \Rightarrow 4Au + Al(Au)$	AuAl	−0.8

Table 5B-2 Volumetric Changes Associated with the Reverse Transformations Across Au-Al Ball Bonds. There is no Au-Au_4Al Interphase Laterally and Hence No Interdiffusion Reactions

place between the Au-Al phases formed across the ball bond and Al/Al alloy from the bond pad, but around the ball bond. A theoretical model predicts that lateral phase transformations also result in volumetric shrinkage, which gives rise to stress concentration in voids at the edge of the ball bond/ void line. Aided by stresses generated by phase transformations across and lateral to the ball bond as well as thermal exposure, these voids grow by a creep mechanism.

Stage 5: *Crack propagation and failure* of Au-Al ball bonds occurs by the coalescence of sufficiently grown cavities along the void line. Due to the stress concentration at the crack tip, which is at the edge of the ball bond, the cavity growth is initially higher at the edge of the ball bond/void line. With the coalescence of cavities, the crack tip moves into the bond and hence the stress concentration eventually leading to the failure of the ball bonds.

Effect of Manufacturing & Service Conditions

Ball bonds are exposed to elevated temperatures during the manufacturing of the electronic packages and further during service. After wire bonding, the packages are molded and cured, followed by surface mounting. Mold temperature is typically about 175°C and the cure is at 175°C over several hours. Ball attach and surface mounting peak temperatures can be as high as 250°C, depending on the solder alloy and the ramp and cooling is typically over 10 min. Growth of the Au-Al phases typically occurs during the manufacturing of the package, but reverse transformations typically take place during the service life of a package. Based on the experimental observations at 175°C and 250°C, it appears that the creep cavities grow significantly only after the completion of the reverse transformations. Hence the time for the completion of reverse transformations gains significance.

Below summarizes the time required for the complete consumption of the Al/Al alloy below the bump for reverse transformations to initiate. Assuming that Au_8Al_3 is the predominant phase formed across the ball bond, time required to consume Al below the ball bump is estimated at

$$t_1 = \frac{(3.62\, X_{Al})^2}{K_{RZ-A}}$$

where t_1 is the time required to completely consume the Al below the ball bump or the time required to initiate reverse transformations
x_{Al} is the thickness of Al below the ball bump
$K_{RZ\text{-}A}$ is the rate constant of the reaction zone across the ball bond
$= 3.20 \times 10^{-7}$ exp (–17954/RT) m^2/sec [1] and R = 1.98Kcal/mol

Figure 5B-2 shows the trends for the complete consumption of the metallization below the bump at various temperatures. It should be noted that these relations are developed assuming that the alloyed

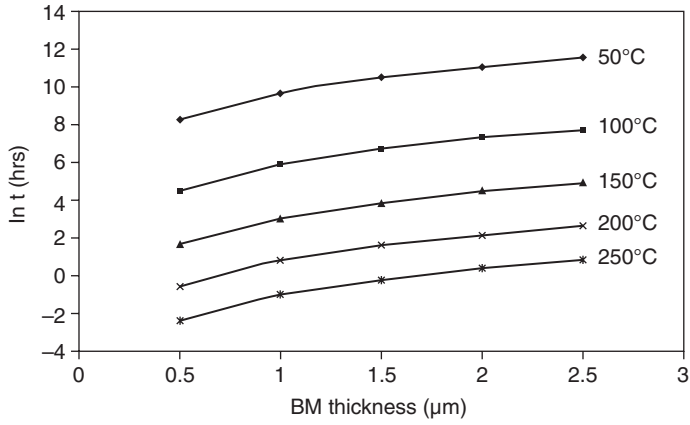

Figure 5B-2 Plot shows the time required for the complete consumption of the metallization below the ball at various metallization thicknesses and temperatures. Note that some other data have shown slower growth but taken/measured under different circumstances or dopants.

zone consists of only Au_8Al_3 during the growth of Au-Al phases across the ball bond and may only provide general trends. If all intermetallics are included the time could be different, usually longer.

SEM images shown in Fig. 5B-1 are from ball bonds thermally exposed at 250°C for various periods of time and are presented to describe the entire degradation process. However, it should be noted that the rate of interdiffusion reactions at 250°C is much higher than that in typical service conditions.

Appendix 5C Various Bond-Related Corrosion Reactions

Halogen-Aluminum Corrosion Reactions

The general chlorine corrosion equations and explanations for aluminum metallization are given below from Paulson [5-29] and Iannuzzi [5-106]. (Similar equations have been given for chlorine [5-43] and for bromine [5-33].) Water is assumed to be present in the package in ≥10,000 ppm range [5-34].

The corrosion mechanism consists of the adsorption of Cl^- on the oxide-solution interface under the influence of an electric field (caused by the electric double layer at the oxide-solution interface and/or the galvanic couple of the bond) in competition with OH^- or H_2O molecules for surface sites on the hydrated oxide surface. This is followed by the formation of a basic hydroxychloride aluminum salt with aluminum oxide cations on the hydrated oxide surface:

$$Al(OH)_3 + Cl^- \rightarrow Al(OH)_2Cl + OH^- \qquad (5C\text{-}1)$$

Once the surface oxide is dissolved, the underlying Al reacts with the Cl^- by the equation

$$Al + 4Cl^- \rightarrow Al(Cl)_4^- + 3e^- \quad (5C\text{-}2)$$

The $Al(Cl)_4$ will then react with the available water by the reaction

$$2AlCl_4^- + 6\,H_2O \rightarrow 2Al(OH)_3 + 6H + 8Cl^- \quad (5C\text{-}3)$$

This process liberates the Cl^- ion, which is then available to continue the corrosion process via Eqs. (5C-1) and (5C-2). In addition, the gold ball bond on aluminum produces a galvanic couple which can accelerate corrosion by acting as the driving force for the aluminum oxidation reaction. The region near the bond is an area of higher chloride ion concentration (compared to the overall surface) because of the reduction reaction of CI_2 by the gold electrode. Although bond-pad corrosion (outside the bond) is not generally considered as a bond failure, the electrical resistance does increase, and the device becomes nonfunctional in a manner similar to that caused by Kirkendall voiding. However, many of the actual bond failures due to halogens are attributed to a corrosion mechanism similar to the above, but occurring to the aluminum under the bond, within the Au-Al intermetallic. The bond pad, away from the bond, is often corrosion-free because the concentration of free Cl^- is highest at the bond, due to the galvanic reaction.

One possible reaction for high-temperature brominated epoxy degradation of bond strength was proposed by Khan [5-33] with the reaction products of Eq. (5C-3). A different proposed mechanism is given below in Eqs. (5C-4) to (5C-7) [5-36]. The possible reaction (unbalanced) might include the liberation of Br from CH_3Br or HBr from the high-temperature breakdown products of the resin.

$$HBrCH_3Br \rightarrow CH_3^+ + Br^- \quad (5C\text{-}4)$$

and

$$4HBr + 2O \rightarrow 4Br^- + 2H_2O \quad (5C\text{-}5)$$

Br^- would react with the Al in Au_4Al forming $AlBr_3$ and Au. The Al once extracted in the corrosion cell as $AlBr_3$ is easily oxidized. This oxidation reaction becomes the driving force until the Au_4AI intermetallic phase is consumed as in the equations below

$$Au_4Al + 3Br^- \rightarrow 4Au + AlBr_3 \quad (5C\text{-}6)$$

$$2AlBr_3 + 3O \rightarrow Al_2O_3 + 6Br^- \quad (5C\text{-}7)$$

Note that Eq. (5C-7) produces aluminum oxide, whereas the normal halogen corrosion, Eq. (5C-3), produces the hydroxide. With the reaction being autocatalytic, the Br^- is freed to start the corrosion over again. These proposed reactions come closest to explaining the lamellar structure found in Refs. [5-30, 5-31]. The equations are based on

Environment	Approximate Compositions in Percent		
	Cu_2O	CuO	Cu_2S
H_2S-O-H_2O	7-10	4-5	80-85
H_2S-SO_2-O_2-H_2O[b]	40-50	10-15	30-35
H_2S-NO_2-O_2-H_2O	15-20	7-10	70-75
H_2S-Cl_2-O_2-H_2O	40-50	35-40	15-20
H_2S-SO_2-NO_2-O_2-H_2O	55-60	30-35	10-20
H_2S-SO_2-NO_2-Cl_2-O_2-H_2O	50-55	30-40	15-20

[a]Reference [5-108] (© IEEE) points out that elemental sulfur vapor has a high occurrence and will also corrode copper.
[b]200 ppb SO_2

Table 5C-1 Film Chemistries for Tarnish Films on Copper [5-107][a]

Au_4Al, which has a low occurrence, except as the final reaction product in a gold-rich couple, see Figs. 5-1 and 5-3. Thus, the probability of this taking place may be low. The most important result of all of these reactions is that ionized halogen is liberated at the end. Thus, only a small amount of the halogen is required to completely corrode a bond pad or a bond interface.

Sulfur-Copper-Chlorine Corrosion Reactions

Copper (as used for ball bonding and lead frames) can be corroded readily (or tarnished) by sulfur and sulfur compounds. Some chemical reactions, including the increased synergistic corrosion by Cl and NO_2, are given in Table 5C-1 [5-107]. These are simple atmosphere reactions, not driven by galvanic couples such as may occur at a Cu-Al bond. Memis [5-108] has discussed copper corrosion by sulfur and that it led to failure in electronic packages. Sulfur and its gaseous compounds easily penetrate silicone materials, but, fortunately, some epoxy seals serve as an effective barrier and can prevent it from entering the package. Nevertheless, Al-Cu or Au-Cu bond studies should include the atmospheres from Table 5C-1 to establish the importance (or lack of it) of shielding the bonds from these omnipresent chemicals.

References

5-1 Philofsky, E., "Intermetallic Formation in Gold-Aluminum Systems," *Solid State Electronics*, Vol. 13, 1970, pp. 1391–1399.
5-2 Philofsky, E., "Design Limits When Using Gold-Aluminum Bonds," *Proc. IEEE Reliability Physics Symp.*, Las Vegas, Nevada, April 1971, pp. 11–16.

5-3 Philofsky, E., "Purple Plague Revisited," Proc. *IEEE Reliability Physics Symp.*, Las Vegas, Nevada, April 1970, pp. 177–185.
5-4 Ramsey, T. H. and Alfaro, C., "The Effect of Ultrasonic Frequency on Intermetallic Reactivity of Au-Al Bonds," *Solid State Technology*, Vol. 34, Dec. 1991, pp. 37–38.
5-5 Hansen, M., *The Constitution of Binary Phase Diagrams*, 2d ed., McGraw-Hill, New York, 1958.
5-6 Koeninger, V., Uchida, H. H., and Fromm, E., "Degradation of Gold-Aluminum Ball Bonds by Aging and Contamination," *IEEE Trans on Components, Packaging, and Manufacturing Tech. Part A,* Vol. 18, Dec. 1995, pp. 835–841.
5-7 Dunn, C. F. and McPherson, J. W, "Temperature-Cycling Acceleration Factors for Aluminum Metallization Failure in VLSI Applications," *Proc. IEEE IRPS,* New Orleans, Louisiana, 1990, pp. 252–255.
5-8 Gerling, W., ""Electrical and Physical Characterization of Gold-Ball Bonds on Aluminum Layers,"" *IEEE ECC*, New Orleans, Louisiana, May 14–16, 1984, pp. 13–20.
5-9 Weaver, C. and Brown, L. C., "Diffusion in Evaporated Films of Gold-Aluminum," *Phil. Mag.*, Vol. 7, 1961, pp. 1–16.
5-10 Kashiwabara, M. and Hattori, S., "Formation of Al-Au Intermetallic Compounds and Resistance Increase for Ultrasonic Al Wire Bonding," *Rev. of the Elect. Communication Lab.* (NTT), Vol. 17, Sept. 1969, pp. 1001–1013.
5-11 Onishi, M. and Fukumoto, K., "Diffusion Formation of Intermetallic Compounds in Au-Al Couples by Use of Evaporated Al Films," *Jap. J. Met. Soc.*, 1974, pp. 38–46.
5-12 Chen, G. K. C., "On the Physics of Purple-Plague Formation, and the Observation of Purple Plague in Ultrasonically-Joined Gold-Aluminum Bonds," *IEEE Trans. on PMP,* Vol. 3, 1967, pp. 149–155.
5-13 Anderson, J. H. and Cox, W. P., "Failure Modes in Gold-Aluminum Thermocompression Bonds," *IEEE Trans. Reliability,* Vol. 18, 1969, pp. 206–211.
5-14 Charles, H. K. Jr. and Clatterbaugh, G. V., "Ball Bond Shearing-A Complement to the Wire Bond Pull Test," *Intl. J. Hybrid Micro.,* Vol. 6, 1983, pp. 171–186.
5-15 Maiocco, L., Smyers, D., Munroe, P. R., and Baker, I., "Correlation between Electrical Resistance and Microstructure in Gold Wirebonds on Aluminum Films," *IEEE Trans. on CHMT,* Vol. 13, Sept. 1990, pp. 592–595.
5-16 Murcko, R. M., Susko, R. A., and Lauffer, J. M., "Resistance Drift in Aluminum to Gold Ultrasonic Wire Bonds," *IEEE Trans. on CHMT,* Vol. 14, Dec. 1991, pp. 843–847.
5-17 Majni, G. and Ottaviani, G., "AuAl Compound Formation by Thin Film Interactions," J. *Crystal Growth,* Vol. 47, 1979, pp. 583–588. Also see, *J. Appl. Phys.,* Vol. 52, June 1981, pp. 4047–4052.
5-18 White, M. L., Serpiello, J. W., Stringy, K. M., and Rosenzweig, W., "The Use of Silicone RTV Rubber for Alpha Particle Protection on Silicon Integrated Circuits," *Proc. 19th IRPS*, Orlando, Florida, April 79, 1981, pp. 43–47.
5-19 Shih, D. Y. and Ficalora, P. J., "The Reduction of Au-Al Intermetallic Formation and Electromigration in Hydrogen Environments," *16th Proc. IEEE IRPS*, San Diego, California, 1978, pp. 268–272.
5-20 Horowitz, S. J., Felton, J. J., Gerry, D. J., Larry, J. R., and Rosenberg, R. M., "Recent Developments in Gold Conductor Bonding Performance and Failure Mechanisms," *Solid State Technology,* Vol. 22, March 1979, pp. 37–44.
5-21 Hund, T. D. and Plunkett, P. V., "Improving Thermosonic Gold Ball Bond Reliability," *IEEE Trans. on CHMT,* Vol. 8, 1985, pp. 446–456.
5-22 Goldstein, J. L. F., Tuckerman, D. B., Kim, P. C., and Fernandez, A., "A Novel Flip-Chip Process," *1995 Proc. SMI,* San Jose, California, Aug. 2931, 1995, pp. 59–71.
5-23 Larson, E. N. and Brock, M. J., "Development of a Single Point Gold Bump Process for TAB Applications," *Proc. of 1993 Intl. Conf. on Multichip Modules,* Denver, Colorado, April 14–16, 1993, pp. 391–397.
5-24 Nowicki, R. S., "Improving Metallization Reliability at the Component Level," *Proc. 1992 Intl. Symp. on Microeletronics (ISHM)*, San Francisco, California, Oct. 1921, 1992, pp. 731–736.

5-25 Tung, C-H., Kuo, Y-S., and Ghang, S-M., "Tape Automated Bonding Inner Lead Bonded Devices (TAB/ILB) Failure Analysis," *IEEE Trans. on CHMT,* Vol. 16, May 1993, pp. 304–310.
5-26 Tjhia, E. and Nguyen, T., "Bump Metallurgies for Tape Automated Bonding (TAB) in Ceramic Packages," *Proc. 1992 Intl. Symp. on Microeletronics (ISHM),* San Francisco, California, Oct. 1921, 1992, pp. 421–426.
5-27 Ueno, H., "Reliable Au Wire Bonding to Al/Ti/A1 Pad," *Jap. J. Appl. Phys.,* Vol. 32, 1993, pp. 2157–2161.
5-28 Horsting, C. W., "Purple Plague and Gold Purity," *10th Annual Proc. IEEE Reliability Physics Symp.*, Las Vegas, Nevada, 1972, pp. 155–158.
5-29 Paulson, W. M. and Lorigan, R. P., "The Effect of Impurities on the Corrosion of Aluminum Metallization," *Proc. IEEE IRPS,* Las Vegas, Nevada, April 2022, 1976, pp. 42–47.
5-30 Thomas, R. E., Winchell, V., James, K., and Scharr, T., "Plastic Outgassing Induced Wire Bond Failure," *27th Proc. IEEE Electronics Components Conf.*, Arlington, Virginia, May 1618, 1977, pp. 182–187.
5-31 Richie, R. J. and Andrews, D. M., "CF4/02 Plasma Accelerated Aluminum Metallization Corrosion in Plastic Encapsulated ICs in the Presence of Contaminated Die Attach Epoxies," *19th IEEE IRPS,* Orlando, Florida, April 7–9, 1981, pp. 88–92.
5-32 Gale, R. J., "Epoxy Degradation Induced Au-Al Intermetallic Void Formation in Plastic Encapsulated MOS Memories," *22nd IEEE IRPS,* Las Vegas, Nevada, April 3–5, 1984, pp. 37–47.
5-33 Khan, M. M. and Fatemi, H., "Gold-Aluminum Bond Failure Induced by Halogenated Additives in Epoxy Molding Compounds," *Proc. 1986 Intl. Symp. on Microelectronics (ISHM),* Atlanta, Georgia, Oct. 6–8, 1986, pp. 420–427.
5-34 Klein, H. P., "Dry Corrosion in Gold-Aluminum Ball Bonds," *Proc. 5th Intl. Conf. on Quality in Electronic Components,* Bordeaux, France, Oct. 7–10, 1991, pp. 889–897.
5-35 Gallo, A. A., "Effect of Mold Compound Components on Moisture-Induced Degradation of Gold-Aluminum Bonds in Epoxy Encapsulated Devices," *Proc. 1990 IEEE IRPS,* 1990, pp. 244–251.
5-36 Ritz, K. N., Stacy, W. T., and Broadbent, E. K., "The Microstructure of Ball Bond Corrosion Failures," *25th Annual Proc. IEEE Reliability Physics Symp.,* April 1987, San Diego, California, pp. 28–33.
5-37 Lum, R. M. and Feinstein, L. G., "Investigation of the Molecular Processes Controlling Corrosion Failure Mechanisms in Plastic Encapsulated Semiconductor Devices," *30th Proc. ECC,* San Francisco, California, April 28–30, 1980, pp. 113–120.
5-38 Nesheim, J. K., "The Effects of Ionic and Organic Contamination on Wirebond Reliability," *Proc. 1984 Intl. Symp. on Microelectronics (ISHM),* Dallas, Texas, Sept. 17–19,1984, pp. 70–78.
5-39 Pavio, J., Jung, R., Doering, C., Roebuck, R., and Franzone, M., "Working Around the Fluorine Factor in Wire Bond Reliability," *Proc. 1984 Intl. Symp. on Microelectronics (ISHM),* Dallas, Texas, Sept. 17-19, 1984, pp. 428–432.
5-40 Lee, W-Y, Eldridge, J. M., and Schwartz, G. C., "Reactive Ion Etching Induced Corrosion of Al and Al-Cu Films," *J. Appl. Phys.,* Vol. 52, April 1981, pp. 2994–2999.
5-41 Graves, J. F. and Gurany, W., "Reliability Effects of Fluorine Contamination of Aluminum Bonding Pads on Semiconductor Chips," *32nd Proc. ECC,* San Diego, California, May 10–12, 1982, pp. 266–267.
5-42 Forrest, N. H., "Reliability Aspects of Minute Amounts of Chlorine on Wire Bonds Exposed to Pre-Seal Burn-In," *Intl. J. Hybrid Microelectronics,* Vol. 5, Nov. 1982, pp. 549–551. (Note: Figures omitted from paper-contact its author.)
5-43 Gustafsson, K. and Lindborg, U., "Chlorine Content in and Life of Plastic Encapsulated Micro-Circuits," *37th Proc. ECC,* Boston, Massachusetts, May 11–13, 1987, pp. 491–499.
5-44 Blish, R. C. II and Parobek, L., "Wire Bond Integrity Test Chip," *21st Proc. IEEE IRPS,* Phoenix, Arizona, April 5–7, 1983, pp. 142–147.

5-45 Ahmad, S., Blish, R. C. II, Corbett, T., King, J., and Shirley, G., "Effect of Bromine Concentration in Molding Compounds on Gold Ball Bonds to Aluminum Bonding Pads," *IEEE Trans. on CHMT,* Vol. 9, 1986, pp. 379–385.
5-46 Koeninger, V., Uchida, H. H., and Fromm, E., "Degradation of Gold-Aluminum Ball Bonds by Aging and Contamination," *IEEE Trans on CHMT, Part A,* Vol. 18, Dec. 1995, pp. 835–841.
5-47 Kern, W., "Radiochemical Study of Semiconductor Surface Contamination, I. Adsorption of Reagent Components," *RCA Review,* June 1970, pp. 224–228.
5-48 Charles, H. K. Jr., Romenesko, B. M., Wagner, G. D., Benson, R. C., and Uy, 0. M., "The Influence of Contamination on Aluminum-Gold Intermetallics," *20th Proc. IRPS,* San Diego, California, March 30–31, 1982, pp. 128–139.
5-49 Khan, M. M., Tarter, T. S., and Fatemi, H., "Aluminum Bond Pad Contamination by Thermal Outgassing of Organic Material from Silver-Filled Epoxy Adhesives," *IEEE Trans. on CHMT,* Vol. 10, 1987, pp. 586–592.
5-50 Plunkett, P. V. and Dalporto, J. F, "Low Temperature Void Formation in Gold-Aluminum Contacts," *32nd Proc. ECC,* San Diego, California, CHMT, May 10–12, 1982, pp. 421–427.
5-51 Sutiono S., Breach C.D., Calpito D., Stephan D., Wulff F., Saraswati P., Seah A., and Chew S., "Intermetallic Growth Behaviour of Gold Ball Bonds Encapsulated with Green Molding Compounds," *IEEE EPTC,* Singapore, Dec. 2005, pp. 584–589.
5-52 Chew, S., Seah, A., Kumar, S., Lin, J., Chin, S., and Soriano, A., "Evaluation of Irregular Inter-Metallic Compound Growth in Gold Wire Bonds Encapsulated with Reliable, Green Epoxy Mold Compound," *Proc. IMAPS, San Jose, California, Nov 11–15, 2007, pp. 624–629.*
5-53 Kurtz, J., Cousens, D., and Dufour, M., "Copper Wire Ball Bonding," *34th Proc. ECC,* New Orleans, Louisiana, May 14–16, 1984, pp. 1–5.
5-54 Hirota, J., Machida, K., Okuda, T., Shimotomai, M., and Kawanaka, R., "The Development of Copper Wire Bonding for Plastic Molded Semiconductor Packages," *35th Proc. IEEE ECC,* Washington, D.C., May 20–22, 1985, pp. 116–121.
5-55 Atsumi, K., Ando, T., Kobayashi, M., and Usuda, O., "Ball Bonding Technique for Copper Wire," *36th Proc. ECC,* Seattle, Washington, May 5–7, 1986, pp. 312–317.
5-56 Levine, L. and Shaeffer, M., "Copper Ball Bonding," *Semiconductor International,* Aug. 1986, pp. 126–129.
5-57 Onuki, J., Koizumi, M., and Araki, I., "Investigation on the Reliability of Copper Ball Bonds to Aluminum Electrodes," *IEEE Trans. on CHMT,* Vol. 10, 1987, pp. 550–555.
5-58 Riches, S. T. and Stockham, N. R., "Ultrasonic Ball/Wedge Bonding of Fine Cu Wire," *Proc. 6th European Microelect. Conf. (ISHM),* Bournemouth, England, June 3–5, 1987, pp. 27–33.
5-59 Khoury, S. L., Burkhard, D. J., Galloway, D. P., and Scharr, T. A., "A Comparison of Copper and Gold Wire Bonding on Integrated Circuit Devices," *IEEE Trans. on CHMT,* Vol. 13, No. 4, Dec. 1990, pp. 673–681.
5-60 Nguyen, L. T., McDonald, D., and Danker, A. R., "Optimization of Copper Wire Bonding on Al-Cu Metallization," *IEEE Trans. on CPMT, Part A,* Vol. 18, June 1995, pp. 423–429.
5-61 Olsen, D. R. and James, K. L., "Evaluation of the Potential Reliability Effects of Ambient Atmosphere on Aluminum-Copper Bonding in Semiconductor Products," *IEEE Trans. on CHMT,* Vol. 7, 1984, pp. 357–362.
5-62 Johnston, C. N., Susko, R. A., Siciliano, J. V., and Murcko, R. J., "Temperature Dependent Wear-Out Mechanism for Aluminum/Copper Wire Bonds," *Proc. Intl. Microelectronics Conf.,* Orlando, Florida, Oct. 23–24,1991, pp. 292–296.
5-63 Totta, P., "Thin Films: Interdiffusion and Reactions," *J. Vac. Sci. Technology,* Vol. 14, No. 26, 1977. Also see Zahavi, J., Rotel, M., Huang, H. C. W., and Totta, P. A., "Corrosion Behavior of AL-CU Alloy Thin Films in Microelectronics," *Proc. of the Intl. Congress on Metallic Corrosion,* Toronto, Canada, June 3–7,1984, pp. 311–316.

5-64 Srikanth, N., Murali, S., Wong, Y. M., and Vath III, C. J., "Critical Study of Thermosonic Copper Ball Bonding," *Thin Solid Films,* Vol. 462–463, 2004, pp. 339–345.
5-65 Wulff, F. W., Breach, C. D., Stephan, D., Saraswati and Dittmer, K.J., "Characterisation of Intermetallic Growth in Copper and Gold Ball Bonds on Aluminum Metallisation," *6th EPTC,* Singapore, Dec. 2004.
5-66 Weston, D., Wilson, S. R., and Kottke, M., "Microcorrosion of Al-Cu and Al-Cu-Si Alloys of the Metallization with Subsequent Aqueous Photolithographic Processing," *J. Vac. Soc.,* Vol. A8, May/June 1990, pp. 2025–2032.
5-67 Thomas, S., and Berg, H. M., "Micro-Corrosion of Al-Cu Bonding Pads," 23rd Proc. IRPS, Orlando, Florida, March 26-28,1985, pp. 153–158.
5-68 Pignataro, S., Torrisi, A., and Puglisi,O., "Influence of Surface Chemical Composition on the Reliability of Al/Cu Bond in Electronic Devices," *Applied Surface Science,* Vol. 25, 1986, pp. 127–136.
5-69 Pinnel, M. R. and Bennett, J. E., "Mass Diffusion in Polycrystalline Copper/Electroplated Gold Planar Couples," *Met. Trans.,* Vol. 3, July 1972, pp. 1989–1997.
5-70 Feinstein, L. G. and Bindell, J. B., "The Failure of Aged Cu-Au Thin Films by Kirkendall Porosity," *Thin Solid Films,* Vol. 62, 1979, pp. 37–47.
5-71 Feinstein, L. G. and Pagano, R. J., "Degradation of Thermocompression Bonds to Ti-Cu-Au and Ti-Cu by Thermal Aging," *Proc. ECC,* Cherry Hill, New Jersey, May 14–16,1979, pp. 346–354.
5-72 Hall, P. M., Panousis, N. T., and Menzel, P. R., "Strength of Gold-Plated Copper Leads on Thin Film Circuits Under Accelerated Aging," *IEEE Trans. on Parts, Hybrids, and Packaging,* Vol. 11, No. 3, Sept. 1975, pp. 202–205.
5-73 Pitt, V. A. and Needes, C. R. S., "Thermosonic Gold Wire Bonding to Copper Conductors," *IEEE Trans. CHMT,* Vol. 5, No. 4, Dec. 1982, pp. 435–440.
5-74 Lang, B. and Pinamaneni, S., "Thermosonic Gold-Wire Bonding to Precious-MetalFree Copper Leadframes," *38th Proc. IEEE Electronic Components Conf.,* Los Angeles, California, May 9–11, 1988, pp. 546–551.
5-75 Fister, J., Breedis, J., and Winter, J., "Gold Leadwire Bonding of Unplated C194," *20th Proc. IEEE Electronic Components Conf.,* San Diego, California, March 30–31, 1982, pp. 249–253.
5-76 Abbott, D. C., Brook, R. M., McLellan, N., and Wiley, J. S., "Palladium as a Lead Finish for Surface Mount Integrated Circuits," *IEEE Trans. CHMT,* Vol. 14, Sept. 1991, pp. 567–572. Also, see *IEEE ECTC,* 1995 (Abbott and Romm), pp. 1068–1072.
5-77 Hall, P. M. and Morabito, J. M., "Diffusion Problems in Microelectronics Packaging," *Thin Solid Films,* Vol. 53, 1978, pp. 175–182.
5-78 Finley, D. W., Ray, U., Artaki, I, Vianco, P., Shaw, S., Reyes, A., and Haq, M., "Assessment of Nickel-Palladium Finished Components for Surface Mount Assembly Applications," *Proc. 1995 SMI Technical Program*, San Jose, California, Aug. 29–31, 1995, pp. 941–953.
5-79 Thiede, H. P., "Bonding Wire Today," *2nd Ann. International Electronics Packaging Conf. IEPS,* Nov. 15–17,1982, San Diego, California, pp. 686–705.
5-80 Bischoff, A. and Aldinger, F., "Reliability Criteria of New Low-Cost Materials for Bonding Wires and Substrates," *34th Proc. IEEE Electronic Components Conf.,* New Orleans, Louisiana, May 14-16, 1984, pp. 411–417.
5-81 Stemple, D. K. and Olsen, D. R., "Kinetics of Palladium-Aluminum Intermetallic Formation," *1983 ISHM Interconnect Conf.,* Session 2, Paper 2, Welches, Oregon, July 27–28, 1983.
5-82 Kyocera Intl. KCILLIUM, *A Report on Properties and Test Results*, Sept. 5, 1980.
5-83 James, K., "Reliability Study of Wire Bonds to Silver Plated Surfaces," *IEEE Trans. on Parts, Hybrids and Packaging*, Vol. 13, 1977, pp. 419–425.
5-84 Kawanobe, T., Miyamoto, K., Seino, M., and Shoji, S., "Bondability of Silver Plating on IC Leadframe," *35th Proc. ECC,* Washington, D.C., May 20–22, 1985, pp. 314–318.

5-85 Baker, J. D., Nation, B. J., Achari, A., and Waite, G. C., "On the Adhesion of Palladium Silver Conductors under Heavy Aluminum Wire Bonds," *Intl. J. for Hybrid Microelectronics,* Vol. 4, 1981, pp. 155–160.
5-86 Kamijo, A. and Igarashi, H., "Silver Wire Ball Bonding and Its Ball/Pad Interface Characteristics," *35th Proc. IEEE Electronic Components Conf,* Washington, D.C., May 20–22, 1985, pp. 91–97.
5-87 Jellison, J. L., "Susceptibility of Microwelds in Hybrid Microcircuits to Corrosion Degradation," *13th Annual Proc. IEEE Reliability Physics Symp.*, Las Vegas, Nevada, April 1975, pp. 70–79.
5-88 Kahkonen, H. and Syrjanen, E., "Kirkendall Effect and Diffusion in the Aluminum Silver System," *J. Matls. Sci. Lett.,* Vol. 5, 1970, p. 710.
5-89 Hermansky, V., "Degradation of Thin Film Silver-Aluminum Contacts," *Fifth Czech. Conf. on Electronics and Physics, Czechoslovakia,* Oct. 16–19, 1972, pp. II. C–11.
5-90 Shukla, R. and Singh-Deo, J., "Reliability Hazards of Silver-Aluminum Substrate Bonds in MOS Devices," *20th Annual Proc. IEEE IRPS,* San Diego, California, March 30 to April 1, 1982, pp. 122–127.
5-91 Nazarova, N. K., Zakharova, S. E., Kharitonov, E. V., and Shetlmakh, S. V., "Degradation in Ag-Al Microcontacts on Prolonged Heating," *Microelectronika,* Vol. 16, July-August, 1987, pp. 320–325.
5-92 Palmer, D. W. and Ganyard, F. P., "Aluminum Wire to Thick Film Connections for High Temperature Operations," *IEEE Trans on. Components, Hybrids, and Manufacturing Technology,* Vol. 1, Sept. 1978, pp. 219–222.
5-93 Palmer, D. W., "Hybrid Microcircuitry for 300 C Operation," *IEEE Trans. on Parts, Hybrid and Packaging,* Vol. 13, Sept. 1977, pp. 252–257.
5-94 Benoit, J., Chen, S., Grzybowski, R., Lin, S., Jain, R., and McCluskey, P., "Wire Bond Metallurgy for High Temperature Electronics", Proc *4th IEEE Int'l High Temperature Electronics Conference,* Albuquerque, NM, June 14–18, 1998, pp. 109–113.
5-95 Jellison, J. L., "Kinetics of Thermocompression Bonding to Organic Contaminated Gold Surfaces," *IEEE Trans. on Parts, Hybrids, and Packaging,* Vol. 13, 1977, pp. 132–137.
5-96 Tse, P. K. and Lach, T. M., "Aluminum Electromigration of 1-mil Bond Wire in Octal Inverter Integration Circuits," *Proc. 45th IEEE ECTC,* Las Vegas, Nevada, May 1995, pp. 900–905.
5-97 Aday, J., Johnson, R. W., Evans, J. L., and Romanczuk, C., "Wire Bonded Thick Film Silver Multilayers for Under-the-Hood Automotive Applications," *Intl. J. of Microcircuits and Electronic Packaging,* Vol. 17, 1994, pp. 302–311.
5-98 Sow, Y. K., Yasmin, A., and Dias, R., "Improving Gold-Silver Wirebond Integrity in Plastic Packages," *Proc. of ECTC,* Orlando, Florida, June 1–4, 1993, pp. 341–347.
5-99 Clarke, R. A. and Lukatela, V., "Inadequacy of Current Mil-STD Wire Bond Certification Procedures," *Proc. 1991 Intl. J. Microcircuits and Electronic Packaging,* Vol. 15, pp. 87–96.
5-100 Harman, G. G. and Wilson, C. L., "Materials Problems Affecting Reliability and Yield of Wire Bonding in VLSI Devices," *Proc. 1989 MRS, Electronic Packaging Materials Science IV,* Vol. 154, San Diego, California, April 24–29, 1989, pp. 401–413.
5-101 5A-1.Au-Al, Aluminum-Gold, *J. of Phase Equilibria*, Vol. 12, 1991 pp.114.
5-102 Noolu, N. J., Murdeshwar, N. M., Ely, K. J., Lippold, J. C., and Baeslack, III, W. A., "Partial Diffusion Reactions and the Associated Volume Changes in Thermally Exposed Au-Al Ball Bonds," *Met. Matls Trans. A*, Vol. 35, April, 2004, pp. 1273–1280.
5-103 Noolu, N. J., Murdeshwar, N. M., Ely, K. J., Baeslack W. A. III, and Lippold, J. C., "Phase Transformations in Thermally Exposed Au-Al Ball Bonds," *J. Electronic Materials,* Vol. 33, No.4, 2004, pp. 340–352.
5-104 Noolu, N. J., Murdeshwar, N. M., Ely, K. J., Lippold, J. C., and Baeslack, W. A. III, "Degradation and Failure Mechanisms in Thermally Exposed Au-Al Ball Bonds," *J. Materials Research,* Vol. 19, No. 5, 2004, pp. 1374–1385.

5-105 Noolu, N. J., Klossner, M. K., Ely, J., Murdeshwar, N. M., Lippold,. J. C., and Baeslack, W. A. III, "The Effect of Copper Additions in The Aluminum Alloy Metallizations on the Formation of Interdiffusion Zones and Voids in Gold Ball Bonds," *6th Ann. Emerging Technology Conference,* Dallas, TX (USA), November, 2000.

5-106 Iannuzzi, M., "Bias Humidity Performance and Failure Mechanisms of Non-Hermetic Aluminum SICs in an Environment Contaminated With C12," *Proc. Reliability Physics Symp.,* San Diego, California, March 30–31, 1982, pp. 16–26.

5-107 Abbott, W. H., "Effects of Industrial Air Pollutants on Electrical Contact Materials," *IEEE Trans. on Parts, Hybrids, and Packaging,* Vol. 10, March 1974, pp. 24–27.

5-108 Memis, I., "Quasi-Hermetic Seal for IC Modules," *30th Proc. Electronic Components Conf,* San Francisco, California, April 28–30, 1980, pp. 121–127.

CHAPTER 6

Introduction to Plating, Section A (Gold) and Section B (Nickel-Based) Bond Pad Technology and Reliability

This chapter is divided into two independent sections. The first, A (bonding to Au) is updated/shortened from the second edition's chapter on gold plating. The second section includes information on newer bonding pad plating materials that are mostly nickel-based, which comprise an increasing number of present substrate pads. This change has occurred because the price of Au has reached astronomical heights and other bonding pad materials have been developed to replace it in many uses. Section B is coauthored by Luke England and Jamin Ling, and their credits appear under their names. Both sections have their own separate references.

Section A Bond Failures Resulting from Gold-Plating Impurities and Conditions

6A.1 Gold Plating

Most of the impurities in Au platings that cause wire bond failures were discovered and explained in the approximate 1970s to 1980s time-frame. They are reviewed here because they and their underlying diffusion principles still result in many current bond failures. Much of the more recent work on such impurities is similar, and usually without fundamental explanations, since such were developed earlier. These early references are usually available from search engines such as Google Scholar.

One of the earliest classes of documented bonding problems resulted from plating impurities in Au films. These impurities have resulted in reducing bondability (low yield), as well as causing premature bond failure during thermal stress tests or later, during the life of the device (reliability). Considerable literature exists on such bond failures; however, much of it is published in plating or thin-film journals that are seldom read by packaging and wire-bonding professionals. Also, much relevant research was published a decade or more ago and is generally unavailable or is ignored. The number of plating variables is so large that there is little quantitative agreement in the literature as to the influence of a particular variable on wire bonds. Also, few experiments by different investigators are similar enough to verify previous results. Factorial statistical experiments should be run to determine the significance of each variable on bondability and reliability.

The first explanation of wedge-bond failures resulting from plating impurities was presented in a classic paper by Horsting [6A-1] titled, "Purple Plague and Gold Purity." He observed that a number of plating impurities resulted in Kirkendall-like voids and early bond failure. He hypothesized that in pure Au films the intermetallic diffusion front moved through the Au to the Ni underplating, forming the alloy phases as shown in Fig. 6A-1*a*, and the bond remains strong. However, for impure Au, the impurities are swept ahead of the intermetallic diffusion front, since most impurities in the Au have lower solubility in the intermetallic compound than in Au or Al as shown in Fig. 6A-1*b*. At some impurity concentration, precipitation occurs, and these particles act as sinks for vacancies produced during the diffusion reaction. Voids develop and join together, leading to weak or zero-strength bonds.

The early impurity analysis methods available to Horsting at that time were limited to spectrographic and chemical analysis. He was unable to identify a specific impurity that caused the problem, but found that the impure Au films contained Ni, Fe, Co, B, and other

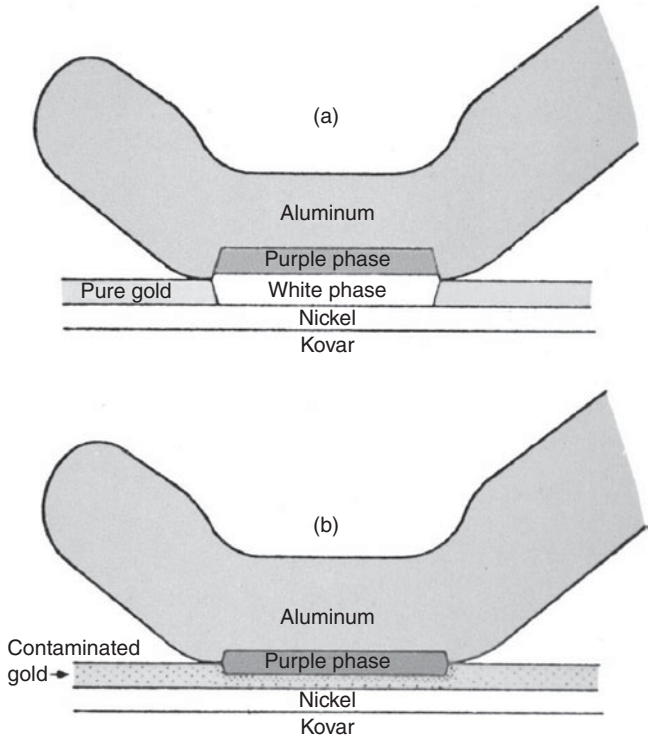

Figure 6A-1 (*a*) Schematic drawing of elevated temperature diffusion results for an aluminum wire bond to a pure gold plating. (*b*) Similar to a contaminated gold plating. (Note that the darkened intermetallic area under bonds is the purple phase.) (*After Horsting [6A-1]; © IEEE*.)

contaminants in lesser concentrations. He devised a pragmatic screening test that could detect such impure Au platings that affected bonding. The plated films (on Kovar headers) were multiply bonded with Al wire. They were heated at 390°C for 1 h after which the wire bonds were pulled. If bonds lifted from the Au during the pull test, the entire header lot was rejected. He observed that well-made Al bonds on pure Au platings always broke in the wire or at the bond heel after this heat treatment. The bond interface remained strong. Horsting's postulate of impurities concentrating ahead of the intermetallic diffusion front was later verified on Au thick films by using SEM, EDAX, and Auger analysis methods [6A-2].

A variation of Horsting's bake test (but at 300°C for 1 h, followed by a pull test) has been adopted as a qualification-test method for bonds in hybrid microcircuits for military usage [6A-3] and has been frequently used by the industry since the 1970s for quickly testing/qualifying Al wire bonds on Au pads or in some cases Au on Al pads.

6A.2 Specific Plating Impurities

Gold-plating baths, intended to deposit bonding films, normally consist of potassium-gold-cyanide, plus buffers, citrates, lactates, phosphates, and carbonates in proprietary mixtures. Thallium, lead, or arsenic may be added to increase plating speed and to reduce grain size. Organic "brighteners" (not recommended for wire bonding) can also be added to the bath. Thus, the problems arising in plating films are very complex, and they are not limited to the bath solution purity alone. It has also been shown that with any given Au bath and impurity level, the plating *deposit* can vary in crystallographic structure, appearance, impurity level, hardness, hydrogen content, and density with changes in the plating waveform or current density. In addition, different plating baths, as well as bath temperatures, can produce different results at the same current density level. The film characteristics and appearance will also vary as the Au solution is depleted. Variations in these film characteristics have all been shown to influence either the bondability or the reliability of wire bonds. It is therefore, not surprising that apparently the same platings obtained from different sources, or even from the same sources at different times, may cause wire-bond problems.

Thallium (TI) was the first identified and is still the most frequently cited impurity causing Al wedge bonding problems in Au platings.* [6A-4 to 6A-11]. Thallium, Pb [6A-8 to 6A-10, 11], and arsenic [6A-8] are commonly added to Au-plating solutions as grain refiners and to permit more rapid plating as well as to change the surface morphology.

Thallium in Au-plated films was first identified as a source of wire-bond failures by the *then new* Auger electron spectrograph [6A-4 to 6A-6]. It could not have been detected by wet chemical, normal spectrographic, or x-ray microprobe methods at those low concentrations. In these studies, the surface concentration of TI was sufficient to degrade thermocompression bondability of Au wire to Au-plated lead frames. It has been found that TI can be transferred to the Au wire from contaminated Au-plated lead frames during the crescent (second) bond break-off [6A-8]. The proposed explanation was that it diffused rapidly during ball formation and concentrated in the grain boundaries above the neck of the ball, where it formed a low melting eutectic. The concentration would be extremely low. It is at least as probable that the EFO, the bonding capillary, the heat stage clamp, or some other bonder setup conditions were not optimized. Many bonding problems often go away after almost any change in the processing schedule and the real reasons are generally not revealed, and the

*There are some inconsistencies in these data, but the overall comparison is considered valid. Several people have commented that modern Au-plating solutions may include Tl apparently without harm. However, such proof for Al wire bonds on Au platings has not been seen by this author in a bonding context.

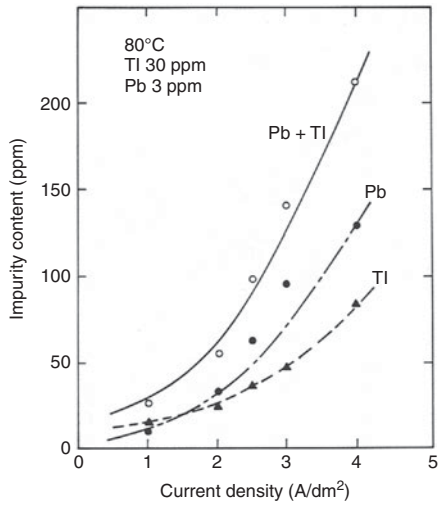

Figure 6A-2 Thallium and Pb content in gold deposits as a function of current density. Initial bath concentration was 3 ppm for Pb and 30 ppm for Tl. These are some impurities that are often intentionally added to the bath. (*After Wakabayashi [6A-10].*)

problem often returns at a later date—a good argument to solve/understand a problem once and for all!

Thallium, as well as high Pb content, in Au platings have also been shown to cause premature Al wire-bond failures during burn-in or other heat treatment, by accelerating cracks or Kirkendall-like void formation under the bond [6A-10, 6A-11]. Such failures have been observed to occur at TI concentrations as low as 14 ppm in the Au plating.

Wakabayashi [6A-10] recommended that the total of all impurities in the film must ***be less than 50 ppm to maintain bond reliability***. Figure 6A-2 shows that increasing the plating-current density increased the codeposited impurity level exponentially. Thus, controlling the bath concentrations alone will not necessarily assure pure films. Endicott [6A-8] studied the effect on bond strength of Tl, Pb, and arsenic at concentrations normally used as grain refiners and compared them to platings made with pure solutions. Adding Tl and Pb resulted in significant bond-strength degradation for both "as bonded" as well as after a 150°C thermal bake for 24 h. However, in low-solution concentrations and low-plating-current density, adding arsenic resulted in improved bond strength under both conditions. Figure 6A-3 is a simplified combination of several figures showing these effects. This figure was chosen because it clearly compared the separate effects of all three additives.*

*There are some inconsistencies in these data, but the overall comparison is considered valid. Several people have commented that modern Au-plating solutions may include Tl apparently without harm. However, such proof for Al wire bonds on Au platings has not been seen by this author in a bonding context.

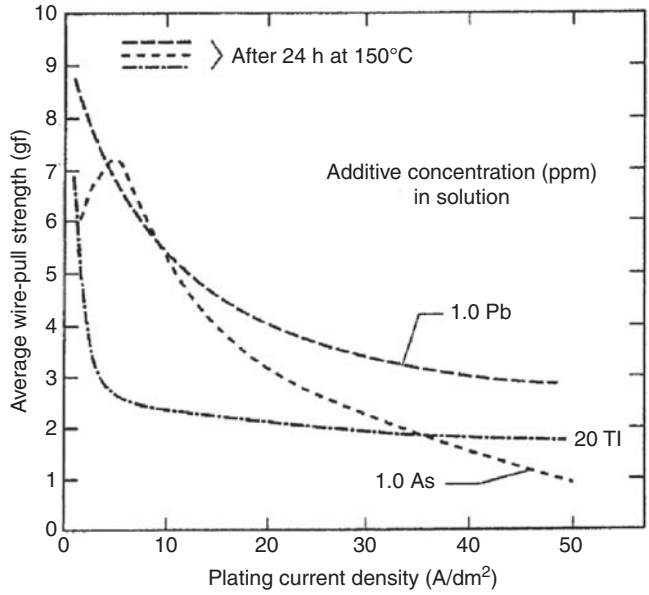

Figure 6A-3 Wire-bond pull strength for 32 μm (1.3 mil) diameter Al 1% Si wire bonds made to 1.25 μm thick plated gold films. The concentrations of grain refiners (T1, Pb, As) are at the recommended parts per million for optimum grain size. (*After Endicott [6A-8].*)

Other workers have shown more decrease in bond strength (to zero), with higher temperature or longer bake times [6A-9, 6A-10]. It is also possible that there may be a cooperative effect between other plating impurities and hydrogen in the film that together may result in very rapid bond-strength degradation.

There have been reports that the best Au surface for bonding is the <111> crystallographic surface. Pure Au or Au with arsenic additives, gives primarily <111> surfaces (desirable), but TI and Pb additives result in increased areas of <311> surfaces [6A-10]. These effects are also complicated by the morphology effect of different plating current densities. There are no data to definitely correlate bond quality with morphology.

6A.3 Hydrogen Gas Entrapments in Plated Films

Although TI is the most frequently cited plating impurity to cause both bondability and Kirkendall-like voiding, other plating impurities or conditions have been shown to cause one or more similar problems. Bondability degradation of Au-coated Cu wire was also found to occur when hydrogen bubbles were present in Au films [6A-12, 6A-13]. These bubbles can occur as a function of plating-current

density and bath-impurity level. Since this was a Au-Au interface, the bondability was addressed rather than the long-term reliability.* The lowest bondability for plated films occurred for plating currents in the 1.6 to 2.7 A/dm^2 region, which corresponded with both the onset of rapid hydrogen evolution at the cathode and a dendritic-like (lenticular) surface morphology. Some plating conditions that can lead to increased hydrogen in the film are high current density, low agitation, and low gold concentration in the bath. In general, any condition that reduces plating efficiency produces more gas at cathode and more entrapment. Any trapped gas can be driven out by heating and the time calculated by the equation time = 0.0033 exp (4062/T K). Hydrogen is typically annealed at ~350°C. Such H_2 filled films are harder, and thermal annealing will remove the H_2, resulting in the desirable hardness of ~70 HKN.[†,‡]

6A.3.1 Failure Symptoms that Appear Similar to Gas Entrapments: Resistance Drift

One reported failure mode that caused Al wedge bond resistance-drift during thermal excursions was found in platings that did not contain any of the known (measurable) impurities or gas entrapments [6A-14]. The authors concluded, after extensive analytical work, using SEM, STM, and AES, that their bad Au platings simply contained more vacancies and other defects than normal, resulting in a more amorphous crystal structure than was observed for reliable Au. Au-Al diffusion is driven by vacancies (Chap. 5) and other defects (increases the diffusion rate), which result in more rapid growth of intermetallic compounds and early failure. The same plating conditions that increased H_2 entrapment (high plating current density, low bath agitation, etc.) were given as causes for the film-defect problem. In addition, the authors found that thinner Au (as described in Chap. 5) also minimized the resistance drift and intermetallic failures. A prebake (before bonding) at 160°C for 48 h eliminated the drift problem, presumably recrystallizing the amorphous-like Au. These conditions and cures, similar to ones found for H_2 entrapment, were first reported by Huettner and verified [6A-12, 6A-13]. It is probable that these two film conditions are interrelated and can exist together or separately, complicating the diagnosis.

---

*For strong gold-to-gold bonds, long-term reliability is seldom a factor—with or without H_2.

†Special "*nano*-hardness testers" are required to make measurements on thin (typically ~1.3 μm, 50 μin) gold platings used for *bonding* in microelectronics. These require loads approximately 1 to 2 g or less. Sometimes platings are made much thicker on special test coupons so that more conventional hardness equipment can be used.

‡Keep in mind that nickel, copper, chrome, or other non-noble undercoats may be thermally diffused to the surface and then oxidized, which can cause bondability and reliability problems resulting from any high temperature annealing to remove H_2.

6A.4 Failures from Metallic Impurities in or on Gold Films That Are Not an Intentional Part of Plating Baths

6A.4.1 Introduction

There are numerous metallic contaminants that can be incorporated into the bond interface and degrade either bondability or reliability. Some may be accidentally introduced into a plating bath, others may be diffused up from the substrate, and still others may occur as a result of some later chemical or "cleaning" step and remain on the Au surface during bonding. These contaminants will be discussed along with any known cleaning techniques. One must be aware, however, that contaminants can be introduced from a source that is unanticipated and unknown at the time of this writing. Most metallic contaminants that affect bonds appear as surface films from 20 to 200 Å thick. If they consist of non-noble metals, they will generally be oxidized by various heat or chemical treatments before bonding, and the oxide may lower bondability (especially for TC bonding) and sometimes lower reliability. Hard-brittle oxides that occur on soft metals (e.g., Al_2O_3 on Al) break up and are pushed into "debris zones" during bonding as the Al deforms and generally have little effect on the bonding process. Softer oxides (e.g., Cu and Ni oxides) are observed to decrease bondability (increase the activation energy required to form a bond), possibly by serving as a lubricant in the bond interface.

Often, failure analyses reported in the literature may reveal contaminants in the interface of a failed bond, without being able to determine the source or even which steps in the packaging process were responsible for their introduction. In other reported cases, it was not clear that any single indicated impurity actually caused the failure. A complete study may have shown that a poor bonding machine setup was as much a cause of the failure as the various contaminants revealed in the failure analysis.

Metals that are deposited under a bondable film (such as metallurgical "glues" or adhesion layers, i.e., Ni, Ti, Cr, etc.) or impurities in the Au film may rapidly diffuse to the surface by grain-boundary diffusion. Figure 6A-4 illustrates grain-boundary diffusion paths for Cr through Au [6A-15]. A diffusing metal moves rapidly along the grain boundaries (which contain many defects) to the surface of the Au film during some high-temperature processing step, die attachment, or other heat treatment. On top, it will rapidly spread horizontally over the Au surface by surface diffusion [6A-16, 6A-17], oxidize (if it is non-noble), and then render the surface less bondable. Palladium (which does not oxidize below ~400°C) can pose an oxide problem if the surface is O_2-plasma or UV-ozone cleaned.

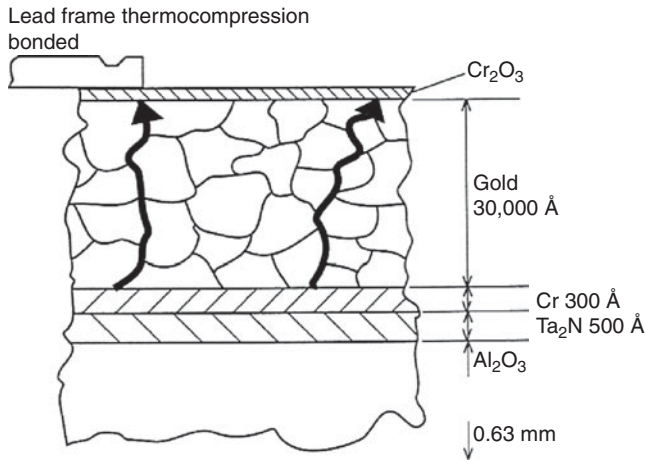

Figure 6A-4 Hybrid microcircuit geometry with Cr_2O_3 layer on the surface. The arrows indicate possible grain boundary diffusion paths. Bulk diffusion would be straight up, across the grains. Grain-boundary diffusion dominates at low temperatures, and bulk at high temperatures (typically higher than used in packaging operations). (*After Nelson [6A-15]; © ASTM.*)

The diffusion characteristics of various metals through Au films (via grain boundary and bulk) are shown in Fig. 6A-5 [6A-17, 6A-18]. In most cases, grain-boundary diffusion is many orders of magnitude faster than bulk diffusion (i.e., single crystal or through the grain), as can be seen in Fig. 6A-5. If a metal appears on the upper right-hand side of the figure (either grain boundary or bulk diffusion) it will move rapidly through the Au film at temperatures in the 100 to 300°C range and in times of an hour or less. Note the single datum point, a circle at the upper right side of the figure, which shows the very rapid grain boundary diffusion of Al through Au at 100°C. This indicates that some Au-Al intermetallics can occur very rapidly and at low temperatures (~100°C) [6A-18]. The diffusion coefficient for Al through Au was determined to be ($D = 5.8 \times 10^{-14}$ cm^2/s) at 100°C, with an activation energy of ~0.66 eV. If a diffusing metal reaches the surface and oxidizes, it can reduce the bondability. Palladium, a rapid diffuser through Au, does not significantly (thermally) oxidize below ~400°C, but can do so if the film is O_2-plasma or UV-ozone cleaned. Metals that appear on the lower left side of Fig. 6A-5 diffuse very slowly and should not reach the surface of the film without exposure to temperatures >300°C. If heated to a lower temperature, then very long times are required. Platinum is in the latter category, as is Ni *by bulk diffusion*, but Ni diffuses so fast through grain boundaries (and oxidizes on the surface) that it poses serious, often major, bondability problems.

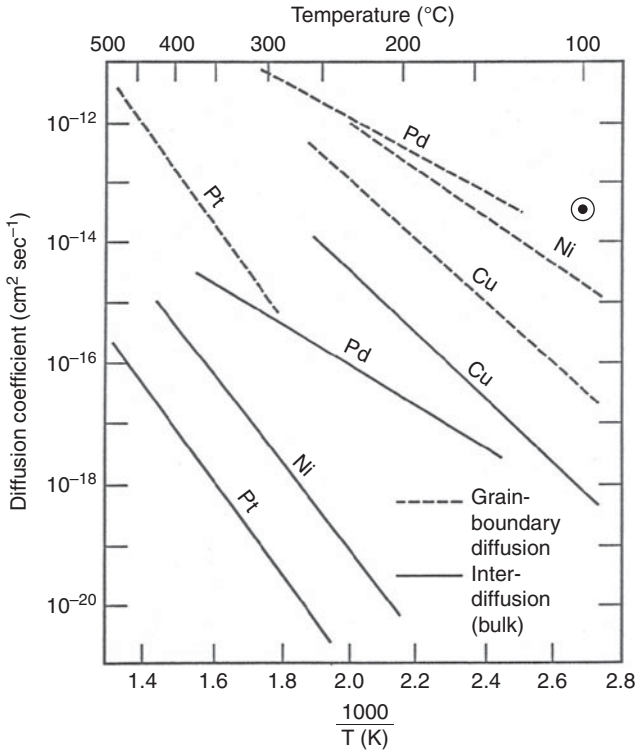

Figure 6A-5 An Arrhenius plot of diffusion coefficients for several metals through gold films (gold was the top layer). The solid lines are by bulk diffusion, and the dashed ones are by grain-boundary diffusion. The single datum point near the upper right is the grain-boundary diffusion of aluminum through gold at 100°C. (*After Hall [6A-17], kind premission of Elsevier; and Bastl [6A-18].*)

6A.4.2 Nickel

After TI (which was extensively discussed in Sec. 6A.2), Ni (as an oxide) is the most frequently cited metal to degrade bond strength on the surface of Au-plated films [6A-1, 6A-16, 6A-17, 6A-19 to 6A-22]. It is generally considered to affect bondability (by raising the bonding activation energy) but is also cited in [6A-1] as affecting reliability. Nickel may be introduced into an Au-plating bath by some accident, such as a Kovar (Fe, Co, Ni-low expansion alloy) lead frame falling into the bath and slowly dissolving. Another mechanism for Ni to enter the Au film is by thermally diffusing upward through the Au (and oxidizing on the surface) from a thin strike or an adhesion layer as described above. The effect of Ni on TC bondability is shown in Fig. 6A-6. As with TI, Ni, and Cu, concentrations in the Au film are strongly dependent on the plating current density, as shown in Fig. 6A-7.

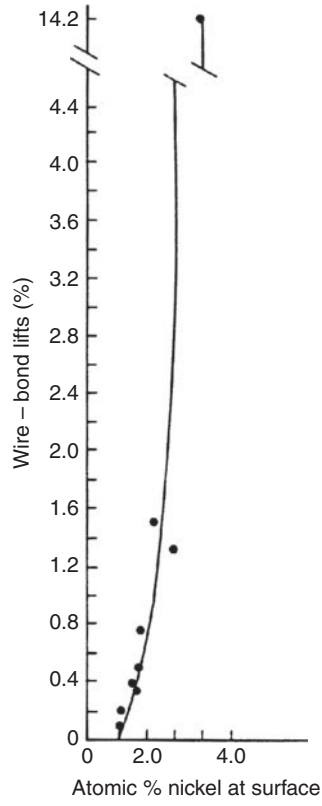

Figure 6A-6 Gold, TC wire-bond lifts versus Auger atomic percent nickel on surface of gold plating. Thermocompression wedge bonds of 38 μm (1.5 mil) gold wire. (Note that thermosonic/ultrasonic bonds are less sensitive to surface impurities than TC bonding, also see Chap. 7, Sec. 7.2.) (*After Casey [6A-19].*)

6A.4.3 Copper

Copper from plating-bath contamination, lead frames, etc., can follow the same diffusion route *to the surface* as Ni, and will oxidize and also decrease the bondability [6A-17, 6A-22 to 6A-26]. Various authors disagree which impurity, Cu [6A-20] or Ni [6A-22], has the most effect on bond-strength degradation, and this controversy may be related to the analysis method, the surface concentration, the impurity plating-out (Fig. 6A-7), the solution concentration, etc. If measured as atomic percent on the Au surface, then Ni is worse [6A-22]. Both Cu and Ni impurities should be avoided since they readily oxidize, and the oxides degrade bondability. Both Cu and Ni are still used as lead frames or as package base/under platings and are often bonded directly with large Al wire. Ultrasonic, TC, or TS bonding can be done at a high yield and maintains reliability only if the surfaces are oxide

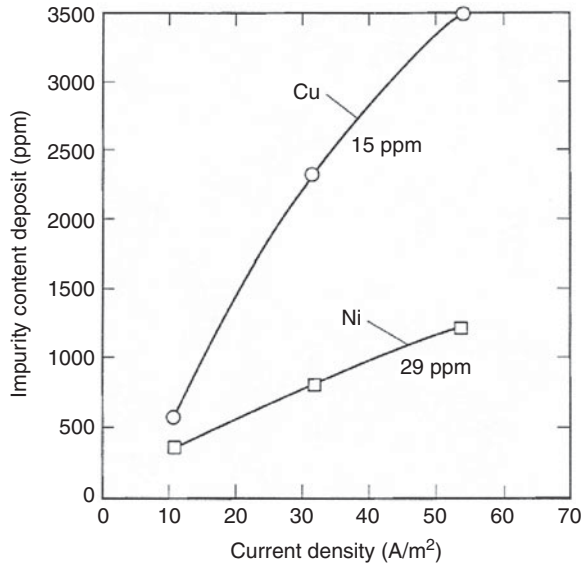

Figure 6A-7 Influence of plating-current density on the impurity content of Cu and Ni in gold deposits. (*After Dini* [*6A-22*]; © *ISHM*.)

free. Thus, for such bonding, an appropriate method of preventing oxide growth during storage or a chemical removal process is essential. It may be helpful in bonding directly to pure Cu or Ni to apply ultrasonic energy as the wire initially contacts the metal. This helps clear the oxide away before microwelds form and wire-to-substrate motion ceases.

6A.4.4 Chromium

Chromium, which has been used to promote adhesion between substrates and vacuum-deposited Au films, can rapidly diffuse through grain boundaries to the surface and oxidize [6A-15, 6A-27 to 6A-29]. Figure 6A-4 illustrates grain-boundary diffusion for Cr through Au; however, other metals (e. g., Ni, Cu) will similarly diffuse. Heating chrome-locked (glued) Au films for 2 h at 250°C was observed to impair the thermocompression bondability of 3 μm thick Au films [6A-27]. Higher temperatures or *thinner films* will decrease the diffusion time significantly. A special cleaning etch, cerric ammonium nitrate, was developed to remove the Cr oxide from Au surfaces and completely restore thermocompression bondability [6A-29].

6A.4.5 Titanium

Titanium, as with Cr, is used in various substrate-metallization systems [6A-30] and can diffuse up to the Au surface or be deposited on it during some part of the processing procedure [6A-31]. It will oxidize

and decrease bondability. A dilute 10:1 HF, HNO_3 etch on the Au surface restores bondability. Note, however, cleaning must be rigorous since any remaining traces of this etch could degrade the reliability of Al wire bonds later put on the surface, although initially strong Au bonds should remain unaffected.

6A.4.6 Tin

Tin has been identified in two studies as leading to bond failures. One found that Sn was deposited (possibly as the oxide, from the Auger analysis) on the Au substrate by a contaminated cleaning solution [6A-32]. Tin thickness in the range of 20 to 30 Å (presumably as an oxide) reduced bondability significantly. A potassium carbonate rinse was used to remove the tin from the substrates. This rinse left traces of potassium on the surface, which might later affect some active devices! Tin was also found to cause Au thermocompression-bond failures to Al pads [6A-33]. Apparently, Sn (as an oxide) prevented a strong bond from forming. This latter work was not clear as to the sources or the extent of the tin problem, since carbon that could have been a contributing factor was also found in the interface (as is typical of the problems we face in complex assembly). Nevertheless, upon aging, tin does form an oxide which is tenacious and impervious enough to reduce solderability in tin-plated lead frames, so it should also be considered a potential hazard for wire bonding. (Note: If you cannot solder to a surface using a nonactivated flux, you cannot wire bond to it either!)

6A.5 Gold Plating Standards

There are no generally accepted standards for platings used for wire bonding, and Horsting's pragmatic screen [6A-1], or equivalent, is still in use and often necessary to qualify a gold plated lot! The accepted plating specifications for Au in electronics are MIL-G-45204 and ASTM B 488-01 (2006). Selected portions of these specifications (listed in Table 6A-1) are minimal for assuring high-quality wire bonds, but are the best standards available and in wide usage.

MIL-G-45204
Type I 99.7 % gold min. (Grade A, B, or C) Type III 99.9 % gold min. (Grade A only) Grade A, Knoop 90 max.
ASTM B 488-01(2006)
Type 1 99.9 % gold min. (Grade A only) Grade A, Knoop 90 max.

Table 6A-1 Specifications for Gold-Plated Films

6A.5.1 Recommendations for Reliable Gold-Plated Films

Gold films with desirable characteristics (bondability, reliability, large bonding window) should, based upon the foregoing, contain no measurable Tl and less than 50 ppm total of Ni, Cu, and Pb impurities. Analysis should be made on a sample basis on the film itself if possible* since many variables can change the correlation between plating solution and film impurity level. Hydrogen and other gas occlusions should be at a minimum. The film should be soft with a hardness of 60 to 80 HKN (*note that these are lower than in both of the above standards*) and nodular in appearance. It should not be shiny (bright), nor have a lenticular surface structure. It is possible that a <111> dominant-surface structure is desirable, but this has not been proven. Unbondable or unreliable Au films that contain hydrogen can be hardness tested, annealed (if appropriate equipment is available†), and, if softer, should be bondable, unless the Au film is thin and was plated over Ni, Cr, Ti, or Cu that has been heated and diffused to the surface. (Note: diffused up surface contaminants can usually be removed by Argon Plasma sputtering before bonding.)

During annealing, any of these metals may diffuse to the surface, oxidize, and render the Au unbondable. This oxide must then be chemically removed if the plating is to be bonded. Gold platings over combination adhesion-barrier coatings, such as titanium-palladium, limit diffusion and can generally be heat treated and used without further cleaning. Since plating conditions, such as waveform, bath temperature, and composition, can affect the film characteristics, there is no specific recommendation for a plating current density (except low) to achieve bondable, reliable films. The literature is contradictory in this regard. If grain refiners or Ni, Cu, etc., are in the bath, then high plating rates will generally increase their incorporation in the films and produce bonding problems.

The wide spectrum of Al-wire to Au-plating bond failures is most perplexing. Such failures have been shown to result from numerous different impurities, H_2 gas in the Au films, or simply a high level of crystallographic defects in an otherwise pure Au plating. Any given Au film could have some combination of these, and an Al bond failure would become impossible to accurately diagnose. The pragmatic test of Horsting for wedge bonds (bond, bake, and pull test) [6A-1] and the observation of a large bonding window appears to be the simplest approach for the user to adopt. The characteristics of reliable platings are summarized in Table 6A-2.

---

*Frequent analysis of plating lots to 50 ppm would be prohibitively expensive. A pragmatic test, such as Horsting's [6A-1] bake test, can be quickly applied to many plating lots and only the ones causing wire bonding failures analyzed further in more detail.

†Special "*nano*-hardness testers" are required to make measurements on thin (typically ~1.3 μm, 50 μin) gold platings used for *bonding* in microelectronics. These require loads approximately 1 to 2 g or less. Sometimes platings are made much thicker on special test coupons so that more conventional hardness equipment can be used.

Gold Films Bond Well and Are Reliable If They:

1. Are pure yellow in color.
2. Are uniform, matte, and lusterless in appearance.
3. Are smooth & free from pits, blisterrs, or other blemishes.
4. Are soft (~80 Knoop), ductile, and dense.
5. Have <50 ppm of total impurity content.
6. Have <1 ppm Tl and low H_2 content.
7. Have a wide bonding parameter window!!

TABLE 6A-2 Characteristics of Plated Gold Films for Bonding

6A.6 Electroless Autocatalytic Gold

In addition to electroplated Au normally used for thicker (~1μm) bonding pads, there are two published autocatalytic electroless Au deposition processes that might be used for such thicker deposits [6A-34, 6A-35]. (These are not the thin (≤0.2 μm) displacement/immersion Au films which are in high volume production—and are usually deposited on Ni to enhance bondability.) The first autocatalytic Au has been extensively used for both Au and Al wire bonding on ceramic as well as on some chemically resistant plastic packages. It is plated from a high pH (13 to 14) solution, which may damage some organic substrates. The second has been used on PC boards and some experimental wire bonding applications. This is plated from a noncyanide solution with a neutral pH. It has been tested for wire bond reliability. However, its solution *shelf life is short,* reducing its usability, especially for laboratory experiments. Both plating methods can deposit Au films in the range of 1 to 3 μm/h. Both offer the possibility of plating to conductor surfaces that are insulated from electrical contact, on boards and ceramic packages. As such, they could be used for bonding applications. However, both take much longer for a comparable thick deposit than electroplating, a disadvantage for production. Currently, thick Au is so costly that alternatives are preferred.

6A.7 Nongold Platings Used in Electronics Packaging

There are several nongold metal platings used in packaging that may affect bonding. The most important are Ni and Pd. Nickel is used in both electroplated and electroless form with the latter dominating in microelectronics applications. There are a number of plating solutions available for each type of deposition, and these are discussed in detail in the second section of this chapter by Luke England and Jamin Ling. The complete physical properties, as well as the chemistry, of various electroless Ni compositions have long been published [6A-36, 6A-37]. Military specifications for electroless Ni are MIL-C-26074 E (for both phosphorus and

boron containing), ASTM, and AMS specifications are maintained. The most used electroplated Ni for bonding (sulfamate) is MIL-P-27418. Typically, Ni is used as a base for other metals platings and, in particular, for Pd and Au. However, Ni is also used directly for bonding with some large-diameter Al wire in power devices. The Ni-Al wire bond interface reliability was discussed in Chap. 5, Sec. 5.3.6, and it is very reliable. Palladium has been used for lead frame and PC board coatings. Its bonding properties and other uses were discussed in Chap. 5, Sec. 5.3.4.

Chapter 6A References

6A-1 Horsting, C., "Purple Plague and Gold Purity," *10th Annual Proc. IRPS*, Las Vegas, Nevada, April 5–7, 1972, pp. 155–158.

6A-2 Newsome, J. L., Oswald, R. G., and Rodrigues de Miranda, W. R., "Metallurgical Aspects of Aluminum Wire Bonds to Gold Metallization," *14th Annual Proc. Rel. Phys.*, Las Vegas, Nevada, April 20-22, 1976, pp. 63–74.

6A-3 MIL Standard 883 G (2006), *Test Methods and Procedures for Microelectronics*, and in MIL-PRF-38534F (2006), APPENDIX C.

6A-4 McDonald, N. C. and Palmberg, P. W., "Application of Auger Electron Spectroscopy for Semiconductor Technology," *Intl. Electron Devices Meeting*, Washington, D.C., October 11–13, 1971, pp. 42–43.

6A-5 McDonald, N. C. and Riach, G. E., "Thin Film Analysis for Process Evaluation, Electronic Packaging and Production," April 1973, pp. 50–56.

6A-6 Czanderna, A. W., Ed., *Methods of Surface Analysis VI*, Chapter 5, Elsevier Scientific Publishing Co., New York, 1975, pp. 212–222.

6A-7 James, H. K., "Resolution of the Gold Wire Grain Growth Failure Mechanism in Plastic Encapsulated Microelectronic Devices," *IEEE Trans. on Components, Hybrids, and Manufacturing Technology CHMT-3*, September 1980, pp. 370–374.

6A-8 Endicott, D. W., James, H. K., and Nobel, F., "Effects of Gold-Plating Additives on Semiconductor Wire Bonding," *Plating and Surface Finishing*, Vol. 68, November 1981, pp. 58–61.

6A-9 Okumara, K., "Degradation of Bonding Strength (Al Wire—Au Film), by Kirkendall Voids," *J. Electrochem. Soc.,* Vol. 128, 1981, pp. 571–575.

6A-10 Wakabayashi, S., Murata, A., and Wakobauashi, N., "Effects of Grain Refiners in Gold Deposits on Aluminum Wire-Bond Reliability," *Plating and Surface Finishing*, August 1982, pp. 63–68.

6A-11 Evans, K. L., Guthrie, T. T., and Hays, R. G., "Investigation of the Effect of Thallium on Gold/Aluminum Wire Bond Reliability," *Proc. ISTFA,* Los Angeles, California, 1984, pp. 1–10.

6A-12 Huettner, D. J. and Sanwald, R. C., "The Effect of Cyanide Electrolysis Products on the Morphology and Ultrasonic Bondability of Gold," *Plating and Surface Finishing*, Vol. 59:88, August 1972, pp. 750–755.

6A-13 Joshi, K. C., Sanwald, R. C., and Annealing, H., "Behavior of Electrodeposited Gold Containing Entrapments," *J. Electronic Materials,* Vol. 2, 1973, pp. 533–551.

6A-14 Murcko, R. M., Susko, R. A., and Lauffer, J. M., "Resistance Drift in Aluminum to Gold Ultrasonic Wire Bonds," *IEEE Trans. CHMT,* Vol. 14, December, 1991, pp. 843–847.

6A-15 Nelson, G. C. and Holloway, P. H., "Determination of the Low Temperature Diffusion of Chromium Through Gold Films by Ion Scattering Spectroscopy and Auger Electron Spectroscopy," *ASTM Special Technical Publication 596, Surface Analysis Techniques*, 1976, pp. 68–77.

6A-16 Loo, M. C. and Su, K., "Attach of Large Dice with Ag/Glass in Multilayer Packages," *Hybrid Circuits* (UK) Number 11, September, 1986, pp. 8–11.

6A-17 Hall, P. M. and Morabito, J. M., "Diffusion Problems in Microelectronics Packaging," *Thin Solid Films,* Vol. 53, 1978, pp. 175–182.
6A-18 Bastl, Z., Zidu, J., and Rohacek, K., "Determination of the Diffusion Coefficient of Aluminum Along the Grain Boundaries of Gold Films by the Surface Accumulation Method," *Thin Solid Films,* Vol. 213, 1992, pp. 103–108.
6A-19 Casey, G. J. and Edicott, D. W., "Control of Surface Quality of Gold Electrodeposits Utilizing Auger Electron Spectroscopy," *Plating and Surface Finishing*, Vol. 67, July 1980, pp. 39–42.
6A-20 McGuire, G. E., Jones, J. V., and Dowell, H. J., "Auger Analysis of Contaminants that Influence the Thermocompression Bonding of Gold," *Thin Solid Films*, Vol. 45, 1977, pp. 59–68.
6A-21 Endicott, D. W. and Casey, G. J., "High Speed Gold Plating from Dilute Electrolytes," *Proceedings American Electroplaters Soc.*, paper 1-d3, 1979.
6A-22 Dini, J. W. and Johnson, H. R., "Influence of Codeposited Impurities on Thermocompression Bonding of Electroplated Gold," *Proc. ISHM Symposium*, Los Angeles, CA, October 1979, pp. 89–95.
6A-23 Panousis, N. T., "Thermocompression Bondability of Bare Copper Leads," *IEEE Trans. on Components, Hybrids, and Manufacturing Technology CHMT-1*, 1978, pp. 372–376.
6A-24 Panousis, N. T. and Hall, P. M., "Application of Grain Boundary Diffusion Studies to Soldering and Thermocompression Bonding," *Thin Solid Films*, Vol. 53, 1978, pp. 183–191.
6A-25 Dini, J. W. and Johnson, H. R., "Optimization of Gold Plating for Hybrid Microcircuits," *Plating and Surface Finishing*, Vol. 67, Jan. 1980, pp. 53-57.
6A-26 Spencer, T. H., "Thermocompression Bond Kinetics—The Four Variables," *Intl. J. Hybrid Microelectronics*, Vol. 5, 1982, pp. 404–408.
6A-27 Panousis, N. T. and Bonham, H. B., "Bonding Degradation in Tantalum Nitride-Chromium Gold Metallization System," *11th Annual Proc. Reliability Physics*, Las Vegas, NV, April 3–5, 1973, pp. 21–25.
6A-28 Harman, G. G., "The Use of Acoustic Emission in a Test for Beam-Lead, TAB, and Hybrid Chip Capacitor Bond Integrity," *IEEE Trans. on Parts, Hybrids, and Packaging*, Vol. 13, 1977, pp. 116–127.
6A-29 Holloway, P. H. and Long, R. L., "On Chemical Cleaning for Thermocompression Bonding," *IEEE Trans. on Parts, Hybrids and Packaging,* Vol. 11, 1975, pp. 83–88.
6A-30 Donya, A., Watari, T., Tamura, T., and Murano, H., "GLO: A New Technology for Fabrication of Fine Lines on Multilayer Substrate," *Proc. IEEE Electronics Components Conference,* Orlando, FL, 1983, pp. 304–313.
6A-31 Thompson, R. J., Cropper, D. R., and Whitaker, B. W., "Bondability Problems Associated with the Ti-Pt-Au Metallization of Hybrid Microwave Thin Film Circuits," *IEEE Trans. on CHMT,* Vol. 4, 1981, pp. 439–445.
6A-32 Vaughan, J. G. and Raut, M. K., "Tin Contamination During Surface Cleaning for Thermocompression Bonding," *Proc. ISHM,* 1984, pp. 424–427.
6A-33 Davis, L. E. and Joshi, A., "Analysis of Bond and Interfaces with Auger Electron Spectroscopy," *Proc. Advance Techniques in Failure Analysis,* Los Angeles, California, October 1977, pp. 246–250.
6A-34 Gaudiello, J. G., "Autocatalytic Gold Plating Process for Electronic Packaging Applications," *IEEE Trans. on CPMT-Part A,* Vol. 19, March 1996, pp. 41–44.
6A-35 Inoue, T., Ando, S., Okudaira, H., Ushio, J., Tomizawa, A., Takehara, H., Shimazaki, T., Yamamoto, H., and Yokono, H., "Stable Non-Cyanide Electroless Gold Plating Which is Applicable to Manufacturing of Fine Pattern Printed Wiring Boards," *Proc. 45th ECTC,* Las Vegas, NM, May 21–24, 1995, pp. 1059–1067.
6A-36 Gawrilov, G. G., *Chemical (Electroless) Nickel-Plating,* Portcullis Press Ltd, Redhill, Surry (GB), 1979.
6A-37 Watson, A. S., "Electroless Nickel Coatings," Nickel Development Institute, NiDI Technical Series No. 10055, 1989 (note other Ni plating pubs. in the series with the same date are 10-047, -048, -049, -052, and -053).

Section 6B Ni-Based Platings Used in Electronics Packaging*

There are several Ni-based metal plating structures used in packaging that may affect bonding. The most important are Ni/Au, Ni/Pd, and Ni/Pd/Au. The plating processes are used in both electroplated and electroless/immersion forms, with the latter dominating in microelectronics applications. There are a number of plating solutions available for each type of deposition, and these are beyond the scope of this book. Therefore, only the basic principles of electroless/immersion plating will be discussed. More detail on this topic can be found in a number of books specializing in the subject. This section will focus on the process and reliability of wire bonding to these Ni-based plated bond pads.

6B.1 Background

In recent years, CMOS technologies have been moving forward with ever shrinking geometries at a much faster rate than the external interconnect technologies. Die size is often limited by bond pad dimensional constraints; therefore, valuable Si surface area may not be maximized for active circuitry areas. There are now strong demands to modify the device design rules to allow both wire bonding and probing on the same pad. Depending on the design of the device, a stronger bond pad structure may be necessary to prevent damage to any sensitive areas under the bond pad such as dielectric layers or actual circuitry in the case of bond pad over active areas [6B-1, 6B-2]. Options to prevent damage include enhanced mechanical properties of underlying dielectrics, reinforcement of layer-to-layer adhesion, and/or changing bond pad metallization to have a stiffer bond pad that can better accept the dual forces of probing and wire bonding on the same location.

Another trend for many semiconductor manufacturing facilities is to use Cu interconnect metallization for their integrated circuit fabrication (see Chap. 10). This is because the Cu has a significantly higher conductivity than the Al used in traditional interconnect metallization structures, which is essential to achieve optimum performance for high-speed applications. Traditional wire bond methods cannot be used consistently or reliably on the Cu metallization due to the tendency for tenacious oxide formation on bare Cu. Even with pre-bond oxide removal, the surface is virtually unbondable because

*By Luke England (Fairchild Semiconductor, luke.england@fairchildsemi.com) and Jamin Ling (Kulicke and Soffa, JLing@kns.com). Both authors contributed equally. Names are listed in alphabetical order.

the Cu rapidly forms an oxide skin over the bond pad surface regardless of the time between cleaning and bonding. Furthermore, even if an oxide layer could be prevented between cleaning and bonding, the temperature increase imposed on the device during the wire bonding process would most certainly drive Cu oxide formation before reliable wire bonds could be made. One common technique for wire bonding to Cu interconnects is the addition of a sputtered Al layer over the bond pad area, which then becomes the wire bonding surface [6B-3]. The cost of adding this Al layer, however, is usually quite high due to the use of expensive metal deposition and photolithography processing techniques required to obtain the Al pad structure. However, it is compatible with traditional bonding technology and therefore in some cases preferable to alternatives.

With recent increases in the price of Au, Cu has regained its traction for wire bonding to potentially replace the very expensive Au wire [6B-4]. Due to the higher potential of Cu to work-harden during ball bonding, a harder and stiffer bonding surface can help prevent bond pad cratering and other damage that is easily induced during Cu ball bonding for both Cu and Al interconnect materials. Alternative bond pad structures have been proposed and adopted recently, which include the addition of a Ni layer directly over the bond pad interconnect. Ni-based bond pads have been extensively used in semiconductor packaging as bond pads for both laminated substrates and metal lead frames. Since the introduction of bare Cu leadframes to replace the more expensive Kovar material, Ni-based bond pads have become prevalent for metal leadframe second bond (stitch bond) locations. Since Ni has a tendency to oxidize, an inert metal such as Pd and/or Au should be deposited on the Ni to prevent oxidation from occurring either before or during wire bonding. Typical bond pad structures include Ni/Au, Ni/Pd, or Ni/Pd/Au layer stacks. Recently, there have been increasing reports and studies using these bond pad structures on semiconductor devices for thermosonic ball bonding [6B-5 to 6B-9]. The Ni, Pd, and Au bond pad metals can be deposited onto either Al or Cu base metals using a plating process (either electrolytic or electroless), and the structures listed previously are now gaining traction in the industry for ball bonding to semiconductor devices.

Other than the obvious advantages of allowing for wire bonding to Cu interconnect structures, the superior mechanical properties of Ni can provide the protection to sensitive underlying pad structures. Ni has a much higher elastic modulus than either Cu or Al. Table 6B-1 shows typical elastic modulus values for pure Ni, Cu, and Al for comparison. The high modulus of Ni leads to high stiffness and fracture toughness, which gives the Ni layer a high potential to resist deflection and absorb energy during the ultrasonic application and downward force applied to the bond pad during the ball bonding process. This makes a Ni base metal an ideal choice for scenarios where probing and wire bonding may be required on the same bond pad.

Elastic Modulus		Poisson's Ratio
Ni	200 GPa	0.31
Cu	130 GPa	0.34
Al	70 GPa	0.35

Source: www.webelements.com

Table 6B-1 Elastic Modulus and Poisson's Ratio Values for Al and Cu (Standard Interconnect Metals) and for Ni (Bond Cap Material)

6B.2 Electroless Plating Processes

As mentioned previously, electroless and electrolytic plating methods can be used to deposit Ni, Pd, and Au onto interconnect pads of either Al or Cu composition. Electroless/immersion plating is a better economic approach than electroplating because it does not require expensive photolithography and etch processes. There are challenges, however, with electroless/immersion plating for wire bond applications. Thicker metal layers are desired for good bondability, and these are more easily obtained using electrolytic methods. Plating selectivity can also be an issue. It is sometimes difficult for plating initiation to occur on very small features depending on processing conditions (i.e., bath composition, temperature, etc.), making good plating bath control imperative. Some possible plating issues/problems are shown in Fig. 6B-1. In spite of these potential issues, electroless/immersion plating remains a viable process for creating bondable surfaces on semiconductor devices.

Typically, the electroless plating process relies on the plating chemistry to react with a catalyst treated substrate in the plating bath to initiate a thin layer of deposit. The substrate is then submerged in another plating bath to further nucleate the element to be deposited. This depositing process continues until the target thickness is reached, which is theoretically unlimited. The plating only occurs on areas of the substrate where metal is exposed; therefore, no masking is needed to cover other areas. The immersion plating process, on the other hand, is a self-limiting chemical reaction. The element to be plated essentially replaces the base metal it is being deposited on. Once the base metal is fully covered with the plated element, the reaction ceases, and the plating process is complete. This section will discuss the electroless/immersion processes of Ni, Pd, and Au plating in detail. Table 6B-2 shows a typical plating process flow for Al and Cu base metals.

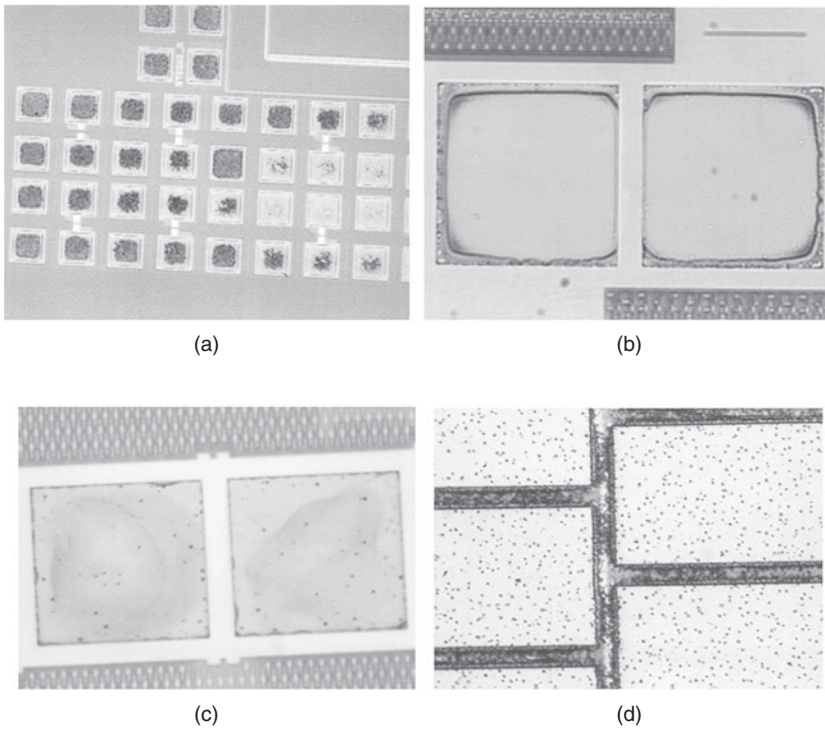

Figure 6B-1 Possible defects that can occur during the electroless/immersion plating process. (*a*) Skip Plating—Plating doesn't initiate onto some or all of the bond pads. (*b*) Step Plating—A plating layer doesn't initiate on all areas of the pad. The result is a "step" from the top plated layer surface to the bottom surface. (c) Blister—Immersion Au plating is thin in areas of the pad. The darker areas are typically caused by oxidation of Ni that is exposed on the surface from the thin Au plating. (*d*) Shorting—Bond pads with a small pitch can plate together during the process.

6B.2.1 Ni Plating

The electroless Ni plating process begins with an initial cleaning to prepare the exposed surface for the catalyst, which is typically a mild acid wash to remove any surface contaminants that may be present. This is followed by an acid rinse that removes any surface oxides present on the surface. For plating on an Al surface, a zincate process is used to etch away a very fine layer of Al from the pad and redeposit a layer of Zn on the pad. This Zn will act as a catalyst for the Ni plating to follow. It is common to perform a second zincate process, which helps to make the surface more uniform for the Ni plating that follows. For plating onto a Cu surface, a Pd activation process is typically used rather than the zincate process [6B-10, 6B-11].

(a) Al Base Metal		
Process	**Temperature**	**Time**
Cleaner	50°C	3 min
Rinse		
Nitric acid rinse	21°C	30 s
Rinse		
1st zincate	21°C	10 s
Rinse		
Nitric acid rinse	21°C	1 min
Rinse		
2nd zincate	21°C	35 s
Rinse		
Electroless Ni	80°C	25 min
Rinse		
Immersion Au	75°C	10 min
Rinse		
Autocatalytic Au	50°C	14 min
Rinse		

(b) Cu Base Metal		
Process	**Temperature**	**Time**
Cleaner	50°C	5 min
Rinse		
Sulfuric acid copper etch	25°C	1 min
Rinse		
Sulfuric acid pre-dip	25°C	1 min
Palladium catalyst	25°C	2 min
Rinse		
Electroless Ni	80°C	25 min
Rinse		
Immersion Au	75°C	10 min
Rinse		
Autocatalytic Au	50°C	14 min
Rinse		

Note: The options shown include immersion Au and autocatalytic Au. It is also possible to use an electroless Pd layer between the Ni and immersion Au, although it is not shown here. *Courtesy of Uyemura.*

Table 6B-2 Typical Process Flow of an Electroless Plating Pond Pad Process for (*a*) an Al Base Metal and (*b*) a Cu Base Metal with Thick Au

An electroless Ni plating bath is very complex as it contains many more chemicals than the Ni source alone (i.e., reducing agent, complexant or chelating agent, stabilizer, etc.). These bath components perform specific functions in the chemical reaction. They are critical to obtain a good quality metal deposit and must be monitored carefully during processing. In order to get the ionized metal in the bath to lower its valence state and plate onto the pad surface, a reducing agent must be used. In the Ni bath, the reducing agent is typically hypophosphite. Equation (6B.1) shows the simplified chemical equation for the electroless Ni plating process.

$$Ni^{2+} + H_2PO_2^- + H_2O \longrightarrow Ni + H_2PO_3^- + 2H^+ \qquad (6B.1)$$

During deposition of the Ni, P from the hypophosphite reducing agent is also deposited on the surface of the base metal. Depending on bath composition, the P levels in the plated Ni(P) layer can vary [6B-10, 6B-12, 6B-13]. For semiconductor applications, the P level is tyically targeted to be roughly 7 to 10%. These levels of P result in an amorphous Ni(P) layer, which is more suitable for a diffusion barrier since no grain boundaries exist. The amount of P that is deposited also helps to determine final mechanical properties of the film such as hardness. As plated hardness for low-P deposits is in the 700 to 750 HK range, while hardness is only 500 HK for high-P deposits [6B-12].

The plating rate of Ni is also a controlable parameter duirng the process, which in turn affects the final surface roughness. Obviously a fast plating rate will increase throughput of the process, but fast plating rates can also result in a rougher Ni surface. Therefore, a careful balance must be maintained between processing speed and surface quality. If the Ni surface is too rough, the next successive metal layers to be plated on the Ni will follow the contours and also result in a rougher surface. As will be discussed in the following section, both surface hardness and roughness have a strong effect on final wire bondability and bond strength. Harder and rougher surfaces typically are less bondable.

6B.2.2 Pd Plating

Pd plating was first investigated as a replacement for Au plating to combat the high cost of Au. Pd and PdNi alloys were initially developed for contact wear resistance in connector applications, but other technical advantages were identified as usage grew. Not only is the pure Pd layer extremely hard (450 to 600 HK) [6B-14], but the Pd deposit is extremely dense and acts as an excellent diffusion barrier coating [6B-5].

For wire bonding applications, pure Pd plating is typically used rather than PdNi alloys. As in electroless Ni deposition, Pd plating requires a catalyst pretreatment to prepare the surface for deposition. The metal source is typically a Pd-ammonia compound with a

hydrazine reducing agent for metal deposition. The major chemical reaction occurring during electroless Pd deposition is shown simplified in Eq. (6B.2).

$$2Pd(NH_3)_4^{2-} + N_2H_4 + 4OH^- \longrightarrow 2Pd + 8NH_3 + N_2 + 4H_2O \qquad (6B.2)$$

6B.2.3 Au Plating

Au has long been a mature plating process for electronic applications. Two types of Au plating processes through chemical reactions exist—immersion and autocatalytic. Immersion Au plating is a self-limiting galvanic displacement process, therefore, no reducing agent is necessary. For microelectronic applications the base metal for immersion Au plating is typically Ni. Equation (6B.3) shows the simplified equation for immersion Au plating onto Ni.

$$\begin{aligned} Ni &\longrightarrow Ni^{2+} + 2e^- \\ 2Au^+ + 2e^- &\longrightarrow 2Au \end{aligned} \qquad (6B.3)$$

The deposited Au atoms physically replace Ni atoms that supply the electrons for the reaction. This reaction ceases when the Ni is completely covered by Au, with a typical final Au layer thickness of <0.05 μm. The immersion Au chemistry must be carefully controlled due to the nature of the process. If the plating is too aggressive, the result will be uncontrolled removal of the Ni layer. This can leave a nonuniform porous Ni surface, which is a poor surface for wire bonding. A secondary effect of uncontrolled Ni removal during plating is the entrapment of Ni atoms within the newly deposited Au layer. This "suspended" Ni is then free to oxidize when exposed to air, which can inhibit wire bondability.

When the base metal for electroless Ni immersion Au plating is Cu, the overall pad structure should be taken into account. Since the plating layers do not adhere to the dielectric sidewall of the bondpad opening, there is a path for the plating chemistries to come in contact with the Cu base metal. Immersion Au chemistries are particularly corrosive to the Cu base metal; therefore, any plating bath that comes into contact with the base metal can result in undesirable removal of the Cu metal. Figure 6B-2 shows a cross-section of a Ni/Au plated Cu bond pad with corrosion at the dielectric/Cu/Ni interface caused by interaction with the immersion Au chemistry. This may contribute to an overall degradation of long-term device reliability. The sketch in Fig. 6B-3 illustrates this concept. The best protection against this phenomenon is to allow the electroless Ni layer to plate thicker than the dielectric layer so lateral plating of Ni occurs. This eliminates the direct path for immersion Au chemistry to penetrate the gap between Ni and dielectric layers. A good rule of thumb is to allow for 3 μm of lateral plating distance to minimize the effects.

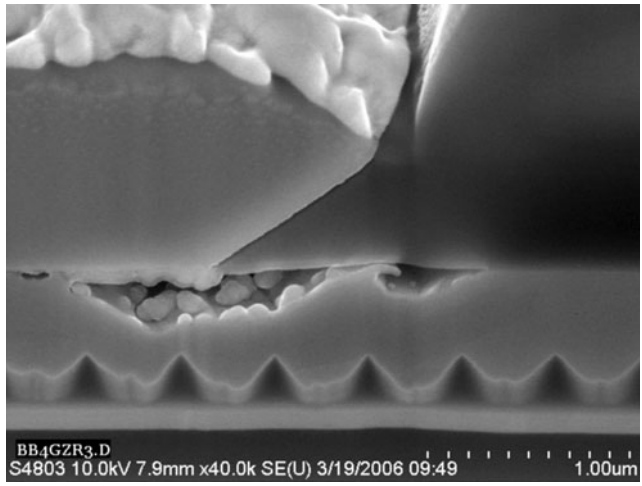

Figure 6B-2 Cross-section image of an ENIG plated Cu bond pad. Notice the Cu corrosion at the point where the Ni plating sidewall begins. This is due to an aggressive immersion Au chemistry attacking the Cu base metal. The severity of Cu corrosion can be controlled by changes to the immersion Au bath (i.e., temperature, pH, chemistry). Figure 6B-3 discusses this in further detail.

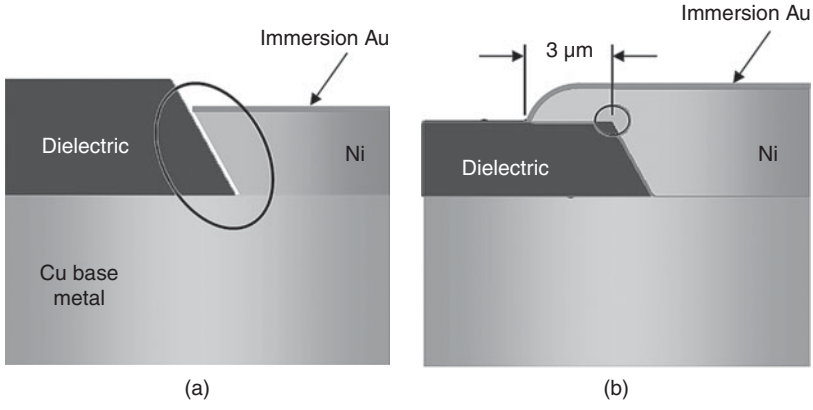

Figure 6B-3 (*a*) Drawing that illustrates electroless Ni immersion Au plating on Cu base metal. Since the plated metals are deposited selectively on other metal only, they cannot adhere to the dielectric. This leaves a small gap, which can be on the atomic scale for width. The gap allows for immersion Au plating chemistry to penetrate the electroless Ni sidewall and corrode the Cu base metal. This could have the potential to cause long-term reliability issues, especially for electromigration, although no study to assess reliability issues with this problem has been published to the author's knowledge. The gap is also a path for surface diffusion of Cu metal atoms throughout the product's life, especially in instances of elevated temperature. (*b*) The recommendation to avoid Au chemistry corrosion of Cu base metal is to plate a thick layer of Ni where 3 µm of lateral plating has been achieved. The Au chemistry penetration is then kept mostly to the point where lateral plating begins (area circled in drawing). *Note: Drawings not to scale.*

Following immersion Au plating with autocatalytic (electroless) Au plating is an excellent way to thicken the overall top layer of Au. Autocatalytic Au chemistries can be placed into two categories, cyanide and non-cyanide based, which refers to the Au source compound. Cyanide based Au plating baths have been used successfully for many years to deposit hard Au films for contact wear resistance on connectors [6B-15]. They can also be used to deposit soft Au films that are desirable for wire bonding applications, but, due to two major shortcomings, non-cyanide based chemistries are typically used. In the cyanide based baths Au is bound with cyanide ions as the metal source, and as Au is broken from the compound and deposited on the base metal surface, free cyanide ions are released. These free cyanide ions are highly toxic. In addition, cyanide plating baths are often operated at a high pH, which is detrimental to many photoresist materials [6B-16]. Therefore, non-cyanide based Au plating baths are typically used for wire bonding applications. The most common type uses a sulfite based Au metal source. Deposition of the Au metal occurs through the simplified chemical reaction shown in Eq. (6B.4).

$$Au(SO_3)_2^{3-} \longrightarrow Au^+ + 2SO_3^{2-} \tag{6B.4}$$

Since the autocatalytic Au reaction requires no external current source, the reaction can continue indefinitely. The result is a thick, nonporous, and highly uniform top Au layer that is well suited for wire bonding. Typical final Au thickness for high reliability wire bonding is >0.5 μm. Modern sulfite based autocatalytic Au baths typically are operated at neutral pH levels, making them more compatible with photoresist materials that are common today.

6B.3 Wire Bond Process Window and Reliability on Plated Bond Pads

6B.3.1 Ni/Au

When using the common electroless Ni immersion Au (ENIG) process for bond pad metal deposition, the result is a thin (<0.1 μm) Au layer on top of the Ni for the primary bonding surface. Although there is an inert Au layer covering the Ni, one must still be concerned about Ni oxidation. The presence of Ni oxide is a common cause of wire bond non-sticks when bonding to an ENIG bond pad structure. Since the immersion Au layer is very thin and usually very porous, Ni can diffuse out to the bonding surface via grain boundaries or partially plated areas, especially at elevated temperatures. The Ni can then oxidize and prevent successful ball bond formation. The immersion plating process itself is also a source of Ni contamination. As the

Au is being deposited onto the Ni base metal, the Ni atoms removed during the replacement reaction can become trapped within the newly deposited Au layer. These Ni atoms "suspended" in the Au layer are then free to oxidize and cause wire bond no stick failures. This phenomenon is a result of poor plating process control that leaves a nonuniform Au layer over the Ni base metal.

Although there is a high potential for wire bond no sticks when using the ENIG process to obtain a wire bondable surface, it is a common semiconductor industry processing technique that is routinely used to obtain highly reliable ball bonds. Several studies have been published on the processing and reliability of wire bonding to Ni/Au bond pads deposited using the ENIG process [6B-9, 6B-17, 6B-18].

Chan [6B-17] characterized Au ball bonding to ENIG pads with a top Au layer thickness of approximately 0.1 μm. By varying the bonding force and ultrasonic power he determined that the overall process window was quite large, which is illustrated in Fig. 6B-4. It was also shown that successful bonding could be done at temperatures as low as 60°C, although a much higher ultrasonic power is needed, and bonding at higher temperatures ultimately gave the largest process window.

Strandjord [6B-9] also determined that the wire bonding process window to ENIG pads was large. He found no strong dependence of any wire bonding parameter on post-bond ball shear or wire pull values. Bonded samples were thermally aged and retested. The results show no significant change in ball shear or wire pull values. It was also shown that there is no Au-Ni intermetallic compound formed during the initial ball bonding process, which can be seen in the cross-section shown in Fig. 6B-5. The post-thermal aging ball shear and wire pull tests also indicate that no detrimental intermetallic growth occurred, which indicates that the wire bonds are highly reliable if proper bonding is performed.

The bonding process window of Au wire on ENIG pads of FR4 printed circuit boards was also studied by Ansorge [6B-19]. They found that thermal aging the boards at 75°C for 1000 h or 125°C for 750 h resulted in the widening of the process window. It was determined that the longer aging time was more critical than aging temperature, with the longer time effectively widening the process window greater than the higher temperature. This is most likely due to the annealing, or softening, of the Au with thermal aging. Lai and Liu [6B-18] also investigated bonding to ENIG pads on FR4 boards. The study looked at low temperature bonding at 105°C. Like Ansorge, they were able to correlate bondability to Au thickness and hardness, and it was determined that thicker and softer Au layers had greater bondability. Although these two studies were done on FR4 printed circuit board pads, they both show that softer bond pad surfaces perform best for Au ball bonding.

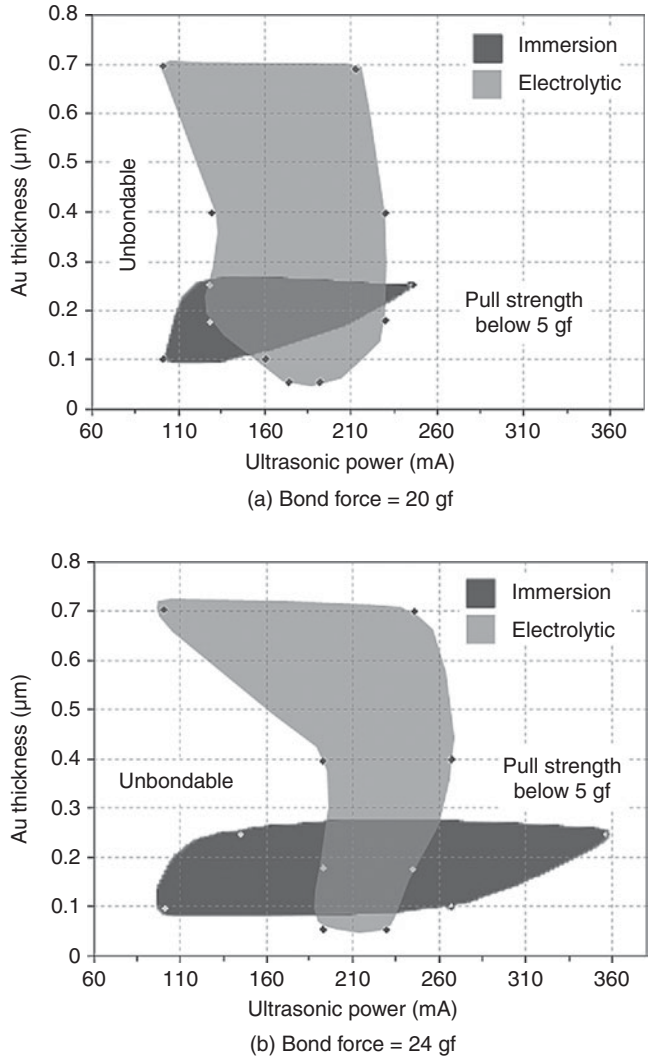

Figure 6B-4 Diagram showing the experimentally determined process windows for low temperature (60°C) Au wire bonding to Ni/Au bond pads of various Au top layer thicknesses based on wire pull testing results. Both immersion and electrolytic methods were investigated. One mil wire diameter was used. Ultrasonic power was varied with bond forces (*a*) 20 gf and (*b*) 24 gf. Notice the larger process window for higher bonding force. It should also be noted that the process window for electrolytic plating is much higher than immersion plating, partly because of thickness limitations of the immersion plating process, but also due to the more uniform plating and lack of contaminants on the surface that can oxidize and prevent good bonding. Areas to the right of the process window were able to be bonded, but their pull strength was low due to excessive wire neck deformation from the high ultrasonic power application. (*After Chan [6B-17]; With kind permission of Springer Science and Business Media.*)

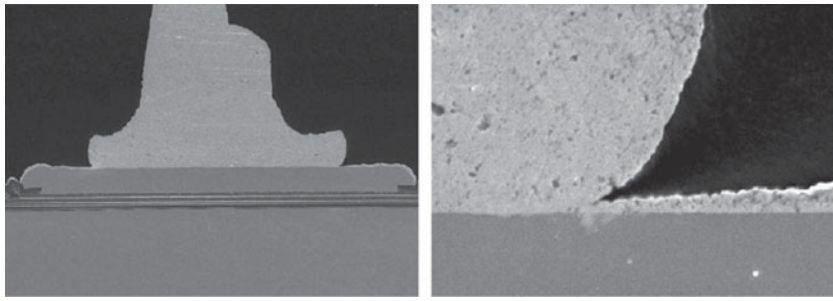

Figure 6B-5 Cross-section of a Au ball bond onto a Ni/Au bond pad (*a*) low Mag (*b*) high Mag. Plating process was electroless Ni immersion Au. Bond pad size was 100 × 100 mm, with 1 mil Au wire. Cross section was taken immediately after bonding with no thermal aging present. Notice the lack of intermetallic compound formation during the bonding process due to the Au wire and Au pad surface. Thermal aging will not result in any detrimental intermetallic compound formation between the Ni and Au layers. (*After Strandjord [6B-9]; © Elsevier.*)

In order to increase the process window of bonding to Ni/Au pads, the Au layer thickness can be increased. One way to do this is to follow the ENIG process with an autocatalytic Au plating process. Since the autocatalytic process is not self-limiting like the immersion Au process, the thickness of this layer can be significantly larger than the immersion Au layer (autocatalytic Au cannot be plated directly onto a Ni surface). A typical autocatalytic Au layer thickness is 0.5 μm, which is 10 times the 0.05 μm immersion Au layer. The thicker autocatalytic Au layer will act to reduce the top layer hardness and also lower the risk of Ni contamination that can oxidize. The thicker Au layer increases the possible diffusion path for any Ni migration, and also covers up any exposed Ni that was "suspended" in the initial immersion Au layer.

Another option to obtain a thicker Au layer is through electroplating. Chan [6B-17] characterized the wire bond process window for various thicknesses of electroplated Au ranging from 0.01 to 0.7 μm over Ni thicknesses of 4 to 8 μm. It was shown that, as the Au thickness increased, the overall surface roughness and hardness both decreased. Thinner Au layers follow the contours of the underlying Ni layer, but the contours become less visible and eventually disappear as Au thickness increases. Surface roughness was shown to play a key role in bondability. Bond pads with higher Au roughness resulted in lower bondability and post-bond wire pull strength. It should be mentioned that a rather large drawback to using electrolytic Ni/Au bond pad structures for wire bonding is the high cost associated with the processing due to the expensive metal sputter/etch and photolithography

processing techniques that are required. Regardless of the Ni/Au deposition method, a thicker Au layer will provide a softer and smoother bonding surface, which allows for easier ball bonding due to the reduction in energy required to form the metallic bonds. Figure 6B-4 shows the process window for varying Au thickness, and it can be seen that the process window shrinks with decreasing Au thickness (rougher and harder surface).

6B.3.2 Ni/Pd/Au

Although the thicker Au layers provided by electrolytic and immersion/autocatalytic methods have shown to be more desirable than the thinner immersion Au layers for ball bonding, the ENIG process is the lowest cost option; hence, it is the most desirable process of the three options for low cost manufacturing even though it exhibits the highest possibility for wire bond no stick failures. Another option to obtain a highly reliable bond pad structure, and maintain low cost, is to apply a layer of Pd between the Ni and Au. This technology has been used extensively in recent years as a Cu leadframe finish for wire bonding and solder attach applications. Pd is an economic alternative to the thick Au because of its lower cost and noble characteristics that it shares with Au. Figure 6B-6 shows a total precious metal

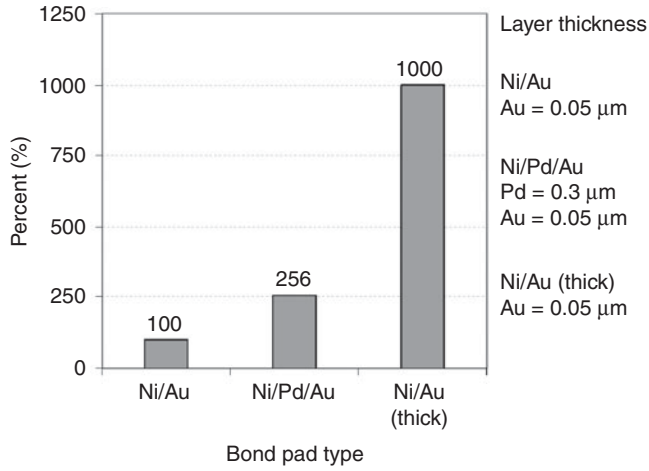

Figure 6B-6 Chart showing the comparative cost of various plating structures for wire bond pads. Electroless Ni Immersion Au is the baseline at 100% cost. The Ni/Pd/Au structure is roughly 2.5× the cost of Ni/Au, but adding thick Au increases the processing cost by roughly 10×. Typical precious metal thickness values for each option are listed above, and these were used for the cost comparison. Cost is estimated based on the following precious metal prices: Au = $913/oz, Pd = $380/oz. (*Note: these exact prices are volatile.*)

cost comparison for a Ni/Pd/Au pad structure and the Ni/Au pad structures with much thicker Au layers. Pd can also be electrolessly plated onto Ni very easily, which makes for seamless integration into an existing plating line (assuming enough tanks are available for the additional chemistry). Unlike the immersion replacement reaction required for Au deposition onto Ni, the Pd is deposited through an electroless reaction. Since no Ni atoms are being removed during the Pd deposition, there is no potential for Ni contamination to be "suspended" in the Pd layer and become available for oxidation. The end result after the Pd deposition process is a highly dense and uniform layer that is very suitable for adding an immersion Au cap. The dense Pd structure will also act to inhibit Ni diffusion for long-term high temperature operation (if the particular device requires) [6B-5]. The additional Au layer on top of the Pd establishes a more robust, well-understood bonding metallization for Au ball bonding.

Johal [6B-6] compared Au ball bonding with 1.2 mil wire to a Ni/Pd/Au pad structure to that of an electrolytic Ni/Au pad structure. Ball shear and wire pull test results exceeded minimum acceptable manufacturing values for both bond pad structures, but the wire bonds on the Ni/Pd/Au bond pads performed better than those on the electrolytic Ni/Au bond pads. Although the mean wire pull values for both conditions were similar, the Ni/Pd/Au condition was much more consistent. Ball shear values for the Ni/Pd/Au condition were clearly higher, and they were also slightly more consistent. These results are summarized in Fig. 6B-7*a* and *b*.

Ng studied the wire bonding process window for Ni/Pd/Au pads [6B-7]. It was determined that the process window for Ni/Pd/Au pads was much higher than that of standard Al pads, and the process windows for both bond pad conditions are shown in Fig. 6B-8. The wider process window allows for bonding with lower bond force, and ultrasonic power, therefore, shows that the Ni/Pd/Au pad structure could be advantageous when bonding over sensitive circuitry or other structures prone to wire bond damage. Ball shear and wire pull testing showed similar results to those of Johal [6B-6]. Values for both tests were higher for the Ni/Pd/Au pad condition than for the Al pad condition immediately after wire bonding. Ng encapsulated samples in a green molding compound and performed thermal aging on specimens from each sample condition. Samples were pulled at specified intervals through 4000 h of aging time and were decapsulated by acid fuming to expose ball bonds for wire pull and ball shear testing. For the Ni/Pd/Au pad condition, it was found that wire pull values remained constant throughout the aging period, while the ball shear values actually improved slightly. This is most likely due to low level Pd grain-boundary diffusion into the Au. Any Pd atoms located on Au grain boundaries could act to impede slip plane movement during ball shear, which would result in an increase in shear strength of the Au. The graphs located in Fig. 6B-9 summarize these data. It

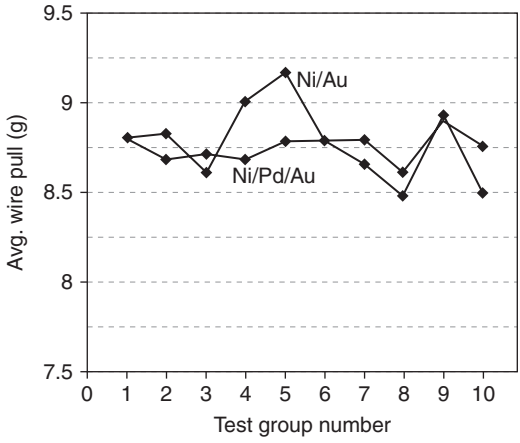

	Ni/Au	Ni/Pd/Au
Avg. pull (g)	8.79	8.76
Min. pull (g)	7.80	7.82
Max. pull (g)	10.27	9.98
Avg. st. dev. (g)	0.46	0.55
Avg. range (g)	1.54	1.78
Avg. CpK	2.10	1.70

(a)

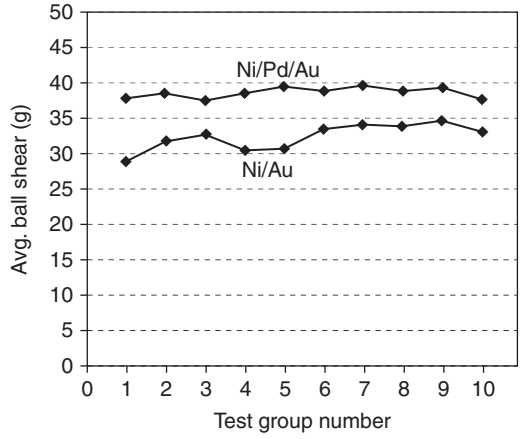

	Ni/Au	Ni/Pd/Au
Avg. shear (g)	32.16	38.39
Min. shear (g)	28.14	35.21
Max. shear (g)	35.94	40.88
Avg. st. dev. (g)	1.15	1.01
Avg. range (g)	3.94	3.32
Avg. CpK	3.32	4.62

(b)

Figure 6B-7 Wire bond integrity test data Ni/Au and Ni/Pd/Au bond pad structures. (*a*) Wire pull—Values for both groups are similar, but notice the variation difference. The Ni/Pd/Au pad structure resulted in the most consistent wire pull values. (*b*) Ball shear—The Ni/Pd/Au pad structure clearly resulted in the best performance for ball shear testing. The test variation was similar for both groups, but the Ni/Pd/Au average values were roughly 6 g higher than the Ni/Au values. Wire was 4N purity with 1.2 mil diameter. Each test group consisted of 20 pulls/shears per group with the average value for each group being plotted. (*After Johal [6B-6].*)

should be noted that throughout the aging process these samples were encapsulated in the green molding compound, which did not inhibit performance or cause any adverse effects throughout the thermal aging process. For the Al pad condition, the values for both wire pull and ball shear tests decreased drastically throughout the aging

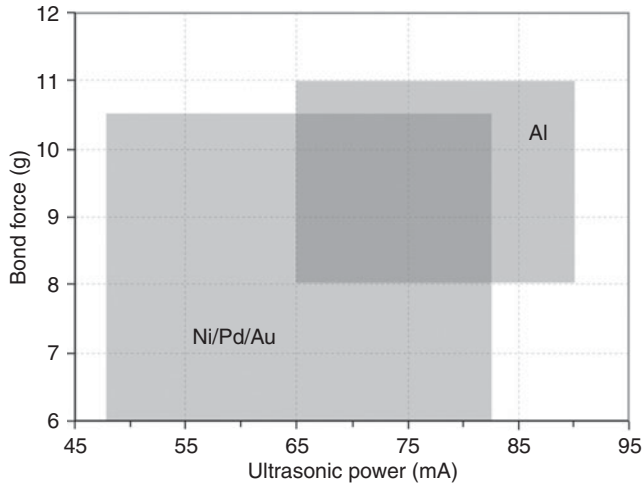

Figure 6B-8 Comparison of wire bond process windows for varying bond force and ultrasonic power on standard Al pads and Ni/Pd/Au plated bond pads. It can be seen that the Ni/Pd/Au structure has a much larger bonding window. It should also be noted that the Ni/Pd/Au bond pads allowed for good bondability at lower force and ultrasonic power settings, which could be beneficial when bonding over sensitive areas of a device. Wire was 4N Au with a 1 mil diameter. Plated bond pad structure was 3 μm Ni + 0.3 μm Pd + 0.05 μm Au, while the Al pad composition was Al-1% Si-0.5% Cu. (*After Ng* [*6B-7*].)

process. This was due to extreme Al-Au intermetallic growth at the ball-to-pad interface, which can be seen in the micrograph shown in Fig. 6B-9*c*. The overall results of this study show that a large process window can be achieved with Ni/Pd/Au bond pads and that long-term reliability can be achieved using the Ni/Pd/Au pad structure for applications where extended operation at elevated temperatures is required.

Hashimoto's wire bond study [6B-5] on Ni/Pd/Au bond pads presents further evidence of the high bondability of the pad structure. They varied both Pd and Au thickness in their experimental setup, and all 16 thickness combinations produced excellent ball shear test results. In their comparison to Ni/Au (ENIG) bond pads, the reliability as measured by ball shear testing was much more consistent throughout the range of Au thicknesses investigated. As the Au thickness increased the ball shear values increased, but for the Ni/Pd/Au conditions the ball shear values remained relatively constant for all Au thicknesses. There was no dependence of ball shear results on the Pd layer thickness. Following this study Hashimoto is recommending an optimum bond pad stack of 5 μm Ni + 0.06 μm Pd + 0.02 μm Au.

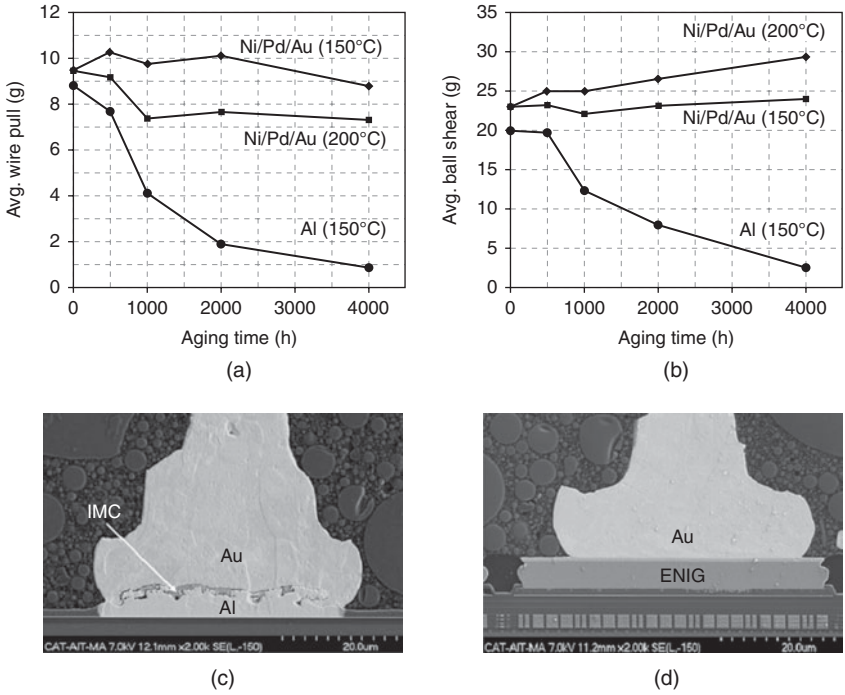

Figure 6B-9 Plots showing effects of high temperature storage on (*a*) Wire Pull and (*b*) Ball Shear test results for Al and Ni/Pd/Au pad structures. Initial results at $t = 0$ for both tests are better for Ni/Pd/Au bond pads. A dramatic decrease in bond strength with aging time can be seen for devices with Al pads. For pull testing, the sole failure mode at $t = 0$ was wire neck breaking. After only 500 h of aging for Al pads, ball lifts began occurring. By 1000 h of aging, ball lifts were common. The wire pull mechanism for Ni/Pd/Au was a consistent neck break throughout the aging process, with the breaking force remaining relatively constant. The Ni/Pd/Au ball shear results show a slight, but clear trend of increasing shear strength with increasing aging time. One possible explanation for this is that low levels of Ni may be diffusing into the Au via grain boundaries, which could act as a strengthening agent. The cross sections of (*c*) Al pad and (*d*) Ni/Pd/Au pad samples clearly illustrate the lack of intermetallic growth with Ni/Pd/Au bond pads and the large presence of intermetallic growth with Al pads. In this case, the source of the images is referring to Ni/Pd/Au as ENIG. (*After Ng [6B-7]*; © *IEEE*.)

6B.3.3 Ni/Pd

Sasangka has recently demonstrated the feasibility and reliability of Au ball bonding directly to Ni/Pd pads [6B-8]. The bond pad stack was composed of 1 to 2 μm Ni + 0.3 μm Pd over Cu interconnects. Thermal aging was performed on encapsulated and unencapsulated samples in order to investigate any possible detrimental intermetallic growth and also to determine how mold compound impurities may affect long-term package reliability at high operating temperatures.

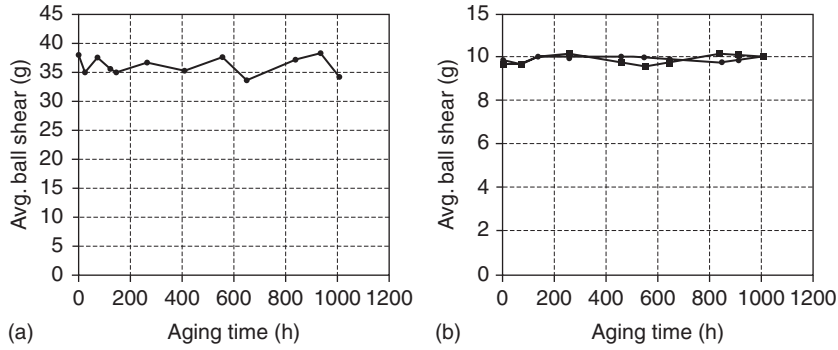

Figure 6B-10 (*a*) Results of ball shear testing of Au wire on Ni/Pd bond pads through 1008 h of high temperature aging at 175°C. The relatively constant results show that there is no impact of thermal aging to ball/pad interface conditions through intermetallic growth. (*b*) Results of wire pull testing of Au wire on Ni/Pd bond pads through 1008 h of high temperature aging at 150°C. The effect of green molding compound on wire bond integrity was investigated using two different molding compounds (with and without ion catcher additive). The results show that there is virtually no difference between mold compounds and, like what was shown for ball shear testing, no degradation of the ball/pad interface throughout the aging process. (*After Sasangka [6B-8]*; © *IEEE*.)

Au ball shear and wire pull testing were performed on as bonded and thermally aged samples (testing was done at regular intervals through 1008 h thermal aging time). Results show that there was no decrease in performance with thermal aging. Figure 6B-10 contains wire pull and ball shear test results. The consistency of wire pull and ball shear values throughout the aging period indicates a lack of intermetallic compound formation, which was later confirmed through cross-sectional analysis of the ball/pad stack. No wire bond process study was disclosed, but manufacturing guidelines provided in an applications note by Micron [6B-20] indicate that there is little difference between wire bond machine parameters for Au ball bonding to Al pads and Ni/Pd pads. Bonding to Ni/Pd requires the USG pre-bleed machine parameter to be activated, which causes the ultrasonic energy to be transmitted prior to free air ball contact to the pad. The recommended bond parameters for bonding to Ni/Pd pads are shown in Table 6B-3. The applications note also shows a cross-sectional comparison of Au ball bonds to Al and Ni/Pd pads that were aged at 150°C for 1008 h. It can be seen that there is no intermetallic compound formation with the Ni/Pd pad, but extensive intermetallic formation is present with the Al pad (see Fig. 6B-11).

In addition to the positive data for Au ball bonding to Ni/Pd pads provided by Sasangka, possible pitfalls for using the process are also presented. Following high temperature aging of encapsulated samples it was found that the Ni/Pd structure provided much better

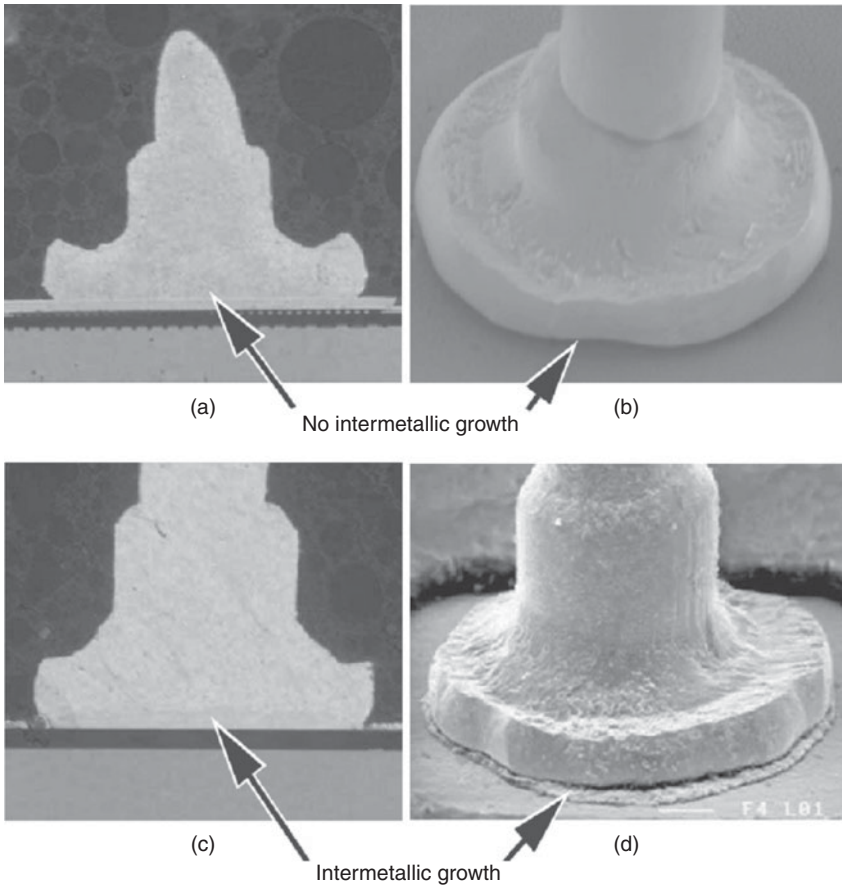

Figure 6B-11 Comparison of Au ball bonds on Ni/Pd and Al bond pads after 1008 h of high temperature storage at 150°C to illustrate the stability of the Au-Pd metallic system. (*a*) Cross section on the Ni/Pd pad. (*b*) Top down image of the same ball bond. There is no intermetallic growth present after aging. (*c*) Cross section on the Al pad. (*d*) Top down image of the same ball bond. Notice the large amount of Au-Al intermetallic growth present after aging. (*After Micron [6B-20].*)

resistance to ionic mold compound impurities over Al pads. There was, however, some pit corrosion present in the surface of the exposed Pd of the bond pads that was most likely caused by ionic impurities reacting with the Pd. The corrosion was found in samples with both high and low amounts of ionic impurities, although it was slightly more severe with the high ionic impurity mold compound. The Pd pit corrosion appears to be minor for both high and low ionic impurity cases (especially when compared to the Al pad cases) and will most likely have little effect on long-term reliability, although the observation may warrant further study.

Bond Pad Material	Ni/Pd	Al
Wire type	23 µm 4N Au	
Platform bonder	Ball bonder	
Finished ball diameter	50–60 µm	
Finished ball thickness	7–11 µm	
Tip offset	127 µm	
Constant velocity	0.3 (0.3–0.4) mil/s	
Ultrasonic generator (USG) profile	Ramp	
USG current	110–140 mW	
Force	18–25 g	
Ramp-up time	10 ms	
Time	7–10 cms	7 ms
USG pre-bleed	10–25%	0%

Note: It can be seen that there is little difference in the parameters other than a slightly longer bond time and the addition of a USG pre-bleed for Ni/Pd pads. The USG pre-bleed essentially begins ultrasonic power transmission prior to the free air ball touching down to the pad surface

Table 6B-3 Wire Bond Process Parameters for Au Wire onto Ni/Pd Bond Pads as Compared to Al Bond Pads

Sasangka also showed that the Pd bond pad surface contained approximately 1% (atomic) Cu contamination as measured by XPS. The Pd surface composition was monitored through the thermal aging process, and the amount of Cu contamination increased steadily with aging time. The cause for contamination was attributed to grain-boundary diffusion of Cu through the Ni and Pd layers to the bond pad surface. Since both the Ni and Pd plated layers are deposited into an amorphous film (no grain boundaries), grain-boundary diffusion is not likely to be the source of Cu contamination. A more likely source of Cu contamination is surface diffusion of Cu up the Ni and Pd pad sidewall. Since electroless Ni and Pd plating occurs through a chemical reaction with exposed metal only, there is no adherence of Ni or Pd to the dielectric layer sidewall that defines the original bond pad opening. The result is an open route for surface diffusion of the very active Cu metal that is the base interconnect metal. This was discussed in the plating section, and the sketch shown in Fig. 6B-3 illustrates the concept. The sidewall diffusion of the Cu base metal cannot be prevented due to the nature of the plating process. The overall risk of this phenomenon affecting wire bondability, however, is relatively low. Typically the only source of high temperature seen by the device

after bond pad plating and before wire bonding is at the die attach epoxy cure step, and this short-term thermal excursion is much less than the long-term thermal aging required to drive significant amounts of Cu diffusion.

6B.4 Plasma Cleaning

The adverse effects of Ni surface contamination (or other metallic contaminant) have been discussed previously. Their effects can be reduced by the use of a plasma clean step immediately prior to wire bonding. Two types of plasma cleaning exist—direct and indirect methods. Indirect plasma cleaning methods involve the use of an active plasma species such as O_2 to chemically combine and remove organic contamination present on bond pad surfaces. In no instance should an indirect O_2-plasma process be used for a Ni-based plated bond pad. Any Ni or other metallic contaminant present on the pad will not be removed, but heavily oxidized, which will further reduce bondability. The preferred method for plasma cleaning Ni-based plated bond pads is direct plasma cleaning, or sputtering. This method uses a highly energetic plasma species such as Ar to physically bombard the metallic contaminants, which then causes them to dislodge from the bond pad surface. One drawback to this method is that the metallic contaminants have the potential to be redeposited if they are all not removed through the plasma systems exhaust. Therefore, to prevent excessive metallic removal and redeposition, care should be taken not to use too long of a cleaning time.

Furukawa [6B-21] has demonstrated the positive effects of direct Ar plasma cleaning on ENIG bond pads. Although there was no discussion of any plasma cleaning parameter optimization, it was clearly shown that Ar plasma treatment improved wire bonding performance. Wire pull test results show low pull strengths for non-plasma treated samples, which indicates ball lift failures due to poor bonding. Plasma treated samples showed consistently higher wire pull values, which indicates wire neck breaking (strong ball bonds). Surface analysis characterization of before-and-after plasma clean samples also showed large decreases in Ni (as well as C) contamination after plasma cleaning.

Chan followed his initial wire bond parameter optimization study [6B-17] with further characterization following plasma cleaning [6B-22]. Direct Ar plasma cleaning was studied for electrolytic and electroless Ni/Au bond pads. Wire bonding process windows for both pad types were able to be increased dramatically following plasma treatment. Plasma power (100 and 400 W) and cleaning time (1 and 5 min) were varied in the characterization. It was determined that the low power/low time combination produced the best results for wire bond process window improvements. This is most likely because higher power and longer times resulted in over-cleaning as described previously.

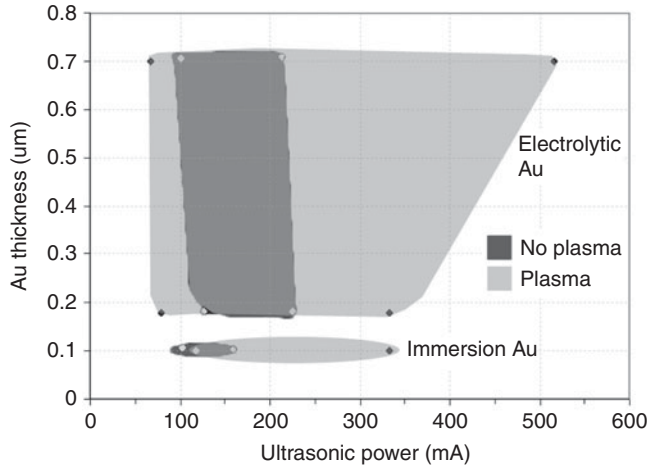

Figure 6B-12 Diagram showing the wire bond parameter processing window for ENIG and electrolytic Ni/Au with and without pre-wire bond Ar plasma clean. It can be seen that implementing an Ar plasma clean prior to wire bonding can significantly increase the bonding process window for both types of Au pads. (*After Chan [6B-22]*; © *IEEE*.)

The wire bond process window for electrolytic and electroless Ni/Au bondpads for both plasma and no plasma clean conditions is shown in Fig. 6B-12.

6B.5 Direct Cu Bonding

Other than bonding to Ni/Au, Ni/Pd, or Ni/Pd/Au bond pads, it should be mentioned that several studies have been done to demonstrate feasibility of ball bonding directly to Cu bond pads. For successful bonding to occur, oxidation of the Cu bond pad surface must be carefully controlled. One proposed method is to deposit a thin film of Ti over the Cu pad to prevent oxidation. Aoh [6B-23] demonstrated that a 3.7 nm thick layer of Ti was sufficient in preventing Cu oxidation while allowing for good bondability using Au wire. Thicker Ti layers resulted in poor bondability and bond strength because the Ti (or its oxide) acted as a barrier between the ball and pad. Another method that has been proposed to prevent Cu oxidation is to apply a self-assembled monolayer (SAM) over the Cu pad surface. This principle is similar to an organic solderability preservative (OSP) coating on a printed circuit board to prevent Cu pad oxidation for soldering. Banda and Whelan [6B-24, 6B-25] have shown that SAM thicknesses of less than 2 nm over Cu bond pads will allow for good bondability when using Cu wire. Cu wire bonded directly to Cu bond pads would allow for very high performance, especially for high frequency

applications. Although these pioneering methods have shown promise in lab applications, the techniques must be perfected before full scale manufacturing can be successful. It should be noted that Banda and Whelan's SAM research was halted shortly after their publications and not continued since.

Chapter 6B References

6B-1 Liu, Y., Irving, S., and Luk, T., "Thermosonic Wire Bonding Process Simulation and Bond Pad Over Active Stress Analysis," *Electronics Packaging Manufacturing, IEEE Transactions*, 2008, **31**(1):61–71.

6B-2 Liu, Y., Irving, S., and Luk, T., "Wafer Probing Simulation for Copper Bond Pad Based BPOA Structure," in *Thermal, Mechanical and Multi-Physics Simulation Experiments in Microelectronics and Micro-Systems, 2007, EuroSime 2007, International Conference, 2007.*

6B-3 Tran, T. A., Yong, L., Williams, B., Chen, S., and Chen, A., "Fine Pitch Probing and Wirebonding and Reliability of Aluminum Capped Copper Bond Pads," in *Electronic Components and Technology Conference, 50th Proceedings*, 2000.

6B-4 England, L. and T. Jiang, "Reliability of Cu Wire Bonding to Al Metalization," in *Electronic Components and Packaging Conference*, 2007.

6B-5 Hashimoto, S., Kiso, M., Oda, Y., Kurosaka, S., Okada, A., and Gudeczauskas, D., "Study of Ni-P/Pd/Au as a Final Finish for Packaging," in *International Wafer Level Packaging Conference (IWLPC)*, 2006.

6B-6 Johal, K., Roberts, H., Desai, K., and Low, Q. H., "Performance and Reliability Evaluation of Alternative Surface Finishes for Wire Bond and Flip Chip BGA Applications," in *Pan Pacific Symposium*, 2006.

6B-7 Ng, B. T., Ganesh, V. P., and Lee, C., "Optimization of Gold Wire Bonding on Electroless Nickel Immersion Gold for High Temperature Applications," in *Electronics Packaging Technology Conference, 2006, EPTC '06, 8th*, 2006, pp. 277–282, (© IEEE).

6B-8 Sasangka, W. A. and A. C. Tan, "High Temperature Performance Study of Gold Wire Bonding on a Palladium Bonding Pad,: in *Electronics Packaging Technology Conference*, 2006, pp. 330–335, (© IEEE).

6B-9 Strandjord, A., Popelar, S., and Jauernig, C., "Interconnecting to Aluminum- and Copper-Based Semiconductors (Electroless-Nickel/Gold for Solder Bumping and Wire Bonding)," *Microelectronics Reliability,* 2002, **42**(2): 265–283.

6B-10 O'Sullivan, E. J., Schrott, A. G., Paunovic, M., Sambucetti, C. J., Marino, J. R., Bailey, P. J., Kaja, S., and Semkow, K. W., "Electrolessly Deposited Diffusion Barriers for Microelectronics," *IBM Journal of Research and Development,* 1998, **42**(5)

6B-11 Rohan, J. F., G. O'Riordan, and J. Boardman, "Selective Electroless Nickel Deposition on Copper as a Final Barrier/Bonding Layer Material for Microelectronics Application." *Applied Surface Science,* 2002, **185**(3–4): 289–297.

6B-12 Baudrand, D. and J. Bengston, "Electroless Plating Processes: Developing Technologies for Electroless Nickel, Palladium, and Gold," *Metal Finishing,* 1995, **93**(9):55–57.

6B-13 Yokomine, K., Shimizu, N., Miyamoto, Y., Iwata, Y., Love, D., and Newman, K., "Development of Electroless Ni/Au Plated Build-up Flip Chip Package with Highly Reliable Solder Joints," in *Electronic Components and Technology Conference, 2001, Proceedings., 51st*, 2001, pp. 1384–1392.

6B-14 Abys, J. A., Kudrak, E. J., Maisano, J. J., and Blair, A. *The Electrodeposition and Material Properties of Palladium Nickel Alloys*, in *WESCON*, 1996.

6B-15 Okinaka, Y. and Hoshino, M., "Some Recent Topics in Gold Plating for Electronics Applications," *Gold Bulletin,* 1998, **31**(1):3–13.

6B-16 Kato, M. and Y. Okinaka, "Some Recent Developments in Non-Cyanide Gold Plating for Electronics Applications," *Gold Bulletin*, 2004, **27**(1–2): 37–44.
6B-17 Chan, Y. H., Kim, J. K., Liu, D., Liu, P. C. K., Cheung, Y. M., and Ng, M. W., "Process Window for Low-Temperature Au Wire Bonding," *Journal of Electronic Materials*, 2004, **33**(2):146–155.
6B-18 Lai, Z. and Liu, J., "Effect of the Microstructure of Ni/Au Metallization on Bondability of FR4 Substrate," in *International Symposium on Electronic Packaging Technology, Proceedings of the 3d*, 1998.
6B-19 Ansorge, F., Bader, V., Zakel, E., and Reichl, H., "Bondability of Electroless Metalfinishes for COB-Technology," in *Recent Progress in Printed Circuit Board Technology. International Workshop*, 1997.
6B-20 Micron, *Technical Note: Micron Wire-Bonding Techniques*, **TN-29-24**: p. www.micron.com.
6B-21 Furukawa, R., "Realizing Low Cost and High Reliability in CSP Packages with Surface Treatment and Material Technology—Plasma Treatment Technology," in *Electronics Manufacturing Technology Symposium, 2004. IEEE/CPMT/SEMI 29th International*, 2004.
6B-22 Chan, Y. H., Kim, J. K., Liu, D., Liu, C. K., Cheung, Y. M., and Ng, M. W., "Effect of Plasma Treatment of Au-Ni-Cu Bond Pads on Process Windows of Au wire Bonding," *Advanced Packaging, IEEE Transactions*, 2005, **28**(4):674–684.
6B-23 Aoh, J. N. and Chuang, C. L., "Thermosonic Bonding of Gold Wire onto a Copper Pad with Titanium Thin-Film Deposition," *Journal of Electronic Materials*, 2004, **33**(4):290–299.
6B-24 Banda, P., Ho, H. M., Whelan, C., Lam, W., Charles J., Vath, I., and Beyne, E., "Direct Au and Cu Wire Bonding on Cu/Low-k BEOL," in *Electronics Packaging Technology Conference*, 2002, pp. 344–349.
6B-25 Whelan, C. M., Kinsella, M., Ho, H. M., and Maex, K., "Corrosion Inhibition by Thiol-Derived SAMs for Enhanced Wire Bonding on Cu Surfaces," *Journal of the Electrochemical Society*, 2004, **151**(2):B33–B38.

This page intentionally left blank

CHAPTER 7

Cleaning to Improve Bondability and Reliability

7.1 Introduction

Molecular cleaning methods have long been used to remove contaminants during various stages of wafer processing and are absolutely essential for high yield. Wire bonds (as with wafers) cannot be made at a high yield unless the bonding surfaces are also clean. Until about the 1990s, there was little consideration given to a cleaning step specifically designed to improve the yield and reliability of wire bonds. Modern ULSI devices can have hundreds or thousands of I/Os and wire bonds, and must meet packaging yield and reliability requirements unheard of only 10 years ago. Since there are so many I/Os per chip, wire bonds (and other interconnection methods) have become the largest packaging yield driver. Modern bond-pad metallizations, which may contain various additives, are often harder than in the past. In addition, reactive ion processing of the wafer can leave halogens and carbon films on the surface. All of these factors can limit yield, inhibit bondability, and/or affect reliability.

Because of contamination resulting from extensive handling, obtaining chips from many sources, sometimes storing them for years, as well as the use of polymer/epoxy die attach, the high-reliability MCM/SIP/hybrid industry was the first to adopt molecular cleaning methods before bonding. Such methods have expanded into other packaging areas and are occasionally used in high-volume IC packaging.

Note that essentially all of the fundamental work on microelectronics cleaning was done in the past (1960s–1990s) when those, "then-new," cleaning processes were being developed. Many of the current published studies are repeats of the past, with perhaps more modern, easier to use equipment or oriented toward a specific device cleaning

problem. Thus, major parts of this chapter are relatively intact, but often rewritten for clarity. Newer work is added, when relevant. Many of the current literature publications are done by the equipment venders, or engineers qualifying some new product. They may be useful for solving specific problems, or to understand equipment improvements but generally do not contain new cleaning technology.

Contaminants on bond pads have long been known to degrade both the bondability and/or the reliability of wire bonds. Table 7-1 lists many of the contaminants that have been found to degrade bonds. The table is only indicative, since the effect on bonds may be concentration-dependent or may only act synergistically (i.e., with moisture or heat, or in Au-Al interfaces). Some contaminants primarily affect bondability, while others reduce reliability. The many important chemical and other contaminants that affect bond intermetallic

Halogens from	
• Plasma (RIE) etching (dry processing)—may leave halogens • Epoxy outgassing—contaminates pads • Silox etch—pads • Solvents (TCA, TCE, chloro-fluro's)—halogens on pads • Photoresist stripper—deposits on pads	
Contaminants from Plating	
• Thallium • Lead • Chromium • Nickel	• Brighteners • Iron • Copper • Hydrogen
Sulfur from Sources—Cause Corrosion, Reduce Bondability	
• Packing containers • Cardboard and paper	• Ambient air • Rubber bands
Miscellaneous Organic Contaminants That Inhibit Bondability	
• Epoxy outgassing • General ambient air (poor storage) • Spittle—currently, rarely seen	• Photoresist
Others That Cause Corrosion or Inhibit Bonding	
• Sodium • Phosphorous • Moisture • Carbon • Copper • Titanium	• Chromium • Bismuth, cadmium • Glass, vapox, nitride • Silver • Tin • Most soft oxides (e.g., Ni, Cu, Ti)

Table 7-1 Impurities That Can Lead to Weak Bonds

reliability are discussed in this book, particularly in Chap. 5, Table 5-5 and Fig. 5-13.

There are many human sources of contamination that are not listed in Table 7-1. These may contain bondability-inhibiting or degrading materials. Some of these may be small particles of skin, hair, sweat, spittle, and mucus. Such may arrive at the device surface by the driving force of talking, coughing, sneezing, yawning, head shaking, scratching, etc. (Face masks and suits prevent most of these.) The various human sources of contamination have been compiled [7-1]. A person sitting motionless generates about 105 particles per minute of greater than 0.3 μm diameter, and up to 50 times more particles while moving. A fully suited person, walking in a class 100 clean room, will distribute up to 50,000 particles in that same period of time [7-2]. Other sources of contamination may enter the air from drinking water (CI and Br) or from dry-cleaned clothes (tetrachloroethylene) [7-3]. Currently, most assembly and packaging facilities operate in clean rooms that are better (lower) than class 10,000, and a few are even near the class 100 level. Assembly equipment (die, wire bonders, etc.) is available for use in lower than class 1000 clean rooms. However, it has not been demonstrated that particulate contamination in clean rooms lowers the wire bond yield.* Presumably, airborne particles that land on bond pads are too small to seriously weaken a normal-sized bond interface, although a fiber from clean room clothing or masks could certainly do so. However, as ball bonds decrease in diameter to fit into fine pitch to ~20 μm pitch (or less) there is increased concern, (see ITRS 2007 tables). In addition, any human particle in a bond interface or on the chip surface could later cause a corrosion reliability problem [7-1]. Perhaps the only way to verify the extent of the particle problem in wire bonding is to use the technique of seeding the device surface [7-4], and then actually performing a controlled experiment including HAST for reliability evaluation. However, modern high-volume IC production is much faster, cleaner, fewer humans are involved in the process, and clean-room/packaging contamination (still near class 10,000) is presumed to be rare.

Considering the large number of possible bond-degrading contaminants, a variety of methods could be required to clean surfaces containing several different ones. Some of these contaminants (e.g., halogens) can become chemically bound to bonding pads and require treatments that can only be performed at the wafer level, such as heating in oxygen for 30 min at 350°C [7-5]. Others, such as glass, nitride, and some metal oxide on pads, cannot be easily removed at the packaging level. Organics, however, may be easily removed before bonding and after die attach. Oxygen, Ar, H_2, and other plasma cleaning gases,

*Such particles can be deliquescent, or oily, and decrease adhesion of plastic mold compound, leading to separation and popcorn effect. Both plasma and UV-ozone cleaning have been used to reduce this problem. On very rare occasions, a particle has actually been found sticking out from the edge of a wire bond.

as well as UV-ozone, can effectively remove carbonaceous contaminants, which cause the majority of bondability problems.

This section will present evidence that contamination can reduce both bondability and reliability and that both UV-ozone and various plasma processes can remove such contamination. These two molecular cleaning methods will be primarily discussed. Various solvent techniques [7-6 to 7-8] (solution, vapor-phase fluorocarbons, ionographic, and DI water) will be discussed only as they compare with the gaseous methods.

7.1.1 Molecular Cleaning Methods to Enhance Bondability and Reliability

Both plasma and UV-ozone cleaning methods have been known for many years [7-8 to 7-16]. Sowell [7-9] gave the clearest comparison between UV (with little or no ozone), argon plasma, and ultra high-vacuum bake-out methods for cleaning gold surfaces. These data are reproduced in Fig. 7-1. The coefficient of adhesion (related to the coefficient of friction) for gold in vacuum is used as the measure of a clean

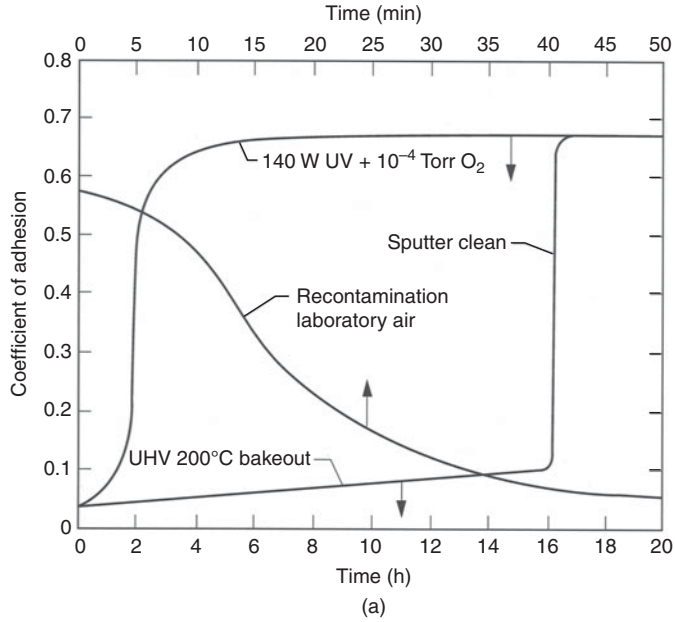

Figure 7-1 (*a*) Cleaning of a gold surface by UHV 200°C bake-out, argon sputtering, and UV-irradiation at 10^{-4} Torr O_2 (lower scale). Recontamination rate in normal laboratory air is also shown. Arrows point to the appropriate time scale. (*After Sowel © JVS, 1974 [7-9].*) (*b*) A similar measurement technique using modern technology and including recontamination from machine shop (or other dirty conditions) as well as clean-room environments. (*Reprinted with permission from the* SVC Education Guides to Vacuum Coating Processing*, by Donald M. Mattox, 2007.*)

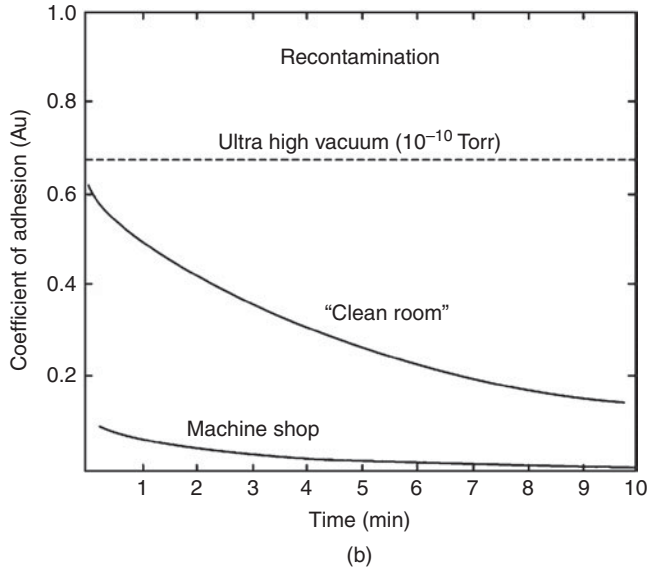

Figure 7-1 (*Continued*)

surface. Recontamination by hydrocarbons in laboratory air is indicated by the center curve (or in 7-1*b*, by machine shop air). These data correlated to data measured for glass surfaces, where the water-drop contact-angle method of evaluation was used. Much of the classical work in cleaning and contamination control was collected and published in a book [7-10] and should be referred to for more detailed fundamental information. The remainder of this section describes work directly applied to the bondability and reliability of wire bonds.

7.1.2 Ultraviolet-Ozone Cleaning

Ultraviolet-ozone cleaners generally consist of a chamber containing banks of quartz-envelope, low-pressure, mercury vapor lamps. These are designed to emit significant amounts of radiation of 1849 and 2537 Å wavelengths. Devices to be cleaned are placed in the chamber as close as practical to the lamps. Since ozone gas is considered dangerous, the units are usually operated in a fume hood or at least in an area where some means of removing the gas exist. Government regulations may apply to the safe use of ozone (USA-OSHA) European Union, or other.

The removal of organic contaminants with UV-ozone takes place as follows. The 1849 Å UV energy breaks up the O_2 molecule into atomic oxygen (O + O), which combines with other O_2 molecules to form ozone, O_3. Ozone has a strong absorption for 2537 Å UV and may break up again into O_2 + O. Any water present may also be broken into the HO free radical. All of these (HO, O_3, and O) can react with hydrocarbons to form CO_2 + H_2O, which leave the device surface as a gas. The strong 2537 Å UV may additionally break the chemical bonds of

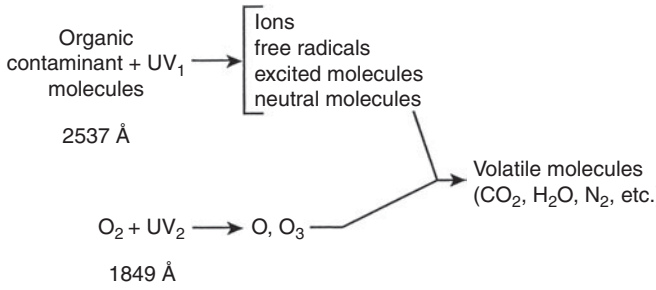

Figure 7-2 A simplified schematic of the UV-ozone cleaning process is shown using two dominant UV wavelengths of mercury-vapor lamps. (*After Vig [7-13]; © IEEE.*)

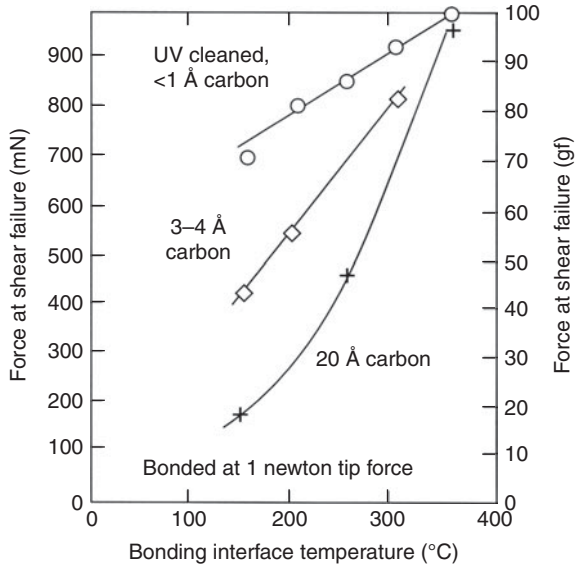

Figure 7-3 Effect of surface contamination on the thermocompression bonding of gold, pulsed bonding. (*After Jellison [7-11]; © IEEE.*)

the hydrocarbon, accelerating the oxidation process. A simplified schematic of the UV-ozone cleaning process is given in Fig. 7-2 [7-13]. Early work [7-11] showed that UV (2537 Å) alone could clean gold metallization of carbonaceous films and increase thermocompression ball-bond shear strength. However, several hours of 2537 Å cleaning could be required, so modern practice combines both wavelengths.

Figure 7-3 shows an example of such cleaning to increase bondability. Even a few angstroms-thick film of carbon* was found to impair

*The total thickness of an organic film is usually 3 to 4 times the measured carbon-equivalent thickness in Auger electron spectroscopy.

bondability, whereas a cleaned gold film (<1 Å carbon) can be strongly TC bonded at 150°C, which is a low temperature to use in thermosonic bonding. Similar cleaning results were found with ozone alone (the UV creating it was shielded from the samples) [7-12], which is similar to an O_2 plasma downstream process. However, it was found that UV and ozone (2537 Å + 1849 Å + ozone) together cleaned much faster than UV or ozone alone, up to 100 times faster, depending on the specific impurities [7-13]. Therefore, present cleaners employ the combination, and with high-intensity lamps may take <10 min to clean typical packages.

The bondability of gold thick-films that were cleaned by vapor degreasing and boiling trichlorethylene were compared to those cleaned with UV-ozone [7-11]. These films were contaminated with beeswax, petrolatum, and halocarbon wax. The results indicated that vapor degreasing was a poor cleaning procedure for removing beeswax (see Fig. 7-4), but quite effective for petrolatum and halocarbon wax. Ultraviolet-ozone, however, effectively removed all of the contaminants. This points out the major problem of solvent cleaning. No one solvent is apt to remove all contaminants that may be on a bond pad, emphasizing the importance of molecular cleaning methods.

Some general aspects of UV-ozone cleaning have been reviewed by the equipment manufacturers. One described applications to ceramic circuit board circuit cleaning, including such components as surface acoustic-wave (SAW) devices [7-15], and another described its application to the cleaning of silicon wafers [7-16].

Devices on laminate and polyimide substrates (including BGAs, SIPs, SOPs, MCMs, etc.) can be safely cleaned with UV-ozone. One study found that the water drop contact angle on a BGA laminate

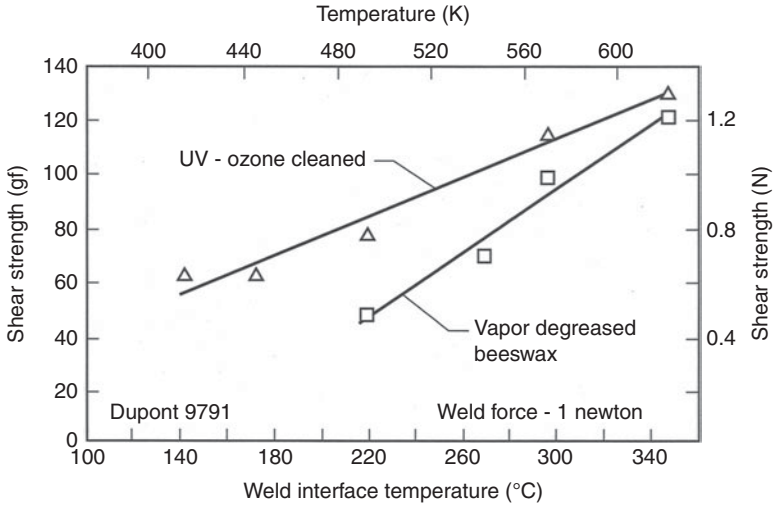

Figure 7-4 Effect of beeswax contamination on gold thick film. (*After Jellison [7-14]; © IEEE.*)

decreased and the plastic adhesion increased to an optimum value in 1 to 5 min of UV/ozone exposure at 150°C. Longer exposure was less reliable in 85°C/85 RH exposure [7-17]. Also, Al bond pad corrosion was eliminated for 240 h pressure cooker testing. Another study found that a 2 min exposure of polyimide to UV-ozone (room temperature) produced optimum cleaning [7-18]. In all cases, too long an exposure can alter the surface of a polymer and possibly lead to reliability problems of one kind or another.

7.1.3 Plasma Cleaning

Plasma-cleaning equipment is generally larger, more costly, and more complicated than UV-ozone equipment. It requires a vacuum pump, a several hundred watt RF-power generator, and pure gases (usually oxygen and argon, or in some cases, hydrogen). By its nature, it is a batch-cleaning method, whereas UV-ozone can be a belt-driven in-line system. In use, devices are placed in a chamber, which is evacuated, the appropriate gas is introduced (typically in the range of 0.1 to 0.5 Torr), and RF power is switched on for about 1 to 15 min to effect the cleaning process.

A simplified and inexpensive type of plasma cleaning system has been introduced in recent years. It is essentially a microwave oven. The plasma and sample to be cleaned are placed in a glass chamber within the microwave oven enclosure. A very high frequency (~2.5 gHz) induced plasma is generated when the magnetron is turned on. This is a commercial product, and is currently used in general laboratory cleaning. However, apparently there have not been independently published comparisons between its cleaning effectiveness for wire bonding with more conventional plasma cleaners, or demonstration of damage-free cleaning of sensitive chips.

The earliest use of plasma cleaning in microelectronics was to remove photoresist contamination from wafers [7-19]. However, more recently, there have been numerous studies applying plasma (O_2 and/or Ar and H_2) to the removal of contaminants. This has been effective on IC bond-pads, hybrid substrates [7-20 to 7-28], from Au bond pads [7-29], chip scale packages [7-30], plastic QFPs, SIPs, SOPs, and lead frames before epoxy molding (to prevent the popcorn effect) [7-29].

Oxygen and Ar plasma have been used for many years to clean ICs, microcircuits, [7-21] to improve bondability and to increase the bonding process window size. (See Fig. 6B-12 for a recent study of this window improvement on modern platings.) Such cleaning was shown to improve the bondability and reliability of gold-wire bonds to aluminum pads on epoxy die-attached devices. An example of the increased reliability after such cleaning is shown in Fig. 7-5. Similar improvements in bondability were obtained for gold ball bonding to gold-plated surfaces [7-22]. In this case, oxygen plasma was used to remove die-attach epoxy "bleed" from bond pads on substrate metallization

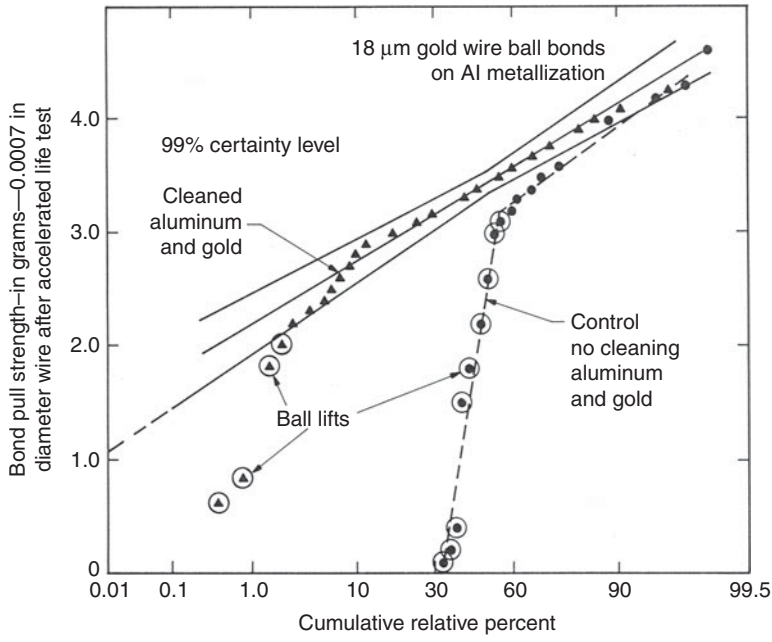

Figure 7-5 Influence of O_2 plasma cleaning on reliability of gold bonds on aluminum metallizations after a thermal stress of 300°C for 4 h. (*After Bonham and Plunkett [7-21]; © Plenum Press.*)

near the chip. The plasma cleaning had no negative effect on the die-shear strength. These results were verified by others [7-25, 7-26].

Graves [7-23] evaluated various plasma processes for improving the bondability of hybrids. He found that the bondability of the particular thick-film gold (Dupont 4290, reaction-bonded) used in their production was not improved by oxygen plasma, possibly because of oxidation of the reaction-bonding elements, such as Cu. His studies showed that the best results were obtained with oxygen-free argon plasma (0.25 Torr, 300 W, 60 min).* This study was also interesting because the author found that optimum results depended not only upon the gas and RF power, but also upon the fixturing, as well as the specific material being cleaned. Presumably, fixturing can shield or otherwise change the concentration of ionized plasma in a local region. In another case, oxygen plasma did not remove fluorine contamination from semiconductor bond pads [7-24]. Presumably, the fluorine had chemically reacted with the aluminum under the surface oxide. Other plasma-cleaning problems have been reported in which bondability

*Note that this cleaning time and power are on the very high side of typical plasma-cleaning parameters and could not be used on sensitive devices or on polymer substrates.

was also degraded rather than improved, as is usually the case. Such problems are often complex synergistic interactions between unlikely coincidences. In one such case, Ar plasma attacked polytetrafluoroethylene (Teflon) bushings in the plasma reaction chamber [7-32]. This liberated F which attacked the Cu as well as the Au in the reaction-bonded thick-film Au. Traces of Cl were also found. The result left copper hydroxyl fluoride on the surface, which degraded Au crescent bondability. It is clear that the interaction of materials and processes must be understood to avoid these and similar problems.

Plastic packages (e.g., BGAs) with epoxy-glass substrates (FR-4, BT, etc.) or polyamide may also be plasma cleaned in O_2/Ar for short times (1 to 5 min) at 300 W [7-18, 7-29, 7-33 to 7-35]. Longer times may heat the substrate or attack the plastic. Some workers use argon for such cleaning to minimize plastic degradation.

Hydrogen and Ar can be used for dc (rather than RF) plasma cleaning [7-36]. When used with about 5% H_2, the plasma breakdown voltage is so low that the authors report no radiation-type damage to sensitive IC devices (see App. 7A for an explanation of such damage). Organic contaminants are converted into hydrocarbon gases. Some inorganic contaminants such as S, P, and N compounds are also volatilized. The authors reported increased bond strength in all cases, but especially higher pull forces from Ag-plated lead frames. The H_2 should reduce any existing silver oxide as well as oxides on Cu lead frames.

Thin gold diffusion problem: With the recent increased price of Au, many companies are using displacement/immersion Au (<0.2 μm thick) directly over Ni platings for wire bonding (see Chap. 6). If there is a thermal treatment before wire bonding, the Ni will diffuse to the Au surface, oxidize, and reduce bondability. An argon plasma clean will "sputter" the NiO_x off and restore bondability, solderability, as well as increase the strength of mold compound adhesion [7-36]. This procedure is frequently used today.

Since plasma cleaning (O_2, Ar, H_2) has been shown to improve bonding, several "in-line" high-volume plasma cleaners have been introduced for cleaning lead frames before bonding [7-36, 7-38]. These are basically batch cleaners, but they automatically load, clean, and then unload the die-attached lead-frame strips, injecting them back into the assembly process. As such, they do not slow the device flow into the wire bonders.

As with UV-ozone, plasma cleaning can be safely used to clean metallization and devices on laminate and polyimide substrates (PBGAs, SIPs, SOPs, MCMs, etc.). In general, plasma is capable of damaging these substrates more than UV-ozone; however, with care, only minimal damage for a depth of about 100 Å may occur on polyimide [7-18] and less on PBGAs, and similar substrates. Often, only a minute or two is adequate for cleaning, and this is harmless to the device and polymer substrate.

7.1.4 Plasma Cleaning Mechanism

The mechanism of oxygen-plasma cleaning is similar to that of UV-ozone. Some of the O_2 can become ionized and other O_2 breaks apart into atomic oxygen, O + O. These react with the hydrocarbons to form H_2O and CO_2 [7-39]. There is also energetic bombardment by the excited oxygen atoms, which assists in breaking up the hydrocarbon molecules, as well as in sputtering off the contaminants. Ionized argon is not known to form stable compounds, although it may form brief metastable compounds with carbon or other contaminants, removing them and then decomposing, and releasing them to be pumped out of the gaseous plasma. Argon has more than twice the atomic weight of oxygen and it can knock off various forms of contamination by impact (sputtering). In general, it takes over twice as long to remove organic contaminants with Ar gas alone as with O_2 plus Ar. Frequently, mixtures of both oxygen and argon are used for plasma cleaning. Table 7-2 compares the various plasma-cleaning system parameters, as well as their reported effect on wire bonds. From these data, it is apparent that a wide range of parameters produces satisfactory cleaning. Parameters, such as an RF power of 100 to 200 W, a gas pressure of 0.5 Torr for either argon, oxygen, or mixtures, with about 10 min of cleaning time have been shown to increase both the bondability and the reliability of wire bonds on ceramic substrates. For removing thick layers of epoxy bleed or other contaminants, more time or power may be required. If the device is easily damaged (see App. 7A), using O_2 plasma with 75 W of RF power for 3 or 4 min may be adequate. Cleaning optimization procedures and schedules have been worked out for bonding [7-21, 7-22]. RF power above 300 W can be detrimental because of excessive heating of the samples and/or by sputtering off the metallization, and can possibly change the electrical characteristics of the devices.

Studies with oxygen plasma (as with UV-ozone) have separated the atomic oxygen, O, and ionized O_2 from the RF plasma (downstream cleaning [7-40]), resulting in effective cleaning of such materials as photoresist.

Procedures as simple as putting the devices inside screen enclosures (Faraday shield) within the RF plasma will shield sensitive devices from electric fields and prevent radiation damage, as discussed in App. 7A. Various specifically designed RF and microwave downstream cleaners are available, and most existing plasma cleaners can be easily modified for that purpose. Unfortunately, no bonding experiments have been performed using this method. Considering that there is no sputtering and many of the activated atoms will decay along the extended diffusion path, it may be presumed that the cleaning time would be increased considerably over normal O_2/Ar plasma. No downstream cleaning would take place with argon gas. Since plasma cleaning can cause problems in some sensitive devices

Power (W)	Gas	Pressure (Torr)	Flow Rate[a]	Time	Effect on Bonds	References
300	O_2	—	300 cm^3/min	10 min	Reduced corrosion	[7-6]
100	O_2	0.5	—	10 min	Increased shear strength	[7-8]
50	O_2, Ar	0.5	—	30 min	Cleaned ceramic	[7-20]
50–150	O_2, Ar	—	130 cm^3/min (various)	2–10 min	O_2 Increased reliability Ar removed Ag black	[7-21]
50–300	O_2	1–2	—	10 min	Increased bond reliability	[7-22]
<300	O_2, N_2, Ar	0.25	—	300 W, 60 min for Ar	Increased bondability See text	[7-23]
100	O_2	—	—	3–5 min	Increased bondability, reliability	[7-25]
75–100	Ar	0.2	113 1/min	5, 10 min	Increased bondability	[7-26]
220	O_2	1	600 cm^3/min	10–15 min	Increased bondability	[7-28]
200	Ar	—	—	2 min	Bonding on laminates	[7-33]
dc 25–30 V	Ar, 5% H_2	—	~70 cm^3/min	5–10 min	Increased bondability	[7-36]

[a]Flow rate to achieve a given pressure is dependent upon the volume and other characterstics of the plasma cleaner.

TABLE 7-2 Various Reported Plasma Cleaning Parameters

and downstream cleaning may not be as effective, then the substitution of UV-ozone can be considered a proven alternative for removing organic contamination (see Sec. 7.1.3). In some cases, gas deposition of thin hydrophilic masks may be used to prevent epoxy bleed buildup, thus eliminating the need for plasma cleaning and its possible damage to sensitive chips [7-41].

7.1.5 Discussion and Evaluation of Molecular and Solvent Cleaning Methods

Both UV-ozone and plasma-cleaning methods improve the bondability as well as the reliability of wire bonds. For ultrasonic and thermosonic bonding, they allow one to use less ultrasonic power and still make a strong weld. This, in turn, will reduce the incidence of another failure due to cratering (see Chap. 8). In addition, strong Au-Al welds have consistently been shown to be more reliable than weak ones. There have been far more published studies using plasma than UV-ozone cleaning for bond-quality improvement, although both methods are routinely used in production and often merely mentioned in publications without any details.

The first major usage of molecular cleaning methods for bond improvement was in hybrid microcircuit production. Here, atmosphere impurities resulting from the long storage of chips combined with a great deal of handling and processing (e.g., from epoxy die-attach outgassing) led to high wire-bond and corrosion failure rates that made cleaning a necessity. These cleaning methods are also currently used for relatively lower-volume expensive Cu/Lo-k and other IC packaging where high reliability is a requirement. Advanced chips are plasma processed and may have colorless fluorocarbon films on their bond pads, which can lead to bondability, as well as plague-like reliability problems. If they are not cleaned, they can require higher ultrasonic energy for strong bonding, which can lead to cratering or Cu/Lo-k materials stack damage.

Direct comparisons between UV-ozone, plasma, and solvent cleaning are rare. Sowell [7-9] did compare UV-ozone, argon sputtering, and high-vacuum bake-out. From his data, Fig. 7-1*a*, the first two appear equivalent in the ability to clean a surface of airborne-organic contaminants. But, in some cases, he could not effectively clean unknown contamination from "as-received" glass slides with UV-ozone, implying that the contamination was inorganic. However, argon plasma cleaning was effective and after that, UV-ozone removed airborne organics. Only one bondability study directly compared UV-ozone, O_2 plasma, acid, and complex solvent cleaning methods [7-8]. Both gold and aluminum bond-pads were intentionally contaminated with photoresist and also the outgas products from two different epoxies. Although some differences were found between the cleaning methods in removing particular contaminants, they were

all essentially equal except for the solvent cleaning. In that case, the bond strength remained as low as for the uncleaned samples. Note also that chlorinated solvents [e.g., trichloroethane (TCA)] can leave free chlorine residues on bond pads [7-28] and result in a serious reliability problem. Oxygen plasma was independently compared with solvents for cleaning incoming die and for epoxy-bleed removal [7-25]. This verified the conclusion that plasma cleaning is effective and that solvent cleaning is not useful in removing general organic contaminants. Iannuzzi [7-6] compared various solvent, plasma, and water-cleaning combinations, using biased aluminum triple-track corrosion in an 85°C/85% RH as the indication of aluminum contamination. It concluded that a freon TMS cleaning step, followed by oxygen plasma followed by cold-deionized water, was the most effective cleaning combination available. This removed both organic and ionic contamination so effectively that open package, biased aluminum triple-tracks withstood 12,000 h of 85°C/85% RH without failure. Uncleaned samples all failed within the first hour. Thus, if heavy organic and/or ionic contaminants are suspected, then the combination of freon TMS, oxygen plasma, and cold DI-water cleaning is recommended. (Note that many freons are currently banned from use by environmental concerns, and their cleaning replacements may offer reliability problems as yet undetermined.)

It should be noted that many solvents, including freons and chlorinated products may affect the environment and/or health, and a facility should verify the safety of all such products before using or disposing them. For instance, ozone (which quickly dissipates in open air) should not be breathed in concentrations more than a few parts per million, and UV-ozone cleaners are required to be vented outside.

7.1.6 Problems Encountered in Using Molecular Cleaning Methods

Both UV-ozone and plasma have been shown to be effective in removing organic contamination from bonding pads, although the degree of effectiveness of each method may vary somewhat, depending on the specific contaminant. Therefore, some evaluation must be made to determine the best choice for a specific application. Detailed studies of the removal effectiveness for a wide range of known contaminants have not been made. It should be noted that some contaminants, such as Cl and F, can become chemically bound and may not be removed by any of these cleaning methods, except sputtering the surface.

UV-ozone can activate electronic "color centers" in white Al_2O_3 ceramic substrates, resulting in a darkening or yellowing of the surface. This coloration may disappear in a few days or weeks, but generally it stays indefinitely. The coloration is completely harmless, but customers of white ceramic packages/substrates may be concerned

about its appearance. If the device can withstand baking over 200°C for 8 to 16 h, the coloration will be removed. Similar coloration may result from plasma cleaning, but it is less noticeable and may decay rapidly. Commercial pin-grid arrays, ceramic multichip packages, SIPS, etc., are usually dark purple or brown and are not further colored by UV-ozone exposure. Oxygen-plasma cleaning will blacken (oxidize) silver metallization and may reduce bondability. However, changing the oxygen to argon near the end of the cleaning process restored the silver to its original color and regained any bondability loss [7-21].

It is well known in plasma processing of reactive-ion etching that the walls of the etching chamber can become contaminated with stable polymers after long usage. These polymers may be redeposited on pads during subsequent operations. Plasma cleaners are subject to the same problems. It is essential, therefore, to occasionally clean the plasma-reaction chamber walls.

There have been reports that some special CMOS devices may display increased threshold voltages after plasma cleaning. A heat treatment of 200 to 300°C for 20 to 30 min will usually restore the threshold voltage (but such temperatures might harm the device or package). Degradations of bipolar devices have also been reported. A similar heat treatment would restore those device characteristics as well. These problems can be reduced and possibly avoided by minimizing the RF power and time. Since oxygen plasma takes less than half the cleaning time of argon, its use should be encouraged. Problems on both CMOS and bipolar devices are presumed to be the result of the energetic gaseous ions impacting on the device insulators (oxides and nitrides). This can generate electron-hole pairs. The holes may diffuse to active areas, degrading device performance. This phenomenon is called radiation damage. Modern dielectrically isolated bipolar devices that are not radiation hard are especially affected by such charges. See App. 7A for a more complete explanation of this effect.

Once a device has been cleaned, it will become recontaminated during storage. Figure 7-1 showed that recontamination of gold surfaces begins within minutes. The recontamination time of several materials by the contact-angle method is shown in Fig. 7-6. It is apparent that different surfaces have different affinities for carbonaceous contaminants from the atmosphere. Of particular interest for bonding is the rapid recontamination of aluminum surfaces. For practical purposes, a period of up to 2-h storage, after cleaning, is acceptable for wire bonding [7-8]. If stored for longer periods (say, overnight), the device should be recleaned. Storing in nitrogen-filled plastic cabinets may help, but this has not been demonstrated to prolong the clean-surface period. The cabinet itself, as well as waffle packs and other plastics inside the enclosure, may outgas organics onto the devices.

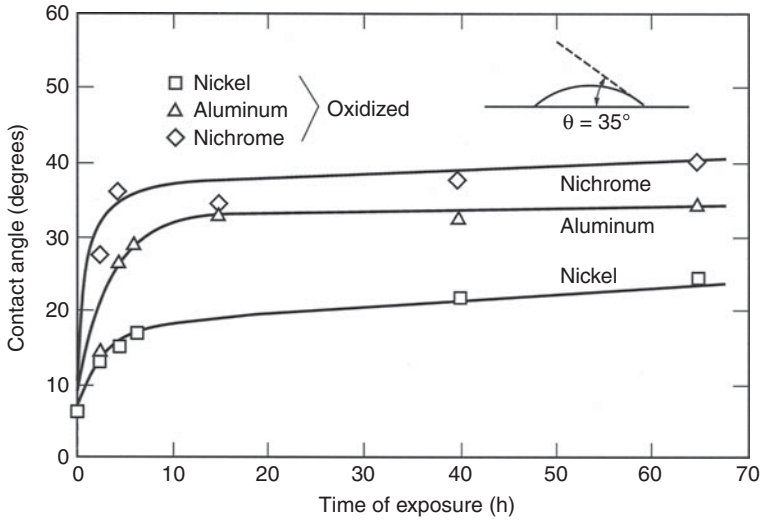

Figure 7-6 A comparison between the recontamination time (in laboratory air) of three metals used as bonding pads in microelectronics, that were cleaned by UV-ozone. Measurements were made by the contact-angle method, illustrated in the upper-right portion of the figure. Note that the aluminum (oxidized as it normally is on bond pads) is rapidly recontaminated. However, nickel (often used on power device packages) is not, but it is often partially oxidized. (*After Vig [7-13]; © IEEE.*)

7.1.7 Burnishing

Although not generally thought of as a cleaning step, various methods of abrading and scraping surfaces have been used for years to improve the bondability of classical thick-film hybrid metallizations. Thick films may have forms of surface contamination (e.g., glass, metal oxides), as well as pits and voids that are not removed by molecular cleaning methods. These contaminants or surface defects can reduce both the bondability and the reliability of a bond. Although there is no substitute for a good cleaning step (such as UV-ozone or oxygen/Ar plasma) before bonding, burnishing, scouring, and coining thick films to increase bondability have been performed since thick-film technology was developed. Burnishing instruments, such as fiberglass brushes, electric erasers (used by draftsmen many years ago) [7-25], various hard scouring tools, as well as prebonding without wire in the tool (coining) [7-44], have been used for this purpose. They remove the top surface layer leaving a clean surface for bonding. These are controversial procedures. Experiments have been published that support [7-42 to 7-44] or criticize [7-45]) such procedures. The controversy over these burnishing methods may result from the exact amount of surface roughness resulting from each operation, as well as how each investigator applied that manual procedure. Surface

roughness (range of ~0.001–0.01 mm) versus bond-pull force was studied for 32 µm (1.25 mil) diameter Al wedge-bonds on Au-Ni-Cu laminate (PCB) metallization. It was found that the rougher the surface, the more likely the bonds will be weak. Failures were revealed with several hundred to a thousand thermal cycles (0–125°C) [7-46]. This appears to be the only study specifically designed to determine the effect of bond strength of Al wedge bonds on surface roughness.

Surface roughness of thick films (not a specific cleaning issue) is considered by all authors to be part of the bondability problem. Coining and electric erasers effectively smooth the thick-film surface, but might leave contaminants. Scouring is effective for smoothing, and it removes all surface contaminants as well, see Fig. 7-7.

The use of various erasers or fiberglass brushes on thick films offer the hazard that particles may be left on the surface or imbedded in the metal film and not be removed by other cleaning steps. These then pose a bondability problem on their own. Erasers, in addition to unspecified abrasive particles, can leave rubber particles containing sulfur that may pose a reliability problem if not removed. One would like to think that the use of various erasers and brushes would have been eliminated. However, these procedures are still found (or thought) to be necessary for bonding to some thick films (We note that thick films are still in use for many applications in 2008.) If thick films present bondability problems related to surface irregularities or oxide and glass contaminants, then scouring (Fig. 7-7) or coining by a bonder, with ultrasonic power turned on, are the best procedures.

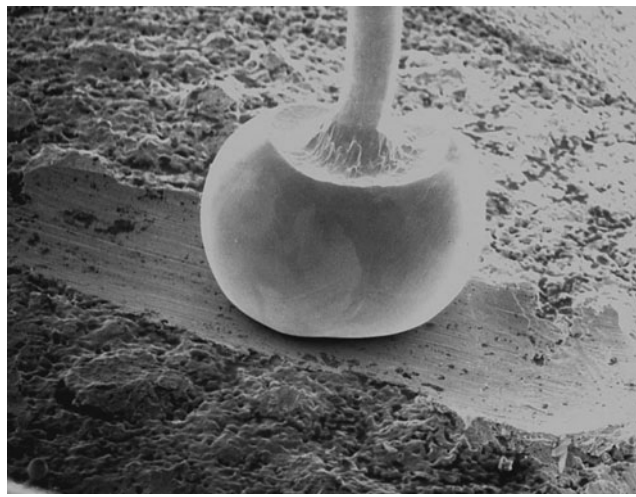

Figure 7-7 A SEM photograph of a 25 µm (1 mil) gold ball bond on a thick film that has been scoured to increase bondability.

7.2 The Sensitivity of Different Bonding Technologies to Surface Contamination

The previous section discussed cleaning methods to improve both bondability and reliability. Many of those bondability studies were made with thermocompression bonds, which have great sensitivity to surface contaminants. Most bonding personnel would agree that ultrasonic aluminum bonding is less sensitive to surface contamination than is thermocompression bonding. However, direct comparisons between bonding methods are rare and the experiments difficult to design. The present section compares the bondability of several methods of bonding through various measured thicknesses of a specific contaminant, photoresist. Significant differences between the bonding methods are revealed, and these should be considered when selecting a bonding technology. This is particularly important for complex devices that undergo considerable handling, such as hybrid microcircuits.

The only formal study comparing the susceptibility of different bonding methods to contamination was done at Sandia [7-47]. The substrates used in this experiment were alumina substrates with a chrome adhesion layer and 3 μm of vapor-deposited gold. These substrates were contaminated with spun-on Shipley 1350H photoresist diluted with acetone to various concentrations to produce specific thicknesses ranging from 50 to 180 Å (effective carbon equivalent thickness of 20 to 60 Å, respectively). The control substrates were UV-ozone cleaned (<5 Å carbon). All bonding parameters (for each bonding technology) were individually optimized on the control substrates and then maintained constant for the various contamination experiments. Thermocompression and thermosonic gold ball bonds (at 60 kHz) were compared as well as ultrasonic-aluminum wedge bonds in Fig. 7-8.

Data for each contamination level and bonding method consisted of 20 to 40 bonds. Selected results from the study are summarized in Fig. 7-8, which was drawn from Bushmire's data. The top of each bar indicates the contamination level required to produce the first lifted wire bond in a pull test. Ultrasonic aluminum wire bonding clearly has superior bondability for this organic film contamination. No pull-test lifts were observed up to the maximum 180 Å of contamination. Limited reliability tests of Al wires bonded to the Au substrates with ~70 Å of photoresist (50 wires at 100°C for 1000 h) showed no pull strength degradation as compared to as-made bonds.

While the results should be valid in the modern electronic-device environment, it would be desirable to repeat the experiment using autobonding machines and a variety of metallizations (i.e., aluminum containing both Si and Cu and various current thick films) and with various organic contaminants and surface films, such as glass

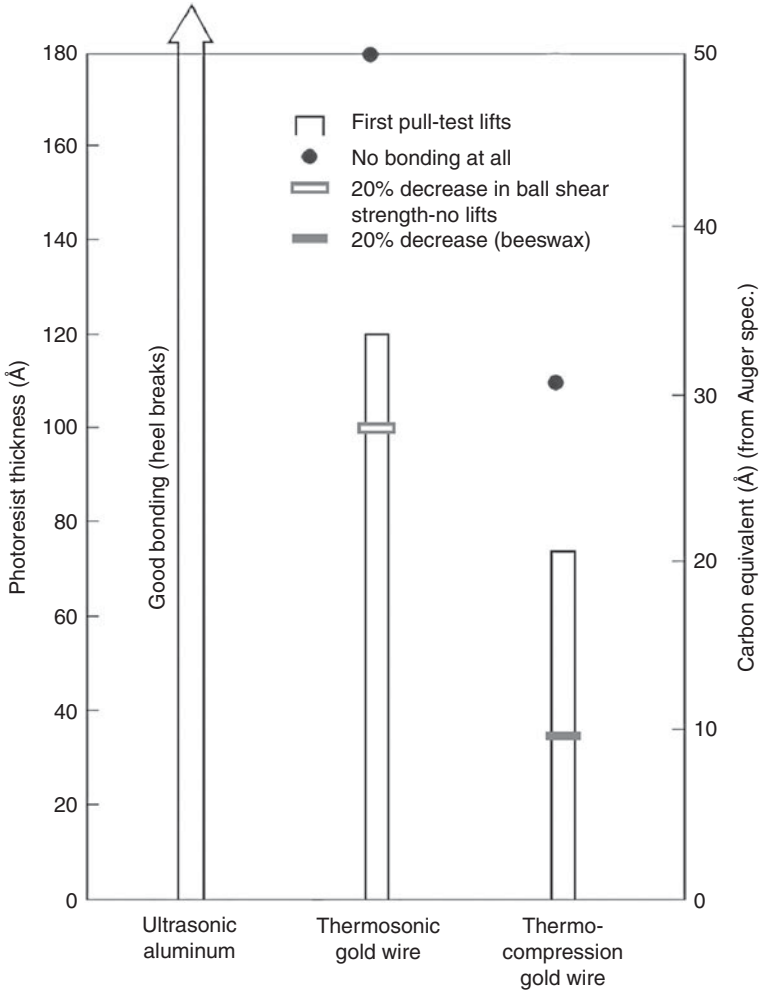

Figure 7-8 Sensitivity of three common wire bonding methods to organic surface contamination. The top of each bar represents the contamination level where the first pull-test lift occurred. The black circles indicate the level where no bonding occurred at all (immediate lifts). (*Redrawn from Bushmire [7-47]; © ISHM.*)

and silicon nitride. There is evidence that during bonding brittle films break up and are swept into "debris" zones, allowing ultrasonic and thermosonic bonds to be made satisfactorily through relatively thick coatings. The bondability through 250 Å of CVD oxide unchanged compared with bonding to uncontaminated pads [7-48]. Similar results in Au ball bonding to O_2 plasma-thickened Al_2O_3 (up to 200 Å) on aluminum bonding pads were found [7-49]. Neither these nor Bushmire's study subjected the bonds to HAST or other high-humidity

reliability testing, which might have revealed other types of problems, as discussed in Chap. 5, Sec. 5.2.1. These experiments should be continued, possibly at universities.

The above studies were primarily concerned with bondability. Although strong bonds are more reliable than weak ones, certain contaminants may affect the reliability of Au-Al bonds later during life (see Chap. 5 and Table 7-1).

Appendix 7A Circuit Damage Caused by Plasma Cleaning During Packaging

Contributed by Peter Roitman, National Institute of Standards and Technology

Integrated circuits can be electrically damaged by relatively benign plasma processing which is a normal part of wafer processing and for some packaging operations. This damage can be and is annealed out during the wafer processing sequence by thermal activation. In particular, a near final step in the process is typically ~350°C anneal to sinter the aluminum metallization. This is sufficient to remove the plasma damage. However, such temperatures are not compatible with modern packaging materials. Thus, a plasma-cleaning step at that time could be harmful and the damage permanent.

Radiation damage in semiconductors is usually associated with high-energy particles or photons that penetrate to sensitive junctions and interfaces in the interior of the device. Such high-energy particles or photons can displace atoms in the silicon lattice, resulting in the formation of defects which act as traps or generation centers. If these occur in the base region of a bipolar transistor, the lifetime is reduced, and the generation current is increased. This results in failure of bipolar devices. In oxides, the major effect of high-energy particles is to create electron-hole pairs. Holes that drift to the silicon interface are trapped, resulting in an interface charge. If the oxide is in the gate of an MOS transistor, the operating point of the transistor is shifted, resulting in failure [7-50].

Plasma damage is more indirect. The threshold for ionization of an electron-hole pair in silicon dioxide is 9 eV. Thus, any ion, electron, or ultraviolet photon that has energy greater than 9 eV and collides with an oxide surface can create an electron-hole pair in that oxide. Depending on plasma and surface conditions (secondary emission from the oxide and trapping near the oxide surface region), the oxide surface can charge either positively or negatively. In either case, electrons and/or holes will drift in the field down to the oxide-silicon interfaces. The mobility of electrons is reasonable in silicon dioxide; the mobility of holes is quite low. However, the hole lifetimes are long enough that these carriers can drift a few microns. The holes are

trapped at the silicon interface creating a positive charge, which can invert the silicon under the oxide. Drift from the top surface of the chip will not normally result in charge under the gate (the classic mode for penetrating radiation damage), but rather in charge under the field oxide. In MOS circuits, inversion of the surface can result in loss of isolation between adjacent transistors, resulting in circuit failure. In modern bipolar circuits, the vertical transistors are oxide-isolated. Thus, charge in the field oxide can short the emitter to the collector. (It is curious how close this mechanism is to that observed by Peck in 1963 [7-51 to 7-53].) The holes at the oxide silicon interface can be annealed at 300°C. Below that temperature, they are stable for very long periods [7-54].

There are a number of other damage modes associated with plasmas, such as interface state formation, neutral trap formation, surface damage due to sputtering, etc. These effects can usually be minimized by the choice of plasma conditions or are of minor concern in the field oxide regions [7-55]. Most of the above problems would not have occurred if H_2 plasma cleaning were used [7-36, 7-37].

References

7-1 Thomas, R. W., and Calabrese, D. W., "The Identification and Elimination of Human Contamination in the Manufacture of IC's," *23rd Annual Proc. on Reliability Physics* , Orlando, Florida, Mar. 26–28, 1985, pp. 228–234.

7-2 Lewis, G. L., and Berg, H. M., "Particulates in Assembly: Effect on Device Reliability," *36th Electronics Components Conference*, Seattle, Washington, D.C., May 5–7, 1986, pp. 100–106.

7-3 Lewis, R. G., and Wallace, L. A., "Toxic Organic Vapors in Indoor Air," *ASTM Standardization News*, Dec. 1988, pp. 40–44.

7-4 Hecht, L., "A New Method to Determine Contamination Limited Yield," *IEEE Trans. CHMT*, Vol. 14, Dec. 1991, pp. 905–906.

7-5 Lee, W. Y., Eldridge, J. M., and Schwartz, G. C., "Reactive Ion Etching Induced Corrosion of Al and Al-Cu Films," *J. Appl. Phys.*, Vol. 52, Apr. 1981, pp. 2994–2999.

7-6 Iannuzzi, M., "Development and Evaluation of a Preencapsulation Cleaning Process to Improve Reliability of HIC's with Aluminum Metallized Chips," *IEEE Trans. on Components, Hybrids, and Manufacturing Technology CHMT-4*, Dec. 1981, pp. 429–438.

7-7 Ameen, J. G., "Ion Extraction Method Improves Reliability," *Proc. of the 32nd IEEE Electronics Components Conference*, San Diego, California, 1982, pp. 401–405.

7-8 Weiner, J. A., Clatterbaugh, G. V., Charles, H. K., Jr., and Romenesko, B. M., "Gold Ball Bond Shear Strength—Effects of Cleaning, Metallization, and Bonding Parameters," *Proc. of the 33rd IEEE Electronics Components Conference*, Orlando, Florida, May 16–18, 1983, pp. 208–220.

7-9 Sowell, R. R., Cuthrell, R. E., Mattox, D. M., and Bland, R. D., "Surface Cleaning by Ultraviolet Radiation," *J. Vac. Sci. Technol*, Vol. 11, Jan./Feb., 1974, pp. 474–475.

7-10 Mittal, K. L., Ed., *Surface Contaminator, Genesis, Detection, and Control*, Plenum Press, New York, Vols. 1 and 2, 1979.

7-11 Jellison, J. L., "Effect of Surface Contamination on the Thermocompression Bondability of Gold," *IEEE Trans. on Parts, Hybrids, and Packaging*, Vol. 11, Sep. 1975, pp. 206–211.

7-12 Holloway, P. H., and Bushmire, D. W., "Detection by Auger Electron Spectroscopy and Removal by Ozonization of Photoresist Residues," *Proc. of the 12th Annual International Conf. on Reliability Physics*, Las Vegas, Nevada, Apr. 1974, pp. 180–186.

7-13 Vig, J. R., and Le Bus, J. W., "UV/Ozone Cleaning of Surfaces," *IEEE Trans. on Parts, Hybrids, and Packaging*, Vol. 12, Dec. 1976, pp. 365–370.
7-14 Jellison, J. L., and Wagner, J. A., "Role of Surface Contaminants in the Deformation Welding of Gold to Thick and Thin Films," *29th Electronics Components Conf.*, 1979, pp. 336–345.
7-15 Clarke, F. K., "UV/Ozone Processing: Its Applications in the Hybrid Circuit Industry," *Hybrid Circuit Technology*, Dec. 1985, p. 42.
7-16 Zafonte, L., and Chiu, R., "UV/Ozone Cleaning for Organics Removal on Silicon Wafers," *SPIE 1984 Microlithography Conferences*, Santa Clara, California, Mar. 11–16, 1984, Paper No. 470–19.
7-17 Ahn, S-H., Yoon, H-G., and Oh, S-Y., "Reliability Improvement of Plastic Ball Grid Array Package by UV/Ozone Cleaning," *Proc. ISHM Symp.*, Los Angeles, California, Oct. 24–26, 1995, pp. 7–12. Also, see "Prevention of Aluminum Pad Corrosion by UV/Ozone Cleaning," *Proc. IEEE ECTC*, Orlando ,Florida, May 28–31, 1996, pp. 107–112.
7-18 Padmanabhan, R. P., and Saha, N. C., "A Comparison of Plasma and Ozone Cleaning Methods for Polyimide Prior To Encapsulation," *Proc. ISHM* Baltimore, Maryland, Oct. 24–26, 1989, pp. 197–202.
7-19 Irving, S. M., "A Plasma Oxidation Process for Removing Photoresist Films," *Solid State Technology*, June 1971, pp. 47–51.
7-20 Mead, J. W., "Cleaning Techniques for an Al_2O_3 Ceramic Wafers," Sandia Report SKND-78-0734.
7-21 Bonham, H. B., Plunkett, P. V., Mittal, K. L., Ed., "Surface Contamination Removal from Solid State Devices by Dry Chemical Processing," published in *Surface Contaminator, Genesis, Detection, and Control*, Plenum Press, New York, Vols. 1 and 2, 1979.
7-22 White, M. L., "Removal of Die Bond Epoxy Bleed Material by Oxygen Plasma," *Proc. of the 32nd IEEE Electronics Components Conf.*, San Diego, California, May 10–12, 1982, pp. 262–265.
7-23 Graves, J. F., "Plasma Processing of Hybrids for Improved Bondability," *The International J. Hybrid Microelectronics,* Vol. c6, 1983, pp. 147–156.
7-24 Graves, J. F., and Gurany, W., "Reliability Effects of Fluorine Contamination of Aluminum Bonding Pads on Semiconductor Chips," *Proc. of the 32nd IEEE Electronics Components Conf.*, San Diego, California, May 10–12, 1982, pp. 266–267.
7-25 Kenison, L. M., Gardner, M. L., and Doering, C. E., "Oxygen Plasma Cleaning to Improve Hybrid Wire Bondability," *Proc. of the 34th Electronics Components Conference*, New Orleans, Louisiana, May 14–16, 1984, pp. 233–238.
7-26 Buckles, S. L., "The Use of Argon Plasma for Cleaning Hybrid Circuits Prior to Wire Bonding," *Proc. of the International Symp. on Microelectronics (ISHM),* Minneapolis, Minnesota, Sept. 28–30, 1987, pp. 476–479. (This has also been published in other conferences and magazines.)
7-27 McKee, J. L. J., Toth, W. D., and Fath, P. M., "The Characterization and Reliability Prediction of a Thermocompression Wirebonding System," *Proc. of the International Symposium on Microelectronics (ISHM)*, Atlanta, Georgia, Oct. 6–8, 1986, pp. 259–264.
7-28 Nesheim, J. K., "The Effects of Ionic and Organic Contamination on Wire Bond Reliability," *Proc. of the 1984 International Symp. on Microelectronics*, Dallas, Texas, Sept. 17–19, 1984, pp. 70–78.
7-29 Casasanta, V. and Wetzstein, J., "Organic Residues and Plasma Treatment for Wirebondable Gold," *IMAPS Proc.,* San Diego, Ca, Nov. 11–15, 2007, pp. 926–932.
7-30 Wood, L., Fairfield, C., and Wang, K.,. "Plasma cleaning of chip scale packages for improvement of wire bondstrength," *Proc. (EMAP 2000). International Symposium on Electronic Materials and Packaging,*, Hong Kong: 11/30–12/02, 2000 , pp. 406–408.
7-31 Djennas, F., Prack, E., and Matsuda, Y., "Investigation of Plastic Packages Delamination and Cracking," *IEEE Trans. on CHMT*, Vol. 16, Dec. 1993, pp. 919–924.
7-32 Gore, S., "Degradation of Thick Film Gold Bondability Following Argon Plasma Cleaning," *Proc. ISHM*, San Francisco, California, Oct. 19–21, 1992, pp. 737–742.

7-33 Robinson, D., Mammo, E., Higgins, L. M., and Baum, J., "Glob Top Encapsulation on Large Die on MCM-L," *Int J. Microcircuits and Electronic Packaging*, Vol. 15, Fourth Quarter 1992, pp. 213–228. Also, see *Proc. ICEMM* (MCM), Denver, Colorado, Apr. 14–16, 1993, pp. 563–574.
7-34 Mukkavilli, S., Pasco, R. W., and Griffin, M. J., "Plasma Processes for Thin Film Surface Treatment," *40th ECTC*, 1990, pp. 737–745.
7-35 Hansen, R. H., Pascale, J. V., DeBenedictis, T., and Rentzepis, P. M., "Effect of Atomic Oxygen on Polymers," *J. Polymer Sci.*, Vol. 3, 1965, pp. 2205–2209.
7-36 Onda, N., Dommann, A., Zimmerman, H., Luchinger, C. H., Jaecklin, V., Zanetti, D., Beck, E., and Ramm, J., "DC-Hydrogen Plasma Cleaning in IC-Packaging," *SEMICON '96 Technical Symposium*, Singapore, Apr. 24–26, 1996, pp. 147–153.
7-37 Haji, H., "Plasma Application Technology," *Proc. SEMICON*, Japan, Dec 3–5, 1997, pp. 9–56 to 9–61.
7-38 Ohzono, M., "Plasma Cleaning for Fine Connection," *Proc. First Intl. Conf. on MCMs (ISHM)*, Denver, Colorado, Apr. 1–3, 1992, pp. 491–498.
7-39 Hansen, R. H., Pascale, J. V., DeBenedictis, T., and Rentzepis, P. M., "Effect of Atomic Oxygen on Polymers," *J. Polymer Sci.*, Vol. 3, 1965, p. 2205.
7-40 Cook, J. M., "Downstream Plasma Stripping," *Solid State Technology,* Vol. 10, Apr. 1987, pp. 147–151.
7-41 Burmeister, M., James, G., and Fierro, L,."Preventing Adhesive Resin Bleed in Microelectronics Assembly through Gas Plasma Technology**,"** *Proc 2005 IMAPS*, Phila, PA, Sept. 25–29, 2005, pp. 771–778.
7-42 St. Pierre, R. L., and Riemer, D. E., "The Dirty Thick Film Gold Conductor and Its Effect on Bondability," *Proc. of the 1976 IEEE Electronic Components Conf.*, San Francisco, California, Apr. 26–28, 1976, pp. 98–102.
7-43 Panousis, N. T., and Kershner, R. C., "Thermocompression Bondability of Thick Film Gold, A Comparison to Thin Film Gold," *IEEE Trans. on Components, Hybrids, and Manufacturing Technology,* Vol. 3, 1980, pp. 617–623.
7-44 Marquis, E., and Wallace, A., "Surface Preparation of Thick-Film Gold for Automatic Thermosonic Gold Wire Bonding," *The International Journal for Hybrid Microelectronics*, Vol. 5, 1982, pp. 559–561.
7-45 Romenesko, B. M., Charles, H. K., Clatterbaugh, G. V., and Werner, J. A., "Thick Film Bondability: Geometrical and Morphological Influences," *Proc. of the 1985 International Symp. on Microelectronics (ISHM),* Anaheim, California, Nov. 11–14, 1985, pp. 408–419.
7-46 DiGirolamo, J.A., "Surface Roughness Sensitivity of Aluminum Wire Bonding for Chip on Board Applications," *IEPS Proc.*, San Diego, California, Sept. 11–13, 1989, Vol. 1, pp. 589–594.
7-47 Bushmire, D. W., and Holloway, P. H., "The Correlation Between Bond Reliability and Solid Phase Bonding Techniques for Contaminated Bonding Surfaces," *Proc. Intl. Microelectronics Symp.* (*ISHM*), Orlando, Florida, Oct. 27–29, 1975, pp. 402–407.
7-48 Harman, G. G., unpublished data.
7-49 Clatterbaugh, G. V., Weiner, J. A., and Charles, H. K., "Gold Aluminum Intermetallics: Ball Bond Shear Testing and Thin Film Reaction Couples," *Proc. of the 34th Electronics Components Conf.*, New Orleans, Louisiana, May 14–16, 1984, pp. 21–30.
7-50 Messenger, G. C., and Ash, M. S., *The Effects of Radiation on Electronic Systems*, Van Nostrand Reinhold, New York, 1986.
7-51 Peck, D. S., Blair, R. R., Brown, W. L., and Smits, F. M., "Surface Effects of Radiation on Transistors" *Bell Syst. Tech. J.*, Vol. 42, 1963, p. 95.
7-52 Srour, J. R., and McGarrity, J. M., "Radiation Effects on Microelectronics in Space," *Proc. IEEE*, Vol. 76, 1988, p. 1443.
7-53 Nicollian, E. H., and Brews, J. R., *MOS Physics and Technology*, John Wiley and Sons, New York, 1982.
7-54 Snow, E. H., Grove, A. S., and Fitzgerald, D. J., "Effects of Ionizing Radiation on Oxidized Silicon Surfaces and Planar Devices," *Proc. IEEE*, Vol. 55, 1967, pp. 1168.
7-55 Mogab, C. J. "Metallization," In: VLSI Technology, S. M. Sze, Ed., McGraw Hill, New York, 1983, pp. 303–344.

This page intentionally left blank

CHAPTER 8
Mechanical Problems in Wire Bonding

8.1 Cratering

8.1.1 Introduction

Many current studies of cratering are described in modeling papers in order to understand the material stresses that cause that failure mode. Such modeling is addressed in Chap. 11 by Yong Liu, Fairchild Semiconductor Corp., "Wire Bonding Process Modeling and Simulation." The subject is also occasionally discussed in the context of work on other subjects, such as wire bonding with Cu wire (i.e., described in Chap. 3). Such specialized work is discussed in that context or in other appropriate chapters.

An overview of the causes of and solutions to cratering problems, such as materials, properties, and bonding conditions are summarized in Table 8-1. One type of bonding failure that is commonly attributed to "overbonding"* appears as damage to the semiconductor, the glass, or to any Lo-k dielectric layers under the bonding pad (see Chap. 10 for Cu/Lo-k cratering). This is often referred to as cratering, because in severe cases a hole is left in the substrate, and a divot is attached to the wire (see Fig. 8-1). However, far more frequently the defects are less severe. They may produce no visible damage, but can degrade the device characteristics. The device failure may then be incorrectly classed as an electrical rather than a wire bonding problem. This entire range of damage is referred to as cratering.

*Overbonding is a term applied to bonding machine parameter setups in which one or more of the bonding parameters (force, time, ultrasonic power, and/or temperature) are significantly greater than is required to produce a normal bond. Usually, this results in the bond being overdeformed (flattened).

1. Materials (Metallurgy)
The harder the wire, the more likely cratering.
Bond-pad thickness: the thinner the pad, the more likely cratering.
Bond-pad hardness: ambiguous, but hard-pad interfacial layers (Ti, W) help.
Stress due to Au-Al intermetallics: occurs after thermal treatment (post-mold curing).
Bond-pad Si precipitates: cracking the under-pad layers.
2. Materials (Substrate-Device)
GaAs craters easily—yield strength and fracture toughness a factor of 2 lower than Si bonding to pads over polysilicon: can separate from underlayer.
3. Bonder and Its Set-up Characteristics
Shape or characteristics of ultrasonic generator pulse; slow rise time is best.
Ultrasonic energy: too high is harmful, contaminated bond pads require more US energy.
Bonding temperature: low and high are harmful—ambiguous.
Tool-wire pad impact force: high may be good for ball bonding, but not on GaAs.
Static-bonding force: too high and too low are harmful for wedge bonding.
Negative electronic flame-off for ball bonding, better than positive flame-off.
4. Failure Symptoms
Marginal cratering (can cause leakage between under layers or in active devices).
Gross cratering (divot comes out at bonding, pull, or shear testing).
Thermal cycling often reveals damage [8-19].
5. Wafer Processes Affecting Cratering
Bond-pad thickness.
Bond pad and interface metal-hardness.
Bond-pad silicon or Cu-, Al-, Si-intermetallic precipitates.
Bond pads over polysilicon.
Time, temperature, and cooling rates of heat treatments
Fracture properties of underlayers. (Thermal oxide better, >Young's Modulus than CVD oxide).

TABLE 8-1 The Causes of Cratering

Although this failure mechanism is often attributed to "over-bonding," there are many materials and equipment problems that can enhance the frequency of its occurrence. A study of each case often reveals a synergistic relationship between the materials, the bonder setup, and/or later stresses such as plastic encapsulation cure or

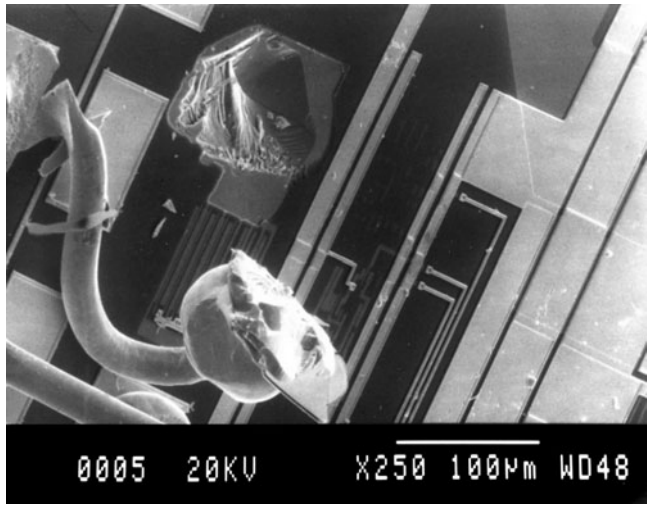

Figure 8-1 An SEM photomicrograph of a bond pad cratering area with the divot still attached to the ball bond. This crater was revealed during ball shear testing.

surface-mount thermal shock. [This problem has been increased since the switch to "green" (no-lead) solders that have higher melting points.] To troubleshoot this problem, one must understand the fracture and deformation of the semiconductor material and possible metallurgical interactions, as well as the wire and bonder characteristics.

There have been two published papers exclusively devoted to studying the causes of cratering during Al ultrasonic (US) bonding and others concerning thermosonic (TS) ball bonding. However, there are many papers that have discussed cratering in some other context, such as developing bonding machine setup schedules or using bonding wires of unconventional or harder materials (e.g., Cu). A compilation of factors that contribute to cratering is shown in Table 8-1. These factors occur in ultrasonic Al- or Au-wedge bonding as well as in Au, Cu, and Ag ball bonding. Cratering usually occurs in only a small percent of the bonds even though the bonds are made at the same time and with the same bond parameters. This small percentage complicates studying the problem and requires experiments with large numbers of bonds and statistical treatments of the data in order to gain an understanding of the process.

Calculations involving cratering often begin with a circle (cylinder or sphere) being pressed against the bonding pad [8-1, 8-2]. The radius of curvature establishes the contact area, and one can easily show (using the Hertz theory of contact pressure) that the initial force creates stresses many times the yield strength and/or the fracture strength of the pad and the semiconductor. It is implied that this

stress is applied directly to the underlying semiconductor, thus initiating a crater. Actually, the metal yields (deforms) far below the yield stress of the semiconductor, deforming the wire (ball) and the bond-pad metal. The wire (ball) flattens, and the stress drops rapidly as the metal-yields. (Ref. [8-2] did calculate the actual stress the Au ball applies to the bond pad, incorporating its yielding.) Ultrasonic energy, with possible stage heater contribution, softens the metal, which further lowers its yield strength, and deformation continues until the bond is mature [8-3]. (Examples and discussion of this are given in Chap. 2.) A major problem with the initial (point) contact-area stress interpretation of cratering is that, according to the Hertz model, the cratering should be initiated at the center of the bonded area. Observations of etch pits due to marginal cratering (under the bond) show that the worst damage occurs along the perimeter of the bond; the marginal damage, (in Fig. 8-2*a* and *b*) was revealed by etching (see Table 8-2). This damage was clearly demonstrated in steam-oxidation studies that revealed ultrasonic bonding-induced stacking faults in Si, as shown in Fig. 8-2*a* and by revealing damage etch-pits in Fig. 8-2*b* [8-4]. Work with peeled or lifted-up bonds [8-3] has shown that the perimeter is also the area where initial welding

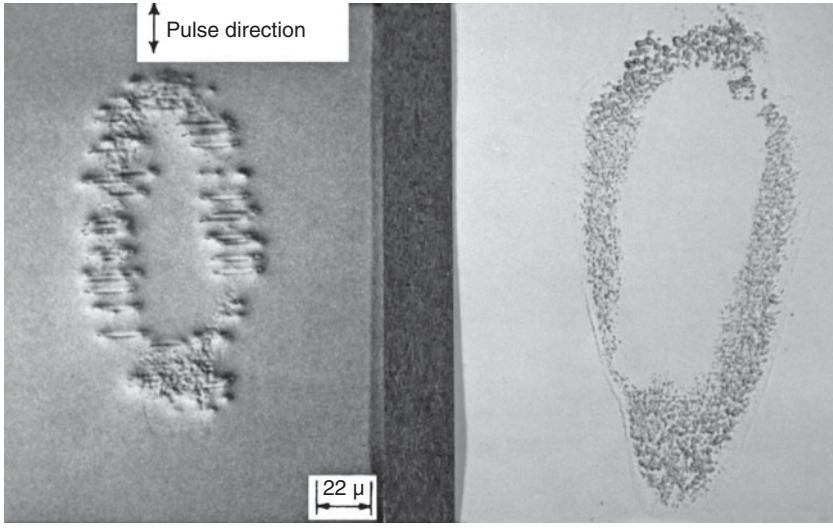

Figure 8-2 (*a*) Stacking faults in <100> Si typically form at the bond periphery from forces in the ultrasonic pulsing direction. Steam oxidation was used to reveal those stacking faults. A 50-μm diameter Al wire had been ultrasonically bonded directly to the Si. (*b*) A chemical-etch-revealed marginal cratering defect pattern on Si. The bond was chemically removed and the Si lightly etched. The bond was made similar to that of Fig. 8-2*a*. (*After Winchell [8-4]; © IEEE*.)

1.	a. Chemically remove metal (bond and pad) and observe with optical microscope.
	b. Lightly etch semiconductor (or SiO_2) surface and use optical microscope with vertical illumination to look for etch pits around bond perimeter (they sparkle).
2.	Bond to pads over active device areas and compare reverse bias leakage (before and after), easiest since no chemicals required.
3.	a. Ball-shear test often results in divoting or gross craters if marginal craters are present.
	b. Pull test on wedge-wedge bonds (with high loops and small to medium deformation) may reveal marginal craters.

TABLE 8-2 Detecting Marginal Craters

takes place (see Fig. 8-4 below for additional evidence of this). Also, force and temperature, without ultrasonic energy, does not cause the form of cratering resulting from Si nodules in the metallization (see Sec. 8.1.7) [8-5]. Thus, the bonding stress that causes stacking faults and other material damage is primarily related to the ultrasonic energy and therefore cannot be modeled by the normal Hertz contact pressure model.* That model, furthermore, is inappropriate because it assumes elastic material properties, whereas bonding results in major plastic deformation of the metals. The fracture toughness, K_c, of the semiconductor (see App. 8A) is a material property closely related to cratering. But it is not obvious how ultrasonic energy initiates cracks or lowers K_c in a single-crystal, defect-free semiconductor, unless this energy is capable of creating defects as it does in polycrystalline metals. If the stress of an electrical probe or other mechanical damage has produced a microcrack in the position of the bond perimeter, that crack can easily propagate during the ultrasonic welding process. Thermocompression (TC) bonding seldom produces cratering and therefore is preferable for use on GaAs devices that are weaker mechanically than Si. If ultrasonic energy is used on GaAs, the bonding process must be carefully optimized and controlled [8-6] with DOE bonder setup (see App. 8B, by Lee Levine).

There can also be a range of hidden damage, such as cracks initiating under ball or wedge bonds that are best revealed by failure

*This does not rule out the possibility that significant tool bounce on initial contact cannot be a contributing process. Bounce-type impact forces can far exceed steady-state ones and can occur before the metal has time to deform. Yield strength and fracture propagation are strong functions of the loading or strain rate. However all modern autobonders have programmed descent and impact, or, if manual-bonders, will have adjustable dash-pots or electronic controls to slow the tool descent rate.

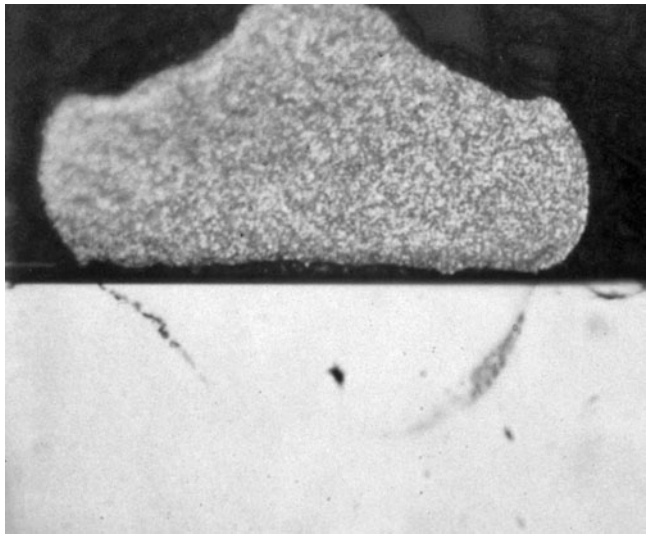

Figure 8-3 A section through a ball bond/silicon revealing hidden Si cracks (cratering). Note that such cratering in ball bonds starts along the bond perimeter, as with wedge bonds. It may or may not have been revealed by an etch-removal process comparable to the one in Fig. 8-2*b*. (*After McKenna [8-10]*; © *IEEE*.)

analysis sectioning-techniques. An example is given in Fig. 8-3. In this case, again, the damage initiated around the perimeter of that bond. Apparently, a slight increase in US power (or possibly a shear test—but not a pull test) would have connected the crack(s) together and opened up a full crater, similar to that shown in Fig. 8-1.

8.1.2 Bonding Machine Characteristics and Setup Parameters

Excessive Ultrasonic Energy

The most common cause of cratering results from improper bonding-machine parameters, and essentially all papers on the subject cite this as a contributing cause. Excessive ultrasonic energy has been cited more often than any other bonding parameter as the cause of craters. This is even more apparent when it is considered that cratering is seldom encountered with TC bonding and that this bonding method is the safest process to use on crater-prone materials like GaAs (assuming the high temperature poses no device or packaging problems). In studying the ultrasonic wedge-bonding process, Winchell found that even though metal mass flow is equal in all directions, stacking faults in Si occur perpendicular to the direction of the ultrasonic bonding tool motion (pulse direction) [8-4]. This verified that

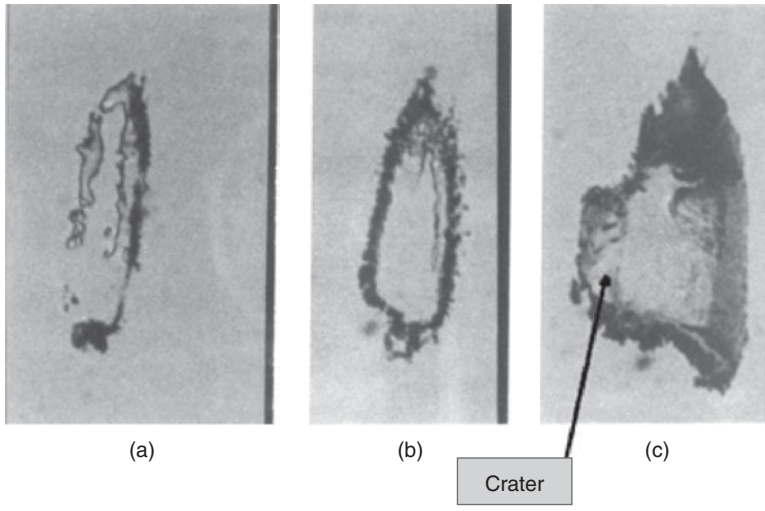

Figure 8-4 Through the underside of a bond pad. The disruption of the bond pad metal observed from the underside of a thin (~0.2 μm) evaporated Al pad, which was deposited on a clear fused quartz substrate. These three patterns were made by bonds on the other side of the substrate. Bonding parameters were constant, except for the ultrasonic power, which was increased for each successive Al wedge bond. Power-supply dial settings were, from left to right, (*a*) 4.5; (*b*) 5.5; (*c*) 9.5. The third bond, made at the highest US power, has cracked (cratered) the quart substrate. This example was also discussed in a different context in Chap. 2.

ultrasonic energy is a major cause of the problem and that it is capable of directly introducing defects into single-crystal Si, although the mechanism is not understood. Figure 8-4 illustrates the cratering (looking up from the bottom of a transparent substrate) as power was increased. Power was the sole variable that changed!

Modern high-speed automated bonders that can bond up to 15 wires/s (30 welds/s) could pose an additional cratering hazard. The time available for ultrasonic energy application to each weld has decreased from an average of 50 ms (for older manual bonders) to less than 10 ms. The ultrasonic energy, bond force, and/or stage temperature must be increased to compensate. This results in a narrower bond-parameter window. If the bond time is decreased below 10 ms, increasing ultrasonic energy is required to produce a reliable weld (at 60 kHz), and the probability of cratering can increase. However, the use of high-frequency US energy (> 60 kHz) could complicate any general conclusions from above, and in many cases it bonds with less power and also shortens the bonding time. See Sec. 2.4, Chap. 2.

It should be known that contaminated bond pads require higher ultrasonic energy and/or temperature for making strong bonds. Since modern processing and packaging may leave polymer or ionic

residues on pads, a molecular cleaning method is recommended, especially where a cratering problem is encountered. (See Chap. 7.)

Modern bonding machines use high-frequency ultrasonic energy for bonding (see Sec. 2.4), and many bondability advantages have been published. However, few studies have made direct comparisons between potential failure modes resulting from different frequencies. Heinen [8-7], has done so in the area of cratering. This work compared cratering over active device areas using approximately 100 kHz energy and concluded, in that case, that such bonding was less crater-prone than if done at 60 kHz. This is encouraging, but more studies are needed for verification for all packaging materials situations. It is noted that cratering while using HF does occur and has been a major problem with Cu/Lo-k bond pads (see Chap. 11).

8.1.3 Bonding Force

Often, for wedge bonds, too high or too low a static-bonding force has been observed to contribute to cratering. This is shown in Fig. 8-5 [8-1]. The conventional explanation for cratering in wedge bonding with low force is that the bonding tool is not held tight enough against the pad, and it chatters across the top of the wire producing high-force spikes to the pad/silicon. This explanation has never been proven. It is generally assumed that the optimum clamping force as in Fig. 8-5 results in more efficient ultrasonic energy transfer, thus lowering the total energy requirements for bond formation. Analysis of data from various sources [8-8, 8-9] indicates that there is a less precise (static) bonding-force effect

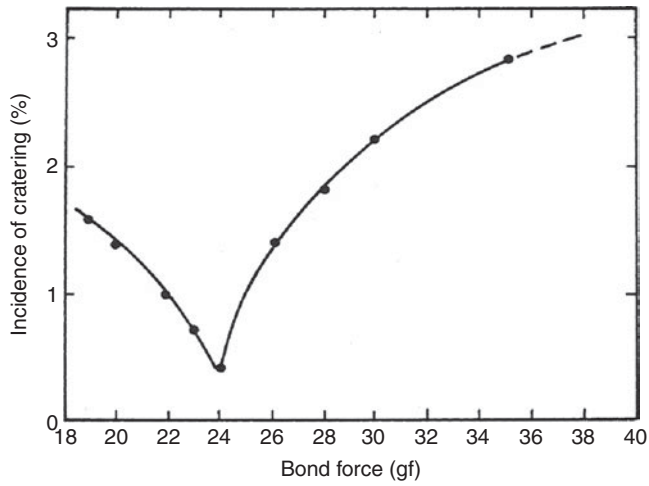

Figure 8-5 The incidence of cratering versus bond force for the ultrasonic bonding of 25-μm diameter Al, 1% Si wire of 15 to 16 gf breaking load. The data were obtained from bonding to various Si devices with 60 kHz power. (*After Kale [8-1]*; © *ISHM*.)

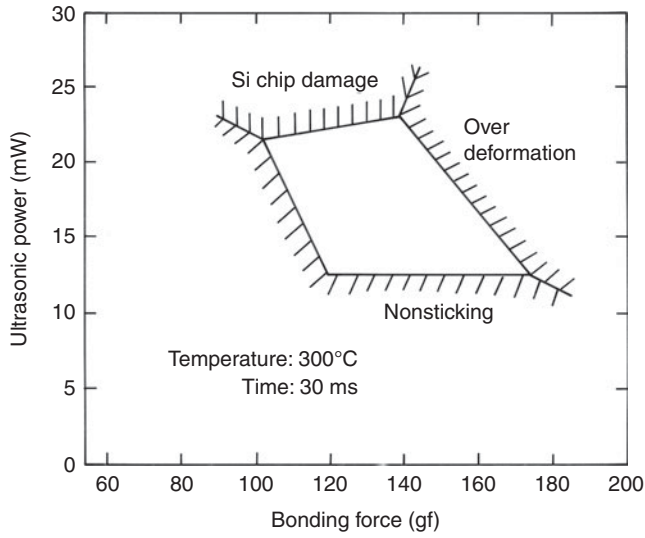

Figure 8-6 The preferred ranges of ultrasonic power and bonding force for copper ball bonding to 1.3 μm of Al, 1% Si, over SiO_2. The wire diameter was 25 μm, the wire was 6-9s purity, and the initial ball diameter was 62 μm. (*Redrawn from Mori [8-8]*; © *IEEE*.)

for cratering during thermosonic (TS) ball bonding. An example of a two-dimensional parameter plot (a bonding window) for Cu ball bonding showing the areas of nonsticking through cratering and over-deformation is given in Fig. 8-6 [8-8]. (Note that two different bonding windows are given in Chap. 6B, Fig. 6B-4. They were set up for a different purpose but show the versatility of using such windows to understand the limits or to optimize a particular bonding situation.)

It is difficult to establish clear comparisons between all variables, since other bonding parameters must be varied to optimize bonding for each experiment [8-4]. If the bond deformation is held constant to make equivalent deformation bonds, then, when the force is reduced, the power, time, and/or temperature would normally have to be increased. Most studies do not give enough data to determine the actual parameters causing the damage. Factorial experiments specifically designed to encompass the entire range of cratering from crystallographic defects to divoting should lead to a better understanding of the cratering problem. Experiments should cover the range from pure thermocompression through pure (no heated stage) ultrasonic ball bonding. Failure analysis of the experiments should be carried out on Si by etching, possibly by steam oxidation and detailed (optical or electron) microscopic observation. On a more fundamental level, it would be desirable to study the mechanism by which ultrasonic energy, during welding, can generate defects (and cracks) in single-crystal semiconductors, using this to study the effect of high-frequency bonding.

8.1.4 Tool Wire-Pad Impact Force

Intuitively, one might think that a zero-impact force on the pad would minimize cratering. Low impact is generally used for wedge bonding, especially for GaAs chips, although documentation for this use to minimize cratering has not been published. However, high-impact bonding has been suggested as a means of reducing cratering during thermosonic ball bonding [8-10]. In this case, the capillary (and ball) rapidly descended to the pad, within 30 ms of ball formation (which required very special bonding-machine modifications, but is possible with some advanced autobonders). This left the ball hot and, therefore, softer at touchdown, and with high-impact force, it deformed essentially to its mature bond deformation on that impact. Ultrasonic energy, applied during and after touchdown, matured the bond interface. As with wedge-bonding, it was found that too low a static bonding force increases cratering significantly. Since the original publication, there has only been only one study on higher force-impact bonding presented at the Third VSLI Packaging Workshop of Japan, Dec. 1996 (unpublished). Thus this technique has not been adopted by the industry. In addition, with the advent of Cu/Lo-k chips (see Chap. 10), having complex bonding stacks susceptible to mechanical damage, it could pose reliability/yield problems.

8.1.5 Causes of Cratering—Materials

Bond Pad Thickness

In addition to being a bonding surface, the bond pad also serves as a cushion to protect the underlying material (SiO_2, Si, polysilicon, GaAs, etc.) from damage due to the stresses of bonding. Winchell [8-4] used an extremely sensitive technique (steam oxidation of the Si surface) to reveal marginal cratering on Si due to Al wedge bonding. He found that the tendency to crater was most prevalent for the thin metallizations, and this has also been found by others. The 0.6 μm metallization thickness represents the transition range in which surface damage to the Si was still observed. For 1.0 to 3.0 μm metallization thicknesses, the surface damage becomes undetectable when using acceptable bonding-machine parameters. An increase of the total metallization thickness from 0.8 to 1.2 μm significantly decreased cratering in GaAs devices [8-6]. Thus, a metallization thickness of 1 μm or greater is desirable to help minimize most cratering damage in GaAs as well as in Si. Unfortunately, modern chip Al metallization is often thin (<1 μm) to facilitate etching of narrow line widths, and this increases the probability of cratering unless there are hard underlayers (see below).

Bond-Pad Hardness

There is no clear evidence that the bond-pad hardness affects the incidence of cratering. One might assume that a softer bonding pad metal would inhibit cratering by absorbing US energy and deforming easily

and that a hard pad should more readily transmit the bonding forces to the substrate. However, the best bonds with the lowest machine-bonding parameters are made when the hardness of the wire and the pad are reasonably matched [8-11, 8-12]. In fact, the combination of a normal Al layer for bonding over a hard interfacial layer (Ti, W, etc.) appears to be less subject to cratering in both Si and GaAs. Hard Cu-doped metallization can be more crater-prone because Cu oxide or Cu-Al corrosion products on the surface require more ultrasonic energy to bond (rather than hardness of the film). The most significant factor may be that the conditions that allow best bond formation also minimize cratering. Generally the pad should be about the same hardness as the ball. In some cases the pad may have ppm-level impurities added to better match the ball hardness to obtain the best welding.

Wire Hardness

It has long been known, but not clearly documented, that harder wire can cause Si craters during Al ultrasonic bonding. Several investigators who have run cratering experiments listed wire hardness as a cratering contributor [8-1, 8-4]. Recently, Cu wire has been used in production for ball bonding as a less expensive replacement for Au. Since Cu balls are significantly harder than Au balls and result in more frequent craters, investigators have studied the relationship between wire/ball hardness and cratering [8-8, 8-11]. See Fig. 8-6 as one possible example of bonding-machine setup for Cu ball bonding. Srikanth has studied the hardness of both Cu and Au bonded balls [8-13, 8-14], and some of his data are listed in Table 8-3. He found that Cu work-hardened significantly during ultrasonic bonding, which suggests the reason the cratering problem persists. See the color CD (after Fig. 3A-2) for a comparison of Cu-ball microhardness before and after bonding.

Investigators have adopted procedures, such as minimizing ultrasonic energy and increasing temperature of the substrate and the tool to help prevent or minimize the problem. Silicon nodule-induced cratering (see Secs. 8.1.7 and 8.1.4) was found to be reduced if the time for ball formation (EFO spark) to pad touchdown was reduced to less than 30 ms ([8-2, 8-11] and Sec. 8.1.4). This left the ball hot (and therefore softer) at touchdown. Such a rapid capillary descent would result in significant impact deformation of the ball, would require less ultrasonic energy for normal deformation during welding, and would presumably decrease cratering.

Table 8-3 compares several hardness measurements made on various bonding wires and metallizations. Some measurements are made directly on the ball. It is very difficult to interpolate between the results of different hardness tester indenters and loads, so the most meaningful information is obtained from data comparisons made by the same investigator and instrument as for the Srikanth data.

The actual role of wire hardness in cratering is not understood, as pointed out by Winchell, because of the synergistic effect of other

Metal	Hardness value (Material)	Load	Reference	Shear Modulus
Gold	40 (HV) (ball) 58–60 (HK) (wire)	1 g	8-8	26 GPa
	37–39 (HK) (free-air ball)	5 g	8-32	
	66–68 (HV) (wire)	—	8–13[a]	
	60–90 (HV) (bulk)	—	8-13	
	71 (HV) (bonded ball)	—	8-31	
Silver	61 (HK) (bulk)	15 g	8–30	30 GPa (bulk)
Aluminum	35–60 (HK) (bond pad)	0.5 g	8-11	26 GPa (bulk)
	20–50 (HV) (bulk)	—	8-31	
Copper	47–53 (HV) (free-air ball) 55 (HV) (ball)	1 g	8-8	48 GPa (bulk)
	77 (HV) (wire) 47–50 (HK) (free-air ball)	0.5 g	8-11	
	64–68 (HK) (wire)	5 g	8-32	
	99 (HK) (bulk)	15 g	8-30	
	89 (HV) (wire)	—	8-14	
	84 (HV) (free-air ball)	—	8-14	
	111 (HV) (bonded ball)	—	8-14	

[a]Microhardness measurements made by different investigators and equipment are difficult to directly compare. Different scales (HV, HK) use different indenters and can use different loads/indentation depths, which are seldom given. References 8-13, and 8-14, by Srikanth, represent unique measurements of both Cu and Au wires and bonded ball hardness, since they were made by the same investigator.

Table 8-3 Hardness and Shear Modulus of Wire Bonding Materials

variables. Harder wires require more ultrasonic energy to bond,* and this energy increase could be the reason for cratering. Papers on the subject do not give enough information to determine the actual cause. Further work is necessary to fully understand the mechanism.

8.1.6 Intermetallic Effects on Cratering

Gold-aluminum intermetallic effects have been studied by using the ball-shear test as a measurement tool [8-15]. It was found that the

*The ultrasonic energy, E, required for bonding is empirically related to the metal hardness by: $E=K(HT)^{3/2}$ where K is a constant, H is the hardness in Vickers, and T is metal thickness. See, for instance, *American Welding Society Handbook,* Vol. 3, part 2, 2007. This specific relationship has not been verified for samples with microelectronic dimensions, but a similar relationship is assumed to be valid.

probability of cratering, as observed in shear testing, increased up to about 4 h during a 250°C bake, and approximately 20% of the ball bonds cratered the Si during that test. However, continued heat treatment resulted in decreased cratering to a level of 4% at 35 h, as shown in Fig. 8-7. The observed Au_2Al could result in a large-volume increase over that of the original Al metallization; up to 30% (see Noolu, Intermetallics App. 5B, Tables 5B-1 and 5B-2) resulted in high stress under the bond, in the order of 90 gf for a typical ball bond. When subjected to the additional stress for balls of this diameter, a shear test (40 to 60 gf), the combination of stresses could result in cratering. The above authors explained the decrease in cratering after a longer time at the baking temperature as an annealing process that resulted in recrystallization, which reduced the stress, also see Ref. [8-16]. (An alternate possibility could be explained by the Noolu App. 5B, in which the different evolving intermetallics cell volumes continue to change with further diffusion and decrease the stress.) This intermetallic volume-induced stress will be referred to as the Clatterbaugh-Noolu (C-N) effect. The results of finite-element modeling of the ball-shear test with the pad converted to intermetallic, were consistent with earlier observations. The shear test can apply approximately 3500 to 7000 kg/cm^2 (50 to 100 K psi). Low-profile balls result in the lower force, while tall ball bonds may exceed the higher-force number. (These values may be reduced somewhat by metal yielding.) This force could easily propagate existing microcracks in Si causing a crater.

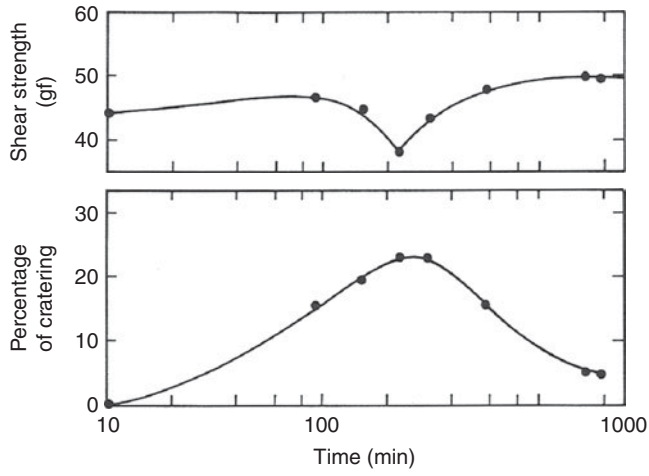

Figure 8-7 Percentage of cratering and shear strength for thermally aged (250°C) gold-ball bonds on bonding pads of 1 μm of pure Al over Si. (*After Clatterbaugh [8-15]*; © *IEEE*.)

Some interesting consequences of this Au-Al stress mechanism have not been explored. For instance, plastic-encapsulated devices require a postmold bake of 3 to 6 h at 175°C, and a calculation indicates that approximately 13 h will completely convert 1 μm of Al to intermetallic compounds.* However, for various reasons, the equivalent time-at-temperature during assembly may be much longer. A midrange of this time at temperature is roughly equivalent to the 10% cratering time temperature† of Clatterbaugh. Thus, most bond pads in plastic-encapsulated devices are at least partially converted to Au_2Al, leaving the underlying structure highly stressed. In some cases, various overcoatings may be applied after bonding and may be cured at various high temperatures. Any anomaly in bonding (and intermetallic is always formed during that process), in the metallization, or in the plastic molding process could increase cratering. These various contributing sources of stress applied in different steps would be easy to overlook.

Cratering under Au-Al bonds, after thermal exposure, has not been directly verified by others. However, the fact that similar cratering has been observed in surface mount thermal shocks during plastic package soldering (illustrated in Fig. 8-8) stands as indirect confirmation.

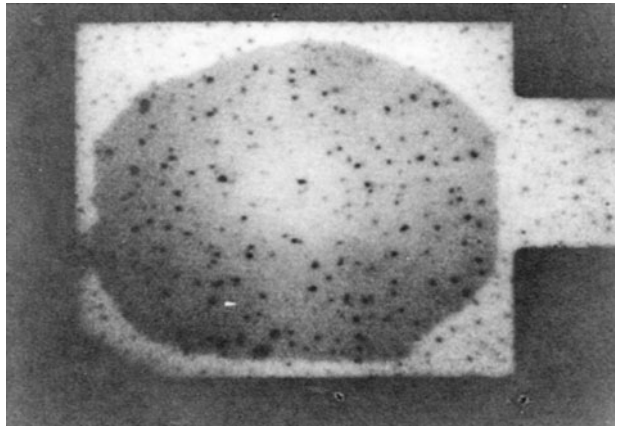

Figure 8-8 An example of an Al, 1% Si bond pad containing large Si participates, as seen through the rear of the chip by an infrared microscope. The larger particles have dimensions of approximately 1 μm. The shadow is the IR image of the ball bond on top of the pad. (*After Footner [8-18].*)

*Modern ULSI metallization is becoming thinner, and the time at temperature for complete intermetallic formation (with a Au ball bond on the Al) is therefore, decreasing.

†Using the Arrhenius equation $t^{1/2} = 5.2 \times 10^{-4} \exp(-15{,}900/kT)$, t = time, T = temperature. Note this is the average diffusion of all phases. Others have measured much shorter times (i.e., ~2 h) for one or another intermetallic phase to diffuse 1 μm into aluminum at comparable temperatures.

There are other examples of the cooperative effect of different stresses in producing cratering. Excess stress from improperly deposited bumps or metal diffusion barriers (i.e., nickel) in the case of TAB (tape automated bonding) has long been known to result in cratering when the TAB bumps are sheared. Stress from Sn-Cu intermetallics under solder bumps in controlled collapse flip-chip devices have led to underlying SiO_2 glass fracture.

More work is needed to clarify the C-N effect. Some investigators have not observed (or at least reported) this effect, but the recent work on intermetallic induced strains by Noolu (see App. 5B) offers a reasonable explanation. Variables such as the Al film and/or the SiO_2 thickness, dopants including Si and Cu, and different temperature bakes (which result in different intermetallics, different diffusion-rate constants, and possibly different strain-reduction characteristics) apparently all affect the process. For completeness, the work should also include different bonding wires, such as Cu, and the effect of bonding-machine variables, such as ultrasonic energy, temperature, and time. Identification of the specific intermetallic(s) causing the problem would be necessary for a complete understanding and to couple the phenomena to Noolu's work.

8.1.7 Silicon Nodule-Induced Cratering

One percent Si is often added to Al metallization to prevent back-diffusion of Si from shallow junctions into that metal. Such back-diffusion could damage the electrical properties of the device. As a result, micrometer-sized Si nodules have been found in Al bond pads, and these can act as stress raisers and crack the underlying glass during thermosonic Au ball bonding [8-17]. Reliability testing revealed electrical leakage between the pad and the underlying Si. Various aspects of the plastic-molding process were shown to add stress to the bond pad. Corrective action to minimize cratering included bonding at higher temperature (250°C), lower ultrasonic power, reducing molding stress, and removing a fracture-prone phosphorus glass layer from under the pad. An example of a bond pad containing such Si participates, as seen by an infrared microscope, is shown in Fig. 8-9 [8-18]. Several others have generally confirmed the Si nodule bond-cratering effect [8-2, 8-5]. One organization solved the problem by changing the structure under the pad (using a 0.3 μm thick layer of hard Ti-W under the Al pad), by modifying the bonding schedules, or by using rapid (hot) ball touchdown. These published experiments apparently did not include plastic encapsulation or application of any other shear forces. However, Si nodule cratering during surface-mount soldering of plastic-encapsulated devices has been observed [8-5]. In this case, ultrasonic energy, rather than force and temperature alone, was found necessary to form the original microcracks that later lead to cratering. (TC bonding did not produce such microcracks.)

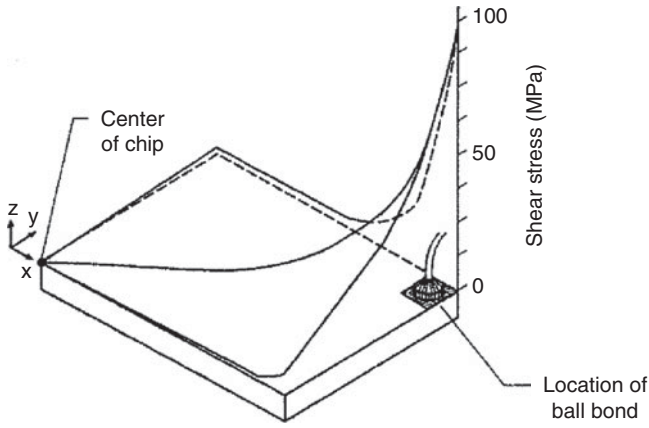

Figure 8-9 An FEM plot showing the high shear-stress that can occur on the corner ball-bond location due to thermal cycling of a plastic molded device. Such stresses have resulted in cratering during surface-mount soldering. (*After Dunn [8-19]*; © *IEEE*.)

Cratering was enhanced if the plastic package had absorbed water. The thermally expanding "wet" plastic applied larger shear forces to the ball bonds during the rapid heating, resulting in cratering. These bond pads would have also included intermetallic stresses from the C-N effect.

Discovery of the Si nodule-cratering mechanism raises questions as to why Si nodules as large as the bond-pad thickness should exist. Bonding-wire manufacturers have long controlled the grain size of nodules in similar 1% Si-doped Al wire by proper heat treatment (rapid cooling from 350 to 100°C). It appears that the metallurgy of Al, 1% Si may occasionally be overlooked by integrated circuit manufacturers. After metal deposition and patterning, the films are annealed (sintered) at temperatures approximately 400°C for up to 30 min. They are cooled without consideration of the Si grain size. Various other processes may require high-temperature wafer heating, such as curing polyimide multilayers. Again, there is no effort to assure a rapid cooling rate to prevent large Si particles from growing. Many processing documents prescribe slow cooling after such heat steps to prevent strains that may lead to wafer bowing. Some compromises must be made to minimize Si nodule growth. In addition, other aspects of device reliability may be improved by this compromise. Large Si nodules will eventually represent most of the Si that was originally added to the Al to prevent back-diffusion from narrow junctions. After nodule formation, such back-diffusion could then take place and damage the device.

When studying cratering after temperature exposure, investigators should be aware that Au-Al intermetallic stresses on the bond pad might result from thermal processing, such as curing various plastic encapsulants, stabilization bakes, etc. Then, the resulting

The Ultimate Synergistic Problem
1. Metal deposition Al, 1% Si (~2+% Cu)
2. Metal sintering (400°C+, 30 min)
3. If >3% Cu then massive Au-Si-Cu alloy nodules form
4. Multilayer insulator (polyimide, oxide, Lo-k)
5. If polyimide coating, *cure* in steps-up to 350°C+
6. More metal deposition and sintering
7. More polyimide (or glass? up to 350°C)
8. Die attach (epoxy cure)
9. Wire bonding (~150°C) if 2% Cu and Si in Al increased US energy, microcracks occur
10. Plastic encapsulation cure (175°C, 3 to 5 h)
11. Storage in various ambients
12. PC-board soldering (surface mount/reflow soldering, etc.)
13. Cratering!

NOTE: All above steps can lead to increased Si nodules (and from 9 on) to Au-Al compound growth, which increases cratering possibility.

TABLE 8-4 Cratering Stresses Resulting from Silicon Nodule and Au-Al Compounds

thermal stresses combined with other stresses (e.g., plastic package shear forces from surface mounting, Si nodules, probe damage, and microdefects marginal cratering due to poor bonding-machine setup) can result in cratering where no single effect alone would cause a problem. The use of several percent of Cu in Al can be expected to form hard Cu-Si-Al intermetallics under various circumstances, and these may be an additional source of crater-forming nodules.

As larger chips have been plastic encapsulated, and surface-mount assembly has increased, another source of potential cratering stress on bonds has been observed. This is a subset of the "popcorn effect," and it might be called "marginal popcorn effect," since it can occur under surface-mounting/reflow-soldering conditions that do not actually rupture (pop) the package. Figure 8-8 is an example of the high stress that can be applied to the corner ball-bond location due to rapid thermal expansion of the mold compound [8-19]. In such cases, cratering can be a result of the synergistic combination of intermetallic stresses (from plastic cure), bonding damage resulting from silicon nodules in the pad, and the large thermal expansion stress resulting from surface-mount soldering of the plastic-encapsulated device. A compilation of such stresses that can synergistically result in cratering is given in Table 8-4.*

*In general, most marginal cratering in this chapter can be revealed in plastic encapsulated devices by several hundred temperature cycles from –65 to 150°C (1% cumulative failures occurred at 200 cycles, and 7% at 1000). Seven times as many cycles are required for 0 to 125°C testing [8-19].

8.1.8 Cratering Over Polysilicon

A high susceptibility for bond cratering under Al pads located over polysilicon has been privately reported numerous times and published at least once [8-9]. The cause of this problem is not clear. Obviously, poor polysilicon adhesion to the underlayer, because of processing problems, is possible. Polysilicon also contains more stacking faults, dislocations, and other defects than single crystals, and it is possible that the ultrasonic energy will interact with them and weaken the structure similar to the manner in which it weakens metals [8-3].

There is an additional possible cause of the problem based on studies of Al metallization effects on polysilicon [8-20, 8-21]. When Al, 1% Si metallization is heated (e.g., sintered at 400°C and for up to 30 min) in contact with polysilicon, the metal can absorb Si from the grain boundaries and can result in relocation and weakening of the polysilicon. In extreme cases, this results in large isolated polysilicon grains that may have lower adhesion to the single-crystal substrate or to the bond pad. Many advanced devices today have a hard barrier layer of Ti or Ti/W, etc., under the Al conductors. If these films are extended under the Al bond pads, which also lowers cratering probability, then the above mechanism would not occur, and cratering would be diminished over polysilicon.

8.1.9 Gallium Arsenide Cratering

Gallium arsenide (along with some other low fracture-toughness compound semiconductors) has long been known to be more susceptible to bond cratering [8-6] and to mechanically induced electrically active defects [8-22] than Si. A number of its material characteristics have been studied [8-23 to 8-27]. Studies of the mechanical properties (where they are linear) indicate that GaAs has approximately a factor of two less strength than Si. The two major characteristics that are the most relevant to cratering, hardness, and fracture toughness of Si and GaAs, are compared in Table 8-5. Hardness is a measure of the resistance of a material to deformation. Fracture toughness is a measure of the stress or energy required to propagate a small existing crack. It is defined in App. 8A.

The properties in Table 8-5 were determined by a number of researchers who, in general, were not concerned with the bond-cratering problem, but rather in studying the general mechanical and fracture properties of the materials. GaAs is so much weaker than Si that it is likely to crater in situations that will not affect Si. It is easy to calculate that the static compressive force on a deformed ball bond [pad contact of 75 g diameter, applied during bonding by a 50 gf (490 mN) thermocompression bonding load] is approximately 1100 kg/cm^2. This is well over half of the compressive force required to create electrical defects in GaAs and is approaching its brittle fracture stress. Only a small variation in bonding parameters or the application of sufficient

Property	GaAs - I	Si - II (Same Refs and Units as I)
Hardness[a] (Vickers HV, 175-g load)	6.9 ± 0.6 GPa [8-26]	11.7 ± 1.5
Hardness[a] (Knoop HK, 100-g load)	590 [8-26]	1015
Young's modulus E	84.8 GPa [8-25]	131
Fracture toughness (energy) [indentation][b]	0.87 j/m^2 [8-22]	2.1
Fracture energy [DCB][c]	1.0 j/m^2 [8-24]	2.1
Compressive force for electrical defects	~ 2000 kg/cm^2 at 380°C [8-22]	—
Thermal conductivity (300 K)	0.48 W/cm/°C	1.57
Expansion coefficient	5.7×10^{-6} [8-25]	2.3

[a]Average approx. 20 impressions perpendicular and parallel to the cleavage axes. Taken on same equipment, same operator (John Smith, NIST, private communication).
[b]Obtained by indentation after initiation of crack (typical of cratering after probe mark or US damage). Data from various orientations on the <100> of GaAs and <111> surface on Si.
[c]Obtained by double cantilever beam method.

Table 8-5 GaAs Properties Compared to Silicon

ultrasonic energy can damage the material. Since both the mechanical and fracture properties are weak, craters could originate from either cause. Studies of the crater surfaces are needed to understand the actual cause of the problem. The GaAs strain-rate dependence of cratering may be different from Si and should be determined.

The "conventional wisdom" (on cratering) from GaAs chip manufacturers, bonder manufacturers, from private communications as well as one publication [8-28], is that thermocompression bonding is the safest to use (if the device/packaging can survive the high temperature). If thermosonic bonding is used, then use a stage heat ≤ 300°C and minimum ultrasonic energy. As with a number of GaAs cratering studies, there have been contradictory recommendations. One study of Au wedge bonding with a grooved tool found that cratering increased for stage temperatures, more than 120°C [8-29].

The use of a negative electronic-flame-off for ball formation in thermosonic-ball bonding is considered helpful to minimize cratering, and currently all ball bonders use it, although the reasons for this are not clear (there are many other reasons to use such, however). Ultrasonic-wedge bonding is the least desirable and has a very

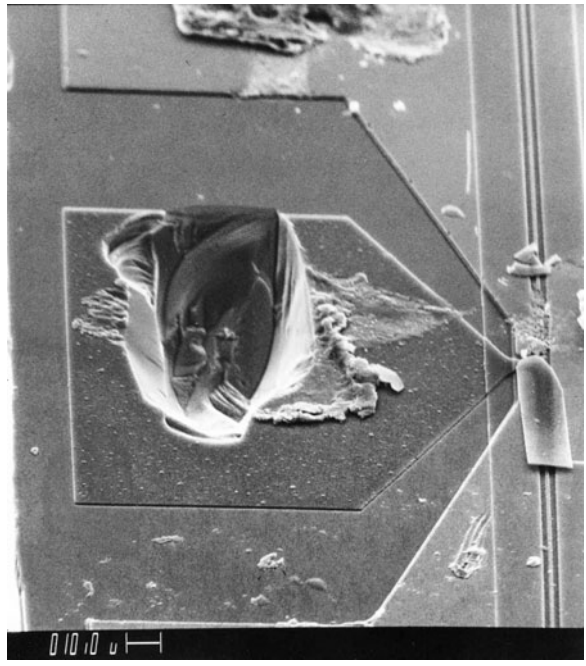

Figure 8-10 An example of GaAs cratering during an Ultrasonic Al wedge bond on a bond pad over a gate. (*Courtesy of Lysette [8-6]*; © *IMAPS*.)

minimal safe bonding window; however, both Au and Al wedge bonding are being successfully used by a number of organizations. In all cases, great care is indicated in bonder setup and monitoring. The ultrasonic energy has been monitored with a capacitor microphone [8-6]. It was found that a slow rise and decay time* for the overall ultrasonic system was helpful. Also, using a thicker metallization with a hard multilayer understructure was found necessary (e.g., either 0.1-μm Ti, 0.08-μm Cr, 0.2-μm Pt, and 0.8-μm of Au on top for bonding, or 0.3 μm of Ti/W under the pad) resulted in essentially crater-free device production. Figure 8-10 is an example of such an early cratering failure before the above improvements were made. (Note that for some multilayer metallization systems, such as Cu/Lo-k devices, special complex support structures are used, see Chap. 10.)

*Modern autobonders can slow application and removal of ultrasonic power and can be programmed after experimentally determining the optimum ramp shape. However, it has not been proven what the desirable ramp is, so it remains empirical. High-speed autobonders having ≤ 10 ms per bond leaves little time for a ramp-up/down, and such would slow the autobonder throughput appreciably.

Fast rise-time ultrasonic systems have long been blamed for cratering problems due to bonding tool "kick or jumping." However, measurements made by this author, with wide band-pass capacitor microphones, monitoring the tool-tip motion during bonding, have never observed such a kick. Therefore, the explanation for power-supply-induced cratering has not been supported by experiment.

Although GaAs is far more susceptible to cratering than Si, the same general procedures that are successful in minimizing cratering on Si are also applicable to GaAs. The use of minimum ultrasonic energy, minimum bonding tool bounce (much more important on GaAs than on Si), and a thick multilayer bond pad structure (thickness >1 μm) is usually successful in reducing the problem. Clean metal requires less ultrasonic energy for bonding; therefore, either UV-ozone or O_2 Ar plasma should be used within 2 h of bonding (see Chap. 7). Since GaAs has a thermal conductivity about one-third that of Si and an expansion coefficient about twice that of Si, it is important to avoid thermal shock. The use of a stage preheater for thermosonic bonding is desirable as well as the use of a heated capillary—not available for autobonders. Since the mechanical strength and the fracture energy of GaAs is so low, the possibility of electrical test probe damage creating an initial microcrack is much greater than for Si, and, once started, a crack can be readily propagated by ultrasonic energy during bonding.

If the GaAs device has Al metallization and the pad is bonded with Au wire (or the reverse), then the Clatterbaugh-Noolu effect (intermetallics, App. 5B) can apply enough calculated intermetallic stress (2000 kg/cm^2) in addition to the shear-force to cause dislocations that degrade the electrical properties under the pad [8-22] as well as predispose it to cratering. Such metal (Au-Al) combinations should be avoided by using monometallic bonding, or the lifetime-temperature environment of the device should stay low.

In addition to weak mechanical properties, GaAs is susceptible to crack propagation enhancement (a 20% lowered fracture toughness) by environmental influences like water, acetonitride, heptane, and presumably other common solvents [8-23, 8-24]. While this type of crack enhancement is most significant for sawed edges of chips, it could also affect probe marks or other subpad damage during cleaning steps within normal assembly-line processing. If a bond is placed over that area, it could have an increased probability of cratering. It is interesting to note that these solvents either have no effect on or actually increase the fracture toughness of Si.

8.1.10 Conclusions of Cratering

The general solutions to the cratering problem are summarized in Table 8-6. These are valid for Si, GaAs, or any semiconductor material. Following are some conclusions about cratering:

1. Set up bonder to minimize ultrasonic energy.
2. Use thicker metallization.
3. Use hard metal layers (e.g., Ti, W) under the bond pad.
4. Do not put pads over polysilicon.
5. Use thermocompression bonding *if possible*.
6. Clean chips (plasma, UV-ozone) to minimize bonding parameters.

TABLE 8-6 Normal Solutions to Cratering Problems (Which Apply to All Semiconductor Bonding)

- Cratering can result from a synergistic combination of stresses beginning with metal deposition and sintering at the wafer level.
- A wide understanding of metallurgy, silicon and multilayer fracture characteristics, bonding-machine variables, handling, processing, soldering thermal shocks, and long-term environments is necessary to eliminate cratering.
- All levels, from chip designers to processing and test engineers to assembly personnel (first and second level) must work together to eliminate the problem (packaging guidelines can be put in the design rules, as some companies have).

8.2 Cracks in the Heels of Ultrasonic Wedge Bonds

Metallurgical cracks in the heels of Al-ultrasonic wedge bonds have been a cause of concern to device users for many years [8-33]. Cracks can be caused, for example, by using a sharp heeled wedge bonding tool,* by operator motion of the micropositioner (if a manual bonder is used) or by bonding machine vibration just before or during bonding tool lift-up from the first bond. However, the most frequent cause is the rapid-tool movement after making the first bond. The tool (and wire) rise high and progress forward before moving backward to form the loop. This bends the wire upward from the heel of the bond and then backward, opening up a crack. The heel of the bond is already overworked (weakened) during ultrasonic welding, and one bend forward and backward is often sufficient to form a crack. [Note, that extra tool (and thus wire) motion is programmed in as part of special loop shaping in autobonders. See App. 9A on Looping by Lee Levine.] Such cracks are enhanced if the second bond is lower than the first, typical of reverse bonding, since the wire is

*A small curvature with a radius approximately 0.3 mil for a 1 mil (7.6 μm, 25 μm) diameter wire generally helps reduce heel cracking.

bent backward more than if bonds are on the same level. Some loop forming processes in autowedge bonders could also contribute to heel cracking, where the wire may be moved back and forth and/or bent in several directions. Note, however, that autoball bonders do not contribute to cracking. (See "Wire Bonder Looping" App. 9A by Lee Levine.)

Also, excessive bond deformation thins and further weakens the heel, which will then crack more easily during loop formation. High loops, desirable for thermal cycling reliability in open cavity devices, can lead to greater tool motion and an increased probability of heel cracking.

Device users often feel that heel cracks predispose bonds to early field failure, and this may be the case if the crack is severe and the device subject to temp cycles. However, many "cracks," when examined at high magnification in an SEM, turn out to be relatively benign tool marks or breaks in the top, amorphous-appearing, surface layer of an ultrasonic bond, as indicated in Fig. 8-11*a*. The metallurgical defects within this "crack" would be partially, if not entirely, annealed during any subsequent heat treatments, such as burn-in. However, the fine inner crack shown in Fig. 8-11*b* with its stress-raising inner "point" may propagate through the wire and cause failure during the device operating life. This crack would be unannealable from the standpoint of thermal-cycle flexure-fatigue life [8-34]. Whether these bonds are annealed or not, there is no reason why otherwise well-made bonds in hermetic packages should fail due to a crack, if the subsequent

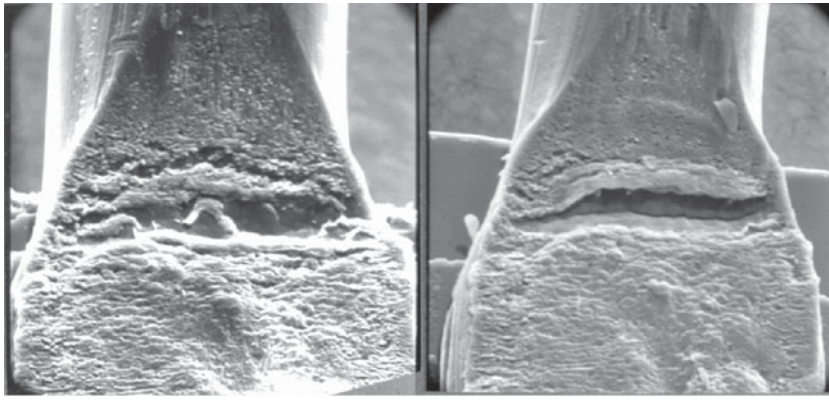

(a) (b)

Figure 8-11 SEM photographs of cracks in the heels of 50 μm (2 mil) diameter Al, 1% Si, ultrasonic wire bonds. The amorphous-appearing surface layer shown in (*a*) reveals no metallurgical cracks in the exposed crystalline Al. (*b*) *clearly* shows an unannealable *inner* crack. Both cracks resulted from the wire-bending forward and then backward during loop formation. (Also see Fig. 8-18 for examples of wedge bond fatigue heel cracks.)

operating field environment does not include stresses produced by temperature cycling or some other force (such as vibration due to ultrasonic cleaning) that may flex the wire loops and propagate the crack.

The main purpose of the above discussion is to examine heel cracks objectively. The discussion is not intended to imply a blank-check acceptance of heel cracks, since some can be so severe that they will significantly degrade the bond-pull strength. Any crack of the type shown in Fig. 8-11*b* can result in long-term reliability problems under thermal-cycle conditions. However, cracks in bonds having small deformation (~1.5 wire diameters) should not significantly reduce the bond pull strength or the device life under favorable bond loop and environmental conditions. The existence of such cracks does indicate that some part of the bonding equipment or procedure is not under proper control and corrective action is indicated.

An additional heel-crack problem was found in which the crack occurred under (rather than on top of) the first (wedge) bond heel [8-35, 8-36]. This is difficult to observe optically and is usually missed with a SEM unless the operator knows what to look for. Figure 8-12 is an example of such a crack. These were revealed by an occasional "freak" low-pull test result (1000 ppm defectives), but the numbers increased to 80% with hard, as-drawn, brittle wire. The entire auto-bonding sequence is involved, including vibration of the wire loop behind the bond. Examination of the (heel) fracture surface revealed a brittle fracture at the bottom (where the crack was) and a ductile fracture above it. In some cases, very weak bonds were observed with a crack on top as well as under the heel.

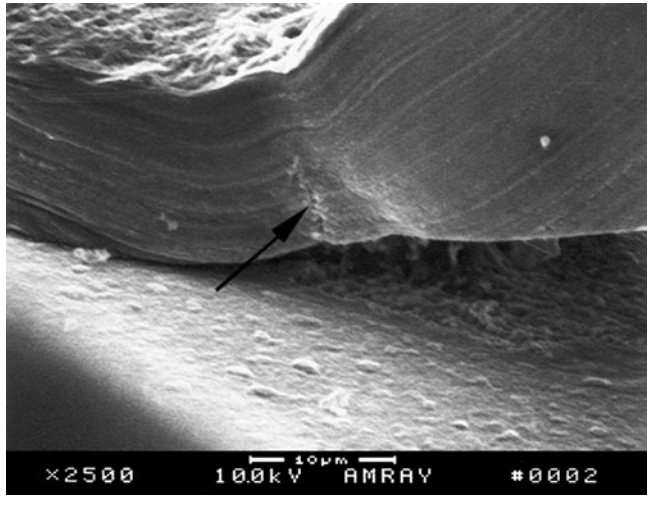

Figure 8-12 A crack under an Al-wedge bond heel, as indicated by the arrow. (*After Fitzsimmons [8-35, 8-36]*; © *IEEE*.)

8.3 The Effect of Acceleration, Vibrations, and Shock on Open-Cavity Packages

Once the bonding process is finished, the package sealed, and various mechanical, thermal, and electrical screens are completed, the variety of possible mechanical bond-failure modes is reduced considerably. Vibrational and centrifugal-type forces that occur in the field are seldom severe enough to cause metallurgical fatigue or other bond damage. In general, the package, its leads, or large components of assembled systems will fail before such forces are sufficient to damage the bonds. The minimum vibrational frequencies that might induce resonance, and thus damage Au- or Al-wire bonds having typical geometries, are approximately 10 and 40 kHz, respectively. The centrifugal forces, in the vertical direction, required to damage well-made 25 μm diameter bonds of Au- or Al-wire are typically greater than 100,000 g. However, Au bonds may be moved sideways (and short circuit with neighbors) or collapse to the substrate with as low as 8 kg of centrifuge forces [8-39] dependent on the length and loop height.

8.3.1 Centrifuge Test for Wire Bond Reliability on Wire Bonds

Centrifuge stress-testing of wire bonds cannot be used for parts that are plastic encapsulated, which includes approximately 95% of all devices. Only some high-reliability, military and space parts, sensors, and unusual devices may need it in 2008. It remains in this book for those special, important, open-cavity parts in such critical/unusual use.

There have been several calculations of centrifuge forces on wire bonds [8-37, 8-38] in open cavity (hermetic) packages. These computations were based on the wire assuming the shape of a catenary during the test, and the equations produced similar forces for similar shapes. The equations derived in [8-37] are given below. The parameters of the system are the same as those on the bond-pull test (see Chap. 4, Fig. 4-1), but the variables are defined below.

It may be shown that the tensile forces in the wire, and F_{wd}, at the contact points to the terminal and die, respectively, are in grams force:

$$F_{wt} = \rho\, \pi r^2 G(\alpha + h) \tag{8-1}$$

$$F_{wd} = \rho\, \pi r^2 G(\alpha + h + H) \tag{8-2}$$

$$\alpha \cong \frac{d^2}{4h(1+\sqrt{1+(H/h)}+2H} \qquad \text{for} \qquad d \geq 2(H+h) \tag{8-3}$$

where ρ = density of the wire (g/cm^3)
r = radius of the wire (cm)
h = vertical distance between the package pad and the peak of the wire loop (cm)

H = vertical distance between the package pad and die bond proofs (cm)
d = horizontal distance between bonds (cm)
G = centrifugal acceleration (in units of gravity).

Using the approximate value of α will only introduce an error of less than 10% in F_{wt} and F_{wd}, even for $d/(h + H)$ as small as 2, which is an unusual case. However, an exact value for α can be obtained from the relation:

$$h + H + \alpha = \alpha \cosh (D/2\alpha) \tag{8-4}$$

where $D/2$ is the lateral distance between the bond at the die and the apex of the wire loop. Actually, the greatest uncertainty may result from the estimate of h, which is the distance between the apex of the wire loop and the package pad surface after the centrifugal forces have deformed the loop to describe the catenary curve. A useful graphical representation of Eq. (8-1) using exact values for α is shown in Fig. 8-13. This gives the tensile force in the wire adjacent to the bonds of

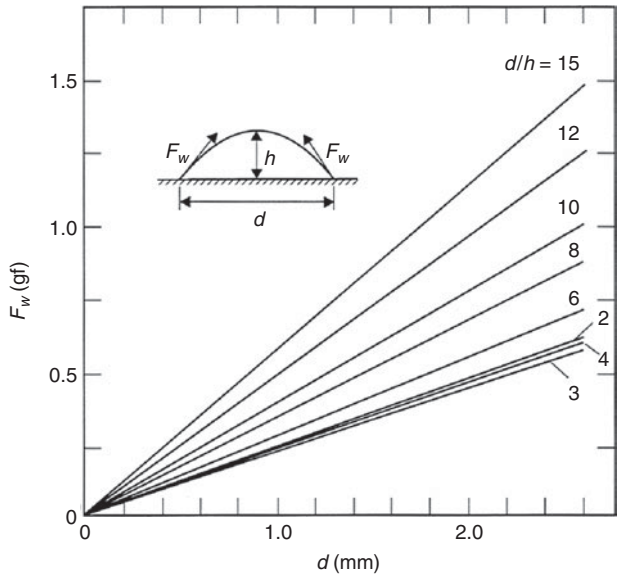

Figure 8-13 Tensile force, F_w, in the wire adjacent to the bonds in a single-level, 25 μm (1 mil) diameter, gold wire bond. This resulted from a centrifugal force of 30,000 g directed perpendicularly away from the bonding surface and is graphed as a function of d for different values of d/h. F_w for a given value of d is a minimum when $d/h \approx 3$. Values for accelerations other than 30,000 g may be obtained by multiplying the value for F_w by the ratio of the acceleration of interest to 30,000 g. Values for F_w for 25-μm (1 mil) diameter Al-wire bonds may be obtained by multiplying F_w, by 0.14. (They are so low that they are seldom significant). (*After Schafft [8-37].*)

a single-level (25 μm diameter) Au-wire bond, subjected to a centrifugal force of 30,000 g, as a function of d for different values of d/h. The figure shows, for example, that for a wire bond with a bond separation of 0.15 cm (≈60 mil) and a loop height of 0.015 cm (≈6.0 mil), the tensile force in the Au wire will be about 0.55 gf. Such a tensile stress could be produced in a pull test if the hook, placed at midspan, were pulled with a force of only 0.25 gf. In the case of an Au ball bond, one must take into account the significant mass of the ball [being made up from 0.03 to 0.050 cm (12 to 20 mil) length of the wire]. If the force on a ball of 3.5 mil diameter is added vectorially to the wire force in the above example, the total force is increased to 0.7 gf. In all cases above, if Al wire is used, the centrifuge forces will be reduced to 0.14 F_{Au} and rarely cause a problem.

Vertical forces generated in the centrifuge test described above are too small to be useful in testing wire bonds. To obtain an equivalent force to the MIL-STD-883G/H nondestructive pull-test requirement [2.0 gf (Al) and 2.4 gf (Au) for 25 μm dia. wire would require accelerating the device to over 100,000 g, an extreme and impractical value.]

Consider that a typical 25 μm diameter Au-ball shear force on a 90 μm (3.5 mil) bonded-ball diameter is in the order of 50 gf (tensile force can be 40% higher), and it is obvious that the centrifuge test is useless to assure quality on such wire bonds. However, this test can damage Au-wire bonds if the device package is accidentally placed in the centrifuge in the wrong orientation (sideways force application), such as may occur in a cannon-launched environment [8-39]. In this case it was found that 30 μm (1.3 mil) diameter Au (ball bond) wire loops can easily move sideways and short against adjacent wires or terminals, as well as collapse downward and short to the edge of the chip. Gold-wire-loop movement was observed to occur with as little acceleration as 5000 g, and shorts occurred in the 8000 to 10,000 g range for wires of approximately 2.5 mm (100 mil) length. Shortening the wire lengths to 1.9 mm (75 mil) resulted in no failures at 11,000 g acceleration in the sideways direction, and also none in the vertical direction at 20,000 g. Thus, considerable care must be exercised when open-cavity electronic packages containing Au wires are subject to centrifuge testing, and in all cases, short wires must be specified. Although not specifically related to wire bonds, a general mathematical analysis of the centrifuge testing of hybrid microelectronic devices is available and may be useful when considering that subject or modern SIP-MCM testing [8-40.]

8.3.2 The Effect of Ultrasonic Cleaning, Launch Vehicles Pyro-shocks, Vibrations, etc., on Open-Cavity-Package Wire Bonds

As with the centrifuge test for wire bonds, most packages today are plastic encapsulated and as a result are not subject to cleaning by ultrasonic or other vibration stresses. Therefore this section is included

for the few, but often important, cases when open-cavity packages are required. This is particularly the case for the less than 5% of devices in high-reliability and unsual devices, such as for space missions, well-logging, sensors, optoelectronic, and the like uses which could not normally be plastic encapsulated.

There have been several published reports and innumerable private communications on bond degradation resulting from the ultrasonic cleaning of hermetic (open cavity) devices [8-33, 8-41, 8-42]. Most reports concern Au-wire bonds. However, only one [8-43] showed such degradation of Al bonds, but without enough details to evaluate the failure. A wire bond, as with any other wire, has a resonance frequency, and if excited, it will vibrate and may fatigue and break. Note that pyro-shocks in space launches and other sources of vibration can cause similar damage. Figure 8-14 is an example of Au-wire bonds that have fatigued during ultrasonic cleaning. The resonant frequencies of wire bonds are generally high (~20 kHz, but vary with material, diameter, and length), and the only source of such excitations are from ultrasonic cleaners, shock tests, and similar stresses. The various vibration modes and the resonant frequencies of wire bonds have been calculated [8-37]. Several vibration modes are possible; however, the lowest resonant frequency, maximum motion, and damage results when the entire loop vibrates side-to-side (lateral mode). A plot of the calculated resonance frequencies for both Au- and Al-wire bonds in various lengths and loop heights is given in Fig. 8-15.

The potential danger of bond failure during ultrasonic cleaning occurs in open-cavity packages because of the many bond configurations (length, loop height, wire diameter, etc.). These may be encountered on a loaded PC board or even within a given package. A single multichip package can contain bonds made with Au and/or Al wire with diameters ranging from 0.018 to 0.038 mm (0.7 to 1.5 mil).

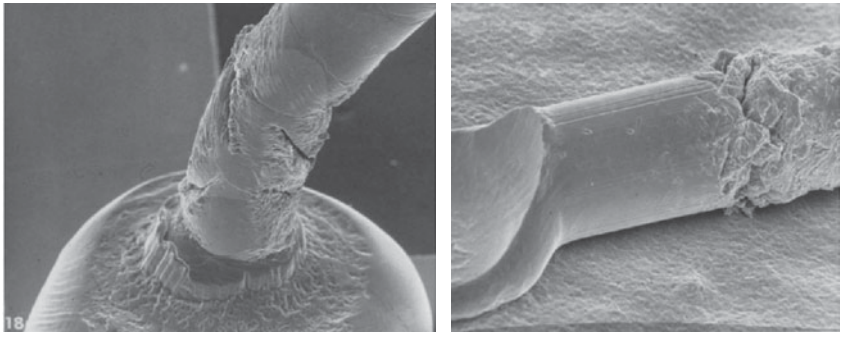

(a) (b)

Figure 8-14 SEM photographs showing 25 μm (1 mil) diameter ultrasonically fatigued bonds. (*a*) A gold-ball bond in a flatpack that had been immersed in an ultrasonic cleaner. (*b*) A wedge bond similarly fatigued. (*After Harman [8-33]*; © *IEEE*.)

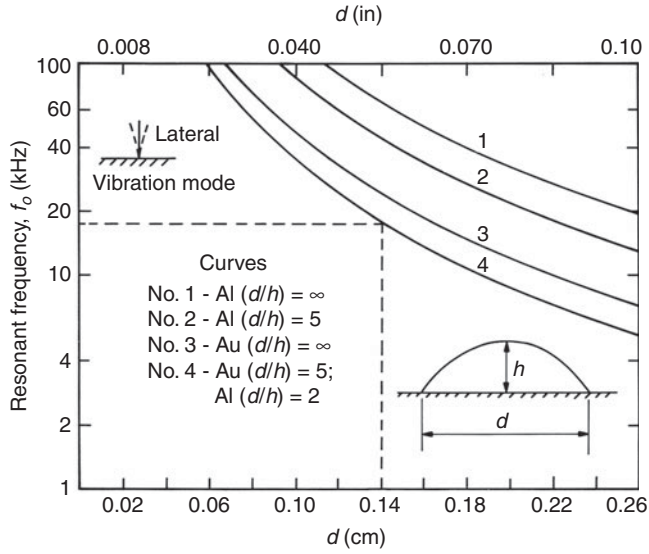

Figure 8-15 Dependence of the resonant frequency on bond separation, *d*, for the lateral mode of vibration for 25 μm (1 mil) diameter Au- and Al-wire bonds with circular-shaped wire spans having the ratios of *d/h* equal to 2 (semicircular), 5 (intermediate), and infinity (straight wire). The height of the span at its apex is *h*. (*After Schafft [8-37].*)

The bond-to-bond lengths, made with autobonders, can range up to approximately 6 mm, (most are <4 mm), and the loop heights may also vary.

A study of PC-board mounted hermetic (open cavity) devices, bonded with 25 μm diameter Al wire, was carried out to determine the extent of damage from US cleaning [8-44]. Wire lengths and loop heights were not given, but the resonant frequencies were calculated as being around 40 kHz. This implies that they were approximately 1 to 1.2 mm (40 to 50 mil), which is shorter than most wire bonds. The cleaning frequencies were 39 to 41, 43, and 66 kHz. No damage was observed, except for a few at high power densities and for long cleaning times (>1 h). Only rarely in the past have Al wires have been reported to fail during US cleaning, and then occurring in poorly defined circumstances [8-43]. Thus, the US cleaning of hermetic devices with *short*, 25 μm diameter Al wires should be generally safe. The problem is that Au wires do fail under US cleaning, and such devices are often mixed with devices having Al wires on any given PC board. Perhaps only in a specified high-reliability equipment situation can the user be assured that no problems will occur.

If many boards are simultaneously cleaned in a large tank, there is the possibility that US-wave resonances/reflections can cause energy maxima in specific areas. Thus, one would expect that only

specific bonds with specific dimensions would be damaged on a given device at a given US cleaning frequency, and the damage would be maximum in specific areas of the board.

The open-package ultrasonic cleaning of some complex packages and ICs that will undergo PIND testing for loose particles would be similar to hermetic-package cleaning. The resonant frequency of the bond will shift downward, only a few percent due to immersion in the cleaning solvent. However, the liquid would dampen the vibration amplitude depending on its viscosity, limiting any damage, but the effect of any cavitation could be severe. Informal tests run in various facilities have indicated that the pull strength of some bonds can be degraded or bonds actually broken by this procedure. The effects are very hard to characterize because of the variables involved.

In the past, most ultrasonic cleaners were designed with frequencies in the 20 kHz range, and most reported failures, as shown in Fig. 8-14, resulted from high-energy industrial cleaners in this frequency range. Currently, ultrasonic cleaner frequencies may be higher, in the range of 40 kHz, broadband (20 to 100 kHz), or in the hundreds of kilohertz range. Considering the resonant frequencies of bonds from Fig. 8-15 and that most wire bonds may be within the geometries of curves 2, 3, and 4, it is unlikely that the high-frequency cleaners (>50 kHz) will damage wire bonds, although definitive tests to verify this on Au-wire bonds have not been performed. One should be aware that open-package cleaning, at any frequency, is capable of damaging semiconductor devices if cavitation is present.

8.3.3 The Effect of Shock and Vibration Tests on Wire Bonds (Problems with Long Wires)

Because the lengths of most wire bonds are short, one seldom considers that normal system-level random vibrations (20 g from 10 Hz to 1 or 2 kHz) as used for screening spacecraft and other equipment would be harmful. However, there have been several failures of very long (25 μm diameter) Au-wire bonds made on stacked memory chips [8-45]. These bonds were between 3.8 and 5 mm (150 and 200 mil) long. They were subjected to random vibration (up to 2 kHz) and 20 g shock in different directions. Failures were observed in which overdeformed crescent bonds were broken loose when vibrated in the side-to-side direction. Extrapolation of Fig. 8-15 to these lengths shows that resonance is possible for such long bonds. This led to their breaking. The actual vibration frequencies were measured with a variation of a magnetic-field technique [8-46]. The resonances for such long wires were in the range as low as 1.4 kHz. In addition, shock in the sideways direction has broken weak crescent bonds, and in one case good bonds were observed to "wrap around one another."

We normally expect Au bonds with normal loops to resonate at frequencies greater than 10 kHz. However, multiple-layer stacked

chips and other unusual devices for space applications often require long nonplastic encapsulated wires. Also, very fine-pitch bond pads on chips can result in long wires fanning out to the coarser package pitch, and modern autobonders "work the loops" so that shorting does not occur. Just because there is adequate as-made clearance, it may not protect the bonds from resonating or shorting under vibration or shock, and failures are possible.

Thus, since modern autobonders can make long wires and these are being used more often than in the past (see App. 9A), both designers and users must understand the potential for low levels of vibration and shock to induce bond failures in special open-cavity packages.

8.4 Effects of Power and Temperature Cycling of Wire Bonds

Wire-bond failures in open-cavity packages due to cyclic temperature changes were first observed by Gaffney [8-47], many years ago, and since then there have been a number of additional studies of such failures [8-48 to 8-51]. These failures resulted from repeated wire flexing due to the differential coefficient of thermal expansion between the Al wire and the package as the device heated up and cooled down during power cycling, see Fig. 8-16. The maximum flexure, and therefore the failure, occurred at the thinned-wedge bond heels. The heel of the chip bond experiences the greater temperature excursion and is observed to fail more frequently than the heel of the package bond. The metallurgical flexure fatigue of a number of Al alloy wires was

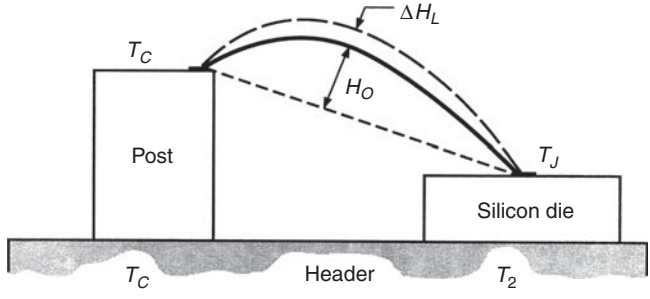

Figure 8-16 A schematic representation of wire-bond flexure due to device power cycling. The solid loop line represents the room-temperature position of the bond, and the dashed line represents the high-temperature position. The wire may be Al or Au, and the package (header) may be kovar, alumina, or other low-expansion substrate/package material. On a first approximation, the expansion of the wire is calculated as the average temperature of T_c, and T_j, and the header is that of T_c and T_2. The flexing, ΔH_L, is approximately inversely proportional to the ratio of the loop height to the bond-to-bond spacing.

experimentally investigated, and it was found that Al, 1% Mg wire was superior to the commonly used Al, 1% Si alloy [8-50], see Chap. 3, Sec. 3.8.

Wire-bond flexing during temperature cycling changes approximately inversely proportional to the loop height. The loop height should be approximately 25% of the bond-to-bond spacing to minimize the bond flexure of small-diameter wires [8-51]. Figure 8-17 shows these results calculated for the flexure of wire bonds with the configuration of Fig. 8-16. This flexure is approximately 20% greater if the loop is triangular (as it would be after a nondestructive wire-bond pull test), but the stress would concentrate at the bend, which should be stronger than at the bond heels. Subsequently, 25 μm (1 mil) diameter Al, 1% Si wire bonds made with high loops survived over 100,000 power cycles even though some bonds had cracked heels [8-51]. Taut (flat) loops resulted in failure after a few hundred to a few thousand power cycles. Villella [8-48] recommended the use of both the magnesium-doped wire and high bond loops to achieve maximum reliability. (However, small diameter Mg-doped wire is not available today except by special order and its ASTM standard has been dropped.) The use of a high loop as protection against flexure fatigue has also

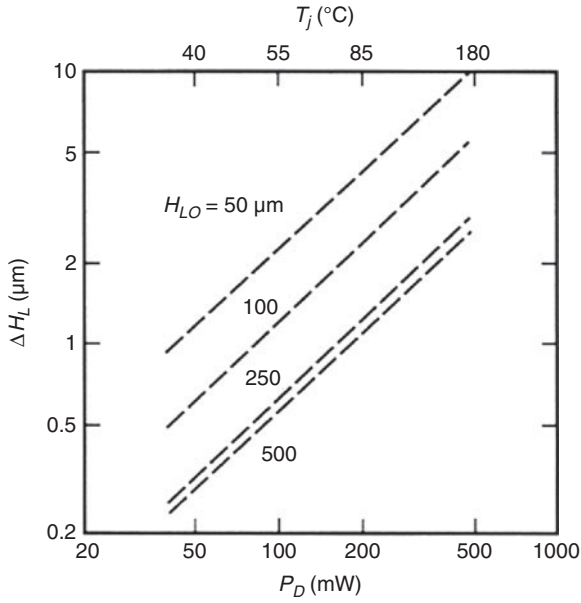

Figure 8-17 Wire-bond flexure, ΔH, as a function of power dissipation, P_D, for circular arc bond loops with various values of initial loop height, H_{LO}. (The analysis was made for 25 μm (1 mil) diameter post-to-die Al-wire bonds in a 500 mW, 50 mA Si transistor in a TO-18 package with package and pad of Au plated kovar. The junction temperature, T_j, is also indicated.)

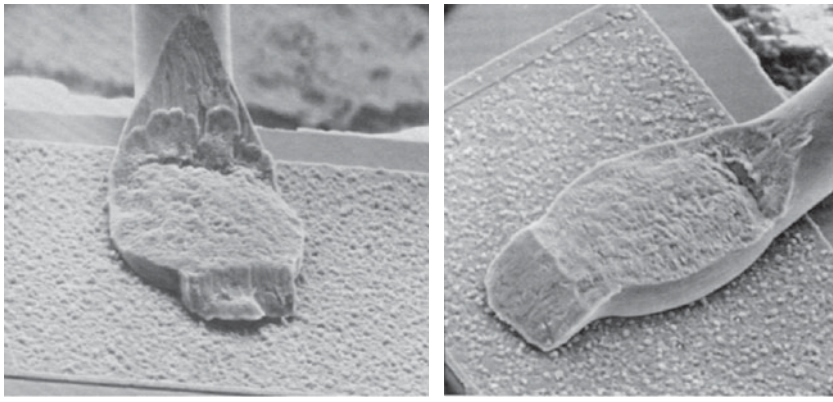

(a) (b)

Figure 8-18 SEM photographs of power cycled 50 μm (2 mil) diameter Al, 1% Si, ultrasonic wire-bonds with loop heights greater than 25% of the bond-to-bond spacing. This device had undergone 227,627 complete power cycles in which the junction temperature ranged from 38 to 170°C, and, yet, no bonds failed. Reconstruction of the Al bond-pad surface resulting from the repeated thermal stress is evident, however, the device still worked.

been verified with 50 μm (2 mil) diameter Al-wire bonds. Figure 8-18 shows typical bonds of a high-frequency power device containing 47 such bonds with high loops (height greater than 25% of the bond-to-bond distance). This device underwent 227,627 complete power cycles, without bond failure, in which the junction temperature ranged from 38 to 170°C. It was characteristic of the production of these bonds that many were made with cracks in their heels, but because of the high loops no failures were encountered.

Although high loops afford stress relief in power and temperature cycling situations, there are many cases where it is not possible or practical to use them. The most obvious case is when the top of the open-cavity package is too low and might contact the wire loop. Another case occurs when the package (chips) run at very high frequencies, and the high loop can increase the inductance of the bond. In such cases, a compromise must be made between performance and reliability. Often the inductance problem is solved by package design where the wires are kept very short and, thus, a lower loop will give adequate stress relief.

When ball bonds are temperature cycled, they typically break just above the ball in the "heat-affected zone." It has been found that if a "worked loop" (App. 9A, Looping) is used with a bend left in the loop away from this "zone," the stress is maximum there rather than above the ball, and the bond fatigue life is improved.

Gold-aluminum intermetallic compounds present an additional thermal cycle problem. They are stronger than the pure metals

providing they are void-free; however, they are also more brittle. If a bond contains intermetallics, it is far more susceptible to flexure damage than pure Au or Al wires alone. An example of a cracked Au wedge bond that had been cycled only 20 times was given in Fig. 5-10 in Chap. 5. In addition to brittleness, the growth of intermetallic compounds is enhanced by temperature cycles. Thus, it is important to be aware that Au-Al couples in devices may fail during repeated temperature excursions.

While failures in small-diameter wire bonds, in open-cavity packages, may be inhibited by high loops, such a solution is only partially helpful for large-diameter wires where the wire stiffness prevents easy flexing (and thus stress relief) of the overall loop. However, large-diameter wire bonds on some power devices may fail after 5000 to 20,000 power cycles due to metallurgical fatigue. See Fig. 8-19 for a typical example of one of these failures.

Note that fatigue occurs at each bend and near the bond heels, which are areas of stress buildup during temperature cycling. These are older bonds/technology. However, the metallurgy is identical to today's large wire (see Chap. 3, Fig. 3-4, lowest curve), and such fatigue would be similar.

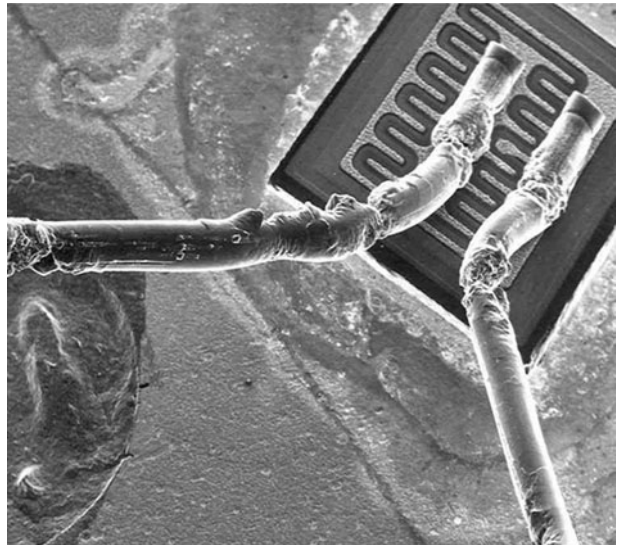

Figure 8-19 An SEM photograph of power-cycled 200 μm (8 mil) diameter 99.99% pure Al bonds on a 2N4863 power transistor. The wires fatigued and the device failed at 18,606 power cycles in which the case temperature ranged from 25 to 125°C (the junction temperature would have reached approximately 180°C). Metallurgical fatigue occurred on the bond heels and at bends in the loops. Although this is an old device (wire bonding technology), the same wire metallurgy is used in 2008, and the wire fatigue would look the same today.

Several possible solutions to the large wire fatigue problem may be applicable. The 200 μm (8 mil) diameter wires in this device were 99.99% pure Al. However, alloying additions invariably increase the fatigue strength of alpha solid solutions of Al [8-52]; thus, the better metallurgical system of magnesium-doped wire should lengthen power-device wire-bond life. The production of smooth loops with no bends should also help. Large cross-sectional area ribbon wire together with high loops may improve reliability. Ribbon is more flexible in the plane of the bond loop and may offer the advantages of small wire with high loops.

Temperature cycling (in which the entire device is externally heated and cooled) is more severe than power cycling described above, since the entire package reaches the temperature extremes. Even so, the loop height-to-bond-length recommendations (25%) are valid and will minimize the effect.

Plastic Encapsulation Failures

The above discussion of wire-bond flexure fatigue is applicable to bonds in open-cavity packages. A variety of different thermal cycle failures have been observed in plastic-encapsulated devices, often where failure occurs above the neck of the Au ball. This failure results from the different thermal coefficient of expansion between the wire, the Si, and the plastic and is not related to the loop height and wire flexing, but rather the stress applied from the expanding/contracting plastic encapsulation. The wire is rigidly held within the plastic. Extended fatigue, as in Fig. 8-19, may occur if compliant-die coatings are used under the plastic encapsulation [8-53]. For normal single-component encapsulation, the wires often partially "neck down" (ductile fracture) and break. At other times, striations (slip) are seen near the wire break. Ball bonds located around the perimeter of the plastic-encapsulated chips may be sheared due to forces exerted by the thermally expanding plastic [8-54] (also see Sec. 8.1.7, Cratering). In general, there is little that can be done at the wire-bonding production level to prevent such failures. Removing moisture from the plastic and minimizing thermal shock during surface mount soldering to boards are reasonably effective in limiting the plastic-expansion problem.

Silicone rubber has been used as a package cavity-fill to prevent moisture failures in some automotive and other devices. However, it may become stiff enough to break wire small bonds during temperature cycles. Silicone gel is currently used, and it is so soft that fine wire bonds remain intact during thermal cycles. This material has been used for years in automotive hybrids without temperature cycle failures. The only caveat is that such cycles must not go below the gel's glass transition temperature (generally about −55°C), or the stiffened gel will break the bonds. Such temperatures do not occur in the normal automotive environment.

Appendix 8A Fracture Toughness Defined Fracture Toughness is the Stress Required to Extend an Existing Crack

Unstable fracture occurs when the stress intensity at the crack tip, K or G, reaches a critical value, K or G_L. For small crack-tip plastic deformation (plane-strain conditions), the critical stress-intensity factor, K_{IC}, for fracture instability is a material property. The K_{ic} is the maximum stress-field intensity at the tip of a crack that the material can withstand without unstable crack extension occurring. Fracture toughness is a generic term for various measures of the resistance of a material to the extension of an *existing* crack. It is frequently represented as K_c, the stress intensity, or as G_c, the energy release rate for a crack extension [8-55]. The relationship between these variables is given below in the Griffith equation:

$$U = \frac{\pi a^2 \sigma^2}{E} \text{ (Griffith equation)} \tag{8A-1}$$

where U = decrease in elastic energy to propagate a crack due to an existing crack of length a (cm) and E = Young's modulus.

$$\text{Stress intensity} = K_c = \sigma_c \sqrt{\pi a} \frac{\text{g}}{\text{cm}^2} \sqrt{\text{cm}} \text{ (Fracture toughness)} \tag{8A-2}$$

$$\text{Energy release rate} = G_c = \pi \sigma_c \ a \text{ over}$$

$$E = \frac{K_c^2}{E} \frac{\text{g}}{\text{cm}^2} \times \text{cm (Fracture toughness)} \tag{8A-3}$$

where $\sigma = \text{Stress} \frac{\text{g}}{\text{cm}^2}$ and a = crack length (cm).

Appendix 8B Design of Experiments (DOE) for Wire Bonder Setup

Process Solutions Consulting. New Tripoli, PA 18066, email: levilr@ptd.net

By Lee Levine

Introduction

In 2008, more than 14 trillion semiconductor interconnections [8-56] will be produced and over 90% will be wire bonds. In high-volume IC production it is desirable for defect rates/wire to be in the less than 10 ppm range. Yields like this are not easily achieved. Statistical process control, design of experiments (DOEs), process capability studies, and machine and material characterization are all tools for

studying the process and making smart decisions for continuously improving that process.

Design of experiments (DOEs) is a topic within the field of statistics [8-57]. It provides an efficient, structured approach to the problem of controlling a process with a large number of variables, like wire bonding. By enabling one to efficiently explore the bonding process using many variables, DOEs allow the engineer to determine which of the variables have significant effects on the process. Once the significant effects are identified through screening experiments, additional experiments provide mapping of the response surface and lead to efficient process optimization.

In contrast, the traditional method for conducting scientific experiments has been to hold everything constant while changing only one variable at a time. Data variation could then be attributed to the shift in that variable. This method poses two problems: it is time consuming and it does not measure the interaction between two variables since they must be varied simultaneously to see the interaction. Often interaction effects are the strongest and most important factors in controlling a process.

The Math is in the Software, the Value You Add is Your Engineering Knowledge

There are many statistical analysis and DOE software packages available [8-58, 8-59]. All have strengths and weaknesses but in general most engineers need a package that provides both statistical analysis and DOE.

The engineering knowledge that you bring to the task is your value added. Your knowledge, judgment, and observation skills are critical. The DOE is the most efficient method for studying the many variables that affect a process but often the observations that you make while observing the experiment are the most valuable result.

What's a Statistic, Effect, and Interaction

A statistic is any quantity calculated from a data sample. Statistics are used to describe the properties of sample populations. Figure 8B-1 graphically defines the main effects of variables A and B on a process. From the graph it can be seen that there is no interaction between variables A and B. Each variable has the same effect on the process independently of the level of the other. Figure 8B-2 shows the effects of variables A and B when there is a strong interaction. Both the effects of A and B change depending on the level of the other; they interact. A major flaw in the classic one-variable-at-a-time method of experimentation is that it is not capable of detecting interactions, and sometimes the interaction effect is the most important experimental result. DOEs are designed to detect interactions between variables and test them to determine whether they are statistically significant. Detecting effects and interactions with statistical confidence in the conclusions that are drawn is a major benefit of the DOE method.

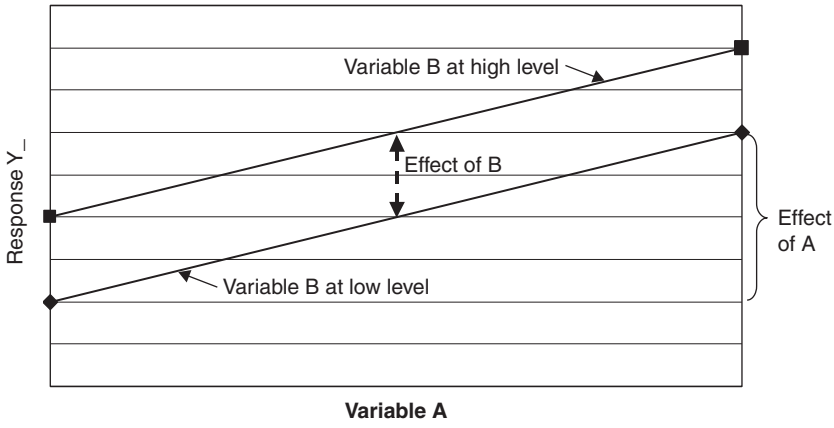

Figure 8B-1 What's an effect? (*No interaction: The effect of A or B is independent of whether the other is high or low.)*

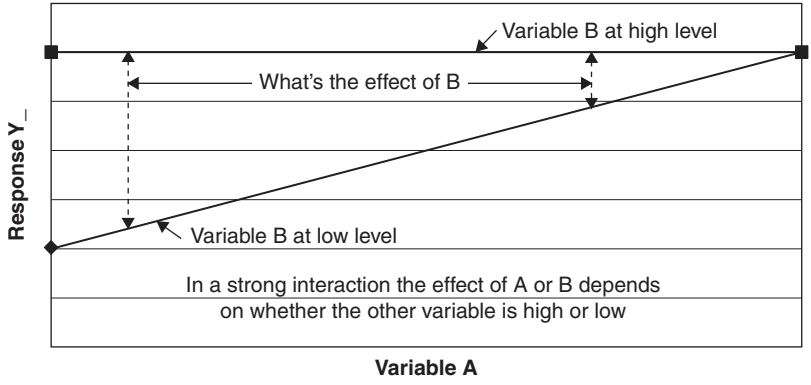

Figure 8B-2 What's an interaction? (*One of the benefits of DOE is statistical validation. Are the effects real or just random variations in the data?*)

What is a DOE?

A DOE is a structured, organized method for determining the relationship between factors (X) and responses (Y) and for testing the relationships to determine whether they are statistically valid. The specific experimental runs chosen are dictated by the experimental design so that valid statistical inferences can be drawn from the results. These runs are the DOE. The results, when shown graphically, are called a response surface.

Choosing Variables and Ranges

Several classes of variables can be used in a DOE. Some, such as programmable bonding parameters, can be changed easily over a

numerical range. Other variables, such as capillary designs and alloy materials, are not easily varied within a DOE. They are called categorical variables. Programmable variables are selected for screening experiments. Repeated DOEs varying categorical variables allows comparisons using a paired t-test.

There are four principal variables in the wire bonding process. In order of importance they are: ultrasonic energy, bonding temperature, bond force, and bond time. A fifth variable, impact velocity (impact force) often has a larger effect than bond time and is often substituted in screening experiments. Figure 8B-3 shows the major wire bonding independent variables. The results of the initial screening experiment will often identify major problems or defects. In subsequent DOEs, variables are chosen to address these problems. For example if weak crescent bonds are detected variables, a DOE using second bond ultrasonic power, bond force, impact velocity, and bond temperature can be chosen to address the problem. Discovery of cratering would change the focus to a DOE using first bond variables. Variables with insignificant effects can be eliminated allowing a more focused effort.

The setting of each variable in a screening experiment should cover a large range, but still be reasonable. Using a large range ensures that the slope of any trends will be correct. However, the intention of the DOE is not to test the extremes of the process, but to sample a reasonable range of the values of interest. If a variable is significant and the results show that extreme values are desirable, subsequent DOEs can explore this new range.

Figure 8B-4 shows a number of wire bonding response variables, but response variables can be anything that is measurable. Numerical measurements like pull test, shear test, number of defects within a sample, loop heights, bond placement, loop height at a fixed distance from second bond, and ball size are all measurements that have been used for wire bonding experiments. More difficult responses include attribute data (good/bad), metallographic cross-section photos, intermetallic growth studies, and thermal aging studies.

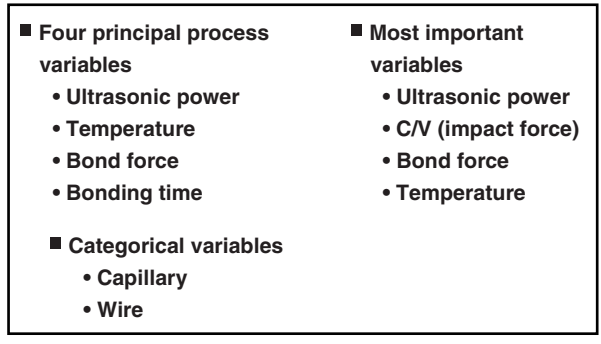

FIGURE 8B-3 Wire bonder independent variables.

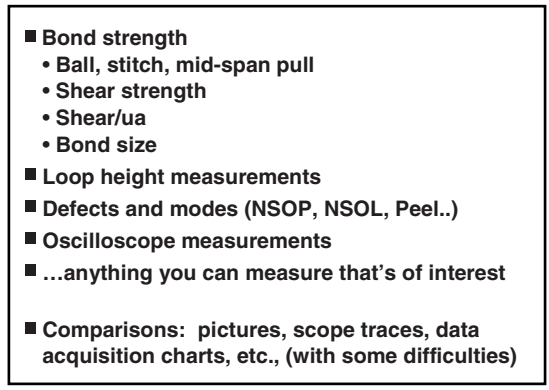

Figure 8B-4 Wire bonder response variables.

With care even these difficult response variables can be used in DOEs. Recent trends in finite element analysis (FEA) using input parameters to the FEA as independent variables and output from the FEA as the dependant variables in a DOE have enabled efficient use of FEA to build a response surface model for the FEA output.

Sequential Experimentation

Designed experiments are the best and most efficient method to control the experimental process while you are waiting for inspiration, but inspiration and knowledge doesn't come quickly. Sequential experimentation, choosing variables, observing and running the DOE, analyzing the data, and using Pareto charts to focus on the most significant problems will make the process evolve to achieve better product and higher yield. Sequential experimentation forces the data to drive continuous process improvements.

Process Capability

Process capability benchmarks (C_p and C_{pk}) are important qualifiers of a high-quality process. Process capability is defined as the natural variation of a process after all of the unnatural, explainable disturbances have been eliminated and the process is operating in a state of statistical control. The value of C_{pk} is a measure of process robustness. Increasing C_{pk} requires a continuous, iterative process using successive DOEs and response surface experiments to reduce the residual error. Process capability studies are a specialized class of DOEs designed to measure normal process variation. They have only one variable, time. They must include enough time to capture the normal drift of the process. The results of each successive experiment are incorporated into the choice of variables, building a database of process knowledge. Process changes, design changes, and materials

changes are all tested against the knowledge baseline, the goal being to reduce the residual error. As residual error decreases, the process is driven toward increased control and higher reliability. Improved yields are an automatic benefit.

Experiments to Improve Yield

Where a process is running, but at unacceptable yields, response surface techniques are useful for optimizing the process. The variation in process output, as adjustments are made, is called a response surface. Typical response surfaces are composed of data from measuring pull strength, shear strength, ball bond diameter, cratering, loop height, straightness, etc. In semiconductor assembly the term "bond window" has been used to describe a response surface. The importance of response surface graphics is that they give a good representation of the process and the interactions of several important variables, simultaneously.

Once the process is running with low defect rates, other techniques are more effective than DOEs. CuSums and the use of special control charts for high-yield processes [8-60, 8-61] will drive the process to higher yields more quickly than DOEs. They use existing process data to determine upper and lower control limits (UCL, LCL) for the process of record (POR) to determine whether the process is still in control. Defect events are tracked against the UCL and LCL. As process changes are made, they are charted against the UCL and LCL to determine whether a new POR has been achieved (operation above the UCL) or whether the change should be discarded (operation below the LCL).

Gage R&R

Every measurement system needs to be characterized to assure that it is repeatable and unbiased. As measurements approach the resolution of the measurement system, it is critical to make sure that the measurement system error is smaller than the measurements themselves. Otherwise poor engineering decisions will be made because the data will not be reliable. In fine-pitch wire bonding, ball and loop specifications measured with optical microscopes are often at the capability limits of the microscopes. A simple gage R&R study, multiple measurements on the same feature, and comparing the paired measurements using a paired t-test will often reveal systemic problems.

Conclusions

A combination of statistical methods and tools is required to control and optimize the wire bonding process. These tools include DOE, response surface methods, process capability, gage capability, and control charts for very high-yield processes. Through the use of these tools and with stringent controls on incoming materials and supplies, it is possible to achieve very high yields and produce high-quality products.

References

8-1 Kale, V. S., "Control of Semiconductor Failures Caused by Cratering of Bonding Pads," *Proc. of the 1979 International Microelectronics Syinp.,* Los Angeles, California, Nov. 13-15, 1979, pp. 311–318.

8-2 Ching, T. B. and Schroen, W. H., "Bond Pad Structure Reliability," *24th Annual Proc., Reliability Physics,* Monterey, California, 1988, pp. 64–70.

8-3 Harman, G. G. and Leedy, K. O., "An Experimental Model of the Microelectronic Ultrasonic Wire Bonding Mechanism," *10th Annual Proc., Reliability Physics,* Las Vegas, Nevada, 1972, pp. 49–56.

8-4 Winchell, V. H., "An Evaluation of Silicon Damage Resulting from Ultrasonic Wire Bonding," *14th Annual Proc., Reliability Physics*, Las Vegas, Nevada, 1976, pp. 98–107, also see Winchell, V. H. and Berg, H. M., "Enhancing Ultrasonic Bond Development," *IEEE Trans. on Components, Hybrids, and Manufacturing Technology*, Vol. 1, 1978, pp. 211–219.

8-5 Koyama, H., Shiozaki, H., Okumura, I., Mizugashira, S., Higuchi, H., and Ajiki, T., "A New Bond Failure Wire Crater in Surface Mount Device," *26th Annual Proc., Reliability Physics,* Monterey, California, 1988, pp. 59–63.

8-6 Lycette, W. H., Knight, E. R., and Hinch, S. W., "Thermosonic and Ultrasonic Wire Bonding to GaAs FETs," *Intl. J. Hybrid Microelectronics*, Vol. 5, Nov. 1982, pp. 512–517.

8-7 Heinen, G., Stierman, R. J., Edwards, D., and Nye, L., "Wire Bonds over Active Circuits," *44th Electronic Components and Technology Conf.,* Washington, D.C., May 1-4, 1994, pp. 922–928.

8-8 Mori, S., Yoshida, H., and Uchiyama, N., "The Development of New Copper Ball Bonding Wire," *Proc. 38th Electronic Components Conf,* Los Angeles., California, May 9-11, 1988, pp. 539–545.

8-9 Chen, Y. S. and Fatemi, H., "Au Wire Bonding Evaluation by Fractional Factorial Designed Experiment," *The International Journal for Hybrid Microelectronics.,* Vol. 10, no. 3, 1987, pp. 1–7.

8-10 McKenna, R. G. and Mahle, R. L., "High Impact Bonding to Improve Reliability of VLSI Die in Plastic Packages," *39th Proc. IEEE Electronics Components Conf.*, Houston, Texas, May 21-24, 1989, pp. 424–427.

8-11 Hirota, J., Machida, K., Okuda T., Shimotomai M., and Kawanaka, R., "The Development of Copper Wire Bonding for Plastic Molded Semiconductor Packages," *Proc. 35th Electronic Components Conference*, Washington, D.C., May 20-25, 1985, pp. 116–121.

8-12 Ravi, K. V. and White, R., "Reliability Improvement in 1-mil Aluminum Wire Bonds for Semiconductors." Final Report (Motorola SPD), NASA Contract NAS8-26636, Dec. 6, 1971.

8-13 Srikanth, N., "Critical Study of Microforging Au Ball on Al Coated Silicon Substrate Using Finite Element Method," *Materials Science and Technology,* Vol. 23, no. 10, 2007, pp. 1199–1207.

8-14 Srikanth, N., Murali, S., Wong, Y. M., Vath III, C. J., "Critical Study of Thermosonic Copper Ball Bonding," *Thin Solid Films*, 462-463, 2004, 339-345 is in Table 8-3.

8-15 Clatterbaugh, G. V., Weiner, J. A., and Charles, H. K. Jr., "Gold-Aluminum Intermetallics: Ball Bond Shear Testing and Thin Film Reaction Couples," *IEEE Trans. on Components, Hybrids, and Manufacturing Technology*, Vol. CHMT-7, 1984, pp. 349–356. Also see earlier publications by Charles and Clatterbaugh, *International Journal for Hybrid Microelectronics*, Vol. 6, 1983, pp. 171–186. Also, more recently, Clatterbaugh, G. V. and Charles, H. K., "The Effect of High Temperature Intermetallic Growth on Ball Shear Induced Cratering," *IEEE Trans on CHMT*, Vol. 13, no. 1, March 1990, pp. 167–175.

8-16 Takei, W. J. and Francombe, M. H., "Measurement of Diffusion-Induced Strains At Metal Bond Interfaces," in *Solid State Electronics*, Pergamon Press, 1968, Vol. 11, pp. 205–208.

8-17 Koch, T., Richling, W., Whitlock, J., and Hall, D., "A Bond Failure Mechanism," *Proc. 24th Annual Proc., Reliability Physics,* Anaheim, California, 1986, pp. 55–60.

8-18 Footner, P. K., et al., "A Study of Gold Ball Bond Intermetallic Formation in PEDs Using Infra-Red Microscopy," *Proc. IEEE IRPS*, 1986, pp. 102–108.
8-19 Dunn, C. F. and McPherson, J. W., "Temperature-Cycling Acceleration Factors for Aluminum Metallization Failure in VLSI Applications," *Proc. IEEE IRPS*, 1990, pp. 252–255.
8-20 Pramanik, D. and Saxena, A. N., "VLSI Metallization and Its Alloys, Part 1," *Solid State Technology*, Jan. 1983, pp. 127–133. See also Pramanik, D. and Saxena, A. N., "VLSI Metallization and Its Alloys, Part II," *Solid State Technology*, March 1983, pp. 131–138.
8-21 Umemura, E., Onoda, H., and Madokoro, S., "High Reliable Al-Si Alloy/Si Contacts by Rapid Thermal Sintering," *26th Annual Proc., Reliability Physics,* Monterey, California, 1988, pp. 230–233.
8-22 Hasegawa, F. and Ito, H., "Degradation of a Gunn Diode by Dislocations Induced during Thermocompression Bonding," *Appl. Phys. Letters,* Vol. 21, No. 3, Aug. 1, 1972, pp. 107–108.
8-23 Forman, R. A., Hill, J. R., Bell, M. I., White, G. S., Freiman, S. W., and Ford, W., "Strain Patterns in Gallium Arsenide Wafers: Origins and Effects, Defect Recognition and Image Processing" in E. R. Weber (ed.), *III-V Compounds II*, Elsevier Science Publishers B. V., Amsterdam, 1987, pp. 63–71.
8-24 White, G. S., Freiman, S. W, Fuller, E. R. Jr., and Baker, T. L., "Effects of Crystal Bonding on Brittle Fracture," *J. Matls. Sci.,* Vol. 3, 1988, pp. 491–497.
8-25 Vidano, R. P., Paananen, D. W., Miers, T. H., Krause, J., Agricola, K. R., and Hauser, R. L., "Mechanical Stress Reliability Factors for Packaging GaAs MMIC and LSIC Components," *IEEE Trans. on Components, Hybrids, and Manufacturing Technology,* Vol. 12, 1987, pp. 612–617.
8-26 Smith, J., NIST, private communication.
8-27 Nishiguchi, M., Goto, N., and Nishizawa, H., "Mechanical Reliability Effects of Back-Grinding upon GaAs LSI Chips," *Proc. of the 43rd Electronic Components and Technology Conf.,* Orlando, Florida, June 1-4, 1993, pp. 1072–1080.
8-28 Riches, S. T. and White, G. L., "Wire Bonding to GaAs Electronic Devices," *Proc. of the 6th European Microelectronics Conf.* (*ISHM*), Bournemouth, U.K., June 3-5, 1987, pp. 143–151.
8-29 Weiss, S., Zakel, E., and Reichl, H., "A Reliable Thermosonic Wire Bond of GaAs-Devices Analyzed by Infrared-Microscopy," *Proc. 44th Electronic Components and Technology Conf.,* Washington, D.C., May 1-4, 1994, pp. 929–937.
8-30 Olsen, D., Wright, R., and Berg, H., "Effects of Intermetallics on the Reliability of Tin Coated Cu, Ag, and Ni Parts," *13th Annual Proc., Reliability Physics,* Las Vegas, Nevada, 1975, pp. 80–86.
8-31 Kashiwabara, M. and Hattori, S., "Formation of Al-Au Intermetallic Compounds and Resistance Increase for Ultrasonic Al Wire Bonding," *Review of the Electrical Communication Laboratory,* Vol. 17, 1969, pp. 1001–1013.
8-32 Douglas, and Davies, G., "The Influence of Electronic Flame-Off-Polarity on the Structure of Gold Wire Balls" and "An Investigation into the Microstructure and Micro Hardness of Various Ball-Formed Copper Wires," A*merican Fine Wire Corp.* Reports, 1988.
8-33 Harman, G. G., "Metallurgical Failure Modes of Wire Bonds," *12th Annual Proc., Reliability Physics Symp.*, Las Vegas, Nevada, April 2-4, 1974, pp. 131–141.
8-34 Plumbridge, W. J. and Ryder, D. A., "The Metallography of Fatigue," *Metallurgical Reviews*, Vol. 14-15, 1970, pp. 129–145. See also Alden, T. H. and Backoffen, W. A., "The Formation of Fatigue Cracks in Aluminum Single Crystals," Acta Metallurgica, Vol. 9, 1961, pp. 352–366.
8-35 Fitzsimmons, R. T., "Brittle Cracks Induced in AlSi Wire by the Ultrasonic Bonding Tool," *IEEE Trans. on CHMT*, Vol. 14, Dec. 1991, pp. 838–847.
8-36 Fitzsimmons, R. T. and Chia, H., "Propagation Mechanism and Metallurgical Characterization of First Bond Brittle Heel Cracks in Al Si Wire," *42nd Electronics Components and Technology Conf.*, May 1992, pp. 162–166.
8-37 Schafft, H. A., "Testing and Fabrication of Wire-Bond Electrical Connections, A Comprehensive Survey," *Nat. Bur. Stands*. (U.S.), Tech. Note 726, 1972.

8-38 Lidbove, C., Perkins, R. W., and Kokini, K., "Microcircuit Package Stress Analysis," *Final Technical Report RADC-TR-81-382*, Rome Air Development Center, 1982, pp. 1–351.
8-39 Poonawala, M., "Evaluation of Gold Wire Bonds in a Cannon-Launched Environment," *33rd Proc. IEEE Electronics Components Conf.*, Orlando, Florida, May 16-18, 1983, pp. 189–192.
8-40 Hartouni, E., "Mathematical Analysis of Centrifuge Testing on a Large-Scale Hybrid Microelectronic Assembly," *The Intl. J. Hybrid Micro.*, Vol. 5, Feb. 1982, pp. 30–33.
8-41 Ramsey, T. H., "Metallurgical Behavior of Gold Wire in Thermal Compression Bonding," *Solid State Technology*, Vol. 16, Oct. 1973, pp. 43–47.
8-42 Riddle, J., "High Cycle Fatigue (Ultrasonic) not Corrosion in Fine Microelectronic Bonding Wire," *Proc. ASM, Third Conf. on Electronics Packaging, Materials and Processes and Corrosion in Microelectronics*, Minneapolis, Minnesota, April 28-30, 1987, pp. 185–191.
8-43 *Microcircuit Manufacturing Control Handbook*, Integrated Circuit Engineering Corporation, Scottsdale, Arizona, 1977, pp. P5–J5, 5A.
8-44 Crawford, T. and Vuono, B., "Ultrasonic Cleaning of Military PWAs," *Proc. NEPCON West*, 1991, pp. 1541–1551.
8-45 Leidecker, H., NASA, Goddard, private communication.
8-46 Tustaniwskyj, J. I., Usell, R. J., and Smiley, S. A., "Progress Towards a Cost Effective 100% Wire Bond Quality Screen," *Proc. 37th IEEE Electronics Components Conf.*, 1987, pp. 557–565. See also US patent 4,677,370, June 30, 1987.
8-47 Gaffney, J., "Internal Lead Fatigue through Thermal Expansion in Semiconductor Devices," *IEEE Trans. Electron Devices*, Vol. 15, 1968, p. 617.
8-48 Villella, F. and Nowakowski, M. F., "Investigation of Fatigue Problem in 1-mil Diameter Thermocompression and Ultrasonic Bonding of Aluminum Wire," *NASA Technical Memorandum, NASA TM-X-64566*, 1970. Also see Nowakowski, M. F. and Villella, F., "Thermal Excursion Can Cause Bond Problems," *9th Annual Proc. IEEE Reliability Physics Symp.*, Las Vegas, Nevada, 1971, pp. 172–177.
8-49 For a summary and recommendations from [8-47], see Villella, F. and Martin, R., "Does Your Bonding Process Doom Devices to Failure?" *Circuits Manufacturing*, Jan. 1973, pp. 22–30.
8-50 Ravi, K. V. and Philofsky, E. M., "Reliability Improvement of Wire Bonds Subjected to Fatigue Stresses," *10th Annual Proc. IEEE Reliability Physics Symp.*, Las Vegas, Nevada, 1972, pp. 143–149.
8-51 Phillips, W. E., in G. G. Harman (ed.), *Microelectronic Ultrasonic Bonding, Nat. Bur. Stands.* (U.S.), Spec. Publ. 400-2, 1974, pp. 80–86.
8-52 Riches, J. W., Sherby, O. D., and Dorn, J. E., "The Fatigue Properties of Some Binary Alpha Solid Solutions of Aluminum," *Trans. ASM*, Vol. 44, 1952, pp. 882–895.
8-53 Kinsman, K. R., Natarajan, B., and Gealer, C.A., "Coatings for Strain Compliance in Plastic Packages: Opportunities and Realities," *Thin Solid Films*, Vol. 166, 1988, pp. 83–96.
8-54 Shirley, C. G. and Blish, R. C., "Thin-Film Cracking and Wire Ball Shear in Plastic DIPS due to Temperature Cycle and Thermal Shock," *25th Annual Proc., Reliability Physics Symp.*, San Diego, California, April 7-9, 1987, pp. 238–249.
8-55 Barsom, J. M. and Rolfe, S. T., *Fracture and Fatigue Control in Structures*, 2d ed., Prentice-Hall, Englewood Cliffs, New Jersey, 1987.
8-56 VLSI Research Inc., 2005.
8-57 G.E.P. Box, W.G. Hunter, J.S. Hunter, *Statistics for Experimenters*, Wiley, New York, 1978.
8-58 Minitab Statistical Software, www.minitab.com
8-59 JMP® Statistical Discovery Software, www.jmp.com
8-60 Bissell, A. F., "Control Charts and Customs for High Precision Processes," Total *Quality Management and Business Excellence*, Vol 1, no. 2, 1990, pp. 221–228.
8-61 Goh, T. N., "A Control Chart for Very High Yield Processes," *Quality Assurance*, Vol. 13, no. 1, March 1987, p. 18.

CHAPTER 9

Advanced and Specialized Wire Bonding Technologies

(Including High Yield, Fine Pitch, PCBs, Soft Substrates, Extreme Temperature Wire Bonding and Specialized Looping)

9.1 The Technology and Problems of High Yield and Ever-Finer Pitch Wire Bonding, and Specialized Looping

9.1.1 Introduction to High Yield in Modern Wire Bonding

Forty years ago, wire bonding yield was considered acceptable if it was around 98%, a figure that could not be tolerated today. At that time, most ICs had only 8 or 10 I/Os, the bonders were manual, and rework for missed bonds took place before the package was removed from the bonder. Today (2008), we have thousands of I/Os per chip, high-speed autobonders (operating 12 wires/second or

greater),* and worldwide competitive pressures. Thus, the current manufacturing thrust assumes high yield for cost-driven as well as performance-driven devices. In assembly and packaging, this usually refers to achieving high yields in each specific operation (e.g., sawing, die attach, wire bonding, plastic encapsulation, surface mounting). Of all chip-assembly steps, wire bonding (and other interconnection methods) can have the greatest assembly impact on device yield because of the large numbers of I/Os on each chip with two bonds per wire. In addition, if the interconnection failure damages the chip (as in cratering), it often results in loss of the package or requires difficult rework, which is prohibitive in current production rates and economics. Thus, to improve device packaging yield, efforts should logically be concentrated on improving interconnection yield.

Bonds can be made with some autobonders at 30 μm pitch, but currently such chips are not available. As the pitch decreases, so does the wire diameter, and 15 μm Au wire is available with finer diameters expected, as demand requires. Thus, fine pitch wire bonding has arrived. Almost every aspect of fine-pitch bonding requires more planning and is more expensive to achieve than bonding at earlier accepted pitches. (We note that many chips are still being made at ≥100 μm pad pitch and will continue for many years.)

Currently (2008), the world semiconductor industry is making about 12 to 14 trillion wire interconnections per year (two bonds and wire loop). The infrastructure to achieve this is so large that no new interconnection method can replace them in the foreseeable future. Thus, we will continue to use wire-bond interconnections for a majority of chips. Flip-chip (C-4) and as yet unknown technologies such as photonic interconnections will be used for the most advanced device production and increase their market share. Today, wire-bonding yield losses in volume production typically range from about 100 to 25 ppm, with some less than 20 ppm. In order to achieve the lower numbers, one must understand all of the conditions that affect both bond yield and reliability (because they are interrelated).

In order to discuss the details of high-yield and fine-pitch bonding, we must assume that the reader understands the normal elements of bonding technology as described elsewhere in this book. These include: bond pad and wire metallurgy (Chap. 3), testing (Chap. 4), but special fine pitch changes are discussed below, intermetallic compound formation (Chap. 5), plating (Chap. 6, Secs. A and B), cleaning

*Defining the bonding speed (number of wires/s) of a high-speed autobonder is complex. The simple straight out, minimum-loop bonding-speed can be much higher than realistic production speeds; even bonding around a chip is slower than a simple straight-out run. Long wires take longer. Complex looping will slow the process considerably—see App. 9A. The cassette loading of chips into bonding position slows the average speed. Thus, a bonder manufacturer could honestly state a very high speed that in real-world usage might never be achieved.

(Chap. 7), and mechanical issues (Chap. 8) such as cratering. In addition, the bonder must be set up by valid statistical design methods [See App. 8B (DOE), by Lee Levine.] Without such understanding and control of the bonding process, it is not possible to even approach high yields and fine-pitch wire bonding. Also, to achieve these ends, everything must be done correctly, and the solution to every solved production problem must be understood! A quick fix (change something and it works), without understanding why it failed, usually results in the problem recurring at a later time.

9.1.2 The Requirements for High-Yield Bonding (Metallization Surface, Hardness, Cleanliness)

The requirements for high-yield bonding are summarized in outline form in Table 9-1. Each of these was discussed in detail in earlier chapters and is summarized below. Also, some of these concepts were described earlier in [9-1].

Bond-Pad Metallization, Aluminum

The first requirement for high-yield bonding is that the metallization on both the chip and the package be bondable. Unfortunately, the characteristics of the chip metallization may be determined by other

1. Good bondable metallization on chip and package
   - Uniform, reproducible characteristics
   - Soft—approximately same hardness as wire
   - Most additives decrease yield (Cu, Ti, etc.)
   - Thickness: 1 to 1.2 μm, pure Al pad caps (0.3 μm thick) can be added at Fab level for bondability and cratering protection
   - Free of organic and inorganic contamination (plasma clean as final Fab process)
2. Uniform wire
   - Close dimensional tolerances (<1.25 μm diameter variation for 25-μm gold ball bonding)
   - Consistent metallurgy (elongation, breaking load)
3. Controllable, consistent bonding machine (force, US energy, etc.)
   - Accurate placement on bonding pad
   - Reproducible, fast, ball formation
4. Package designed around the characteristics and limitations of the specific autobonder
5. Bonding machine package clamping designed for the specific package
6. Accurate and flat (horizontal) die-attach

TABLE 9-1 High Yield and Fine Pitch Bonding Requirements

considerations. For example, adequate electromigration performance often requires that additives be incorporated in or under the Al metallization. Titanium nitride or Ti-W layers are sometimes sandwiched within or under the pad and occasionally (process dependent) the Ti may diffuse to the surface [9-2] and oxidize, lowering bondability. Copper is often added to the Al variously from about 0.5 to 2% by weight. Generally, if the amount of Cu exceeds –2%, the bondability decreases. In most cases, 1% Cu is adequate for electromigration purposes, this low percentage may result in the growth of theta phase (Al_2Cu) hillocks/aggregates during various wafer heat treatments [9-3]. This level of copper doping increases the metallization's susceptibility to corrosion [9-1, 9-4] and may result in copper oxide on the surface, which requires the bonding engineers to deal with the resulting poorly bondable metal. The metallurgical part of this problem was discussed in Chap. 5, Sec. 5.3.2. A solution to this can be to apply approximately 3000 Å of pure Al on top of the Cu doped metallization as shown in Fig. 9-1. This does add another step to fabrication but increases the bonding yield, which should pay for that process. (Also, there are other ways to avoid Cu, TiN, or other additives, and some devices use special underlayers, sandwiches of metals, etc., which can leave pure Al on top in the process.)

The effect of bond pad hardness on bondability is shown in Fig. 9-2 [9-5, 9-6]. (Note: these experiments are difficult to perform and should be repeated with modern equipment.) In general, for the highest bondability between Au and Al, the hardness of both the wire

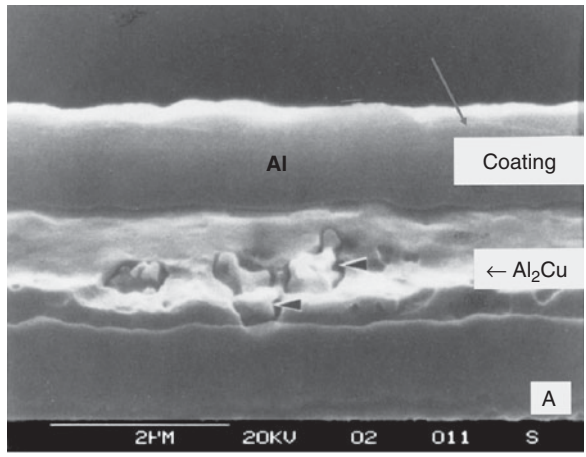

Figure 9-1 A bond pad containing 1.5% Cu with Al-Cu intermetallic compounds which decreases bondability. A 3000 Å cap of pure Al was deposited over the layer of Al-Cu which will increase the bondability [9-1]. (Composite figure showing an Al-1.5% Cu-bond pad metallization including Al-Cu intermetallics, with a cap which can be pure Al or Al-1%Si *[9-1]*; © *IEEE*.)

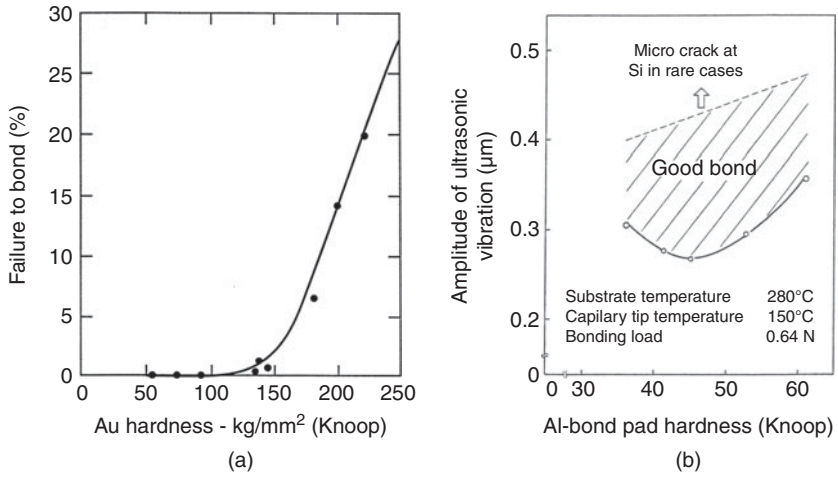

Figure 9-2 (*a*) The effect of a gold film hardness versus gold bond lifts (bondability) [9-5]. (*b*) Ultrasonic energy to bond versus hardness of aluminum bond pad, for Cu ball bonding [9-6]. In (*a*), a minima should be reached below the ball hardness (~40 HK). For Cu balls (hardness ~55 HK), it occurs on (hardened) Al pads near 45 HK (© *IEEE*).

and the bond pad should be approximately matched [9-6, 9-7]. Titanium has also been alloyed into Al in concentrations of about 0.2% for electromigration protection. No increased corrosion has been reported for this additive; however, some Ti may diffuse to the surface of the pad, lowering bond yields. Also, it will increase the hardness to over 100 HK (Knoop hardness), requiring an increase of the thermosonic energy or bonding temperature to ~320°C in order to achieve a high yield. This, in turn, requires a high-temperature die-attach epoxy which, if not already in use, necessitates expensive qualification tests. In general, any dopant (except silicon) added to pure Al will reduce its bondability to some degree.

A solution to many bondability problems that could eliminate bond yield loss from Fab-metallurgical bond-pad conditions has been known for some time. This requires capping (or coating) the Cu-doped bond-pad metallization with –0.3 μm of pure aluminum as indicated in Fig. 9-2. Fortunately, today, many IC Fabs have design rules that are intended to produce high-bondability chip pads. Some of this has been a result of Cu/Lo-k chips that were originally impossible to bond at high yield. (See above and in Chap. 10.)

Metallization Cleanliness

Regardless of the specific metal(s) making up the pad, its surface must be clean in the assembly area if high-bond yields are expected. There have been numerous studies on cleaning methods and procedures, and many of these are reviewed in Chap. 7. One recent study

was oriented specifically toward cleaning/bonding to the Ni-based metallizations that are used for wire bonding on PCBs, PBGAs, etc., [9-8] (also see Sec. 6B). Oxygen/argon plasma and UV/ozone are the best cleaning methods, but one must be aware that any silver, copper, or nickel in the package or chip may oxidize and lower the yield for bonds made on these metals. Such cleaning is economically mandatory for low-volume, high-reliability hybrids, MCMs, SIPs, sensors, and the like, and large single-chip packages but not, in general, for high-volume IC production (although automatic, in-line plasma cleaners are available). Investigations of bond-pad cleanliness on wafers have shown that several significant contaminants may be left by the wafer processing steps [9-5, 9-7]. These may include S, Cl, Fl, TiN, fluoropolymers, glass, and carbonaceous materials. Some of these are shown in the Auger spectra of a bond pad on a wafer (see Fig. 9-3). This figure also demonstrates how effective oxygen plasma is in removing most residual Fab contamination. However, oxygen plasma will not remove glass or other inorganics from the pad, except by sputtering, so it is imperative that they be removed earlier during processing. Wafers may be shipped to packaging foundries (often continents away) with the processing contaminants remaining on the bond pads. These will not be removed by washing accompanying

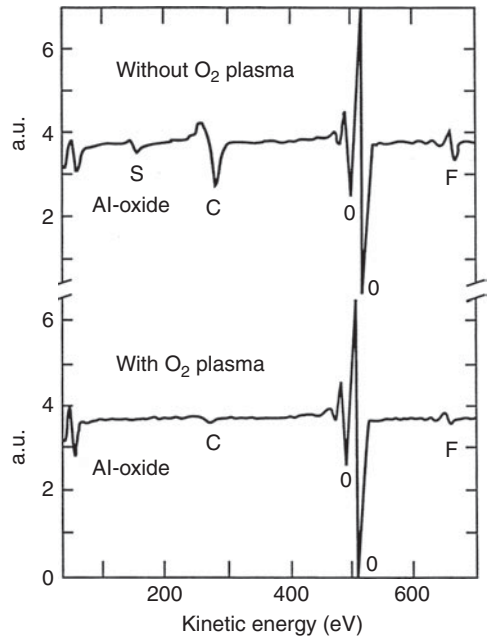

Figure 9-3 The effect of O_2 plasma cleaning on an Al-bond pad surface. This Auger cleaning was done at the wafer level in order to remove wafer processing contamination. (*After Klein [9-5]; © IEEE.*)

saw-separation and can, therefore, reduce bondability. It is a simple matter for the wafer Fab to plasma clean the wafers, in oxygen (or oxygen-argon), before shipment or storage. Then, Fab-induced contaminants will not contribute to bond-yield or reliability problems as in the past!

After the wafers are cleaned, they must be properly packaged for storage or shipment to avoid recontamination. The effect of wafer storage on contamination was studied [9-9]. It was found that storage and shipment of wafers should take place in sealed aluminum cans having aluminum wafer holders. Storage in plastic will eventually result in a buildup of organic contamination. As an alternative, if wafers must be shipped and stored in plastic then the wafers should be plasma or UV-ozone cleaned before saw-separation at the packaging facility. Cleaning whole wafers is quick and economical.

Advanced, High-Performance Devices now Use Cu (Rather than Al) On-chip Interconnects

These Cu-bond-pad areas on the chip are protected by a diffusion barrier and have ~1 μm of pure Al deposited on top as the actual bond pad. Thus recent Cu/Lo-k devices do not have the same bond-pad problems as many traditional Al interconnected devices. However, they must be cleaned as described above. See Chap. 10 for a description of that technology. At the present time, the vast majority of devices are still based on Al interconnects, but this will change in the future.

The Package Metallization

The off-chip metallization, be it on a leadframe, ceramic, laminated plastic substrate for a BGA, etc., can result in as serious a bond-yield problem as the chip metallization. Gold, Ag, Pd, and Ni are the most frequently used off-chip metallizations, see Chap. 6 (A and B). Cleaning is equally as important as for the chip pads (discussed in Chap. 7). This problem is complicated because of the variety of different metals used for bond pads in the many types of packages. Each metal usually requires different cleaning and storage conditions. Metals that oxidize (i.e., Ni, Cu) cannot be removed with UV/ozone or oxygen plasma, but rather by sputtering/reduction with Ar or H_2 + Ar. Electroplated metal films may vary in hardness, crystal structure, impurity, and gas content, all of which can affect bondability. Appropriate quality evaluation tests must be run for each bonding method (pull test for wedge and shear test for ball bonds).

9.1.3 The Bonding Machine and Its Control

As indicated above, the characteristics and setup procedures of individual bonding machines are beyond the scope of this book, since these vary greatly and will continue to change as newer models are

introduced. Specific information for each bonder is available from the manufacturers, who usually offer training courses in their use. All bonders for production use, must be set up for the intended chip and package metallization using appropriate experimental design methods, DOE (see Chap. 8, App. 8B). However, the set up and control of bonders to produce high-bond yields in hybrids, SIPs, stacked chips with overhanging pad areas, etc., are much more difficult than for the high-volume production of ICs. The latter have been discussed earlier in this chapter. Most sensors, hybrids, and MCMs are produced in relatively low volume, but stacked chips, SIPs, etc. can be very high. These all may include a number of chips from different manufacturers, and each chip can have different metallizations or at least have undergone different heat treatments. The contamination left on bond pads by different wafer Fabs and subsequent handling is apt to be different. As production progresses, chips ordered later from the same vendors can be from different wafer lots/designs, and the metallization and residual contamination may vary. Thus, cleaning with UV-ozone or O_2 plasma, after polymer die-attach (which produces its own contamination) and within several hours of bonding becomes important in order to obtain the highest bond yields. Following these procedures, the highest yields have been achieved when bonding to chips in ceramic packages [9-5]. The choice of specific bonding technology, in addition to all other factors, can have an impact on the yield in a given situation. Numerous other machine conditions and factors can affect yield in the 10 to 100 ppm region (e.g., design of the bonding tool, as well as maintaining the vertical position with respect to the bonding pad).

9.1.4 Reliability for Small Numbers of Bonds (Small Sample Statistics)

Bondability, as well as reliability data for set up on low-volume chip and substrate metallizations, is often obtained by bonding across metallization pads on electrical reject substrates and chips. However, the main high-yield problem is less than 100 ppm yield production control when using small sample sizes. One approach to achieve bond-production control with small sample sizes used the deformed width of wedge bonds (which fitted a normal distribution as determined by the Chi-square statistic) in conjunction with reliability test data. This was used to predict bond reliability (lifetime) of chip-on-board (COB) devices on PC boards [9-10]. While not a generic solution, this concept may be used as a starting point to develop a more universal small sample bond-process control. An example of fine-pitch bond-yield prediction was used by Shu [9-11] who measured the gaps between adjacent ball bonds on fine-pitch bonding test die, assumed that they were normally distributed, and used that assumption to calculate the probability of shorting between adjacent balls in a variety of fine-pitch wire-bonding situations. Based on these

examples, one possible approach to small sample yield or reliability control would be to study the failure modes, establish and then combine the distributions of the most likely failures, and use the results to predict yield or reliability. As production continues, confidence in the method would increase based on cumulative production control charts. In the above examples, the predictions based on a measurable bond parameter would apply to a wide variety of products so that in time a large amount of yield or reliability data could be obtained, even though low-volume production runs are small. Discussions, including cause-and-effect (fishbone) diagrams, of the procedures necessary to bring low-volume wire bonding under statistical process control have been published [9-12]. The process can be improved using DOE setup of bonders in the beginning (see Chap. 8, App. 8B, by Lee Levine).

The generic *reliability* prediction (defects per thousand device hours) for wire bonds is often requested by designers of low-volume systems, such as SIPs, MCMs, specialized devices/systems, as well as small-volume IC production. While such a value would be desirable, it is not realistic to expect that any definitive numbers will emerge. There are so many variables in the manufacture and long-term environment of devices that such a hypothetical value, if used to predict bond life, would be equivalent to the computer jargon of "garbage in, garbage out." Some variables that make such general prediction almost impossible are: type of bond and metallurgy (Au-ball-wedge, Al- and Au-wedge-wedge, Al, Au, Ag, Ni, Pd, etc., pads), quality of bond set up (DOE or other), any cleaning procedures used before bonding (plasma, UV-ozone, solvent, other, or none), loop heights (if open cavity), plastic molded (if so then which resin), fine pitch or not, cratering probability, and chip metallization structure, environment (temperature, power, or temperature cycle-number), range, dwell time, duration, and humidity. However, the reliability of a specific known type of device can be determined by performing stress tests on appropriate numbers and evaluating the results by statistical methods. If all chips from different vendors had pure, uniform aluminum metallization caps, as described in Fig. 9-1, then high-yield low-volume bonding set up and control would be greatly simplified, and such reliability predictions could be more valid. The same admonition for manufacturing low-volume systems as for high-yield bonding is appropriate. To achieve these ends, everything must be done correctly, and the solution to every solved production problem must be understood (or the problem may reappear)!

9.1.5 Package Related Bond-Yield Issues

The effect of different package types on bonding yield as well as its dependence on leadframe clamping has been studied by Klein [9-5]. In general, he found that the rigid ceramic packages are best, and that small packages (perhaps because they are difficult to clamp) are worse.

Leadframe and package clamping have long been known to affect bond yield. A poorly clamped package results in the dissipation of ultrasonic energy by resonating (vibrating) rather than concentrating that energy in the bond interface area.* The observable symptom of poor clamping is a large variation of bond deformation across the sample/substrate. Ceramic packages, because of their rigidity, generally result in higher bond yields than bare leadframes. Also, thin, small-outline, and also fine-pitch leadframes, have lower bond yields than large leadframes. Thus, the choice of package, as well as its clamping, can have a significant impact on wire-bond yield.

9.1.6 Possible Yield Problems and Solutions

Wire Diameter Variations

It has been shown that variations in the diameter of gold bonding wire (within the currently allowed ASTM specifications of ±3%, or a 6% maximum diameter variation) for 25 μm wire, ASTM F 72-06 in Chap. 3, App. 3A, can result in variations of ball-formation diameter for ball bonding [9-13]. If the wire diameter is slightly larger, then more of the thermal energy from the EFO is conducted away from the melt zone, and the resulting ball is smaller. The maximum difference in the unbonded, free air-ball diameter is only about 5 μm for a typical 25 μm diameter wire ball. However, this can combine with other variables of the EFO wire-machine system increasing the difference. Different ball sizes require slightly different optimum bonding machine set ups, so this may affect yield in the high-yield range. To achieve the very highest bond yields (e.g., <25 ppm defects, wire should be purchased under a tighter diameter control of ±1 to 2%. Similar variations in wire for wedge bonding should not affect bonding, since thermal conductivity does not play a role as it does with ball bonding. (A ball size shift, with constant wire diameter, can be experimentally simulated by varying the EFO setting in a designed experiment.)

Probe-Mark Damage

Probe-mark damage left on the pads is an example of a problem that chip packaging personnel cannot avoid, if left during wafer test. However, they can be observed, and could be a reason to reject a wafer lot, if bonding problems occur. Such probe marks only became a problem when fine pitch was implemented [9-14, 9-15, 9-16]. It was found that

*This resonance can be easily demonstrated by spreading *lycopodium* powder (or equivalent) over the package before the bonding-clamping experiments. Poorly clamped packages will show powder accumulations at resonance nodes and clean areas on maxima. Such resonant patterns are very prominent in large-diameter wire bonding experiments. (Note: this very fine powder tends to get all over the bonder workstage, so it should be handled with care. Such experiments are usually run on manual bonders.) All such large wire experiments show some resonances, but it is still helpful.

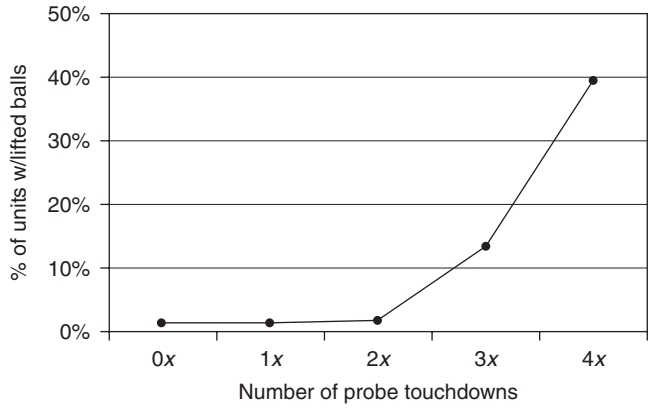

Figure 9-4 The number of lifted balls versus probe touchdowns for ~60 µm pitch pads [9-14] (© IEEE).

probe damage was acceptable for 60 µm pitch pads, only if the probe touchdowns exceeded 2/pad, as shown in Fig. 9-4. However, the finer the pitch, the more lifts occurred. For 35 µm pitch, the ratio of non-stick-on-pads (NSOP) due to probe marks could be as high as 84%, with only *one probe touchdown* [9-16]. Although several solutions for pad design have been investigated (hardened, laminated, and corrugated pads, etc.), it was found by several studies that the most practical solution was to off-set the probe testing part from the bonding area, as shown in Fig. 9-5. In those cases the extended pads can overlap into active areas that would not be damaged by the probe stress. This design would not require larger chip size. It would, however, require different visual inspection criteria which could require changes in such documents.

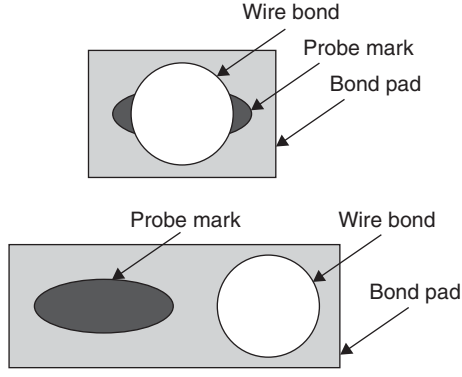

Figure 9-5 Top, normal fine-pitch pad. Bottom, pad is elongated to avoid damage during probing. (This configuration may require different visual inspection criteria.) [9-16] (© IEEE).

9.1.7 Other Considerations That May Affect Overall Device Yield

The Ultrasonic Systems

The ultrasonic systems of wire bonders in the past used 60 kHz ultrasonic energy. However, starting in the 1990s the bonding frequency has been increased to ~120 kHz. Publications of that period indicated that the bond yield could be improved by increasing the ultrasonic frequency. This work offered a new parameter that may increase the bond yield. High-frequency systems currently have been universally adopted by production autobonder manufacturers. See Chap. 2, Sec. 2.4, for a more detailed discussion of high-frequency bonding technology including additional references.

Wire Sweep

Wire sweep refers to the movement of the wire-bond loops during the transfer-molding process. In worst cases, adjacent wires will touch and short one another. Technically, wire sweep is not a part of wire bonding, but it can affect the yield of plastic devices. As such, it must be considered in designing such wire-bonding process.

During the molding process, enough hydrostatic force is generated by the hot plastic to deform and occasionally push the wires into one another, leading to short circuits. The latter seldom occurs, but some deformation of the wire loops is common. Many industry specifications permit up to a 5% (permanent) displacement or deformation of the loop. However, this is an arbitrary value that is not appropriate for long fine-pitch wires in molded devices. Course pitch can normally safely accept an even greater displacement. The smaller the wire diameter, the higher and longer the loop, the more rejects will be encountered due to wire sweep. Fine-pitch packages have less fanout and often longer wires for higher lead count, resulting in greater possibility of wire shorting from minimal wire sweep. The looping shapes can also affect the shorting possibility. Additional complications can result from area array bonding.

Wire sweep is a complex subject and depends on the wire diameter, its stiffness (Cu stiffer than Au), the shape of the loop, its orientation with respect to the plastic flow (position and size of the mold gates), the height and position of the chip, and the mold design. In addition, it is affected by the viscosity and other parameters of the mold compound [9-17, 9-18, 9-19]. Although many experiments have been run using x rays and/or plastic removal, most current work consists of finite element modeling to design the mold, gates, and plastic flow, in order to minimize the effect. The dynamic flow properties of the hot filled resin must often be estimated, and FEA results that are not confirmed with experiments may not be accurate. Wire sweep modeling is often done with large, general, FEA software packages, and these can be adapted to wire sweep design [9-20].

9.1.8 Wire Looping

Appendix 9A by Lee Levine has a specialized discussion on wire looping, illustrated with many examples of long wires, shapes, etc. As with wire sweep, looping is not directly a bonding issue. It is controlled by the machine and its looping software. However, looping can affect the reliability and yield of a ball bonded package, so such capabilities should be understood by the user. Often packages require very low loops only about 50 to 75 μm (2 to 3 mil), such as in stacked chips, CSPs, BGAs, etc. Other packages require long flat loops or ones with special shapes to avoid contacting part of the chip or package. The simplest and oldest of these looping techniques moves the wire initially in a reverse (opposite) direction from the second bond position before moving toward it. This forms a smooth loop that does not sag. More recently, bonder manufacturers have learned to form very special loop shapes by a series of tool motions (back and forth, up and down, etc.) during loop formation. There have been patents and papers describing these complex loop-forming motions [9-21 to 9-23]. These motions can produce long flat loops, as well as loops with kinks and discrete bends. Some variations of these are named "worked loops," "smart loops," etc. Without such loop control it would not be possible to wire bond many of the special packages used today as fully described in App. 9A. We note, however, that any special loop shaping slows the bonder throughput significantly. Unusual loop shapes have been designed for special purposes. One, for especially low stable loops, is shown in Fig. 9-6.

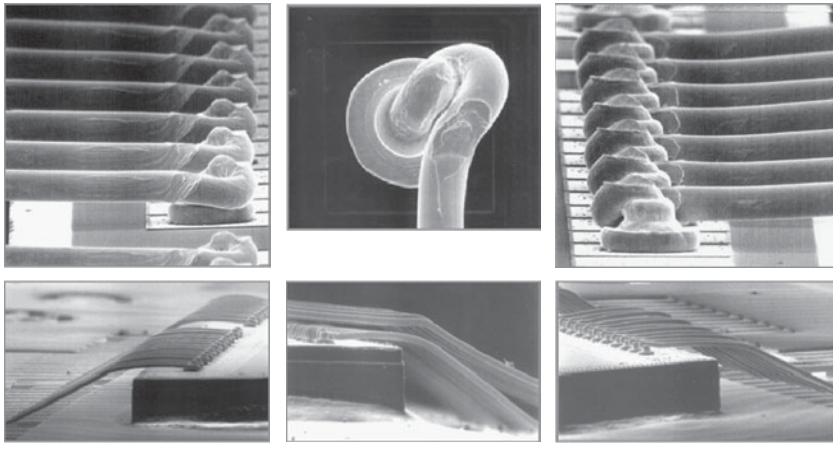

Figure 9-6 Ultralow "Escargot" loops that are less than 40 μm high. (*Courtesy of ASM, Singapore*)

Stacked Chips

Another area that requires very special looping and other unusual wire bonding techniques is that of stacked chips. These chips are first thinned to 50 to 200 μm and bonding often takes place to overhanging chips. This leads to very special bonders/programming for that unique purpose. There is a glue layer, or interposer, between offset chips. These stacks are built in layers, with bonding as each layer is applied. Normally, memory chips are used because of their low thermal dissipation. However, when power chips are used, they are placed at the bottom of the stack for heat-sinking. Currently, most of these stacks are used in very high volume for portable devices, such as cell phones. Although stacks have been demonstrated as high as 25 or 30, most have less than 10 layers. Several such stacks are shown in Fig. 9-7*a*.This is a specialized subject and interested persons should

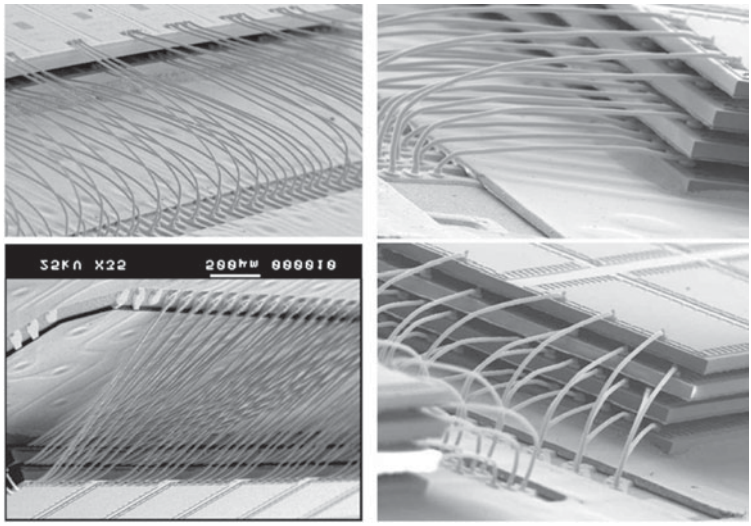

(a)

Maximum numbers of dies stacked (and in volume production)									
Year	*2008*	*2009*	*2010*	*2011*	*2012*	*2013*	*2014*	*2015*	*2018*
Wire bonded	8	10	10	12	12	12	14	14	16

(b)

Figure 9-7 (*a*) Examples of stacked dies connected with wire bonds. (Stud bumps are first bonded to dies and the-crescent of a ball bond to-the-package is bonded to it. Then the next layer is applied, etc.) In this case 4- stacked dies are shown on the right. The wire bond complexity is obvious **(*Courtesy of Amkor*)**. (*b*) An excerpted section of the 2008 ITRS A&P roadmap for wire-bonded stacked chips predicting the years that the number of stacked dies will be entering high-volume production, somewhere in the world.

start with the ITRS 2008 A&P Roadmap, and the ITRS "SIP white paper 2008," manufacturers' literature, etc. A section of the 2008 A&P Roadmap predicting the future number of dies stacked is given in Fig. 9-7*b*. Note that the roadmap also discusses another stacking technology (e.g., "Through Silicon vias"-TSV), which is predicted to have only 5 chips/stack by 2018, but its performance would be much higher than wire bonded ones. We note that some totally different method of increasing active chip density could be invented by that date.

9.1.9 Fine-Pitch Ball and Wedge Bonding

Fine-pitch bonding is evolving faster than a book can possibly follow. It is the leading edge of wire bonding. Although the author believes that the current state of the art (2008) is reasonably represented below, the situation will probably change (improve) even before this book is published. Most of the advances result from improvements in autobonders, capillary design, wire doping, and associated equipment, rather than user-based improvements. Currently, advanced autobonders for IC production are capable of 30 to 35 μm pitch, and some might go still finer, but implementation is delayed by the availability of appropriate chips/infrastructure. There are many papers/articles on this subject each year, in conferences, as well as from the bonding machine manufacturers. The reader should obtain these and contact those companies to assess the state-of-the-art at any given time. Fine-pitch bonding requires special capillaries that are generally called bottleneck capillaries, because of their shape. These avoid hitting adjacent wires, as shown in Fig. 9-8.

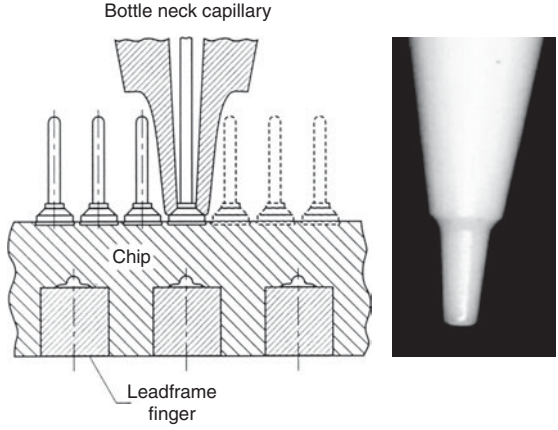

Figure 9-8 Left: drawing of a bottleneck capillary, bonding from the left to right direction. It is designed to avoid contacting the last-made-bond (on the left). These capillaries are fragile and break easily. Right: a photograph of the constricted tip. For very fine pitch, the tip is much more constricted and more fragile.

It should be noted that as the pitch decreases, more interface reliability and other problems have appeared. Some will be described below. The introduction of new dopants for Au wires is the major change related to reliability of the Au-Al interface. As a reality check, one should realize that most chips and packages are not (in 2008) classified as fine pitch. These are usually the most advanced or specialized chips. Later as new Fabs are built, and the feature size shrinks, finer pitch moves to more conventional chips.

Fine-Pitch Ball Bonding

A majority of devices made in 2008 still have low pin-counts (<100), and the bonding-pad-pitch for such ball bonds is still in the 80 to 100 μm range. However, 40 μm pitch is currently in production for high-end devices. An example of ball-bonds made with a similar fine pitch is given in Fig 9-12, and 35 μm ball bond pitch devices are nearing volume production in 2008. Figure 9-7 gives an example of 70 μm pitch ball bonds made with 25 μm diameter Au wire. Such bonds are made with bottleneck capillaries to avoid displacing adjacent bond wires. See Fig. 9-8 for an example of such capillaries. Very fine-pitch ball bonds can be visually different from the familiar coarser pitch ones, as shown in Chap. 4, Fig. 4-18 in which the bonded ball is only a little larger than the wire.

Some wires in use are only 15 μm in diameter, and 12 μm has been tested. These wires will be more subject to wire-sweep failures during plastic molding unless a solution to that problem is achieved. In time, insulated wire, lower viscosity molding compounds, or improved mold gates may extend the limit somewhat. Finer pitch-ball bond pitch (<30 μm) has been achieved in experiments but may not be used until chips having such pitch are available.

Typical bond parameters for fine-pitch ball bonding are given in Table 9-2. Note that the bonded ball size for this 70 μm process is about 47 μm, less than twice the wire diameter. For 50 μm pitch the bonded ball is only ~40 μm diameter and having ~12 gf shear, with a shear force of ~7.5 gf. Below −60 μm pitch, the bond-pull test would adequately evaluate the weld strength of ball bonds, and the shear test would be used only for set up purposes. This is desirable since shear testing of fine pitch balls is slow, difficult, and error prone. See Chap. 4, Sec. 4.7 for a discussion of this alternative. A caveat of such testing is that for long-term reliability of Au-Al ball bonds, the bond shear force should be more than 5.5 gf/mil^2 (also see Ref. [9-24] and Chap. 4, Fig. 4-23).

Fine-Pitch Wedge Bonding

Currently, wedge bonds can be made at 25 μm pitch using wires of 18 to 20 μm diameter, and bonding with high frequency (~120 kHz) US energy. This results in very low bond deformation (see Chap. 2, Sec. 2.4). It is not clear if this is in actual production, but if not, it certainly will be in the near future.

Machine or Test Parameter	100 μm Process	90 μm Process	80 μm Process	70 μm Process	50 μm[b] Process	40 μm[b] Process	35 μm[b] Process
Free-air ball diameter (μm)	50	—	43.2	40.6	32.4	31	29.5
Bonded ball diameter (μm)	74	61.3	55.8	47	~40	32	27
Bonded ball height (μm)	16.1	13.5	12.5	5.9	~6	~7	~7

[a]Values are typical and were collected from the literature, since the ball diameter can be changed during setup, it may not result in a consistent table.
[b]Wire diameter <25 μm, for fine pitch (from K&S [9-25]), as low as 17 and 15 μm diameter.

TABLE 9-2 Four Fine-Pitch Ball Bonding Parameters for Processes Using 25 μm Diameter Gold Wire[a]

Fine-Pitch Capillaries (Caps) and Wedge-Bonding Tools

Everything must undergo a change for fine pitch, and the capillaries and bonding tools are no exception. In order to avoid deforming the already formed loops, the tools must be reduced in diameter. Examples for both ball-bonding capillaries and wedge-bonding tools are given in Figs. 9-8 and 9-9. Note that these shapes are typical, but for instance, caps can also be long and finely tapered, rather than bottleneck shaped.

9.1.10 Reliability and Testing Problems of Fine-Pitch Bonding

The bond pitch is the distance between wire bond centers (also the distance between the center of one bond pad to the next). However, part of this space must be used to separate (insulate) the pads; thus, the bondable area on the pad itself is further reduced by the overlapping passivation. One of the concerns expressed about very fine-pitch bonding is that bonder inaccuracy can place the bond on that passivation. It may not be far enough off-pad to be rejected, but it can crack the passivation, and the cracks sometimes propagate outside the pad. There have been no documented reports that this presents a reliability problem in hermetic packages. The primary concern is for devices in moisture permeable plastic molded packages where leakage paths may develop. Also, some bonds can overlap and short with

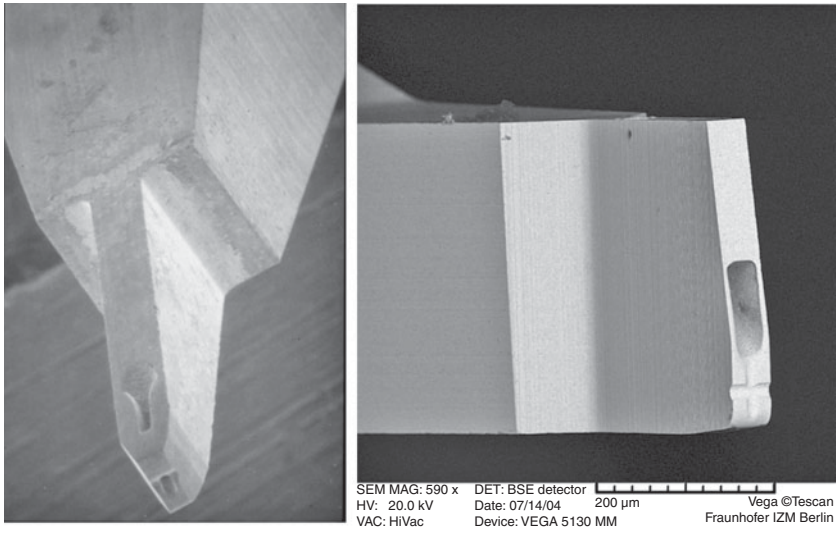

Figure 9-9 Fine-pitch wedge bonding tools. The left is an older design. (*Courtesy of Microminiature Tech.*) On the right is a recent design that is stronger (less fragile). This tool has a cross-groove in its foot, and is intended for fine-pitch wedge bonding with gold wire. (*Courtesy of Franuhoffer IZM.*)

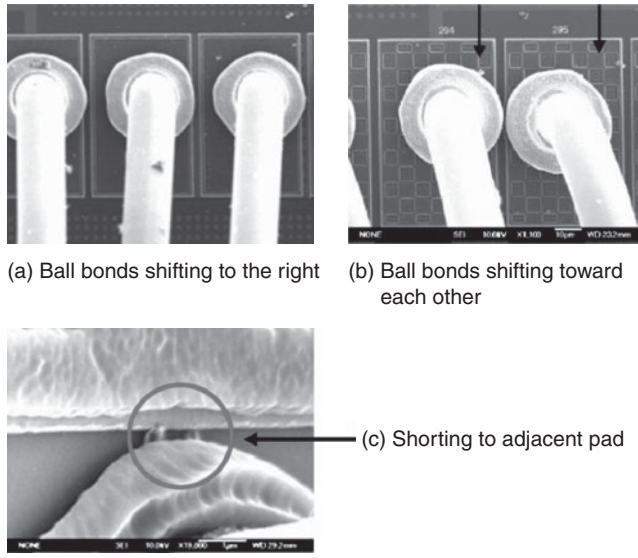

Figure 9-10 Three possible shorting problems of 47 μm fine-pitch (and finer) ball bond placement [9-24] (© IEEE).

adjacent pads or ball bonds. Ruston [9-24] gave examples of several possible placement problems with 47 μm pitch ball bonds. These are shown in Figure 9-10. Solutions included finer diameter wire (which could lead to more wire sweep), but produced smaller balls, and new machines with closer placement tolerance. Ultimately, the balls passed the ball shear strength and maintained the minimum industry-standard value of 5.5 gf/mil^2 after extended thermal aging. It should be noted that similar problems can arise with each new *finer pitch chip* generation!

The New Mechanical Testing Problems for Fine Pitch Ball Bonds

Table 9-3 shows the predictions of the ITRS roadmap for wire-bonding pitch until 2016. Ball-bonding pitch reduces to its minimum of 25 μm by 2015, and the wedge-bonding minimum is expected to be reached sometime in 2009 (see the table footnote). (All such ITRS predictions are subject to modification each year and assume that high-volume production at such pitch will exist somewhere in the world by that date.)

The decreasing pitch indicates possible future wire-bond problems or at least changes in manufacturing and testing (see Fig. 9-11). Both pull testing and shear testing are affected by finer pitch bonds.

The ball-shear test has been described as indispensable to evaluation of ball bonds (see Chap. 4, Sec. 4.3). However, as the pitch decreases to below ~50 μm, it is harder to position the ever smaller

Year of Production	2007	2008	2009	2010	2012	2014	2016
Wire bond, ball, single in-line (μm)	**40**	**35**	**35**	**35**	**30**	**30**	**25**
Two-row staggered pitch (μm)	55	50	45	45	40	40	35
Three-tier pitch (μm)	60	60	60	55	55	45	45
Wire bond—wedge bond pitch (μm)	**25**	**25**	**20**[a]	**20**[a]	**20**[a]	**20**[a]	**20**[a]

Excerpted from ITRS 2008 A&P roadmap, Table AP3.
[a]These values are proposed and may be postponed or never reach production. The bonders could, but other factors may prevent or slow implementation.

Table 9-3 Chip-to-Package Substrate Technology Requirements—Near-Term Years

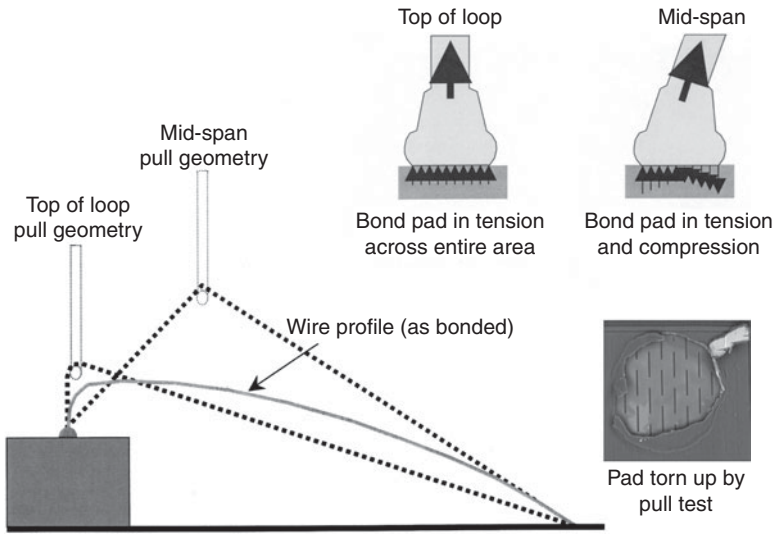

Figure 9-11 A merged figure showing two pulling geometries. The Top of loop (left) vertical pull (will never be perfectly straight up) will minimize pad tearing. An example of a pad, torn up during a pull test is shown on the lower right. (*Courtesy of Jon Brunner, K&S.*)

shear probe without hitting the adjacent ball bond, resulting in inaccurate data. (Accurate placement takes longer and requires more operator skill. At some point even this is not possible.)

The first work to have investigated the pull test to replace the shear test for fine-pitch ball bonds was done by Sundararaman [9-26]. He found that when a fine-pitch ball bond is made over a probe mark, the pull-test stress at the normal center-pull angle is large enough to lift-peel that ball. This starts in the probe mark area, which is poorly bonded and serves as a stress raiser, and the ball lifts before the wire can break normally at the HAZ. The results from such a lift/peel test should be interpreted with caution. A bond pull should be considered a failure only if the *ball* lifts and examination shows that there was poor intermetallic formation.

This test is mostly used on Cu/Lo-k chips, which often have low pad or sublayer to *pad* adhesion and the *pad* may lift or tear, even without a probe mark-stress raiser. Other work found that if the angle of pull is vertical, then the "tear" component is minimized and more normal HAZ (wire) breaks occur. An example of the desired (vertical) configuration is shown in Fig. 9-11. Note that even for "attempted" top-of-loop pulling, some tear stress still exists and tearing may be occasionally observed since the angle is not exactly vertical. For some very fine-pitch bonds with balls shaped as in Fig. 4-18 (Chap. 4), this tearing problem can occur if the pull force exceeds the tensile adhesion of the pad to SiO_2 in normal (non-Cu/Lo-k) structures.

Almost every aspect of fine-pitch bonding requires more planning and is more expensive to achieve than bonding at relatively course pitch. The shape, size, and placement of the bond pads must be coordinated with the selection of the autobonder and die-attach machine (with their known positioning accuracy and repeatability), as well as the specific package layout. For vertically integrated companies this is done during the early chip-design phase. Problems can exist for packaging foundries, but they often work closely with high-volume chip designers. The finest pitch wedge bonding is achieved with narrow (rectangular or parallelogram shaped) bond pads, but these would not be amenable to ball bonding even if there were compelling reasons for doing it at a later time. Because of these limitations such pad designs are not often used except in vertically integrated companies, or as a help in testing fine-pitch pads using displaced probes (in Fig. 9-5). The throughput from an auto-wedge bonder is less than that from an equivalent ball bonder (2 to 4 wires/s vs. >10/s, respectively). Thus, wedge bonds cost more than ball bonds, and as a result, only represent about 5% of the total number of bonds made.

Some packages have bonding pads on two or more vertical shelves (tiers). It is possible for bond wires to cross over one another, particularly when bonding around corners of the package where the wires fan out. Shorting between rows is a possibility, and it is necessary to

carefully design and control the bond loops to meet minimum clearance requirements (see App. 9A). This is both a high-yield and a fine-pitch bonding problem. Proprietary spreadsheet programs for tolerance analysis have been designed for this purpose, which includes bond-loop and wire-spacing prediction, as well as all package tolerances. Software with some modern autobonders has some of this capability. However, the bonding machine will operate faster, the positioning will be more accurate, bond loops more highly controlled, and the yield higher if all wires are bonded straight out from the chip (no fanout). This requires complete coordination between the chip and the package designer. Bonding straight out in fine-pitch ceramic packages is usually achieved by bonding to two or more tiers. However, some modern high-density SIPs, MCMs, etc., can have bond pads with pitches approaching those on chips, simplifying bonding and improving the yield.

Area Array Wire Bonding

As autobonders have increased in capability and chips have more I/Os, the concept of area-array wire bonding became both possible and essential for high leadcount devices. This has pushed the limits on all aspects of wire-bonding technology. These bonders have fine-pitch, extremely precise, long loops, with minimum possible sag of the loop. It is thus possible to have a greater number of wire bond I/Os than area-array flip chips in the same chip area. (Cross-talk, inductance, and other electrical problems can be improved by design, but of course, will still not have the high-frequency performance of flip chips.) An example of area-array chip bonding is shown in Fig. 9-12.

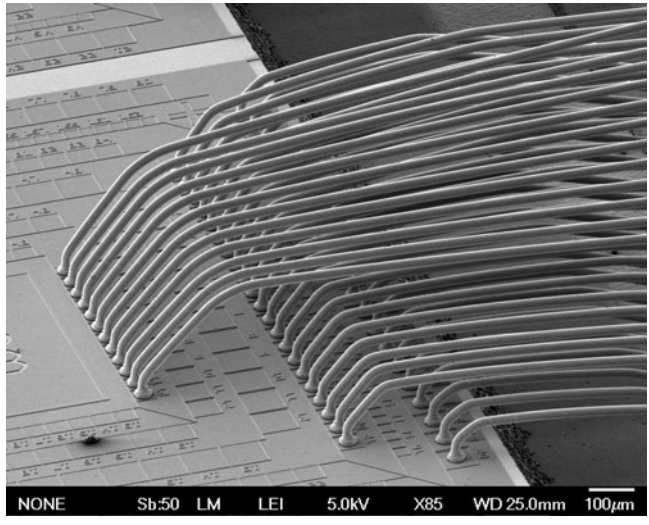

Figure 9-12 An example of fine-pitch area-array wire bonding. These bonded balls are 40 μm in diameter. (*Courtesy of ASM, Singapore.*)

9.1.11 Conclusions of High Yield and Fine Pitch

1. To even hope to approach high-yield and fine-pitch wire bonding, you have to do everything right and understand everything you do!
2. If vertically integrated, you should *cooperatively* design the chip, the package, and choose the bonding and die-attach process as well as the actual equipment before chip production can begin.
3. You have to understand both the wafer Fab's metallurgical processes (what's under the pad) as well as all assembly processes (e.g., die attach) that affect bonding.
4. You must remove contamination from the bond pads, including those remaining from the wafer Fab and assembly processes. (However, it should be the responsibility of the wafer Fab to deliver wafers that have clean, bondable metal.)
5. You have to understand both your wire bonder's limitations and the bonding process, and control them as well as your incoming materials. (Form keiretsu-like relationships with your suppliers.)
6. For fine pitch you must upgrade your equipment (bonders, caps, cleanliness, etc.) continually.
7. Your management must be completely committed to the fine-pitch and high-yield process.
8. If you are manufacturing SIPs, hybrids, MCMs, MEMS or other complex, low-volume products, you start with two strikes against you. You will have to work twice as hard as the IC industry to even approach high-yield bonding, but fine pitch can be achieved with the same effort.

9.2 Wire Bonding to PC boards, Flex, BGAs, MCMs, SIPs, and Various Soft Substrate Devices and High-Performance Systems

9.2.1 Introduction

The classical thick-film hybrid uses a ceramic substrate. Bond pads are of thick-film Au or Ag (alloy) applied directly over that ceramic. This poses no more special problems than bonding to a ceramic package [9-27]. As such, high yields (≤50 ppm defective) are attainable if the best metallurgy and bonding procedures are followed. However, other plastic-based substrates (PC boards, BGAs, SIPs, etc.) can pose significant bonding problems. These are normally epoxy-like

polymers laminated with fiberglass or other fillers and may bond well above their glass transition. In some cases, a layer of thin-film dielectric and metallization is deposited on the surface of a ceramic- or laminate-based substrate to improve the high-frequency signal characteristics (build-up layers). In other cases, plastics without lamination (such as flex substrates) may be used. Some complex IC chips have multilevel polymer-insulated metallization or special Low-k dielectrics such as SiOC (see Chap. 10). If pads are placed on top of these polymers rather than on the traditional Si/SiO_2, then bonding can be similar to bonding on soft substrates. Microwave hybrids are often made on polytetrafluoroethylene (PTFE) "soft" substrates and require special knowledge and bonding machine set up. These plastic substrates may be laminated or have fillers similar to PC boards. Some are hard and easily bonded.

The discussion that follows describes all aspects of soft-substrate wire bonding, including the polymer and bond-pad metal material properties, the bonding-machine requirements, as well as the considerations for using wire bonds in high-clock-rate systems. The important point is that if one expects to wire bond to multilayer polymer substrates, or other soft substrates, then one must design the system (both polymer and metallization) with that objective in mind. Otherwise, the wire-bond yield may be unacceptable and the redesign time consuming and costly [9-28].

9.2.2 Bonding to Thin-Film Dielectric Substrates

Bond pads usually consist of gold-plated thin-film Cu, or Al, placed on top of one or more layers of relatively soft polyimide (PI) or other plastics. But the first soft substrates were microwave hybrids that used laminated or filled PTFE (soft) substrates. One of the first solutions to bonding over PTFE was to solder thick gold-plated Cu disks to the thin-metal bond pads, which produced a rigid platform for bonding [9-29]. Most of the later work on soft substrates has followed equivalent solutions, although often without realizing it. As an example, when using Cu conductors, Ni films are often applied as diffusion barriers between the Au surface plating (for high bondability) and the Cu to prevent Au-Cu interdiffusion. But, fortuitously, this Ni layer also stiffened the bond pads, improving their bondability.

Other approaches that improved thermosonic (TS) ball bonding yields onto pads over PI are to add hard 0.5 μm thick Ti or Ti/W layers under Al-bonding pads on PI (over Si chips) [9-30, 9-31, 9-32, 9-33]. (Such hard metal layers have long been used under Al and GaAs IC chip pads to prevent cratering.) In addition, it was reported that greater ball deformation resulted with the same bonding machine parameters, a normal indication of improved bondability. Various reliability tests used in both studies verified the improved bond quality.

As with PI-coated chips, hard underlayers of Ti, Cr, etc., are also used to stiffen Cu-bond pads on thin-film high-performance substrates. (These hard metals are often required for adhesion, as well as corrosion protection on PI substrates, but because these metal films are lossy, they must be thin, ≤1000 Å, for high clock-rate systems; see Sec. 9.2.6.) To improve Au-plated Cu bond pads, a thick layer of Ni (~3 to 8 μm) can be plated on top of the Cu pad and then overplate it with ~1 μm of soft, bondable Au. All of these hard layers can reduce the pad deformation during bonding, increasing the bonding yield. Although the terms cupping, bending, copper-trace sag, and pad deformation of the bond pads have been used in the field for several years, it remained for Takeda [9-34] to actually measure this effect on bond pads over flexible polyimide PCBs. He wedge bonded to 18 μm thick Cu-bond pads (overplated with 2 μm of Au) using 35 μm diameter gold-plated Cu wire. (Since this is much harder than Au or Al wire, it easily demonstrated the cupping phenomena.) The bonding process left a significant pad indentation (measured with a profilometer), as shown in Fig. 9-13. The indentation depth was shown to be dependent on both the ultrasonic energy and the bonding force. They also found that the larger the bond-pad area, the higher the wire-bond yield. The fact that the Cu-bonding wire was harder than the usual Au or Al wires presumably made the indentation more prominent and, thus, easier to measure. The cupping was accompanied by poor bonding yield. After plating 3 μm of Ni between the Cu base and the top bondable Au, the

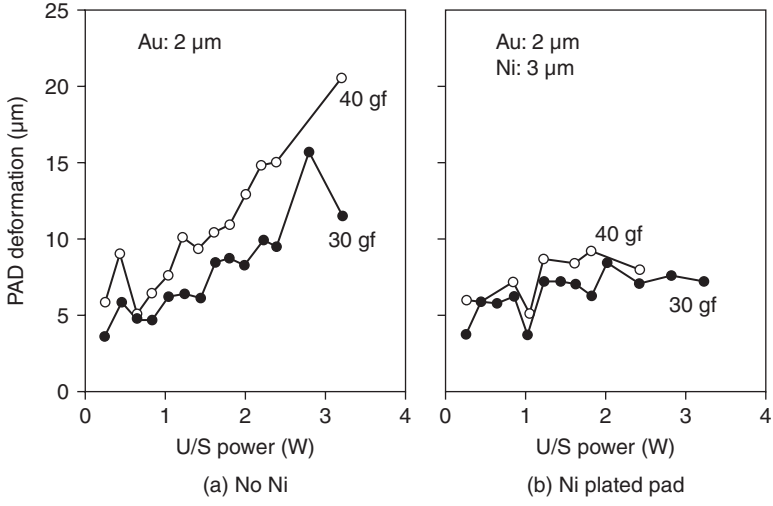

Figure 9-13 The depth of bond-pad indentation (cupping) on polyimide flex substrates as a function of ultrasonic energy and bond force. (*a*) with only 2 μm thick Au over 18 μm thick Cu; (*b*) with a 3-μm thick Ni layer between the Cu and Au layers [9-34] (© IMAPS).

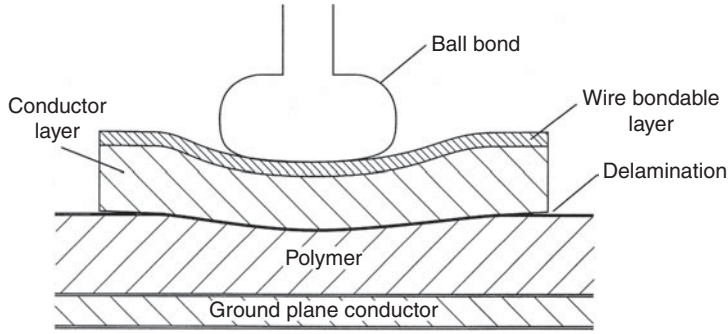

Figure 9-14 Deformed bond pad and polymer structure after wire bonding. This illustrates the bond-pad cupping phenomena (metal and polymer yielding) that occurs during wire bonding to copper-gold metallization deposited over a soft polymer. The edge of the metal pad may delaminate (as shown) from the polymer due to high-vertical stress. The figure is drawn from the results of a finite element model [9-30] (© IMAPS).

cupping decreased, and the bonding yield increased enough for volume manufacturing. Figure 9-14 illustrates the cupping phenomena. The edge of the metal pad may delaminate (rupture) from the polymer due to high-vertical stress. In such cases, the addition of an adhesion layer (usually Cr or Ti) will prevent separation [9-32].

Some workers in the past have developed bonding parameters for Au-TS bonding with the substrate maintained at room temperature using a heated capillary. This was intended to minimize the thermal softening of the flex-PI film and allow a low bonding force. The combination could help to prevent bond-pad cupping, but a hard Ni layer (platform) appears to be the better solution. In addition, heated capillaries are unavailable on modern autobonders; therefore, hard Ni layers or bond-pad support structures (similar to those used in Cu/Lo-k, see Chap. 10) have become a necessity under the bond pad.

Bonding at temperatures above the T_g for glass-laminated substrates is often possible if the bond-pad metallization is rigid (e.g., having adequate hard metal top layers or underlayers and covers a large area to inhibit sinking). Once a sufficiently rigid, non-cupping platform is achieved, then lowering the bonding temperature (to decrease softening of the polymer) has less effect on bonding. Nevertheless, because of changing expansion coefficient, the effect on any metal adhesives, and in some cases elastic compression of the entire rigid bond pad into the soft plastic, bonding above the substrate's T_g is not recommended.

Several investigators have presumed that it is the soft plastic under the bond pad that absorbs the ultrasonic energy, reducing wire-bonding yield, but this has never been proven. However, if cupping can be minimized by hard-metal layers, bonding will take place

over the softest of substrates, PTFE and polyethylene, implying that the cupping (metal yielding) is more detrimental than the soft plastic in dissipating the ultrasonic energy (assuming that the pad dimensions are large enough to prevent the pad from dynamically sinking into the soft substrate during US application and bonding). Also, for the best bond yield, the application of US energy should be delayed until all mechanical cupping and sinking has stabilized.

The design solution for dynamic sinking and cupping is to apply a hard metal layer, such as Ti, Ti/W, or Ni, directly under the bond pad or between the metallization and the polymer. This reduces or prevents cupping and results in reliable bonding. An example of a structure (with all variations) that achieves this is shown in Fig. 9-15.

9.2.3 Bonding to Laminate Substrates, Such as PCBs, BGAs, SIPs, and Buildup Layers

The wire bonding on most laminate substrates (plastic-ball grid-arrays, system in packages, etc.), which are generally made of glass-epoxy laminates, resembles bonding to PCBs. The metal pads are relatively thick and are often designated in "ounces" of Cu ("1 oz Cu" is 36 µm or 1.4 mil thick) from PCB industry usage. The most common thickness for laminate board Cu conductors is 18 µm (0.5 oz). The epoxy-fiberglass substrate (other polymers and fibers may also be used) is hard and rigid below its glass transition temperature (T_g). This technology offers few problems when bonding at low to moderate temperatures. Aluminum-wedge bonding at 25°C is done with little concern for rigidized bond pads (using ≤2 µm of Ni under a Cu pad). Chip-on-board (COB) devices using similar substrates have been used for many years, and watch-modules are made on them. BGAs, SIPs, etc. on single or multilayer substrates are also similar. These types of substrates can be bonded with both Au-TS (heated work-stage-below T_g) and cold Al-US methods.

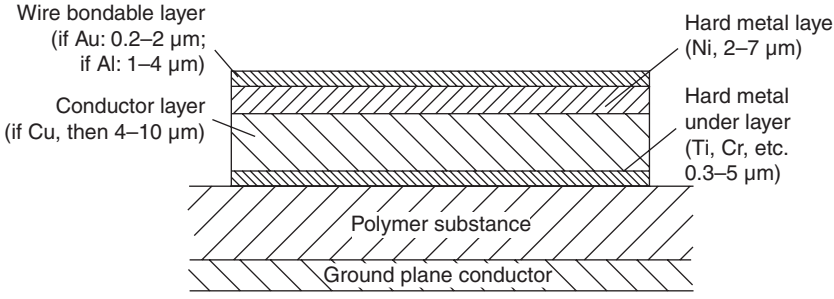

Figure 9-15 Structure of a generic, stiffened-metal bond pad and polymer substrate for wire bonding to high-performance substrates/systems [9-30]. The ground plane is included for discussion in Sec. 9.2.6. (© IMAPS).

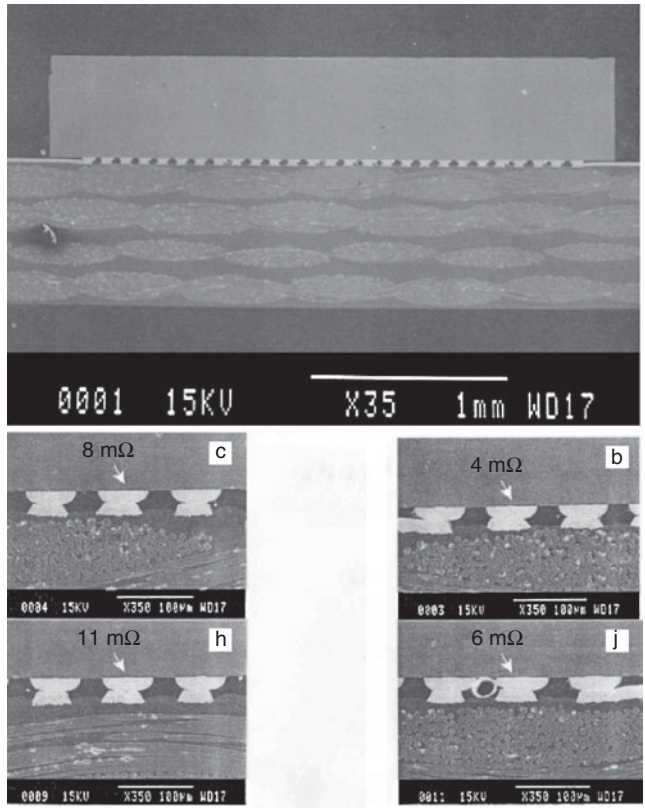

Figure 9-16 A cross-section of a glass-fiber-filled printed circuit board, showing how the existence/absence of glass fibers, depending on position, either can or cannot mechanically support any bond pads on the surface. As the temperature approaches T_g the plastic becomes soft. Sinking (and low-bond yield) during the bonding process will more easily occur over areas with no fiber support on the left. (*After Liu [9-35].*)

The problem of bonding to any type of fiberglass-laminated polymer substrate is illustrated in a PC board cross-section with conductive epoxy flip-chip connections in Fig. 9-16. This provides limited support in specific areas under some of the bond pads. It should be pointed out that some boards use a nonwoven polymer "paper" for support. If its T_g is high (such as aramid), then it uniformly supports all bond pads, even above the epoxy board's T_g.

In some cases, the polymer (being above T_g, or because of applied US) may become soft enough so that an entire rigid bond pad literally sinks into the soft plastic during bonding. Dynamic bond-pad sinking changes (lowers) the effective bond force over the first few milliseconds after the capillary (tool) drops (normally during the time that US energy is applied) leading to a changing bond force and lowering

the bond quality/yield. This was first observed when bonding to a polymer substrate above its T_g [9-30] but can also occur with low modulus substrates at room temperature.

9.2.4 Buildup Layers

These are pure polymer (usually epoxy) films without any reinforcing glass fiber (as was shown in Fig. 9-16). They are deposited on top of a normal PC board, and thin, fine-line metallization is applied on top. This can then be laser drilled, and fine vias applied through the layer. The fine vias/metallization lines permit much higher frequencies to be used on a normal low-frequency board/substrate. Often many such layers are built up in this way resulting in high-density, high-performance systems at a nominal cost. They are often used for cell phone boards and other high-density/high-frequency, but cost-driven, applications. If the board or buildup layer has a T_g, near the bonding temperature, then wire bonds (but not flip chips), are subject to sinking and low yield. An example of such dynamic sinking during gold crescent-bonding to an Au plating on a *buildup layer* is given in Fig. 9-17.

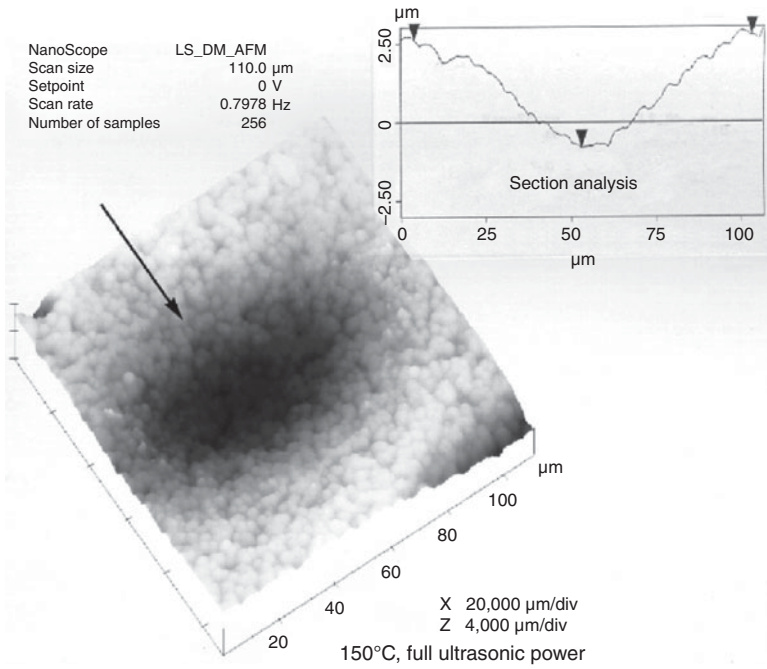

Figure 9-17 The sinking phenomena (indicated by arrow) of a 25-µm Au crescent (wedge) bond into an Au-plated pad on an epoxy buildup layer over a PC board (the wire did not weld to the Au plating). The bonding temperature was 150°C, which was near the buildup layers' T_g. The measured depth of the sinking as indicated in the AFM section analysis was about 2.5 µm. (*The AFM measurement was made by J. Kopanski, NIST.*)

Dynamic bond-pad sinking changes (lowers) the effective bond-to-pad force over the first ~10 to 100 ms after the capillary (tool) drops. This sinking occurs during the time that US energy is normally applied and the bond weld is forming (optimum delay experimentally determined). The dynamically changing bond force requires more US energy or the welding will be incomplete. (The solution is to delay application of US energy.) Thus, bonding near or above the substrate or buildup layer's T_g is not recommended for production unless the bond pad is both rigid *and* large enough to prevent sinking, or (*experimentally* determined) delay application of US energy until the dynamic sinking stabilizes [9-36]. The effectiveness of such a delay has been verified informally many times. The sinking phenomenon can also occur in PTFE, PI, and other soft substrates at room temperature, if the bond pad is small. A similar delay usually improves bonding.

In general, large PCB panels (typically made of FR-4, T_g ~120°C) having bare chips (COB) are usually bonded with Al wire by cold US methods to prevent heat warping of the board and possible softness complications that might result from exceeding the material's T_g. TS bonding at moderate temperatures (≤110°C) is often possible, and using a heated tip tool also helps. Special resins with higher T_g (170 to 190°C) are used to permit higher temperature thermosonic bonding (and soldering) to PBGAs and equivalent. If these are processed as large panels, then special substrate clamps (often assisted by vacuum) to hold the structure firmly against the workstage are required and can be a design challenge. Even small, thin-laminate module substrates must be firmly clamped for TS ball bonding to avoid warping, which will lower the bonding yield. However, in some cases, vacuum hold-down has proven adequate for individual BGA-sized substrates. The thicker the PCB/BGA substrate, the less important special clamping becomes. Thermosonic bonding over an unsupported center was successfully achieved on two sides of a small, 28 mm square, 1 mm thick, glass fiber-reinforced BT-resin module [9-37]. When bonding problems are encountered in such substrates, they can usually be solved by methods described above, using bond-pad structures illustrated in Fig. 10-11 (Chap. 10) and delaying application of US energy, if necessary.

9.2.5 The Effect of a Polymer Substrate's Material Properties on Wire Bonding

The best polyimide for thermosonic bonding over active areas on IC chips was found to have the highest elastic modulus, E (stress divided by the strain, below the elastic limit) [9-33]. This material property is related to the stiffness of the polymer and, therefore, should be correlated with cupping, or indentation, of the material during bonding. (The compression modulus in an anisotropic material should give a better indication of softness, but the tensile modulus is often the only

modulus property measured.) The total deformation of an unsupported pad and the polymer during the bonding process was shown in Fig. 9-14 results in the absorption of considerable ultrasonic energy. Such deformation can also result in delamination/rupture of the bond-pad metal from the polymer [9-32]. Elastic modulus data for several substrate polymers are given in Table 9-4. These values range from about 0.5 to 30 GPa. Values on the high end come from harder materials, which will better support a bond pad and, therefore, inhibit cupping during bonding. Polymers having low-modulus values require thicker layers of hard metal (e.g., 4 to 12 μm of Ni) and possibly larger area bond pads to prevent them from sinking into the soft polymer under the bonding load.

Material	Elastic modulus (E) GPa @ (25°C)	E, GPa @(T°C)	Glass Trans. (T_g) T°C	Reference
FR-4	23, varies by mfg. and meas. direction, range 11–25	21 (100); 15.4 (150)	115–125	Fu, Brown, Ume Ref. [9-38]
Epoxy-glass (BT)	17	–	>170	Manufacturer
Epoxy-Aramid-Paper filler	30	–	194	Sanyu Rec Co., Ltd, Osaka,
Polyimide (unfilled films)	2.5 (flex, films) 7–13 (used as Si chip coatings)	2.0 (200)	–350	E. I. Dupont, Various Mfg., and Ref. [9-33]
BCB	~2–2.5	~1.4–1.8 (200) cure-dependent	>350	Dow Chemical, Midland, MI and Ref. [9-39]
PTFE composite (filled)	0.5–0.9 (ceramic) 1–1.3 (glass micro)	0.45–0.49 (100)	>300, if any, minor trans. ≈75	Rogers Corp., Chandler, AZ, others

[a]Some E values depend on the type of filler and the axis chosen for measurement. Values, therefore, are considered typical. Polyimides and BCB may change properties with different cures. Values obtained from manufacturers' literature, except as noted.

Table 9-4 Modulus for Several Electronic Packaging Polymers[a]

For comparison with polymers, Table 9-5 gives the properties of the metals often used (in combination) for bond pads on them. Note that the modulus of Ti is too low to explain its successful use in supporting Al pads on polyimide over Si chips [9-6, 9-7]. However, both the yield strength and the hardness appear to be good indicators of the bond pad's ability to prevent plastic deformation (cupping) during bonding. The yield strength has been used in a finite-element model with general agreement to observations of cupping, that was illustrated in Fig. 9-14. From Table 9-5 it is apparent that both electroplated and electroless Ni and Cu can have a wide range of yield strengths and hardness. The consequences are that the extent of cupping, for a given metal thickness, will depend upon the specific properties of the metal films in use. As an example, electroless Ni with 1 to 3% P will have much higher yield strength than with 8 to 12% P. The quantitative effect of ultrasonic energy on the softening of both the polymers and the metal layers is a major unknown. Little information is available on this subject. Aluminum, Cu, and Au soften significantly with ultrasonic energy (see Chap. 2) and bond (weld) readily. Nickel, Ti, and W do not soften at normal ultrasonic bonding energy densities and therefore should make good rigid platforms during

Metal	Modulus GPa	Yield Str. MPa	Micro-hardness (Films) kg/mm²	Brinell hardness (Bulk) kg/mm²
Al, 1% Si	70	35 (anneal dependant)	50–120	30
Au	80	low, 1–3 (dopant and anneal dependant)	40–100	30
Cu	130	27–40	140–170	35
Ni	207	60–130+	450–800 EL 150–800 EP	75
Ti	**110**	140		200
W	410	140	460	365

[a]EL is electroless and EP is electroplated (films). Most values are for bulk samples at room temperature and are considered indicative only. (For example, Ti values are sensitive to oxygen and nitrogen content, electroless Ni is sensitive to P content, etc.) *Values from Mechanical Behavior of Materials*, by McClintock and Argon, Addison-Wesley, 1966, and *ASM Metals Handbook*, Vol. 2, 9th ed. Also Safranek, W. H., *The properties of Electrodeposited Metals and Alloys*, 2d ed., ASEF, 1986.

Table 9-5 Selected Properties of Metals Used on PC Boards and "Soft Substrates[a]"

bonding. Nickel has much lower yield strength and hardness than Ti and W, but is higher than copper. As such, Ni should require thicker layers to stiffen a bond pad, which has been observed (3 to 8 μm Ni vs. 0.3 to 0.5 μm Ti or Ti-W). (Note: very thick Ni-plated layers on fine-pitch pads may produce nodular or rounded bonding surfaces that can lower autobonder yield.)

Many HPS substrate materials have anisotropic (directional) characteristics and/or ones that vary with the type of filler or lamination [e.g., some PTFE substrates may have compressive moduli of ~1 GPa at 23°C for microparticle fills (either ceramic or glass), but ~10 GPa for woven glass fills]. The latter should be better for wire bonding. In some cases (e.g., flex PI, some filled polymer substrates), the metal films have been bonded to the substrate by a different polymer (i.e., acrylic, T_g ~45 to 55°C), and this layer can be of significant thickness (~25 μm). The various polymer-based glues often have relatively low values of thermo-mechanical properties (i.e., T_g and melting point, modulus <50% of PI films, etc.), and these can limit the wire-bonding temperature and affect other bonding characteristics as much or more than the known substrate properties. (Note also that any tiny air bubbles remaining in the glue layer under the pad that do not otherwise present problems may inhibit wire bonding [9-40].) Often, the material characteristics of the glue layer are not readily available to polymer-substrate assembly personnel and, in fact, may not be considered by them when purchasing the substrate. High-T_g glues are available, but direct-bonded Cu is better for wire bonding than gluing with a different polymer on flex substrates.

The temperature characteristics of the substrate must also be taken into consideration when TS bonding at high temperatures. As the polymer's T_g is approached, the modulus decreases (the material becomes softer), and this can affect bonding by offering less resistance to dynamic sinking by a relatively soft- or thin-metal pad. An example of this ($>T_g$) softening on the most frequently used PC board material, a low-temperature FR-4, is given in Fig. 9-17 [9-38]. Equivalent data were not available for other epoxy-based board materials, but they should have similar shaped curves, being displaced toward higher temperatures for higher T_g. Note that the modulus value of the FR-4 board (above) at 150°C is ~15.5 GPa, which is still considerably higher than PTFE boards and PI (on flex or as-deposited films). We note, however, that the imbedded glass fiber limits the lowest value on the right of the curve. Without its support, the modulus would be only a few GPa (see Fig. 9-16 for a cross-section of typical PC boards).

A new measurement is needed that would better reflect the resistance to bond-pad cupping. The compressive modulus of anisotropic materials is better than the tensile elastic modulus but, even when available, is not the optimum measurement. If a small bond pad happens to be located over an area of voids between the woven-glass fiber bundles in Fig. 9-16, the board will be locally softer above the T_g,

and no general modulus measurement will reveal a problem. A better measurement could be made by recording the depth of depression, of a ball-type probe, into the bond pad, the glue film (if any), and the polymer substrate, by a given force. It should be measured as a function of temperature and would reflect the overall material properties related to wire bonding much better than a modulus measurement of the polymer substrate alone.

Bonding Optimization

Other actions that can improve bonding over polymers are using *finer diameter wire* (e.g., 18 μm vs. 25 μm diameter), and making *smaller balls* if ball bonding. These permit bonding with *lower machine parameters* (force/power) and thus reduce dynamic cupping, everything else being equal. If using US Al wedge bonding, then the same result will follow from using a softer wire (12 to 14 gm vs. 16 to 18 gm breaking load for 25 μm diameter wire) and/or smaller diameter wire. In general, it is easier to wedge bond with Al wire at room temperature than to use Au wire (wedge or ball) at high temperatures because of the polymers' softening, especially if any glue layers are under the metallization. It is also slow and difficult to conduct heat from the heat-stage through a relatively thick glass-filled polymer and obtain even temperature distribution over an area. However, the specific material properties of the polymer(s) in question should be considered before making such decisions. Often, Al wedge bonding at 25°C can be accomplished on epoxy-laminate substrates (e.g., FR-4) without special thick or hard bond-pad structures. Because the problem in bonding to small-bond pads is related to sinking, which dynamically changes the bond-interface force until it stabilizes, some improvement should be realized by delaying application of US power as discussed above. This delay time should be empirically determined for each type of substrate at its bonding temperature, while approaching its T_g.

Wedge-bond machine parameters for bonding to pads over polyimide-type substrates have been compared to those for bonding to pads over ceramics. If all machine variables were held constant, then bond-pull strengths will be lower (particularly low-modulus ones), compared to normal ceramic bonding. In other examples [9-32, 9-33], when ball bonding to Al IC chip pads over PI, even with 0.5 μm of Ti under the pad, a higher bonding force was found to be necessary (≈110 versus 80 gf). In addition, it was found that bonding to Au/Cu (with no hard Ni) pads on 90 μm thick PI required 350 ms versus 50 ms compared to bonding over ceramic [9-41]. Also, more power was required. The long bonding time may have delayed most of the welding until sinking and any load-induced cupping had stabilized. This is another option if the bonder has no adjustable delay in applying the US energy after tool touchdown.

High-volume, high-yield wire bonding on very soft substrates may require the combined use of high-frequency energy, pad metallurgy

optimized for bonding (i.e., soft bondable gold), DOE-machine set up, delayed application of US energy, and plasma or UV-ozone cleaning before bonding. Certainly, a full understanding of all normal bond reliability and yield issues is required, as discussed in this chapter and elsewhere in this book.

9.2.6 Additional Considerations When Using Wire Bonds in Packages Running at High Clock Rates in High-Performance Systems (HPS)

Inductance of Wire Bonds

Flipchips have the lowest inductance of any chip-interconnection method. However, short wire bonds have long been used in circuits operating over 1 GHz. A simple calculation, based on classical formulas for the self-inductance of a straight wire, can easily be made and gives a *quick estimate* that is adequate for many computations. (FEA modeling can be used for an exact solution.) Such an equation was given years ago by Terman [9-42] and is in modern electrical engineering handbooks as well.

$$L = 2 \times 10^4 \times \ell \times (\ln [4\ell/\mathrm{d}] - 1 + \mu\varepsilon) \qquad (9\text{-}1)$$

where L is inductance in nanohenries, ℓ is the wire length, d is its diameter (both in μm), and μ is the permeability (assumed to be 1). The skin-effect correction factor, E, is a function of wire diameter and frequency. For 25 μm and 33 μm diameter Au wires at 1 GHz, its value is approximately 0.07 and can be neglected. For low frequencies, <100 kHz, E is 0.25. Larger diameter wires produce slightly smaller values of inductance. From Eq. (9-1), it can be seen that a wire bond has an inductance of approximately 1 nH/mm. A graph of measured values of bond inductance and mutual inductance is shown in Fig. 9-18 [9-43]. This figure includes values of both self- and mutual-inductance from nearby wires. Parallel signal wires were also shown to reduce the inductance somewhat. Another technique is to use special interspaced ground and signal wire structures with 50 Ω terminations to achieve performance at 2.4 GHz or higher [9-44].

The most important consideration in using wire bonds for high clock-rate packages is to design them as short as possible (~1 mm long). This can be accomplished by thinning the chips, recessing the chips, and placing the pads on the package-/board-substrate as near to the chip as practical, which usually means no long diagonal bonds.

9.2.7 Skin-Effect in Typical Package/Board Conductor Metal Structures

In most wire-bonded systems, it is necessary to have metallization structures consisting of two or more metal layers, as described above

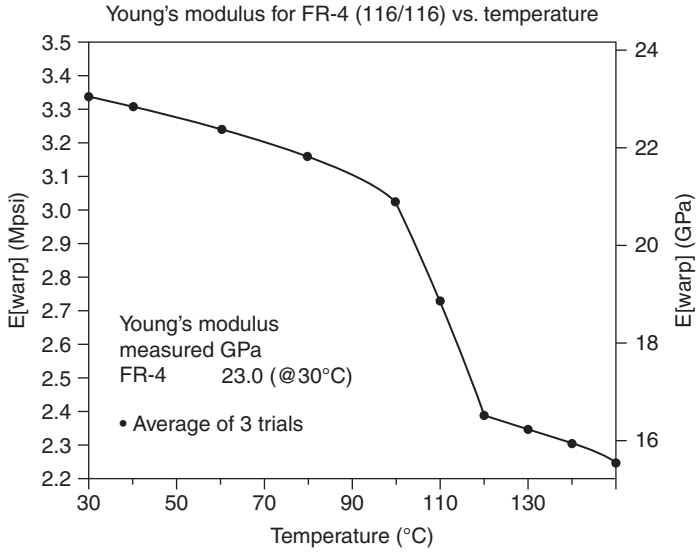

Figure 9-18 A typical plot of Young's modulus as a function of temperature for FR-4 glass-laminated epoxy printed-circuit boards. This particular board had a T_g of ~110°C, but different manufacturers' FR-4 boards T_g can vary up to approximately 140°C [9-38] (© IEEE).

and shown in Fig. 9-15. The primary conductor is typically Cu or Al, but the structures may include a layer(s) of resistive (lossy) conductor(s) such as Cr, Ti, Pd, W, and/or Ni, the latter being both lossy and magnetic. These lossy layers are applied to serve several purposes in high-performance boards. These purposes may be to improve adhesion of the primary conductor to the polymer, to provide corrosion protection, and, in some cases, to act as a diffusion barrier. If thick enough, they also improve bondability by providing a rigid, noncupping bonding platform as discussed above.

The resistive layer or film can result in skin-effect losses at high frequencies, assuming that the same metal structure is used to conduct the signals. The extent of these losses will depend upon both the metal-film properties, its thickness, and its position with respect to any ground plane. From Fig. 9-15, if the resistive metal film lies between the primary conductor and the ground plane, the current will concentrate in that film, and losses will occur in the gigahertz-frequency range. See Table 9-6 for a listing of skin depths for metals used in high clock-rate conductors. These will depend upon the film-resistivity thickness and magnetic properties. Adhesion and corrosion-prevention layers can be quite thin (~1000 Å) and, if so, will introduce negligible losses [9-45]. However, the layer must be relatively thick (3000 to 4000 Å for Ti) to act as a rigid platform for bonding on a soft substrate. At some combination of thickness and frequency, the skin effect will result in significant

Metal	Resistivity (μΩ-cm)	Skin depth, δ (μm) at Frequency			
		1 GHz	10 GHz	20 GHz	40 GHz
Aluminum	2.65	2.59	0.82	0.58	0.41
Chromium	12.9	5.71	1.81	1.28	0.91
Copper	1.67	2.05	0.65	0.46	0.33
Gold	2.35	2.43	0.77	0.55	0.39
Nickel[b]	6.84-(*60*)	0.59-(*12.3*)	0.19-(*3.9*)	0.13-(*2.8*)	0.093-(*1.9*)
Titanium	42.0	10.3	3.26	2.31	1.63

[a]Values from Ref. 45 but with Ni corrected for (permeability) and all metals recalculated for 40 GHz (© IEEE).

′$\delta = (\rho / f \times \mu \times \pi)^{1/2}$ where ρ = resistivity, f = frequency, $\mu = 4 \times \pi \times 10^{-7}$.

[b]Range for Ni is calculated with a permeability of (*50*), first number for bulk Ni, and second number (in parenthesis) for high-phosphorus electroless Ni. Lower phosphorus content gives intermediate permeability values. All electroless Ni resistivity values are much higher than bulk Ni values and resistivity must be changed for calculations, due to *P* and other impurities.

Table 9-6 Skin-Effect Depth for Typical MCM Metallizations as a Function of Frequency[a]

electrical losses! These losses can be avoided entirely if the hard-lossy metal layer is confined to the bond-pad region. To do this, the bond pads must be processed separately from the rest of the signal conductors, with some cost penalty. Alternatively, the signal could pass through a via to a good-quality conductor below the surface.

Most PCBs have the hard-resistive layer (usually Ni) on top of the primary conductor (usually Cu). Assuming that a ground plane lies below, as shown in Fig. 9-15 (without the hard under-layer), this will not cause skin-effect losses at high frequencies. The skin effect and other high-frequency losses in HPS have been extensively studied [9-45, 9-46, 9-47].

9.2.8 Conclusions

The solutions to increased wire-bond yields on pads over soft substrates are to increase the bond-pad metal thickness and area and apply a hard-metal underlayer (e.g., ~0.3 μm thick Ti), a hard-metal top layer (e.g., 3 to 8 μm thick Ni), or some combination of these, capped with a highly bondable metal (e.g., Al or Au). This converts the pad into a rigid platform that does not "cup" or "sag" during bonding. Most workers using stiffened pads report that essentially "normal," or with ~10 to 20% higher than normal, bonding parameters are required for various soft substrate bonding. The material properties of the polymer were discussed, and bonding was generally correlated to the elastic modulus of the polymer or

laminate and to the yield strength of the metal bond-pad layers. The higher these values, the more rigid the material and the less cupping during bonding for a given pad structure. If the polymer has a low modulus (or is bonded near its T_g), then the pad must be larger to prevent it from dynamically sinking into the soft material or the application of the US energy should be delayed (5 to 10 ms) until the pad sinking has stabilized. Sinking, as well as cupping, can lower the bond yield. Thus, the material properties are at least as important as the actual bonding-machine set up in achieving high-yield bonding on soft substrates. Even when using the above solutions, high-yield bonding will occur only if the best metallurgical, bonding, and cleaning (UV-ozone or plasma) procedures are followed, as given in Chaps. 5, 6, and 7.

9.3 Wire Bonds in Extreme Temperatures/Environments*

9.3.1 Introduction

This is a brief introduction to the materials and requirements for wire bond interconnections that can be used in packaging chips for extreme high- and low-temperature (HTE and LTE, respectively) environments. Devices capable of operating in these environments are needed for future space probes on other solar system planets, well-logging, geothermal measurements, sensors near rocket and jet engines, automobile engines, etc. Modern SiC and other high-temperature devices are capable of operation up to 500°C, although packaging materials/technology for such high temperatures can be both challenging and expensive! The normal metallurgy used for Si chip interconnections, Au-Al (wire bonds, aluminum metallization) fail in *HTE*, but generally can be used in *LTE.* The required material changes, such as Au-Au, (or other noble and monometallic interfaces), substrate/chip CTE matching, etc., are necessary for systems to survive in these thermal and changing-temperature environments. Some of the concepts/problems below are described in Chaps. 2 and 5, and in the literature [9-48, 9-49, 9-50, 9-51, 9-52]. Reference [9-48] is a comprehensive overview of materials, and wire bonding for extreme environment devices.

9.3.2 High Temperature Interconnection Requirements

The most commonly used Au-Al wire bonds should be avoided in the *HTE* range, along with any other metallurgical interfaces that form brittle intermetallics and/or Kirkendall voids. Gold-gold bonds can improve with time and temperature rather than degrade (see Chap. 5,

*Part of this material is from a chapter in: Suhir, E., Lee, Y. C., and Wong, C. P., *Micro-and Opto-Electronic Materials and Structures*, Springer, 2007, Vol. 2, Chapter 4, Harman, G. G., *Metallurgical Interconnections for Extreme High and Low Temperature Environments*, pp. 121–133.

Fig. 5-16). Therefore, a clear preference is given for high-melting point monometallic interfaces or metals that form solid solutions—gold (or other noble metals) in the HTE environments for both wire and flip-chip bonds. Gold bumps/balls can be used in place of the normal solder-ball flip-chip interconnections. Such chips can be ball-bumped or stud-bumped to Au pads, and the entire chip thermocompression/thermosonic bonded to gold metallization on (matched CTE) ceramic substrates. This results in reliable HTE flip-chip interconnections (provided the chip and substrate have approximately matched TCEs, with the substrate a little higher than the chip).

Metallurgical fatigue damage to wires can occur during large ΔT temperature/power-cycling in both HTE and LTE. Also, deep well-logging, and sensor applications can be cycled through wide temperature ranges. McClusky [9-50, 9-51] has reported that high-temperature-annealed Al wires have decreased fatigue life as well as the wire interconnection integrity, even if the bonded interface (the bond nugget) remains strong. In this case temp-cycling went up to 200°C. No data exist for higher temperature cycling of large (or any) diameter Al round and ribbon wires. One could assume that large ribbon wire, since it is flexible in the plane of the bond loop, will have a longer fatigue life at high temperature than equivalent cross-section/metallurgy round wire. An example of large-diameter Al wire fatigue was shown in Chap. 8, Fig. 8-19. Large-diameter

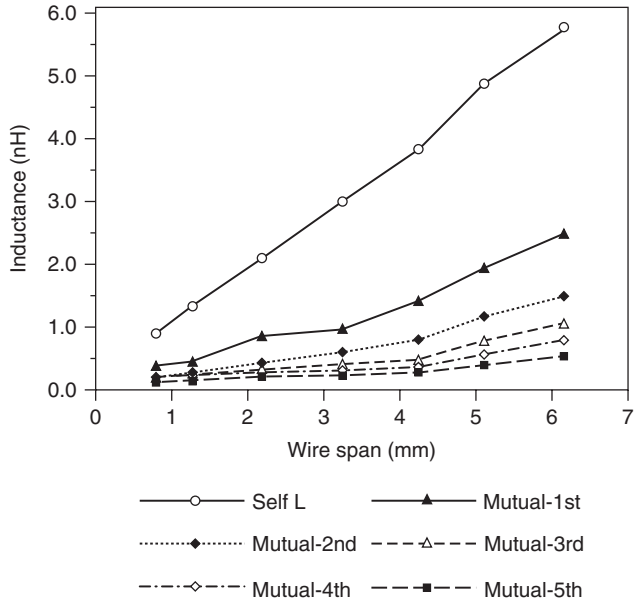

Figure 9-19 Gives plots of both self- and mutual-inductance of wire bonds as a function of wire span [9-43] (© IMAPS).

round wires are stiff, and stress is concentrated at all bends and at the weld attachment (bond heel), where the fatigue failures usually occur. Small-diameter wire (e.g., 25 μm) is flexible, and most fatigue stress is applied to the heels of the bonds, where the failures occur. A variety of factors (wire diameter, shape, loop height, metallurgy, including additives/dopants, and strain-rate) determine the fatigue susceptibility and life of a wire bond (high, smooth loops and *low*-bond deformation give best protection against fatigue, for fine-diameter wires). Gold wire is more fatigue resistant than Al wire at typical thermal cycle, low-strain-rates, and temperatures up to 125°C [9-53]. No equivalent data are available for higher temperatures.

In HTE (but not LTE), the current carrying capacity of wire bonds must be appropriately derated to avoid burnout. Al wire (with its 660ºC melting point) must be derated more than Au (melting point 1064ºC). HTE will result in annealing *small-diameter* Al wires causing the breaking load and bond-pull strength to decrease to less than 30% of their initial values. *Large-diameter* Al wire (≥100 μm) is normally annealed when produced, so its breaking load will decrease only slightly. Aluminum-aluminum or Al-Ni welded bond interfaces will remain strong at high temperatures, so any annealing of the wire (tensile strength decrease) is not normally considered a reliability problem. However, its temperature-cycle fatigue-life may be shortened, as above [9-51], and this must be determined before implementation. Gold wire for ball bonding is already annealed, and its strength will change minimally. However, the strength of small-diameter gold wire used for wedge bonding will anneal (soften), but less than equivalent Al wire. Little work has been done to determine the effect of high-temperature cycling on fine-diameter Au and Al wire fatigue. Temperature studies, up to 125°C, have shown a general decrease in fatigue lifetime with temperature, and also a significant dependence on strain rate [9-53]. (See comments in Chap. 3.) Modern gold wires have special stabilizing impurities, and it is assumed that these improve the high-temperature fatigue life from the past studies; however, typical aluminum wires are unchanged from the past.

Platinum wire is used in HTE, but it requires high-bonding force and work-hardens significantly during US wedge bonding, similar to Cu (Chap. 3). Wedge bonding with it can crater SiC, one of the hardest known materials [9-49]. Pt and Pd have much lower electrical conductivity, only ~20% of Au or Al, as well. In general, Pt and Pd wedge bond best at high temperatures (≥300°C) (thermosonic bonding). Both can be ball bonded, but little information has been published on that. Sometimes Pt and Pd are used in LTE systems *because* of their *low thermal conductivity* (~20% of Au). In the 75 to 150 μm (~3 to 6 mil) diameter range, Pt and Pd may be welded to substrates and packages by electrical discharge methods, if appropriate for an application (see Chap. 2).

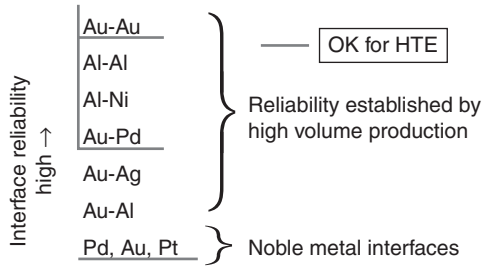

Figure 9-20 Metallurgical interfaces that can be used reliably in both extreme environments. All are acceptable for LTE. However, only the underlined/boxed ones are acceptable for HTE.

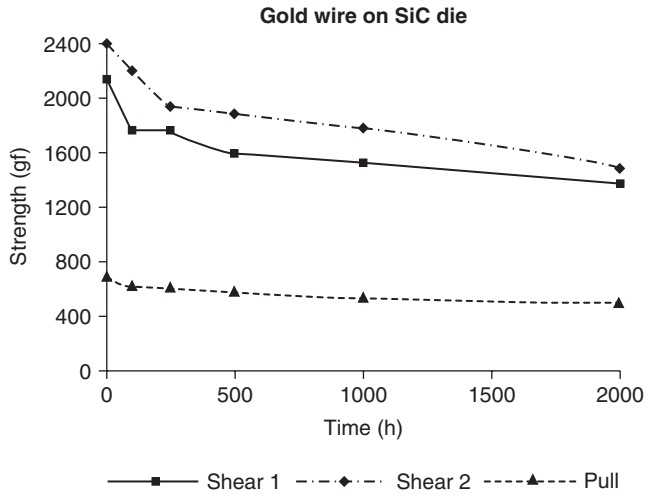

Figure 9-21 Average pull/shear strength of 250 µm diameter Au wire, wedge bonded at 225°C to Ti/Ti:W/Au die metallization (Au plating was 3 µm thick), as a function of storage time at 300°C [9-49] (© IEEE).

An overview of metallurgical interface (bonding) reliability for both HTE and LTE is shown in Fig. 9-20.

Examples of gold bond interface lifetimes, stored at 300°C, were given by Johnson as shown in Fig. 9-21. This stable life is in agreement with discussions in Chap. 5 for Au-Au bonds.

9.3.3 Low-Temperature Environment Interconnection Requirements

For LTE and intermediate temperature ranges, up to about 125°C, conventional interconnections (Au and Al wire bonds) to Al chip metallization (bond pads) are acceptable. One would not use a normal

Component	Material	CTE (ppm/°C)	Thermal Cond. (W/cm-°C)
Chip	Si	2.6	1.57
	SiC	1–3 (T-dep)	~5 (>T dep)
	GaN	~3	1.3
	GaAs	5.7	0.48
Substrate	SiC	1–3	0.8–2
	Si_3N_4	2.5–3.3	0.3–0.6
	AlN	4.6	1.75
	Al_2O_3	~6	0.35
	BeO	~6–7	~3

Components should be chosen to minimize thermal expansion differences. In the table, similar color chip and materials are appropriate matches.
(Color distinctions wash out in B & W and should be checked in the color CD.)
Note: *thermal-conductivity values can/will change at low temperatures and exact data may not be available. (Data from SRC-CINDAS.)*

Table 9-7 Some Material Properties of Chips and Substrates for Use in both High and Low Temperature

laminate substrate, but rather a ceramic one. See Table 9-7 for some material property choices in designing packages. Components should be chosen to minimize the expansion differences for temperatures down to about 55°C.

9.3.4 Packaging Effects at Extreme Temperatures

The packages for HTE will usually be made of metal/glass/ceramic (classical hermetic hybrid packages). Package reliability problems from hysteresis, creep, and/or cracking of normal glass-metal seals (Kovar-glass) in hermetic packages can cause failure during temperature cycling in both HTE and especially in LTE. The glass-metal seals undergo expansion/contraction hysteresis possibly resulting in cracking or delamination in the range starting below −100ºC. In HTE, any leads extending through the softened glass seals, at ~300ºC, will yield under mechanical stress resulting in possible damage to any wire bonds connected to them. Diffusion processes generally follow the Arrhenius equation and will be greatly accelerated in HTE. Possible failure of metal adhesion layers between gold metallization and ceramic, as well as any diffusion barriers under/over the chip metallization, must be considered as potential reliability hazards that could weaken wire bonds attached to them.

Although chips used in LTE can be Si based, those used in HTE will not be. Most likely they will be SiC or possibly GaP, GaAs, with Si-Ge being used in the low HTE range. Their metallization will most

likely be complex layers with noble metals and diffusion barriers between the chip and the conductors. The die attach for HTE will have to be metallurgical rather than polymer (epoxy), as currently used on normal devices. In some intermediate temperature ranges, silver-glass (maximum T ~350ºC) may be an acceptable die-attach material. For SiC chip die attach, some possibilities could be Ni/Ti/$TaSi_2$, Ti/$TaSi_2$/Pt, Ni/Ti/Pt/Au, or Au-Sn. Currently, neither these nor any other die-attach materials have been qualified for HTE (up to 500ºC). Thus high-temperature wire-bond development is far more advanced than die attach and other packaging materials/technologies.

9.3.5 Summary

The material properties and requirements for wire bond and Au ball-bumped flip-chip interconnections that can be used in packaging chips for extreme high- and low-temperature environments [from ~500°C (HTE) down to about –100°C (LTE)] have been described. The most commonly used Au-Al wire bond interfaces should be avoided in the HTE range, along with any other metallurgical interfaces that form brittle intermetallics and/or Kirkendall voids. Gold-gold bonds (and other noble metals) are stable or improve with time and temperature (see Chap. 5); thus a clear preference is given for gold (or other noble metals) in the HTE environment for both wire and flip-chip bonds. Monometallic interfaces, such as Al-Al are also reliable. For LTE, and in intermediate temperature ranges, conventional interconnections (Au-Al wire bonds) to Al-chip metallization (bond pads) are acceptable. (Also, normal flip-chip solder bumps are acceptable, without plastic under-fill.) Information on other materials, such as CTE matching between chip and substrate, was given. It is concluded that, with the proper selection of materials, interconnections can be reliable over a wide range of extreme temperature environments. For an overview of the entire high-temperature electronics field see Kirschman [9-54].

Appendix 9A Wire Bonder Looping

Process Solutions Consulting. New Tripoli, PA 18066, email <levilr@ptd.net>

By Lee Levine

9A.1 Introduction

In its simplest form a wire bond is a segment of wire interconnected (bonded) at each end to allow completion of an electrical circuit. The segment of wire between the bonds is called the loop. Historically ball-bond loops were 10 to 15 mil in height with a smooth, unstressed shape. As wire-bonding machines were automated, producing

low-stress loop shapes without stretching the heat affected zone (HAZ) directly above the ball became more difficult because the dynamics of automated machines were different from manual, operator-controlled machines. The HAZ is the region above the ball that was heated by the melting of the wire that formed the ball. Its properties are significantly different from the bulk wire because the heat recrystallizes the grain structure and recrystallized grains are weaker than the cold worked grains in the wire. Controlling the chemistry of the 99.99% (100 ppm residual trace elements) became necessary to both refine the grain size in the recrystallized HAZ and provide additional strength. The addition of Beryllium in the 7 to 10 ppm range provided these properties and allowed the development of high-speed automated wire bonders. Today all 99.99% gold bonding wire is alloyed within the 100 ppm residual impurities range. However, some special purpose wires can have a higher level of dopant than this (not 99.99/Au). Each wire manufacturer has a variety of alloys with different properties tailored to provide optimized performance for difficult applications. Specialized machine motions were developed to mimic the behavior of manual machine operators. Observations that manual machine operators often made a motion away from second bond after forming the first bond lead to the development of the reverse bond motion. Bending the wire in the HAZ cold works the wire, changing its mechanical properties. Specific bending motions, such as reverse motion bending (bending first away from and then toward second bond), are used to control final loop height and shape and to reduce sag near second bond. Pulling the wire just before bonding the second bond straightens the wire and reduces the final loop height.

Currently state-of-the-art packages have wire pitch (the distance between adjacent wires) of 30 μm. The demands of fine-pitch bonding in turn drive the requirements for longer wire length, smaller wire diameter, smaller capillary tip diameter, straighter wire loops with less sagging, and better machine motion control. Because fine-pitch devices typically have more wire interconnections they require faster bonding motions and higher acceleration to maintain productivity and profitability. These demands have been met by continuously studying the wire-bonding process; wire, tools, hardware, and software. All have been continuously improved through the use of designed experiments and advanced analytical tools that have enabled improved process controls and enhanced capabilities.

9A.2 Machine Motions and Trajectories

Wire bonders move in smooth, continuous, coordinated motions, with all three axes (X, Y, and Z) moving simultaneously. Wire is fed through the capillary and bent by the machine motion to provide the required shape. Motions are calculated on the fly and adjusted so that each machine axis travels along a precisely calculated trajectory.

Motion trajectories must be controlled and coordinated to within only a few microns of tracking error. A variation of a few microns can significantly affect loop shape and repeatability. Wire payouts and bends need to be adjusted on the fly to account for changing wire lengths caused by die placement variation. All this needs to be accomplished while bonding up to 16 wires/s, with acceleration rates exceeding 12Gs in XY and 150Gs in Z. The latest wire-bonding equipment employs new, faster, and more accurate servo controls, which enable more repeatable looping and more complex shapes. The simplest standard wire-bond loop employs four separate motions from the ball bond to second bond. The formation of more complex loop shapes may employ more than 12 motions. Kinks, bends, flat segments, and smooth curved portions are all formed by programmable loop parameters within the software. Wire lengths are controlled and adjusted based on both the modeled loop shape and actual calculated distances between the ball and second bond. As each die is indexed to the bond site, the machine vision system uses pattern recognition to locate the die and leads. Machine intelligence, then, corrects the location of each bond and adjusts the metered wire length for repeatable loop shape and height.

Accurate servo controls enable more repeatable looping and more complex shapes. The simplest standard wire-bond loop employs four separate motions from the ball bond to second bond as shown in Fig. 9A-1. The formation of more complex loop shapes may employ

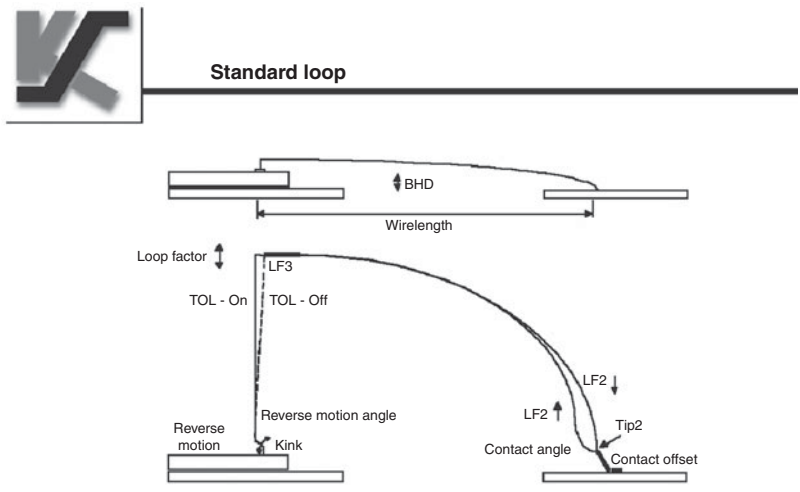

Packages: QFP (<170 mil wire), discrete
Status: Common basic loop shape
Motions: 4 XYZ between first and second

Figure 9A-1 The formation of a standard loop.

more than 12 motions. Kinks, bends, flat segments, and smooth curved portions are all formed by programmable loop parameters within the software. Wire lengths are controlled and adjusted based on both the modeled loop shape and actual calculated distances between the ball and second bond. As each die is indexed to the bond site, the machine vision system uses pattern recognition to locate the die and leads. Machine intelligence, then, corrects the location of each bond and adjusts the metered wire length for repeatable loop shape and height.

9A.3 Loop Shaping

The main reasons for shaping a wire loop are to provide clearance and avoid interference (electrical short circuits) from adjacent wires as well as from the die or substrate. Some wedge-bonding applications demand controlled impedance where the wire length, height, and shape are controlled to tight tolerances. The shape and features of the wire, the wire "loop," have changed significantly over time as machine capabilities and device requirements have evolved and package density has increased.

9A.4 Prebending, Cold Work During Looping Trajectory

Bonder motions within the HAZ can be used for cold working and bending functions. Standard wire-bond loops use a reverse motion in the HAZ to bend the wire away from second bond initially, cold working the HAZ. When the looping trajectory bends the wire in the

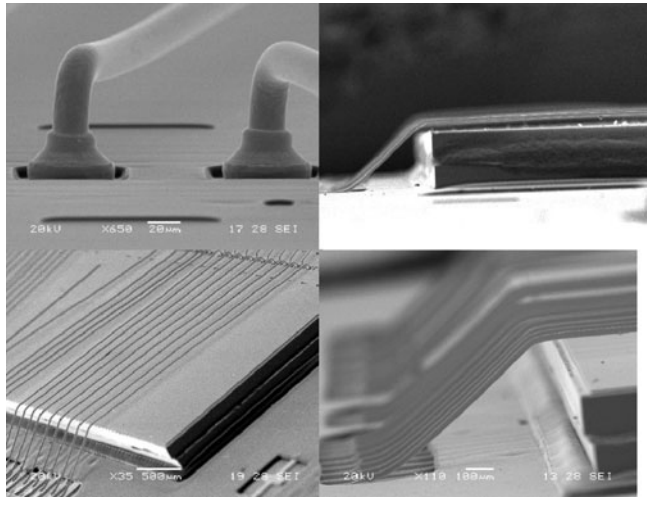

Figure 9A-2 Examples of long low loops. (*Courtesy of Oerlikon.*)

HAZ back into a vertical position, the cold worked HAZ will be stiffer and the wire loop will be more erect with less sagging than it would have been without the cold work from the reverse motion. Other motions can be used to provide additional bends in the wire, providing useful shapes. These shapes can provide additional standoff near second bond, as required in ball grid array (BGA) packages, with power and ground rings in the vicinity of second bond. They can also provide flat (parallel to the die surface) portions of the loop with sharp bends descending to the second bond, as in the chip scale packages (CSP) or worked loop. Wire stiffness needs to be optimized so that these bends can be produced uniformly. New wire types are being developed to provide both a high stiffness above the HAZ and a soft ball for improved bondability.

9A.5 CSP and BGA Looping

The ability to shape a wire-bond loop, with well-controlled bends and kinks, has been in continuous development for over 12 years [9A-1, 9A-2]. The first worked loop shape patents were granted in 1993 [9A-3]. These shapes enabled the development of the CSP loop. The CSP loop, with additional wire bends designed to provide buss bar clearance near second bond, evolved into BGA looping. Now, the demand for thin-profile, *stacked-die, and multichip packages* is pushing development of even lower loop height levels. Today's state-of-the-art wire bonders may offer the capabilities to support a library of as many as 20 loop shapes. Additional new loop shapes are continually being developed to accommodate packaging design requirements. Loop shapes within the bonder library have programmable

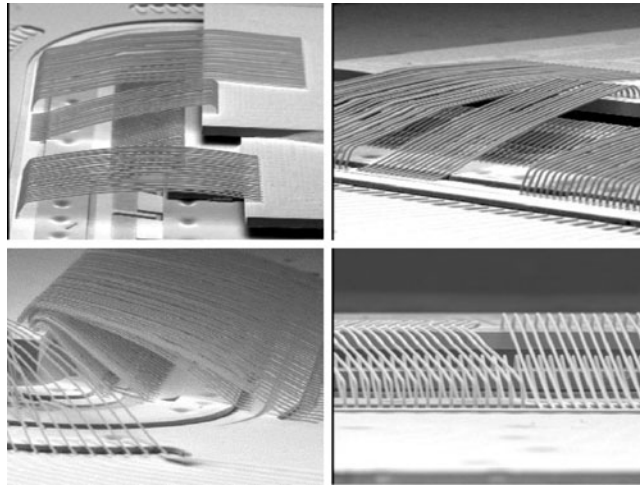

Figure 9A-3 Stacked die looping. (*Courtesy of K&S.*)

parameters that enable formation of the desired shape but also provide flexible controls for the large variety of packages that are encountered.

9A.6 Stacked Die and Multi-Chip Packages

The advent of stacked die packages has also placed new demands on wire bonders. More die layers need to be integrated into thinner and thinner packages. Production dice, commonly thinned to 100 μm thickness, are now down to 75 μm. Even 50 μm dice are being introduced into mass production. Stacked thin cantilever dice, with cantilever exposure of up to 5 mm, deflect significantly during bonding. This deflection effects bonding. Differences in deflection between bond pads located in the corner of the die and those located in the center of the die edge are large; therefore, bonding variability as a function of pad location has to be taken into consideration. In addition, finite element modeling (FEM) and high-speed video photography of the die deflection have enabled good understanding of this process and provided good working solutions to this problem. Time delays required for the die to deflect and recover are significant and reduce throughput.

Multichip packages often require several different type loops, at different second bond elevations (Z axis) within the same package. Often they require chip-to-chip bonding. Chip-to-chip bonding has a whole range of additional requirements because the capillary cannot touch the die face without damaging sensitive components on the die. The stand-off-stitch bond (SSB) is a sequence of three bonds that addresses this application. First a ball bump is bonded on Die 1 and terminated forming a new ball under the capillary. The second ball is then bonded to Die 2 as a standard wire bond. The second bond is then bonded on top of the bump bond on Die 1 completing the 3-bond sequence. The SSB is called a reverse bond because the ball bond is

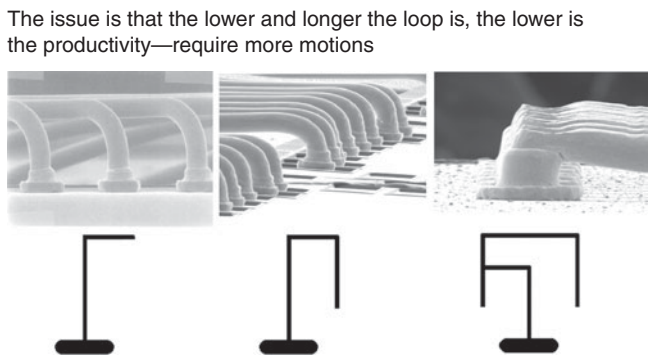

Figure 9A-4 Loop height reduction using the capillary. (*Courtesy of K&S.*)

normally on the lead and the second bond/bump are on the upper die. This avoids placement of a second bond directly on the die surface, which would be a reliability risk. SSB height is very low because the second bond and bump are normally on the upper die. However, bond speed for the 3-bond sequence is slower than standard bonding because of the additional process steps.

9A.6 Capillary Forming for Lower Loops

Recently, new forward bonded loop shapes have been introduced that can produce heights of less than 75 μm without sacrificing throughput. Achieving these ultra-low loop shapes is very important for the lowest die of a stacked dice package, especially when the wires are underneath an overhanging cantilever die. In this loop profile the ball bond is produced and as the capillary is moving from reverse bond position the capillary descends to the ball-bond surface, compressing the wire against the ball bond. The capillary then moves to second bond position and completes the second bond. This loop profile can achieve loop heights less than 50 μm with only a small throughput cost.

9A.7 Capillary Shape and Its Effect on Drag/Friction

Capillaries transfer ultrasonic energy to the bond and control weld size and shape. Their internal and external shapes and dimensions provide the necessary features that form the bond. They also are a source of friction during wire feed. Friction and drag are necessary to control the flow of wire and provide tension, but too much friction can break bonds and wire, stretch the ball neck in the HAZ, result in deformed loop shape, and scrape and tear the wire surface.

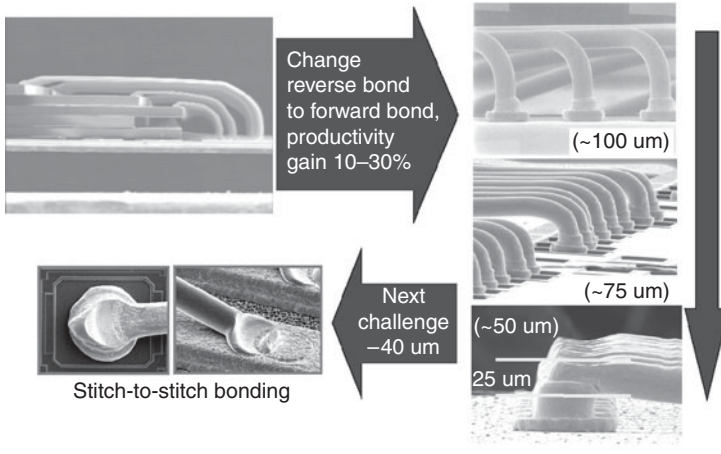

Figure 9A-5 Ultralow loops. (*Courtesy of K&S.*)

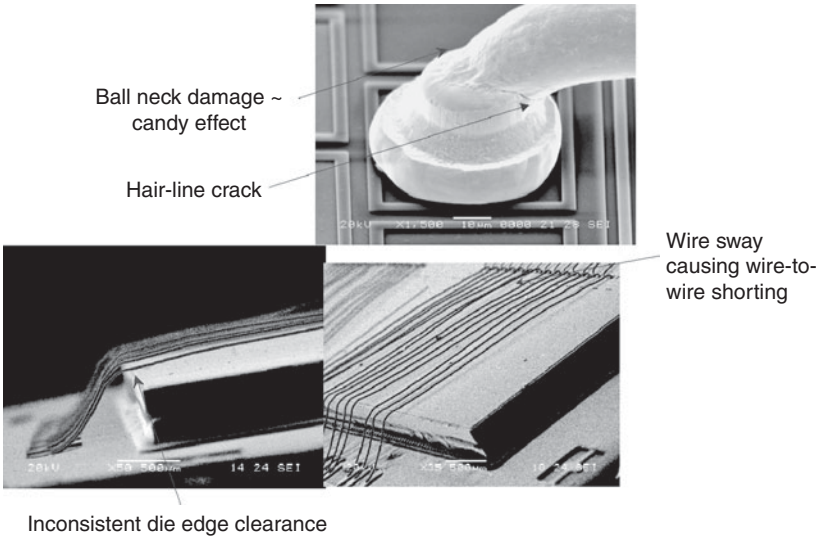

Figure 9A-6 Wire bond loop defects. (*Courtesy of Oerlikon.*)

Controlled low-drag capillaries, with design features optimized for long capillary life, can add value to the process. When implemented in the wire-bonding process, these unique bonding tools provide greater loop height control and shape stability, significantly reducing looping failures typically found on wires formed with a conventional capillary.

9A.8 Role of Wire

Wire properties play a significant role in a wire bonder's ability to produce accurate, repeatable loops. Over the years these properties have undergone continuous improvements to enable the production of the longer, lower, straighter loops required by today's packages. Gold bonding wire is normally specified as 99.99% (four 9s) purity, while chemistry within the residual 100 ppm impurities is carefully controlled to provide the required mechanical and electrical properties. New alloys that have recently been introduced to the market are in the high three-9s range to provide improved long-term reliability in very fine pitch (<50 μm ball diameter) applications without significantly sacrificing electrical properties.

9A.9 Ball and Stud Bumping

Ball and stud bumping can be classified as looping variants because the bonder terminates the wire above the ball without making a loop. There are three varieties of stud bumps. Normal ball bumps terminate within the HAZ because this region is the weakest region of the

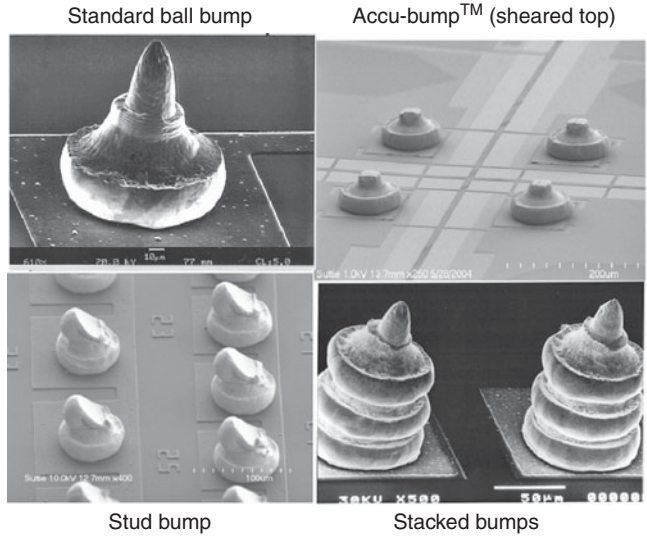

Figure 9A-7 Variants of bump bonding. (*Courtesy of K&S.*)

wire and the wire preferentially breaks in the weakest region. The bonder forms the ball bond and then rises to the correct height for a new ball, the wire clamps close, and the bond head again ascends to the EFO firing position. The wire breaks within the HAZ during this motion. Wire alloying can significantly affect the wire recrystallization temperature and have a large effect on the height and variability of the broken wire tip. An alloy with a higher recrystallization temperature will have shorter tails and less variability.

Newer bonders, with better Z axis control, are capable of forming the ball, rising a controlled distance of only a few microns, and then moving horizontally to shear the wire above the ball bond and produce a flattened bump. The additional motions require additional time but the process is still very fast (>20 bumps/second). Planarity is adequate for many applications.

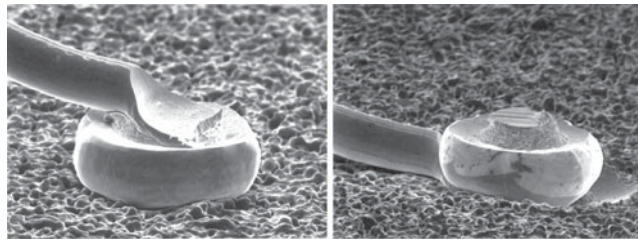

Figure 9A-8 Bumps for improved reliability. (*Courtesy of K&S.*)

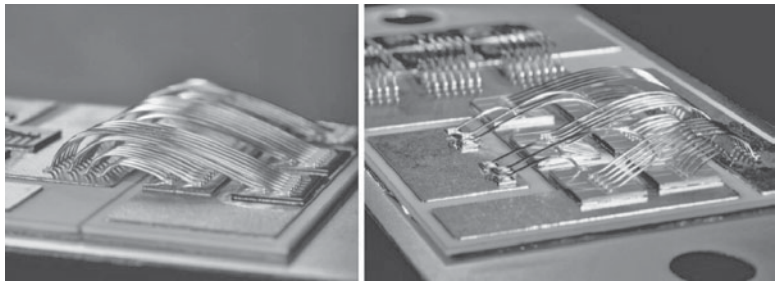

Figure 9A-9 Heavy wire wedge and ribbon bonding. (*Courtesy of Orthodyne.*)

Stud bumps are produced by first forming the ball bond; the head rises a short distance then descends and forms a second bond on the edge of the ball. The wire/loop has the appearance of a cotter pin with a total loop height of approximately 3 to 5 mil. In most cases stud bumps are dipped in a conductive adhesive for interconnection of the bump to the substrate.

Wedge bonding has required an additional machine motion axis in order to align the wedge tool, which is directional during bonding. This additional axis resulted in the wedge-bonding process being significantly slower and it also had less bond placement accuracy. Historically, both fine and heavy wire-wedge bonding had simpler motions, "H" or "trapezoidal" motions were most common. In an "H" motion the tool lifted straight up off first bond, moved to top of loop, moved horizontally toward second bond and then down. In a trapezoidal motion loop the tool lifted off at an angle, usually close to the angle of the tool feed hole, reached top of loop and moved towards second bond. At a programmed point the tool began an angled descent toward second bond. Recently more complex loop shapes, with pull-out motions near second bond and better axis controls, have become available. Bond shift is now available so that first and second bonds do not have to be as closely aligned as previously required.

Because of its low inductance and high current carrying capacity, ribbon wire is often required. Often in microwave, Rf devices design

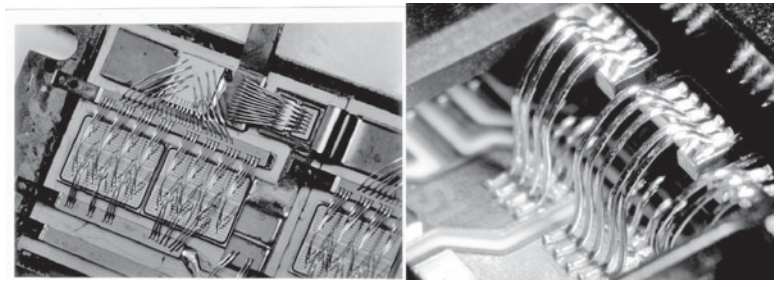

Figur 9A-10 Heavy wire wedge bonded modules. (*Courtesy of Orthodyne.*)

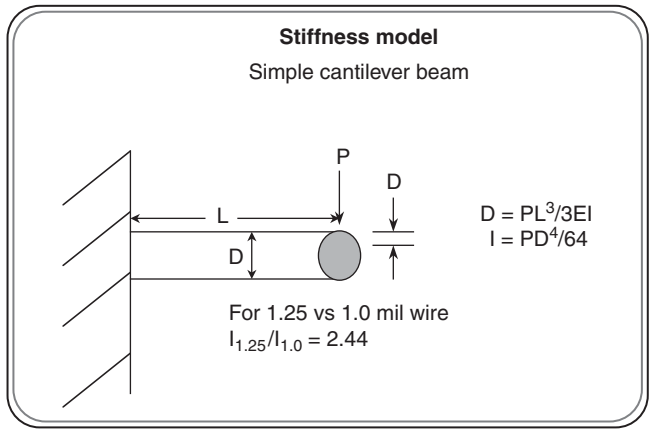

Figure 9A-11. Wire stiffness model.

criteria requires ribbon bonds that are nearly horizontal, the shortest length between first and second bonds.

Ribbon bonding is a variant of wedge bonding. Ribbon wire is normally produced by roll forming round wire to flatten it.

9A.10 Stiffness—Young's Modulus

Even though wire is thin, it should be understood as a structural element. The simplest model of a round cantilever beam provides adequate understanding of the relationships between the significant variables (deflection, length, diameter, material). Stiffness, defined as the resistance to deflection under a load, has a cubic relationship with length and a quartic relationship with diameter (a 10% increase in length will have a 33% increase in deflection and a 10% decrease in diameter will have a 46% increase in deflection). Wire chemistry and treatments can have a smaller effect on Young's modulus (E), but the effect is linear.

References

9-1 Harman, G. G., "Wire-Bonding-Towards 6σ Yield and Fine Pitch," *IEEE Trans. on CHMT,* Vol. 15, Dec. 1992, pp. 1005–1012.

9-2 Onoda, H., Hashimoto, K., and Touchi, K., "Analysis of Electromigration-induced Failures in High-temperature Sputtered Al-Alloy Metallization," *J. Vac. Sci. Technol*., Vol. A 13, 1995, pp. 1546–1555.

9-3 Puttlitz, A. F., Ryan, J. G., and Sullivan, T. D., "Semiconductor Interlevel Shorts Caused by Hillock Formation in Cu-Al Metallization," *IEEE Trans. on CHMT,* Vol. 12, Dec. 1989. pp. 619–626.

9-4 Thomas, S. and Berg, H. M., "Micro-Corrosion of Al-Cu Bonding Pads," *23rd Ann. Proc. IEEE Reliability Physics Symposium,* March 26–28, 1985, pp. 153–158.

9-5 Klein, H. P., Durmutz, U., Pauthner, H., and Rohrich, H., "Aluminum Bond Pad Requirements for Reliable Wirebonds," *Proc. IEEE Intl. Symp. on Physics and Failure Analysis of ICs,* Singapore, Nov. 7–9, 1989, pp. 44–49.

9-6 Hirota, J., Machida, K., Okuda, T., Shimotomai, M., and Kawanaka, R., "The Development of Copper Wire Bonding for Plastic Molded Semiconductor Packages," *35th Proc. IEEE Electronic Components Conf.*, May 20–22, 1985, pp. 116–121.

9-7 Lowery, R. K. and Linn, J. H., "How Microcircuit Bond Pads Effect Device Yield," *Semiconductor International,* Vol. 14, May 1991, pp. 174–176.

9-8 Jang-Kyo, K. and Benny, P. L., "Effects of Metallization Characteristics on Gold Wire Bondability of Organic Printed Circuit Boards," *J. Elect. Mat.*, Vol. 30, No. 8, 2001, pp. 1001–1011.

9-9 White, M. L., "Detection and Control of Organic Contaminants on Surfaces," *Proc. 27th Ann. Symposium on Frequency Control*, Cherry Hill, New Jersey, 1973, pp. 79–88. Also see U.S. Patent #3,505,006, April 1970.

9-10 Heleine, T. L., Murcko, R. M., and Wang, S-C., "A Wire Bond Reliability Model," *Proc. 41st IEEE Electronic Components and Technology Conf.,* May 11–16, 1991, p. 378.

9-11 Shu, B., "Fine Pitch Wire Bonding Development Using a New Multipurpose, Multi-pad Pitch Test Die," *Proc. 41st IEEE Electronic Components and Technology Conf.*, May 11–16, 1991, pp. 511–518.

9-12 Eisenberg, H. B. and Jensen, I., "When Control Charting is Not Enough. A Wirebond Process Improvement Experience," *Proc. 1990, Intl. Microelectronics Symposium,* Chicago, IL, Oct. 15–17, 1990, pp. 61–66.

9-13 Shaeffer, M., "Creation of a New High Yield Wire Specification, presented at the ASTM F1.07 Meeting," Andover, MA, June 28, 1990.

9-14 Hotchkiss, G., Ryan, G., Subido, W., Broz, J., Mitchell, S., Rincon, R., Rolda, R., and Guimbaolibot, L., "Effects of Probe Damage on Wire Bond Integrity," *Electronic Components and Technology Conference,* May 29–31, 2001, Orlando FL, USA, pp. 1175–1180.

9-15 Sauter, W., Aoki, T., Hisada, T., Miyai, H., Petrarca, K., Beaulieu, F., Allard, S., Power, J., and Agbesi, M., "Problems with Wirebonding on Probe Marks and Possible Solutions," *Electronic Components and Technology Conference,* May 27–30, 2003, New Orleans, LA, USA, pp. 1350–1358.

9-16 Yong, L., Tran, T. A., Lee, S., Williams, B., and Ross, J., "Novel Method of Separating Probe and Wire Bond Regions Without Increasing Die Size," *Electronic Components and Technology Conference,* New Orleans, LA, USA. May 27–30, 2003, pp. 1323–1329.

9-17 Reusch, R. K., "Wire Sweep in Small-Outline Packages," *Proc 6th IEPS Conf.,* San Diego, CA, Nov 17–19, 1986. pp. 25–34. (A thorough paper, discusses transfer mould process-stress strain curve for 1.3 mil Be- doped Au wire—6% elongation—wire sweep vs diameter 1 mil and 1.3 mil wire, factorial experiment.)

9-18 Nguyen, L. T., "Reactive Flow Simulation in Transfer Molding of IC Packages," *Proc. of the 43rd Electronic Components & Technology Conf.,* June 1–4, 1993, Orlando, Fl, pp. 375–390.

9-19 Tay, A. A. O., Yeo, K. S., and Wu, J. H., "The Effect of Wirebond Geometry and Die Setting on Wire Sweep," *IEEE Trans. on CPMT-Part B* Vol. 18 No 1, Feb. 1995, pp. 201–209.

9-20 Tummala, R. R. and Rymaszewski, E. J, ed., *Microelectronics Packaging Handbook*, Van Nostrand Reinhold, 1989, and second edition, Springer, 1997.

9-21 Holdgrafer, W. J., Levine, L. R., and Gauntt, D. L., "Method of Making Constant Clearance Flat Link Wire Interconnections," U. S. Patent # 5,205,463, April 27, 1993.

9-22 Grover, R., Shu, W. K., and Lee, S. S., "Wire Bond Profile Development for Fine Pitch-Long Wire Assembly," *IEEE Trans. on Semiconductor Mfg.*, Vol. 7, Aug. 1994, pp. 393–399.

9-23 Egger, H. and von Flue, D., "Improved Looping for Gold Ball Bonding," *Proc. Semicon Tech. Symp.*, Singapore, April 24–26, 1996, pp. 27–30.

9-24 Ruston, M, Tran, T. A., Yong L., Youngblood, A., Ravenscraft, D., Fuaida Harun, K., "Assembly Challenges Related to Fine Pitch In-line and Staggered Bond Pad Devices," *2003 Electronic Components and Technology Conference*, New Orleans, LA, pp. 1334–1343.

9-25 Beleran, J., Wulff, F., and Breach, C. D., "Gold Ball-Bond Mechanical Reliability at 40 μm Pitch: Squash Height and Bake Temperature Effects," *Proc. IEEE EPTC*, Dec. 8–10 2004, pp. 701–706.
9-26 Sundararaman, V., Edwards, D. R., Subido W. E, and Test, H. R., "Wire Pull on Fine Pitch Pads: An Obsolete 'Test for First Bond Integrity?," *Proc ECTC,* May 21–24, 2000, Las Vegas, NV, pp. 416–420.
9-27 Charles, H., "Chip Level Interconnect: Wire Bonding for Multichip Modules," in *Chip on Board Technologies for Multichip Modules*, J. Lau, Editor, Van Nostrand, 1994, pp. 124–185.
9-28 Harman, G. G., "Wire Bonding—Towards 6σ Yield and Fine Pitch," *Proc. Trans. on CHMT,* Vol. 15, Dec. 1992, pp. 1005–1012.
9-29 Brathwaite, N. E., "Chip and Wire Assembly for MCMs," *Electronic Packaging and Production,* Vol. 34, Feb. 1994, pp. 70–72.
9-30 Harman, G. G., "Wire Bonding to Multichip Modules and Other Soft Substrates," *Proc. 1995 Intl. Conf. on Multichip Modules,* Denver Colorado, April 19–21, 1995, pp. 292–301. Also see updated version, *Proc. NATO ARW on MCM & Sensor Technologies,* Budapest, Hungary, May 18–20, 1995. Kluwer Academic Pub., 1997.
9-31 Conroy, B. L. and Cruzan, C. T., "Ultrasonic Bonding to Metallized Plastic," NASA Tech Brief Vol. 10, Jan./Feb. 1986, pp. 48, item # 29.
9-32 Murali, V., Gasparek, M., Bahansali, A., Chen, S. H., and Dais, R., "Wirebonding of Aluminum/Polyimide Multilayer Structures," *Int. Rel. Physics Symposium Proc. (IRPS),* San Diego, California, March 31–April 1, 1992, pp. 24–30.
9-33 Heinen, G., Stierman, R. J., Edwards, D., and Nye, L., "Wire Bonds Over Active Circuits," *44th Electronic Components & Technology Conference,* Washington, D.C., May 1–4, 1994, pp. 922–928.
9-34 Takeda, K., Ohmasa, M., Kurosu, N., and Hosaka, J., "Ultrasonic Wirebonding Using Gold Plated Copper Wire onto Flexible Printed Circuit Board," *Proc. 1994 IMC* (Japan), April 20–22, 1994, pp. 173–177.
9-35 Liu, J., Lai, Z., Kristianses, H., and Khoo, C., "Overview of Conductive Adhesive Joining Technology in Electronics Packaging Applications," *Proc. 3rd Intl. Conf. on Adhesive Joining & Coating Technology in Electronics Mfg*. (Adhesives '98) Binghamton, NY, Sept. 28–30, 1998, MS. 1-1.)
9-36 Benton, B. K., Palomar Technologies, Carlsbad, CA, Private communication, <bbenton@bonders.com>.
9-37 Anderson, H., "Wire Bonding Dual-Sided MCM-L Modules," *Proc. Intl. Conf. Multichip Modules,* April 13–15, 1994, Denver, Colorado, pp. 424–429.
9-38 Fu, C., Brown, R. C., and Ume C., "Temperature-Dependent Material Characterizations for Thin Epoxy FR-4/E-Glass Woven Laminate," *Proc. 43rd Elect. Comp. Tech. Conf.,* June 1–4, 1993, Orlando, Florida, pp. 560–562. Note: authors will send figures on request.
9-39 Strandberg, J., Theide, H., Karlsson, A., and Weiland, A., "High Reliability 4-metal Layer MCM-D Structure with BCB as Dielectric," *Proc. Intl. Conf. Multichip Modules,* April 19–21, 1995, Denver, Colorado, pp. 223–228.
9-40 Christiansen, R. A., "Wire Bonding Chip on Board," in *Chip on Board Technologies for Multichip Modules,* J. Lau, Editor, Van Nostrand, 1994, pp. 275–341; also numerous private communications.
9-41 Nii, M., Omori, J., et al., "Evaluation of Copper/Polyimide Thin Film Substrate for Multi-chip Module," *Proc. Intl. Microelectronics Conf.*, Yokahama, Japan, June 3–5, 1992, pp. 259–264.
9-42 Terman, F. E., *Radio Engineers' Handbook,* McGraw Hill, New York, 1943, pp. 47–5.
9-43 Tsai, C. T., Anderson, H., and Yip, W-Y., "Electrical Characterization of Bonding Wires," *Proc. Intl. Symp. Microelectronics* (ISHM) Boston, Massachusetts, Nov. 15–17, 1994, pp. 479–484.
9-44 Hayashi, K., Nagayama, Y., Shirai, Y., Nakamura, A., Otsuka, K., Nagai, K., and Imaizumi I., "A Wire Bonding Structure Package for 2.4 GHz Frequency," *Proc. VLSI Packaging Workshop,* Yorktown Heights, New York, October 1993, Paper IV-1.

9-45 Gilbert, B. K. and Pan, G. W., "Packaging of GaAs Signal Processors on Multichip Modules," *IEEE Trans. on CHMT,* Vol. 15, Feb. 1992, pp. 15–28.
9-46 Hwang, L. T. and Turlik, I., "A Review of The Skin Effect as Applied to Thin Film Interconnections," *IEEE Trans. on CHMT,* Vol. 15, Feb. 1992, pp. 43–55.
9-47 Salmon, L. G., "Evaluation of Thin Film MCM Materials for High-Speed Applications," *IEEE Trans. on CHMT*, Vol. 16, June 1993, pp. 388–391.
9-48 Johnson, R. W., "Electronics Packaging for Extreme Environments," *Proc. of the International Planetary Probe Workshop,* Bordeaux, France, June 25–29, 2007.
9-49 Johnson, R. W., Wang, C., Liu, Y., and Scofield, J. D., "Power Device Packaging Technologies for Extreme Environments," *IEEE Transactions on Electronics Packaging Manufacturing,* Vol. 30, No. 3, July 2007, pp. 182–191.
9-50 Hansen, P. and McCluskey, P., "Failure Models in Power Device Interconnects," *Proc. 2007 European Conference on Power Electronics and Applications,* Sept. 2–5, 2007, pp. 1–9.
9-51 Benoit, J., Chen, S., Grzybowski, R., Lin, S., Jain, R., and McCluskey, P., "Wire Bond Metallurgy for High Temperature Electronics," *Proc. 4th IEEE Int'l High Temperature Electronics Conference,* Albuquerque, NM, June 14–18, 1998, pp. 109–113.
9-52 Salmon, J. S., Johnson, R. W., and Palmer, M., "Thick Film Hybrid Packaging Techniques for 500°C Operation," *Proc. 4th Intl High Temp. Elect. Conf.,* Albuquerque, NM, June 16–19, 1998, pp. 103–108.
9-53 Deyhim, A., Yost, B., Lii, M., and Li, C-Y., "Characterization of the Fatigue Properties of Bonding Wires," *Proc.ECTC,* Orlando FL, May 28–31, 1996, pp. 836–841.
9-54 Kirschman, R. K., High Temperature Electronics, 1999 - IEEE Press.s
9A-1 Levine, L. and Sheaffer, M., "Wire Bonding Strategies to Meet Thin Packaging Requirements," Part I, *Solid State Technology*, March 1993.
9A-2 Holdgrafer, W. J., Sheaffer, M. J., and Levine, L. R., "Method of Making Low Profile Fine Wire Interconnections," U.S. Patent 5,111,989 (5/12/1992).
9A-3 Holdgrafer, W. J., Levine, L. R., and Gauntt, D. L., "Method of Making Constant Clearance Flat Link Fine Wire Interconnections," U.S. Patent 5,205,463, (4/27/1993).

CHAPTER 10

An Overview of the Materials and Material Science of Copper, Low-k Devices That Affect Bonding and Packaging

10.1 Introduction

It is absolutely essential for anyone involved in advanced wire bonding to understand the properties of all layers below the bond pad that may affect (or be affected by) the bonding process. This chapter presents an overview for understanding the materials, material science, engineering of copper, and low-dielectric-constant (Cu/Lo-k) devices; discusses their effect on wire bonding problems, and has some comments on flip-chip problems as well. It is not intended to be an advanced paper with new technology on this subject, but rather to serve as background material to understand the complexities of this recent technology and its implications for wire bonding production and reliability.

Cu/Lo-k devices represent a challenge for packaging/wire bonding because of their complex multilayer structures and low-modulus materials below the bond pads. This chapter describes the different dielectrics, how the damascene copper structures are made and differ

from the normal planar deposition we grew up with. Also, the device packaging related failure modes and methods of minimizing are discussed. Following this chapter is one on bond modeling, including the bonding effect on Cu/Lo-k.

Most Lo-k materials used today (2008) are some form of CVD OSG [organo-silicate glass (SiOC)]—which has a much lower modulus of elasticity (softer/weaker) than pure SiO_2 (the normal dielectric/insulator used on traditional chips in the past). The Lo-k modulus is even lower when it has pores added to further decrease the dielectric constant. This dielectric, often stacked in 5 to 12+ layers [with as many levels of copper interconnects (wiring)], challenges the packaging process and later the device reliability. In addition, all copper interconnects imbedded in the dielectric must be coated with thin (<10 nm, 100 Å) diffusion barriers to prevent device degradation and reliability failure (since Cu degrades both Si and the dielectrics). These buried barriers and dielectrics can be damaged during the wire bonding process, or by flip chip (FC) stresses in systems during temperature cycling. These can lead to long-term failures that are not detectable in the production, packaging, or normal qualification processes.

Therefore, it has become necessary for reliable wire bonding (a metallurgical welding process) to include the material properties of complex under-layers of dielectrics and diffusion barriers as being equally important in the bonding reliability/yield process as the metallurgy. In cases where the Lo-k has a low modulus as well, it is necessary to have special support structures to prevent damage from bonding stresses.

10.2 The Cu/Lo-k Technology

Modern chips are usually intraconnected with multilayers of Cu and insulated with various low-modulus, low-dielectric-constant insulators (Cu/Lo-k). These chips are very different from traditional ones that have a single layer of aluminum over oxide or nitride. A comparison of the two technologies is shown in Fig. 10-1*a* and *b*. Wire bonding too (Fig. 10-1*a*) is traditional and does not require special knowledge or care. Figure 10-1*b* gives a simplified example of the layered stacks used in Cu/Lo-k chips. Great care must be exercised when bonding to these structures, since the layers may delaminate or warp during the wire bonding and packaging process. Flip chips can have these problems as well during packaging but especially during temperature cycling in operation. Further, any damage to the materials stack for wire or flip chips may not be evident at the time it occurs, but can result in failure after installation and long operation, resulting from Cu diffusion into the dielectric or semiconductor.

Copper has approximately 35% better electrical conductivity than Al (see Chap. 3). This decreases both the delay time and the electrical

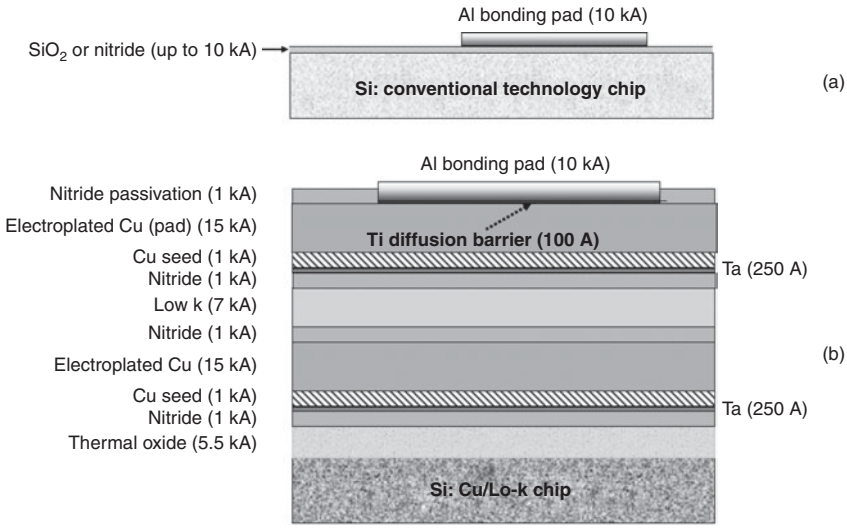

Figure 10-1 Comparison of the materials stacks of a conventional aluminized chip (*a*) with a very simple Cu/Lo-k chip. (*b*) The complexity and potential damage susceptibility during bonding is apparent. With all this complexity, there is only one layer of Lo-k dielectric in this figure. (*Figure 10-1b is from SEMATECH with modifications*.) In general, new designs result in reducing the thickness of nitride and barrier layers.

loss between active devices on a semiconductor chip. However, since Cu cannot be etched into fine-line width conductors, as can Al, it was necessary to develop a different method of depositing and delineating fine pitch structures. Figure 10-2 details the Cu damascene process. Figure 10-2*a* shows the final Cu plated up from the bottom of the trench. This was previously etched into the dielectric, and a thin barrier deposited on its inner surfaces. Next, a Cu seed was deposited, and finally the Cu was electroplated up from the bottom and CMP-polished flat, as shown in Fig. 10-2*a*. Figure 10-2*b* gives more details of manufacture [10-1]. If two trenches are formed and then filled with copper at the same time, such as a trench overlying a via, then it is a *dual-damascene structure*. The resulting fine pitch structure is capable of being used down to at least the 45 nm semiconductor manufacturing node.

A more complex Cu/Lo-k structure, shown in Fig. 10-3, is a cross-section of four metal layers of damascene-Cu imbedded in Lo-k dielectric. A more complex structure (up to five metal layers), with its dielectric etched out for illustration, is given in Fig. 10-4. The complex Cu-conductor, barrier encased structure is normally supported/imbedded in damascene trenches in the Lo-k material. If bonding (or other packaging) stresses are high, damage can occur. Thus it is apparent that modern chips can pose new problems for wire bonding

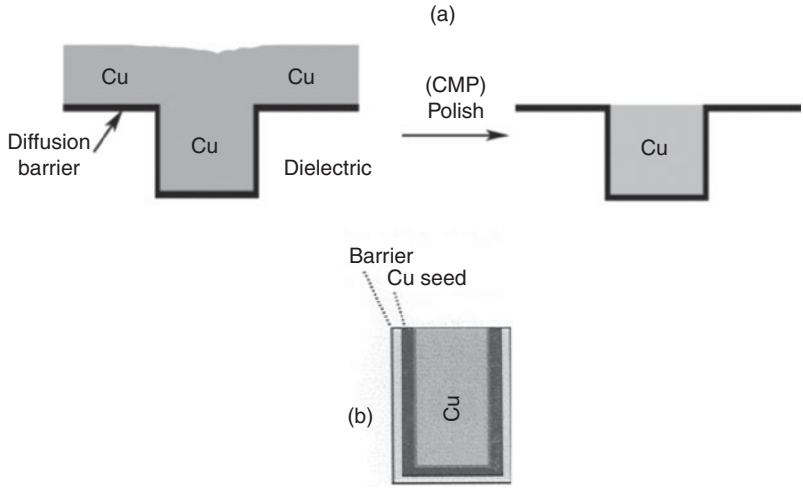

Figure 10-2 Details of the basic Cu-damascene (trench) process. First the trench is etched in the Lo-k dielectric, then a thin diffusion barrier is deposited on its inner surfaces, next a Cu seed is deposited, and finally Cu is electroplated up from the bottom. Then the surface is CMP-polished flat, leaving a well-delineated conductor, as shown in (*a*). (*b*) gives more details of the metal deposition steps [10-1].

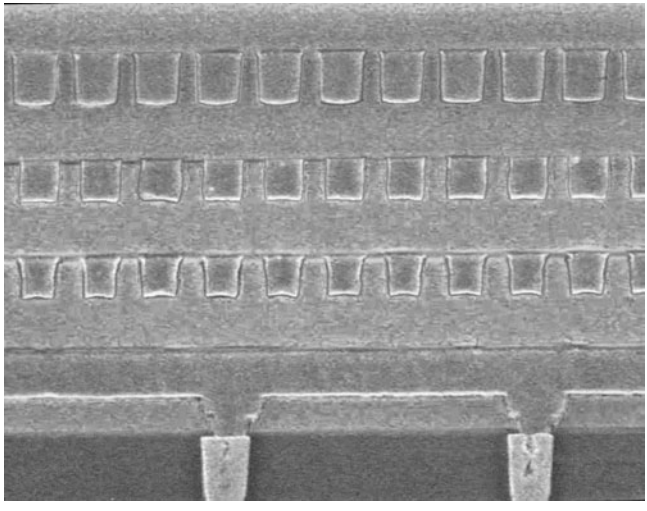

Figure 10-3 A four-metal-layer Cu-damascene structure imbedded in a Lo-k dielectric. This cross-section shows the individual Cu metallization lines in their damascene trenches. The trench is surrounded by Lo-k dielectric. (*Courtesy of IBM.*)

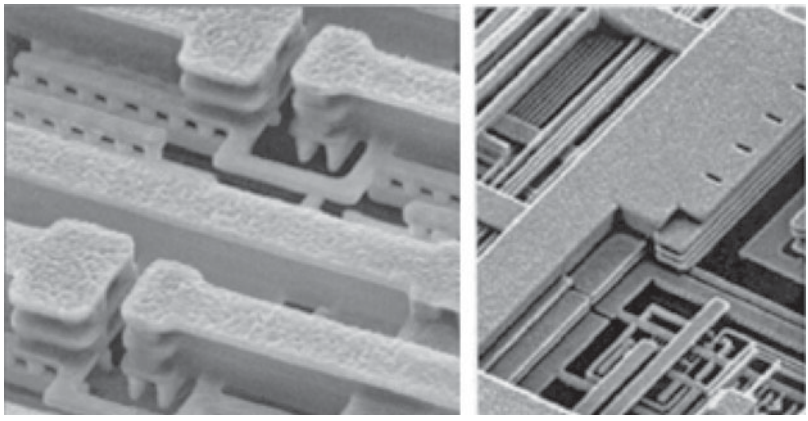

(a) (b)

Figure 10-4 This presents a classical example of the metal structure of copper low-dielectric constant (Cu/Lo-k) chips with the dielectric etched away. It reveals the extremely complex damascene Lo-k structure of modern Cu-metallization chips. (*Courtesy of IBM.*)

or flip chip interconnections, which can result in damaging the complex Cu-damascene structure and lowering the device reliability.

10.2.1 The Lo-k Dielectrics

The standard dielectric, used on chips since the beginning of Si technology, is SiO_2. This material has a dielectric constant k (ε) of ~4. Lo-k materials (by definition) have $\varepsilon < 3$ and 2.4 to 2.8 is typical. Currently, most Lo-k's are some form of OSG (Organo-Silicate Glass), which is SiO_2 with carbon-hydrogen added as part of the chemical-vapor-deposition (CVD) process. The range of dielectric constants (k) obtainable from silicon dioxide with CH_3 added in the CVD process is shown below. The more CH_3 added, the lower the modulus, which ranges from (a) ~70 GPa (no CH_3: strong and hard) down to (c) ~4 GPa (max CH_3: weak and soft).

Dielectric constant changes with C additions

(a) $SiO_2 \approx 4$; (b) $SiO_{1.5}CH_3 \approx 3.1$; (c) $SiO_{0.5}(CH_3)_3 \approx 2.5$

(Still lower k is obtained by adding pores, but this lowers the mechanical properties and can result in poor wire bondability as well as unreliable chips.)

An example of the decreasing mechanical properties of OSGs is given in Fig. 10-5 [10-2] (in which both the hardness and the modulus decrease dramatically as the amount of carbon-hydrogen increases). To go below k ~2.4 requires pores, which further lowers (degrades) the mechanical properties. Unfortunately the lower k dielectrics are

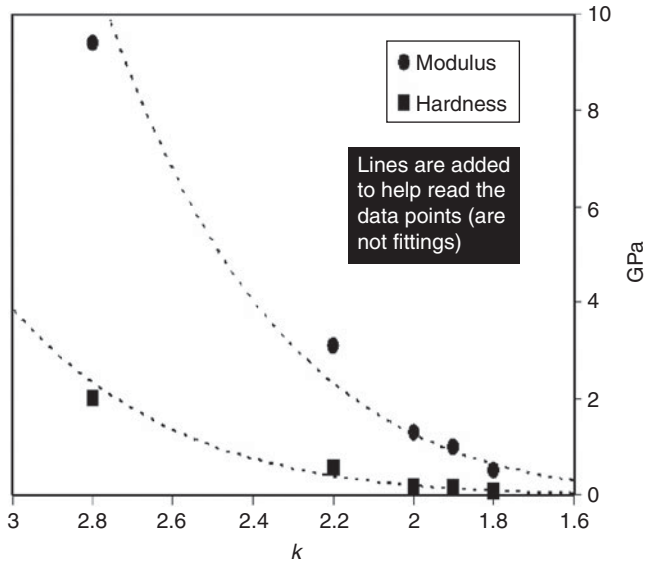

Figure 10-5 The reduction of mechanical properties of organo-silicate glass as the amount of C-H is increased. For these materials, *k* can be decreased below 2.4 only by introducing pores [10-2]. (*Courtesy of Intel.*)

required for future chip technologies and will be implemented in one form or another.

These OSG materials are clearly much weaker than SiO_2, but better than earlier Lo-k organics, and they are compatible with wafer fab requirements. Table 10-1 gives the relevant properties of current Lo-k materials and compares them with SiO_2. SiLK (an acronym) at the top, is the last of the organics to be considered, but never reached production. Its modulus was too low and the CTE was too high for incorporation on a chip, typical problems of the organics. (It should be noted that exact values in the table may depend on the details of the measurement and can vary considerably as parameters, such as indentation depth, loading or unloading of the nano-indenter tool, etc., change.) Many details and measurement techniques for OSG Lo-k's are given in Ref. [10-3].

The development of Lo-k dielectrics continues rapidly, and the OSG Lo-k materials and their properties listed in Table 10-1 will presumably be superseded. Unusual solutions such as airgaps, mixed dielectrics, etc., may be incorporated into the Lo-k structures in order to further reduce *k*. Recent announcements indicate that nanomaterials may be used to generate partial air gaps with $k \sim 2.0$ (vs. 1.0 for vacuum). Development of such will increase device performance, but may introduce problems for wire bonding to such chips using those materials.

Material[a]	Organic—O Inorganic—I	*k* (ε) @ 25°C	Modulus (GPa) @ 25°C	Hardness (GPa)	Fracture-Toughness (MPa-$m^{1/2}$)[c]	CTE[b] (10^{-6}/°C)	Reference
SiLK Y[b]	O	2.6–2.2	2.45	0.31	0.66–0.42	62	Dow Chem.
Black Diamond II (SiO_2 + C)	I/O (OSG)[e,f]	2.7 → 2.4	7.7 → 6	3.6–1.3	0.3–0.2	17–23	Applied Matls.
Corel	I/O OSG[e,f]	2.7	~7	—	—	—	Novellus
Aurora	I/O OSG[e,f]	2.8–2.4	12–6	2.2–1.1	—	17	ASM
Nanoglass silica (gels) pores <5 nm	I	1.3–2.5	0.5–2.3	0.03–0.1	<0.04–0.14	4 up (varies)	Many sources
SiO_2	I	3.8–4.1	72–100	9.5	0.46	1–2	Many sources

[a]Trade names are used to describe a material when no other identifier is available. This does not imply any endorsement.
[b]CTEs of organic Lo-k matls. generally increase with temperature. Reported values are average and in the range of 25 to 100°C.
[c]Fracture toughness of material interface with SiO_2, SiN, Ta, or TaN
[d]**Discontinued product** (included for comparison)
[e]**Organo Silicate Glass SiO_2 + C**
[f]The properties of OSGs can be changed in the wafer-fab by changing the pressure, concentrations, etc., which changes the amount of C-H (see Eq-1) in the material, which may lower the modulus and hardness and increase the CTE. Thus, values above are not absolute and not necessarily different for each of these products.

TABLE 10-1 Low Dielectric Constant Materials Used/Proposed for Cu/Lo-k Structures

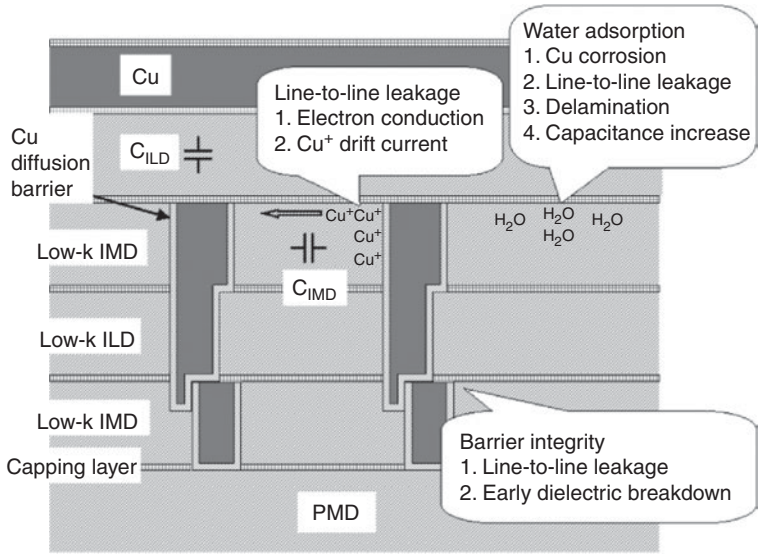

Figure 10-6 A cartoon of a dual-damascene structure showing several potential reliability hazards. If a bond is made to the Cu pad on top, barriers could be damaged, accelerating failures. IMD is the intermetal dielectric, ILD is the interlevel dielectric, and PMD is the premetallization dielectric (above the Si) [10-4] (© IEEE).

All copper conductors imbedded in the Lo-k dielectrics must be encased in thin diffusion barriers to prevent copper from drifting/diffusing into the dielectric or the Si, which would change their properties, eventually degrading or destroying the device. Such diffusion barriers today are usually made of TaN/Ta or TiN/Ti and are currently ~5.4 nm thick, decreasing to one-half by 2013. The integrity of such thin barriers is always a potential chip reliability problem, and may be damaged by wire bonding stresses permitting Cu and water vapor diffusion and lowering the device reliability. In addition it is necessary to prevent water vapor from entering the Lo-k stack. This is sometimes accomplished by adding a top layer of SiO_2. Figure 10-6 illustrates some of the potential reliability hazards, such as the diffusion of water and Cu into the Lo-k layers of a dual damascene (Lo-k) structure [10-4].

10.2.2 Top Surface Protective and Bondability Coatings for Copper Bond Pads

Traditionally, wire bonds on chips have been made to aluminum pads over silicon or silicon dioxide. This presented both an ideal metallurgy and a rigid platform for thermosonic bonding (Fig. 10-1*a*). However, copper bond pads may be located over low modulus dielectrics

encased in thin brittle diffusion barriers, which can crack during bonding to the Lo-k structures as shown in Fig. 10-1*b*. This can result in low-bond yield and/or device reliability problems. In addition, it is necessary to protect the top surface of the copper bond pads from oxidation, sulfiding, etc. Such can be achieved with various metallurgical coatings over the Cu, that is, gold or aluminum protected by a barrier. (This is the most common method today and is illustrated in Fig. 10-1*b*.) Aluminum pads are both wafer-fab compatible and ideal for wire bonding. However, the chip fabrication requires diffusion barrier deposition, masking, and etching steps and is therefore expensive. There is also the possibility that, if the bonding process cracks the Al to Cu diffusion barrier, the reliability can be worse than if no diffusion barrier existed. Such could happen if a low-modulus dielectric was below the bond pad and *cupping* or *sinking* occurred (Chap. 9). Another possible problem is that the Al/barrier/Cu method has been patented [10-5], and it may not be available, or may be costly.

Table 10-2 gives some possible non-aluminum protective coatings over the Cu bond pad, and some of these may offer simplicity or other cost advantages over the Al/barrier/Cu pads mostly used today. The reliability of the several interfaces (Au on Au/Ni, Cu on Au/Ni, Cu on Cu, and Au on Cu) is indicated in Fig. 10-7 for 150°C storage times up to 1500 h [10-6]. All of these interfaces are easily bondable, so economic or other conditions would be used to determine the production choice. None of the materials in Table 10-2 are wafer-fab compatible and must be applied later outside of the fab, a disadvantage when compared to the Al/barrier/Cu metallization system. (Note: Wafer-fab preferences usually dominate over those of the packaging community.)

Top Surface Metals for Bondability
1. Copper itself (oxidation lowers/kills bondability)
2. Possible metals/stacks to enhance bondability a. Au/barrier/Cu, Au/Ni/Cu, or just Au/Cu (all known to be reliable) b. Al/barrier/Cu, also a well known bonding surface and the most used in 2008 c. Ag/Cu, known reliable interface (Ag migration on fine pitch may be a problem) d. Pd/Cu (or with Ni, etc.), a well known reliable interface e. Other (combinations of above)

Table 10-2 Copper-Pad Top-Surface Coatings for Protection and Wire Bondability

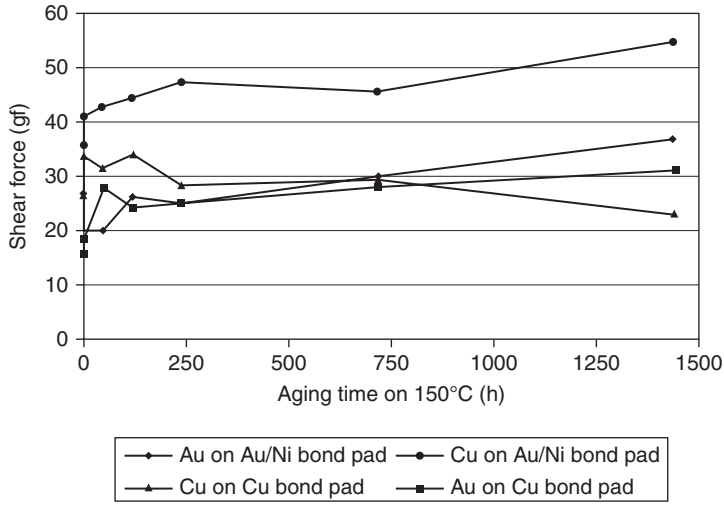

Figure 10-7 The high-temperature storage of several interfaces, reversing the bond pad with the bonded ball. All are reliable at 1500 h, but the shear force of the Au on Al (below Au on Cu curve) begins to decrease as expected. It is apparent that any combination of Au with Cu is adequately reliable for use in normal devices [10-6]. (*Courtesy of IMEC.*)

10.3 Wire Bonding to Integrated Circuits with Copper Bond Pads over Lo-k Material

After appropriate surface bondability and Cu oxidation protection are achieved, the problems of wire bonding to pads over low-modulus substrates must be addressed. This incorporates the knowledge obtained from the past on bonding to multichip modules, where bond pads are often located over similar low-modulus dielectrics. Cu/Lo-k chips and multichip SiPs are part of the same problem and share some of the same solutions (see Chap. 9).

In any laminated structure, delamination is a potential failure mode. The dynamic stresses of wire bonding and other packaging process can create such delaminations. Several finite element models of bonding stress on pads over Lo-k and their under-layers have been published. All show that high stress is generated under and around the bond. Figure 10-8 depicts a typical FEA of the mechanical stress profile for a Cu ball at touchdown onto a Cu bond-pad [10- 8]. (Note that an Au ball would generate ~20% less stress.). None have been able to model the direct atomic interface welding effect of ultrasonic energy. However, some good approximations have been published [10-8]. Several studies also indicate that bonding over low-modulus materials produces major stress contributions to pad peeling as illustrated in Fig. 10-9 [10-9, 10-10]. Such physical damage is clearly illustrated

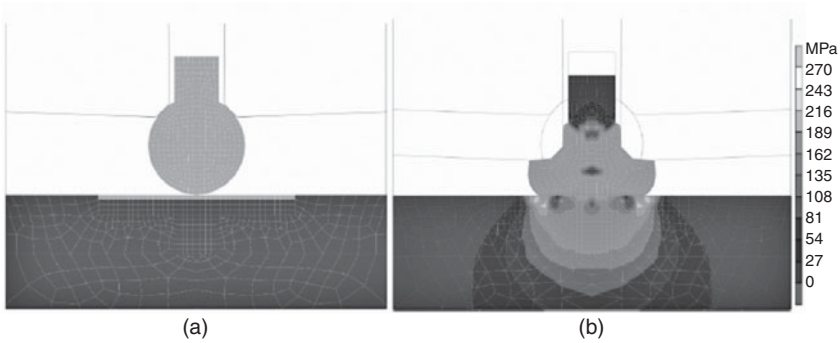

Figure 10-8 FEA of a Cu ball to Cu bond pad during the initiation of wire bonding, giving the Von Mises stress in the ball, the pad, and the dielectric below. Much of this stress would be applied to the Lo-k and the copper diffusion barriers below as bonding is started. The stress would increase with the application of ultrasonic energy, possibly damaging the Lo-k as well as the Cu diffusion barriers. The Von Mises stress at the end of ball touchdown is given (in MPa) on the right [10-7] (© IEEE).

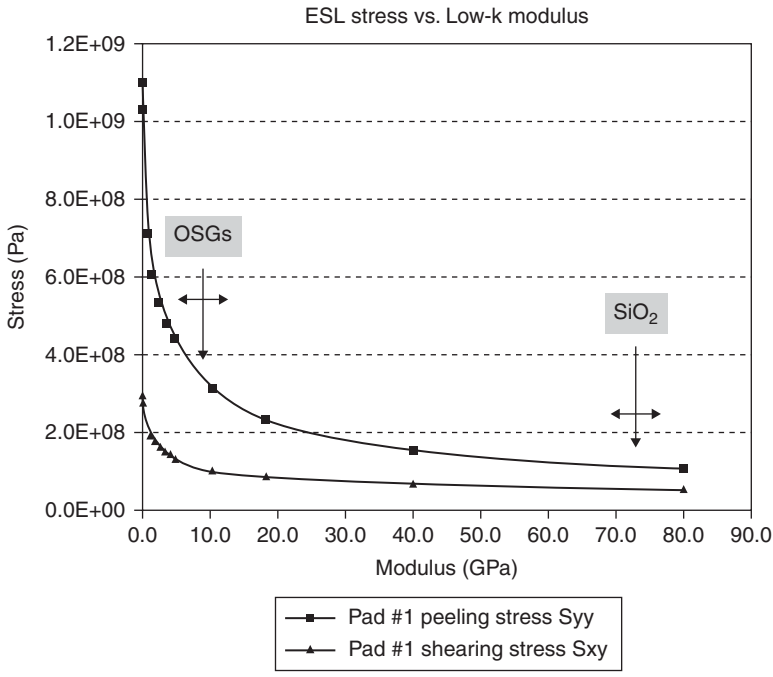

Figure 10-9 Wire bonding stress versus the (Low-k) dielectric's modulus. The lower the modulus during wire bonding, the greater the possibility of pad peeling. Since the modulus decreases with ε, and higher performance requires lower ε, pad peeling is a common problem with Lo-k devices [10-9] (© IEEE).

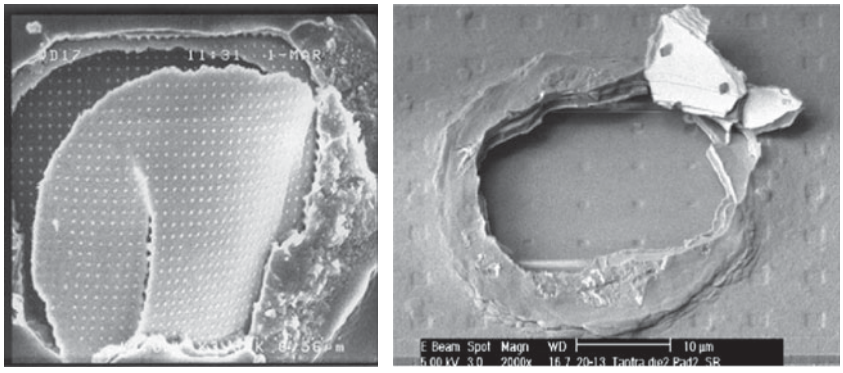

(a) (b)

Figure 10-10 Typical examples of bond pad peeling after bonding over Lo-k dielectrics. (This is also referred to as cratering even though the Si was intact [10-10]; © *IEEE*).

in Fig. 10-10*a* and *b*. Such pad peeling is frequently referred to as cratering, although technically this is incorrect unless there is damage to the dielectric or Si. These figures offer some reasons why the earlier, low-modulus, organic Lo-k materials (e.g., SiLK in Table 10-1 and many others) were not successful.

In order to prevent such damage, a number of underpad support systems have been developed by the IC industry. One such structure is shown in Fig. 10-11 and discussed in Ref. [10-9]. Typically these consist of a number of metal vias below the pad, extending down to the chip or its oxide protection layer. These transmit the bonding stress from the pad directly to the high-modulus Si chip below, where it is dissipated or transmitted to the package, thus protecting the Lo-k dielectric, the Cu, and the diffusion barriers.

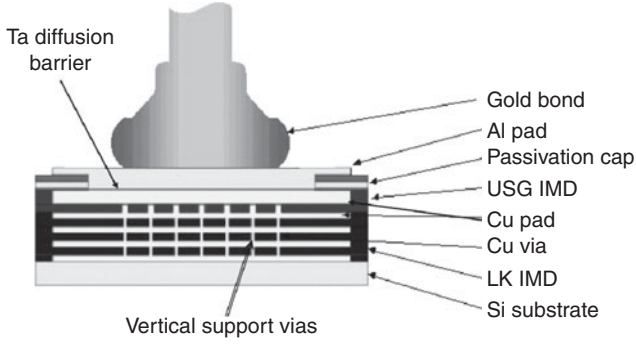

Figure 10-11 An example of a typical underpad support structure that limits damage to the bond pad from the bonding process. This prevents Cu diffusion barriers from cracking, as well as stressing the (Lo-k) dielectric material. Mechanical stresses are transmitted to the high strength silicon-oxide below [10-9] (© *IEEE*).

These ICs have copper metallization as well as low-dielectric constant, low-modulus dielectrics (Cu/Lo-k) beneath the bond pads, as opposed to older ICs that had SiO_2 or silicon there as shown in Fig. 10-1. The Lo-k materials are partly processed with the wafer at relatively high temperatures (up to 425°C) compared to normal thermosonic bonding temperatures (125 to 200°C). Therefore, their T_g's are designed to be high and will not pose temperature-dependent bonding problems as some MCM-SiP substrates do. In some cases, the already low modulus of the OSG Lo-k material will decrease at bonding temperatures, and can affect bonding.

An important difference between bonding to most devices on MCM-SiPs and on advanced Cu/Lo-k chips is that bond pads on the latter are generally small (<60 µm and ultimately down to 20 µm pitch, ITRS 2007 Roadmap) resulting in sinking into, and/or mechanically damaging the low-modulus material and barrier films beneath. Also, the metal/dielectric stack is multilayered and extremely complex. Often there can be more than 12 metal layers, dielectrics, barriers, and oxides above the silicon, as discussed above. In addition, support structures as shown in Fig. 10-11 are required to protect the Lo-k material during bonding. Without these, any resulting dielectric sinking or cupping can crack/damage barrier layers below the bond pad, leading to pad peeling, electrical leakage, and/or degraded high-frequency properties. Possible wire bonding damage to the Lo-k layers, Cu interconnects, and diffusion barriers can be minimized by optimizing the bonding machine parameters and materials. These can be summarized as (1) minimizing the US energy and the clamping force, (2) reducing the ball diameter or wire hardness (if wedge bonded), (3) delaying application of US energy after tool touchdown, and (4) plasma cleaning the pads before bonding. These are summarized in Table 10-3, and are similar to those recommended in Chap. 9.

1. Use finer diameter wire (e.g., 18 vs. 25 µm dia.); if ball bonding, make smaller balls (requires lower force/power).
2. If Al wedge bonding, use softer wire (12–14 gm vs. 16–18 gm BL for 25 µm dia.) (requires lower force/power).
3. May still require 10–20% higher bonding machine parameters for same wire if the pad/dielectric sinks (but this would damage a Lo-k chip).
4. Delay applying ultrasonic energy (~10–25 ms) to allow pad bond force stresses to stabilize before US stresses begin.
5. Clean pads before bonding which lowers US energy required to make the bond.

TABLE 10-3 Cu/Lo-k Bonding Machine Considerations

Wire bonding damage in chips having Lo-k materials below the pad are summarized as follows: Various dielectric and metallurgical damage can occur, resulting in long-term packaged-device reliability problems. These include cracked diffusion barriers, copper diffusion into the Lo-k dielectrics, cracking and delamination of the Lo-k materials, and bond pad indentation ("cupping"). Lo-k materials, with high-expansion coefficients and low-thermal conductivities, can increase the temperature cycle stress and further extend any existing damage. Many of the above problems have previously been encountered when bonding to pads over low-modulus dielectrics in MCM-SiPs, polymer buildup-layers on PCBs, PBGAs, flex circuits, etc. (see Chap. 9), and they share some of the same solutions. Well-designed Lo-k underpad structures should have no negative effect on bonding parameters and in fact should be invisible to the bonding process.

10.3.1 Lo-k Flip Chip Damage

Although it is beyond the scope of this book to detail the problems or solutions for Lo-k devices interconnected with flip chips, it is useful to point out that FC connections in such devices also have packaging problems. They are different from those of wire bonded devices. Any wire bond damage occurs during the manufacturing process, resulting from dynamic bonding, stresses on the pads and under-layers. For FC, the manufacturing stresses of solder reflow are generally minimal or nonexistent. The problems occur later in service, especially in high-performance devices that generate considerable heat and result in temperature cycle stresses. The problems typically occur on devices that are mounted on organic substrates (e.g., plastic BGAs, etc) and the choice of underfill properties becomes a critical compromise [10-11].

Figure 10-12 [10-12] is a pictorial example of temperature-cycle damage to flip chip devices mounted on organic substrates. Cracks and delaminations occur at the solder bump interfaces and in the Lo-k layers (better seen in the enclosed color CD). In some cases, special stress buffers have been proposed to minimize damage to both chip and plastic package structures [10-13], and these or other developments can be expected in the future.

10.4 Conclusions

The Cu/Lo-k interconnects represent a new technology. Instead of one metal for both bond pads and intraconnections (within the chip), and one dielectric (SiO_2), there are now many possibilities to choose from. Each organization makes material choices optimized for their special needs and capabilities. Currently (2008), the preferred top pad surface for wire bonding is Al/barrier/Cu and the preferred Lo-k dielectric is an OSG as shown in Table 10-1 (or in some advanced cases-air gaps). New classes of dielectrics are continually being

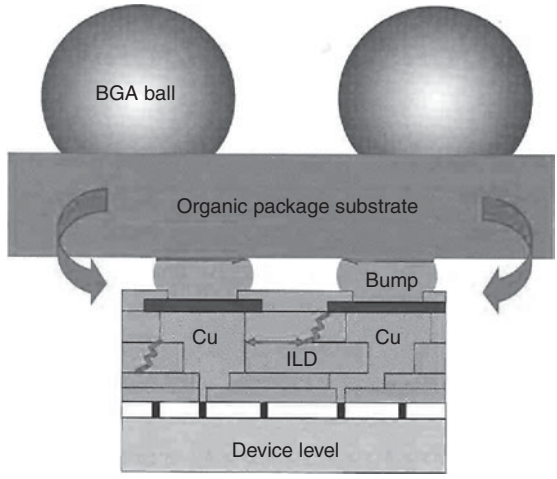

Figure 10-12 A pictorial example of temperature-cycle stress-induced cracks on flip chip devices mounted on organic substrates. Cracks and stresses are indicated in red (in the CD). Cracks originate at the bump-to-substrate, UBM-to-substrate, and damascene Cu-to-substrate material interfaces (*red in the CD*) [10-12]. (*Courtesy of Chip Scale Review.*)

investigated, so these may change. The underpad bonding-support structures are still evolving with each new design. The desire is that the chosen materials/structures will be invisible to the assembly/packaging operation. However, work at some laboratories involves developing a compatible gold bond pad process (plated Au directly over Cu); thus, even the metallization may change.

If one plans to wire bond to pads over "soft substrates," be they multichipped-packages, SiPs or Cu/Lo-K devices, then one must design the entire system (dielectric/metallization/support structures) with bonding in mind; otherwise, the wire-bond and device yield and/or device reliability may be unacceptable and later redesigning will be costly. Wire bonding in microelectronics is entering a new area in which understanding the materials/metallurgical structures beneath the pad is at least as important as understanding and controlling the wire bonding process itself.

References

10-1 Ho, P. S., "Material Issues and Impact on Reliability of Cu/Low k Interconnects," Microelectronics Research Center University of Texas at Austin Talk Presented at the AVS Chapter meeting 10/2002 (on university web site).

10-2 Garner, C. M., Kloster, G., Atwood, G., and Mosley, L., "Challenges for Dielectric Materials in Future Integrated Circuit Technologies," *Presented at the 13th Workshop on Dielectrics in Microelectronics*, Kinsale, Ireland, June 2004, summarized in *Microelectronics Reliability*, Vol. 45, No. 5-6, May-June 2005. pp. 919–924.

10-3 Vella, J. B., Adhihetty, I. S., Junker, K., and Volinsky, A. A., "Mechanical Properties and Fracture Toughness of Organo-Silicate Glass (OSG) Low-k Dielectric Thin Films for Microelectronic Applications," *International Journal of Fracture*, Vol. 119/120, 2003, pp. 487–499.

10-4 Tsu, R., McPherson, J. W., and McKee, W. R., "Leakage and Breakdown Reliability Issues Associated with Low-k Dielectrics in a Dual-damascene Cu Process," *Proceeding. 38th Annual IEEE Reliability Physics Symposium*, San Jose, CA, 04/10-23/2000, pp. 348–353.

10-5 Cheung R. W. and Ming-Ren Lin, "Advanced Copper Interconnect System That Is Compatible with Existing IC Wire Bonding Technology", U.S. Patent 5,785,236, issued July 28, 1998.

10-6 Ho, M., Lam, W., Stoukatch, S., Ratchev, P., Vath, C., and Beyne, E., "Direct Gold and Copper Wires Bonding on Copper," *Microelectronics Reliability*, Vol. 43, No. 6, 2003, pp. 913–923.

10-7 Chen, J., Degryse, D., Ratchev, P., and Wolf, de I.,"Mechanical Issues of Cu-to-Cu Wire Bonding," *IEEE Trans. on CPT*., Vol. 27, No. 3, Sept. 2004, pp. 539–544.

10-8 Liu, Y., Irving, S. T., and Luk, T., "Thermosonic Wire Bonding Process Simulation and Bond Pad over Active, Stress Analysis," *Proc. 54th ECTC*, Vol. 1, pp. 383–391. Las Vegas, NV, 1–4 June 2004. Also see; Chang-Lin Yeh, Yi-Shao Lai, and Jenq-Dah Wu, "Dynamic Analysis of Wirebonding Process on Cu/low-K Wafers," *Electronics Packaging Technology*, (*EPTC 2003*), Singapore, Dec., 10-12, 2003, pp. 282–286.

10-9 Huang, T. C., Liang, M. S., Lee, T. L., Chen, S. C., Yu, C. H., and Liang, M. S., "Wire Bonding Analysis and Yield Improvements for Cu Low-K IMD Chip Packaging," *6th VLSI Packaging WS*, Kyoto, Japan, Nov. 12-14, 2002. Also in *Advanced Metallization Conf*., pp. 67–73, 2002.

10-10 Lee, C-C., Tran, TuAnh., and Miller, C., "Overview of Metal Lifted Failure Modes During Fine-Pitch Wirebonding Low K/Copper Dies with Bond Over Active (BOA) Circuitry Design," *57th Electronic Components and Technology Conference*, Reno, NV, May 29-June 1, 2007, pp. 1775–1781.

10-11 Paquet, M. C., Gaynes, M., Duchesne, E., Questad, D., Bélanger L., and Sylvestre, J., "Underfill Selection Strategy for Pb-Free, Low-K and Fine Pitch Organic Flip Chip Applications," *Electronic Components and Technology Conference*, 2006, pp. 1063–1595, and IBID, L. Li, J. Xue, M. Ahmad and M. Brillhart, "Materials Effects on Reliability of FC-PBGA Packages for Cu/Low-k Chips," pp. 1590–1594.

10-12 Lanzone, R., "How Flip-Chip Package Interactions Affect the Manufacture of High-Performance ICs," *Chip Scale Review*, Jan.-Feb. 2006, pp. 25–45.

10-13 Lee, C. C., Liu, H. C., Chiang, K. N., "3-D Structure Design and Reliability Analysis of Wafer Level Package With Stress Buffer Mechanism," *IEEE Trans CPT*, Vol. 30, March 2007, pp. 110–118.

CHAPTER 11

Wire Bonding Process Modeling and Simulation*

In this chapter, a transient nonlinear dynamic finite element framework is developed which integrates the wire bonding process and the silicon devices under the bond pad. Two major areas are addressed: one is the impact of assembly first wire bonding process and another one is the impact of device layout below the bond pad. Simulation includes the ultrasonic transient dynamic bonding process and the stress wave transferred to bond pad device and silicon in the first bond. The Pierce strain rate dependent model is introduced to model the impact stain hardening effect. Ultrasonic amplitude and frequency are studied and discussed for the bonding process. In addition, different layouts of device metallization under the bond pad are analyzed and discussed to reduce the dynamic impact response of the bond pad over active design. Modeling discloses the stress and deformation impacts to both wire bonding and pad below device with strain rate, different ultrasonic amplitudes and frequencies, different friction coefficients, as well as different bond pad thickness and device layout under pad. The residual stress, after cooling down to a lower temperature, is discussed for the impact of the substrate temperature.

Most of the figures in this chapter are easier to understand in color, especially the Von-Mises stress distributions. Therefore see the book color-CD for a clearer understanding/presentation. Several animations are included as well.

11.1 Introduction

Wire bonding is a critical process stage in the assembly process for the connection between the semiconductor chip and the external

*This chapter was written by Yong Liu (Fairchild Semiconductor, Inc.; Yong.Liu@fairchildsemi.com)

world [11-1]. By this stage, most of the device's costs have been absorbed, especially for the high density wire bonding and the bond pad over active (BPOA) design [11-2, 11-3]. To reduce the cost and obtain the optimized wire bonding solution, modeling of the wire bonding process has been used to help to determine the optimized wire bonding parameters and to help identify the potential failure mechanisms [11-4]. Currently, there are a number of modeling studies on the wire bonding process [11-5 to 11-10]. Dominiek et al. [11-7] and Vincent et al. [11-9] have considered Cu/Lo-k interconnects under the bonding pad; Liu et al. [11-11] studied the wire bonding loop formation in the electronic packaging assembly process. Yeh et al. [11-12] made the transient simulation of wire pull test on Cu/Lo-k wafers. However, most authors only consider pure mechanical bonding loads with static or quasi-dynamic methods to simulate the free air ball (FAB) under compressive bonding process. Few simulations include both the dynamic nonlinear wire bonding process and silicon device stresses in the same model due to difficulties in achieving convergence. In reality, wire bonding is a complicated, multi-physics, transient dynamic process that is completed within a very short period of time. The dynamic impact to both the wire bond and devices on silicon is critical and significant. Therefore, previous modeling methods seem to be insufficient [11-10].

It is known that the common failure modes when making the wire binds are bond pad cratering, peeling, and cracking below the bond pad. There are five major factors that relate to the failure modes and affect the quality of bonding process and bond pad devices [11-10, 11-13]: bonding force or deformation, ultrasonic amplitude and frequency, friction and intermetallic compounds between FAB and bond pad, substrate temperature, and time duration. The challenges here are how to describe the ultrasonic dynamic effects? If we change the bond pad design, how does it affect the bonding process and stress distribution? When the system cools down to room temperature, how does the residual stress impact the bond pad device? In this chapter, the methodology of wire bonding modeling and simulation is presented and the finite element framework for both static and transient nonlinear dynamic wire bonding analysis are developed, which integrates both wire bonding process and the interconnects/silicon under the bond pad. Dynamic simulation focuses on the ultrasonic transient dynamic bonding process and the stress wave transferred to the bond pad device and silicon. The bonder capillary is considered as a rigid body due to high hardness. This results in a rigid and elastic plastic contact pair between the capillary and the FAB, while the contact surfaces between the FAB and the bond pad are a nonlinear contact pair with consideration of the dynamic friction. The Pierce strain rate dependent model is introduced to model the impact stain hardening effect.

Four topics of interest will be presented in this chapter: (1) wire bonding process with different parameters which includes ultrasonic amplitude, frequency, friction between the FAB and the bond pad, the

bond pad and the below device, residual stress after substrate cooling down; (2) comparison of the impacts between the wire bonding and the wafer probing for a bond pad over active device (BPOA); (3) wire bonding above a laminate substrate; and (4) impact of the wedge bonding versus the thermal-mechanical stress.

11.2 Assumption, Material Properties, and Method of Analysis

Simulation may help us to understand the stress impact and to examine the relative effects of elements within the bond pad structure over the active device on the stresses developed during wire bonding. However, modeling cannot solve every part of the bonding process. To conduct an effective simulation, the following assumptions are made:

1. Assume that the temperature of the FAB is the same as substrate (in reality, there is some difference due to the transient temperature cooling from FAB forming and moving to contact bond pad).
2. Assume that the FAB is rate dependent elastic plastic material during the bonding process. Bond pad and rest metal layers are elastic plastic material. All the other materials are linear elastic.
3. The contact intermetallic effect and diffusion in the bond formation due to ultrasonic energy will not be considered in this chapter. It will require further work to determine an equivalent way to model the intermetallic impact, such as the equivalent material parameters over certain local ranges and the coefficient of friction between FAB and bond pad.
4. Assume the capillary is a rigid body due to a much higher Young's modulus and hardness. The inertia force from capillary transferred to FAB is not considered here.
5. The heat and temperature induced by the friction between FAB and bond pad is not included.

When ultrasonic energy is applied to the FAB by capillary, it causes a reduction in yield strength and increases the mobility and density of dislocations after some dwell time [11-13]. The strain rate is in the "slip by dislocation shifting region," as the deformation occurs, the material strain hardens. When the hardening material transmits energy to the ball-pad interface, slip planes shift at the interface, opening up new metal surfaces. Contact diffusion bonding (with intermetallic effects at certain temperature rises by dynamic friction), enhanced by ultrasonics, occurs at the newly exposed metal surfaces; as the frequency increases, after some point (e.g., 120 kHz or above), the FAB material may not be significantly softened at the beginning, while the strain rate is in the "simultaneous several lattice slip region,"

Material	Modulus (GPa)	CTE (ppm/C)	Poisson Ratio	Yield Stress (GPa)
Silicon	169.5	3.2	0.23	
ILD	70.0	4	0.25	
TiW	117.0	10.2	0.25	
Al(Cu)	70.0	10	0.35	0.2 (25°C) 0.05 (45°C)
Au(FAB)	60.0	14	0.44	0.0327 (200°C)
W (plugs)	409.6	4.5	0.28	

TABLE 11-1 Materials Parameters

the material behaves as a hard material transmitting energy to the ball-pad interface [11-14, 11-15]. Ikeda et al. indicated [11-1]: a gold ball is impacted by a capillary at the loading speed of 0.98 N/s, which may result in the strain rate of the gold ball more than 1000 1/s locally. Based on the Hopkinson impact bar tests by Ikeda, the yield stress of FAB with strain rate hardening may be approximated by

$$\sigma_s = \sigma_0 + H'\dot{\varepsilon}^{pl} \tag{11.1}$$

where σ_0 = 0.0327GPa, H′ = 0.00057 GPa·s

Equation (11.1) can be further expressed as the rate dependent Peirce model

$$\sigma_s = \left[1 + \frac{\dot{\varepsilon}^{pl}}{\gamma}\right]^m \sigma_0 \tag{11.2}$$

where m = 1 and γ = 561.4 (1/s)

The material parameters are listed in Table 11-1, FAB, bond pad, and metal layers are nonlinear (bi-linear) materials, all of the rest of the materials are considered to be linear elastic.

A general finite element code, ANSYS®, is used in the modeling. A nonlinear large deformation and transient dynamics implicit algorithm with the above rate dependent Peirce model is selected. Since the bonder capillary is considered as a rigid body due to high hardness, this leads to the rigid and elastic plastic contact pair between capillary and FAB. While the contact surfaces between FAB and bond pad are a nonlinear contact pair with consideration of the dynamic friction.

11.3 Wire Bonding Process with Different Parameters [11-10]

A conceptual 2D model is shown in Fig. 11-1, which is a cut from a typical die with three layer metallization and three dielectric (ILD)

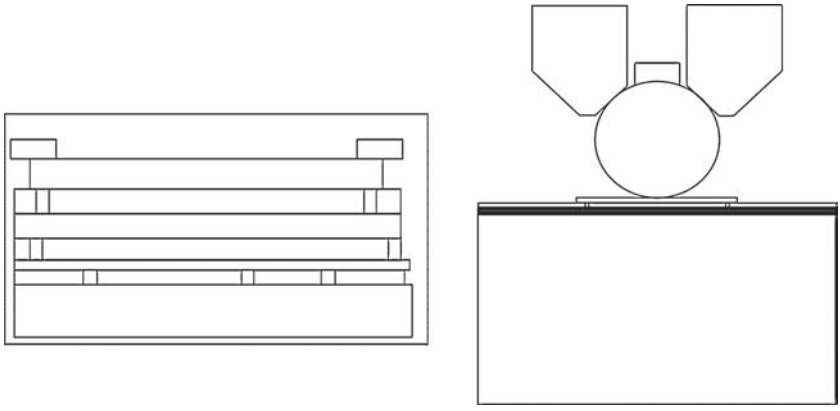

Figure 11-1 Conceptual bond pad system.

layers above the silicon. The typical diameter of a FAB is 70 μm, the bond pad length is 90 μm. The bottom of silicon is fixed and two sides are constrained in horizontal direction. Figure 11-2 gives the meshes of FAB and bond pad system. The capillary moves down a certain height (bonding height) to press the FAB with a high speed and different frequency. The ultrasonic horizontal motion cycle of the capillary

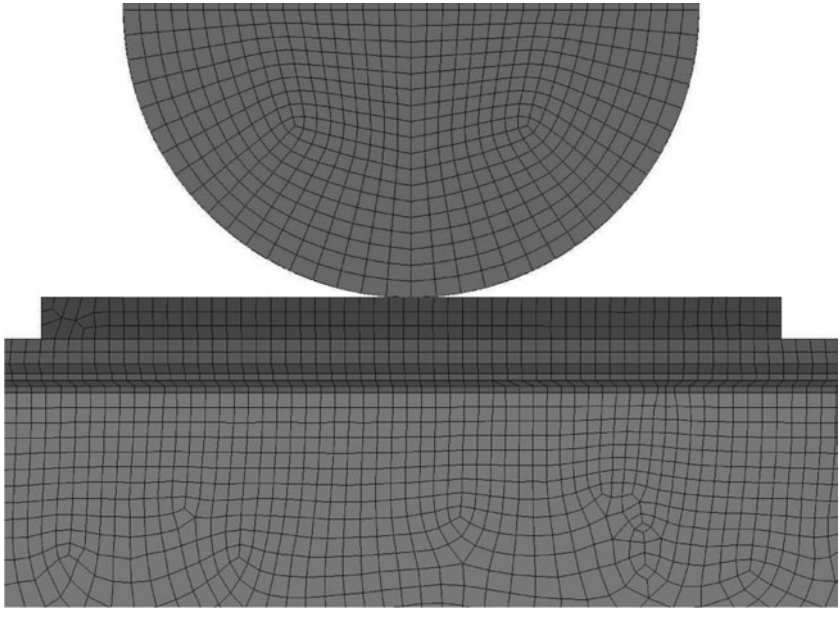

Figure 11-2 Meshes of FAB and bond pad model.

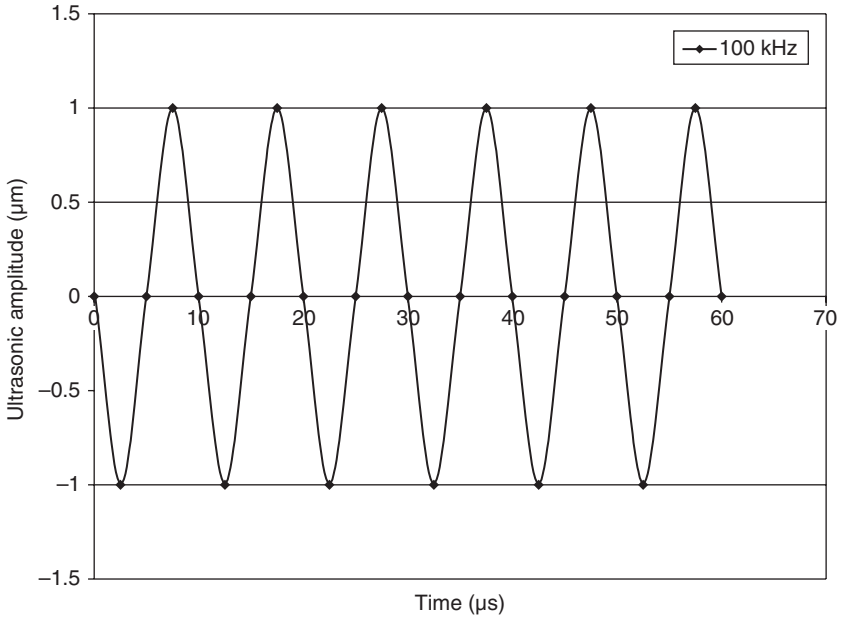

Figure 11-3 Ultrasonic cycle movement versus time (US) with a amplitude of 1 µm and 100 kHz.

with a typical amplitude of 1 µm and a typical frequency of 100 kHz is showed in Fig. 11-3.

Figure 11-4 shows the typical bonding force versus time. Two phases are defined in Fig. 11-4, phase one includes the contact impact with strain hardening and after about 100 to 150 ultrasonic cycles

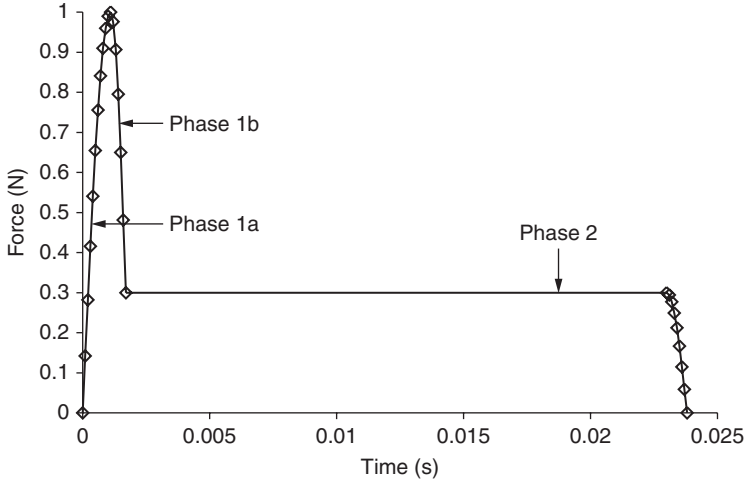

Figure 11-4 Typical bonding force versus time.

later, it becomes softened (similar to Ref. [11-16]); and goes into the second phase with a lower constant bonding force.

11.3.1 Impact of Ultrasonic Amplitude

The results of impact of ultrasonic amplitude are showed in Figs. 11-5 to 11-10. These results are obtained under a fixed ultrasonic frequency 138 kHz.

Figure 11-5 shows that the stress in bonding processing moves as the capillary moves and symmetric case only appears when the capillary moves to the center area. Figure 11-6 shows that the von-Mises stress at amplitude of 1.0 μm is about 37% greater than that at 0.25 μm amplitude.

Figure 11-7 shows that the maximum principal stress in pad below device increases as the ultrasonic amplitude increases. However, the maximum von-Mises stress and shear stresses decrease at the beginning, after amplitude is larger than 0.5 μm, their values increase. Figure 11-8 gives similar situation in stresses transferred to silicon. Figure 11-9 discloses that as the amplitude increases, cratering deformation in horizontal direction increases, while the cratering deformation in vertical direction reduces. Strains in both direction increase as the amplitude value increases. Figure 11-10 shows all the stresses in bond pad (metal 3) increase as the ultrasonic amplitude increases. The above results show that the ultrasonic amplitude has significant impact to the stress and cratering deformation during wire bonding process.

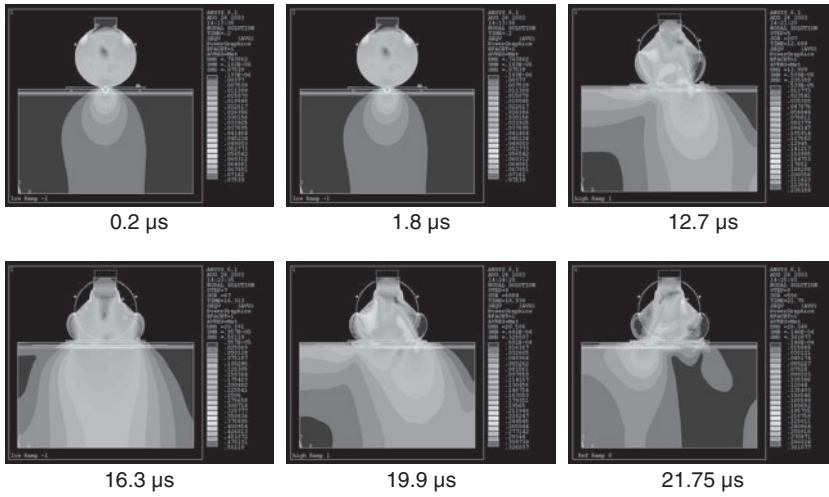

Figure 11-5 Von-Mises stress distribution at different time.

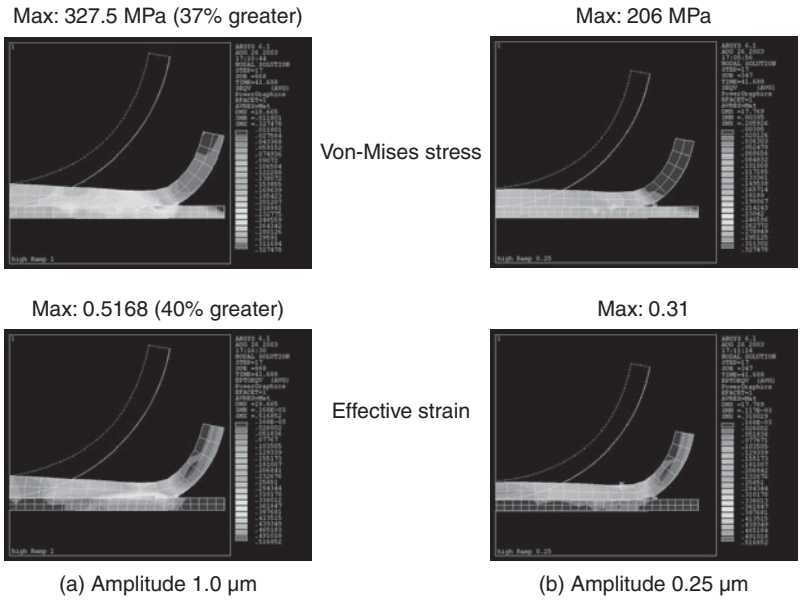

Figure 11-6 Contact layers between pad and ball with ultrasonic amplitude 1.0 μm versus 0.25 μm.

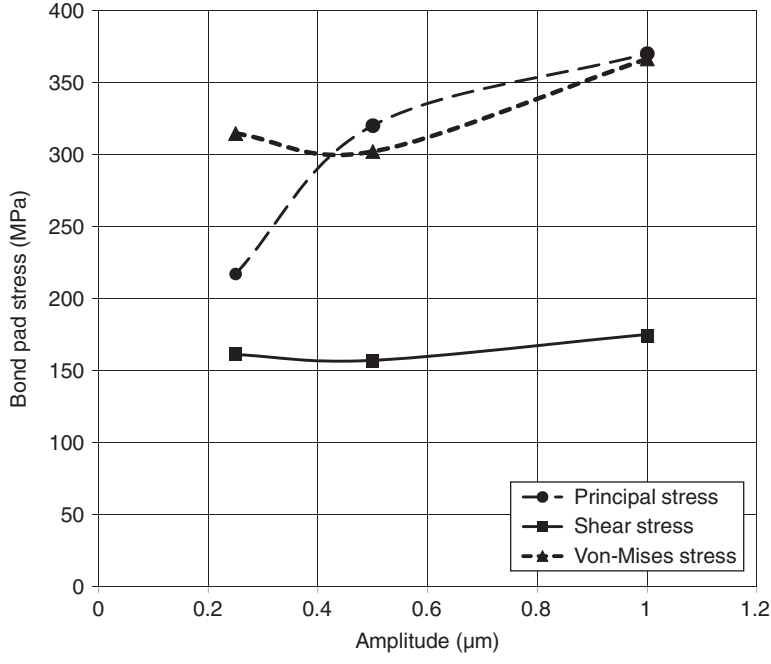

Figure 11-7 Stresses in pad below device versus ultrasonic amplitude.

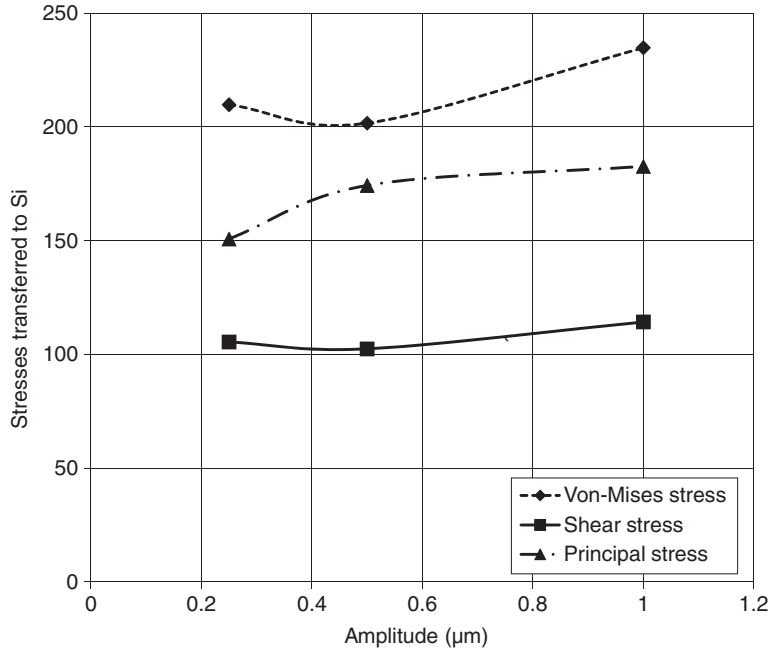

Figure 11-8 Stresses transferred to silicon.

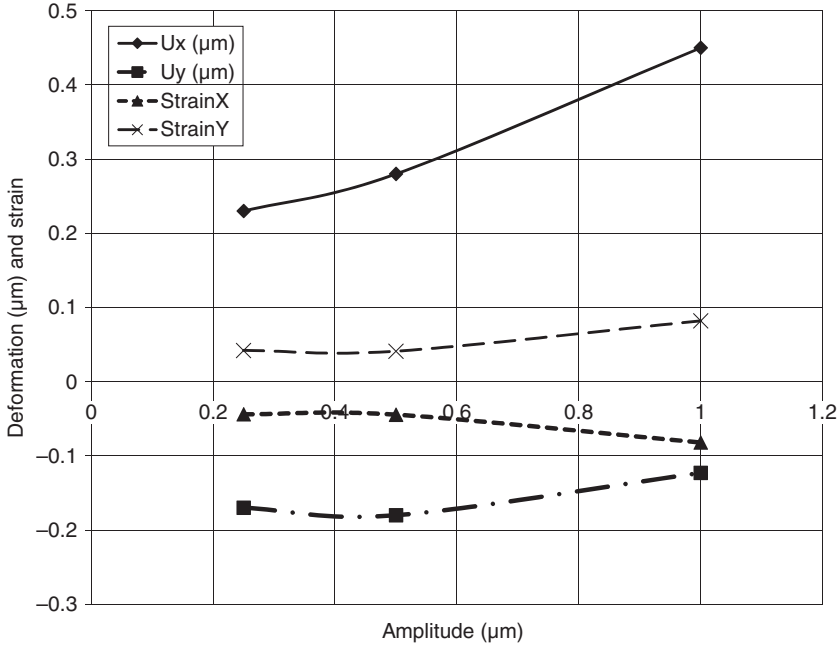

Figure 11-9 Bond pad cratering deformation and strains.

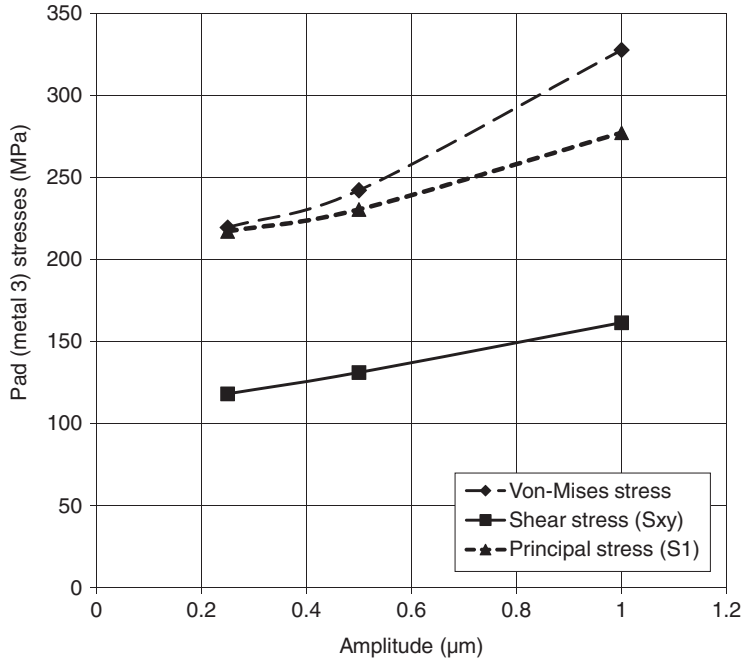

Figure 11-10 Bond pad stresses versus ultrasonic amplitude.

11.3.2 Impact of Ultrasonic Frequency

The results under different ultrasonic frequency and a fixed amplitude of 1 μm are listed in Figs. 11-11 to 11-15. Figure 11-11 gives the comparison of von-Mises stress and strain under 60 kHz and 138 kHz frequencies. The von-Mises stress increases about 7.5% with 138 kHz, and effective strain increases about 8.5%.

Figure 11-12 shows the maximum principal stress in pad below device increases as the ultrasonic frequency increases. However, the maximum von-Mises stress and shear stress decrease at the beginning, when the frequency is larger than 100 kHz, their value increases. This may explain the effects of frequency, at the beginning, FAB becomes softened at lower frequency, and after 100 kHz the strain hardening properties due to rate dependence become dominant and make the stresses increase. However, the changes are not so significant. Figure 11-13 shows that all the stresses transferred to silicon have similar properties, that is, at the beginning the decrease after the frequency is larger than 100 kHz, their values increase. Figure 11-14 shows there is no significant difference in bond pad cratering strain and deformation as the frequency goes up, though vertical cratering deformation has the same properties. Figure 11-15 shows stresses in bond pad increase as the ultrasonic frequency increase. In overall,

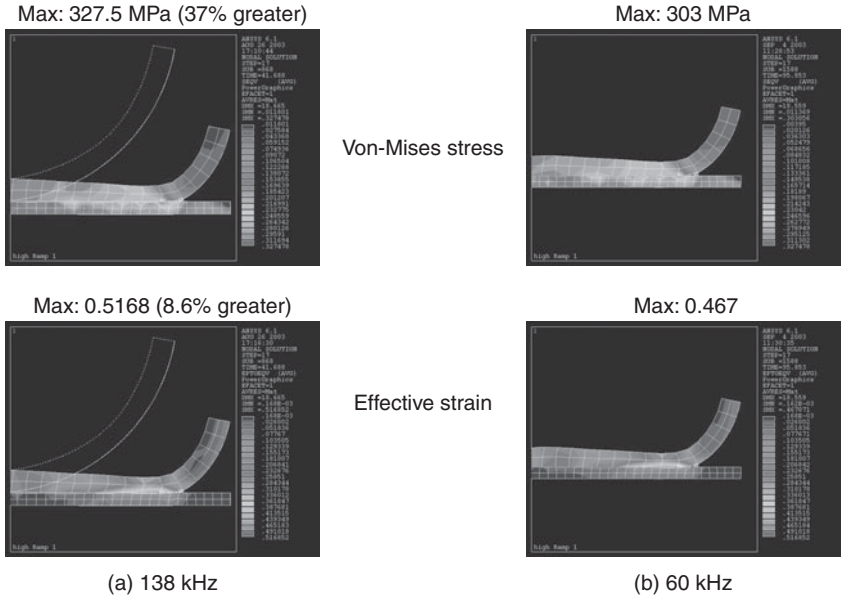

Figure 11-11 Contact ball and pad layers with 138 kHz and 60 kHz.

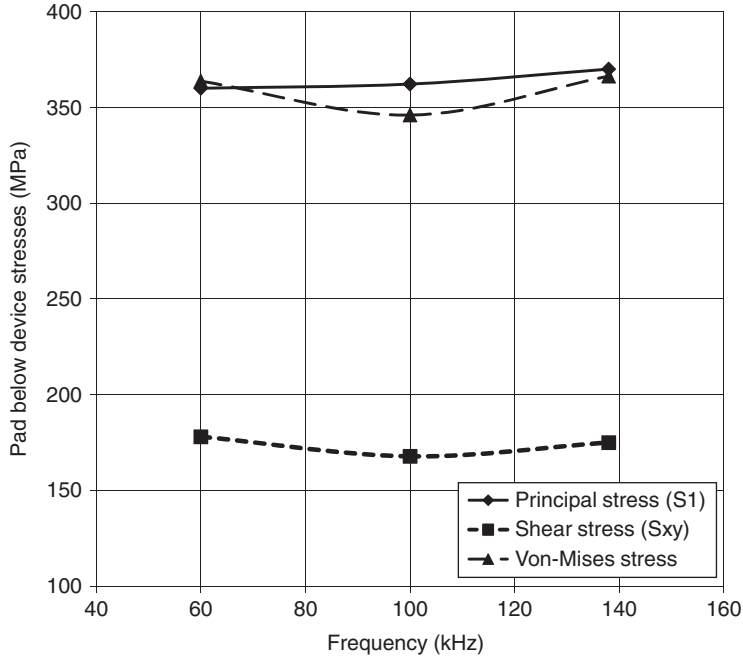

Figure 11-12 Stresses of pad below device under different frequencies.

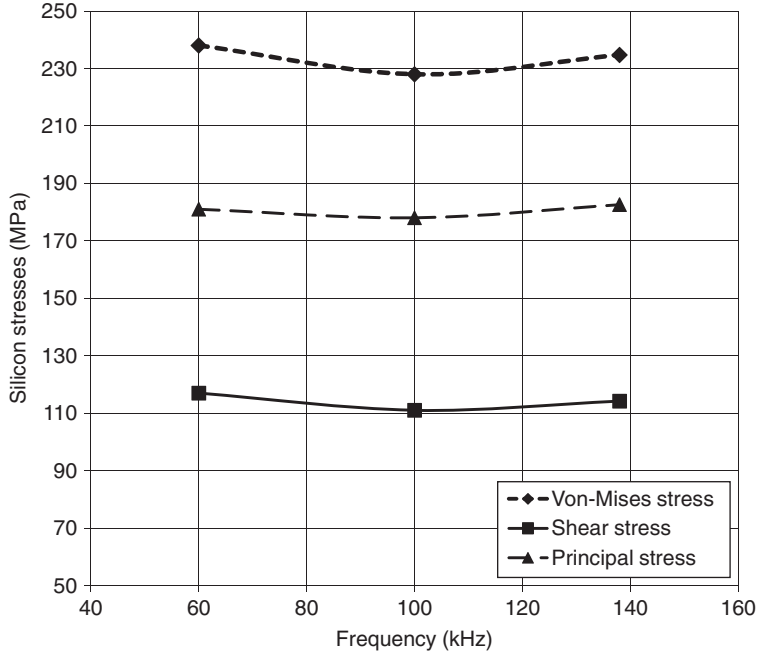

Figure 11-13 Stresses transferred to silicon under different frequencies.

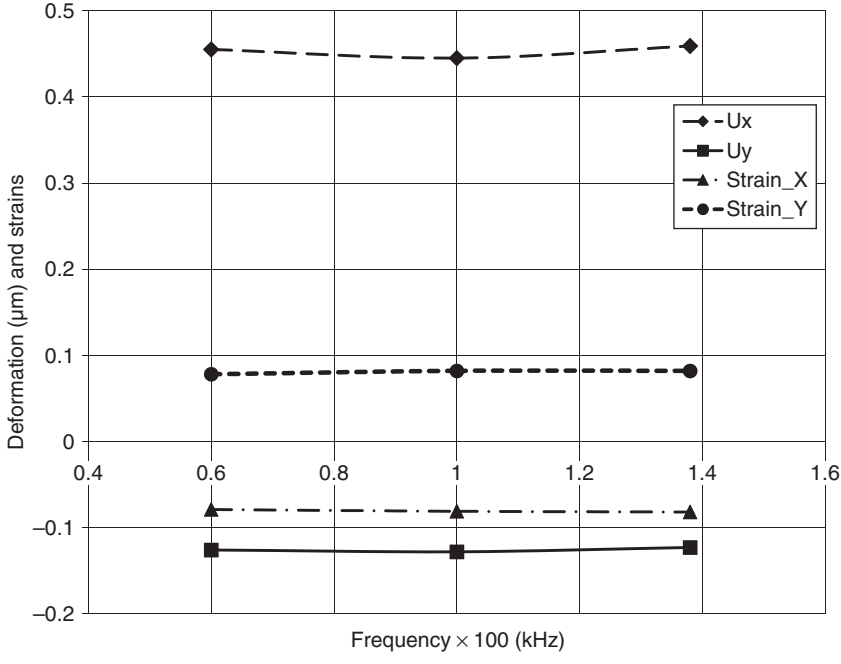

Figure 11-14 Bond pad cratering deformation and strain versus frequency.

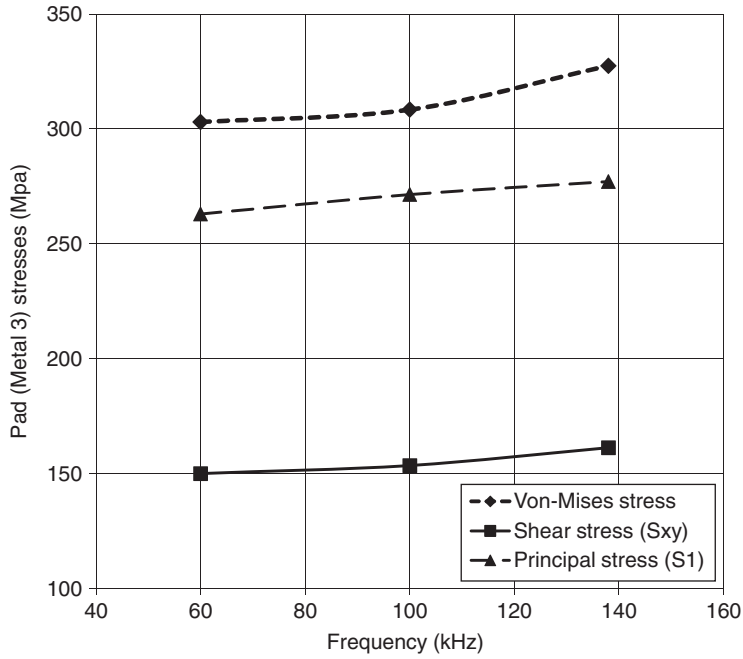

Figure 11-15 Bond pad stresses versus frequency.

impact of ultrasonic frequency is not as significant as the impact of ultrasonic amplitude. Perhaps when in our modeling assumptions, the inertia force from capillary is not considered, that could induce an error.

11.3.3 Impact of Friction Coefficients between Bond Pad and FAB

Bonding friction is a complicated multiple physics process at interface between ball and pad, bonding occurs when the ample energy is available to overcome the active energy of barrier and surface oxidation; and the relative motion at the interface of ball and pad is zero. Based on the assumption, the heat induced by friction and thereby induced intermetallic diffusion problem are not considered. The results are listed in Figs. 11-16 to 11-20 with different friction coefficients.

Figure 11-16 shows the von-Mises stress comparison at different phase with a higher friction and a lower friction. The results have disclosed that at final phase, although the stress in a higher friction case is about 1.18 times greater than the lower friction case, radius of ball/pad bonding is about 10% greater than that of lower friction.

Lower friction

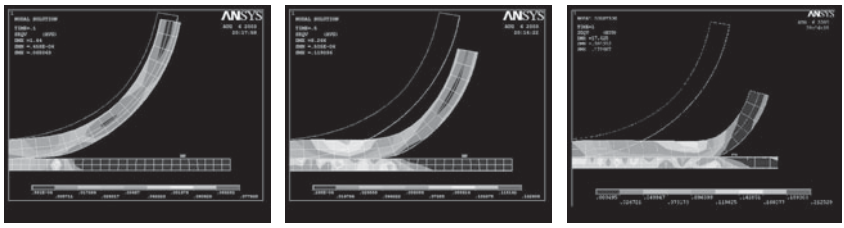

65.06 MPa 119.04 MPa 178.67 MPa

Higher friction

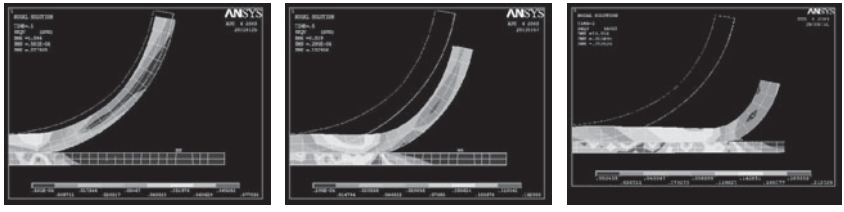

77.94 MPa 132.91 MPa 212.53 MPa
(radius 10% greater)

Figure 11-16 Von-Mises stress comparison of higher (friction coefficient is 1.5) and lower friction (friction coefficient is 0.2).

Figures 11-17 to 11-19 show that pad deformation is very nonuniform in horizontal (radial) direction. Higher friction makes larger ball/pad contact area and codeformed bonding. However, this may result in higher stress and greater cratering. If the stress and deformation induced in wire bonding process are within the failure criterion, it would be better to increase the friction coefficient.

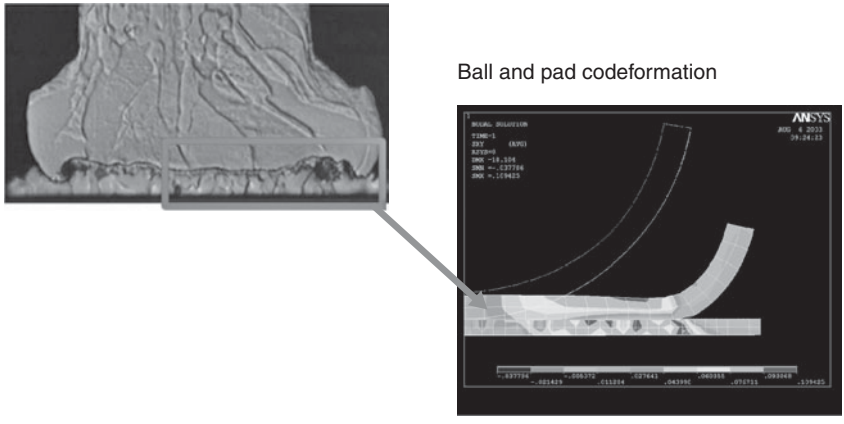

Figure 11-17 Codeformed ball/pad with friction. (*Courtesy from KNS: C-SAM Picture*)

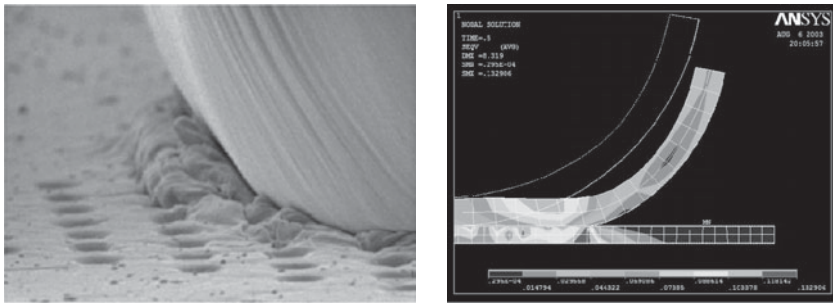

Figure 11-18 Deformed ball/pad during bonding process (maximum stress appeared at the contact edge interface). (*Courtesy from KNS: C-SAM Picture*)

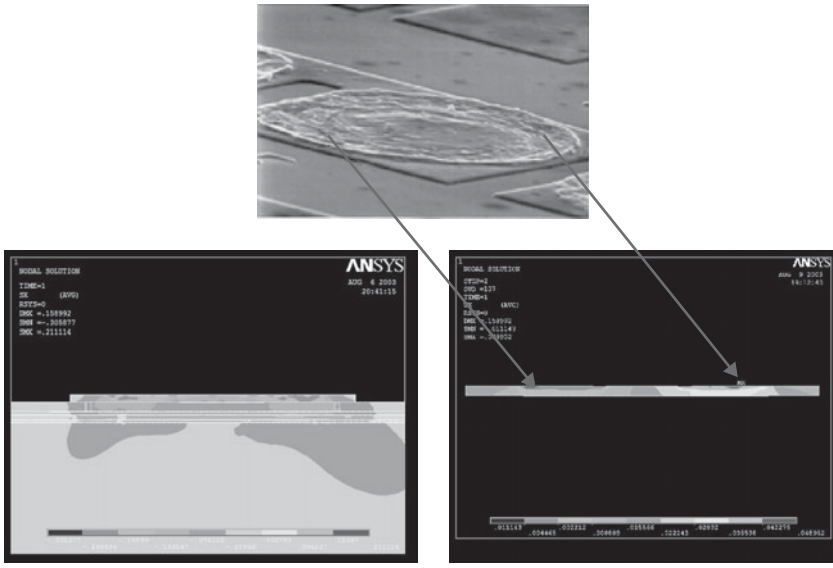

Figure 11-19 Pad cratering and 2D section modeling results. (*Courtesy from KNS: C-SAM Picture*)

Figures 11-20 and 11-21 give the profiles of bond pad stresses and deformation versus the friction coefficients. As the friction coefficient increases, the stress and deformation increases. After some point (1.5), stress and deformation do not change significantly. This is understandable, because as the friction coefficient becomes big enough, the ball and pad become stuck together and initial relative movement is not possible.

Optimation of wire bonding assembly process is one way to reduce the cratering and crack failure of a BPOA design. Another way is to test different bond pad structures above the device, and determining

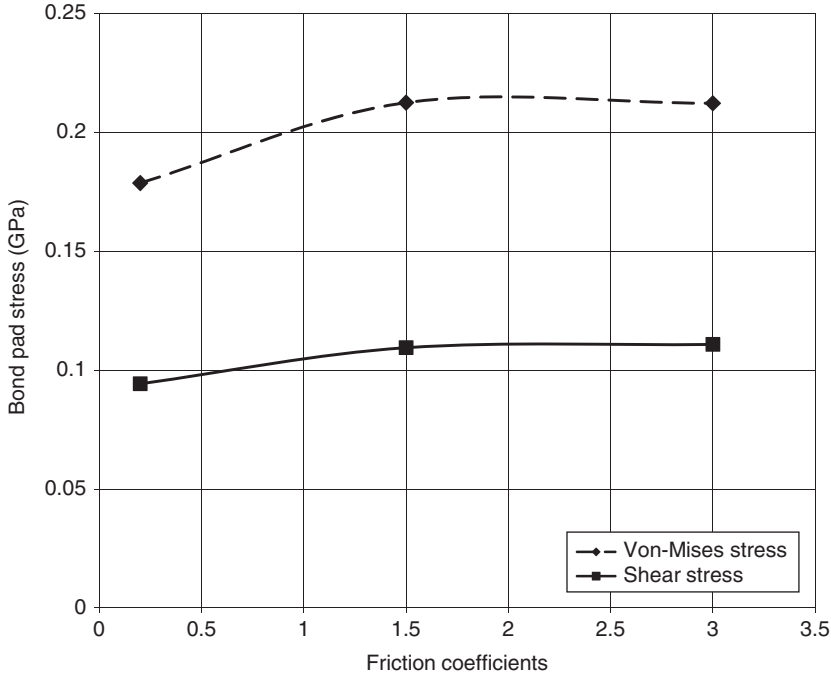

Figure 11-20 Bond pad stresses versus friction coefficient.

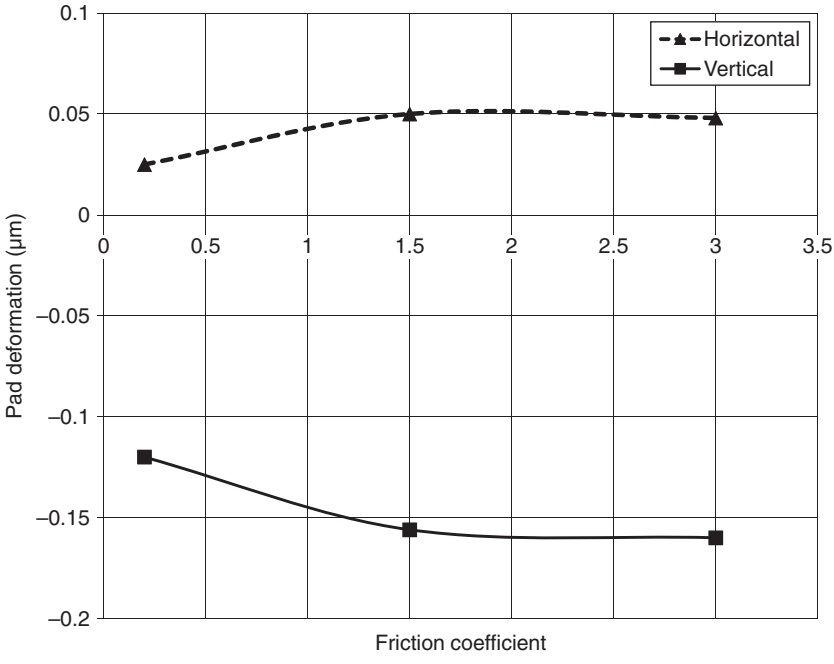

Figure 11-21 Bond pad deformation versus friction coefficient.

how much stress is transferred to the silicon. This section discusses the impact of different bond pad thickness and pad structure.

11.3.4 Impact of Different Bond Pad Thickness

Increasing bond pad thickness is an easy and low cost way to reduce cratering. The simulation results for different bond pad thicknesses are listed in Figs. 11-22 to 11-25.

Figure 11-22 gives the maximum principal stresses comparison for die under three different bond pad thicknesses. Figure 11-23 gives the profiles' comparison of stresses transferred to silicon interface. Both have shown that as the bond pad thickness increases, the stresses transferred to silicon see no significant reduction. However, the plastic effective strain and plastic strain density in bond pad reduces rapidly (see Figs. 11-24 and 11-25). It is this property of bond pad that reduces the cratering during wire bonding.

11.3.5 Impact of Different Bond Pad Structures

Here we discuss two different layouts below bond pad, one layout adds a thin TiW layer under the bond pad (Fig. 11-26) and another layout is to make a higher uniform density of plugs in the three ILD layers (Fig. 11-27).

Table 11-2 gives the von-Mises stress comparison of two structures with and without the TiW thin layer. These data show that adding TiW thin layer could reduce the stress transferred to silicon a small amount. However, this induces greater stress in ILD and metal layers.

Table 11-3 and Fig. 11-28 show the von-Mises stress comparison with and without higher density plugs in ILD. The results show that with a uniform high density of plugs, it reduces the stress transferred to silicon. However, the stress in ILD layers increases.

From the above it can be seen that there is a trade-off in changing the bond pad structure. One needs to do reliability testing to make sure the new device can withstand the wire bonding process.

11.3.6 Modeling Results and Discussion for Cooling Substrate Temperature after Wire Bonding

The residual stress after wire bonding is an interesting topic, which relates to the substrate temperature and bond pad peeling failure [11-17, 11-18]. Reference [11-17] studied the optimization of thermosonic ball bonding process with different substrate temperatures. Here, an ultrasonic wire bonding with amplitude 0.25 μm and frequency 138 kHz, its substrate temperature is 240°C. After wire bonding, the system cools down to 50°C. The simulation of a fully transient dynamic wire bonding modeling at substrate temperature 240°C is done first, then remove the capillary and cool down to 50°C. The results show that most of the stresses in the ball decrease when the

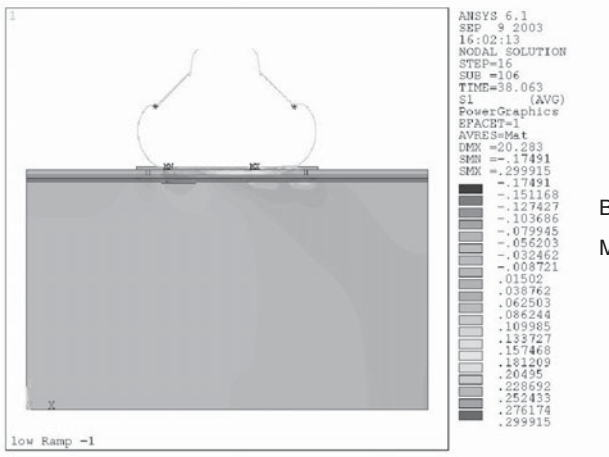

Bond pad: 1.2 μm

Max tensile: 299 MPa

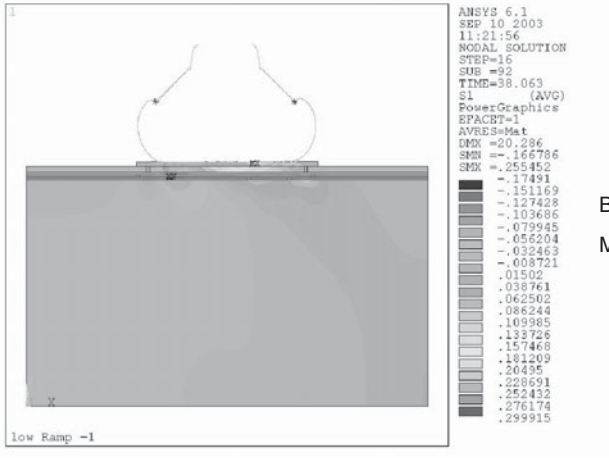

Bond pad: 2.4 μm

Max tensile: 255 MPa

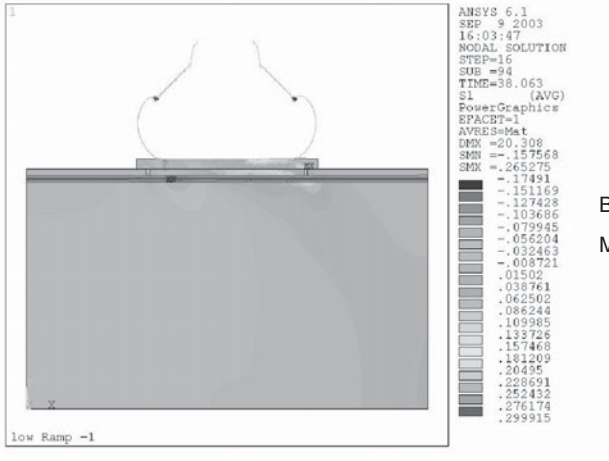

Bond pad: 5.0 μm

Max tensile: 265 MPa

Figure 11-22 Maximum principal stresses in die versus bond pad thickness at the first step of cycle 6 (capillary toward left).

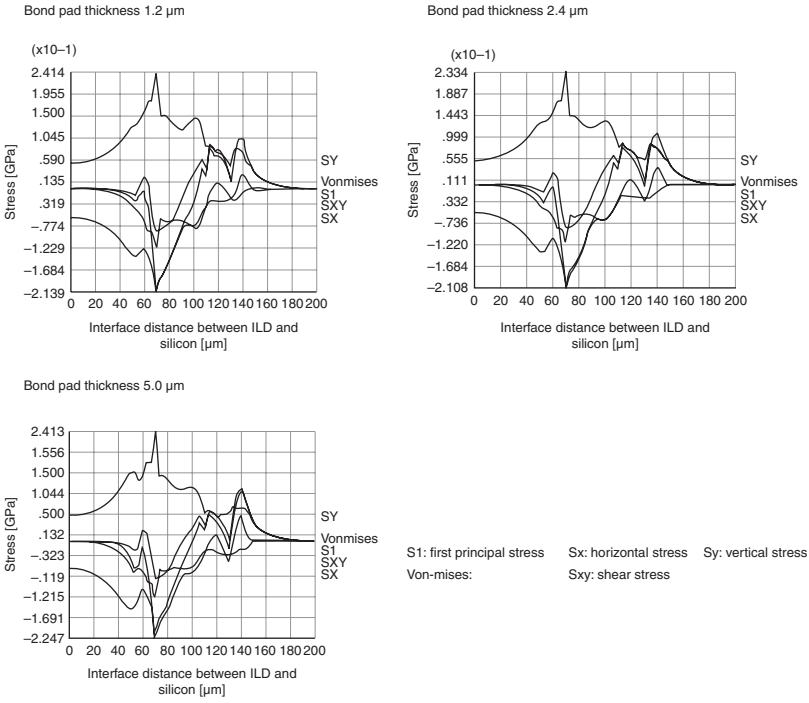

FIGURE 11-23 Stresses transferred to the interface between ILD and silicon at the first step of cycle 6 (capillary toward left and 35-135 is the pad area).

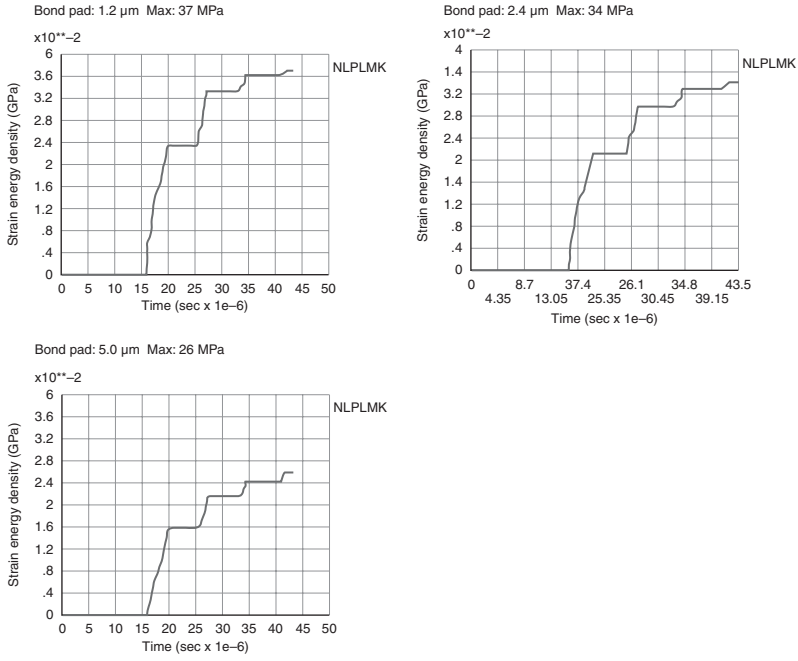

FIGURE 11-24 Bond pad plastic strain energy density at the end of cycle 6.

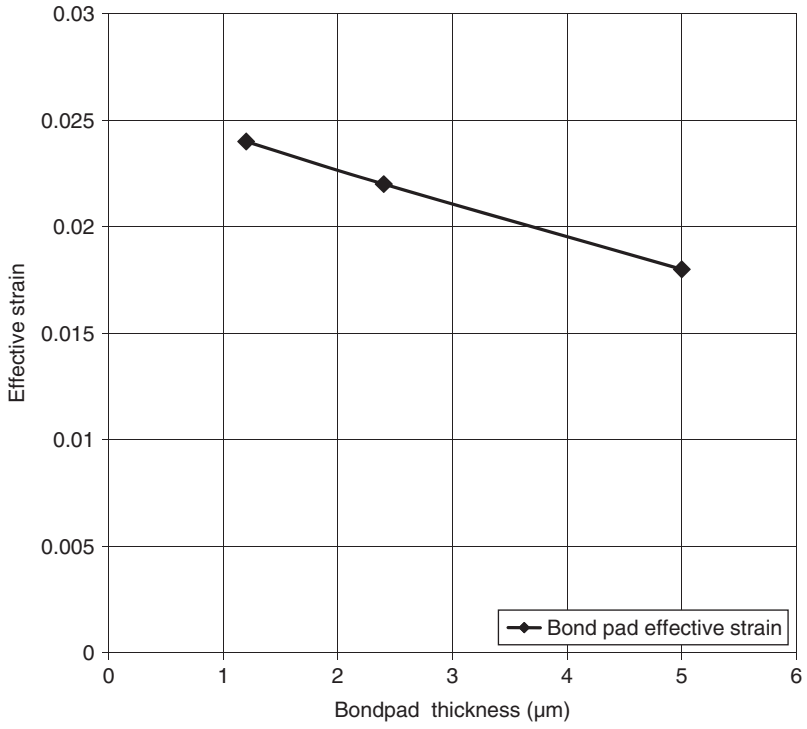

Figure 11-25 Bond pad maximum plastic strain versus pad thickness.

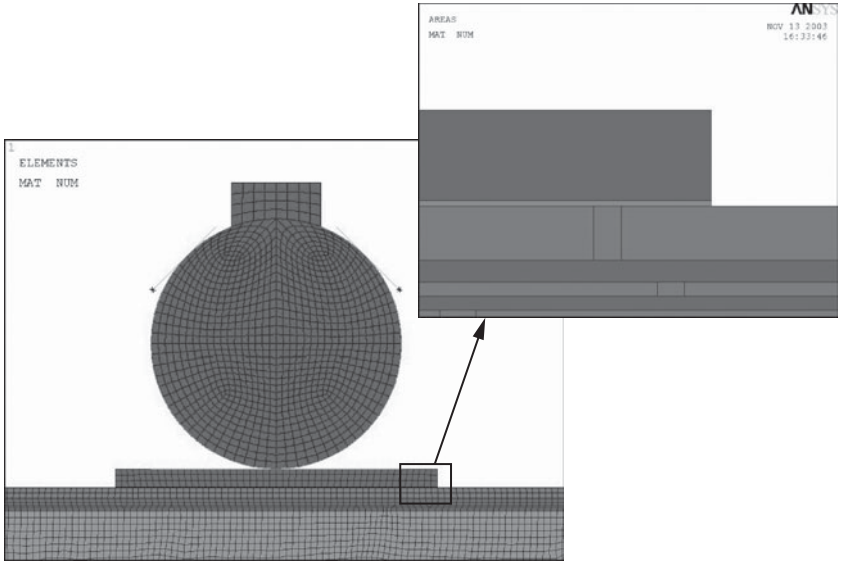

Figure 11-26 A TiW layer (0.3 μm) is added under bond pad.

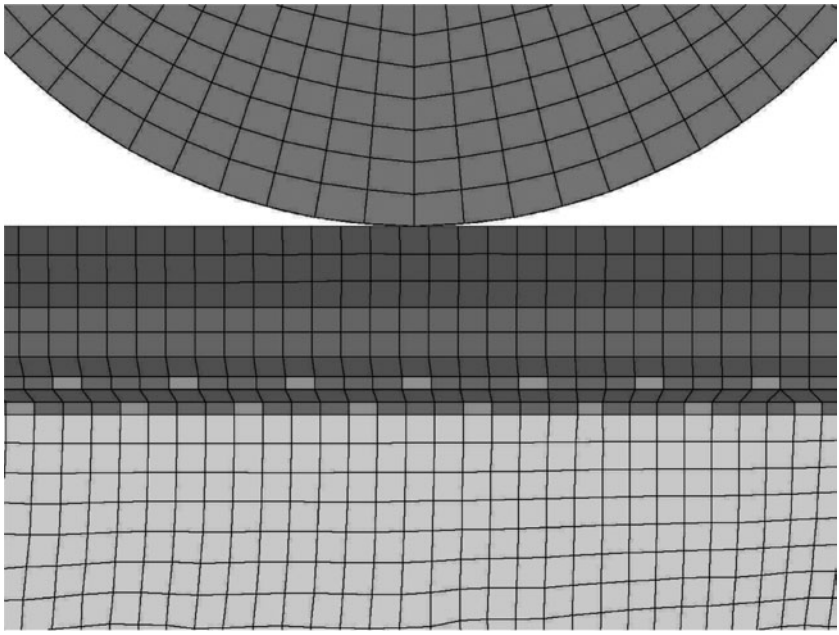

Figure 11-27 A higher density plugs in ILD layers.

Quasi-Dynamics	With TiW	No TiW
Maximum stress in ILD	281 MPa	276 MPa
Stress transferred to silicon	268 MPa	272 MPa
Maximum stress in metal layers	180 MPa	171 MPa

Table 11-2 Von-Mises Stress Comparison for Layout First w/o TiW

temperature cools down to 50°C. Figure 11-29 gives an example of shear stress distribution before and after the cooling. However, the stresses below the ball increases, the maximum von-Mises stress appears at the interface between plug and ILD (see Fig. 11-30).

Figure 11-31 gives the shear stress distribution at the contact interface between ball and pad, the position value stands for the shear stress toward the counterclockwise direction, it reduces after cooling to 50°C, however, the shear stress along the clockwise direction increases significantly. Figure 11-32 gives the comparison of stresses transferred to the interface between ILD and silicon, after cooling down, the stresses increase due to CTE mismatch. However, since the capillary is removed, stress jumping at the ball and pad contact edge relaxes.

Quasi-Dynamics	With Higher Density Uniform Plugs	Current Design
Maximum stress in ILD	294 MPa	276 MPa
Stress transferred to silicon	260 MPa	272 MPa
Maximum stress in metal layers	173 MPa	171 MPa

TABLE 11-3 Von-Mises Stress Comparison for Layout Two

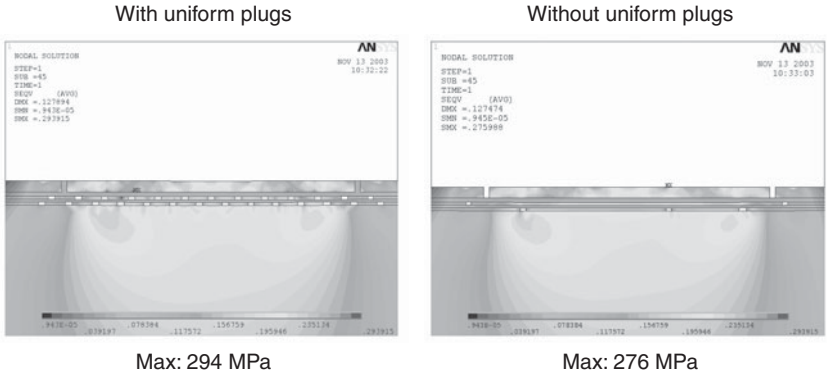

FIGURE 11-28 Von-Mises stress comparison with and without higher density uniform plugs.

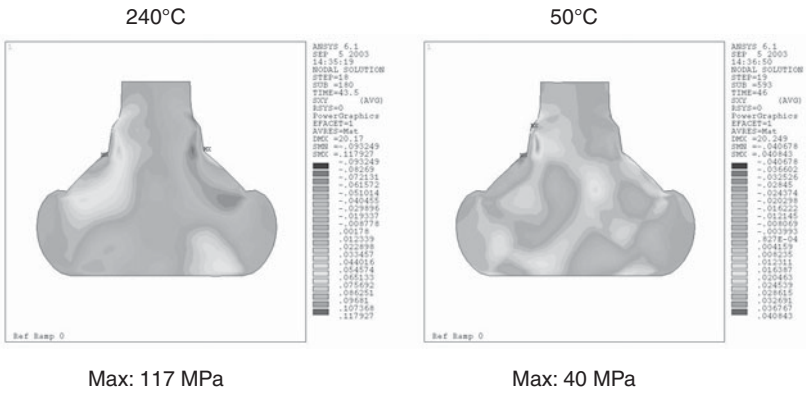

FIGURE 11-29 Shear stress after ball cools to 50°C.

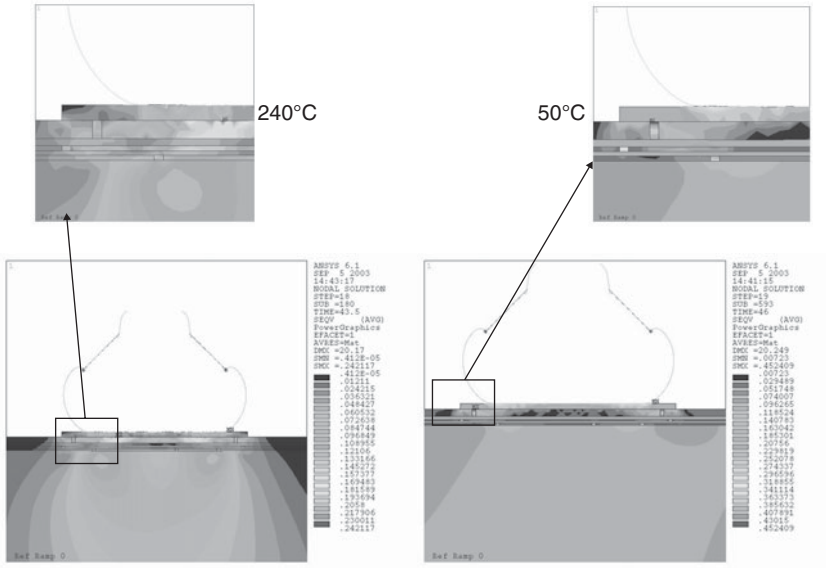

Figure 11-30 Maximum stress appear at the plugs interface after cooling to 50°C.

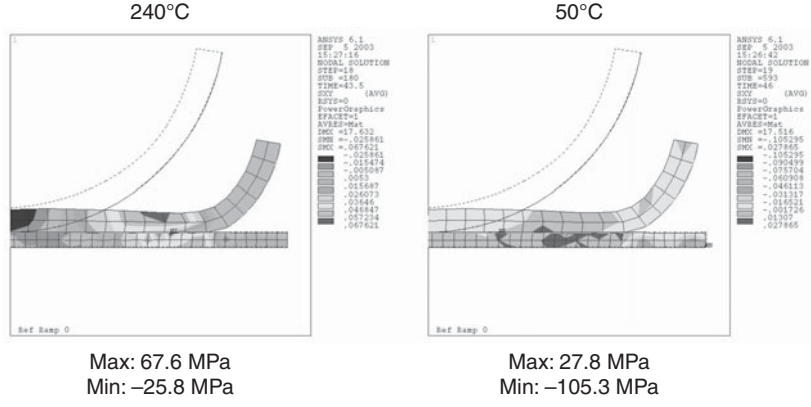

Figure 11-31 Shear stress comparison at the ball and pad interface layers.

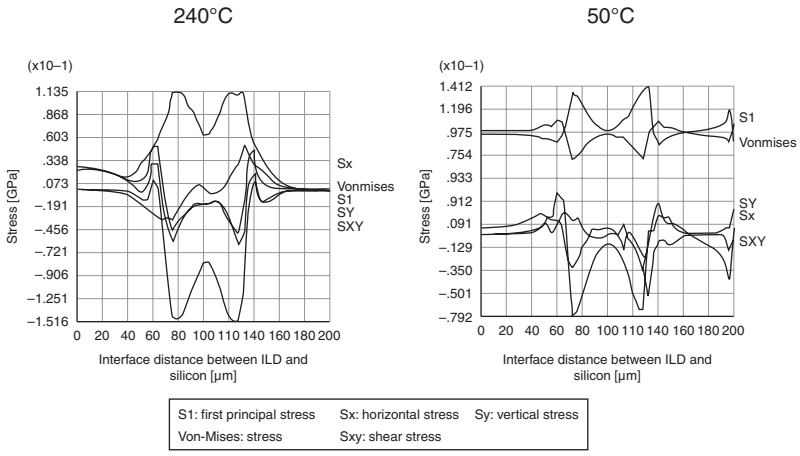

Figure 11-32 Stress transferred to the interface between ILD and silicon.

11.3.7 Summary

Wire bonding is a complicated multi-physics problem; this section develops the simulation framework and tries to target both the assembly wire bonding process and bond pad structure with a fully transient nonlinear dynamic FEM. A summary of the work follows:

1. For the wire bonding assembly process, increasing the ultrasonic amplitude will certainly increase the wire bonding stress, the stress transferred to silicon as well as the cratering in radial direction. Increasing the ultrasonic frequency seems to have an optimum point, the stress decreases at the beginning, and increases again after some point. However, the increment seems less significant than the impact of amplitude; this may be partly due to our not considering the inertia force of the capillary during the wire bonding process. Increasing the friction coefficient between the FAB and bond pad will increase the wire bonding stress and stress transferred to silicon, however, higher friction contact will result in better codeformed bonding.
2. For the bond pad and structure below, increasing the bondpad thickness can reduce the bondpad plastic energy density and strain, this helps to reduce the cratering failure, but the stresses seem not significantly reduced. Changing the bond pad structure, such as adding a thin TiW layer under the bond pad and introducing higher density plugs in ILD can reduce the stress transferred to silicon, however, this will induce higher stress in ILD. There is an optimum trade-off in the design for the BPOA structure.

3. The impact of substrate temperature is remarkable during cooling process. The stresses in ball are reduced by cooling down to 50°C, and stresses below the ball increase due to CTE mismatch. The maximum stress appeared at the plug interface between plug and ILD. However, stress jumping at the position of contact edge of ball and pad relaxes. This shows after the cooling process, the stresses becomes more uniform as compared to before cooling.

11.4 Comparison of the Impacts between Wire Bonding and Wafer Probing for a Bond Pad Over Active (BPOA) Device [11-19, 11-20]

The region below the bond pad may be utilized for active devices to minimize the die area and the die cost. Modeling is an approach to understand the stress impact to both wire bonding process and BPOA, and may further help us to improve the bonding process and BPOA design for avoiding die failure such as crack/debonding. What degree of wafer probe induced failure is equivalent to wire bonding process failure with the same bond pad structure? Wire bonding or wafer probe, which make things worse? This section provides the modeling comparison of probe test versus wire bonding for bond pad structure. Therefore, this section will address to compare the impacts of wire bonding and wafer probing for a BPOA structure.

11.4.1 Probe Test Model

The probe test structures are shown in Figs. 11-33 and 11-34. Because the geometry size of the probe beam is much larger than the probe tip, in order to conduct an effective simulation and analysis, the following assumptions are made:

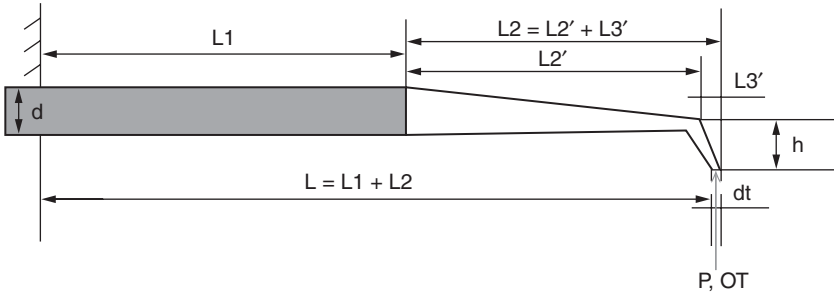

Figure 11-33 Probe test structure.

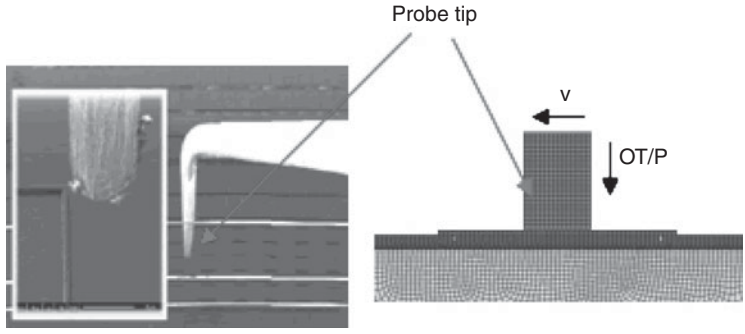

(a) A typical probe tip [11–19] (b) A probe tip model

Figure 11-34 Probe test model: probe tip contact with bond pad.

1. The probe beam follows Euler Beam theory, therefore the relationship of probe over travel (OT) distance and probe tip force (P) could be analytically obtained

$$P = \frac{\pi E \Delta}{64\left\{\dfrac{d + C_d(L_1 - L)}{3C_d^2[d + C_d(L_1 - L)]^2} + C_1 L + D_1\right\}} \tag{11.3}$$

where Δ is the OT, $C_d = \dfrac{d - d_t}{L_2}; I = \dfrac{\pi d^4}{64}$

$$C_1 = \frac{(LL_1 - L_1^2)}{EI} - \frac{32[d + 2C_d(L - L_1)]}{3\pi E C d_d^2 d^3}$$

$$D_1 = \frac{(LL_1^2/2 - L_1^3/6)}{EI} - C_1 L_1 - \frac{32[2d + C_d(L - L_1)]}{3\pi E C_d^3 d^2} \tag{11.4}$$

for a particular probe test pin used in this study, the relationship between OT and probe tip force is listed in Table 11.4 in terms of Eq. (11.3).

2. Based on assumption 1, the FEA model may be set up for a local probe tip and BPOA structure (see Fig. 11-34), which includes a contact pair for probe tip and bond pad.

Figure 11-35 gives the wire bonding model that is used for the comparison of the damage degree of probe test and wire bonding. The material parameters are listed in Table 11-5, FAB, bond pad and metal layers are nonlinear (bilinear) materials, all of the rest of the materials including probe pin are considered to be linear elastic.

OT(mil)	Probe Force *P* (g)	Probe Tip Force *P* (mN)	Probe Tip Pressure *p* (GPa)
2	4.31	42.2	0.0833
4	8.62	84.4	0.167
6	12.93	126.7	0.25
8	17.2	168.9	0.333
10	21.55	211.1	0.417

Note: Probe size: L = 4.874 mm, L_1 = 2.169 mm, L_2 = 2.705 mm, d = 0.254 mm, dt = 0.0254 mm (probe tip diameter), BCF = 2.15 g/mil

TABLE 11-4 OT versus Contact Force

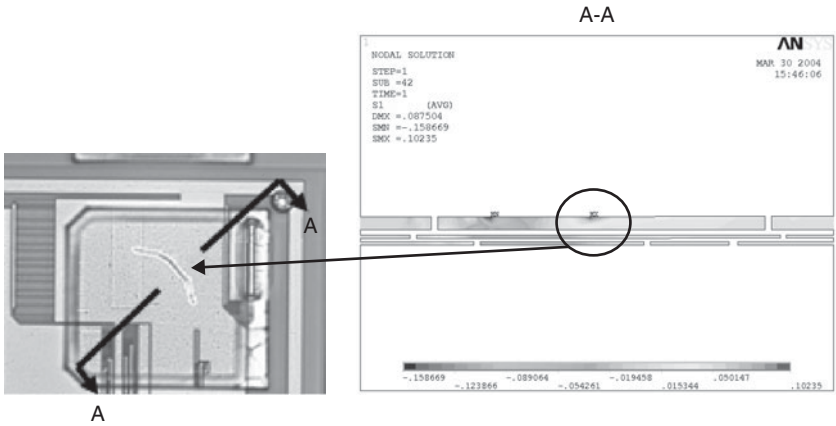

FIGURE 11-35 Failure comparison of modeling and test with OT = 6 mils, the max. first principle stress is 102.3 MPa.

11.4.2 Probe Test Modeling

During the probe over travel, electrical contact is made as the probe breaks through the thin surface oxide of the pad. Since the contact area of probe tip is very small, it can induce some local bending deformation and tensile stress in the bond pad layers, both metals and dielectric of the BPOA structure. Normal dielectrics like TEOS have very strong compressive strengths, but are weak with regard to the tensile strength. One of the key BPOA failure criteria is to examine the dielectric failure in reliability screening. Therefore, the dielectric layer failure criterion is used to judge the modeling and test results.

The modeling results for probe test are shown in Table 11-6 and Fig. 11-35.

Material	Poisson Ratio	Modulus (GPa)	Yield Stress (GPa)
Silicon	0.23	169.5	
ILD	0.25	70.0	
TiW	0.25	117.0	
Al(Cu)	0.35	70.0	0.2 (25°C) 0.05 (450°C)
Au(FAB)	0.44	60.0	0.0327 (200°C)
W	0.28	409.6	
75W/Re25 (probe)	0.3	430.3	

Table 11-5 Materials Parameters

Met3 Thks / ILD3 Thks	2.16(–10%) µm	2.4 µm	3.0 (+20%) µm
2.7 (–10%) µm	4 mil 51 MPa	6 mil 103.2 MPa	6 mil 91.8 MPa
3 µm	4 mil 52 MPa	6 mil 102.3 MPa	6 mil 91.7 MPa
3.6 (+20%) µm	6 mil 105 MPa	6 mil 101 MPa	8 mil 129.3 MPa

Table 11-6 Modeling Results for First Principle Stress in ILD, The Maximum Tensile Strength for ILD is 76 MPa[20] OT = 6 mil, and The Maximum First Principle Stress is 102.3 MPa

Table 11-6 gives the probing test modeling results of first principal stress in ILD with different metal and ILD thickness in BPOA structures. From Table 11.6 we may see that due to the maximum tensile yield strength of ILD is 76 MPa, so all the yellow area data beyond this yield strength will induce the crack (see the color CD). The simulation results match the experimental results [11-20]. Figure 11-10 has shown the failure comparison, it may be seen that during the probe touch down, the local bend, and tensile stress (first principal stress) is induced. When the local tensile stress exceeds the ILD tensile yield strength, the crack appears. That is the root cause of ILD failure in probing.

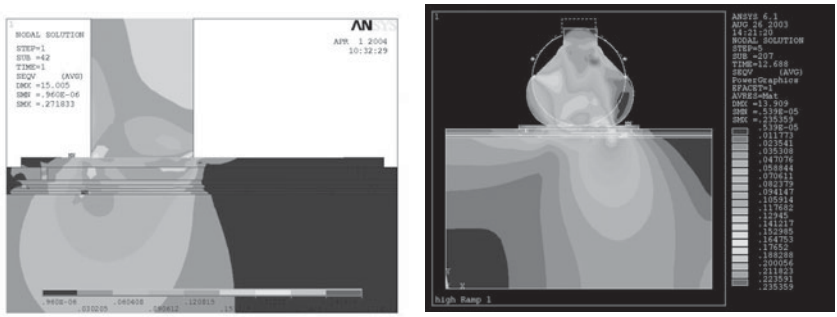

(a) Probing test (b) Wire bonding

Figure 11-36 Modeling for wire bonding and probing test.

11.4.3 Probe Test versus Wire Bonding Modeling

This section provides the modeling comparison of probe test versus wire bonding for bond pad structure. Figure 11-36 shows the results of a wire bonding process modeling with a frequency 138 kHz and a probing test modeling.

The first principal stress S1 in wire bonding with different ILD and metal thickness are shown in Table 11-7.

Compared the probe test modeling results in Table 11-6 with wire bonding results in Table 11-7, we may see that the ILD first principal stress in probe test is not sensitive to ILD3 thickness, while wire bonding is sensitive to both ILD3 and metal 3 thickness. The wire bonding trial 3 in Table 11-7 is equivalent to a probe test case with 2.7 μm thick third ILD, 2.4 μm thick metal 3 under OT 6 mil in Table 11-3. For a normal ILD and metal layers of BPOA structure in wire bonding, its ILD first principal stress is 89 MPa (see Fig. 11-37), that is equivalent to the same BPOA structure under OT 5.47 mil in probe test based on interpolation in Table 11-6. However, normal probe test only uses OT no more than 3 mil, therefore the damage to ILD layer from normal wire bonding is greater than probe test.

Trial	ILD3 Thickness (μm)	MET3 Thickness (μm)	S1 MPa
1	3	2.4	89
2	3	3	71
3	2.4	2.4	100
4	2.4	3.0	76

Table 11-7 Wire Bonding Modeling Results

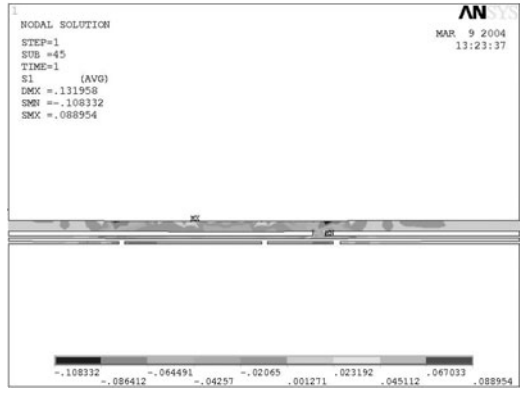

FIGURE 11-37 First principal stress of ILD in wire bonding.

11.4.4 Summary

1. The probe test modeling has shown that the probe test OT, probe type, and probe scrub of probe tip on surface of bond pad are important parameters for the damage contribution. Modeling results have revealed that local bending or tensile first principal stress in ILD, once it exceeds the ILD tensile yield strength, will induce the ILD crack. This might be the root cause of ILD failure.
2. By comparison of the probe test and the wire bonding modeling with the same BPOA structure, it has shown that for a normal BPOA structure in wire bonding and a normal probe test, the damage of ILD from wire bonding is greater than probe test.

11.5 Wire Bonding above a Laminate Substrate [11-8]

Wire bonding on a laminate substrate is an interesting topic. Because of the laminate substrate which absorbs large amount of wire bonding energy, to generate a wire bond is a challenge, especially for a laminate substrate with partial support. The goals of this section are to investigate the stress and deformation mechanism of the bonding process on a laminate substrate and to understand the impact of different wire bonding parameters to the stress balance and deformation of a bond pad with partial support at the bottom of laminate. The simulation will consider both the ultrasonic transient dynamic bonding process and the stress wave transferred to the interface between bond structure and laminate substrate. Different laminate material parameters are studied to understand their impact on the bond pad

structure. Different ultrasonic parameters such as bonding force and frequency are studied and discussed for the effects of the bonding process on laminate substrate structures with partial supports. Experimental test work includes a DOE study with different parameters of ultrasonic power and bonding force. Ball shear strength is used for the DOE test response. The trend comparison and discussion of modeling and experimental results are presented.

11.5.1 Problem Definition and Material Properties

The basic bond pad structure with laminate substrate, shown in Fig. 11-38, is created using Cu, Ni, and Au layers plated onto the laminate material. The wire bonding area is located near the via, which is also very close to the edge of the die. Furthermore, due to the substrate design the bottom is only partially supported. This increases the difficulty of wire bonding to generate a good bond. The FAB is considered as a rate dependent elastic plastic material during bonding process. The bond pad and other metal layers are treated as elastic plastic material. All the other materials are considered to be linear elastic. The related material properties are listed in Table 11-8.

Figure 11-39 illustrates the capillary on a FAB before compression. Figure 11-40 shows the local (with half via) deformed meshes of FAB and bond pad system in the wire bonding process in which the yellow area is space/air, light blue area is laminate and dark blue area is the copper (see the color CD).

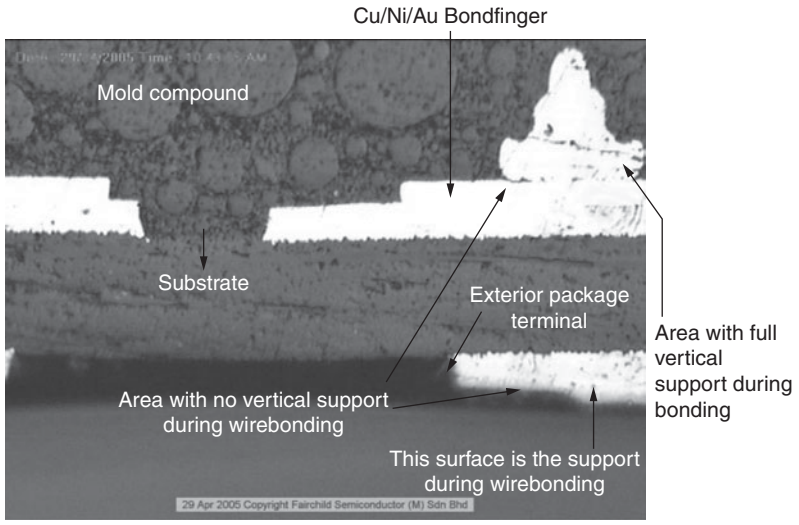

Figure 11-38 Wire bond structure—a laminate substrate with partial support at the bottom.

Material	Modulus (GPa)	Poisson Ratio	Yield Stress (GPa)
Laminate	20.5	0.39	
Ni	205	0.3	
Cu	110	0.3	
Al(Cu)	70.0	0.35	0.2 (25°C) 0.05 (450°C)
Au(FAB)	60.0	0.44	0.0327 (200°C)

TABLE 11-8 Materials Parameters

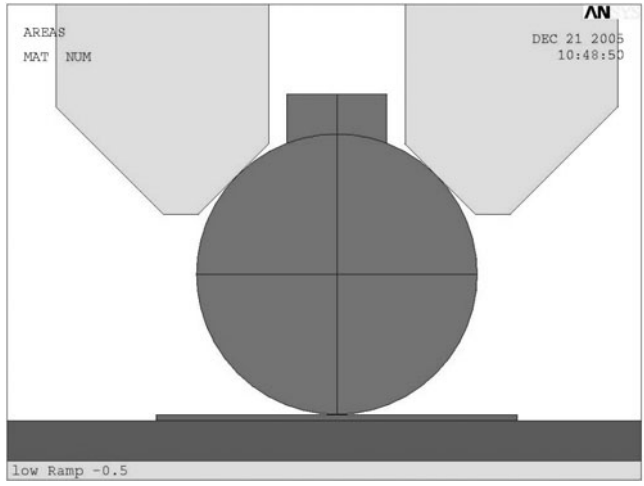

FIGURE 11-39 Ultrasonic capillary on a FAB above a laminate substrate.

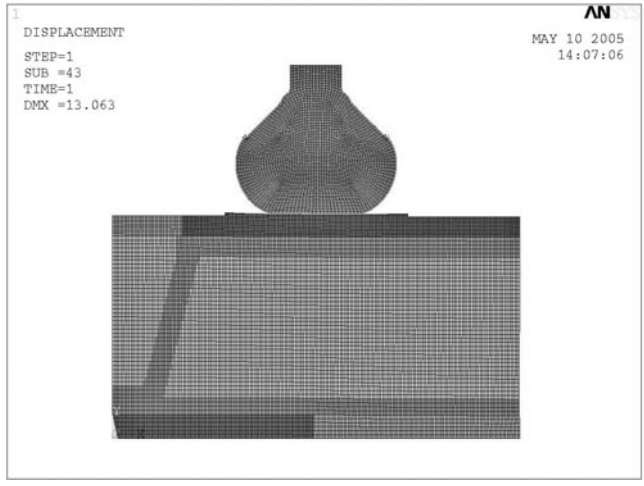

FIGURE 11-40 Meshes of a deformed FAB and bond pad model with patial supported laminate substrate.

11.5.2 Modeling Results and Discussion

Impact of Wire Bonding Force on the Wire Bonding above Laminate Substrate

The results of impact of wire bonding force are shown in Figs. 11-41 to 11-45. These results are obtained under a fixed ultrasonic frequency 128 kHz.

Figure 11-41 shows the whole von-Mises stress field of wire bonding (650 mN bonding force) with partial support under laminate. It shows there is some imbalance at both left and right sides of the bond pad structure. Higher stress is also seen at the interface between laminate and the copper material. Figure 11-42 shows the stresses (von-Mises, shear, principal stress, and vertical stress) vary along the interface of bond pad and ball. The maximum von-Mises stress at left side is 16% greater than the right side. Figure 11-43 provides the von-Mises stress and shear stress distribution on the contact layer of ball and bond pad. Figure 11-44 indicates the friction stress distribution on the ball and bond pad surface. Forty five percent of stress imbalance is found between left and right sides. Figure 11-45 illustrates the bond tilt profile. Due to the imbalance of stresses, it is very likely to induce the partially unbonded area seen on the right-hand side (see Fig. 11-42).

In order to examine the stress balance and the bond pad tilt during wire bonding process, different wire bonding forces are applied to the model.

Figure 11-45 graphs the wire bonding force applied against the resultant bond pad tilt. As the wire bonding force increases, the bond pad tilt increases. Figure 11-46*a* gives the bonding cross-section

Figure 11-41 Von-Mises stress distribution under wire bonding force 650 mN.

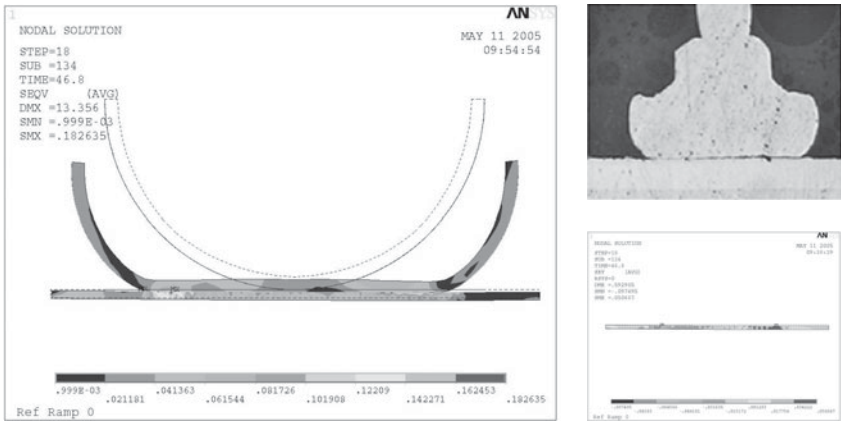

Von-Mises stress Shear stress

Figure 11-42 Von-Mises stress and shear stress at the interface layers under partial left support.

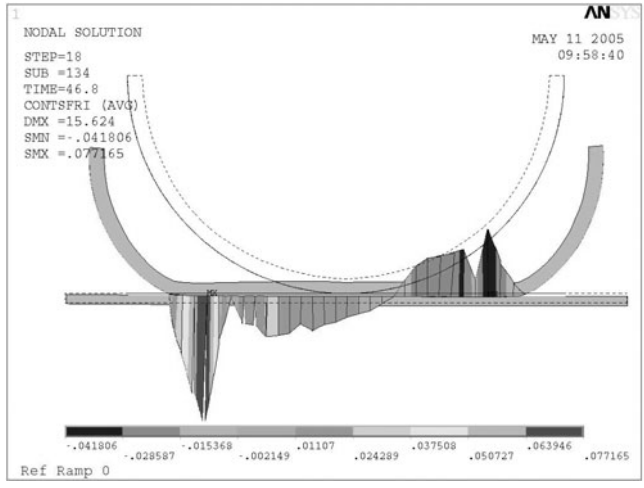

Figure 11-43 Friction stress distribution. Left side is about 45% greater than right side.

picture under wire bonding force of 200 mN. It shows at lower wire bonding force case, there is an unbonded area. Figure 11-46*b* gives the stress imbalance on bond pad varies with wire bonding force. In the ideal case the imbalance is 0%, then the two sides of the bond pad get the same stress level. From Fig. 11-46, it can be seen that for von-Mises stress as the wire bonding force increases, its imbalance is reduced. However, if the wire bond force is too big, the wire bonding will be overloaded which will reduce bonding quality. As we have

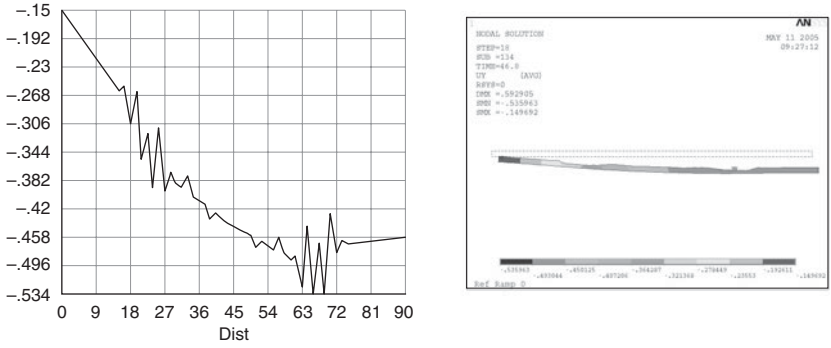

Figure 11-44 Bond pad tilt during wire bonding under partial left side support.

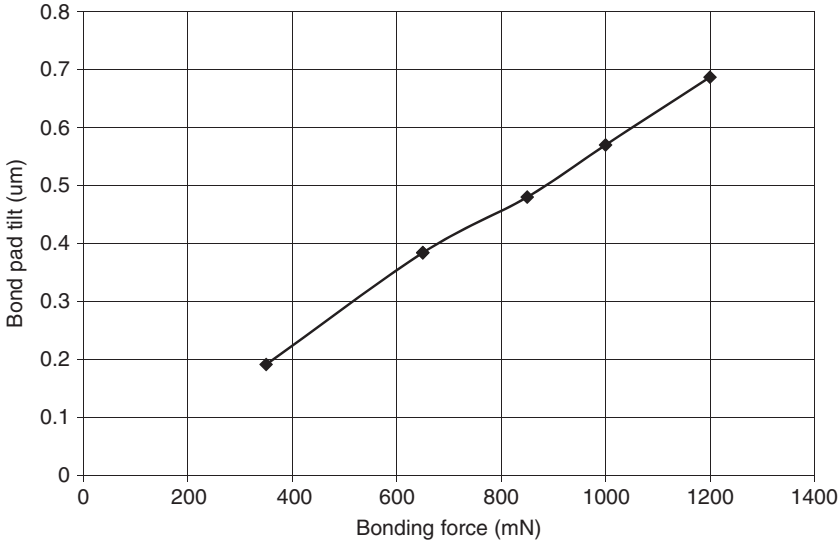

Figure 11-45 Bond pad deformation versus wire bonding force.

seen from the Fig. 11-46 the left side has been overstressed, resulting in the stress balance becoming negative when the wire bonding force exceeds 1000 mN. Therefore, if we control the wire bonding force so that it cannot overstress the bond pad, we can reduce the stress balance as much as possible.

Impact of Ultrasonic Frequency on Wire Bonding above the Laminate Substrate

The results under different ultrasonic frequency and a fixed wire bonding force 650 mN are shown in Figs.11-47 and 11-48. Figure 11-47

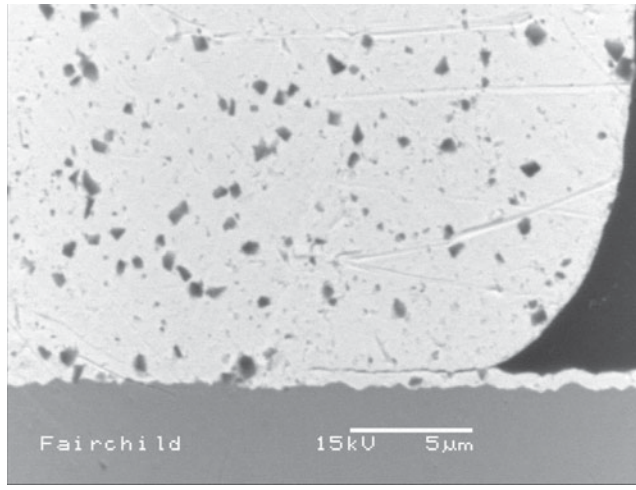

(a)

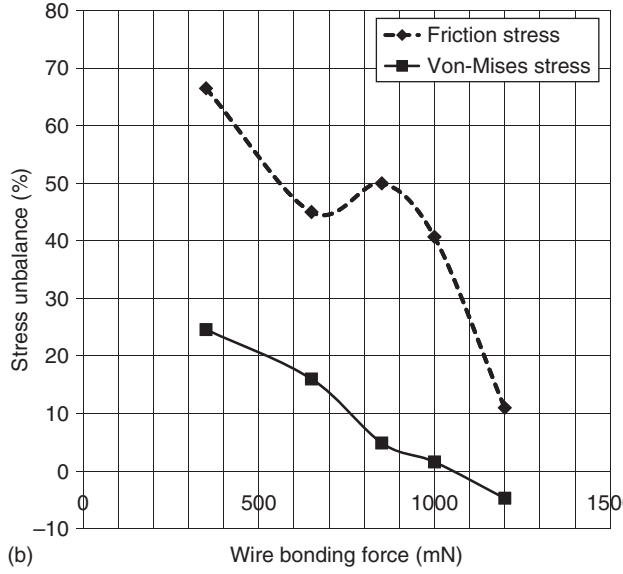

(b)

FIGURE 11-46 (*a*) Unbonded area (on right side) under bonding force 200 mN. (*b*) Stress imbalance (Stress_left-Stress_right)/Stress_left on bond pad vs. wire bonding force.

gives the bond pad tilt under different ultrasonic frequency. It looks like the impact of ultrasonic frequency is not significant.

Figure 11-48 compares the stress imbalance of friction and von-Mises stress at the contact surface of FAB and bond pad. It can be seen from this figure that the von-Mises stress imbalance becomes smaller at lower frequency and bigger at higher frequency. While

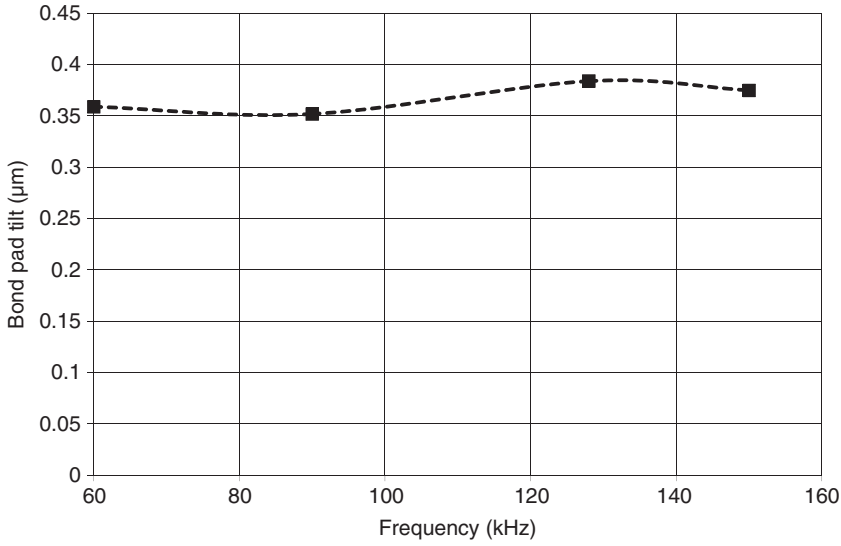

Figure 11-47 Bond pad tilt versus different ultrasonic frequencies.

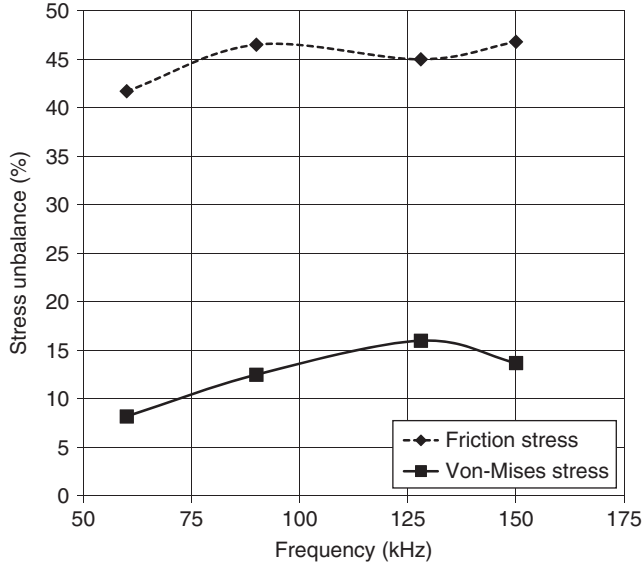

Figure 11-48 Stress imbalance (Stress_Left-Stress_Right) /Stress_Left on bond pad versus ultrasonic frequency.

the friction stress imbalance has slightly increased at higher frequency. This may be because at the higher frequency the horizontal acceleration of capillary is greater, which induces a greater inertia force on a tilted bond pad.

Impact of the Modulus of Laminate to the Bond Pad Tilt

The laminate material is considered to be an orthotropic elastic material. The out-of-plane modulus is very important to the bondpad tilt. Figure 11-49 shows that as the out-of-plane modulus of the laminate increases, the bond pad tilt decreases. This indicates that higher out-of-plane modulus of laminate is helpful to optimize the wire bonding on laminate substrate.

11.5.3 Experimental Result

The DOE test run legs for wire bonding above laminate substrate are listed in Table 11-9 with different wire bonding force and power. There are three power settings for each bonding force. The test results are shown in Figs. 11-50 and 11-51.

Figure 11-50 has shown that the capillary print mark on bond pad with two different wire bonding forces. It clearly shows that with smaller wire bonding force 25 g, the print mark on bond pad is less than half circle due to imbalance force. However, when the wire bonding force is increased to 85 g, the capillary print mark seems to be a full circle. This agrees with our modeling results regarding the stress imbalance ratio versus wire bonding force (see Fig.11-46).

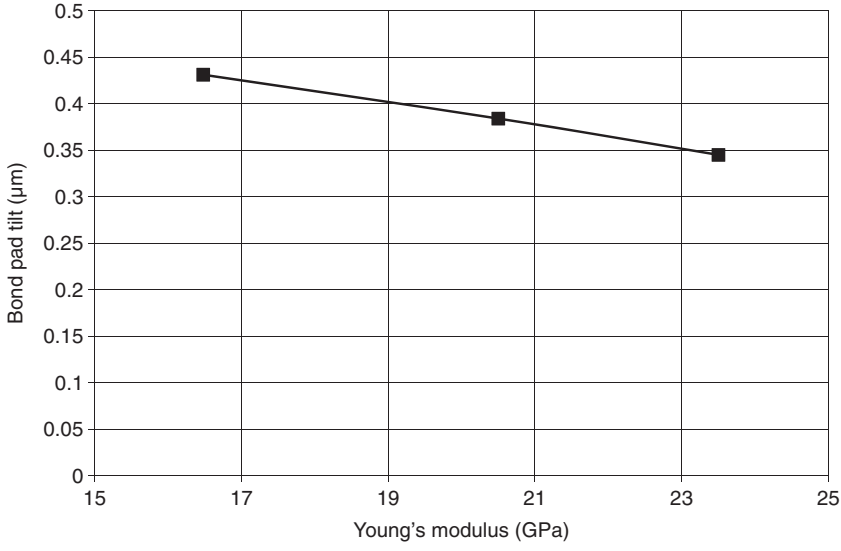

Figure 11-49 Bondpad tilt versus out-of-plane modulus of laminate.

Test Run Leg	Bonding Power (mW)	Bonding Force (g)
1	120	25
2	160	25
3	200	25
4	120	50
5	160	50
6	200	50
7	120	75
8	160	75
9	200	75
10	120	100
11	160	100
12	200	100

Table 11-9 Test DOE (Fixed Frequency—128kHz)

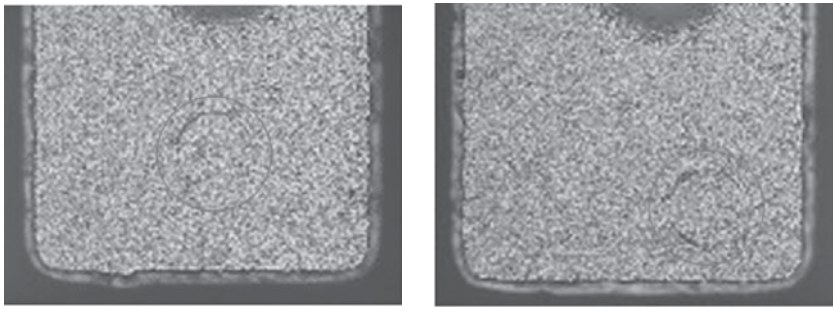

(a) Less half capillary mark with 25 gf

(b) Full circle capillary mark with 85 gf

Figure 11-50 Bonding capillary images at 25 and 85 gf showing imbalance compensation effect.

Figure 11-51 shows that at a power of 120 W, as the wire bonding force increases, the bonding ball shear strength increases significantly. However, for the higher power cases, when the bonding force increases, the ball shear strength decreases slightly. The results are consistent with our modeling results, at the frequency 128 kHz, as the wire bonding force increases, the stress imbalance becomes smaller. This induces better bonding strength. On the other hand,

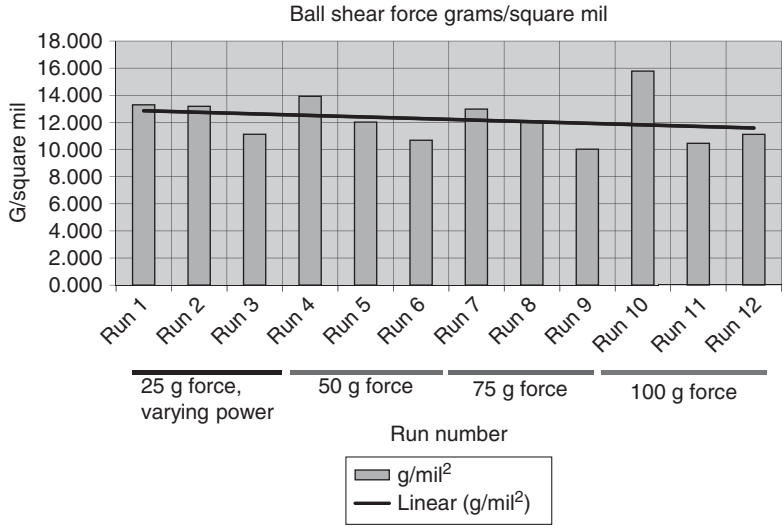

Figure 11-51 DOE of wire bonding test for a laminate substrate.

the modeling has shown the trends that as the frequency increases, the friction stress imbalance increases slightly.

11.5.4 Summary

This section studies the wire bonding process above laminate substrate with partial support by both FEA and experimental DOE. Summary of the work are as follows:

1. For the wire bonding above laminate with partial support, increasing the wire bonding force will increase the bond pad tilt, but it will reduce the stress imbalance and get better ball shear response. However, too high a wire bonding force will induce overstress on the bonding interface which will decrease the ball shear performance
2. With higher ultrasonic frequency, the stress imbalance will increase slightly. However, the ultrasonic frequency does not impact the bond pad tilt. There is a trade-off between ultrasonic power and wire bonding force.
3. For laminate material under bond pad with partial support, the greater the out-of-plane modulus, the smaller the bond pad tilt. So selecting the higher out-of-plane modulus laminate material is a good way to generate better BSOB bonding.

The methodologies of the above models may be used for optimization, relative comparison, analysis of different process parameters,

or selection of different BPOA layouts. However, since wire bonding is such a complicated process, there are a lot of challenges which need to be further investigated. Major further work includes the optimization of the capillary shape and the reliability/failure analysis by combined test with the modeling. Investigation of the intermetallic compounds between the FAB and the bond pad, and the development of an effective modeling methodology which includes the material dynamic constitutive relation of the FAB and bond pad would be a key research work of wire bonding modeling. Failure modes and the material test criteria will also be a major work to be conducted in the future.

11.6 Acknowledgments

The author wishes to thank the support from Automation Development and Process Development, Fairchild Semiconductor Corp., Fairchild Assembly Suzhou and Penang. Thanks to KNS and ASM for sharing the bonding information.

References

11-1. Ikeda,T., Miyazaki, N., Kudo, K. et al, " Failure Estimation of Semiconductor Chip During Wire Bonding Process," *ASME J. of Electronic Packaging*, Vol. 121, 1999, pp. 85–91.

11-2. Hess, K. J., Downey, S. H., and Hall, G. B., et al, "Reliability of Bond Over Active Pad Structures for 0.13-µm CMOS Technology," *Proceedings of 53th Electronic Components and Technology Conference,* New Orleans, May 2003.

11-3. Awad, E., "Active Devices and Wiring under Chip Bond Pads: Stress Simulations and Modeling Methodology," *Proceedings of 54 Electronic Components and Technology Conference,* Las Vegas, NV, May 2004, pp. 1784–1787.

11-4. Takahashi,Y. and Inoue, M., "Numerical Study of Wire Bonding-Analysis of Interfacial Deformation between Wire and Pad," *ASME J. of Electronic Packaging*, Vol. 121, 2002, pp. 27–36.

11-5. Gillotti, G. and Cathcart, R., "Optimizing Wire Bonding Processes for Maximum Factory Portability," *SEMICON West 2002 SEMI Tecgnology Symposium: International Electronics Manfacturing Technology Symposium*, 2002.

11-6. Van Driel, W. D., Janssen, J. H. J., and Van Silfhout, R. B. R., **"**On Wire Failures in Micro-electronic Packages," *EuroSimE2004*, 004, pp. 53–57.

11-7. Degryse, D., Vandevelde, B., and Beyne, E., "Mechanical FEM Simulation of Bonding Process on Cu LowK Wafers," *IEEE Transactions on Components and Packaging Technologies*, Vol. 27, No. 4, Dec., 2004, pp. 643–650.

11-8. Liu, Y., Allen, H., and Luk, T., "Simulation and Experimental Analysis for a Ball Stitch on Bump Wire Bonding Process above a Laminate Substrate," *Proceedings of 56th Electronic Components and Technology Conference*, 2006, pp. 1918–1923.

11-9. Fiori, V., Beng, L. T., and Downey, S., "3D Multi Scale Modeling of Wire Bonding Induced Peeling in Cu/Low-k Interconnects: Application of an Energy Based Criteria and Correlations with Experiments," *Proceedings of 57th Electronic Components and Technology Conference,* ECTC, 2007, pp. 256–263.

11-10. Liu, Y., Irving, S., and Luk, T., "Thermosonic Wire Bonding Process Simulation and Bond Pad Over Active Stress Analysis," *IEEE Transactions on Electronics Packaging Manufacturing*, Vol. 31, 2008, pp. 61–71.

11-11. Liu, D. S., Chao, Y. C., and Wang, C. H., "Study of Wire Bonding Looping Formation in the Electronic Packaging Process Using the Three-Dimensional

Finite Element Method," *Finite Elements in Analysis and Design*, Vol. 40, No. 3, Jan., 2004, pp. 263–286.
11-12. Yeh, Chang-Lin, Lai, Yi-Shao, and Kao, Chin-Li, "Transient Simulation of Wire Pull Test on Cu/Low-K Wafers" *IEEE Transactions on Advanced Packaging*, Vol.29, No. 3, Aug., 2006, pp. 631–638.
11-13. Harman, G., *Wire Bonding Microelectronics Materials, Processes, Reliability, and Yield*, McGraw-Hill, Vol. 1, 1997.
11-14. Langenecker, B., "Effects of Ultrasound on Deformation Characteristics of Metals," *IEEE transactions on Sonics and Ultrasonics*, Vol. SU-13, 1, 1966.
11-15. Shirai, Y., Otsuka, K., Araki, T. et al, "High Reliability Wire Bonding by the 120 KHz Frequency of Ultrasonic," *ICEMM Proceedings*, 1993, pp. 366–375.
11-16. Levine, L., "The Ultrasonic Wedge Bonding Mechanism: Two Theories Converge," *ISHM 1995, Proc*, Los Angeles, California, Oct.24-26, 1995, pp. 242–246.
11-17. Mayer, M., Paul, O., Bolliger, D., and Baltes, H., "Integrated Temperature Microsensores for Characterization and Optimization of Thermosonic Ball Bonding Process," *Proceedings of 49 th Electronic Components and Technology Conference*, San Diego, California, May 1999, pp. 463–468.
11-18. Tan, C. T. and Gan, Z. H., "Failure Mechanisms of Aluminum Bond Pad Peeling During Thermosonic Bonding," *IEEE Transactions on Device and Materials Reliability*, Vol. 3, No. 2, June, 2003, pp. 44–50.
11-19. Liu, Y., Desbiens, D., Luk, T., and Irving, S., "Parameter Optimization for Wafer Probe Using Simulation," *Proceedings of the EuroSimE 2005*, Berlin, Germany, 2005, pp. 156–161.
11-20. Liu, Y., Desbiens, D., Irving, S., and Luk, T., "Probe Test Failure Analysis of Bond Pad over Active Structure by Modeling and Experiment," *55th Electronic Components & Technology Conference*, Lake Buena Vista, FL, USA, May, 2005, pp. 861–866.

Glossary

Following are definitions of less familiar bonding, metallurgical, and packaging terms and abbreviations. In some cases, terms have been defined in context. If so they will not be redefined here, but referenced to the appropriate chapter. The definitions are not intended to be rigorous, but rather to give an introductory explanation for those who are new to wire bonding. There are several Web glossaries available, and the interested reader can try them for more help (such Web material may change).

Autoclave A temperature-humidity stress test used for assessing the reliability of plastic packages. Usually defined as 121°C, 15 PSI, and 100 % RH (similar to HAST, below; the same comments apply).

Ball Bond A wire bond usually made with gold or copper wire, in which the wire extending below the capillary is sparked (and melted) by an EFO to form a ball. The ball is then pressed against a heated bond pad, ultrasonic energy is applied, and a TS weld is made. (See Chaps. 1 and 2.)

Ball Bumping This consists of bonding a gold ball to a chip pad, breaking off the wire above the ball (sometimes coining to flatten), and using the resulting bump in place of a plated bump for TAB bonding. The wire typically contains ~1 % Pd to shorten the HAZ breakoff. The technique is also used for flip-chip bumps (often without coining). Sometimes two or three bumps are stacked to give stress relief. A variation, bonding the wire back onto the ball, is called Stud Bumping. The machine setup parameters and reliability of such bumps are generally equivalent to those of a normal ball bond. Recently "chopped" bonds in which the capillary is moved and cuts off the wire, leaving a bonded bump. Each bonder manufacturer uses its own name for the procedure. See Chap. 9, its appendix, and also the color CD for an animation of the process.

BGA Ball grid array is a package that has I/O connections made with solder bumps (similar to flip chips but larger). The bumps are placed along the bottom side of the substrate or package. The chip(s) is/are usually attached on the top of the substrate using either wire bonding or C4 interconnections.

Bonding Tool It is used for wedge bonding. Sometimes it is called a bonding "wedge" or a bonding "tip." If used for ball bonding, it is generally called a bonding "capillary."

Bonding Window (also called process windows) This is a plot of at least two bonding parameters to show the safe or preferred (optimal) operating parameters for the chosen bonder or bonding pad (materials). Examples are in Chap. 6B and Fig. 8-4. The larger/wider the window, the more tolerant the system is to making good bonds over a range of bond-parameter variations.

Breaking load (BL) The strength of a wire and its actual force (usually given in grams, grams-force, mN, etc.) required to break a particular wire in a tensile pull. It is not tensile strength, which by definition is the force per unit area.

Build-up Layers Polymer layer (usually epoxy) thin films *without* reinforcing fiber, on top of normal PC boards. Thin film metallization is applied and fine vias are made by laser drilling, yielding high performance boards. Several such layers are usually stacked and interconnected.

C4 See flip chip; has solder-bump interconnections. Could be ball bumped.

Capillary A bonding tool used for ball bonding. Its name is derived from the hole through the length of its tapered cylinder.

CERDIP Ceramic dual-in-line package, usually a glass-sealed ceramic package based on a lead frame construction.

Chemical-mechanical polishing (CMP) More related to wafer preparation and Cu/Lo-k than wire bonding. See Chap. 10.

Chemical Symbols (Too numerous to define here; see a chemical handbook.) The most commonly used symbols in this book are: Al_2O_3 = aluminum oxide, Ag = silver, Au = gold, Cu = copper, GaAs = gallium arsenide, Fe = iron, Ni = nickel, Pb = lead, Pd = palladium, Pt = platinum, Si = silicon, Sn = tin, Ti = titanium, W = tungsten, and WC = tungsten carbide.

Chip on board (COB) A bare chip attached to a PCB. Usually, it is wire bonded or C4 interconnected, but could be connected with TAB or any other method.

Chip on flex (COF) Similar to COB, except the substrate is a flex circuit (usually made of PI).

Chip on glass (COG) Similar to COB, except that the substrate is glass. An example might be placing chips on the reverse side of a flat-panel display.

Couple Used as a metallurgical couple, two metals (usually different) that have been joined together by some welding method.

Crescent Bond The final (not the ball) bond made with a capillary bonding tool. Also called a stitch bond, but strictly speaking that is an

intermediary bond, when more than one are made to different pads or positions. Sometimes it is called a wedge bond.

CSP Chip sized package or chip scale package. A package that is only a little larger than the chip itself, usually defined as being no more than 20 % larger than the perimeter of the chip. The concept is new and rapidly changing (1996). There are many variations of the designs, and most are proposed rather than in high production. The chip is protected by a thin layer of plastic. The I/O interconnections may be solder bumps (C4) or conventional leads.

CTE Coefficient of thermal expansion.

Cu/Lo-k Complex technology of using copper conductors and low dielectric-constant insulators, described in Chap. 10.

CVD Chemical vapor deposition, a gaseous method of depositing films (metal or insulator) to a substrate.

DCA Usually refers to some form of face-down flip-chip attachment, whereas COB usually refers to face-up attachment to board or substrate by wire bonding or TAB.

Design of Experiment (DOC) Usually done in a software package. Optimizes the variables for machine set up for wire bonding. Described in an appendix by Levene in Chap. 8.

Direct chip attach (DCA) Refers to attaching a bare chip directly to a board or substrate. Related to COB, SIP, etc.

Dopant Also called doping agent. An impurity element added to a crystal, semiconductor lattice in low concentrations (usually $<10^{-3}$ ppm) in order to alter the optical/electrical/mechanical properties of a material. In electronic packaging, it also is used to indicate small quantities of impurities put in bonding wire, plastics, solders, or other materials. In such cases, it is usually added at <1 % level, typically by weight.

Electronic flame-off (EFO) This supplies the spark that melts the wire, thus forming the ball that is used in a ball-bonding process. Polarity of the wire when making ball bonds positive or negative. (Negative does not sputter the gold and thus results in longer tool life and also in more uniform balls for high yield and fine pitch.)

Eutectic An alloy of two or more metals that has a sharp melting point (e.g., for tin-lead solder this is 63 % Sn and 37 % Pb, MP = 183°C), and also the lowest melting point of alloys containing those metals.

Fatigue A metallurgical process in which the metal weakens after repeated applications of stress. See Chaps. 3 and 8.

Flip Chip Also called C4. A face-down chip mounting technique. The Al chip I/O pads are protected with a diffusion barrier, then coated with solder or other conductors. Electrical contact to the package is made by soldering the inverted chip pads to equivalently placed pads on the

package. Variations include ball-bond bumping, conductive polymer bumping, etc.

Fracture Toughness See Sec. 8.5 (App. 8A).

Hardness Measurements In microelectronics one measures, with a *Microhardness tester*, the hardness of bonding wire, balls, and other relatively thick objects. As the test material thickness decreases to ~1 μm, the measurement accuracy can be affected by hard substrate properties. For that, *Nano-, Ultramicro-, and Tribo-indenters (different company names for similar instruments)* are used to measure thin films, such as bond pads and even thinner films. These latter testers apply a low load, to achieve shallow penetration. The load versus penetration depth-curve is recorded during penetration using a three-sided diamond pyramid indenter into the material at very low loads. The test results come solely from analysis of force/displacement data. They can also obtain the elastic modulus and other properties (which microhardness testers do not). These instruments are expensive and mostly used in research laboratories in universities and corporations. The joke is that each nanohardness tester is accompanied by a PhD.

HAZ The heat affected zone above a ball bond. Discussed in Chap. 3.

HF High Frequency (Not hydrofluoric acid!). Used to indicate that the ultrasonic bonding (power supply) frequency is higher than the traditional 60 kHz. Frequencies that have been used range from 80 kHz to about 300 kHz.

Highly accelerated stress test (HAST) Often referred to as a pressure-cooker test. It is intended to reveal reliability failures in plastic packages very quickly. The usual conditions are 130°C, 85 % RH, at 18 psig (EIA-JEDEC-JC-13). The problem with such highly accelerated tests is that they may hydrolyze the plastics and create failure modes that would not otherwise exist. Nevertheless, they are often required.

Input/output (I/O) Usually refers to the electrical connections to a chip, package, or module. In this book, the term usually refers to the number of bond pads.

ITRS The International Technology Roadmap for Semiconductors. It is sponsored by the five leading chip manufacturing regions in the world: Europe, Japan, Korea, Taiwan, and the United States. Provides a roadmap (assessment) of the needs and challenges facing the semiconductor industry over 15 years.

Known good die (KGD) A pretested (often burned-in) die that can be put in a multichip module (SIP, SOP) with confidence that it will not fail. Thus, no rework is required.

Kovar Iron, nickel, and cobalt alloy with low expansion that matches the CTE of some glasses. It was extensively used for packages in the past, but only occasionally today, primarily in hybrid packages.

Miscible When two liquids mix completely. In metallurgy it would result in a single phase.

Multichip module (MCM) Any package containing several chips (currently, preferred terminology is SIP, SOP, etc.). It may also contain chip capacitors and other passive components. If the dielectric is ceramic, then it is -C; if deposited film dielectrics (e.g., polyimide), it is -D; if laminate (e.g., PCB material), it is -L. Bonding conditions to MCMs are described in Chap. 9.

Nondestructive Pull Test (NDPT) A wire bond is tested at a preselected (nondestructive) force that is below the normal force that causes failure (described in Chap. 4).

Nugget A term applied to the remaining welded part of a wedge bond, usually after a pull test that removed the free wire.

Overbonding This is a generic term applied to bonding machine parameter setups in which one or more of the bonding parameters (force, time, ultrasonic power, and/or temperature) are significantly greater than is required to produce a normal bond. Usually, this results in the bond being overdeformed (flattened) and sometimes damaging the pad underlayers (cratering).

Pad Usually referred to as the bond pad. It is a small area of a bondable metal onto which the wire is bonded (one of the weldments).

Peeling Tweezer pulls for "quality" and troubleshooting of wedge bonds and crescent (tail) bonds of ball bonds. Peel testing of tail bonds.

PGA Pin grid array (package). A package that usually has many I/Os in the form of extending pins. It may be made of ceramic or plastic (usually laminate).

PGW Parallel gap welding, sometimes called split electrode welding. An electrical discharge welding method that can be used for wires ~75 μm or greater (described in Chap. 2).

PIP Package in a package, see Chap. 9.

Polyimide (PI) An insulating polymer with a high T_g that is used in MCMs.

Polytetrafluoroethylene (PTFE) Called Teflon and other trade names.

POP Package on a package, see Chap. 9.

Popcorn Effect A complex interaction between moisture absorbed in a plastic molding compound, the die-attach polymer, the lead frame, and temperature during surface-mount soldering. When the plastic cracks or separates from the chip or lead frame, a popping sound is heard, as when cooking popcorn. The device is destroyed.

Printed circuit board (PCB) A laminated polymer, usually epoxy, reinforced with woven fibers of glass or other fiber materials. It has copper-based conductors on the surface and usually inside as well.

QFP Quad flat pack.

SOP System on a package, see ITRS SIP White paper (from Web site in Bibliography).

SPC Statistical process control.

Stud Bump A generic term applied to a ball bump bonded to a bond pad. It includes variations of making ball bonds, with the wire neck bonded-off, cut-off, or pulled-off, leaving a bonded ball which may be used for flip chip or other applications. See Chap. 9, appendix.

System in a package (SIP) May resemble a traditional thick film Hybrid but often made with an organic substrate.

T_g The glass-transition temperature of a plastic. It is the point or region where a plastic (usually thermosetting) begins to rapidly soften. Wire bonding becomes difficult above T_g; see Chap. 10. An example is FR-4 PCBs, which usually soften in the 110 to 130°C range, see Chap. 9.

Tape automated bonding (TAB) A non-wire bonding process discussed in Chap. 2.

TCE Thermal coefficient of expansion, sometimes rearranged and called CTE.

TS An abbreviation for *Thermosonic Bonding*. Ultrasonic bonding in which the bond pad/chip/package is heated ~100 to 200°C to help form a better, faster bond.

TSOP Thin, small outline package. A small plastic-encapsulated-chip package, but larger than a CSP.

Tweezer Welding An older electrical discharge welding method used for bonding large-diameter Al wires, usually 400 μm or larger, to extended posts in power device packages. This method is described in Chap. 2.

US Used as abbreviation for "ultrasonic" and "ultrasonic energy" in context. (Not to be confused with other common abbreviations using that symbol.)

Wedge Bond A bond made by a bonding tool or capillary directly pressing against a round or ribbon wire (not a ball). (See Chaps. 1 and 2.)

Weldment One of the materials being welded; for example, the wire or the bond pad.

WH Work holder, sometimes called work stage or bonding stage. It holds the device or package during wire bonding. It contains a means of rigidly clamping the device, and, if used for thermosonic bonding, it will be heated, usually to 150°C or higher. It is usually placed on an automated or manual movable stage. If used for high volume production, it may be a part of an automatic feed system.

Bibliography

Note that some of these suggestions are books and reports, while many others are Web sites. These have been verified by the author on 6/25/09. All are thought by this author, to be potentially useful; however, a reader should be aware that after this book was published, some of the Web sites could be changed (be discontinued, improved, etc.) in the future. The entries are generally in alphabetical order of their author(s) or for Web sites, their titles, since their information is widely diverse. Only Web sites that give substantial technical information, such as materials, properties, technical papers, etc., are included. Sites that are primarily equipment sales platforms are omitted since these change frequently and are easily accessible from general Web searches. (It may be necessary to paste the address directly into the Web browser, and then click.)

For those who are not familiar with Web searching, we note that one can enter the authors' names and (perhaps) a title into Google Scholar or Yahoo and it will usually give the paper with abstract download available. If an organization has contract with the publisher, example IEEExplore (see below), Science Direct, etc., one can usually download the full pdf of such paper in minutes. Some publishers require payment for each download, but they are still quickly available!

http://www.asminternational.org/asmenterprise/apd/help/Intro.aspx
ASM Society Information on metallurgical phase diagrams, with *excellent explanations*.

Charles, H. K., The Wirebonded Interconnect: A Mainstay for Electronics, Chapter in: Suhir, E., Lee, Y. C., and Wong, C. P., *Micro- and Opto-Electronic Materials and Structures*, Springer, 2007, V-2, pp. 71–120.
A good overview/summary of wire bonding technology.

http://www.dage-group.com/technical-papers-bondtesters

http://nepp.nasa.gov/wirebond/
NASA basic and advanced information on wire bond failures, with many links and references.

http://www.gaisertool.com/catalog/2.pdf
The CoorsTech/Gaiser catalogue has a great deal of explanation of bonding tools as well as considerable wire bonding trouble shooting information.

Nordic Electronics Packaging Guideline:
http://extra.ivf.se/ngl/#Level%200.%20Guideline%20structure
A wide ranging introduction/applications of packaging and interconnection technologies. Site is updated from time to time.

http://ieeexplore.ieee.org/
Web site that has most IEEE transactions and proceedings. These are usually available for full pdf download if the seeker is a member/or the organization is, of the IEEE, or through technical libraries. We note that essentially all IEEE transactions for approximately 50 years and somewhat less for proceedings have been scanned into this service.

Fraunhoffer IZM listing of papers (with abstracts) that they have published in electronic packaging.
http://www.izm.fhg.de/EN/publi_download/papers/index.jsp

S. K. Prasad, *Advanced Wirebond Interconnection Technology*, Bangalore, India, Kluwer Academic Publishers, 2004.
A book on wire bonding including extensive elementary explanations for training.

R. R. Tummala, E. J. Rymaszewski, and A. G. Klopfenstein, *Microelectronics Packaging Handbook*, Van Nostrand Reinhold, NY, 1989. Also Part II, Semiconductor Packaging, Chapman & Hall, NY, 1997. (Springer)

http://www.kns.com/Templates/showpage.asp?TMID=111&FID=114&PID=14121
Includes downloads or links to all K&S wire bonding papers. Some tutorial and others very advanced and specialized. Also see,
http://www.kns.com/knsnew/library/articles/ballbondcapillaries.htm, has detailed pictures of bonding motions http://www.kns.com/_Flash/CAP_BONDING_CYCLE.swf

http://www.utilisegold.com/products_suppliers/directory/4/bonding_wire
The World Gold Council has many links to wire sources and papers.

http://www.itrs.net/Links/2007ITRS/Home2007.htm
http://www.itrs.net/Links/2007ITRS/2007_Chapters/2007_Assembly.pdf
The ITRS 2007 for Assembly and Packaging Roadmap is available from the WEB, includes much information and special reports, such as the SIP Report, requirements for bond and flip-chip pitch, etc.

http://www.itrs.net/Links/2007ITRS/LinkedFiles/AP/AP_Paper.pdf
ITRS SIP White Paper, V-9, 2007, 127 Pages (tables updated for 2008). It describes the totality of "system in a package" technology, POPs, PIPs, stacked chips, optoelectronic integration, etc. It will be kept up to date, and is recommended to all as a complete overview of that entire advanced assembly technology. All of the ITRS roadmaps are available for free downloading from http://www.itrs.net/reports.html

Index

Note: Page numbers referencing figures are followed by an "*f*"; page numbers referencing tables are followed by a "*t*".

C

G

H

M

N

O

P

T

U

V

W

Y

Z

CD WARRANTY

This software is protected by both United States copyright law and international copyright treaty provision. You must treat this software just like a book. By saying "just like a book," McGraw-Hill means, for example, that this software may be used by any number of people and may be freely moved from one computer location to another, so long as there is no possibility of its being used at one location or on one computer while it also is being used at another. Just as a book cannot be read by two different people in two different places at the same time, neither can the software be used by two different people in two different places at the same time (unless, of course, McGraw-Hill's copyright is being violated).

LIMITED WARRANTY

McGraw-Hill takes great care to provide you with top-quality software, thoroughly checked to prevent virus infections. McGraw-Hill warrants the physical CD-ROM contained herein to be free of defects in materials and workmanship for a period of sixty days from the purchase date. If McGraw-Hill receives written notification within the warranty period of defects in materials or workmanship, and such notification is determined by McGraw-Hill to be correct, McGraw-Hill will replace the defective CD-ROM. Send requests to:

McGraw-Hill
Customer Services
P.O. Box 545
Blacklick, OH 43004-0545

The entire and exclusive liability and remedy for breach of this Limited Warranty shall be limited to replacement of a defective CD-ROM and shall not include or extend to any claim for or right to cover any other damages, including but not limited to, loss of profit, data, or use of the software, or special, incidental, or consequential damages or other similar claims, even if McGraw-Hill has been specifically advised of the possibility of such damages. In no event will McGraw-Hill's liability for any damages to you or any other person ever exceed the lower of suggested list price or actual price paid for the license to use the software, regardless of any form of the claim.

McGRAW-HILL, SPECIFICALLY DISCLAIMS ALL OTHER WARRANTIES, EXPRESS OR IMPLIED, INCLUDING, BUT NOT LIMITED TO, ANY IMPLIED WARRANTY OF MERCHANTABILITY OR FITNESS FOR A PARTICULAR PURPOSE.

Specifically, McGraw-Hill makes no representation or warranty that the software is fit for any particular purpose and any implied warranty of merchantability is limited to the sixty-day duration of the Limited Warranty covering the physical CD-ROM only (and not the software) and is otherwise expressly and specifically disclaimed.

This limited warranty gives you specific legal rights; you may have others which may vary from state to state. Some states do not allow the exclusion of incidental or consequential damages, or the limitation on how long an implied warranty lasts, so some of the above may not apply to you.